LEABHARLANN CHOLÁISTE NA TRÍONÓIDE, BAILE ÁTHA CLIATH | TRINITY COLLEGE LIBRARY DUBLIN
Ollscoil Átha Cliath | The University of Dublin

Terms and Conditions of Use of Digitised Theses from Trinity College Library Dublin

Copyright statement

All material supplied by Trinity College Library is protected by copyright (under the Copyright and Related Rights Act, 2000 as amended) and other relevant Intellectual Property Rights. By accessing and using a Digitised Thesis from Trinity College Library you acknowledge that all Intellectual Property Rights in any Works supplied are the sole and exclusive property of the copyright and/or other IPR holder. Specific copyright holders may not be explicitly identified. Use of materials from other sources within a thesis should not be construed as a claim over them.

A non-exclusive, non-transferable licence is hereby granted to those using or reproducing, in whole or in part, the material for valid purposes, providing the copyright owners are acknowledged using the normal conventions. Where specific permission to use material is required, this is identified and such permission must be sought from the copyright holder or agency cited.

Liability statement

By using a Digitised Thesis, I accept that Trinity College Dublin bears no legal responsibility for the accuracy, legality or comprehensiveness of materials contained within the thesis, and that Trinity College Dublin accepts no liability for indirect, consequential, or incidental, damages or losses arising from use of the thesis for whatever reason. Information located in a thesis may be subject to specific use constraints, details of which may not be explicitly described. It is the responsibility of potential and actual users to be aware of such constraints and to abide by them. By making use of material from a digitised thesis, you accept these copyright and disclaimer provisions. Where it is brought to the attention of Trinity College Library that there may be a breach of copyright or other restraint, it is the policy to withdraw or take down access to a thesis while the issue is being resolved.

Access Agreement

By using a Digitised Thesis from Trinity College Library you are bound by the following Terms & Conditions. Please read them carefully.

I have read and I understand the following statement: All material supplied via a Digitised Thesis from Trinity College Library is protected by copyright and other intellectual property rights, and duplication or sale of all or part of any of a thesis is not permitted, except that material may be duplicated by you for your research use or for educational purposes in electronic or print form providing the copyright owners are acknowledged using the normal conventions. You must obtain permission for any other use. Electronic or print copies may not be offered, whether for sale or otherwise to anyone. This copy has been supplied on the understanding that it is copyright material and that no quotation from the thesis may be published without proper acknowledgement.

The telomere-associated (*TLO*) genes of *Candida dubliniensis*

A thesis submitted to the University of Dublin, Trinity College, in fulfillment of the requirements for the degree Doctor of Philosophy (Ph.D.) by

John Haran

September 2014

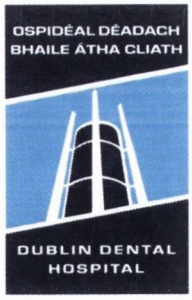

Microbiology Research Unit,
Division of Oral Biosciences,
Dublin Dental University Hospital,
Trinity College,
Dublin, 2.

TRINITY COLLEGE
1 4 MAY 2015
LIBRARY DUBLIN
Thesis 10501

Declaration

I declare that this thesis has not been submitted as an exercise for a degree at this or any other university and it is entirely my own work.

I agree to deposit this thesis in the University's open access institutional repository or allow the library to do so on my behalf, subject to Irish Copyright Legislation and Trinity College Library conditions of use and acknowledgement.

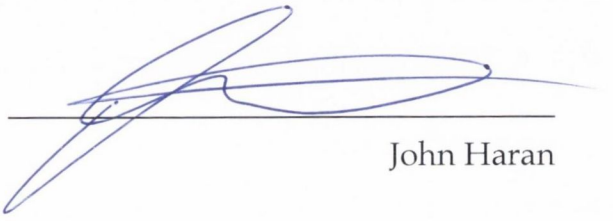

John Haran

Summary

Candida species are members of the *Saccharomycetaceae* and are the most common cause of fungal infections in humans. Diseases caused by these yeasts range from superficial infections (e.g. oropharyngeal & vulvovaginal candidiasis) to life-threatening systemic infections (e.g. candidemia). *C. albicans* is the most prevalent species associated with such infections. *C. dubliniensis* is a closely related species, yet is significantly less virulent. Evidence for this disparity has been supported with *in vivo* and *in vitro* virulence models. Genome comparisons were carried out to identify differences in gene content in an attempt to explain the contrasting virulence between these closely related species. The TeLOmere-associated (*TLO*) gene family had the largest difference in copy number between the species, with 14 (plus one pseudogene) in *C. albicans* compared to 2 in *C. dubliniensis*. The *TLO*s were originally identified as putative transcriptional activators with some homology to the Med2 subunit of the Mediator complex in *Saccharomyces cerevisiae*

A range of *in silico* analyses, as well as molecular techniques such as Southern immunoblotting and polymerase chain reaction (PCR) were performed to characterise the *TLO* gene family. Quantitative real-time PCR (qRT-PCR) was used to measure expression of the genes and it was observed that expression of both genes increases with growth stage, with *TLO1* expression higher than *TLO2*. Homology to Med2 in *S. cerevisiae* was confirmed *in silico*, which supports previous assertions by other groups. Interestingly, allelic heterozygosity was observed for *TLO2*, with one intact and one truncated copy in Wü284.

Both *TLO* genes were deleted separately in *C. dubliniensis* and phenotypic analyses were carried out under a range of conditions. No difference in antifungal susceptibility was observed. One of the main phenotypes observed was a defect in filamentation (including hyphal formation and chlamydospore formation), a process that is important to both virulence and nutrient acquisition. Upon deletion of both *TLO*s, *C. dubliniensis* could no longer form true hypha, instead exhibiting a cell separation defect. Moreover, biofilm formation, which is a major challenge in healthcare settings, was affected by deletion of the *TLO*s. As well as these, defects in the response to oxidative, osmotic and cell wall stress were observed in strains lacking *TLO*s. Growth was also retarded upon disruption of *TLO*s, particularly in media with alternate carbon sources.

In conjunction with the phenotypic analyses, DNA microarrays (with qRT-PCR to confirm) were used to characterise the transcriptional change upon deletion of *TLO*s in order to identify any regulatory pathways affected by their deletion. Expression of genes

vital to processes such as filamentation, response to stress, nutrient acquisition and the starvation response were significantly altered in a double *tlo* mutant. As well as this delayed changes in expression suggested a requirement for *TLO* expression in mediating rapid transcriptional responses to growth in serum.

Chromatin immunoprecipitation (ChIP), both on a global level and single-gene level, was carried out to explore the relationship of Tlo1 with DNA. Tlo1 was observed to be enriched at most coding genes as well as (sub-)telomeres and the Major Repeat Sequence (MRS). Data from these experiments, in conjunction with the bioinformatic, phenotypic and expression data, point towards a functional relationship with the Mediator complex.

Our data suggest that the Tlos are part of the Mediator complex, specifically that they are the previously unidentified orthologs of Med2 in *C. albicans* and *C. dubliniensis*. This study suggests that the *TLO* genes have evolved to expand across all sub-telomeres in *C. albicans* compared to *C. dubliniensis*, which has conferred an evolutionary advantage in the increased ability to modulate specific transcriptional responses. As well as this, our data have shown that expression of *TLO* genes is essential for optimal growth, filamentation and response to stress in *C. dubliniensis* making the *TLO* genes important regulators of fungal virulence.

Table of Contents

	Index of Figures	i
	Index of Tables	iv
	Abbreviations	v
	Acknowledgements	ix
	Publication	xi
Chapter 1.	**Introduction**	1
1.1.	***Candida* – a species of pathogenic yeast**	2
1.2.	**Development of *Candida* infections**	3
1.3.	**Epidemiology of *Candida* infections**	5
1.4.	**Treatment of Candidiasis**	6
1.5.	***C. albicans* and *C. dubliniensis***	8
1.6.	**Morphology as a virulence determinant of *Candida* species**	9
1.7.	**Biofilm formation in *Candida* spp.**	11
1.8.	**Virulence and the stress response**	13
1.9.	**Genomic comparisons**	14
1.10.	**The *TLO* genes**	16
1.11.	***TLO* genes and the Mediator complex**	17
1.12.	**Rationale for this study**	18
Chapter 2.	**Materials and Methods**	19
2.1.	**General microbiological methods**	20
2.1.1.	Strains and isolates	20
2.1.2.	Growth conditions and culture media	20
2.1.3.	Buffers and solutions	21
2.1.4.	Reagents, enzymes, chemicals, antibiotics and antifungal agents	21
2.1.5.	Oligonucleotides	22
2.1.6.	Storage of isolates for future use	22
2.1.7.	Cell counting	22
2.1.8.	Quantification and quality assessment of nucleic acids	23
2.1.9.	Agarose gel electrophoresis	23
2.1.10.	Microscopy	24
2.1.10.1.	*Light microscopy*	24
2.1.10.2.	*Phase contrast microscopy*	24
2.1.10.3.	*Fluorescent microscopy*	25
2.1.10.4.	*Scanning electron microscopy (S.E.M.)*	25
2.2	**DNA techniques**	25
2.2.1.	Whole genomic DNA purification	25
2.2.2.	Rapid extraction of genomic DNA from *Candida* strains	27
2.2.3.	DNA ligation	28
2.2.4	Plasmid DNA isolation	28

2.2.5.	DNA sequencing	29
2.2.6.	Basic analysis of DNA sequences	29
2.2.7.	Restriction enzyme digestion of DNA	29
2.2.8.	Transformation of *Candida* strains by electroporation	30
2.3.	**Polymerase chain reaction (PCR)**	31
2.3.1.	Routine PCR	31
2.3.2.	Cleanup of PCR products	31
2.3.3.	Quantitative real-time PCR (qRT-PCR)	32
2.3.3.1.	*Relative quantification*	32
2.3.3.2.	*Absolute quantification (Standard curve)*	33
2.4.	**Southern Immunoblot hybridisation**	34
2.4.1.	Amplification and labelling of DNA probe	34
2.4.2.	Sample preparation and membrane transfer	35
2.4.3.	Pre-hybridisation	36
2.4.4.	Hybridisation	36
2.4.5.	Washing	37
2.4.6.	Detection	37
2.4.7.	Development	38
2.5.	**RNA techniques**	38
2.5.1.	RNA extraction	38
2.5.1.1.	*Rapid method*	38
2.5.1.2.	*Freeze-fracture method*	39
2.5.2.	cDNA synthesis	40
Chapter 3.	**Characterisation of the *TLO* genes in *C. dubliniensis***	43
3.1.	**Introduction**	44
3.2.	**Materials and Methods**	46
3.2.1.	Chemicals, buffers, solutions & oligonucleotides	46
3.2.2.	Bioinformatic analyses of *TLO* genes	46
3.2.3.	Bioinformatic analyses of Tlo proteins	46
3.2.4.	Construction of Tlo-Gfp fusion proteins	47
3.3.	**Results**	48
3.3.1.	Confirming the genotypes of *C. dubliniensis TLO* mutant strains.	48
3.3.1.1.	*Using PCR to confirm genotype*	48
3.3.1.2.	*Using Southern immunoblotting to determine genotype*	49
3.3.2.	Bioinformatic analysis of *TLO* genes	50
3.3.2.1.	*Basic analyses of the TLO genes in C. dubliniensis*	50
3.3.2.2.	*Comparison of TLO genes in C. dubliniensis*	50
3.3.2.3.	*Synteny and homology with other species*	51
3.3.3.	Confirmation of expression of *TLO* genes	51
3.3.4.	Bioinformatic analysis of the Tlo proteins	53
3.3.4.1.	*Tlo proteins across the CTG clade*	53
3.3.4.2.	*Tlo1 and Tlo2 display homology to ScMed2*	54
3.3.5.	Tlo proteins may encode proteins that localise to the nucleus	54
3.4.	**Discussion**	56

3.4.1.	*TLO* genotype	56
3.4.2.	Tlo proteins	57
Chapter 4.	**Phenotypic analysis of *tlo* mutant strains of *Candida dubliniensis***	61
4.1.	**Introduction**	62
4.2.	**Materials and Methods**	66
4.2.1.	Spot plate assay	66
4.2.2.	Antifungal susceptibility screening	66
4.2.3.	Induction of the white-opaque switch	67
4.2.4.	Induction of chlamydospore formation	67
4.2.5.	Growth rate determination	68
4.2.6.	Agar invasion experiments	69
4.2.7.	Hyphal production assay	69
4.2.7.1.	*Large-scale method*	69
4.2.7.2.	*Small-scale method*	70
4.2.8.	Biofilm formation assay	70
4.2.8.1.	*Induction of biofilm formation*	70
4.2.8.2.	*Quantitative measurement of biofilm formation*	71
4.2.8.2.1.	*XTT Method*	71
4.2.8.2.2.	*Biomass (staining) method*	72
4.3	**Results**	73
4.3.1.	Effect of temperature on the growth of *C. dubliniensis tlo* mutants	73
4.3.2.	Antifungal susceptibility of *C. dubliniensis tlo* mutants	73
4.3.3.	Effect of *TLO* disruption on cell wall integrity	73
4.3.4.	Effect of detergent on *tlo* mutant strains of *C. dubliniensis*	74
4.3.5.	*TLO* disruption causes a defect in cell separation	74
4.3.6.	Effect of *TLO* disruption on the response of C. *dubliniensis* to osmotic stress	76
4.3.7.	Effect of *TLO* disruption on the response to oxidative stress	76
4.3.7.1.	*Spot plate assay*	76
4.3.7.2.	*Broth micro-dilution test*	77
4.3.8.	White-opaque switching frequency in *C. dubliniensis TLO* strains	78
4.3.9.	Effect of *TLO* disruption on the formation of chlamydospores in C. *dubliniensis*	78
4.3.10.	*TLO* disruption affects growth of C. *dubliniensis*	79
4.3.10.1.	*Effects of TLO disruption on growth in nutrient-rich conditions*	79
4.3.10.2.	*Effects of TLO disruption on growth in alternate carbon sources*	79
4.3.10.3.	*Effects of TLO disruption on growth in minimal media*	80
4.3.10.4.	*Effects of TLO disruption on growth in Spider Medium*	81
4.3.11.	Effect of *TLO* disruption on filamentous colony morphology	81

4.3.12.	Effect of *TLO* disruption on filamentation in liquid culture	82
4.3.13.	Effect of *TLO* disruption on the ability of C. *dubliniensis* to form and maintain biofilms	83
4.3.14.	Ability of *C. dubliniensis tlo* mutant strains to invade solid substrates	80
4.4.	**Discussion**	85
4.4.1.	The *TLO*s regulate the morphological state of *C. dubliniensis*.	85
4.4.2.	The *TLO*s affect the tolerance of *C. dubliniensis* to environmental stress.	86
4.4.3.	*TLO1* versus *TLO2*.	88
Chapter 5.	**Expression analysis of *tlo* mutant strains in *Candida dubliniensis***	91
5.1.	**Introduction**	92
5.2.	**Materials and Methods**	94
5.2.1.	Two-colour DNA microarray analysis	94
5.2.1.1.	*Sample preparation*	94
5.2.1.2.	*Labelling & Amplification*	94
5.2.1.3.	*Cleanup & Purification*	95
5.2.1.4.	*Hybridisation*	96
5.2.1.5.	*Washing*	97
5.2.1.6.	*Scanning & image processing*	97
5.2.1.7.	*Analysis*	97
5.3.	**Results**	98
5.3.1.	Investigation of the effects of deletion of *TLO* genes in C. *dubliniensis* under nutrient-rich conditions	98
5.3.1.1.	*Basic analysis*	98
5.3.1.2.	*Genes expressed at higher levels in the tlo deletion mutant*	99
5.3.1.3.	*Genes expressed at lower levels in the tlo deletion mutant*	100
5.3.2.	Investigation of the effects of deletion of *TLO* genes in C. *dubliniensis* under early hypha-inducing conditions	101
5.3.2.1.	*Genes expressed at higher levels in a tlo deletion mutant*	101
5.3.2.2.	*Genes expressed at lower levels in a tlo deletion mutant*	102
5.3.3.	Investigation of the effects of deletion of *TLO* genes in C. *dubliniensis* under later hypha-inducing conditions	102
5.3.3.1.	*Genes expressed at higher levels in a tlo deletion mutant*	103
5.3.3.2.	*Genes expressed at lower levels in a tlo deletion mutant*	103
5.3.4.	Comparison of data sets	104
5.3.5.	Confirmation of select expression patterns	104
5.4.	**Discussion**	107
5.4.1.	Filamentation & biofilm formation	107
5.4.2.	Stress responses	108
5.4.3.	Nutrient acquisition & starvation response	112
5.4.4.	Closing remarks & additional observations	116

Chapter 6.	**The relationship between Tlo1 and DNA in *C. dubliniensis***	119
6.1.	**Introduction**	120
6.1.1.	Opening remarks	120
6.1.2.	ChIP-on-chip	121
6.2.	**Materials and Methods**	123
6.2.1.	Estimating extent of cell lysis and breakage	123
6.2.1.1.	*Visual estimation of lysis*	124
6.2.1.2.	*Bradford assay*	124
6.2.2.	Chromatin immunoprecipitation (Berman Laboratory Method)	125
6.2.2.1.	*Growth and chemical fixation*	125
6.2.2.2.	*Spheroplasting*	126
6.2.2.3.	*DNA fragmentation*	127
6.2.2.4.	*Pre-binding of Antibody*	127
6.2.2.5.	*Immunoprecipitation*	128
6.2.2.6.	*Washing*	128
6.2.2.7.	*Elution*	129
6.2.2.8.	*Reverse cross-linking and cleanup*	129
6.2.3.	ChIP-on-Chip	130
6.2.3.1.	*Blunt-end DNA preparation*	130
6.2.3.2.	*Blunt-end ligation*	130
6.2.3.3.	*Amplification*	131
6.2.3.4.	*Labelling*	132
6.2.3.5.	*Microarray hybridisation*	133
6.2.3.6.	*Scanning*	133
6.2.3.7.	*Analysis*	134
6.2.4.	Chromatin immunoprecipitation (Fleming Laboratory, TCD)	134
6.2.4.1.	*Growth and chemical fixation*	135
6.2.4.2.	*Cell lysis*	135
6.2.4.3.	*DNA fragmentation*	135
6.2.4.4.	*Pre-binding of Antibody-protein complexes*	136
6.2.4.5.	*Immunoprecipitation*	136
6.2.4.6.	*Washing*	136
6.2.4.7.	*Elution*	137
6.2.4.8.	*Reverse cross-linking & pronase digestion*	137
6.2.4.9.	*DNA cleanup*	137
6.2.5.	ChIP-qRT-PCR	138
6.2.6.	Western immunoblot	138
6.3.	**Results**	139
6.3.1.	Whole genome chromatin immunoprecipitation	139
6.3.1.1.	*Optimisation of spheroplasting for ChIP-on-chip*	139
6.3.1.2.	*Whole genome ChIP-on-chip*	140
6.3.2.	Design of single gene ChIP-qRT-PCR assay	141
6.3.2.1.	*Breakage optimisation*	142
6.3.2.2.	*Sonication optimisation*	142
6.3.2.3.	*Immunoprecipitation optimisation*	143

6.3.3.	Confirmation of global ChIP-on-chip with single gene ChIP-qRT-PCR	143
6.3.4.	Gene ontology analysis of chromosomal enriched regions (ChERs)	145
6.3.5.	Relationship between expression and Tlo1 enrichment	146
6.4.	**Discussion**	148
6.4.1.	General remarks	148
6.4.2.	Enrichment at repetitive regions	149
6.4.3.	Enrichment at open reading frames (orfs)	150
6.4.4.	Other remarks	151
Chapter 7.	**General Discussion**	153
7.1.	General Discussion	154
References		163
Appendices		183

Index of Figures

Chapter 1

1.1. *TLO* genes of *Candida albicans* and *Candida dubliniensis* 16
1.2. Mediator complex in *C. albicans* 18

Chapter 3

3.1. Amplification of *TLO1* and *TLO2* 48
3.2. Southern immunoblot used to confirm *TLO* genotypes 50
3.3. Specificity of DNA probe used in Southern immunoblotting 50
3.4. Global alignment of *C. dubliniensis TLO* genes 52
3.5. Repeat motifs found in *C. dubliniensis TLO1* and *TLO2* 52
3.6. *C. dubliniensis TLO1* does not show synteny with regions of other genomes 52
3.7. *C. dubliniensis TLO2* displays synteny with regions of other genomes 52
3.8. *TLO* homology across other *Saccharomycetaceae* 52
3.9. Expression of *TLO* genes in *C. dubliniensis* 52
3.10. Amino acid composition of Tlo proteins 54
3.11. Tlo protein sequence alignment 54
3.12. Gfp fluorescence indicates localisation of Tlos to the nuclear compartment 56
3.13. Gentoype of *TLO* genes in Wü284 56

Chapter 4

4.1. Effect of temperature on the growth of *C. dubliniensis tlo* mutants 74
4.2. Growth of *C. dubliniensis* in the presence of Calcofluor White 74
4.3. Growth of *C. dubliniensis* in the presence of Congo Red 74
4.4. Growth of *C. dubliniensis* in the presence of SDS 74
4.5. Calcofluor white-stained *C. dubliniensis tlo* mutant strains 74
4.6. Visualisation of cell-cell contacts in wild-type *C. dubliniensis* and *tlo* mutant 76
4.7. Growth of *C. dubliniensis* in the presence of calcium chloride 76
4.8. Growth of *C. dubliniensis* in the presence of Sodium Chloride 76
4.9. Effect of sorbitol on the growth of *C. dubliniensis tlo* mutants 76
4.10. Effect of hydrogen peroxide (H_2O_2) on the growth of *C. dubliniensis tlo* mutants. 76
4.11. Effect of menadione on the growth of *C. dubliniensis tlo* mutants 78
4.12. Growth of *tlo* mutants under oxidative stress. 78
4.13. Chlamydospore formation in *C. dubliniensis tlo* mutants 78
4.14. Growth behaviour of *C. dubliniensis tlo* mutants in nutrient-rich conditions 80

4.15. Growth behaviour of *C. dubliniensis tlo* mutants in galactose-based media 80
4.16. Growth behaviour of *C. dubliniensis tlo* mutants in succinate-based media 80
4.17. Growth behaviour of *C. dubliniensis tlo* mutants in minimal media 80
4.18. Growth behaviour of *C. dubliniensis tlo* mutants on solid minimal media 82
4.19. Growth of *C. dubliniensis tlo* mutants in liquid Spider medium 82
4.20. Growth of *C. dubliniensis tlo* mutant strains on solid filament-inducing medium 82
4.21. True-hyphal formation in *C. dubliniensis tlo* mutant strains 82
4.22. Hyphal formation in *C. dubliniensis tlo* mutants. 82
4.23. Determination of the effects of *TLO* disruption on biofilm initiation and maintenance 84

Chapter 5

5.1. Distribution of entities on DNA microarrays 98
5.2. Profile plot of expression of *tlo* mutant compared to Wü284 104
5.3. Overview of overlap in DNA microarray datasets 104
5.4. Expression patterns of genes involved in galactose metabolism upon deletion of *TLO* genes is confirmed by qRT-PCR 104
5.5. Expression patterns of *SOD* genes is confirmed by qRT-PCR 106
5.6. Expression patterns of genes involved in filamentation analysed by qRT-PCR 106
5.7. DNA microarray analysis of genes involved in the regulation of filamentation 108
5.8. The network of regulators and transcription factors involved in hyphal formation 108
5.9. DNA microarray analysis of genes specific to the fungal cell wall 108
5.10. DNA microarray analysis of genes involved in the cellular response to stress 110
5.11. Deletion of *TLO* genes in C. *dubliniensis* alters the expression of genes involved iron uptake and homeostasis 112
5.12. Expression of genes involved in galactose degradation is affected by the deletion of *TLO* genes in C. *dubliniensis* 114
5.13. DNA microarray analysis of genes involved with N-acetyglucosamine-associated processes 116

Chapter 6

6.1. Overview of Chromatin immunprecipitation (ChIP) and ChIP-on-chip methodology 122
6.2. Confirmation of HA-epitope on Tlo1-HA fusion protein 140
6.3. Distribution of enrichment scores over chromosomes 140
6.4. Tlo1 enrichment across chromosome 5 of *C. dubliniensis* 140
6.5. Significance of distribution of Tlo1 enriched regions is dependent on threshold 140

6.6. Enrichment of Tlo1 is not biased towards 5-prime or 3-prime regions of genes 142
6.7. Determination of cell lysis & breakage 142
6.8. Visualisation of extent of cell breakage & lysis in experimental samples 142
6.9. Optimisation of sonication step in Chromatin immunoprecipitation protocol 142
6.10. qRT-PCR was used to confirm Tlo1 enrichment at *PUT1* (*Cd36_52370*) 144
6.11. qRT-PCR was used to confirm Tlo1 enrichment patterns at an intergenic region (*NEG*) 144
6.12. qRT-PCR was used to confirm Tlo1 enrichment at *CLN1* (*Cd36_51640*) 144
6.13. qRT-PCR was used to confirm Tlo1 enrichment at *Cd36_52970* 144
6.14. qRT-PCR was used to assess Tlo1 enrichment at *Cd36_51290* 144
6.15. qRT-PCR was used to confirm Tlo1 enrichment at *FGR6-3* (*Cd36_52975*) 144
6.16. qRT-PCR was used to confirm Tlo1 enrichment at *ACT1* (*Cd36_12690*) 146
6.17. qRT-PCR was used to confirm Tlo1 enrichment at *MTLalpha2* (*Cd36_51540*) 146
6.18. qRT-PCR was used to confirm Tlo1 enrichment at *Cd36_17440* 146
6.19. RNA Polymerase II ChIP 146
6.20. Gene-specific relationship between expression and Tlo1 enrichment 146
6.21. Expression of significantly enriched gene groups 148

Chapter 7

7.1. Proposed models of Tlo-mediated regulation 162

Index of Tables

Chapter 2

2.1. *Candida* strains used in this study 20

2.2. Oligonucleotide primers used in this study 22

Chapter 4

4.1. Susceptibility of *C. dubliniensis* to common antifungals 74

4.2. Doubling times of *tlo* mutant strains 80

Chapter 5

5.1. Filtering applied to DNA microarray data 98

Supplementary figures (Appendices)

S1. Sample script used in R/Bioconductor to process ChIP-on-chip data.

Supplementary tables (Appendices)

S1. Changes in gene expression greater than 1.5-fold in ΔΔ*tlo* compared to Wü284 during mid-exponential growth in YEPD.

S2. Changes in gene expression greater than 1.5-fold in ΔΔ*tlo* compared to Wü284 at 1 h growth in WS.

S3. Changes in gene expression greater than 1.5-fold in ΔΔ*tlo* compared to Wü284 at 3 h growth in WS

Abbreviations

AEBSF	4-(2-Aminoethyl) benzenesulfonyl fluoride hydrochloride
AIDS	Acquired Immune Deficiency Syndrome
ATP	Adenosine triphosphate
BLAST	Basic Local Alignment Search Tool
blastP	BLAST-Protein
bp	base pair(s)
BSI	Bloodstream Infection
CaCl2	Calcium Chloride
cDNA	Complementary DNA
CGD	Candida Genome Database
ChER	Chromosomal Enriched Regions
cm	centimetre
CO2	Carbon Dioxide
cRNA	Complementary RNA
Ct	Threshold Cycle
CTD	C-terminal Domain
CTP	cytidine triphosphate
DAPI	4'6-diamidion-2-phenylindole
dATP	deoxyadenosine triphosphate
dCTP	deoxycytidine triphosphate
dGTP	deoxyguanosine triphosphate
DIG	Digoxigenin
DMA	Dimethylapidimidate
DNA	Deoxyribonucleic Acid
dsDNA	Double Stranded DNA
DTT	Dithiothreitol
dTTP	deoxythymidine triphosphate
E	Efficiency
e.g.	For Example
ECM	Extracellular Matrix
EDTA	Ethylenediaminetetraacetic acid
EPC	Esophageal Candidiasis
FCS	Foetal Calf Serum
g	Gravity
GEWB	Gene Expression Wash Buffer
gfp	Green Fluorescent Protein
GI Tract	Gastrointestinal Tract
GlcNAc	N-Acetylglucosamine
GO	Gene Ontology
GTP	guanosine triphosphate

h	Hour(s)
H_2O	Water
H_2O_2	Hydrogen Peroxide
HAI	Healthcare Associated Infections
HCl	Hydrochloric Acid
HIV	Human Immunodeficiency Virus
Hsp	Heat Shock Protein
IP	Immunoprecipitation
kbp	kilobase Pair(s)
kV	kiloVolts
LiCl	Lithium Chloride
LTR	Long Terminal Repeat
M	Molar
m	Slope
m	metre
MAPK	Mitogen Activated Protein Kinase
Mbp	Megabase Pair(s)
mg	Milligram
MgCl2	Magnesium Chloride
MIC	Minimum Inhibtory Concentration
min	Minute(s)
mM	Millimolar
mm	millimetre
mRNA	messenger RNA
MRS	Major Repat Sequence
MSA	Multiple Sequence Alignment
MYA	Million Years Ago
NaCl	Sodium Chloride
NADPH	Nicotinamide adenine dinucleotide phosphate
NaOH	Sodium Hydroxide
NAT	Nourseothricin
NGS	Next Generation Sequencing
NHSN	National Healthcare Safety Network
nm	nanometres
NTD	N-terminal Domain
O.D.	Optical Density
ODU	O.D. Units
OH-	Hydroxyl Radical
OPC	Oropharyngeal Candidiasis
orf	Open Reading Frame

p:c:i	Phenol:Chloroform:Iso-amyl Alcohol
PAMP	Pathogen-Associated Molecular Pattern
PBS	Phosphate-Buffered Saline
PCR	Polymerase Chain Reaction
pH	decimal logarithm of the reciprocal of the hydrogen ion activity
PI	Protease Inhibitor(s)
PIC	Pre-Initiation Complex
PMSF	Phenylmethanesulfonylfluoride
PRR	Pattern Recognition Receptor
PTFL	Polytetrafluoroethylene
qRT-PCR	Quantitative Real Time PCR
r.p.m.	Revolutions Per Minute
RHE	Reconstituted Human Epithelium
RNA	Ribonucleic Acid
ROS	Reactive Oxygen Species
s	Second(s)
SAGE	Serial Analysis Of Gene Expression
SAP	Secreted Aspartyl Protease
SAPK	Stress Activated Protein Kinase
SDS	Sodium Dodecyl Sulphate
SDS-PAGE	SDS-Polyacrylamide Gel Electrophoresis
SEM	Scanning Electron Microscopy
SNR	Signal-To-noise Ratio
spp.	Species
SSC	Saline-Sodium Citrate
ssDNA	Single Stranded DNA
TE	Tris-EDTA
T_{hyb}	Hybridisation temperature
T_m	Melting Temperature
U	Units
UTP	uridine triphosphate
UV	Ultraviolet
V	Volt
v/v	volume per volume
vsn	Variance Stabilisation And Normalisation
VVC	Vulvovaginal Candidiasis
W	Watt
w/v	weight per volume
w/w	weight per weight
WS	Water + 10 % serum

XTT	2,3-Bis-(2-Methoxy-4-Nitro-5-Sulfophenyl)-2H-Tetrazolium-5-Carboxanilide
YEPD	Yeast Extract, Peptone, Dextrose
YNB	Yeast Nitrogen Base
ΔCt	Delta Ct
ΔΔCt	Delta Delta Ct
µg	Micrograms
µl	microlitre(s)
µm	Micrometre(s)
µM	Micromolar
%	Percentage
<	Less than
>	More than

Acknowledgements

Firstly, I'd like to thank my supervisor Dr. Gary Moran, whose feedback and support was an immense help over the past four years and without whom I would never have reached this stage. I'd also like to thank my co-supervisor Prof. Derek Sullivan for his support and encouragement over the course of my PhD. I'd like to extend a special thanks to Dr. Moran and Prof. Sullivan for the many opportunities they have allowed me to travel to present my work. Over the past four years, my project has taken me to Paris, Minnesota, Berlin, Belfast, Newcastle, Cork, Galway, New Orleans, Maynooth and more. Apologies for all the 'expensed' coffees!!

I'm extremely grateful to Prof. David Coleman, Dr. Mary O' Donnell for all their help and support throughout my time in the lab as well as to the DDUH for being my home for the past 4 years. Also, sincere thanks to Matt Anderson and Judith Berman for allowing me to undertake work in Minneapolis on an unforgettable trip.

A special thanks to my friends in the Microbiology Laboratory at the Dublin Dental University Hospital - I consider myself extremely lucky to have spent what was an eventful and inevitably stressful four years amongst some of the nicest, most supportive people. Thanks for all the great evenings in the Lincoln's Inn, cheeky Pav pints, random nights out, trips beyond the pale and of course for the karaoke!

Particular thanks to my ex-bay buddy Orla for all the laughs and my current bay-buddy Maria for the company on walks home and for always putting a smile on my face. Thanks to Aoife for bringing some much-needed style to 'Michael Bay'! Thanks to Aisling for help with photography and for generally just being an awesome friend over the past 4 years. Thanks also to Peter H and Emily, go class of '09! Thanks to Alexandros and Peter F for always joining me in laughing at the most inappropriate & offensive things and for the fun times with the 5H's! Thanks to Hannah for all the help with Tlo-related goings-on and for always being there for a rant/chat. Thanks to Sarah for all the advice and laughs, to Izzy for being the soundest hipster around and thanks to Anna for all the words of wisdom :) Thanks to Brenda, Peter K, Eimear, Phillipa and Hal as well for all the help and coffee over the past 4 years.

Thanks to Chris Davitt and Mick Church for all the banter over the past 8/9 years and for keeping in touch, especially thanks to Chris for the support as we

both came to the end of the PhDs! Also, thanks to Cristín for forcing me to take breaks every now and again :)

To my parents, thanks for all the encouragement and for helping to support me over the past 20 + years of education! In particular, thanks to my Mam for all the help during the PhD and for supporting me in everything I did. Finally, but certainly by no means least, thanks to Paul for all of the adventures and for being there for me over the past few years ,as well as putting up with all the stress! I certainly couldn't have come anywhere close to finishing without his constant support...and now, as promised, I have my weekends back!

Publication

Haran, J., Boyle, H., Hokamp, K., Yeomans, T., Liu, Z., Church, M., Fleming, A.B., Anderson, M.Z., Berman, J., Myers, L.C., Sullivan, D.J. & Moran, G.P. (2014).
Telomeric *ORFs* (*TLOs*) in *Candida spp.* encode Mediator subunits that regulate distinct virulence traits. *PLoS Genetics* **10**, e1004658.

OPEN ACCESS Freely available online

PLOS | GENETICS

Telomeric *ORFs* (*TLOs*) in *Candida* spp. Encode Mediator Subunits That Regulate Distinct Virulence Traits

John Haran[1☯], Hannah Boyle[1☯], Karsten Hokamp[2], Tim Yeomans[1], Zhongle Liu[3], Michael Church[2], Alastair B. Fleming[2], Matthew Z. Anderson[4¤], Judith Berman[4,5], Lawrence C. Myers[3], Derek J. Sullivan[1]*, Gary P. Moran[1]*

1 Division of Oral Biosciences, Dublin Dental University Hospital, University of Dublin, Trinity College Dublin, Dublin, Ireland, **2** School of Genetics and Microbiology, University of Dublin, Trinity College Dublin, Dublin, Ireland, **3** Department of Biochemistry, Geisel School of Medicine at Dartmouth, Hanover, New Hampshire, United States of America, **4** Department of Genetics, Cell Biology and Development, University of Minnesota, Minneapolis, Minnesota, United States of America, **5** Department of Microbiology and Biotechnology, George S. Wise Faculty of Life Sciences, Tel Aviv University, Ramat Aviv, Israel

Abstract

The *TLO* genes are a family of telomere-associated ORFs in the fungal pathogens *Candida albicans* and *C. dubliniensis* that encode a subunit of the Mediator complex with homology to Med2. The more virulent pathogen *C. albicans* has 15 copies of the gene whereas the less pathogenic species *C. dubliniensis* has only two (*CdTLO1* and *CdTLO2*). In this study we used *C. dubliniensis* as a model to investigate the role of *TLO* genes in regulating virulence and also to determine whether *TLO* paralogs have evolved to regulate distinct functions. A *C. dubliniensis tlo1Δ/tlo2Δ* mutant is unable to form true hyphae, has longer doubling times in galactose broth, is more susceptible to oxidative stress and forms increased levels of biofilm. Transcript profiling of the *tlo1Δ/tlo2Δ* mutant revealed increased expression of starvation responses in rich medium and retarded expression of hypha-induced transcripts in serum. ChIP studies indicated that Tlo1 binds to many ORFs including genes that exhibit high and low expression levels under the conditions analyzed. The altered expression of these genes in the *tlo1Δ/tlo2Δ* null mutant indicates roles for Tlo proteins in transcriptional activation and repression. Complementation of the *tlo1Δ/tlo2Δ* mutant with *TLO1*, but not *TLO2*, restored wild-type filamentous growth, whereas only *TLO2* fully suppressed biofilm growth. Complementation with *TLO1* also had a greater effect on doubling times in galactose broth. The different abilities of *TLO1* and *TLO2* to restore wild-type functions was supported by transcript profiling studies that showed that only *TLO1* restored expression of hypha-specific genes (*UME6, SOD5*) and galactose utilisation genes (*GAL1* and *GAL10*), whereas *TLO2* restored repression of starvation-induced gene transcription. Thus, Tlo/Med2 paralogs encoding Mediator subunits regulate different virulence properties in *Candida* spp. and their expansion may account for the increased adaptability of *C. albicans* relative to other *Candida* species.

Citation: Haran J, Boyle H, Hokamp K, Yeomans T, Liu Z, et al. (2014) Telomeric *ORFs* (*TLOs*) in *Candida* spp. Encode Mediator Subunits That Regulate Distinct Virulence Traits. PLoS Genet 10(10): e1004658. doi:10.1371/journal.pgen.1004658

Editor: Geraldine Butler, University College Dublin, Ireland

Received July 9, 2014; **Accepted** August 11, 2014; **Published** October 30, 2014

Copyright: © 2014 Haran et al. This is an open-access article distributed under the terms of the Creative Commons Attribution License, which permits unrestricted use, distribution, and reproduction in any medium, provided the original author and source are credited.

Data Availability: The authors confirm that all data underlying the findings are fully available without restriction. Genomic data files are available from Gene Expression Omnibus at NCBI (accession numbers: GSE59113, GSE60173).

Funding: This project was funded by Science Foundation Ireland, grant numbers RFP.1/GEN/3044, RFP.1/GEN/3042 and O4/IN3/B463 to GPM and DJS (www.SFI.ie). JB was supported by the NIH, grant number R01AI075096. JH was supported by the Faculty of Health Sciences, Trinity College Dublin and by an award from the Society for General Microbiology President's fund to visit the laboratory of JB. The funders had no role in study design, data collection and analysis, decision to publish, or preparation of the manuscript.

Competing Interests: The authors have declared that no competing interests exist.

* Email: Derek.sullivan@dental.tcd.ie (DJS); gpmoran@dental.tcd.ie (GPM)

☯ These authors contributed equally to this work.

¤ Current address: Department of Molecular Microbiology and Immunology, Brown University, Providence, Rhode Island, United States of America

Introduction

Candida albicans is a commensal yeast commonly recovered from mucosal surfaces in humans. *C. albicans* is also a versatile opportunistic pathogen, responsible for a variety of superficial infections as well as more severe, life threatening infections in severely immunocompromised patients. Phenotypic versatility is an important characteristic of *C. albicans* and this flexibility allows *C. albicans* to adapt to this wide range of niches in the human host [1–3]. Over the past decade, transcriptional profiling of *C. albicans* using microarray and RNA-seq technologies has revealed that rapid adaptation to local environmental conditions involves elaborate, programmed shifts in transcription pattern. The biochemistry of transcriptional regulation has been studied intensively in the model yeast *S. cerevisiae*. Most genes transcribed by RNA polymerase II (PolII) require a carefully orchestrated series of events to initiate transcription. The formation of the pre-initiation complex and recruitment of PolII requires the function of Mediator, a large multi-subunit protein complex [4,5]. Mediator is thought to be required to bridge DNA-bound transcription factors with the rest of the transcriptional machinery [6,7]. The complex is generally divided into three modules: a head, middle and tail. The tail region includes Med2, Med3 and Med15/Gal11 and is thought to be the part of Mediator that

Author Summary

Candida albicans and *C. dubliniensis* are fungal pathogens of humans. Both species possess *TLO* genes encoding proteins with homology to the Med2 subunit of Mediator. The more virulent pathogen *C. albicans* has 15 copies of the *TLO* gene whereas the less pathogenic species *C. dubliniensis* has only two (*TLO1* and *TLO2*). In this study we show that a *C. dubliniensis* mutant missing both *TLO1* and *TLO2* is defective in virulence functions, including hyphal growth and stress responses but forms increased levels of biofilm. Analysis of gene expression in the *tlo1Δ/tlo2Δ* mutant revealed extensive differences relative to wild-type cells, including aberrant expression of starvation responses in nutrient-rich medium and retarded expression of hypha-induced transcripts in serum. Tlo1 protein was found to interact with genes and this was associated with both gene activation and repression. *TLO1* was found to be better at restoring hyphal growth compared to *TLO2* and but was less effective than *TLO2* in supressing biofilm formation in the *tlo1Δ/tlo2Δ* strain. Thus, Tlo proteins regulate many virulence properties in *Candida* spp. and the expansion of the *TLO* family in *C. albicans* may account for the increased adaptability of this species relative to other *Candida* species.

interacts directly with transcription factors such as Gal4 and Gcn4 [8].

Most components of Mediator are highly conserved between *S. cerevisiae* and *C. albicans* [9]. However, completion of the *C. albicans* genome sequence [10,11] revealed a family of up to 15 telomeric (*TLO*) genes that were subsequently found to encode a domain with homology to the Mediator tail subunit Med2 of *S. cerevisiae* [9,12,13]. This *TLO* gene expansion is unique to *C. albicans*, as most of the less pathogenic non-*albicans Candida* species such as *C. tropicalis* and *C. parapsilosis* have only one *TLO* gene. *C. dubliniensis*, the closest relative to *C. albicans* has two *TLO* genes, namely *TLO1* and *TLO2*. *TLO1* (*Cd36_72860*) is located internally on chromosome 7 and *TLO2* (*Cd36_35580*) is at a telomere-adjacent locus on the right arm of chromosome R [14]. *C. dubliniensis TLO2* appears to be the ancestral locus, based on synteny with, and homology to, the single *C. tropicalis* orthologue CTRG_05798.3 [14]. All candidal *TLO* genes share the Med2-like domain of the *C. albicans TLOs* and appear to be the *MED2* orthologs in these species. Indeed, biochemical studies have shown that like the *S. cerevisiae* Med2 protein, Tlo proteins co-purify with the *C. albicans* orthologs of mediator tail module components Med3 and Med15 [9].

The 15 *TLO* genes in the *C. albicans* type strain SC5314 can be classified into four distinct clades based on gene structure, including the highly expressed *TLOα* clade (6 members), a single *TLOβ* gene, the poorly expressed *TLOγ* clade (7 members) and a single *TLOψ* gene which is a pseudogene [12]. Biochemical studies have shown that the levels of Tloα and Tloβ proteins is in vast excess to the amount necessary to be a stoichiometric subunit of Mediator (9) and stands in stark contrast to the situation in *S. cerevisiae*, where the Med2 subunit is expressed at roughly equivalent amounts to other subunits of the complex. Due to the large numbers of *TLO* genes in *C. albicans*, functional analysis of Mediator has largely been restricted to other subunits, including Med3 (tail domain), Med31 (middle domain), Med20 (head domain) and Med13/Srb9 (kinase domain). Med31 and Med20 are required for the transition of *C. albicans* yeast cells to filamentous hyphae and for biofilm formation, two important pathogenic traits of the organism [9,15]. Med31 is required for expression of the genes *ALS1* and *ALS3* that encode cell-surface proteins involved in biofilm production, consistent with the poor biofilms produced by *med31Δ* mutants. In addition, Med31 is required for the expression of genes regulated by the transcription factor *Ace2*, which regulates many genes involved in cell wall remodelling during cell separation. Consistent with this, the *med31Δ* mutant exhibits defective cytokinesis. Deletion of *MED3* resulted in a stronger filamentous growth defect, resulting in short pseudohyphae in serum or liquid media supplemented with GlcNac [9]. Deletion of Mediator subunits also has complex effects on the transcriptional circuit governing the white-opaque switch, a phenotypic transition involved in mating [16].

C. albicans is the most prevalent pathogenic fungal species. The closely related species *C. dubliniensis* is responsible for far fewer infections and is a minor component of the human oral flora [14,17]. The yeast-to-hypha transition is an important virulence trait of *C. albicans* and *C. dubliniensis* forms fewer hyphae than *C. albicans* in response to most *in vitro* and *in vivo* hypha-inducing stimuli [17]. *C. dubliniensis* requires much stronger environmental cues, including nutrient depletion, in order to activate a transcriptional response that will induce the yeast-to-hypha transition [18–20]. Less effective transcriptional responses may also account for the increased susceptibility of *C. dubliniensis* to environmental stress relative to *C. albicans* [21]. It has been suggested that the expansion of the *TLO* family in *C. albicans* may account for the greater transcriptional flexibility and adaptability of this species relative to *C. dubliniensis* and the other non-*albicans Candida* species [22]. However, direct analysis of *TLO* null mutants has not been attempted in *C. albicans*, due to the large number of *TLO* genes and the likelihood of redundancy in the *TLO* family.

In this study, we exploited the closely related species *C. dubliniensis* as a model to study *TLO* gene function and to construct the first *tlo* null strains. We found that *C. dubliniensis* mutants lacking both *TLO1* and *TLO2* (*tlo1Δ/tlo2Δ*) exhibit widespread changes in the transcription of virulence-associated genes. ChIP analysis detected Tlo1 within the coding regions of ORFS, as well as subtelomeric regions and the Major Repeat Sequence (MRS). Interestingly, in strains lacking only one of the two *TLO* genes, expression of distinct subsets of genes was altered. We propose that expansion of the *TLO* family, even to only two members, has facilitated the evolution of functional diversity and may be of particular importance in the evolution of an expanded set of *TLO* paralogs together with the increased virulence in *Candida albicans*.

Results

Candida dubliniensis possesses two expressed *TLO* paralogs

The two *Candida dubliniensis TLO* genes, *TLO1* and *TLO2*, encode proteins of 320 and 355 amino acids, respectively, and share 58% identity. Homology to each other and to the *C. albicans* Tlo proteins is concentrated in the N-terminal 120 residues of the proteins. Tlo1 and Tlo2 share 81% identity in this N-terminal region, which also exhibits homology to *S. cerevisiae* Med2 (Figure 1A). The amino acid sequence of Tlo2 is 25 residues longer and contains a central triplet repeat of the motif KAAAKVKEEQ. *C. dubliniensis* is a diploid organism and gene deletion studies (see below) and Southern blot analysis confirmed that *C. dubliniensis* strain Wü284 has two alleles of *TLO1* (Figure S1). However, Southern blot experiments could detect only one allele of *TLO2* at the telomere of chromosome R (ChR) in strain

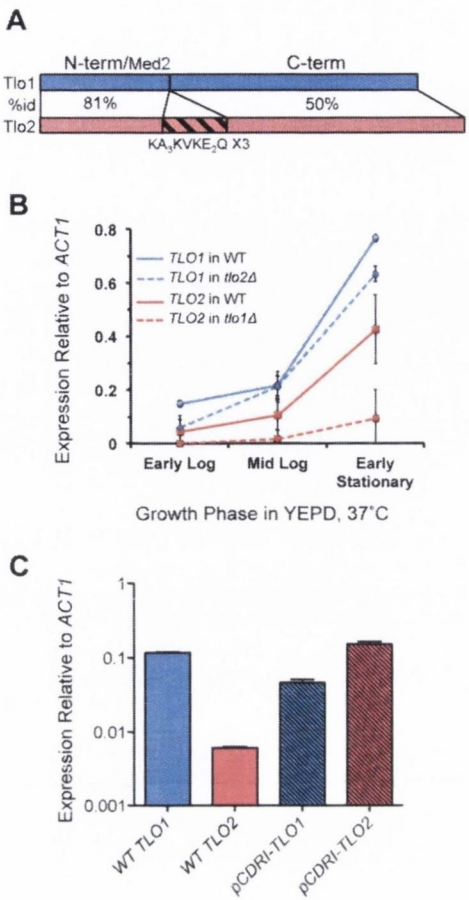

Figure 1. Structure and expression of *C. dubliniensis TLO* genes. (A) *TLO1* and *TLO2* encode proteins of 320 and 355 amino acids respectively that exhibit 81% identity in the N-terminal Med2-like domain, and 50% identity in the C-terminal portion of the protein. In addition, Tlo2 has an internal triplet repeat, indicated. (B) Expression of *TLO1* and *TLO2* was measured by QRT-PCR using gene-specific primers during growth in YEPD broth at 37°C in early exponential (1.5 h-post inoculation), mid-exponential (8 h) and early stationary phase (18 h) in strain Wü284 (WT). The effect of deletion of either *TLO1* or *TLO2* on the expression of the other paralog was also analysed. (C) Expression of reintegrated copies of *TLO1* and *TLO2* in plasmid pCDRI in the *tlo1*Δ/*tlo2*Δ strain.
doi:10.1371/journal.pgen.1004658.g001

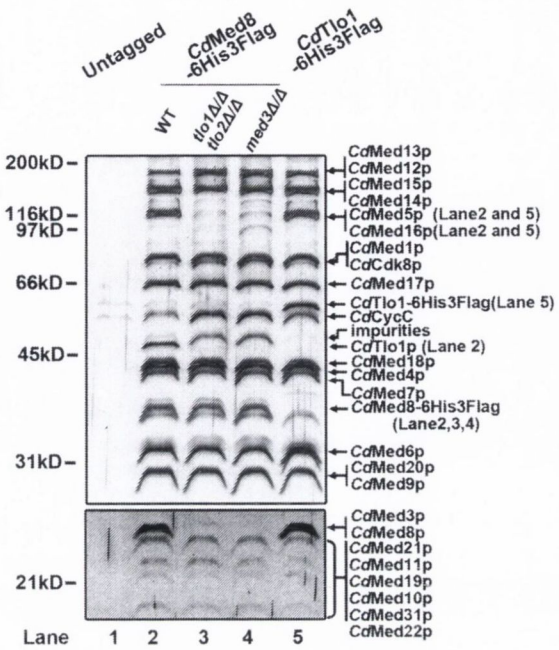

Figure 2. Biochemical analysis of Mediator in *C. dubliniensis* wild-type and *tlo1*Δ/*tlo2*Δ. Lysates from untagged WT *C. dubliniensis* (Lane 1), a Med8-6His-Flag-tagged WT strain (Lane 2), a Med8-6His-Flag-tagged *tlo1*Δ/*tlo2*Δ strain (Lane 3), a Med8-6His-Flag-tagged *med3*Δ strain (Lane 4) and a Tlo1-6His-Flag-tagged WT strain (Lane 5) were subjected, in parallel, to multiple chromatographic separations. The elutions from the IMAC (Talon) step were analyzed by 8% SDS-PAGE. Proteins were revealed by staining with silver. Bands that are present in WT but clearly absent in the *tlo1*Δ/*tlo2*Δ and *med3*Δ Mediator are indicated in parenthesis on the right. The absence of these proteins in the *tlo1*Δ/*tlo2*Δ Mediator was confirmed by mass spectroscopy.
doi:10.1371/journal.pgen.1004658.g002

Wü284, indicating that one copy of ChR in Wü284 was truncated resulting in loss of one allele of *TLO2* (Figure S1). PCR analysis of the *tlo2Δ* strain confirmed that bases 1 to 918 of the second *TLO2* allele are deleted due to this truncation, with only a small 150 bp remnant of the ORF remaining. Analysis of gene expression by QRT-PCR revealed that *TLO1* mRNA is expressed over 2-fold higher than *TLO2* mRNA in YEPD at 37°C (Figure 1B).

C. dubliniensis Tlo proteins and Med3 are components of the Mediator tail module

We first asked if *C. dubliniensis* Tlo is a component of Mediator. To address this, we purified Mediator from whole cell extracts of *C. dubliniensis* wild-type and *tlo1Δ/tlo2Δ* mutant cells using a dual affinity tag on the *C. dubliniensis* ortholog of the conserved Med8 subunit of Mediator. The resulting Mediator complex was analyzed for purity by SDS-PAGE and for composition by mass spectroscopy with untagged WT *C. dubliniensis* serving as a control. Biochemical analysis showed that the *C. dubliniensis* Mediator, like *C. albicans*, is composed of a complete set of orthologs of the *S. cerevisiae* complex (Figure 2). Mediator purified from the *tlo1*Δ/*tlo2*Δ mutant lacked tail subunits Med3, Med15, Med16 and Med5 subunits (Figure 2, Lane 3). Importantly, Mediator purified from the *C. dubliniensis tlo1*Δ/*tlo2*Δ strain or from a *med3*Δ null strain had equivalent composition, lacking tail components Tlo1, Med3, Med5, Med15 and Med16 (Figure 2, Lanes 3 and 4).

To determine the relative abundance of Tlo proteins compared to other Mediator subunits, we constructed strains carrying Tlo1-HA, Med3-HA and Med8-HA tagged derivatives. Immunoblotting of whole cell extracts revealed that *C. dubliniensis* Tlo1 Mediator subunit is expressed in amounts comparable to the Med3 Tail Module and Med8 Head Module subunits (Figure S2). Consistent with this finding, purification of an affinity tagged Tlo1 protein from *C. dubliniensis* yielded only the Mediator associated form (Figure 2, Lane 5) and no free Tlo1 protein. Thus, in *C. dubliniensis* Tlo1 appears to be acting solely as a component of Mediator.

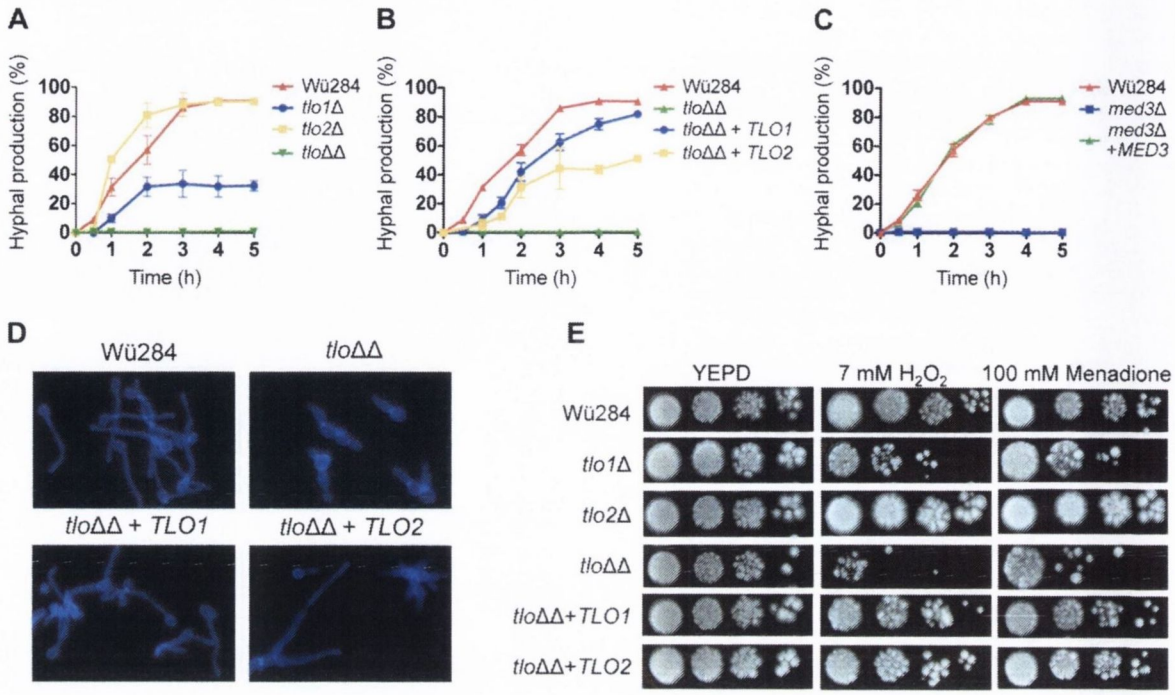

Figure 3. Phenotypic analysis of *C. dubliniensis tloΔ* and *med3Δ* mutants. The rate of formation of true hyphae in water supplemented with 10% serum was measured in the *tlo1Δ*, *tlo2Δ* and *tlo1Δ/tlo2Δ* (*tloΔΔ*) mutants relative to Wü284 (A), in the *TLO1* and *TLO2* reintegrants (*tloΔΔ+TLO1/2*)(B) and in the *med3Δ* mutant (C). Measurements were taken over a period of 5 h by counting the number of cells producing unconstricted germ-tubes and expressing this value as a percentage of the whole population. (D) Cellular morphology of Wü284, the *tlo1Δ/tlo2Δ* (*tloΔΔ*) mutant and *TLO1* and *TLO2* reintegrated strains in 10% serum following staining with calcofluor white. (E) Oxidative stress susceptibility in *tloΔ* mutants. Susceptibility to oxidative stress was assessed by spotting 20 µl aliquots of 10-fold serially diluted suspensions (10^6 to 10^3 cells/ml) of the indicated strains on YEPD agar plates containing 7 mM H_2O_2 or 100 mM menadione. Plates were incubated for 48 h at 37°C.
doi:10.1371/journal.pgen.1004658.g003

TLO1 activates hyphal growth to a greater extent than *TLO2*

Deletion of *TLO2* did not reduce filamentous growth significantly (Figure 3A), while deletion of *TLO1* resulted in reduced hyphal production (Figure 3A), as reported previously [14]. However, the double *tlo1Δ/tlo2Δ* mutant (*tloΔΔ*) had a more severe filamentation defect than the *TLO1* deletion alone, suggesting that *TLO2* partly compensates for the deletion of *TLO1* in the single mutant (Figure 3A, 3D). The cellular morphology of the *tlo1Δ/tlo2Δ* mutant in 10% serum was characteristically pseudohyphal (Figure 3D).

In order to investigate if *TLO1* and *TLO2* are functionally different, we reintroduced *TLO1* and *TLO2* individually to the *tlo1Δ/tlo2Δ* mutant using a previously described integrating vector pCDRI. This strategy was employed as it allowed us to express both *TLO1* and *TLO2* to similar levels (Figure 1C) thus allowing a direct comparison of their ability to complement the phenotypes of the *tlo1Δ/tlo2Δ* mutant. Introduction of *TLO1* could restore true hypha production to almost wild-type levels, whereas *TLO2* restored hypha formation to approximately 50% of wild-type levels (Figure 3B, 3D). These data show that *TLO1* and *TLO2* differ in their ability to activate filamentous growth.

Deletion of *TLO1* and *TLO2* produces multiple phenotypes

The colony morphology of the *tlo1Δ*, *tlo2Δ* and *tlo1Δ/tlo2Δ* mutant strains following growth on nutrient-rich solid medium (YEPD agar) at 37°C was indistinguishable from that of wild-type. At the cellular level, the *tlo1Δ/tlo2Δ* mutant grew as short chains of 3–4 cells, which is indicative of a defect in cytokinesis (Figure S3A). A similar phenotype was described by Uwamahoro et al. [15] in a *C. albicans med31Δ* mutant. Wild-type cytokinesis was restored in the *tlo1Δ/tlo2Δ* mutant following reintroduction of *TLO1* but not *TLO2* (Figure S3A). Growth defects of *tlo* mutants became apparent when grown on non-optimal media. On Spider agar, the wild-type strain formed smooth white colonies, typical of *C. dubliniensis* on this medium. However, the *tlo1Δ/tlo2Δ* mutant formed heavily wrinkled colonies on this medium (Figure S3B). Wild-type smooth colonies could be restored by complementation of the *tlo1Δ/tlo2Δ* mutant with either *TLO1* or *TLO2* (Figure S3B). Following 5 days incubation on Pal's medium, the double mutant produced extensive levels of pseudohyphae, but unlike wild-type which produced copious amounts of chlamydospores on this medium, no terminal differentiation of these pseudohyphae to chlamydospores was observed (Figure S4A). The *TLO1* mutant and the *tlo1Δ/tlo2Δ* double mutant also exhibited longer doubling times in several different liquid media, including YEPD (Table 1). When galactose was substituted for glucose in YEP medium (YEP-GAL), the growth rate of the *tlo1Δ* and the *tlo1Δ/tlo2Δ* mutants was reduced with doubling times 1.4 to 1.6 times longer than wild-type doubling times, respectively (Table 1). Growth in synthetic liquid Lee's medium was also retarded, with a doubling time 1.6 fold higher than that of wild-type. The addition of 1% peptone restored growth to WT levels in the *tlo1Δ/tlo2Δ* mutant

Table 1. Doubling times (min) of *tlo*Δ mutants and complemented strains *in vitro*.*

Growth Media	Wü284	*tlo1*Δ	*tlo2*Δ	*tlo*ΔΔ	*tlo*ΔΔ+*TLO1*	*tlo*ΔΔ+*TLO2*
YEPD	94.92	104.6	91.72	102.9	*nd*	*nd*
	0.9865	*0.9502*	*0.9783*	*0.9044*	*nd*	*nd*
YEP-Galactose	95.17	129.2	106.8	149.3	84.29	103.1
	0.9828	*0.9933*	*0.9995*	*0.9821*	*0.9916*	*0.9974*
YEP-Succinate	89.31	110.8	91.88	132	94.46	112
	0.9228	*0.9835*	*0.9826*	*0.9037*	*0.9707*	*0.8614*
Lee's defined medium	100.6	106.6	97.27	157.6	127.3	130.1
	0.978	*0.9598*	*0.9836*	*0.7243*	*0.8682*	*0.9675*
Spider medium	152.4	168.2	145.4	178.7	161.1	175.9
	0.9535	*0.9842*	*0.9528*	*0.966*	*0.9464*	*0.9456*

* The coefficient of determination (r^2) value is shown italicised below each doubling time value as an indicator of confidence in the data when analysed using regression.

doi:10.1371/journal.pgen.1004658.t001

(Figure S4B) while the addition of carbon sources or individual amino acids to solid Lee's medium did not.

Reintroduction of either *TLO1* or *TLO2* in the *tlo1Δ/tlo2Δ* double mutant background restored doubling times to wild-type levels in YEP-GAL. However, reintroduction of *TLO1* had a significantly greater effect on doubling time compared to complementation with *TLO2*. In contrast, either *TLO1* or *TLO2* restored the growth defect on Lee's medium to the same degree (Table 1).

We next investigated if *TLO* genes affect a range of stress responses. Supplementation of YEPD agar with H_2O_2 (7 mM) or menadione (100 mM), which generate reactive oxygen species, inhibited growth of the *tlo1Δ/tlo2Δ* mutant, partly inhibited growth of the *tlo1Δ* mutant, while growth of the *tlo2Δ* single mutant was largely unaffected by these oxidizing agents (Figure 3E). Reintroduction of either *TLO1* or *TLO2* to the *tlo1Δ/tlo2Δ* strain restored wild type growth in the presence of both H_2O_2 and menadione, indicating that both *TLO* genes have a role in the growth of cells under oxidative stress.

med3Δ phenocopies a *tlo1Δ/tlo2Δ* mutant

Tlo proteins are components of the Mediator complex, which is thought to facilitate interactions between Mediator and DNA-bound transcriptional activators [8]. As Tlo protein and Med3 are required for the stability of the Mediator tail in *C. dubliniensis* (Figure 2), we hypothesized that deletion of *MED3* and *TLO* genes should result in similar phenotypic effects. To test this, we compared the phenotypes of *C. dubliniensis tlo1Δ/tlo2Δ* and *med3Δ* mutants. The *C. dubliniensis med3*Δ mutant, similar to the *C. albicans med3*Δ mutant [9] and the *C. dubliniensis tlo1Δ/tlo2Δ* mutant was unable to form true hyphae in 10% serum (Figure 3C) and exhibited extended doubling times in YEP-Gal (Figure S5A) and increased susceptibility to H_2O_2 (Figure S5B). All of these properties could be restored to wild-type levels in the *med3*Δ mutant with the reintroduction of a wild-type copy of *MED3* on pCDRI (Figure 3C, S4A, S4B).

Tlo proteins regulate the transcription of a diverse set of genes

Since Mediator is important for transcription regulation, we analysed RNA expression patterns in the *tlo1*Δ/*tlo2*Δ mutant relative to wild-type cells grown in nutrient-rich growth conditions (YEPD at 37°C) and grown in hyphal inducting conditions (water plus 10% serum, optimal for *C. dubliniensis* hypha formation). During exponential growth in YEPD, a total of 746 genes exhibited a 1.5-fold or greater increase in expression and 635 genes exhibited a 1.5-fold or greater reduction in expression ($Q \leq 0.05$; Figure 4A). This scale of differential gene expression observed in our *tlo1Δ/tlo2Δ* is similar to that seen in *S. cerevisiae* Mediator tail mutants [23,24]. In the nutrient-rich YEPD broth, the *tlo1Δ/tlo2Δ* mutant exhibited a transcriptional profile that resembled a response to nutrient starvation (Figure 4B). The induced set of genes was enriched for processes associated with catabolism of alternative carbon and nitrogen sources such as *N*-acetyl-glucosamine (*NAG1, NAG3, NAG4, NAG6*), amino acids (e.g. *GDH2*, *CAR1*, *PUT2*, *PUT1*, *LPD1*, *FDH1* and *FDH3*) and fatty acids. The *tlo1*Δ/*tlo2*Δ mutant cells also up-regulated key genes of gluconeogenesis (*PCK1* and *FBP1*) and the glyoxylate cycle (*ICL1* and *MDH1*) (Figure 4B). In concert with this, the *tlo1*Δ/*tlo2*Δ mutant also caused down-regulation of genes encoding glycolytic enzymes (*PFK1*, *PFK2*, *FBA1*, *GPM1* and *ENO1*) and the glycolytic regulator *TYE7*. The *tlo1*Δ/*tlo2*Δ mutant also exhibited a greater than 2-fold decrease in expression of genes encoding proteins important for sulphur amino acid biosynthesis (e.g. *SAM2, MET1, MET6, MET10, MET14, MET16*) and ergosterol biosynthesis (*ERG1, ERG9, ERG25*). In addition, some hypha-specific genes were induced in the *tlo1*Δ/*tlo2*Δ mutant grown in YEPD. This included *IHD1*, *RBT5* and *SAP7* (induced in *C. dubliniensis* hyphae) as well as several regulators of biofilm and hyphal growth (*BCR1*, *NRG1*, *SFL1*, *TEC1* and *EED1*).

Gene Set Enrichment Analysis (GSEA) was used to compare the *tlo1*Δ/*tlo2*Δ regulated genes with published microarray datasets. GSEA indicated that the set of genes differentially expressed in the *tlo1*Δ/*tlo2*Δ mutant was enriched for genes induced during infection of RHE [25] and genes both induced and repressed during infection of bone-marrow derived macrophages [26] (Figure S6).

We also examined the transcript profile of the *tlo1Δ/tlo2Δ* mutant in 10% serum relative to wild-type (Figure 4A). After 1 h, 868 genes were significantly up-regulated 1.5-fold or greater and 816 ORFs downregulated ($Q \leq 0.05$) relative to wild-type expression at the same time point. In this medium the *tlo1Δ/tlo2Δ* mutant exhibited reduced expression of several key regulators of filamentous growth including *RAS1*, *RIM101*, *EFG1* and *UME6*. In addition, the hyphal growth regulating cyclins *CLN3* and

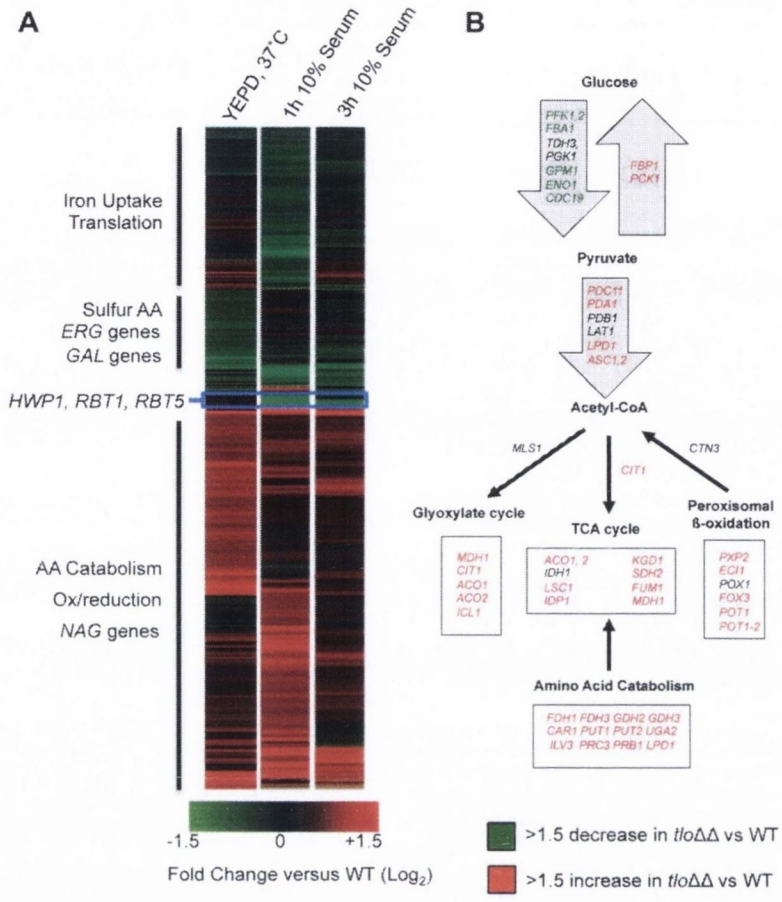

Figure 4. Microarray gene expression profiling of the *tlo1Δ/tlo2Δ* (*tloΔΔ*) mutant in YEPD and 10% serum. (A) A heat map generated in GeneSpring GX12 showing all 1.5 fold regulated genes in the *tlo1Δ/tlo2Δ* (*tloΔΔ*) mutant relative to wild type strain Wü284 during exponential growth in YEPD broth and following inoculation in 10% (v/v) serum (1 h and 3 h). The fold change (Log_2) relative to wild-type is color coded as indicated in the lower panel. GO terms associated with up and down regulated clusters are indicated on the left. (B) A cartoon metabolic map of the *tlo1Δ/tlo2Δ* (*tloΔΔ*) mutant showing the changes in expression of genes involved in energy metabolism during growth in YEPD. Genes in green exhibit a 1.5-fold or greater reduction in expression relative to wild-type whereas those in red exhibited a 1.5-fold increase in expression. Genes in black were not significantly changed.
doi:10.1371/journal.pgen.1004658.g004

HGC1 were also down regulated in the *tlo1Δ/tlo2Δ* mutant. The *tlo1Δ/tlo2Δ* mutant also exhibited reduced expression of many cell wall proteins whose induction is chracteristic of the yeast-to-hypha transition in *C. dubliniensis*, including *HWP1*, *RBT1*, *RBT5* and *SOD5* [20]. Paradoxically the *tlo1Δ/tlo2Δ* mutant exhibited a more rapid induction of the hypha-specific gene *ECE1* following 1 h incubation in serum, and expression remained elevated relative to wild-type at 3 h. In addition to hyphal genes, the *tlo1Δ/tlo2Δ* mutant exhibited reduced expression of galactose metabolic genes *GAL1*, *GAL7* and *GAL10*.

After 3 hours in 10% serum, a similar number of genes were differentially expressed 1.5-fold or greater (n = 1726). However, the level of differential expression at many genes had decreased by 3 h (Figure 4A).

TLO1 and *TLO2* restore expression of different subsets of genes

In order to investigate whether *TLO1* and *TLO2* regulate similar or different sets of genes, we analysed the transcript profiles of the *TLO1* and *TLO2* complemented mutants rather than the *tlo1Δ* and *tlo2Δ* single mutants, as the complemented strains exhibited equivalent expression of *TLO1* or *TLO2* (Figure 1B, 1C). Both *TLO1* and *TLO2* largely restored the transcript profile of the *tlo1Δ/tlo2Δ* mutant back to wild-type levels in both YEPD and 10% serum (Figure 5A, 5B). However, some *TLO*-specific transcript patterns were also detectable. Sixty-one genes were regulated in a *TLO*-specific manner in YEPD (Table S1). In comparison to the *TLO1*-complemented strain, the *TLO2*-complemented strain showed a greater reduction in expression of many *tlo1Δ/tlo2Δ* induced genes, including many hyphal genes (*IHD1*, *SAP7* and *EED1*), negative regulators of hyphal growth (*NRG1* and *SFL1*) and some starvation-induced genes such as *CAR1*, *GDH3*, *NAG3* and *NAG4* (Figure 5C). The *TLO2* complemented strain was also better at restoring wild-type levels of *SOD6* expression relative to the *TLO1* complemented strain (Figure 5C).

In 10% serum, *TLO1* was more effective at restoring expression of several genes required for induction of, and induced during,

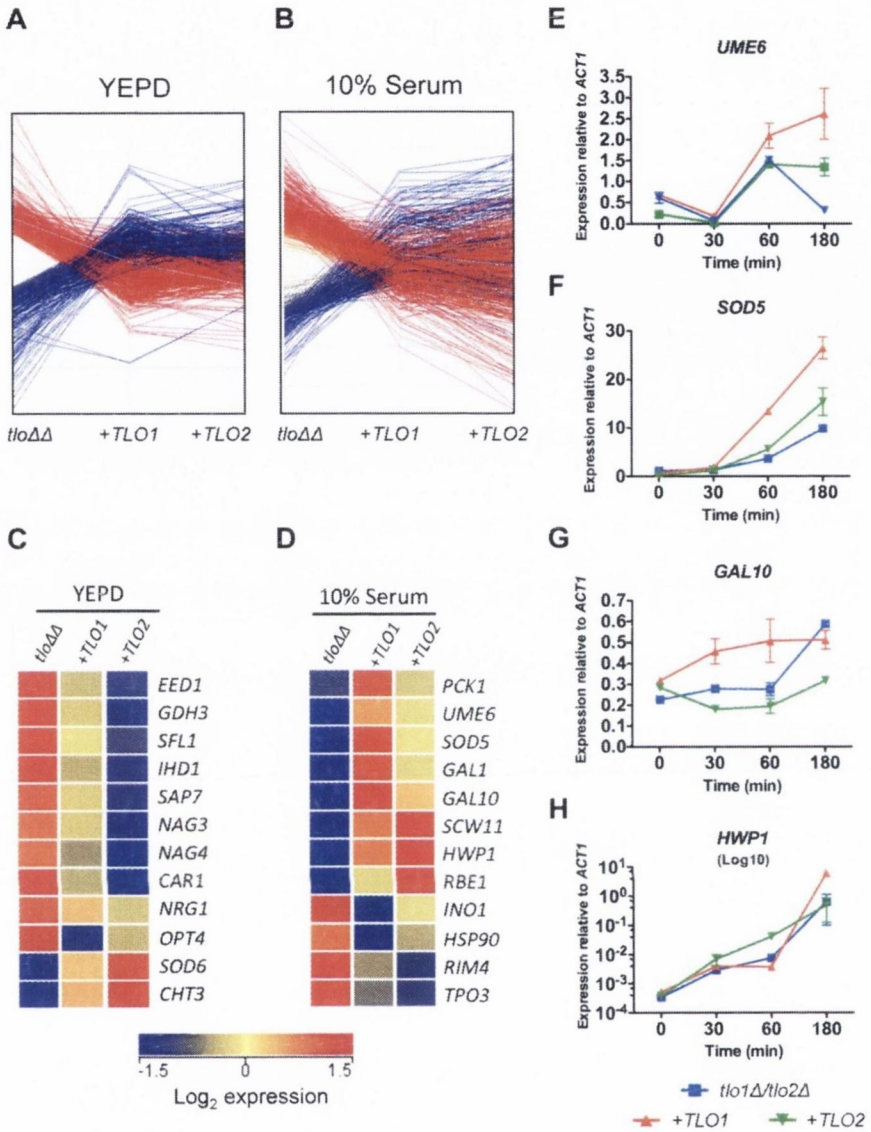

Figure 5. Reintroduction of *TLO1* or *TLO2* in the *tlo1*Δ/*tlo2*Δ (*tlo*ΔΔ) mutant restores wild-type levels of expression of overlapping and distinct sets of genes. (A) A graph plotting the change in expression of genes up regulated (red lines) or down regulated (blue lines) in the *tlo1*Δ/*tlo2*Δ (*tlo*ΔΔ) mutant following complementation with either *TLO1* (+*TLO1*) or *TLO2* (+*TLO2*) in YEPD or (B) 10% (v/v) serum. (C) Heat map of selected genes that were differentially expressed in the *tlo1*Δ/*tlo2*Δ (*tlo*ΔΔ) mutant during growth in YEPD broth (C) or 10% (v/v) serum (D) that exhibited a *TLO1* or *TLO2* specific restoration to wild-type in expression. Colors in the first column (*tlo1*Δ/*tlo2*Δ) represent the fold change in expression of the indicated genes in *tlo*ΔΔ vs wild-type; colors in columns 2 and 3 (+*TLO1* and +*TLO2*) represent the fold change in expression of the indicated genes following reintegration of *TLO1* or *TLO2* versus *tlo*ΔΔ. (E to H) QRT-PCR of the indicated genes was carried out following 30, 60 and 180 min incubation in 10% (v/v) serum at 37°C. Gene expression was determined using Sybr green technology and gene-specific levels are expressed relative to *ACT1*. Primer sequences are listed in Table S5.
doi:10.1371/journal.pgen.1004658.g005

filamentous growth including *UME6* and *SOD5* (Table S2, Figure 5D). *TLO1* was also a more effective inducer of *GAL1* and *GAL10* expression, which may explain why restoration of growth in galactose medium was more effective in the *TLO1* reintegrant relative to the *TLO2* complemented strain (Figure 5D). In contrast, *TLO2* was more effective at inducing *HWP1* expression (Figure 5D). More detailed analysis of hyphal-induced gene expression by QRT-PCR corroborated these microarray findings and supported the existence of a temporal defect in the induction of hypha specific genes in the *tlo1*Δ/*tlo2*Δ mutant. QRT-PCR showed that *UME6* and *SOD5* exhibited weak levels of induction in the *tlo1*Δ/*tlo2*Δ mutant relative to the *TLO1* reintegrant (Figure 5E, 5F). Although addition of *TLO2* led to a minor increase in *SOD5* expresssion, complementation with *TLO1* restored high-level induction of *SOD5*. Similarly, induction of *GAL10* also occurred more rapidly in the *TLO1*-reintegrated

strain relative to both the *tlo1Δ/tlo2Δ* mutant and the *TLO2*-reintegrated strain (Figure 5G) Conversely, QRT-PCR confirmed that *TLO2* restored more rapid induction (~10-fold) of the *HWP1* transcript following 1 h incubation in serum relative to the *TLO1* reintegrant (Figure 5H). However *HWP1* expression in the *tlo1Δ/tlo2Δ* mutant and *TLO1* reintegrant reached similar levels following three hours incubation in serum (Figure 5H).

This transcriptional analysis of the *TLO1* and *TLO2* complemented strains for the first time demonstrate functional diversification of Tlo proteins and show that different Tlos can regulate distinct subsets of genes.

Deletion of *MED3* disrupts transcription of a similar set of genes

This study has shown that deletion of *MED3* in *C. dubliniensis* results in similar phenotypes to those observed in the *tlo1Δ/tlo2Δ* mutant. In order to determine whether these gene deletions resulted in similar changes in transcript profile, we compared gene expression in the *tlo1Δ/tlo2Δ* and the *med3Δ* mutant in YEPD broth and in 10% serum. Hierarchical clustering was used to compare all 1.5-fold regulated genes in strains *tlo1Δ/tlo2Δ* and *med3Δ* during exponential growth. This comparison demonstrated the similarity of the transcriptional changes in both mutants relative to wild-type cells (Figure 6A). A large number (n = 47) of these commonly down-regulated genes were associated with the GO term "ribosome biogenesis" ($P = 3.89 \times 10^{-19}$; FDR = 0.0). In YEPD, both mutants exhibited aberrantly increased expression of the hypha-specific genes *IDH1*, *RBT5* and *SAP7* as well as the regulators *TEC1* and *EED1*. Activation of starvation responses was also evident in the *med3Δ* strain, which like the *tlo1Δ/tlo2Δ* strain exhibited increased expression of genes involved in gluconeogenesis (*PCK1, FBP1*) and the glyoxylate cycle (*ICL1, MDH1*). Decreased expression of glycolytic genes was less pronounced in *med3Δ*, however we could detect decreased expression (>1.5-fold) of *PFK1*, *PFK2*, *CDC19* the glycolytic regulator *TYE7* (Figure S7). Similar to *tlo1Δ/tlo2Δ*, *med3Δ* also exhibited increased expression of genes involved in oxidation/reduction processes, including amino acid catabolism (Figure 6B) in addition to reduced expression of genes involved in sulphur amino acid metabolism (*CYS3, MET1, 2, 4, 10*) and ergosterol metabolism (*ERG1, ERG251*).

Following 1 h growth in water plus 10% serum the *med3Δ* and *tlo1Δ/tlo2Δ* mutants again exhibited a common set of co-regulated genes, however in serum many *med3Δ* mutant-specific responses could also be identified (Figure 6B, 6C). The common gene set included regulators of filamentous growth, cell wall proteins and galactose metabolic genes (Figure 6B). Importantly, the *med3Δ* mutant specifically exhibited an increase in expression of glycolytic genes (n = 11; Figure 6C, S6) and genes encoding histones and proteins involved in chromatin assembly (n = 18). The *med3Δ* mutant also exhibited reduced transcription of genes associated with the GO terms "DNA replication" (n = 43) and "telomere maintenance" (n = 18) (Figure 6C).

These data indicate that in exponentially growing cells, Tlo proteins and Med3 are involved in regulating very similar processes. However, in response to specific environmental cues, these proteins may be required for regulation of specific sets of genes.

Deletion of *TLOs* has different effects on virulence traits compared to a *C. albicans med31Δ* mutant

Uwamahoro *et al.* [15] showed that in *C. albicans* deletion of *MED31*, encoding a middle subunit of Mediator affected cytokinesis, filamentous growth and biofilm formation. Similarly the *C. dubliniensis tlo1Δ/tlo2Δ* mutant described here also grew as chains of cells, typical of mutants with defects in cytokinesis (Figure S3A). However, the *C. albicans med31Δ* mutant was capable of filamentous growth in response to serum, whereas the *C. dubliniensis tlo1Δ/tlo2Δ* mutant is incapable of forming true hyphae in serum. GSEA analysis of our *C. dubliniensis tlo1Δ/tlo2Δ* mutant transcript data identified a significant enrichment for genes that are also affected in a *C. albicans med31Δ* mutant [15]. Interestingly, while the *tlo1Δ/tlo2Δ* and the *med31Δ* deletions affected similar genes, the *C. dubliniensis tlo1Δ/tlo2Δ* mutant showed increased expression of genes that were both Med31-activated and -repressed in *C. albicans* (Figure 7A). Inspection of these differentially expressed genes identified several genes required for biofilm formation that were downregulated in the *C. albicans med31Δ* mutant and induced in the *C. dubliniensis tlo1Δ/tlo2Δ* mutant, including *ALS1*, *TEC1* and *SUC1*. Uwamahoro *et al.* [15] showed that reduced *ALS1* expression in the *C. albicans med31Δ* mutant was largely responsible for the defect in biofilm formation. As the *C. dubliniensis tlo1Δ/tlo2Δ* mutant exhibited increased expression of *ALS1*, we examined whether this mutant was affected in biofilm formation. In contrast to the *med31Δ* mutant phenotype, deletion of *TLO1* and *TLO2* in *C. dubliniensis* enhanced biofilm growth on plastic surfaces (Figure 7B). In this case, complementation with *TLO2* reduced the amount of biofilm formation more than complementation with *TLO1* (ANOVA $P<0.05$) (Figure 7B). Thus the mediator middle domain has a different effect on biofilm formation than does the mediator tail domain.

Tlo proteins regulate a core set of Med2 regulated genes

The genetic and biochemical data presented here and by Zhang *et al.* [9] support a hypothesis that Tlo proteins are the candidal orthologs of *S. cerevisiae* Med2. In order to support this, we decided to compare the transcript profile of the *C. dubliniensis tlo1Δ/tlo2Δ* mutant and the *S. cerevisiae med2Δ* mutant to identify if there is an evolutionarily conserved core regulon controlled by these proteins [27]. Although the experimental details of the two studies vary, a comparison of all genes regulated 1.5-fold or greater in both mutants could identify a small but significant overlap in regulated genes (Figure S8). Carbohydrate metabolism genes that were downregulated in both mutants included the carbohydrate metabolism master regulator *TYE7* and genes regulating carbohydrate catabolism and glycerol biosynthesis (*PFK1, FBA1, GPH1, GDB1*). One of the signatures of the *tlo1Δ/tlo2Δ* mutant profile was the downregulation of sulphur amino acid metabolism and in *S. cerevisiae*, we could also detect down regulation of *MET6* and *MET13* as well as several other conserved genes regulating amino acid catabolism (*GCV1, GCV2, SHM2*). Both mutants exhibited a general increase in the expression of genes encoding enzymes involved in oxidation-reduction processes (Figure S8).

ChIP supports a role for Tlo1 in transcriptional activation and repression

In order to characterise Tlo1-DNA interactions, we carried out chromatin immunoprecipitation and high-density *C. dubliniensis* microarray (ChIP-chip) of HA-tagged Tlo1 from cells grown in YEPD broth at 30°C. On a genome wide level, we found extensive binding of Tlo1 to all chromosomes. The regions exhibiting the greatest enrichment included subtelomeric and telomeric regions and the Major Repeat Sequence (MRS) (Figure 8A). Outside of these regions, the interaction of Tlo1 was closely associated with the coding regions of genes (Figure 8A). Excluding subtelomeric

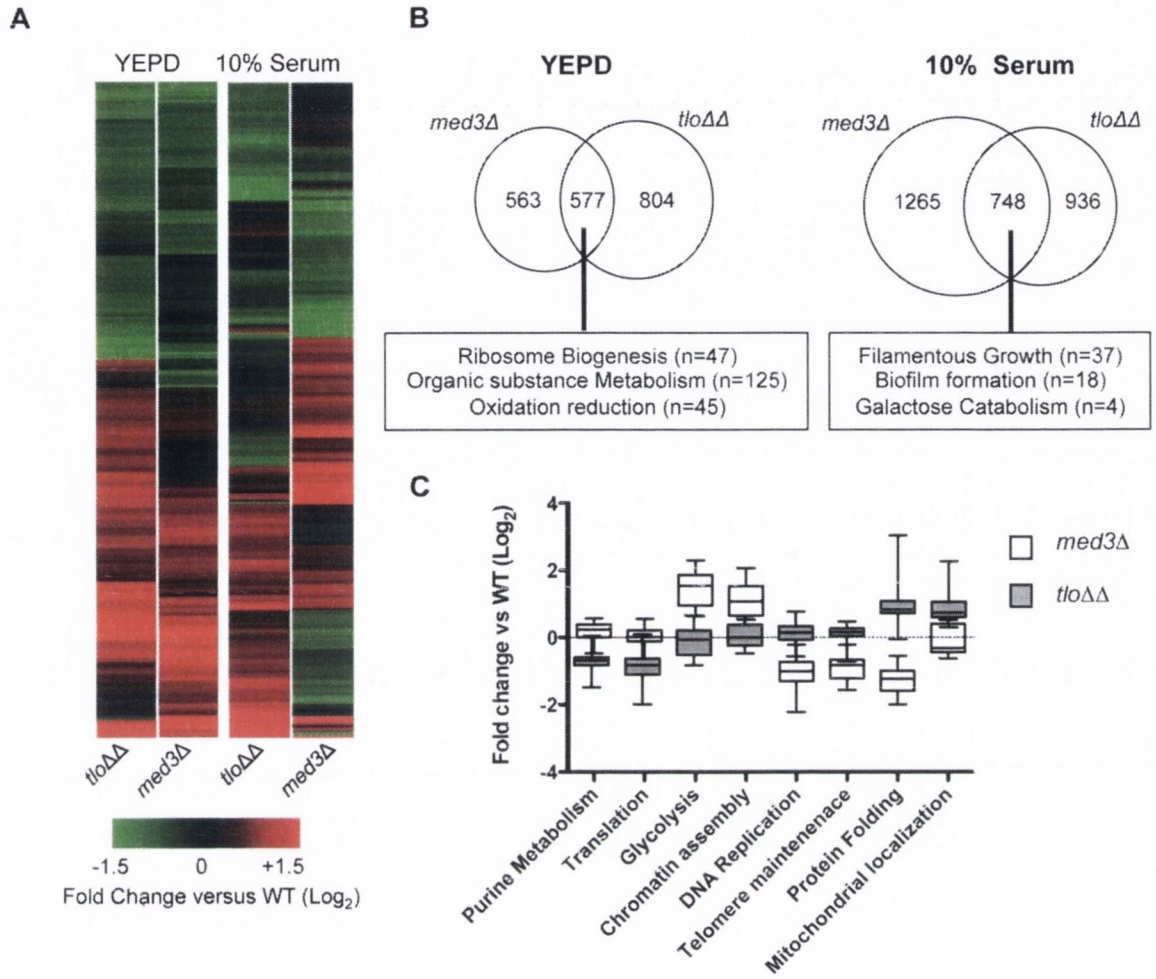

Figure 6. Microarray gene expression profiling of the *med3Δ* mutant in YEPD and 10% (v/v) serum. (A) A heat map generated in GeneSpring GX12 showing all 1.5 fold regulated genes in the *tlo1Δ/tlo2Δ* (*tloΔΔ*) and *med3Δ* mutants relative to wild type strain Wü284 during exponential growth in YEPD broth and following inoculation in 10% serum (1 h). The fold change (Log_2) relative to wild-type is color coded as indicated in the lower panel. (B) Venn diagrams illustrating the numbers of genes commonly regulated greater than 1.5-fold in the *tlo1Δ/tlo2Δ* (*tloΔΔ*) and *med3Δ* mutants following growth in YEPD broth or 10% serum. The box below indicates major functional classes of commonly regulated genes identified by GO term analysis using the GO Term finder at CGD (http://www.candidagenome.org/). (C) Graph plotting the expression levels (Log_2 fold change versus wild-type) of genes associated with selected GO terms in the *tlo1Δ/tlo2Δ* (*tloΔΔ*) and *med3Δ* mutants during growth in 10% (v/v) serum.

doi:10.1371/journal.pgen.1004658.g006

regions, only 45 intergenic regions exhibited a significant enrichment peak not associated with a coding region. In addition, we did not observe any association between Tlo1 and 57 putative Pol III transcribed tRNAs and snRNAs. Tlo1 was enriched at 1,617 ORFs in the *C. dubliniensis* genome (27% of all nuclear genes; Ringo Peak Score 0.8).

Due to recent discussions in the literature regarding artefacts in ChIP data [28–30], we restricted detailed analysis to a group of 367 genes that exhibited highly significant Tlo1-enrichment (Ringo peak score 0.9; Table S3). The region of Tlo-enrichment was centred on the coding region with extension into 5′ and 3′ flanking non-coding regions (Figure S9A). The level of Tlo-enrichment at the 5′ region was variable and was generally <100 bp in length, however extensions up to 1000 bp in length were observed (Figure S9B). QRT-PCR analysis of DNA generated in replicate ChIP experiments confirmed the high levels of enrichment observed at *PUT1* and *ACT1* and low enrichment levels observed at non-enriched genes such as *CLN1* and Cd36_51290 and an intergenic region on chromosome 5 (bp 521680–521729) (Figure 8B, 8C). Due to the repetitive nature of the repeat sequences in the MRS, it was not possible to accurately determine the level of enrichment in this region by QRT-PCR.

Using fluorescence intensity data extracted from our gene expression microarrays, we compared the expression levels of the Tlo1-associated ORFs relative to non-Tlo1 associated ORFs. Tlo1-associated ORFs were found to exhibit higher expression levels (average 1.8-fold) in YEPD compared to those genes that are not occupied (Figure S9C). However, a plot of enrichment score versus expression level did not identify a direct correlation between Tlo1 enrichment and expression. Importantly, the most highly

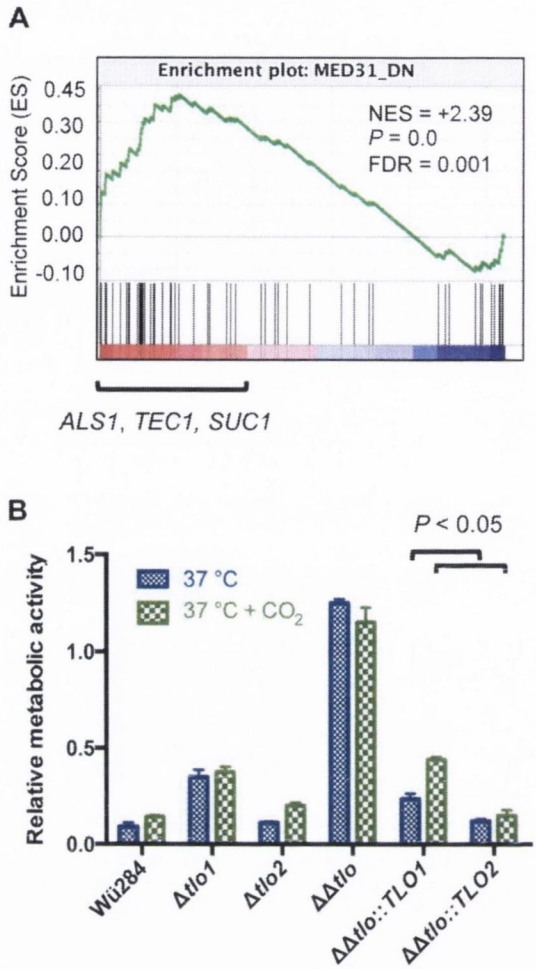

Figure 7. Deletion of *TLOs* has different effects on biofilm formation compared to a *med31Δ* mutant. (A) Gene Set Enrichment Analysis (GSEA) plot showing differential expression of genes down-regulated in a *C. albicans med31Δ* mutant in the *tlo1Δ/tlo2Δ* mutant (i.e. they are upregulated in the *tlo1Δ/tlo2Δ* mutant) (B) Biofilm formation was assessed in the indicated strains on plastic surfaces at 37°C in the presence or absence of 5% CO_2 as indicated. Adherent biomass determined by an XTT reduction assay. The experiment was carried out in triplicate on three separate occasions (n = 9) and error bars represent the standard deviation from the mean. *P* values above figure are the result of one-way ANOVA with Tukey's post hoc test.
doi:10.1371/journal.pgen.1004658.g007

enriched genes (n = 367; Ringo peak score 0.9) covered a broad spectrum of expression levels, including genes expressed at high and low levels in YEPD (Figure 9A). We analysed the GO terms associated with these Tlo1-enriched genes and identified significant numbers of highly expressed genes associated with the GO categories glycolysis (n = 7; $P = 0.003$) and the TCA cycle (n = 7; $P = 0.048$)(Figure 9A). Manual inspection of the gene list also identified highly expressed genes involved in translation (n = 5) and sulphur amino acid metabolism (n = 4). Tlo1-enriched genes that are poorly expressed in YEPD were associated with the GO categories glyoxylate cycle (n = 3; $P = 0.09$), GlcNac catabolic process (n = 6, $P = 0.094$), amino acid catabolic process (n = 10; $P = 0.018$) and hexose transport (n = 9; $P = 0.057$). Manual inspection also identified poorly expressed genes encoding nitrogen scavenging transporters (e.g. *FRP6, MEP21, MEP22, DAL1, UGA6*) and genes involved in gluconeogenesis (*PCK1* and *FBP1*). Many YEPD repressed, hypha-specific genes were also enriched including *EED1, RBT1, HWP1, HWP2* and *IHD1*.

These data show that Tlo1 is present at many highly expressed metabolic genes in addition to genes normally repressed in YEPD (starvation, hyphal genes) indicating a dual role in transcriptional activation and repression. In order to support this hypothesis, we analysed the transcription of these categories of Tlo1-enriched genes in our *tlo1Δ/tlo2Δ* mutant. This analysis found that the highly expressed genes involved in glycolysis and sulfur amino acid metabolism exhibited significantly reduced expression (ANOVA; $P<0.05$) in the *tlo1Δ/tlo2Δ* mutant relative to wild type cells, indicating that Tlo1 occupancy is required for maintaining the high level of expression of these genes (Figure 9B). The exceptions to this finding were the genes encoding enzymes of the TCA cycle, which although highly expressed in wild-type cells, exhibited increased expression in the *tlo1Δ/tlo2Δ* mutant. In addition, highly Tlo1-occupied, low expression genes exhibited increased expression in the *tlo1Δ/tlo2Δ* mutant, including genes involved in starvation responses, nitrogen scavenging mechanisms, *N*-acetyl glucosamine catabolism and the hyphal GPI-anchored proteins (Figure 9B). These data indicate that Tlo1 and the Mediator complex are involved in both transcriptional activation and repression of different classes of genes. The fact that Tlo1-enriched genes exhibit regulation in the *tlo1Δ/tlo2Δ* mutant also provides support for hypothesis that Tlo proteins interact with these ORFs.

Discussion

Despite the importance of Mediator in transcriptional regulation, few studies have investigated the role of Mediator in regulating virulence-associated characteristics in pathogenic eukaryotic microrganisms. The discovery of a widely dispersed telomeric gene family with homology to Med2 in the pathogenic yeast *C. albicans* has accelerated the level of interest in Mediator in this fungus. Published data suggest important roles for Mediator in regulating important biological processes in *C. albicans*, including filamentous growth (Med3), biofilm formation (Med31, Med20) and white-opaque switching (multiple subunits) [9,15,16]. Because functional analysis of the 15 *TLO* paralogs in *C. albicans* remains technically challenging, we turned to *C. dubliniensis*, which shares many characteristics with *C. albicans* but contains only two *TLO* orthologs, thereby providing an ideal genetic background in which to investigate the degree to which *TLO* gene function(s) have diverged between the two *TLO* paralogs. It has been hypothesized that in *C. albicans*, Mediator could form variant complexes that contain different Tlo/Med2 subunits that could be differentially recruited to activate or repress different subsets of genes in response to specific stimuli [9,12]. *C. dubliniensis*, which has only two Tlo proteins that appear to associate primarily with Mediator, provides an invaluable tool to understand first, how different *TLO* genes may affect Mediator function and second how the presence of multiple variant *TLO* genes contributes to virulence.

In *C. dubliniensis*, *tlo1Δ* deletion mutants are defective in hyphal growth [14]. Here, we constructed a null *tlo1Δ/tlo2Δ* double mutant strain of *C. dubliniensis*. The *tlo1Δ/tlo2Δ* strain exhibits a wide range of phenotypic defects, indicating that they play a central role in global transcriptional control. Consistent with a role in regulating hyphal growth, deletion of both *TLO* genes reduced expression of many of the key regulators of

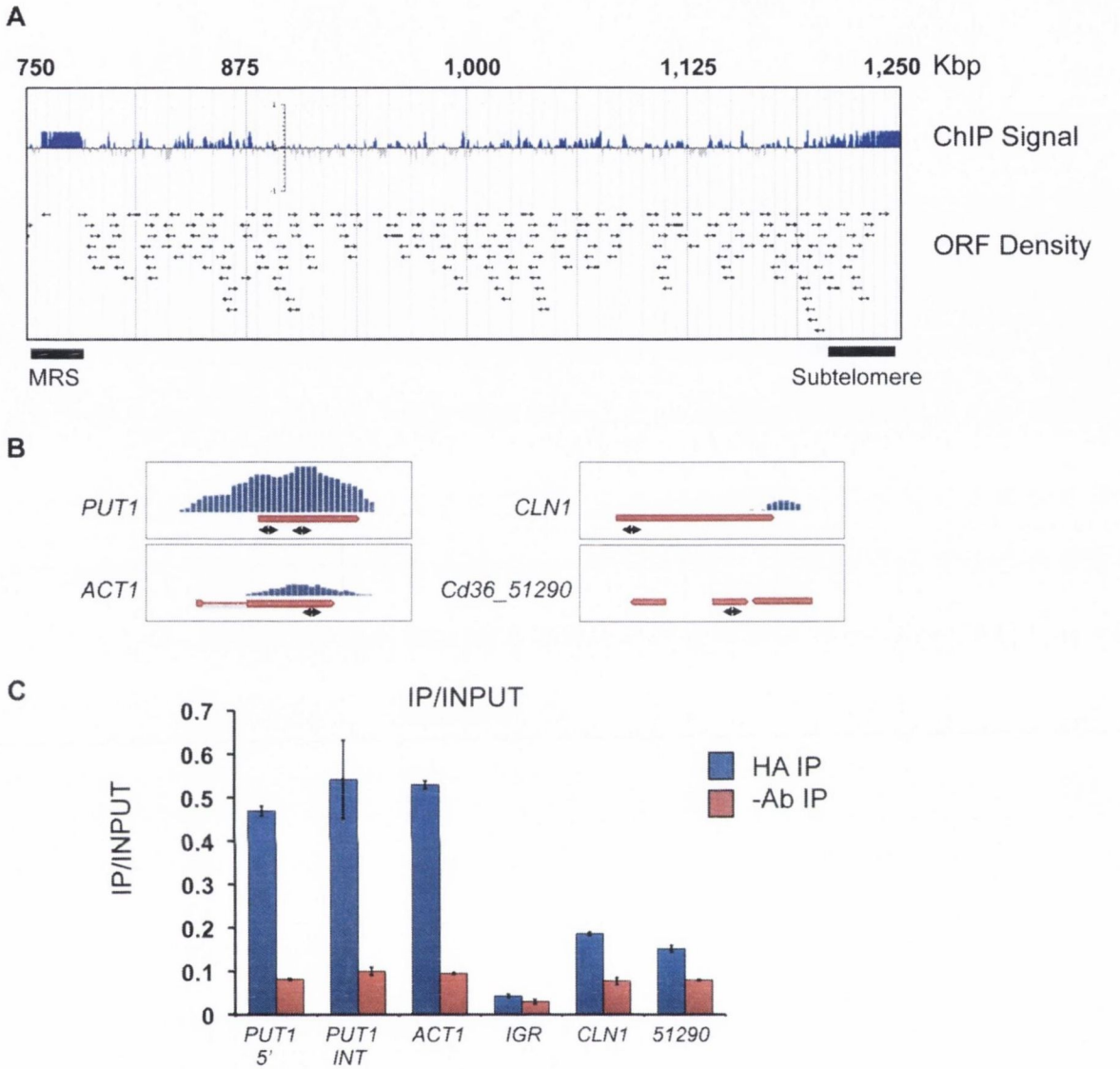

Figure 8. Localization of Tlo1-DNA interaction by ChIp-Chip analysis. (A) A map of the right arm of *C. dubliniensis* chromosome 5 showing Tlo1-HA enriched areas, including the subtelomeric and Major Repeat Sequence (MRS) regions. Arrows indicate the position of individual ORFs. All chromosomes can be visualised here: http://bioinf.gen.tcd.ie/jbrowse/?data=cdub. (B) ChIP-chip Enrichment profiles for *PUT1*, *ACT1*, *CLN1* and CD36_51290. Double headed arrows show approximate positions of amplimers used in QRTPCR confirmation experiments. (C) QRT-PCR confirmation of the enrichment levels shown in panel B using gene-specific primers and an intergenic region (IGR)-specific primer set (Chr5 521680–521729 bp)(Table S5). Amplification was carried out on immunoprecipitated chromatin in anti-HA antibody samples (HA-IP) and no antibody (-AB IP) negative control samples. Relative enrichment values refer to the quantity of DNA amplified from anti-HA immunoprecipitated samples ('enriched') relative to total input chromatin ('non-enriched').
doi:10.1371/journal.pgen.1004658.g008

morphogenesis including signal transducers (*RAS1*, *RIM101*) transcriptional regulators (*EFG1*, *UME6*) and kinases (*HGC1*), resulting in largely pseudohyphal growth phenotypes with reduced expression of key hyphal genes (*SOD5*, *RBT5*, *HWP1*). The *tlo1*Δ/*tlo2*Δ mutant also exhibited increased susceptibility to oxidative stress and reduced growth in the presence of alternative carbon sources. These data demonstrate that the *TLO*s of *Candida* spp. have evolved to regulate many key processes, including those important for virulence and growth in the host. In addition, the importance of Tlo in mediating transcriptional responses important for pathogenicity is shown in the similarity of our transcript profiles to those observed during infection of RHE and bone marrow-derived macrophages (Figure S6) [25,26]. Indeed, a *tlo1*Δ/*tlo2*Δ mutant grown in YEPD mounts a transcriptional response akin to that observed following phagocytosis by macrophages [1]. Recent studies have also shown that Mediator is an important regulator of the *Candida*-macrophage interaction [31]. One key observation regarding the transcriptional changes

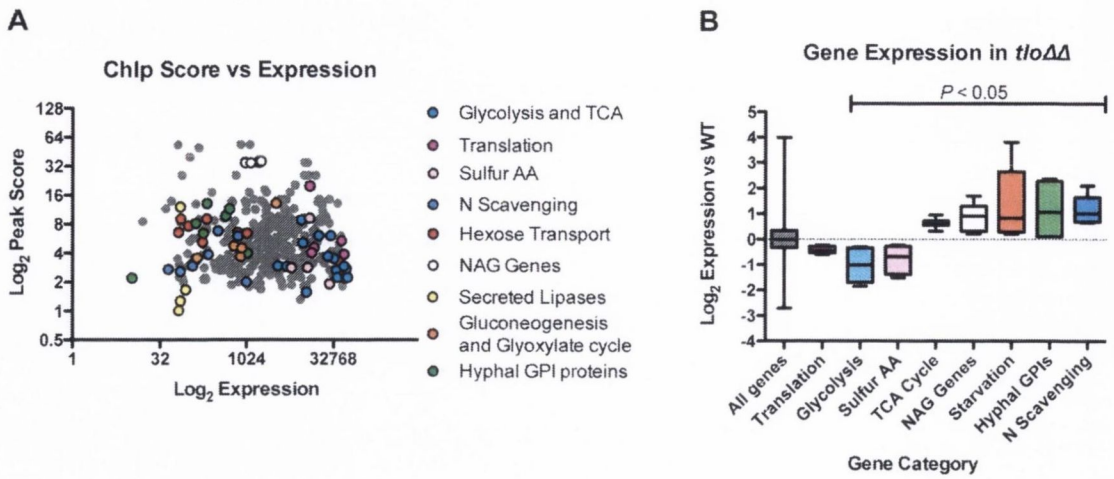

Figure 9. The relationship between Tlo1 binding and gene expression. (A) A plot of Tlo1 enrichment scores for the 367 most highly enriched genes versus the expression levels of those genes in YEPD broth (extracted from microarray data). The categories of highly expressed and repressed genes are color-coded; TCA = Tricarboxylic acid cycle; Sulfur AA = sulphur amino acid biosynthesis; N scavenging = Nitrogen scavenging; NAG = GlcNac metabolism; GPI = glycophosphatidylinositol anchor). (B) Analysis of the expression of Tlo1-enriched groups of genes in the wild type in the *tlo1*Δ/*tlo2*Δ (*tlo*ΔΔ) mutant indicated that the highly expressed, highly enriched genes exhibited reduced expression whereas the poorly expressed and repressed genes exhibited increased expression in the *tlo1*Δ/*tlo2*Δ (*tlo*ΔΔ) mutant. The change in expression in these groups, with the exception of the genes involved on translation, was significant (ANOVA, $P<0.05$).
doi:10.1371/journal.pgen.1004658.g009

observed in the *tlo1*Δ/*tlo2*Δ mutant was the alteration in the kinetics of induction of hypha-specific transcripts. Complementation of the *tlo1*Δ/*tlo2*Δ mutant with Tlo1 resulted in more rapid and higher levels of transcriptional induction of *SOD5*, *UME6* and *GAL10*. Some induction of these transcripts could be observed in the *tlo1*Δ/*tlo2*Δ mutant, however the amplitude of the response was greatly retarded relative to the complemented strains. These data suggest that Tlo proteins play an important role in maximizing the speed and magnitude of transcriptional changes in response to environmental cues. This characteristic is likely to be of great importance in the host where rapid responses could be important for survival, e.g. following phagocytosis or translocation to a different part of the gastrointestinal tract.

In *S. cerevisiae*, the Mediator tail regulates stress responses and the metabolism of carbohydrates and amino acids [23,24,27]. A direct comparison of the genes regulated in our *tlo1*Δ/*tlo2*Δ mutant and an *S. cerevisiae med2*Δ mutant supports this evolutionarily conserved role for Mediator tail in eliciting transcriptional responses to deal with changing environments [27]. In *S. cerevisiae* this effect has been shown to be centred on SAGA-regulated genes [24].

In this study, we also explored the relationship of Tlo proteins with other subunits of Mediator. A defect in filamentous growth was described by Zhang *et al.* in *C. albicans* following deletion of *Med3*, encoding another Mediator tail subunit that interacts with Tlo proteins [9]. Biochemical analysis of the Mediator complex in the *tlo1*Δ/*tlo2*Δ null mutant and the *C. dubliniensis med3*Δ mutant revealed the absence of Med5 and Med16 in Mediator purified from both mutants, suggesting that the entire tail complex is destablilized by loss of Tlo or Med3 proteins. Consistent with this idea, the *C. dubliniensis med3*Δ and *tlo1*Δ/*tlo2*Δ null mutants exhibited remarkably similar phenotypes and transcriptional profiles when cultured in YEPD. However, in response to hyphal stimulating conditions, many differences in transcriptional responses could be observed in the *tlo1*Δ/*tlo2*Δ strain and the *med3*Δ mutant strain (Figure 6), suggesting that Mediator complexes with different tail substituents may exist *in vivo* in response to specific environmental conditions. Alternatively, the deletion of either Med3 or Tlo protein may release the remaining Tail module Mediator subunits to form a sub-complex that can interact with cellular components independently of the remainder of the complex.

We next examined the relationship of Tlo with the Mediator middle subunit, Med31, described by Uwamahoro *et al.* [15]. The *C. dubliniensis tlo1*Δ/*tlo2*Δ null mutant exhibited a defect in cell separation and *CHT3* expression, which is consistent with the defect in cytokinesis described in the *C. albicans med31* mutant by Uwamahoro *et al.* [15]. These data support previous studies that suggest that regulation of cytokinesis and possibly Ace2-regulated genes is a conserved function of mediator in yeast [15,32]. However, a *med31*Δ mutant was still capable of true hyphal growth in liquid medium whereas the *tlo1*Δ/*tlo2*Δ null mutant was completely unable to form true hyphae under the same conditions. The most striking difference in phenotype was the increased ability of the *C. dubliniensis tlo1*Δ/*tlo2*Δ mutant to form biofilm. The *C. albicans med31*Δ mutant exhibits reduced biofilm growth relative to wild-type and decreased expression of the biofilm regulator *TEC1* and the adhesin *ALS1* (Figure 7A). The *C. dubliniensis tlo1*Δ/*tlo2*Δ null mutant exhibited increased expression of many *med31*Δ downregulated genes, including *TEC1* and *ALS1*, although the roles of these genes in biofilm formation in *C. dubliniensis* have yet to be confirmed. These data illustrate the very different and possibly opposing roles that mediator tail and middle subunits may have in transcriptional regulation in *Candida* spp.

Our ChIP analysis of Tlo1 for the first time indicates the level of Tlo and Mediator occupancy across the *Candida* genome. Although Mediator tail subunits are unlikely to interact directly with DNA, they associate closely with DNA-bound transcription factors and histones and have been successfully isolated in association with DNA in other yeasts [8,33]. We identified extensive Tlo1 binding across all *C. dubliniensis* chromosomes.

Tlo1 was closely associated with Pol II transcribed ORFs as well as the telomeres and the MRS. Binding of Mediator to telomeres and sub-telomeric genes has been described in *S. cerevisiae* and Mediator has been shown to have an additional role in heterochromatin maintenance [33,34]. Our data suggests that Mediator could play a similar role in *Candida* spp. The significance of Tlo1-enrichment at the MRS is more difficult to explain as the function of this repeat element is unknown. Further studies will be required to verify this interaction.

In order to limit the numbers of possible ChIP artefacts, often associated with highly expressed genes, we have used a very stringent cut off to define highly enriched genes. This Tlo1-enriched gene set includes repressed and moderately expressed genes, supporting the assumption that our data set is not biased for highly expressed ORFs. In addition, the highly expressed genes identified in our ChIP analysis are regulated following deletion of Tlo, supporting a direct, functional interaction with these ORFs.

The association of Mediator subunits with the coding regions of Pol II transcribed ORFs has been observed in Mediator ChIP localization experiments in other yeasts and suggests that Tlo1 may be involved in transcript elongation or in chromatin interactions at coding regions [35,36]. We observed that although Tlo1-occupied genes on average were expressed higher than non-occupied genes (average 1.8-fold), Tlo1 was associated with ORFs having a range of expression levels. To further investigate the significance of Tlo1 ORF occupancy and Tlo1-dependent gene expression, we compared the regulation of specific classes of Tlo1 occupied genes in our *tlo1*Δ/*tlo2*Δ mutant. Highly expressed genes encoding enzymes involved in amino acid synthesis, glycolysis and translation required Tlo1 to maintain high levels of expression. In contrast, genes that exhibited low levels of expression under the conditions analysed were repressed by Tlo1. These data suggest a dual role for Tlo1 in mediating transcriptional activation and repression. Specifically, Tlo1 was required to maintain transcription of genes involved in glycolysis and translation and to repress starvation responses (glyoxylate cycle, gluconeogenesis) and several hypha-specific genes. Localisation of Mediator to both expressed and repressed genes has been observed in *S. cerevisiae* and the ability of the complex to carry out opposing regulatory functions is likely due to its ability to adopt different modular conformations [36]. Specifically, the kinase module in *S. cerevisiae*, consisting of Cdk8, Cyclin C, Srb8 and Srb9 has been shown to associate with Mediator to repress transcription [36]. A specific role for the kinase module in transcriptional repression has yet to be determined in *Candida* spp.

The *C. dubliniensis* genome harbors two *TLO* orthologs, two alleles of *TLO1* and one allele of *TLO2*. One of the central goals of our study was to determine whether different *TLO* genes could regulate different processes. To compare the effects of single copies of *TLO1* and *TLO2*, we complemented the *tlo1*Δ/*tlo2*Δ mutant independently with either *TLO1* or *TLO2*. Each of the *TLO* genes complemented *tlo1*Δ/*tlo2*Δ mutant phenotypes, albeit to different degrees; *TLO1* was better at restoring true hyphal growth and growth in galactose. *TLO2* supressed biofilm growth to a greater extent than *TLO1*. With regard to *TLO2*, it should be noted that the level of expression of the reintegrated allele was significantly higher than the wild-type allele, which may have resulted in higher levels of Tlo2 activity. However, despite this, the reintegrated *TLO2* allele did not restore filamentous growth to the same extent as wild-type *TLO1*.

Support for these functional differences was obtained when the transcript profiles of the *TLO1* and *TLO2* complemented strains were compared. It was observed that *TLO1* could restore *GAL* gene induction to a greater extent than *TLO2*. During hyphal growth, *TLO1* also restored expression of *UME6* and *SOD5* to a greater degree than *TLO2*. In contrast, during growth in YEPD *TLO2* was required for repressing transcription of aberrantly expressed hyphal genes such as *IHD1*, *SAP7* and *EED1* and the negative regulators of hyphal growth *SFL1* and *NRG1*. *TLO2* was also required for suppression of many starvation induced genes involved GlcNac metabolism (*NAG3, NAG4*) and amino acid metabolism (*CHA1, GDH3*). The data suggest that the two *TLO* paralogs in *C. dubliniensis* have evolved to regulate overlapping as well as distinct subsets of genes. Under standard growth conditions, both *TLO1* and *TLO2* are expressed in *C. dubliniensis*, suggesting that two distinct pools of Mediator exist at any one time, with the ability to regulate different subsets of genes. The implications of our study for *C. albicans* biology, where there are potentially 15 different Tlo-Mediator complex varieties with differing transcriptional activating activities, are immense. It is tempting to speculate that this variety in Mediator activity, or a varying pool of non-Mediator associated Tlo protein, could contribute to the phenotypic plasticity and adaptability of this fungus and may go towards explaining why its incidence as a commensal and opportunist is far greater compared to its close relatives *C. tropicalis* and *C. dubliniensis* which do not have this expanded repertoire of Med2 paralogs.

Over the last decade, a wealth of studies have described the global transcriptional responses of *C. albicans* to environmental stress, pH changes and nutrient availability amongst others. It is clear from these studies that one of the characteristics of *C. albicans* is its ability to rapidly respond to environmental change by mediating rapid transcriptional responses. The current study suggests a vital role for the Tlos in mediating the speed and scale of these responses, which are associated with characteristics required for commensalism (nutrient acquisition, metabolism) and pathogenicity (starvation responses, filamentation) indicating a key role for Tlo-regulated responses in the lifestyle of *C. albicans*. This, coupled with the potential diversity in the activity of the different Tlo paralogs may have contributed to the ability of *C. albicans* to colonise many diverse niches and thus to evolve to be a highly successful commensal and pathogen.

Materials and Methods

Candida strains and culture conditions

All *Candida* strains were routinely cultured on yeast extract-peptone-dextrose (YEPD) agar, at 37°C. Solid Lee's medium and Spider medium were used as described previously [37,38]. Pal's agar medium was also used for chlamydospore induction as described previously [39]. For liquid culture, cells were grown shaking (200 rpm) in YEPD broth at 30°C or 37°C. In order to determine the doubling time of each strain, the optical densities (600_{nm}) of cultures in the exponential phase of growth were plotted and analysed using the exponential growth equation function in Graphpad Prism (GraphPad, CA, USA). Doubling times and r^2 values in Table 1 were calculated from three replicate growth curves. Glucose (2% w/v) was substituted with galactose (2% w/v) where indicated. Hyphal induction was carried out in sterile Milli-Q H_2O supplemented with 10% (v/v) fetal calf serum at 37°C. Samples were randomized and the proportion of germ-tubes or true-hyphae in 300 cells was assessed at intervals by microscopic examination of an aliquot of culture with a Nikon Eclipse 600 microscope (Nikon U.K., Surrey, U.K.). Experiments were performed on at least three separate occasions.

Genotypes of strains used in this study are listed in Table S4. Gene disruption of *TLO1* (Cd36_72860) and *TLO2* (Cd36_35580)

was achieved through use of the *SAT1* flipper cassette system [40]. Deletion constructs were created by PCR amplifying the 5′ flanking regions of *TLO1* or *TLO2* with the primer pairs CTA21KF/CTA1X and CTA22KF/CTA2X respectively and the 3′ flanking regions with the primer pairs CTA1S/CTA21SIR and CTA2S/CTA22SIR, respectively (Table S4). Ligation of these products in the corresponding restriction sites in plasmid pSFS2A resulted in the construction of plasmids pTY101 (*TLO1*) and TY102 (*TLO2*) as described [19]. The deletion construct was used to transform *C. dubliniensis* Wü284 as described previously [19] and deletion of genes was confirmed by Southern blotting (Figure S1). A single transformation with TY102 was sufficient to delete *TLO2* in strain Wü284 which was found to have a truncation in one copy of ChrR, resulting in the presence of only one copy of *TLO2*. Deletion of *MED3* was carried out using a primer tailing method with the primers MED3M13F/MED3M13R as described [41]. Reintroduction of wild-type *TLO* genes or *MED3* was achieved by PCR amplification of the entire ORF plus their upstream and downstream regulatory sequences using primer pairs CdTLO1FP/CdTLO1RP for *CdTLO1*, CdTLO2FP/CdTLO2RP for *CdTLO2* and MED 3FP/MED3RP for *MED3* (Table S5) and ligation of these into the *C. dubliniensis* integrating vector pCDRI to yield plasmids pCdTLO1, pCdTLO2, and pCdMED3 respectively. These plasmids were transformed as described previously [19].

Biochemical analysis of mediator

Mediator was purified from *C. dubliniensis* strains containing Mediator subunits tagged at their C-terminus with either HA or 6His-FLAG. *CdMED8-* and *CdTLO1*-tagging cassettes were amplified from pFA-3HA-SAT1 or pFA-6His3Flag-SAT1 using the primer pairs pZL420/pZL421 and pZL422/pZL423, respectively, as described previously [9]. Whole-cell extracts were made from strains that were untagged or had a single copy of Tlo1 or other Mediator subunit tagged with a HA or 6His-FLAG and subjected to multiple chromataographic separations as described previously [9]. The elutions from the immobilized metal affinity chromatography (IMAC; Talon Kit, Clontech Laboratories, CA, USA) step were analyzed by SDS-PAGE as indicated and proteins were revealed by staining with silver as described previously [9].

Induction of biofilm formation

Biofilm mass was determined using an XTT reduction assay to assess metabolic activity. Prior experiments with planktonic cells indicated that wild-type and *tlo*Δ mutant strains exhibited similar rates of XTT reduction. To induce biofilm growth, a suspension of 1×10^6 cells of each strain was prepared in 10% (v/v) foetal calf serum from 18 h cultures grown in YEPD broth at 30°C with shaking at 200 rpm A 100 µl volume of each suspension was added to triplicate wells of a 96-well, flat-bottomed polystyrene plate (Greiner BioOne) with lid. Plates were then incubated for 24 h or 48 h in a static incubator (Gallenkamp) set to 37°C. Growth in the presence of 5% (v/v) CO_2 was carried out in a static tissue culture incubator with 5% (v/v) relative humidity (Gallenkamp). All wells were then washed 5 times with 200 µl sterile PBS to remove non-adherent cells. After the final wash, 200 µl of 200 µg/ml XTT supplemented with 50 µg/ml CoEnzyme Q (Sigma-Aldrich) was added to each well and incubated at 37°C in the dark for 50 min. A 100 µl aliquot of this suspension was transferred to a fresh plate and the absorbance measured at 480 nm using a Tecan Plate Reader system (Tecan). Results were analysed and graphed using Microsoft Excel (Microsoft).

Transcriptional profiling with oligonucleotide microarrays

The *C. dubliniensis* whole genome oligonucleotide microarray used in this study was previously described [20]. RNA was extracted from cells grown to an OD 600 nm of 0.8 in YEPD broth at 37°C or from cells (1×10^6) inoculated in 10% (v/v) fetal calf serum at 37°C. Cell pellets were snap frozen in liquid N_2 and disrupted using the Mikro-Dismembrator S system (Sartorius Stedim Biotech, Göttingen, Germany). RNA was prepared using the Qiagen RNeasy mini-kit. A 200 ng aliquot of total RNA was labelled with Cy5 or Cy3 using the Two-Color Low Input Quick Amp labeling Kit (Agilent Technologies) according to the manufacturer's instructions. Array hybridization, washing, scanning and data extraction was carried out in GenePix Pro 6.1 (Axon) as described [20]. For each condition, four biological replicate experiments were performed, including two dye swap experiments. Raw data were exported to GeneSpring GX12 and signals for each replicate spot were background corrected and normalized using Lowess transformation. Log_2 fluorescence ratios were generated for each replicate spot and averaged. Genes differentially expressed (1.5-fold) relative to wild-type were identified from those that passed a *t*-test ($P\leq0.05$) and satisfied a post-hoc test (Storey with Bootstrapping) with a corrected Q value ≤0.05. Hierarchical clustering was used to compare gene expression in each condition using the default settings in Genespring GX12. The Gene Set Enrichment Analysis (GSEA) PreRanked tool (available to download at www.broadinstitute.org/gsea/index.jsp) was used to investigate whether our data sets were enriched for particular genes present in published data sets [42]. This analysis required the use of a database of publicly available genome-wide data sets, constructed by Andre Nantel (National Research Council of Canada, Montreal), that can be downloaded from the Candida Genome Database (CGD). This database included 171 lists of up- and down-regulated genes from microarray experiments, *in vivo* promoter targets derived from ChIP-chip experiments performed on 36 transcription factors, members of 3,601 Gene Ontology (GO) term categories, and 152 pathways, as curated by CGD, amongst others, and is fully described by Sellam *et al.* [43]. Genes in our expression data sets were first 'ranked' based on Log2 values from highest to lowest. The GSEA PreRanked tool was then used to determine if particular gene sets in the database were enriched towards the top or bottom of this ranked list. Enrichment plots show the level of enrichment towards the top (red) or bottom (blue) of the ranked list. The normalized enrichment score (NES) indicates the level of enrichment at the top (positive NES) or bottom (negative NES) of the ranked list and is supported by a p value and a False Discovery Rate (FDR) value to indicate the likelihood of false positive results.

Microarray data have been submitted to Gene Expression Omnibus (GEO), accession number: GSE59113.

Real-time PCR analysis of gene expression

RNA for QRT-PCR was isolated using the RNeasy Mini-kit (Qiagen). Cells were disrupted using a FastPrep bead beater (Bio101). RNA samples were rendered DNA free by incubation with Turbo-DNA free reagent (Ambion, Austin, TX). cDNA synthesis was carried out using the Superscript III First strand synthesis sytem for RT-PCR (Life technologies) as described by Moran et al. [19] Reactions were carried on an ABI7500 Sequence Detector (Applied Biosystems, Foster City, CA) using MicroAmp Fast Optical 96-well Reaction plates (Applied Biosystems) in 20 µl reactions using 1X Fast SYBR Green PCR Master Mix (Applied Biosystems), 150 nM of each oligonucleotide (Table S4) and 2 µl of diluted template (10 ng). Cycling conditions used

were 95°C for 20 sec, followed by 40 cycles of 95°C for 3 sec and 60°C for 30 sec, the latter of which was the point of detection of fluorescence. This was followed by a melt curve stage as a quality control point. Gene expression levels were normalized against the expression levels of the constitutively expressed *ACT1* gene in the same cDNA sample. Gene specific primers are shown in Table S5. Each gene-specific set was shown to amplify at a similar efficiency (within 10%) to the control *ACT1* primer set in primer optimization experiments.

Chromatin immunoprecipitation and microarray hybridisation (ChIP-chip)

C. dubliniensis strain Tlo1-HA, derived from strain Wü284, was grown at 30°C degrees and harvested at an OD 600 nm of 2.0. A secondary cross-linking strategy was employed to fix chromatin that involved initial treatment of cells with dimethyl adipimidate (10 mM) for 45 min with agitation at room temperature followed by cross-linking with 1% formaldehyde. Cells were washed twice in PBS prior to spheroplasting in 5 ml of spheroplasting buffer (1.2 M sorbitol, 20 mM 4-(2-hydroxyethyl)-1-piperazineethanesulfonic acid [HEPES] pH 7.4) containing 0.4 mg/ml Zymolyase 100T (Seikagaku Corp., Japan) and incubated for 2.5 h 30°C with rotation. DNA isolation and fragmentation was carried out as described in Ketel *et al* [44] using a Branson sonifier to yield DNA fragments of 500–600 bp. Chromatin immunoprecipitation (ChIP) was carried out as described by Ketel et al. [44] using an anti-HA mouse monoclonal antibody (clone 12CA5) which was incubated overnight at 4°C on a rotating wheel. The following day, 70 µl of Protein A agarose beads (Santa Cruz Biotech, California, USA) were added and mixed at 4°C for 4 h. DNA was recovered as described by Ketel et al [44] and resuspended in 80 µl TE buffer for downstream applications.

Microarray chip analysis (CGH Microarray) was carried out as described in the Agilent Yeast ChIP-on-chip analysis protocol handbook (Version 9.2, 2007). Competitive hybridization was carried out on a whole genome *C. dubliniensis* oligonucleotide microarray consisting of 175,758 unique 60mer probes, spaced at 20 bp intervals (Agilent Technologies). Experiments were performed with triplicate biological replicate samples. The IP samples were labelled with Cy3 and input samples (total lysate control) were labelled with Cy5. One sample was dye swapped. Array hybridisation and washing were carried out using standard Agilent Technologies CGH hybridisation buffers and washes. Scanning of the array was carried out on an Agilent G2565B rotating multi-slide hyb-scanner (Agilent Technologies) using a 5 µm resolution and PMT settings at 100% for both channels (Green/Red). The scan area was set to 61×21.6 mm. The raw images were processed using Agilent Feature Extraction software suite v 10.5.1.1. and feature extraction was automatically carried out using the 'CGH automatic' programme to align and normalise fluorescent probe spots on the array.

Data were read into the Bioconductor [45] package Ringo [46] and pre-processed with the "nimblegen" method. This was followed by merging of replicates and smoothing with a window half size of 500 bp. ChIP-enriched regions were calculated with an enrichment threshold based firstly on a 0.8 percentile, followed by a more stringent 0.9 percentile which was used for the analysis presented here. Genes were assigned to an enrichment region if they overlapped up to 500 bp away from the gene boundaries. For visualisation of the data a JBrowse [47] instance was set up on http://bioinf.gen.tcd.ie/jbrowse/?data=cdub. The ChIP data have been submitted to GEO, accession number GSE60173.

Supporting Information

Figure S1 Southern immunoblots of *Nde*I digested genomic DNA from *C. dubliniensis*. Hybridizing fragments were detected using a digoxigenin-labeled probe homologous to bases +51–250 of *TLO1* (100% homology) and bases +51–248 of *TLO2* (87% homology). *TLO1* and *TLO2* hybridizing Fragments were predicted to be 14.07 Kb and 5.96 Kb in size. Only one copy of *TLO2* was detected in Wü284, hence the absence of a second hybridizing allele in lane 3 (*tlo2*Δ).
(TIFF)

Figure S2 Immunoblotting of whole cell extracts of *C. dubliniensis* using an anti-HA antibody for detection Tlo1-HA, Med8-HA and Med3-HA. Whole-cell extracts were made from strains that were untagged or had a single copy of a Tlo or other Mediator subunit tagged with the HA epitope. The strain used for each extract is listed above the lanes. Multiple volumes were loaded for each strain to allow normalization with an anti-tubulin antibody.
(TIFF)

Figure S3 (**A**) Microscopic appearance of *tlo1*Δ/*tlo2*Δ (*tlo*ΔΔ) mutant cells and reintegrant strains (+*TLO1* or +*TLO2*) stained with calcofluor white. (B) Colony morphology of *tlo1*Δ/*tlo2*Δ (*tlo*ΔΔ) mutants and reintegrant strains (+*TLO1* or +*TLO2*) on Spider agar medium.
(TIFF)

Figure S4 Additional phenotypes in the *tlo1*Δ/*tlo2*Δ mutant. (A) Production of pseudohyphae and chlamydospores (indicated by arrow) following growth on solid Pal's medium (B) Comparative growth on solid Lee's medium. Lee's medium was supplemented with 1% (w/v) peptone in the lower panel, as indicated.
(TIFF)

Figure S5 Phenotypes in the *C. dubliniensis med3*Δ mutant. (A) Growth of the *med3*Δ mutant in YEP-Gal. (B) Susceptibility of the *med3*Δ mutant to hydrogen peroxide.
(TIFF)

Figure S6 Enrichment plots from Gene Set Enrichment Analysis (GSEA) of the transcript profile of the *tlo1*Δ/*tlo2*Δ mutant showing enrichment for genes regulated during infection of reconstituted human epithelium (RHE, [25]) and bone marrow derived macrophages (BMDM, [26]).
(TIFF)

Figure S7 Heat map showing the expression of glycolytic and gluconeogenic (highlighted) pathway encoding genes in the *tlo1*Δ/*tlo2*Δ mutant and the *med3*Δ mutant during growth in YEPD broth and 10% serum. Each gene is represented by data from duplicate microarray spots.
(TIFF)

Figure S8 Tlo proteins regulate similar processes to Med2 in *S. cerevisiae*. Venn diagrams illustrating the numbers of orthologous genes commonly regulated in an *S. cerevisiae Scmed2* mutant and the *C. dubliniensis tlo1*Δ/*tlo2*Δ (*tlo*ΔΔ) mutants following growth in YEPD broth. *P* values were generated by hypergeometric probability testing (http://www.geneprof.org/GeneProf/tools/hypergeometric.jsp).
(TIFF)

Figure S9 (A) Composite, smoothed Tlo1-enrichment plot generated with a sliding window of 100 bp from the plots of the 367 highly-enriched genes (Ringo peak score 0.9) (B) Box-plot graph showing the distribution and length of Tlo1 enrichment at the 5′ and 3′ ends of 367 highly-enriched genes (Ringo peak score

0.9) (C) Graph showing average expression levels of Tlo1 occupied genes (n = 1613, mean 4783) and non-occupied genes (n = 3744, mean 2620) in wild-type *C. dubliniensis*. Expression data are raw, background corrected fluorescence intensity signals extracted from microarray data sets. *P* value generated with unpaired, two-tailed t-test.
(TIFF)

Table S1 List of genes exhibiting *TLO1*- or *TLO2*-specific regulation following complementation of the *tlo1Δ/tlo2Δ* (*tloΔΔ*) mutant with either *TLO1* (+*TLO1*) or *TLO2* (+*TLO2*). Transcript profiles were generated on cells grown to OD 600_{nm} 0.8 in YEPD at 37°C. Expression values are to Log_2 ratios.
(XLSX)

Table S2 List of genes exhibiting *TLO1*- or *TLO2*-specific regulation following complementation of the *tlo1Δ/tlo2Δ* (*tloΔΔ*) mutant with either *TLO1* (+TLO1) or *TLO2* (+TLO2). Transcript profiles were generated on cells grown for 1 h in 10% serum at 37°C. Expression values are to Log_2 ratios.
(XLSX)

Table S3 List of genes considered highly enriched for Tlo1-HA (Ringo peak score 0.9) in ChIP-chip experiments in YEPD broth. Column '*tloΔΔ* vs WT YEPD' indicated Log_2 gene expression ratios in the *tlo1Δ/tlo2Δ* (*tloΔΔ*) mutant relative to wild-type generated in gene expression microarrays. 'YEPD Expression level' refers to the raw, background corrected, Loess normalised fluorescent intensity level for that gene in gene expression microarray experiments.
(XLSX)

Table S4 Strains of *Candida* spp. used in this study.
(DOCX)

Table S5 Oligonucleotide primers used in this study.
(DOCX)

Acknowledgments

Mass spectroscopy was carried out by Scott Gerber (Geisel School of Medicine at Dartmouth). Files for running Gene Set Enrichment Analysis (GSEA) on microarray data were kindly supplied by Andre Nantel (Biotechnology Research Institute, National Research Council of Canada, Montreal, Quebec) *via* the Candida Genome Database (CGD).

Author Contributions

Conceived and designed the experiments: JH HB TY ZL LCM MC ABF MZA JB DJS GPM. Performed the experiments: JH HB TY ZL. Analyzed the data: JH HB ZL LCM KH ABF MZA JB DJS GPM. Contributed reagents/materials/analysis tools: LCM JB ABF DJS GPM. Wrote the paper: GPM.

References

1. Lorenz MC, Bender JA, Fink GR (2004) Transcriptional response of Candida albicans upon internalization by macrophages. Eukaryotic Cell 3: 1076–1087.
2. Pérez JC, Johnson AD (2013) Regulatory Circuits That Enable Proliferation of the FungusCandida albicans in a Mammalian Host. PLoS Pathog 9: e1003780.
3. Kadosh D, Johnson AD (2005) Induction of the Candida albicans filamentous growth program by relief of transcriptional repression: a genome-wide analysis. Mol Biol Cell 16: 2903–2912.
4. Conaway RC, Conaway JW (2011) Origins and activity of the Mediator complex. Seminars in Cell and Developmental Biology 22: 729–734.
5. Malik S, Roeder RG (2010) The metazoan Mediator co-activator complex as an integrative hub for transcriptional regulation. Nature Reviews Genetics 11: 761–772.
6. Björklund S, Gustafsson CM (2005) The yeast Mediator complex and its regulation. Trends in Biochemical Sciences 30: 240–244.
7. Thompson CM, Young RA (1995) General requirement for RNA polymerase II holoenzymes in vivo. Proc Natl Acad Sci USA 92: 4587–4590.
8. Ansari SA, Morse RH (2013) Mechanisms of Mediator complex action in transcriptional activation. Cell Mol Life Sci 70: 2743–2756.
9. Zhang A, Petrov KO, Hyun ER, Liu Z, Gerber SA, et al. (2012) The Tlo Proteins Are Stoichiometric Components of Candida albicans Mediator Anchored via the Med3 Subunit. Eukaryotic Cell 11: 874–884.
10. Braun BR, van Het Hoog M, d'Enfert C, Martchenko M, Dungan J, et al. (2005) A human-curated annotation of the Candida albicans genome. PLoS Genet 1: 36–57.
11. van Het Hoog M, Rast TJ, Martchenko M, Grindle S, Dignard D, et al. (2007) Assembly of the Candida albicans genome into sixteen supercontigs aligned on the eight chromosomes. Genome Biol 8: R52.
12. Anderson MZ, Baller JA, Dulmage K, Wigen L, Berman J (2012) The Three Clades of the Telomere-Associated TLO Gene Family of Candida albicans Have Different Splicing, Localization, and Expression Features. Eukaryotic Cell 11: 1268–1275.
13. Bourbon H-M (2008) Comparative genomics supports a deep evolutionary origin for the large, four-module transcriptional mediator complex. Nucleic Acids Res 36: 3993–4008.
14. Jackson AP, Gamble JA, Yeomans T, Moran GP, Saunders D, et al. (2009) Comparative genomics of the fungal pathogens Candida dubliniensis and Candida albicans. Genome Res 19: 2231–2244.
15. Uwamahoro N, Qu Y, Jelicic B, Lo TL, Beaurepaire C, et al. (2012) The Functions of Mediator in Candida albicans Support a Role in Shaping Species-Specific Gene Expression. PLoS Genet 8: e1002613.
16. Zhang A, Liu Z, Myers LC (2013) Differential Regulation of White-Opaque Switching by Individual Subunits of Candida albicans Mediator. Eukaryotic Cell 12: 1293–1304.
17. Moran GP, Coleman DC, Sullivan DJ (2012) Candida albicans versus Candida dubliniensis: Why Is C. albicans More Pathogenic? Int J Microbiol 2012: 205921.
18. Stokes C, Moran GP, Spiering MJ, Cole GT, Coleman DC, et al. (2007) Lower filamentation rates of Candida dubliniensis contribute to its lower virulence in comparison with Candida albicans. Fungal Genet Biol 44: 920–931.
19. Moran GP, MacCallum DM, Spiering MJ, Coleman DC, Sullivan DJ (2007) Differential regulation of the transcriptional repressor NRG1 accounts for altered host-cell interactions in Candida albicans and Candida dubliniensis. Mol Microbiol 66: 915–929.
20. O'Connor L, Caplice N, Coleman DC, Sullivan DJ, Moran GP (2010) Differential filamentation of Candida albicans and C. dubliniensis is governed by nutrient regulation of UME6 expression. Eukaryotic Cell: doi:10.1128/EC.00042-10.
21. Enjalbert B, Moran GP, Vaughan C, Yeomans T, MacCallum DM, et al. (2009) Genome-wide gene expression profiling and a forward genetic screen show that differential expression of the sodium ion transporter Ena21 contributes to the differential tolerance of Candida albicans and Candida dubliniensis to osmotic stress. Mol Microbiol 72: 216–228.
22. Moran GP, Coleman DC, Sullivan DJ (2011) Comparative genomics and the evolution of pathogenicity in human pathogenic fungi. Eukaryotic Cell 10: 34–42.
23. Miller C, Matic I, Maier KC, Schwalb B, Roether S, et al. (2012) Mediator Phosphorylation Prevents Stress Response Transcription During Non-stress Conditions. Journal of Biological Chemistry 287: 44017–44026.
24. Ansari SA, Ganapathi M, Benschop JJ, Holstege FCP, Wade JT, et al. (2011) Distinct role of Mediator tail module in regulation of SAGA-dependent, TATA-containing genes in yeast. EMBO J 31: 44–57.
25. Zakikhany K, Naglik JR, Schmidt Westhausen A, Holland G, Schaller M, et al. (2007) In vivo transcript profiling of Candida albicans identifies a gene essential for interepithelial dissemination. Cell Microbiol 9: 2938–2954.
26. Marcil A, Gadoury C, Ash J, Zhang J, Nantel A, et al. (2008) Analysis of PRA1 and its relationship to Candida albicans- macrophage interactions. Infect Immun 76: 4345–4358.
27. van de Peppel J, Kettelarij N, van Bakel H, Kockelkorn TTJP, van Leenen D, et al. (2005) Mediator Expression Profiling Epistasis Reveals a Signal Transduction Pathway with Antagonistic Submodules and Highly Specific Downstream Targets. Molecular Cell 19: 511–522.
28. Park D, Lee Y, Bhupindersingh G, Iyer VR (2013) Widespread misinterpretable ChIP-seq bias in yeast. PLoS ONE 8: e83506. doi:10.1371/journal.pone.0083506.
29. Teytelman L, Thurtle DM, Rine J, van Oudenaarden A (2013) Highly expressed loci are vulnerable to misleading ChIP localization of multiple unrelated proteins. Proceedings of the National Academy of Sciences 110: 18602–18607.
30. Fan X, Struhl K (2009) Where Does Mediator Bind In Vivo? PLoS ONE 4: e5029. doi:10.1371/journal.pone.0005029.t002.
31. Uwamahoro N, Verma-Gaur J, Shen HH, Qu Y, Lewis R, et al. (2014) The Pathogen Candida albicans Hijacks Pyroptosis for Escape from Macrophages. mBio 5: e00003–14–e00003–14. doi:10.1128/mBio.00003-14.
32. Mehta S, Miklos I, Sipiczki M, Sengupta S, Sharma N (2009) The Med8 mediator subunit interacts with the Rpb4 subunit of RNA polymerase II and Ace2 transcriptional activator in Schizosaccharomyces pombe. FEBS Lett 583: 3115–3120.
33. Liu Z, Myers LC (2012) Med5(Nut1) and Med17(Srb4) are direct targets of mediator histone H4 tail interactions. PLoS ONE 7: e38416.

34. Peng J, Zhou JQ (2012) The tail-module of yeast Mediator complex is required for telomere heterochromatin maintenance. Nucleic Acids Res 40: 581–593.
35. Zhu X, Wirén M, Sinha I, Rasmussen NN, Linder T, et al. (2006) Genome-Wide Occupancy Profile of Mediator and the Srb8-11 Module Reveals Interactions with Coding Regions. Molecular Cell 22: 169–178.
36. Andrau J-C, van de Pasch L, Lijnzaad P, Bijma T, Koerkamp MG, et al. (2006) Genome-Wide Location of the Coactivator Mediator: Binding without Activation and Transient Cdk8 Interaction on DNA. Molecular Cell 22: 179–192.
37. Liu H, Köhler J, Fink GR (1994) Suppression of hyphal formation in Candida albicans by mutation of a STE12 homolog. Science 266: 1723–1726.
38. Lee KL, Buckley HR, Campbell CC (1975) An amino acid liquid synthetic medium for the development of mycellal and yeast forms of Candida albicans. Med Mycol 13: 148–153.
39. Al-Mosaid A, Sullivan DJ, Coleman DC (2003) Differentiation of Candida dubliniensis from Candida albicans on Pal's agar. J Clin Microbiol 41: 4787–4789.
40. Reuss O, Vik A, Kolter R, Morschhäuser J (2004) The SAT1 flipper, an optimized tool for gene disruption in Candida albicans. Gene 341: 119–127.
41. Spiering MJ, Moran GP, Chauvel M, MacCallum DM, Higgins J, et al. (2010) Comparative transcript profiling of Candida albicans and Candida dubliniensis identifies SFL2, a C. albicans gene required for virulence in a reconstituted epithelial infection model. Eukaryotic Cell 9: 251–265.
42. Subramanian A, Tamayo P, Mootha VK, Mukherjee S, Ebert BL, et al. (2005) Gene set enrichment analysis: a knowledge-based approach for interpreting genome-wide expression profiles. Proc Natl Acad Sci USA 102: 15545–15550.
43. Sellam A, van het Hoog M, Tebbji F, Beaurepaire C, Whiteway M, et al. (2014) Modeling the Transcriptional Regulatory Network That Controls the Early Hypoxic Response in Candida albicans. Eukaryotic Cell 13: 675–690.
44. Ketel C, Wang HSW, McClellan M, Bouchonville K, Selmecki A, et al. (2009) Neocentromeres form efficiently at multiple possible loci in Candida albicans. PLoS Genet 5: e1000400.
45. Gentleman RC, Carey VJ, Bates DM, Bolstad B, Dettling M, et al. (2004) Bioconductor: open software development for computational biology and bioinformatics. Genome Biol 5: R80.
46. Toedling J, Skylar O, Sklyar O, Krueger T, Fischer JJ, et al. (2007) Ringo–an R/Bioconductor package for analyzing ChIP-chip readouts. BMC Bioinformatics 8: 221.
47. Westesson O, Skinner M, Holmes I (2013) Visualizing next-generation sequencing data with JBrowse. Brief Bioinformatics 14: 172–177.

Chapter 1

General Introduction

1.1. *Candida* - a species of pathogenic yeast

Fungi make up an estimated 7 % (611,000) of all eukaryotic species, 600 of which are human pathogens (Mayer *et al.*, 2013). Fungi account for up to 17 % of all healthcare-associated infections and *Candida* species for 90 % of these (Delaloye & Calandra, 2014). The most prevalent fungal pathogen is *Candida albicans* and accounts up to 70 % of all major infections attributed to *Candida* species (Falagas *et al.*, 2010). *C. albicans* is a eukaryotic fungus and is part of the *Saccharomycetaceae* family of organisms alongside other important pathogenic and non-pathogenic fungi, including the distantly related, non-pathogenic model organism *Saccharomyces cerevisiae* (Kim & Sudbery, 2011).

Candida species can cause a wide variety of pathologies in humans ranging from superficial and mucocutaneous infections to more serious systemic infections (Lim *et al.*, 2012) depending on the interplay of host, pathogen and environmental factors. The clinically relevant *Candida* species are opportunistic pathogens, existing mainly as commensal organisms of the vaginal and oral mucosae and the gastrointestinal (GI) tract (Hube, 2004). As commensals, various *Candida* species can survive in such areas of the body without significant impact on human health. In fact, *Candida* strains are present in the oral cavity in up to 75 % of the population (Mayer *et al.*, 2013). However, in the case of compromised host immune defence, *Candida* species can be formidable pathogens. *Candida* species have been attributed to 96 % of all opportunistic mycoses (Bondaryk *et al.*, 2013)

Perhaps the most common of all infections caused by *Candida* species are the well-described infections of the mucosal surfaces observed in cases of oropharyngeal candidiasis (OPC), and vulvovaginal candidiasis (VVC), both more commonly referred to as oral- or vaginal- 'thrush'. Thrush of the oral cavity or pseudomembranous candidiasis, is the typical presentation of *Candida* infections observed in the mouth. It is characterised by white-yellow plaques on oral mucosae, particularly on the tongue which consists of fungi and desquamated epithelium (Akpan & Morgan, 2002). Infections are generally acute in nature and in many cases can be addressed by improving oral hygiene and treating any causative factors (e.g. other illness, drug therapy, etc.) (Fathilah *et al.*, 2012; Ramage *et al.*, 2011). In some cases, antifungals (e.g. nystatin) can be administered topically and in more serious cases, where risk of systemic infection is moderate to high or where the underlying cause cannot be controlled, antifungal agents such

as members of the azole family of drugs (e.g. fluconazole, itraconazole) can be prescribed (Akpan & Morgan, 2002; Bensadoun *et al.*, 2011). Often, these drugs are also prescribed as preventative prophylaxis in high-risk patients with prolonged immunodeficiency. OPC infections can also present as erythematous (atrophic) candidiasis which is generally localised to the palate and dorsal area of the tongue typically in patients undergoing antibiotic and steroidal therapies or in HIV-infected individuals (McCullough & Savage, 2005). Angular cheilitis is similar to erythematous candidiasis except it affects folds and angular regions of the mouth, commonly in denture wearers (Farah *et al.*, 2010). Hyperplastic candidiasis is found predominantly on the buccal mucosae and cases have been observed to contain premalignant lesions or leukoplakia (Lodi *et al.*, 2006; Sitheeque & Samaranayake, 2003)

These various types of infections can all range from mildly acute to more serious and difficult to treat chronic mycoses (Akpan & Morgan, 2002). VVC is another extremely common infection caused by *Candida* species that is characterised by inflammation caused by *Candida* growth leading to discharge and pruritus (Cassone, 2014). It is estimated that 75 % of women are affected by VVC at one or more instances in their lives with 5 % experiencing chronic infections (Fischer, 2012). VVC is usually treated with over-the-counter antifungal therapies but in some cases more advanced antifungals may be required. Both VVC and OPC can occur in healthy individuals, but more frequently occur in those with an underlying predisposing factor.

1.2. Development of *Candida* infections

There are many predisposing factors that can lead to reduced immunity to and increased risk of *Candida* overgrowth and infection. Immunosuppression, either intrinsic (e.g. acquired and inherited defects in cellular immunity) or extrinsic (e.g. drug-mediated immunosuppression in transplant recipients) increases the likelihood of the development of *Candida* infections (Coronado-Castellote & Jiménez-Soriano, 2013). The development of acquired immunodeficiency syndrome (AIDS) after contraction of the human immunodeficiency virus (HIV) is a well-studied example of pathological immunosuppression that can lead to increased risk of *Candida* infection. In fact, since the late 1980's, OPC and esophageal candidiasis (EPC) have often been used

as an indication of the progression of the disease (Cassone & Cauda, 2012; Klein *et al.*, 1984). Cancers of the lymphoid and hematopoietic tissues (e.g. lymphomas) similarly increase the likelihood of *Candida* infection. Changes in the endocrine system can also lead to a predisposition for infection with *Candida* species. Patients suffering from long-term diabetes mellitus have been shown to be highly susceptible to *Candida* infection (de Leon *et al.*, 2002) due to hyperglycemia, neuropathy and angiopathy (Dorko *et al.*, 2005). Other endocrine disorders, including renal disorders, hyperthyroidism as well as pregnancy can influence the susceptibility to *Candida* overgrowth. Hormonal imbalances are particularly relevant in cases of VVC, where oestrogen levels are a triggering factor (Fischer, 2012). There are numerous other host factors that can increase the likelihood of *Candida* infection and many high quality reviews have been published on the subject (Bondaryk *et al.*, 2013; Calderone & Fonzi, 2001; Delaloye & Calandra, 2014; Smeekens *et al.*, 2013; Yapar, 2014)

Diseases and defects affecting the immune system however are not the only causes of increased risk of infection. A wide variety of drug therapies, some used in serious cases of illnesses (e.g. chemotherapy and radiotherapy in cancer patients) can alter the body's defense against *Candida* infection (Bensadoun *et al.*, 2011; Coronado-Castellote & Jiménez-Soriano, 2013). Likewise, some commonly prescribed drug treatments (e.g. corticosteroids, steroid inhalers, antidepressants and antibiotics) can increase susceptibility to *Candida* infection (Farah *et al.*, 2010). In addition, tobacco and alcohol ingestion along with lack of adequate hygiene (including of dental prostheses and implants for OPC and intra-uterine devices for VVC) can create favourable conditions for *Candida* growth (Farah *et al.*, 2010).

When risk factors such as those above are not recognised or controlled, or when infections are left untreated, superficial candidiasis can develop into much more serious systemic infections. This can be due to the risk factors outlined above, but also factors such as lengthy stays in hospital settings, use of indwelling devices including catheters, various surgical procedures and in particular, severe neutropenia (Kim & Sudbery, 2011). *Candida* infections can spread to give rise to candidemia which have mortality rates of up to 50 % (Koehler *et al.*, 2014; Pfaller & Diekema, 2010). Candidemia, like septicemia is difficult to quickly diagnose and upon preliminary diagnosis, intravenous anti-fungal treatment is started without delay as mortality rates have been shown to double over a 48 h period in some cases (Kibbler *et al.*, 2003; Koehler *et al.*, 2014). *Candida* infections can quickly

disseminate to a number of organ sites, which means quick diagnosis and treatment is of utmost importance.

1.3. Epidemiology of *Candida* infections

Fungi account for 15 % of healthcare associated infections (HAIs) and *Candida* infections represent up to 90 % of these (Delaloye & Calandra, 2014) with species like *Aspergillus* accounting for the rest. *Candida* are reportedly the fourth most common causative agents of nosocomial infections overall (Yapar, 2014). In the period 2009-2010, *C. albicans* accounted for 5.3 % of all HAIs reported to the national healthcare safety network (NHSN) in the USA (Sievert *et al.*, 2012). Moreover, in the period between 1995 - 2002, 9 % of all nosocomial bloodstream infections (BSIs) reported were attributed to *C. albicans* (Wisplinghoff *et al.*, 2004). In Europe, this figure is closer to 3 % (Méan *et al.*, 2008).

Of the *Candida* species isolated in infection, *C. albicans*, *C. glabrata*, *C. parapsilosis*, *C. tropicalis* and *C. krusei* account for roughly 95 % (Yapar, 2014). *C. albicans* remains the most common of the *Candida* species, although it has been suggested that due to improved diagnostic techniques combined with overuse of certain antifungals, the prevalence of non-*albicans* species is increasing. For example, a 5-year study in Italy attributed 40 % of fungaemia cases to *C. albicans* and 23 % and 15 % to *C. parapsilosis* and *C. glabrata* respectively (Bassetti *et al.*, 2006). *C. albicans* generally accounts for over half of BSIs attributed to *Candida* species (Jackson *et al.*, 2009; Odds *et al.*, 2007). Isolates associated with infections appear to vary depending on geographical and patient-specific parameters, for example *C. glabrata* is more prevalent in older adults and in infections associated with indwelling devices, whereas *C. tropicalis* is seen mostly in leukemic patients (Yapar, 2014).

1.4. Treatment of Candidiasis

Unlike antibacterial chemotherapy, there exists only a small range of antifungal drugs used to combat *Candida* infections. This is in part due to the lack of selective targets in *Candida* that are not present in humans. Antifungal drugs currently used can be split into several classes. The polyene antifungals include commonly prescribed drugs such as Amphotericin B and Nystatin. These drugs work by targeting sterols within the cell membrane causing leakage of the intracellular contents (Dixon & Walsh, 1996). At low doses, these drugs work well and are specific for ergosterol in *Candida*. However, at higher doses, interaction with human cholesterol can occur (Myers, 2006). The azole class of antifungals work by inhibiting lanosterol demeythylase which is integral in ergosterol biosynthesis, which in turn disrupts the cell membrane. They include drugs of three main subclasses: the imidazoles (e.g. clotrimazole, ketoconazole), the triazoles (e.g. fluconazole, itraconazole, voriconazole) and the thiazoles (e.g. abafungin). Echinocandins (e.g. caspofungin and micafungin) work by inhibiting β(1,3)-glucan synthase in the cell wall of *Candida* species. Allylamines such as naftifine work by inhibiting squalene epoxidase thereby affecting ergosterol biosynthesis (Bondaryk *et al.*, 2013; Cannon *et al.*, 2009). Some other drugs exist outside these classes which include flucytosine (targets nucleic acid metabolism), griseofulvin (affects mitosis) and ciclopirox (targets metabolism) (Bondaryk *et al.*, 2013; Cannon *et al.*, 2009; Dixon & Walsh, 1996; Rubin *et al.*, 2002).

Many of these drugs are toxic in high doses and can cause renal or hepatic toxicity. In addition, many are contraindicated against each other. As such, with minor infections, there is usually no need to prescribe an aggressive course of antifungal therapy. Courses of treatment are largely based on severity, site of infection, host immune status and ongoing risk (Hidalgo & Vasquez, 2014). Treatments of superficial *Candida* infections mostly involve making changes to host factors, e.g. cessation of alcohol or tobacco intake or ending courses of drug therapy, which can in many cases allow the host to recover. In other cases, topical antifungals such as Nystatin (in the case of oral thrush) are prescribed with relatively high success. This treatment may be combined with oral administration of azoles if the infection is particularly aggressive, or if the patient is part of an at-risk cohort (e.g. patients with HIV, neutropenia etc.). For patients suffering with VVC, over the counter medications are available that have good rates of success,

in particular topical application of clotrimazole and oral administration of fluconazole. In otherwise healthy individuals, the prognosis is excellent and treatment is usually successful (Akpan & Morgan, 2002).

Systemic infections are significantly more difficult to treat, partly due to difficulty in early and definite diagnosis (Cannon *et al.*, 2009). However as outlined above, *Candida* infections often occur in patients with underlying conditions (e.g. neutropenia) and the already fragile state of some of these patients demands aggressive and effective antifungal therapy to halt the spread of the disease. Careful selection of therapy is required so as not to promote the development of resistance. Most serious cases are treated intravenously or parenterally with either an azole or Amphotericin B, the former being less nephrotoxic but more prone to resistance (Charlier *et al.*, 2006; Sanglard & Odds, 2002) with transition to oral formulations after the infection is under control (Hidalgo & Vasquez, 2014). For those with neutropenia, an enchinocandin is usually administered. Several studies have been published which set out to recommend guidelines on the treatment of *Candida* infection (Alothman *et al.*, 2014; Leroux & Ullmann, 2013; Pappas *et al.*, 2009).

A growing concern is the continued emergence of resistance to antifungal drugs, particularly since there are relatively few commonly prescribed. Development of resistance to azoles has been well-documented, with several mechanisms allowing *Candida* to survive in their presence, including increased efflux pump expression, amino acid substitution at target sites (e.g. Erg11), up-regulation of *ERG11* and alteration of biosynthetic pathways (e.g. the ergosterol biosynthetic process via Erg3) (Cannon *et al.*, 2009; Paul & Moye-Rowley, 2014; Sanglard & Odds, 2002). Many antifungals have common targets, so development of resistance to one drug can often mean resistance to other members of that class. In addition, it has been postulated that increased use of antifungal agents such as fluconazole has played a role in allowing non-*albicans* species to increase their prevalence (Sanglard & Odds, 2002).

1.5. *C. albicans* and *C. dubliniensis*

The primary focus of this study is on the most prevalent of the *Candida* species, *C. albicans* and its closest known relative, *C. dubliniensis*. As discussed in the preceding sections, *C. albicans* is the primary causative agent in infections attributed to *Candida* species. In addition to this, it is widely considered to be the most pathogenic of the *Candida* species for a variety of reasons, which will be discussed later. In 1995, *C. dubliniensis* was identified and characterised from isolates recovered from HIV-infected patients with OPC (Moran *et al.*, 2012; Sullivan *et al.*, 1995). *C. dubliniensis* is the closest known relative to *C. albicans*, sharing numerous phenotypes. Both species have the ability to form long germ-tube structures known as true hyphae. In addition, both can form spore-like structures known as chlamydospores. Prior to the discovery of *C. dubliniensis*, both of these abilities were attributed exclusively to *C. albicans*. In fact, *C. dubliniensis* was probably misidentified for many years as *C. albicans* because of these striking similarities and because the two species often co-isolate together in oral cavities (Moran *et al.*, 2012; Sullivan & Coleman, 1998). Methods of discriminating between these two species include growth at 42 °C (at which *C. dubliniensis* exhibits slower growth) and growth on CHROMagar, a differential culture medium that displays chromogenic changes for specific species (Coronado-Castellote & Jiménez-Soriano, 2013; Loreto *et al.*, 2010; Odds & Bernaerts, 1994).

However, despite these striking similarities, there is a stark contrast in virulence between the two species. Epidemiological data has demonstrated that *C. dubliniensis* is responsible for around 2 % of *Candida* BSIs compared to *C. albicans* causing around 50 % of candidemias (Jackson *et al.*, 2009; Odds *et al.*, 2007). *In vivo* experiments in a tail-vein murine model demonstrated that while *C. albicans* systemic infection resulted in almost 100 % mortality within 24 h, *C. dubliniensis* infections displayed significantly lower mortality (Gilfillan *et al.*, 1998). This was later confirmed in similar models, but also using histopathological techniques, which found that while *C. albicans* was mostly hyphal in the infected organs, *C. dubliniensis* was mainly in yeast form (Vilela *et al.*, 2002). Interestingly, it has been suggested that while *C. dubliniensis* displays generally poor levels of invasiveness, it can be successful at dissemination once it has bypassed the immune system and is within the bloodstream of the host. Moreover, the virulence of *C. dubliniensis* strains can vary depending on isolate origin, and it has even been suggested that a

compounding factor in the lower virulence of *C. dubliniensis* can sometimes be due to the competition of other, more pathogenic *Candida* species (Asmundsdóttir *et al.*, 2009).

The success of *C. albicans* as a diverse and persistent pathogen lies in its ability to colonise and infect a variety of sites/niches in the host as well as its impressive arsenal of virulence factors and regulatory networks. Although *C. dubliniensis* possesses many of these attributes, its virulence is greatly reduced relative to *C. albicans*. In the following sections, some of the more important virulence determinants will be described and discussed in the context of the differing virulence of *C. albicans* and *C. dubliniensis*.

1.6. Morphology as a virulence determinant of *Candida* species

As mentioned above, the formation of true hyphae was once thought to be exclusive to *C. albicans* until the identification of *C. dubliniensis*. Both *C. albicans* and *C. dubliniensis* possess the ability to grow as typical budding yeast cells, hyphae and chlamydospores. Hyphae are elongated filamentous structures, which are an important mode of growth. True hyphal cells (henceforth referred to as hyphae) are highly elongated, highly polarised cells, with parallel cell walls and no septal constrictions. Pseudohyphae are can be closer in appearance to either yeast or true hyphae, except for that septation and significant branching along with inconsistent cell width is often observed (Berman & Sudbery, 2002; Mayer *et al.*, 2013). More detailed characteristics for distinguishing between these morphologies are discussed in Chapter 4.

This ability to switch between morphologies is important in adapting optimally to a particular niche and as such, certain morphologies are either induced or inhibited by specific environmental conditions. The formation of hyphae is promoted by a range of conditions including alkaline pH, nutrient limitation, a temperature shift to 37 °C, low nitrogen, the presence of serum, N-acetylglucosamine (GlcNAc), solid matrix, quorum sensing molecules, methionine and higher than normal levels of CO_2 (O'Connor *et al.*, 2010; Sudbery, 2011). These environmental signals are translated through several complex regulatory networks to either induce and/or maintain both filamentous regulators and hypha-specific genes. While commensal, non-invasive *Candida* isolates tend to

grow as yeast cells, invasion and penetration of tissue along with tissue damage is commonly associated with the hyphal morphology (Moran *et al.*, 2012).

Hyphal formation is thought to be an important virulence determinant and is a shared phenotype between *C. albicans* and *C. dubliniensis* (Moran *et al.*, 2012). However, *C. dubliniensis* is much less efficient at forming true hyphae. It has been suggested that this reduced ability to filament is implicated in the contrast in virulence between the two strains, a hypothesis which is supported *in vivo*, whereby lower filamentation rates were associated with lower dissemination and faster gastrointestinal clearing in an oral-intragastric murine model (Stokes *et al.*, 2007; Vilela *et al.*, 2002) as well as *in vitro* (Moran *et al.*, 2012; Spiering *et al.*, 2010). Hyphal growth is associated with increased invasiveness and increased tissue damage and in RHE models, *C. albicans* forms hyphae whereas *C. dubliniensis* does not, remaining in the yeast form (Moran *et al.*, 2012). The yeast form of *Candida* has been associated with dissemination during infection (Saville *et al.*, 2003). It has been demonstrated that this differing ability in forming hyphae is due to a complex regulatory network, which includes the higher expression of some virulence-associated, hypha-specific genes such as *ECE1* and *HWP1* during initiation of hyphal growth. However, the differences in regulation between the two species are relatively unknown. One study has shown that deletion of *NRG1* in *C. dubliniensis*, a key filamentous regulator which has a repressive effect on induction of hyphal formation, can partially restore hyphal growth (Moran *et al.*, 2007). However, fully true hyphal growth in either wild-type *C. dubliniensis* or *nrg1* mutant strains still required nutrient depletion, suggesting the involvement of other regulatory pathways. Once hyphal growth is initiated in *C. dubliniensis*, similar genes to those in *C. albicans* are expressed, with the exception of those that are not present in *C. dubliniensis* (e.g., *ALS3, HYR1*). It is therefore likely that the contrasting morphological traits are due to a more global change in regulation.

Besides filamentous dimorphism, *C. albicans* and *C. dubliniensis* can form chlamydospores, which are large thick-walled, spore-like, round structures that often grown on the ends of 'suspensor filaments' when grown on specific nutrient limiting media e.g. cornmeal agar (Staib & Morschhäuser, 2007). *C. dubliniensis* cultures are better at forming chlamydospores than *C. albicans*, by mechanisms which are only beginning to become clear. It has recently been suggested that differential regulation of genes such as *NRG1*, *CSP1* and *CSP2* is involved in this process (Palige *et al.*, 2013). However, their definite function *in vivo* remains

unknown and despite their name, are unlikely to act as typical spore structures (Citiulo *et al.*, 2009). Despite this, chlamydospore formation on Staib agar is exclusive to *C. dubliniensis* and has aided in the differentiation from *C. albicans* (Staib & Morschhäuser, 2007)

Filamentation is also important for the adherence to host cells during colonisation and invasion. In *C. albicans,* adhesins on the fungal cell surface promote adherence of *Candida* to mucosal surfaces via proteins found in serum. As well as this, such adhesins promote development of an extracellular matrix and interaction with cell molecules such as E-cadherin (Williams *et al.*, 2013). The agglutinin-like sequence (Als) proteins, hyphal wall protein 1 (Hwp1) and the enhanced adherence to polystyrene (Eap1) protein are examples of such adhesins. The adhesin Als3, for which no direct ortholog exists in *C. dubliniensis,* acts as an invasin which binds to E-cadherin on the epithelial surface promoting induced endocytosis (Mayer *et al.*, 2013). Hwp1 is expressed in association with the hyphal morphology in both *C. albicans* and *C. dubliniensis* and promotes covalent attachment to the mucosal surfaces of the host (Sundstrom *et al.*, 2002; Williams *et al.*, 2013). As well as stimulating endocytosis, hyphal cells can actively penetrate host cells, which is promoted by secretion of specifically regulated effectors such as the secreted aspartyl proteases (SAPs) (Mayer *et al.*, 2013; Williams *et al.*, 2013). The differences in expression and copy number of such adhesins and invasins has been suggested as a likely factor in the differing virulence between the two species (Moran *et al.*, 2012).

1.7. Biofilm formation in *Candida* spp.

Intricately linked to the morphological switch in *C. albicans* and *C. dubliniensis* is the formation of biofilms. Biofilm formation is becoming an area of increasingly high interest, in both bacterial and eukaryotic species. Growth as part of a biofilm is the ideal reservoir for infection in indwelling medical devices and as such has huge health as well as economic implications (increases length of stay in hospitals, costs of medicines, etc.) (Cuéllar-Cruz *et al.*, 2012; Tumbarello *et al.*, 2012). Biofilms form first as adherent yeast cells, which multiply and eventually form hyphae in the upper biofilm, followed by the formation of an extracellular matrix (ECM). Yeast cells then detach and disperse to reinitiate biofilm or infection at other sites (Mayer *et al.*, 2013). Like all other virulence-associated traits, biofilm

formation is regulated by a complex network of proteins, including Bcr1, Tec1, Efg1 and Hsp90 (Mayer *et al.*, 2013). Both *C. albicans* and *C. dubliniensis* can form biofilms well, however the impaired hyphal formation in *C. dubliniensis* compared to *C. albicans* is associated with a decrease in the adherence of biofilms *in vitro* (Kolecka *et al.*, 2011). Besides acting as a reservoir of infection, biofilms can also act as a physical barrier to drug therapies and are more resistant to inflammatory responses and killing by neutrophils, and so can prove challenging to eliminate (Fanning & Mitchell, 2012; Mayer *et al.*, 2013).

The other morphological 'switch' that *C. albicans* and *C. dubliniensis* can undergo is the white-opaque switch which can occur spontaneously and reversibly (Huang *et al.*, 2010). The process is controlled by the *WOR-1* locus and other global regulators. White cells are typical round yeast-type cells, whereas opaque cells are 'bean' shaped and smaller than white cells and exhibit cell wall pimples and a large vesicle containing vacuole (Soll, 2007). The switching process is intricately linked to mating of *Candida*, in that white cells are mating incompetent and opaque cells are mating competent, the specifics of which are extensively reviewed by Soll (2014). Both species undergo mating in the same way, but *C. dubliniensis* does so less efficiently and can form an atypical oversized opaque-type cell not observed in *C. albicans* (Pujol *et al.*, 2004). White cells have been shown to be more virulent in mouse models, but opaque cells were shown to better colonise the skin (Soll, 2014). White-opaque switching is also linked with biofilm formation (Soll, 2014) and expression of invasins and adhesins (Morrow *et al.*, 1992; White & Agabian, 1995) as well as immunomodulation via the expression of chemo-attractants (Geiger *et al.*, 2004).

1.8. Virulence and the stress response

While the relationship between morphology and virulence is probably the most intensely studied area of *Candida* biology, it is only one of many processes that allow *C. albicans* to be a successful pathogen (and commensal). *C. albicans* and *C. dubliniensis* possess similar signal transduction pathways and gene regulatory networks that govern the response to harsh environments. In possessing tailored responses to non-optimal environments, *Candida* increases its fitness and the range of niches it can occupy, a hallmark of any 'good' pathogen.

Osmotic stress is encountered commonly within the environment, for example exposure to high salt/sugar concentrations (e.g. sweat on skin surface) or sudden exposure to high water concentrations (Hohmann, 2002). This type of shock is dealt with by alterations in intracellular glycerol concentration via expression of a glycerol 3-phosphatase encoded by *GPP1* and glycerol 3-deydrogenase encoded by *GPD2* which compensates for osmotic shock in the environment (Mayer *et al.*, 2013). Response to unsuitable temperatures is mediated by heat shock proteins (Hsps) such as the Hsp90 chaperone, which in combination with low trehalose intra-cellular concentrations helps prevent temperature-induced protein unfolding as well as inducing hyphal formation via the Ras-PKA pathway (Robbins *et al.*, 2011). The expression of these Hsps is mediated by heat shock factor 1 (Hsf1) which acts as a regulator of their expression through direct binding to promoters (Mayer *et al.*, 2013). Detoxification of reactive oxygen species (ROS), which are commonly generated by phagocytic cells of the immune system is also a highly specialised process, with regulatory proteins (e.g. Hog1) and enzymes such as the superoxide dismutases (e.g. Sod1) and catalases (e.g. Cat1) playing a central role in this response (Brown *et al.*, 2014). These examples are just some of the individual processes that these species have evolved to deal with a variety of environmental pressures.

The response to these environmental shocks is governed by several large protein/gene networks that are responsible for the induction of responses to such stresses. These mitogen-activated protein kinase (MAPK) pathways maintain tight control over the responses to environmental stresses. One well-studied example is the high osmolarity glycerol response (Hog1) –mediated pathway which is involved in regulating transcriptional responses to thermal, oxidative and osmotic stresses (Cheetham *et al.*, 2011; Mayer *et al.*, 2013). Another is the Mck1 pathway

which, in response to osmotic and oxidative stress, is important in maintaining cellular integrity (Mayer *et al.*, 2013). The various pathways relevant to this study are described in more detail in each relevant chapter.

The dichotomy in virulence between *C. albicans* and *C. dubliniensis* is difficult to attribute to any one particular process. While there are orthologs of several major virulence genes missing in *C. dubliniensis* (*HYR1, ALS3*, etc.) there is a level of functional redundancy within these gene families that may compensate for this. In addition, most comparisons were, until recently based on single gene experiments with predictive annotation based on *S. cerevisiae*. Also, while levels of biofilm formation, hyphal formation and mating differ, *C. dubliniensis* is still a successful commensal and pathogen in its own right. With the advent of high throughput sequencing and genomic comparison techniques, more detailed knowledge of the genomes of these organisms has become available allowing us to compare and contrast the genomes in an attempt to pinpoint differences that may account for the disparity in virulence.

1.9. Genomic comparisons

C. albicans and *C. dubliniensis* are thought to have diverged approximately 20 million years ago (MYA) (Mishra *et al.*, 2007). Both *C. albicans* and *C. dubliniensis* are members of the CTG-clade of yeasts, which consists of over 75 *Candida* species and numerous others, e.g. some *Lodderomyces* spp. and *Debaryomyces* spp. (Santos *et al.*, 2011). These yeasts have evolved to 'mistranslate' the CUG codon to serine instead of the more widespread translation to leucine. Interestingly, some of the CTG-clade species have been shown to translate CUG to either serine or leucine dependent on the presence of specific tRNA molecules (Santos *et al.*, 2011) which may confer an as yet unknown evolutionary advantage. It is estimated that this evolutionary split of CTG *Candida* species from non-CTG species occurred approximately 170 MYA (McManus & Coleman, 2014).

The publication of the improved annotated assembly of the *C. albicans* genome in 2007, (van het Hoog *et al.*, 2007) allowed simple DNA microarray hybridisation experiments to be carried out comparing the overall genomes of these two closely related species (Moran *et al.*, 2004). It was found that 4 % (n = 247) of the genes in *C. albicans* were absent or highly divergent in *C. dubliniensis* (Moran *et al.*, 2004, 2012). Building on this, the genome of *C. dubliniensis* was

sequenced in 2009 which allowed large-scale comparison of the two genomes *in silico* (Jackson *et al.*, 2009). It was found that 96.3 % of genes displayed significant identity (> 80 %) with 98 % of genes co-localising on the same chromosomal locations (i.e. syntenic) (Jackson *et al.*, 2009; Moran *et al.*, 2012). This information confirmed previous assertions (Mishra *et al.*, 2007; Moran *et al.*, 2004) of the relatedness of the two species.

Many genes that *C. dubliniensis* lacked, could be directly attributed (although not uniquely) to virulence, e.g., *ALS3* and *HYR1* are not present in *C. dubliniensis*. Homologous genes were grouped into families to allow direct comparison of copy number between species. It was found that although *C. dubliniensis* possessed the other 7 *ALS* genes, it appeared that both species had evolved their own novel *ALS* genes that show significant interspecies orthology but not homology. Likewise, the secreted aspartyl proteases (*SAP*s) differed in copy number (8 in *C. dubliniensis* versus 10 in *C. albicans*). The second largest disparity in copy number between species was identified in the *IFA* gene family, which encodes putative transmembrane proteins, with 31 in *C . albicans* and 21 in *C. dubliniensis*. However, the largest difference was observed in the telomere-associated (*TLO*) genes, with 14 (plus one additional pseudogene) identified in *C. albicans* versus only 2 genes in *C. dubliniensis*. With such large disparity, it was suggested that elucidating their functions might help to understand the reason behind such extreme differences in virulence phenotypes between these two closely related species.

1.10. The *TLO* genes

The *TLO* genes were originally identified as the *CTA* genes by Kaiser *et al.* (1999), a putative family of transcriptional activators identified from yeast-one-hybrid screens (Kaiser *et al.*, 1999). Interestingly, Zakikhany *et al.*, (2007) demonstrated that *TLO* expression was up-regulated during RHE infection models. Whole genome sequencing of *C. albicans* strain SC5314 revealed the presence of these genes at telomeric and sub-telomeric loci across all 8 chromosomes, so they were renamed telomere-associated (*TLO*) genes in 2007 (van het Hoog *et al.*, 2007). Figure 1.1 shows the organisation of the *TLO* genes across *C. albicans* and *C. dubliniensis*. Outside of *C. albicans* and *C. dubliniensis*, a homolog to the *TLO*s was identified in *C. tropicalis*, but homologs were not described in the rest of the *Candida* species. In the current study, this has been shown to be inaccurate as *MED2* homologs exist across the *Candida* species, which show significant homology to the *TLO* genes. This is discussed in detail in Chapter 3. Phylogeny predictions (Jackson *et al.*, 2009) based on sequence divergence suggest that the *TLO* genes in *C. albicans* expanded independently (Figure 3.7). In addition to this, the *TLO* genes in *C. albicans* are significantly more homogenous in sequence (96.5 % average identity) than in *C. dubliniensis* (74.9 % identity), with the latter more closely aligning to *C. tropicalis CTRG05211.3* than the *TLO*s in *C. albicans*. It was predicted that beginning with the ancestral *TLO* gene on chromosome R, *TLO*s have expanded independently in the closely related *C. albicans* and *C. dubliniensis*, with additional expansion to all but one chromosome in *C. albicans* and a single transposition to a locus on chromosome 7, leading to *TLO1* in *C. dubliniensis* (Jackson *et al.*, 2009).

In a recent study by Anderson, *et al.* (2012), it was suggested that the *TLO* genes could be divided into clades based on the structure of the *TLO* genes in *C. albicans* (Figure 1.1). The *TLO* genes contain three distinct regions - a 5-prime region with Med2 homology (Bourbon, 2008), a central variable length linker and a 3-prime end that determines the clade designation assigned by Anderson, *et al.* (2012). Each clade is labelled in Figure 1.1. The *TLOα* clade is made up of 6 genes that contain a single continuous sequence at the 3-prime end of the gene. The *TLOβ* clade consists of only one gene (*TLOβ2*), which contains additional sequences not present in *TLOα* genes. The *TLOγ* clade contains the other 7 *TLO*

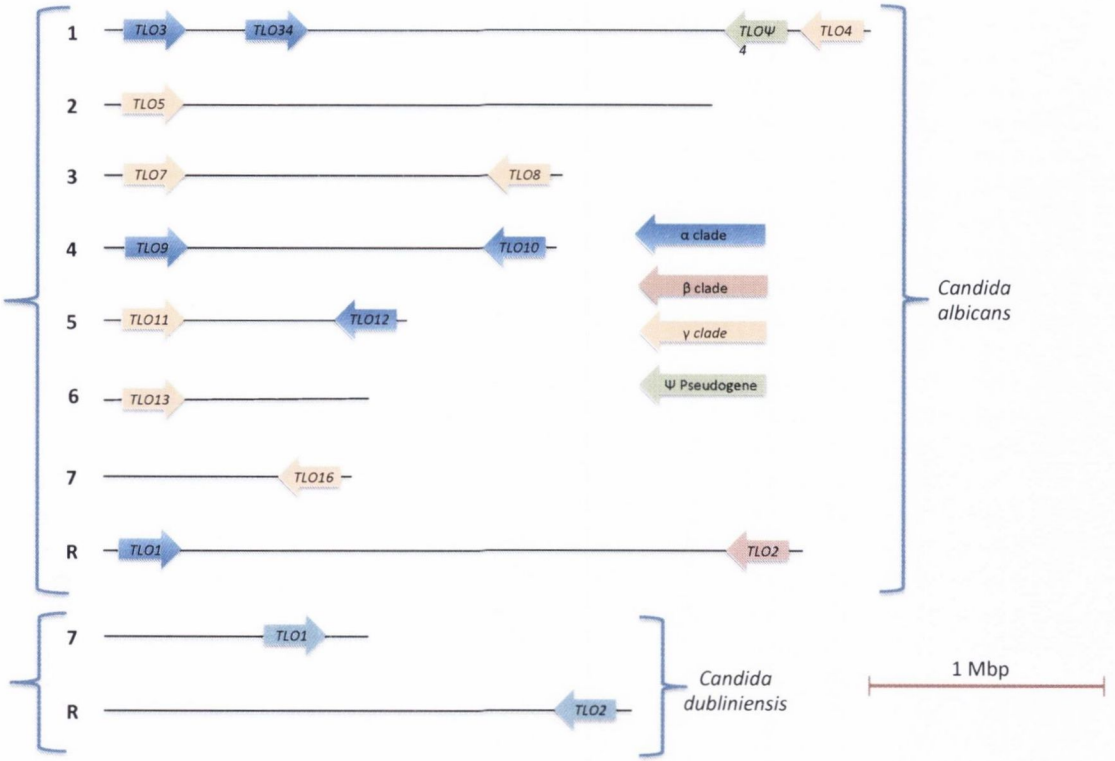

Figure 1.1. *TLO* genes of *Candida albicans* and *Candida dubliniensis*.

Illustration of *TLO* genes in *C. albicans* and *C. dubliniensis*. Chromosomal gene locations and orientations are shown. Direction of arrows indicates direction of transcription. Chromosomes are labeled to the left of the illustration. While specific karyotypes are not accurate, scale of 1 Mbp is shown. Re-assignment of *TLO* genes in *C. albicans* as proposed by Anderson, *et al.*, (2013) into clades is shown using the indicated colour scheme. *C. dubliniensis TLO*s are not assigned to a clade.

genes which display alternative spliced transcripts (Anderson *et al.*, 2012). The pseudogene (*TLOΨ34)* was not assigned to a clade.

1.11. *TLO* genes and the Mediator complex

Bourbon, *et al.* (2008) suggested that the *TLO* genes in *C. albicans* encoded paralogs of the Med2 subunit of the Mediator complex in *S. cerevisiae* (Bourbon, 2008). The Mediator complex (Figure 1.2) is an aggregate of proteins that associates with RNA Polymerase II. It is highly conserved amongst eukaryotes and is essential in transcriptional regulation (Uwamahoro *et al.*, 2012). In fact, recent work by Zhang, *et al.* (2013) determined that the structure of Mediator in *C. albicans* is indeed highly similar to that of *S. cerevisiae*. The complex consists of between 25 and 31 subunits (depending on species) organised into core, middle, tail and kinase modules. Work in *S. cerevisiae* has demonstrated various roles for specific subunits of the complex, for example the tail subunit is directly associated with activation domains of transcription factors (van de Peppel *et al.*, 2005; Zhang *et al.*, 2013). Mediator has been shown to be indispensable in transcriptional regulation by acting as the intermediary in the relationship between the main transcriptional machinery (RNA Polymerase II and general transcription factors) and transcriptional activators which are bound to DNA (Ansari & Morse, 2013). As well as this, the Mediator promotes the formation of pre-initiation complex (PIC) (Poss *et al.*, 2013). The Mediator in *S. cerevisiae* has been implicated in maintaining and stimulating low, basal levels of transcription (all modules), chromatin remodeling & heterochromatin maintenance (middle and tail modules), silencing of genes at telomeres and sub-telomeres (middle and tail modules), regulation of expression of genes in response to environmental stimuli (tail and middle modules) and even transcriptional repression (Cdk8 module) (Miller *et al.*, 2012; Tsutsui *et al.*, 2013; Uwamahoro *et al.*, 2012; Wang *et al.*, n.d.; Zhu *et al.*, 2011). While the study of *C. albicans* Mediator is relatively novel, it has recently been described as important in regulation of the white-opaque switch in *C. albicans* (Zhang *et al.*, 2013). The Med2 subunit is situated in the tail region and in conjunction with Med3 and Med15 has been implicated in direct interaction with transcriptional activators (Ansari *et al.*, 2012).

The idea that *TLO*s could encode orthologs of the Mediator subunit Med2 is supported by the original identification of the *TLO* (*CTA*) genes as encoding

proteins with trans-activating potential (Kaiser *et al.*, 1999). All of the *TLO* genes in *C. albicans* and *C. dubliniensis* contain a Med2-like domain (see Figure 3.10). Recent work by Zhang, *et al.* (2012) has experimentally proven this functional orthology by demonstrating co-purification of the Tlo genes in *C. albicans* with components of the Mediator complex tail subunit. Moreover, evidence suggests that Tlos are components of the Mediator complex via anchoring to Med3, as determined in *med3* deletion mutants in both *C. albicans* and *C. dubliniensis* (Personal Communication, Boyle, 2013; Zhang *et al.*, 2012).

1.12. Rationale for this study

The highest disparity in gene content between the closely related, yet pathogenically distinct *C. albicans* and *C. dubliniensis* is found in the *TLO* gene family. As such, identifying the role(s) of the *TLO*s may help in explaining the differences between these species as well as increasing our understanding of this relatively unexplored gene family. In order to properly identify the functions of *TLO* genes and their proteins in this study, we utilise a range of molecular techniques. The focus of this study was on *C. dubliniensis TLO* genes for a number of reasons. There are 14 *TLO* genes (plus one pseudogene) in *C. albicans*, all of which are very similar which might suggest a functional redundancy of sorts. It is therefore possible that deletion of *TLO* genes in *C. albicans* may be compensated for, by the remaining copies. Furthermore, *C. dubliniensis* only contains two *TLO* genes, which are much more divergent and therefore likely to have distinct functions. As a result, *C. dubliniensis TLO* deletion is not only a quicker process (less genes to disrupt), but might allow the determination of different phenotypes based on deletion of either or both of *TLO1* and *TLO2*. As well as this, because of the close relationship with *C. albicans*, the determined functional phenotypes can most likely be related between species and complementation with *C. albicans TLO* genes would help to confirm this.

Each section in this study explores different aspects of the *TLO* genes and by the conclusion of the study, a much greater picture of the roles that this relatively uncharacterised gene family play in *C. albicans* and *C. dubliniensis* is uncovered.

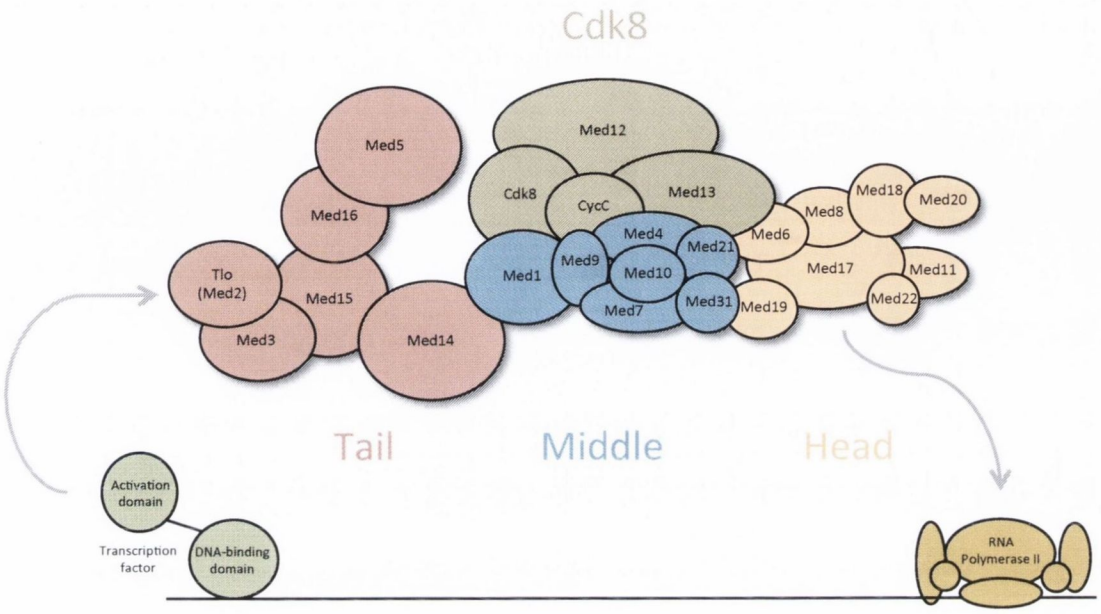

Figure 1.2. Mediator complex in *C. albicans*.

Illustration of the Mediator complex and its relationship with DNA/transcription. The complex is composed of the tail, middle, head and Cdk8 domains, which are colour coded. The tail region interacts with transcriptional activators and the head region interacts with RNA polymerase II (and associated general transcription factors). Structure is derived from Zhang, Liu & Myers (2013) and Zhang *et al.*, (2013). Middle, Head and Cdk8 modules are derived from *S. cerevisiae* Mediator complex structure. Illustration was adapted from Zhang, Liu & Myers (2013) .

Chapter 2

Materials and Methods

2.1 General Microbiological Methods

2.1.1. Strains and isolates

Strains of *Candida* spp. used in this study are outlined in Table 2.1. Unless otherwise stated, strains were acquired from the Dublin Dental University Hospital microbiological strain collection at Dublin Dental University Hospital, University of Dublin, Trinity College, Lincoln Place, Dublin 2.

2.1.2. Growth conditions and culture media

Strains of *Candida* spp. were routinely grown on Yeast Extract Peptone Dextrose (YEPD) agar (1 % [w/v] yeast extract [Sigma-Aldrich, Co. Wicklow, Ireland], 2 % [w/v] peptone [Oxoid, Cambridge, UK], 2 % [w/v] glucose [Sigma-Aldrich], 1.5 % [w/v] Bacto Agar [Becton, Dickinson & Co. , Oxford, UK]) at 37 °C for 24 - 48 h in a Gallenkamp static incubator (Gallenkamp-Weiss Tecknik, Gwent, UK). At 24 – 48 h of growth, single colonies from such plates were used as initial inocula, unless otherwise stated.

For liquid culture, strains of *Candida* spp. were routinely grown in YEPD broth (1 % [w/v] yeast extract [Sigma-Aldrich], 2% [w/v] peptone [Oxoid] and 2 % [w/v] glucose [Sigma-Aldrich]). Incubation was carried out in an orbital incubator (Gallenkamp-Weiss Tecknik) at either 30 °C or 37 °C with shaking at 200 r.p.m. During preparation of YEPD broth, glucose was not added prior to sterilisation. After autoclaving, the yeast extract and peptone components of the medium were supplemented with sterile glucose/dextrose (Sigma-Aldrich) to a final concentration of 2 % (w/v).

YEPD agar and liquid broth were also supplied by ForMedium (Norfolk, UK) as pre-made powders (without glucose) at the same concentrations as outlined above. Bacterial strains were routinely grown in Luria-Bertani Lysogeny Broth (Becton, Dickinson & Co.) (1 % [w/v] Bacto Tryptone [Becton, Dickinson & Co], 0.5 % [w/v] yeast extract, 1 % [w/v] NaCl) with selective antibiotics if required.

All other modified and optimised growth media are described in specific sections preceding each experiment.

Species	Strain	Genotype	Parent	Source
Candida albicans	SC5314	Wild-type	n/a	Gillum *et al*, 1994
Candida dubliniensis	Wü284	Wild-type	n/a	Morchhäuser *et al*, 1999
	Δ*tlo1/TLO1*	*tlo1*Δ::FRT/*TLO1*	Wü284	Jackson *et al*, 2009
	Δ*tlo1/*Δ*tlo1*	*tlo1*Δ::FRT/ *tlo1*Δ::FRT	Δ*tlo1/TLO1*	Jackson *et al*, 2009
	Δ*tlo2/*Δ*tlo2**	*tlo2*Δ::FRT/ *tlo2*Δ::FRT	Δ*tlo2/TLO2*	Jackson *et al*, 2009
	ΔΔ*tlo*	*tlo1*Δ::FRT/ *tlo1*Δ::FRT, *tlo2*Δ::FRT/ *tlo2*Δ::FRT	Δ*tlo1/*Δ*tlo1*	This study
	ΔΔ*tlo-TLO1*	*tlo1*Δ::FRT/ *tlo1*Δ::FRT, *tlo2*Δ::FRT/ *tlo2*Δ::FRT, *CDR1/cdr1*Δ::pCDRI-*TLO1*	ΔΔ*tlo*	This study
	ΔΔ*tlo-TLO2*	*tlo1*Δ::FRT/ *tlo1*Δ::FRT, *tlo2*Δ::FRT/ *tlo2*Δ::FRT, *CDR1/cdr1*Δ::pCDRI-*TLO2*	ΔΔ*tlo*	This study
	Δ*tlo1*-Ca*TLO11*	*tlo1*Δ::FRT/ *tlo1*Δ::FRT, *tlo2*Δ::FRT/ *tlo2*Δ::FRT, *CDR1/cdr1*Δ::pCDRI-Ca*TLO11*	Δ*tlo1/*Δ*tlo1*	Jackson *et al*, 2009
	Δ*tlo1*-Ca*TLO12*	*tlo1*Δ::FRT/ *tlo1*Δ::FRT, *tlo2*Δ::FRT/ *tlo2*Δ::FRT, *CDR1/cdr1*Δ::pCDRI-Ca*TLO12*	Δ*tlo1/*Δ*tlo1*	Jackson *et al*, 2009
	Δ*tlo1*-Ca*TLO34*	*tlo1*Δ::FRT/ *tlo1*Δ::FRT, *tlo2*Δ::FRT/ *tlo2*Δ::FRT, *CDR1/cdr1*Δ::pCDRI-Ca*TLO34*	Δ*tlo1/*Δ*tlo1*	Jackson *et al*, 2009
	TLO1-HA	*TLO1*::*TLO1-HA-NATR/TLO1*	Wü284	This study
	TLO1-GFP	*tlo1*Δ::*TLO1-GFP-NATR/TLO1*	Wü284	This study
	TLO2-GFP	*tlo2*Δ::*TLO2-GFP-NATR/TLO2*	Wü284	This study

Table 2.1. *Candida* strains used in this study.

Strains of *Candida albicans* and *Candida dubliniensis* used in this study are listed, with each genotype/source detailed.

* It was determined during the course of this study that there is only one intact allelic copy of *TLO2* in Wü284, as detailed in Chapter 3, hence the lack of heterozygous *tlo2* mutant strain.

2.1.3. Buffers and solutions

Formulations for specific buffers and solutions used in this study are described in the relevant experiments during which they were used. If necessary, sterilisation by filtration or autoclaving was carried out as described below. All solutions were made up to final volume with sterile, ultrapure (Milli-Q) water processed using a MilliQ Biocel system (Merck-Millipore, MA, USA), unless otherwise stated.

When a specific pH solution was required, pH was measured using a Thermo Scientific Orion 3-Star bench-top pH meter (Thermo Fisher Scientific, Ballycoolin, Dublin, Ireland) and adjusted to lower pH using 37 % (v/v) Hydrochloric acid (HCl) (Sigma-Aldrich) or adjusted to higher pH using 5 M Sodium Hydroxide (NaOH) (Sigma-Aldrich).

Sterilisation by filtration involved passing a solution or liquid through Steritop Vacuum-driven filtration systems with a 0.22 µM membrane (Merck-Millipore) assisted by a vacuum pump, into sterile glassware. Sterilisation of solutions by autoclaving was carried out in a Tomy SX-700 portable autoclave (Digital Biology, Tokyo, Japan), which was set to 121 °C for 15 min. Defend autoclave tape (MyDent International, NY, USA) was used to monitor successful cycles of sterilisation.

1 X TE Buffer was composed of 10 mM Trizma base (Sigma-Aldrich), brought to a pH of 8.0 with HCl as well as 1 mM Ethylenediaminetetraacetic acid (EDTA) (Sigma-Aldrich).

2.1.4. Reagents, enzymes, chemicals, antibiotics and antifungal agents

Suppliers for specialist reagents, chemicals, antifungals and antibiotics are outlined in the relevant sections of this study. The main suppliers are detailed below.

Enzymes were obtained from Promega, WI, USA, New England BioLabs (c/o Brennan & Co.), Stillorgan, Co. Dublin) and Roche Diagnostics Ltd., East Sussex, UK. Preparation of a DNase-free RNase A (Sigma-Aldrich) stock solution involved making a 10 mg/ml solution of RNase A in 10 mM Tris-HCL (pH 7.5). The resulting mix was boiled at 100 °C for 20 min on a heat block. The solution was then cooled and stored at – 20 °C until required.

2.1.5. Oligonucleotides

All oligonucleotides were designed as part of this study unless otherwise stated (Table 2.3). Prior to ordering, all oligonucleotide sequences were uploaded to BLAST (primer-BLAST) servers (Ye *et al.*, 2012) and tested against the relevant genome sequence to ensure specificity for the intended target.

Custom synthesised oligonucleotides (primers) were ordered and obtained from Sigma-Aldrich with the exception of those oligonucleotides ordered as part of work carried out in Minneapolis, MN, USA, which were ordered from Integrated DNA technologies (IDNA), Iowa, USA. Oligonucleotides were received in a lyophilised (dried) form and were re-suspended in the appropriate volume of sterile Milli-Q water (Merck-Millipore) to make a stock concentration of 100 µM.

2.1.6. Storage of isolates for future use

All strains used in this study were stored for future use at - 80 °C and were processed in the same way regardless of species. Single colonies from pure cultures on freshly incubated agar plates were used to inoculate 1.5 ml vials containing cryogenic beads and cryopreservative (Microbank, Pro-Lab Diagnostics, Cheshire, UK). The vial was gently mixed by hand. After sufficient homogenisation, the excess cryopreservative fluid was discarded. Vials were labelled and stored at - 80 °C in an ultra-low temperature freezer.

To reactivate cultures, vials were removed from storage at -80 °C and a single 'cryobead' was removed from the vial and was placed onto suitable media for incubation, as outlined in section 2.1.2.

2.1.7. Cell counting

In order to accurately count cells, washed pellets of the desired cell types were re-suspended in sterile PBS to a final volume of 1 ml. For more dense cultures (e.g. overnight cultures of yeast), this suspension was diluted to a factor of 100 in order to simplify counting and reduce errors. 10 µl of the cell suspension (diluted or not) was added directly to the central chamber of a clean Neubauer Haemocytometer (Marienfeld Glassware, Germany) and covered with a 0.13 – 0.17 mm coverslip (Thermo Fisher Scientific). The sample was allowed to rest for up to 2 min prior to counting.

Using a light microscope (Nikon instruments, c/o/ Aquilant Scientific, Dublin) at X 400 magnification, cells were counted in the central grid of the

Primer	Nucleotide Sequence (5′ – 3′)	Gene or region	*TLO* gene co-ordinates	Source
ACT1-FW	AGCTCCAGAAGCTTTGTTCAGACCAG	*ACT1*		Vaughan, C. (2006)
ACT1-RE	TGCATACGTTCAGCAATACCTGGG	*ACT1*		Vaughan, C. (2006)
TLO1SFW	AAAGGCCTCAGGGTACATCTT	*TLO1*	+51, +71	This study
TLO1SRE	TCTCAATCATAACGGCGACA	*TLO1*	+231, +250	This study
TLO1L	AAACAAGACTAGAGAACTCACTCAACG	*TLO1*	+17, +43	This study
TLO1R	TGACTTGATTGTCGTTGTTGC	*TLO1*	+896, +916	This study
TLO2L	GCTGGACCCAACAATGAACT	*TLO2*	+112, +131	This study
TLO2R	TTCAATTGCCACTGCTCTTG	*TLO2*	+599, +618	This study
CTA21KF	ATGGGGTACCTTTCTGACAACCGCTTCACG	*TLO1*	-484, -464	(Jackson, *et al.*, 2009)
CTA21SIR	GGCCGAGCTCAAGAGGGACCCGACCAAGAC	*TLO1*	+1280, +1299	(Jackson, *et al.*, 2009)
CTA2F	ATCCGAGCTCGACCCTGAAGTTGTTACGTG	*TLO2*	-365, -346	(Jackson, *et al.*, 2009)
CTA2R	ATCGTCTAGAGACTTGACGGAAAACTTGTC	*TLO2*	+1227, +1246	(Jackson, *et al.*, 2009)
TLO1BF	TAAGGTCGCCAATATGGAC	*TLO1*	+786, +804	This study
TLO1BR	GTCTCAAATACGATCGG	*TLO1*	+1086, +1102	This study
TLO2BF	CGACAGCGCCAGTCTCGAC	*TLO2*	+918, +936	This study
TLO2BR	TTGTGACACCAGTAAAGG	*TLO2*	+1257, +1274	This study
T1GFPF	GACAATAGCAACAACGACAATCAAGTCAATGAAGAGTTTGATGTAGATAGC TTCTTGAACCAATTTGGTAATGGTGGTGGTTCTAAAGGTGAAGAATTATT	*TLO1*		This study
T1GFPR	AATTGAACTGATTGTTCACCCTCATAAAAGCCCACAGATGACCACAACCAAG AGTAAGTCTAACAAATGATGTTGTCCGCGTTAGTATCGAATCGACAGC	*TLO1*		This study
T2GFPF	CTTGATGACGCCAACACCTTCAACGATAATGAAGAGTTTGATGTGGATAGTT TCTTAAACCAGTTTGGTAATGGTGGTGGTTCTAAAGGTGAAGAATTATT	*TLO2*		This study
T2GFPR	AATGTTTGGTGAGGTAAGGCCAAGGATAACTTCAAGGCGTCTGAAGACACAG CAGATTCAGTGGCATAGGTTCTTGTGACGTTAGTATCGAA TCGACAGC	*TLO2*		This study
TLO1F	CGGAAAGACAAGCGATAAGGT	*TLO1*	+771, +779	This study
TLO1R	CCATCCAAGCCTCCATCAAG	*TLO1*	+868, +887	This study
TLO2F	TGGTGTGTTGCCGTTATGAT	*TLO2*	+226, +245	This study
TLO2R	TTTTTGTCTTTCTCCGTCTTC	*TLO2*	+283, +303	This study
GFPR	CACCTTCACCGGAGACAG	*GFP*		This study

Table 2.2. Oligonucleotide primers used in this study.

Co-ordinates for *TLO*-specific primers are shown. Restriction sites are underlined where relevant.

IGR = Intergenic Region

Primer	Nucleotide Sequence (5′ – 3′)	Gene or region	*TLO* gene co-ordinates	Source
GAL1FW	CCAATTTCCCTAATGCATCG	*GAL1*		This study
GAL1RE	CCATGGGTAAAACAGGGAAG	*GAL1*		This study
GAL7FW	CCACCATTGTTACGTTCAGC	*GAL7*		This study
GAL7RE	ATCCCCATCCAATTCTTGC	*GAL7*		This study
GAL10FW	GTGCAGGCTATTGAAACTGTG	*GAL10*		This study
GAL10RE	TCACCAGGGCCAATATCTC	*GAL10*		This study
SOD3FW	AGATACCAATTCCCCCTTGG	*SOD3*		This study
SOD3RE	AAGCTCCTCCGTTTTGCTTG	*SOD3*		This study
SOD5FW	GTCCATTCCCATATCATGTCC	*SOD5*		This study
SOD5RE	AGGGGTTGAAATGGTTCTCG	*SOD5*		This study
SOD6FW	AGGAAACGCGGTGTTTAGTG	*SOD6*		This study
SOD6RE	ACCGACCGTTCATGGATATG	*SOD6*		This study
HWP1FW	CAGCTGGTATTAAAACTAACCCAGC	*HWP1*		This study
HWP1RE	ATTCTAATGTGGTTGGAATAGCACC	*HWP1*		This study
RBT5FW	TTGGCTAAAGCTGGTGAAGC	*RBT5*		This study
RBT5RE	TCAGCAGCAGTGGTTTCTTG	*RBT5*		This study
ECE1FW	ATTGCTGATATGCCATTGTTGTTAG	*ECE1*		This study
ECE1RE	CAATCTGACGATGGCATTAGTAACAT	*ECE1*		This study
UME6FW	TACCACCACCACCACCAAT	*UME6*		This study
UME6RE	TATCCCCATTTCCAAGTCCA	*UME6*		This study
NRG1FW	ACCAACACCACCACCATATCC	*NRG1*		This study
NRG1RE	TGAGGTTGTTGTAGTGTTTGTT	*NRG1*		This study
oJW102	GCGGTGACCCGGGAGATCTGAATTC	-		
oJW103	GAATTCAGATC	-		
PUT1AF	GGGTCACCAAACCAACCAAC	*PUT1*		This study
PUT1AR	TCGTGCAATCTCAATCCCGT	*PUT1*		This study
PUT1BR	GGCGGCATCTTTAGCAAACC	*PUT1*		This study

Table 2.2. Oligonucleotide primers used in this study (contd.)

Primer	Nucleotide Sequence (5′ – 3′)	Gene or region	*TLO* gene co-ordinates	Source
PUT1BF	TGAGATTGCACGAACGTGGT	*PUT1*		This study
NEG1F	AATTAATGAGAATTGCAGTGAGTGT	IGR*		This study
NEG1R	AATGCATGAATGACGGATTGAA	IGR*		This study
CLN1AF	AACGTCGACCATATCATCCAA	*CLN1*		This study
CLN1AR	TGGTTGTAAATCAATCATGGCCG	*CLN1*		This study
IDH1AF	TCAACTCCGAAAGAATTGCCA	*Cd36_52970*		This study
IDH1AR	GCCACAACATCGACTTGTCC	*Cd36_52970*		This study
IDH1BF	CCAGGTGCTAACTTTGGCAGA	*Cd36_52970*		This study
IDH1BR	GCTTCTGTTCATGTCTCGACG	*Cd36_52970*		This study
CD36_51290AF	ACAACTGATTCCCAGTGTTCCA	*Cd36_51290*		This study
CD36_51290AR	AATGGAGCACGTTTCTGGGC	*Cd36_51290*		This study
CD36_51290BF	GGGTGGATCTGCGATTGATGT	*Cd36_51290*		This study
CD36_51290BR	TGTAGTGCACCAGAGACCAA	*Cd36_51290*		This study
FGR6-3AF	AGCCCAATGAAAGAGCACCA	*FGR6-3*		This study
FGR6-3AR	CGGCAGTTTGCAAGTTGTGA	*FGR6-3*		This study
FGR6-3BF	GGTTGCAGATACCCTTGACCT	*FGR6-3*		This study
FGR6-3BR	ACCGCCAAAGGGTCAATGAA	*FGR6-3*		This study
MTLαAF	AGATGGCGATGACAGGAAGAC	*Cd36_51540*		This study
MTLαAR	ACCATCCCTCCAACACAAGC	*Cd36_51540*		This study
Cd36_17440AF	GCAAGACAGGTTAGGGGGTC	*Cd36_17440*		This study
Cd36_17440AR	TGGAAGGGTTGCAGGTTGTT	*Cd36_17440*		This study
Cd36_17440BF	CAGCCGGAGAGATCCACTTG	*Cd36_17440*		This study
Cd36_17440BR	GGTTTGCGCCAGACTCAATG	*Cd36_17440*		This study
Cd36_17440CF	GATTTTGTGCCGAGCAGGAC	*Cd36_17440*		This study
Cd36_17440CR	TTCCAAATCACGTCGCAGGA	*Cd36_17440*		This study

Table 2.2. Oligonucleotide primers used in this study (contd.)

haemocytometer (Marienfeld Glassware) in a total of 5 separate and non-adjacent 0.20 mm x 0.20 mm squares. An accurate estimation of the total cell count per ml was calculated by the use of the following formula:

$$Cells\ per\ ml = Total\ cells\ counted\ x\ \frac{dilution\ factor}{0.2}\ x\ 10{,}000\ cells/ml$$

In some cases, cells were difficult to visualise, in which case the use of Calcofluor White (Sigma-Aldrich) was incorporated into this protocol at the re-suspension stage (one drop of Calcofluor White stain was used for each prepared slide).

2.1.8. Quantification and quality assessment of nucleic acids

Prior to downstream applications, it was often necessary to quantify the amount of dsDNA or RNA in solution. This was done using a Nanodrop spectrophotometer (Thermo Fisher Scientific) or Qubit 2.0 fluorometer system (Life Technologies, CA, USA). The solution in which the DNA or RNA was suspended was used to blank the Nanodrop spectrophotometer to a baseline absorbance. A 1 µl volume of DNA or RNA was then loaded onto the stage of the Nanodrop spectrophotometer and DNA or RNA concentration was quantified in ng/µl using Nanodrop 2000c software (Thermo Fisher Scientific) on a PC running Windows XP (Microsoft, CA, USA). The 260 nm/280 nm and 260 nm/230 nm absorbance ratios were used to assess purity of the DNA/RNA.

To measure DNA or RNA using the Qubit system, each assay required calibration prior to sample reading. The relevant assay kit was selected (dsDNA, ssDNA, RNA), the system was calibrated and samples were measured as outlined in the Qubit 2.0 fluorometer user manual (Life Technologies Corporation, 2010)

2.1.9. Agarose gel electrophoresis

Agarose (Sigma-Aldrich) was prepared in 0.5 X TBE (5.4 g/l Trizma Base (Sigma-Aldrich), 2.75 g/l Boric Acid (Sigma-Aldrich), 1mM EDTA (Sigma-Aldrich) pH 8.0) and melted to molten agarose using a domestic microwave (Bosch, Stuttgart, Germany). Gel Red (Biotium, CA, USA) was added to a final concentration of 100 µl/l. Molten agarose was cast in gel tanks (Thermo Fisher Scientific). Well-spacing combs (Thermo Fisher Scientific) with 5 to 25 spaces were placed in the casts and the gels were allowed to set. Once solid, the gel tanks were

filled with sufficient 0.5 X TBE to submerse the gel and the well spacing combs were removed.

A 2 µl volume of Green/Blue loading dye (Promega) and 5 µl of sterile water were added to 5 µl PCR product and loaded on onto the gel. When size estimations were required, 100 bp or 1 kbp DNA ladders (Promega) were run in a single lane. The gel was run at 100 V, 20 W on a high-power electrophoresis power supply unit (Mason Technologies, Dublin, Ireland) until the dye fronts had reached the end of the gel. The gel was then visualised on an Alpha Imager Mini (Alpha-Innotech c/o Protein Simple c/o Medical Supply Company, Mulhuddart, Dublin, Ireland) using ultraviolet light at wavelength of 312 nm to allow visualisation of the fluorescently stained DNA.

When a more sensitive image was required, Gel Red was omitted from the agarose. Instead, after completion of the electrophoresis, the agarose gel was placed in a solution of Gel Red (Biotium) diluted 1 in 3,300 with 400 ml Milli-Q ultrapure water (Merck-Millipore) and 0.1 M NaCl (Sigma-Aldrich). The gel was incubated in this solution for 30 min in the dark, with gentle agitation. After this, the gel was washed in Milli-Q (Merck-Millipore) ultrapure water which had been heated to 37 °C and was immediately visualised on the Alpha Imager as described above.

2.1.10. Microscopy

2.1.10.1. Light Microscopy

Light microscopy was used in this study was carried out on either Nikon Eclipse E600 light microscope or Nikon TMS-F/TS-100 Inverted Light microscope (Nikon Instruments) using lenses with X100 or X400 magnification (Nikon Instruments)

2.1.10.2. Phase Contrast Microscopy

Phase contrast microscopy was carried out when viewing more dense cultures such as those in tissue culture dishes, or for easier discrimination of pseudohyphae and true hypha (Chapter 4). For this the above models of microscopes were used with addition of a phase-contrast filter ring.

2.1.10.3. Fluorescent Microscopy

Fluorescent microscopy was carried out on a Nikon eclipse E600 microscope with fluorescence vertical illuminator and 100 W mercury high-pressure lamp with Gfp fluorescent filter set (Nikon Instruments).

2.1.10.4. Scanning electron microscopy (S.E.M.)

Samples for S.E.M. were prepared by applying either a colony, or a 200 µl volume of a dense YEPD culture directly to a nitrocellulose membrane (Corning Life Sciences, UK) with a pore size of 0.2 µm. Samples were labelled and placed in an airtight container in order to prevent drying.

For all samples, fixation was performed using glutaraldehyde-osmium tetroxide as described by Staniszewska *et al.*, (2013). Fixation was carried out by submerging the membrane and specimen in 2.5 % (w/v) glutaraldehyde solution (Sigma-Aldrich) in 100 mM potassium phosphate (Sigma-Aldrich) for 2 h at room temperature. The membrane and specimen were washed twice with 100 mM phosphate buffer (pH 7.5) (Sigma-Aldrich).

Additional sample processing and scanning electron microscopy (S.E.M.) was carried out in the Centre for Microscopy and Analysis (CMA), Trinity College Dublin. Samples were subjected to an improvised supercritical point drying protocol (Bagshaw, 2010) and were visualised using a Zeiss Supra scanning electron microscope (Carl Zeiss Ltd, Welwyn Garden City, UK) set to 5 kV output.

2.2. DNA techniques

2.2.1. Whole genomic DNA purification

Colonies of the required *Candida* strain(s) were grown on YEPD agar for 48 h at 30 °C in a static incubator. From these plates, one colony was used to inoculate 50 ml of YEPD in 250 ml borosilicate Erlenmeyer narrow-neck flasks (Thermo Fisher Scientific) and incubated at 37 °C with shaking at 200 r.p.m., in an orbital incubator (Gallenkamp) overnight. The overnight culture was transferred to 50 ml polystyrene tubes (Greiner Bio-One, c/o Cruinn Diagnostics Ltd., Dublin, Ireland) centrifuged in a bench-top swing-bucket centrifuge (Eppendorf, Hamburg, Germany) at 2,000 x *g* for 5 min. The supernatant was discarded and cell pellet was re-suspended carefully in 5 ml of sterile P-buffer (20 mM Citrate-phosphate buffer [14.32% {w/v} disodium hydrophosphate {dodecahydrate}

{Sigma-Aldrich}, 4.2 % {w/v} Citric acid {Sigma-Aldrich}], 40 mM EDTA [Sigma-Aldrich], 1.2 M Sorbitol [Sigma-Aldrich], pH 5.6). 15 mg of Zymolyase 20T (AMS Biotechnology, Abingdon, UK) was added to the suspension and the mixture was incubated at 37 °C with shaking at 200 r.p.m. for 90 min (*Candida albicans*) or 3 h (*Candida dubliniensis*).

The suspensions were then centrifuged at 2,000 x *g* for 5 min in a bench-top swing-bucket centrifuge (Eppendorf) and the supernatant was discarded. The cell pellet was re-suspended in 7.5 ml 10 X TE with the addition of 10 % (v/v) sodium dodecyl sulphate (SDS) (Sigma-Aldrich) to a final concentration of 1 % (v/v). A volume of 2.5 ml of 5 M Potassium acetate (Sigma-Aldrich) was added followed by incubation on ice for 30 min. Cells were then centrifuged for 10 min at 8,600 x *g* at 4°C in a Sorvall SS-34 rotor (Beckman Coulter, Co. Clare, Ireland).

The supernatant was transferred into a new 50 ml polystyrene tube (Greiner Bio-One) and mixed gently with 10 ml ice-cold isopropanol (Sigma-Aldrich). The mixture was incubated on ice for 5 min and centrifuged at 2,500 x g in a bench-top swing-bucket centrifuge (Eppendorf) for 5 min at 4 °C. The supernatant was then discarded.

The cell pellet was allowed to air dry and was then re-suspended in 1 ml of 1 X TE buffer. RNAse A (Sigma-Aldrich) was added to a final concentration of 1 mg/ml and the suspension was incubated at 37 °C for 1 h. Subsequently, Proteinase K (Sigma-Aldrich) was added to a final concentration of 1 mg/ml and the suspension was incubated at 37 °C for 2 h.

The solution (≈ 1.2 ml) was split into two equal fractions in 1.5 ml microcentrifuge tubes (Eppendorf) and 600 µl of phenol:chloroform:isoamyl-alcohol at a 24:24:1 ratio (P:C:I-24:24:1) (Sigma-Aldrich) was added to each, followed by vigorous mixing for 30 s and centrifugation at maximum speed for 1 min in a bench-top microcentrifuge (Eppendorf). The aqueous phase (top layer) was removed and subjected to two additional rounds of P:C:I purification. An additional round of purification was sometimes carried out using chloroform:isoamyl-alcohol (24:1) to reduced phenol carryover.

The extracted aqueous layers from the two fractions were combined (approx. 600 µl) in a 2 ml tube (Eppendorf) and 2 volumes of ice-cold 100 % (v/v) ethanol (Sigma-Aldrich) was added. The DNA was 'spooled' from the mixture using a sterile glass Pasteur pipette tip (Thermo Fisher Scientific) and transferred

to a new polystyrene tube (Greiner Bio-One). The DNA was washed with 70 % (v/v) ethanol for 5 min. The DNA was then air-dried and re-suspended in 150 µl of 1x TE buffer. The DNA was quantified and checked for integrity by measurement using a Nanodrop spectrophotometer (Thermo Fisher Scientific) or Qubit fluorometer (Life Technologies) as described in section 2.1.8. and by performing agarose gel electrophoresis as described in section 2.1.9.

2.2.2. Rapid extraction of genomic DNA from *Candida* strains

Strains of *Candida* spp. were plated onto YEPD agar plates and incubated at 30 °C in a static incubator (Gallenkamp). Fresh colonies were used to inoculate 2 ml of YEPD in 15 ml screw-capped tubes (Sarstedt Ltd, Wexford, Ireland) which were incubated at 30 °C overnight (18 h). A 1.5 ml volume of culture was transferred to a 2 ml microcentrifuge tube (Eppendorf) and the cells were harvested by centrifugation in a bench-top microcentrifuge (Eppendorf) at 10,000 x *g* for 2 min. The supernatant was discarded and the cell pellet was re-suspended in 200 µl of Breaking Buffer (2% [v/v] Triton X-100 [Sigma-Aldrich], 1% [w/v] SDS [Sigma-Aldrich], 10 mM Tris-HCL [Sigma-Aldrich], pH 8.0, 1 mM Ethylenediaminetetraacetic acid [EDTA] [Sigma-Aldrich], 100 mM NaCl [Sigma-Aldrich]).

The resulting suspension was added to a screw-capped 2 ml tube (Sarstedt) containing 300 mg glass beads with 425 – 600 µm diameter (Sigma-Aldrich). 200 µl of P:C:I (Sigma-Aldrich) was added to the tube, which was then processed in a FastPrep cell disruptor (Thermo Fisher Scientific) for 2 rounds of 45 s, with rest periods on ice for 2 min after each round of disruption.

The tube was removed from the cell disruptor and centrifuged at 25,000 x *g* for 10 min at room temperature in a bench-top microcentrifuge (Eppendorf). The aqueous phase was transferred to a new 1.5 ml microcentrifuge tube (Eppendorf). To prevent phenol carryover, an equal volume of a 24:1 mix of chloroform (Sigma-Aldrich) and isoamyl alcohol (Sigma-Aldrich) was added and mixed by vortexing. The mix was centrifuged at 25,000 x *g* for 3 min at room temperature and the aqueous phase was transferred to a new microcentrifuge tube (Eppendorf).

The DNA was precipitated by adding 1 µl of 3 M Sodium acetate (Sigma-Aldrich) per 10 µl of sample and two volumes of ice-cold 10 % (v/v) ethanol (Sigma-Aldrich). This mix was incubated at -80 °C for 30 min and centrifuged in a bench-top microcentrifuge (Eppendorf) at 25,000 x *g* at 4 °C for 10 min. The

resulting DNA pellet was washed with ice-cold 70% (v/v) ethanol (Sigma-Aldrich), with gentle mixing. The 70% (v/v) ethanol (Sigma-Aldrich) was carefully pipetted away from the pellet and the pellet was allowed to dry at room temperature. Once dry, the pellet was re-suspended in 50 µl 1 X TE Buffer for further processing.

2.2.3. DNA ligation

DNA ligations were carried out in microcentrifuge tubes (Eppendorf). DNA was suspended in 1 X T4 DNA ligase buffer (New England Biolabs) and 1 µl (400 U) of T4 DNA ligase (New England Biolabs) was added to a final volume of 20 µl. Reactions were incubated for 2 h at room temperature.

2.2.4. Plasmid DNA isolation

Plasmids used in this study were routinely maintained in *Escherichia coli* strain XL-10 {Tet^{r}Δ(*mcrA*)183 Δ(*mcrCB-hsdSMR-mrr*)*173 endA1 supE44 thi-1 recA1 gyrA96 relA1 lac* Hte [F′ *proAB lacIqZDM15* T*n10* (Tet^r) Amy Cam^r]}. Strains were grown on L-agar (Becton, Dickinson & Co) containing the relevant selective antibiotic and incubated at 37 °C overnight. 2 ml cultures of *E. coli* were inoculated using single colonies from these plates and incubated overnight at 37 °C with shaking at 200 r.p.m. A 1.5 ml volume of this overnight culture was transferred to a microcentrifuge tube (Eppendorf) and centrifuged at 13,000 x *g* for 2 min in a bench-top microcentrifuge (Eppendorf). The supernatant was discarded and the plasmid was purified using the PureYield Plasmid Miniprep System (Promega) with an altered protocol optimised for higher yields as described below.

A 100 µl volume of Cell Lysis Buffer (Promega) was added directly to the cell pellet. The cells were re-suspended by scraping the microcentrifuge tube back and forth over a hard surface (e.g. wire tray) 15 times. Care was taken to ensure the tube was sealed properly prior to re-suspension. A 350 µl volume of ice cold Neutralisation Solution (Promega) was added to the mix and the tube was sealed and scraped back and forth over a hard surface 15 times to mix. The resulting solution was centrifuged at 16,000 x *g* for 5 min. The supernatant was transferred to a PureYield mini-column and the pellet was discarded.

The protocol was carried out from this point as is described in the manufacturer's protocol (Promega Corporation, 2009). Plasmid DNA was eluted

from the column with sterile water and was kept at 4 °C for short-term storage or -20 °C for longer-term storage.

2.2.5. DNA sequencing

Sequencing performed in this study was carried out commercially in St. James's Hospital, Dublin on behalf of the Oral Biosciences Division, Dublin Dental University Hospital, by Source BioSciences (Nottingham, UK). Unless otherwise stated, the method used was single-read Sanger sequencing on an ABI 3730xl DNA analyser (Applied Biosystems, Life Technologies). Sequence reads were supplied by email in the form of .seq and .ABI files.

2.2.6. Basic analysis of DNA sequences

Raw sequence files obtained from sequencing in the form of .AB1 files were imported as chromatograms and analysed/interpreted using 4Peaks software for Mac OSX (Mekentosj, CA, USA). The validated sequences were then exported as .txt files and imported into genetic analysis software of choice.

For most instances in this study, genetic sequences were analysed and annotated using ApE Plasmid Editor (Jorgensen Laboratory, Department of Biology, University of Utah, Salt Lake City, UT, USA). Previously published or annotated DNA sequences were obtained from GeneDB (Sanger Institute, Cambridge, UK) or the *Candida* genome database (Inglis *et al.*, 2012) in FASTA format and uploaded to ApE Plasmid Editor (Jorgensen Lab) for further editing.

2.2.7. Restriction enzyme digestion of DNA

DNA was prepared and cleaned prior to digestion as outlined in section 2.2.2. Restriction digestions using New England Biolabs products were carried out in a 50 µl volumes containing 1 µg of target DNA, 10 U of the relevant restriction enzyme (New England Biolabs), 1 X NEBuffer (New England Biolabs) and sterile ultrapure water. Double digests included an additional enzyme at a concentration of 10 U. Other restriction digest systems (e.g. Promega, Roche) were performed in similar manners according to the relevant manufacturer's protocol. Reactions were incubated overnight at 37 °C. The success of the DNA digestion was determined by agarose gel electrophoresis as outlined in section 2.1.9.

2.2.8. Transformation of Candida strains by electroporation

The recipient *Candida* strain was sub-cultured and incubated for 48 h at 37 °C on YEPD agar. From these plates, a single colony was used to inoculate 50 ml of YEPD broth which was incubated at 30 °C in an orbital incubator with shaking at 200 r.p.m until grown to an approximate $O.D._{600nm}$ of 2.0. The culture was transferred to 50 ml polystyrene tubes (Greiner Bio-One) and centrifuged for 5 min at 2,500 x *g* in a bench-top centrifuge (Eppendorf). The supernatant was discarded and the cell pellet was re-suspended in 10 ml of 1X TE (pH 7.5). Lithium acetate (pH 7.5) was added to a final concentration of 100 mM. The resulting mixture was incubated for 1 h at 30 °C with shaking at 200 r.p.m in an orbital incubator. DTT was added to a final concentration of 25 mM and the mixture was incubated at 30 °C with shaking at 200 r.p.m for a further 30 min.

A 40 ml volume of sterile ultrapure water was added to the mixture, which was then centrifuged at 2,500 r.p.m for 5 min as before. The supernatant was discarded and cells were washed with 50 ml of ice-cold sterile ultrapure water, followed by another round of centrifugation as before. The supernatant was discarded and the cell pellet was re-suspended in 50 µl ice-cold 1 M Sorbitol.

A 40 µl volume of cell mixture was transferred to a 1.5 ml electroporation cuvette (Sigma-Aldrich) and donor DNA was added to a concentration of approximately 0.5 µg in a final volume of 10 µl. Prior to transformation, donor DNA was linearised by restriction enzyme digestion as described in section 2.2.7. Transformation was induced by electroporation at 1.6 kV in a Minipulser (BioRad). 1 ml of warm YEPD broth was immediately added to the mixture and the cuvettes were incubated at 37 °C for 2 h in an orbital incubator with shaking at 100 r.p.m. in order to allow the cells to recover. Afterwards, 100 µl volumes of the transformed strains were spread-plated out onto YEPD agar containing 100 µg/ml of nourseothricin (Sigma-Aldrich) for *C. dubliniensis* strains or 200 µg/ml in the case of *C. albicans* strains. Plates were incubated for 48 h to allow resistant (transformed) colonies to grow, which were then confirmed by subculturing on YEPD-NAT and by PCR (section 2.3.1.) using gene-specific oligonucleotides.

2.3. Polymerase Chain Reaction (PCR)

2.3.1. Routine PCR

Template DNA was diluted to a concentration of 100 ng/μl in sterile MilliQ water (Merck-Millipore). Reagents were prepared as a master mix and added appropriately so that the final contents of each tube were as follows: 1X Colourless Go-Taq Flexi Buffer (Promega), 2.5 mM $MgCl_2$ (Promega), 0.2 mM each of dATP, dTTP, dGTP, dCTP (Promega), 1 μM of forward oligonucleotide primer (Sigma-Aldrich), 1 μM of reverse oligonucleotide primer (Sigma-Aldrich), 1.25 U GoTaq DNA Polymerase (Promega), 100 ng template DNA and sterile, nuclease free water (Sigma-Aldrich) up to a final volume of 50 μl in 0.2 ml polystyrene tubes (Molecular BioProducts).

Reactions were carried out in a thermal cycler (Kyratech, Queensland, Australia) with an initial denaturation step at 95 °C for 2 min. This was followed by 30 cycles of the following: denaturation at 95 °C for 1 min, annealing at 58 °C for 1 min, extension at 72 °C for 1 min per kilobase of amplicon length. There was then a final extension step at 72 °C for 5 min, followed by an indefinite hold at 4 °C. Annealing temperatures and extension times were adjusted appropriately for each experiment, the former being dependent on the primer melting temperature (usually 3 °C less). Agarose gel electrophoresis was carried out in order to visualise PCR products as described in Section 2.1.9.

2.3.2. Cleanup of PCR products

Different methods were used to clean PCR products depending on the requirements of downstream reactions and experiments. If products were to be used for cloning, the GenElute PCR Clean-Up Kit (Sigma-Aldrich) was used according to the standard protocol (Sigma-Aldrich, 2012). Alternatively, if a specific product needed to be separated from others, gel purification was carried out. Briefly, this involved performing agarose gel electrophoresis as described in section 2.1.9. and using the Wizard SV Gel and PCR Clean-up System (Promega) as outlined in the manufacturer's protocol (Promega Corporation, 2010)

2.3.3. Quantitative real time PCR (qRT-PCR)

For quantitative real time PCR (qRT-PCR), cDNA was prepared as outlined in section 2.5.2. using normalisation of input RNA template to 100 ng/µl to ensure relative quantification of cDNA templates for qRT-PCR.

Primer pairs specific for the desired target were designed (Table 2.2.) using stringent criteria, which included a melting temperature (Tm) of 59 °C - 60 °C, keeping the intended amplicon length between 50 and 200 bp and ensuring a comprehensive BLAST search was carried to ensure complementarity was specific for the gene/region of interest. Primer BLAST (Ye *et al.*, 2012) was commonly used to ensure these criteria were met.

Reactions were carried out on MicroAmp Fast Optical 96-well Reaction plates (Applied Biosystems) in 15 µl or 20 µl reactions using 1X Fast SYBR Green PCR Master Mix (Applied Biosystems), 150 nM of each oligonucleotide primer, 2 µl of diluted template (less than 10 ng) and sterile water. Cycling conditions used were 95 °C for 20 sec, followed by 40 cycles of 95 °C for 3 sec and 60 °C for 30 sec, the latter of which was the point of detection of fluorescence. This was followed by a melt curve stage as a quality control point.

Using a proprietary algorithm (Applied Biosystems), the Threshold Cycle (Ct) value is computed for each reaction. The Ct value is the intersection between an amplification curve and a threshold line, with the average being calculated over technical replicates. The reliability of the qRT-PCR run was also determined by analysing the R^2 value and standard deviation between replicates.

Results were determined in three separate ways, depending on the type of experiment set up:

2.3.3.1. Relative Quantification

Relative quantification involves the detection of a control target run in tandem with the experimental target detection. The 'endogenous control' target is normally a gene that has a relatively constant expression level, so that experimental samples can be compared directly to it. For the case of *C. dubliniensis*, it has previously been shown in this laboratory (O'Connor, 2009) that *ACT1* is a suitable endogenous control. Reactions with ACT1-FW and ACT1-RE (Table 2.2) were setup, using the same template DNA as the experimental reactions and using the same cycling conditions.

After the PCR had completed, the ΔCt was calculated as follows:

$$\Delta Ct = Ct(Experimental\ Target) - Ct(Endogenous\ control)$$

The results were presented by transforming the data logarithmically to $2^{-\Delta Ct}$, which inverts the data, making an increase in value, equal an increase in expression.
Sometime, it was necessary to compare separate groups of targets. In this case the ΔΔCt was calculated using the following formula:

$$\Delta\Delta Ct = \{Ct(Experimental\ Target\ 1) - Ct(Endogenous\ control\ 1)\} - \{Ct(Experimental\ Target\ 2) - Ct(Endogenous\ control\ 2)\}$$

The ΔΔCt was, like the ΔCt, represented logarithmically as $2^{\Delta\Delta Ct}$.
For relative quantification to be accurate, the efficiency of oligonucleotides needed to be tested. This was done by running serial dilutions of the same cDNA sample with a set of oligonucleotides and plotting the Ct values against Log_{10} dilution of cDNA and deriving the slope (m) of the standard curve using the formula:

$$m = \frac{y_2 - y_1}{x_2 - x_1}$$

where, x_1, y_1 and x_2, y_2 are separate co-ordinates of the curve.
Then, using the following equation, the efficiency (E) of the oligonucleotide pair was computed:

$$E = 10^{-1/m}$$

2.3.3.2. Absolute quantification (Standard Curve)

Quantification using a standard curve involved running reactions as described above, but with the absence of an endogenous control. Instead, serial dilutions of Wü284 genomic DNA, from 100 ng/μl to 1 μg /ml were included as templates for each oligonucleotide pair used and a standard curve was plotted from the Ct values of these. From this curve, concentrations of qRT-PCR products were extrapolated, assuming that they fell within the range of the standards. With

this method, primer efficiency could also be calculated using the standard curve data.

2.4. Southern Immunoblot hybridisation

All chemicals used in the following protocol were supplied by Sigma-Aldrich unless otherwise stated. All buffers were sterilised prior to use as described in section 2.1.3.

2.4.1. Amplification and labelling of DNA probe

A digoxigenin (DIG) -labelled probe (200 bp) was amplified with primers TLO1SFW and TLO1SRE using a modified PCR protocol. The 50 µl reaction mixture contained 1X GoTaq PCR buffer (Promega) with 1.5mM MgCl (Promega), 1x PCR DIG probe synthesis mix (Roche Diagnostics) consisting of 2mM dATP, 2mM dCTP, 2mM dGTP, 1.3 mM dTTP, 0.7 mM DIG-dUTP, pH 7.0, 1 µM TLO1SFW oligonucleotide, 1 µM TLO1SRE oligonucleotide, 10 ng template gDNA (Wü284) and 5 U GoTaq DNA polymerase (Promega). The mixtures were incubated in a thermal cycler (Kyratech) with an initial denaturation of 2 min at 95 °C for 30 s. This was followed by 10 cycles of 95 °C for 30 s, 60 °C for 30 s, 72 °C for 30 s. Following this, there were a further 23 cycles of 95 °C for 30 s, 60 °C for 30 s, 72 °C for 40 s. There was then a final step of 72 °C for 7 min. Control reactions, one with 2mM of all dNTPs without DIG-dUTP and one with no template were also run in parallel.

Products were then separated by 1 % (w/v) agarose gel electrophoresis alongside 1 Kb DNA ladder (Promega) to assess size and purity of probe. If required in the case of non-specific amplification, the probe was extracted using agarose gel extraction & cleanup as in Section 2.3.2.

2.4.2. Sample preparation and membrane transfer

Whole genomic DNA samples were prepared as described in Section 2.2.1. DNA samples were digested using the 40 U of the restriction enzyme *NdeI* (New England Biolabs) with 1 X Buffer 4 (New England Biolabs) and 1X Bovine Serum Albumin (BSA) (New England Biolabs) in a final volume of 100 µl at 37 °C overnight in a circulating waterbath (Thermo Fisher Scientific)

The following day, 5 µl of the digested DNA sample was electrophoresed on a 0.8% (w/v) agarose gel at 120 mV for 1 h and post-stained for 10 min with a 1 in 3,300 diluted solution of Gel Red (Biotium) in water, to monitor digestion. Gels were imaged as described in Section 2.1.9. Following satisfactory digestion, 30 µl (approximately 10 µg) of each digest was combined with 1 X Green/Blue Loading Dye (Promega) and subjected to 1 % (w/v) agarose gel electrophoresis (without pre-staining) at 20 mV overnight to allow full resolution of samples. DIG-labelled, DNA molecular weight marker III (Roche Diagnostics) was also run on each edge well of the agarose gel, as a size marker.

The following morning, the gel was post-stained for 10 min with Gel Red (Biotium) and rinsed briefly in water. The gel was visualised to ensure correct running prior to downstream processing. The gel was de-purinated in 100 ml of 250 mM HCL in a clean glass dish for 10 min with gentle shaking. The gel was rinsed with water and then incubated with denaturing solution (500 mM NaOH, 1.5 M NaCl) for 15 min in a clean glass dish with gentle shaking. This wash was repeated for an additional 15 min with fresh denaturing solution. After a brief rinse with water, the gel was incubated in neutralisation solution (500 mM Tris, 1.5 M NaCl, pH 7.5). This was repeated for an additional 15 min with fresh neutralisation solution. The gel was then equilibrated in sterile 20X SSC buffer (3 M NaCl, 300 mM Sodium Citrate, pH 7.0) prior to setup of the capillary transfer sandwich.

A capillary transfer sandwich was setup as follows: A glass dish (reservoir) was filled with 20X SSC buffer. On a suspended glass plate, a filter paper bridge was set up using Whatman 3 mm blotting paper (Whatman, GE Healthcare Life Sciences, Wien, Austria) pre-soaked in 20X SSC buffer. The agarose gel was placed face-down on the bridge, followed by a piece of positively charged Nylon membrane (Roche Diagnostics) cut to fit the gel. Ensuring not to capture air bubbles, 3 pre-soaked blotting paper layers were placed on the bridge, followed by two stacks of paper towels (>10 cm high) evenly on top of the layers to absorb

and draw the liquid from the reservoir. The sandwich was weighted using books and the entire setup was enclosed with cling film to prevent evaporation. The transfer apparatus was left overnight to transfer.

The next day, the transfer sandwich was dismantled and the nylon membrane was placed on Whatman 3mm blotting paper (GE Healthcare Life Sciences) that had been pre-soaked in 2 X SSC Buffer (0.3 M NaCl, 30 mM Sodium Citrate, pH 7.0) ensuring not to directly touch the membrane. This was then exposed to 0.120 Joules of ultraviolet light (UV) (1.5 min) in a UV cross-linker (Biometra, Goettingen, Germany) to cross-link the DNA to the membrane. The membrane was flipped over and exposed again to 0.120 Joules of UV light (Biometra). The membrane was then rinsed with MilliQ ultrapure water (Millipore-Merck) and allowed to air dry. The orientation of the membrane was noted and the membrane was stored dry at 4 °C until ready to proceed to hybridisation.

2.4.3. Pre-hybridisation

The membrane, henceforth referred to as the blot, was placed into a hybridisation roller bottle (Thermo Fisher Scientific). 10 ml of reconstituted DIG Easy-Hyb (Roche Diagnostics) was added per 100 cm^2 of blot. The roller bottle was sealed and incubated with slow rotation in a hybridisation oven (Thermo Fisher Scientific) for at least 30 min, up to 3 h at the appropriate hybridisation temperature. Hybridisation temperature (T_{hyb}) was calculated based on the melting point of the probe-target hybrid (T_m) using the formulae below:

$$T_m = 49.82 + 0.41(\%\text{ of G/C residues in probe}) - 600/\text{ probe-target hybrid length}$$

$$T_{hyb} = T_m - (22.5\ °C)$$

2.4.4. Hybridisation

Immediately prior to commencement of hybridisation experiment, the clean, DIG-labelled DNA probe was denatured at 95 °C for 5 min in a thermal cycler (Kyratech) and placed immediately on ice for a further 5 min. The roller bottle was decanted and 3.5 ml of DIG Easy Hyb (Roche Diagnostics) was added per 100 cm^2 of blot. 2 µl of denatured DNA probe was added per ml of solution. The bottle was sealed and incubated for 16 h at the previously calculated T_{hyb} with gentle rotation in a hybridisation oven (Thermo Fisher Scientific).

2.4.5. Washing

The blot was removed from the hybridisation solution and washed with 200 ml of Low Stringency Buffer (2X SSC Buffer, 0.1 % [w/v] SDS) for 10 min with vigorous shaking on a Unimax 2010 mixing tray (Heidolph, Germany). This was repeated with fresh Low Stringency Buffer for a further 10 min. The blot was then transferred to a new roller bottle (Thermo Fisher Scientific). 200 ml of pre-warmed (65 °C) High Stringency Buffer (0.5 X SSC Buffer, 0.1 % (w/v) SDS) was added and incubated at 65 °C with rotation for 15 min in a hybridisation oven (Thermo Fisher Scientific). This was repeated with 200 ml of fresh High Stringency Buffer for a further 15 min.

2.4.6. Detection

The blot was incubated in a glass dish in 100 ml of Wash Buffer (1% [w/v] Maleic Acid Buffer [100 mM Maleic Acid, 150 mM NaCl, pH 7.5], 0.3 % [w/v] Tween-20) with gentle shaking. The Wash Buffer was discarded and the blot was then incubated with 100 ml of 2% (w/v) Blocking Reagent (Roche Diagnostics) suspended in Maleic Acid Buffer in a roller bottle (Thermo Fisher Scientific) in a hybridisation oven (Thermo Fisher Scientific) with slow rotation for 3 h at room temperature.

The Block solution was discarded and replaced with 2% (w/v) Blocking Reagent (Roche Diagnostics) re-suspended in Maleic Acid Buffer with the addition of 2 µl of Anti-Digoxigenin-AP, fragment-antigen-binding (Fab) fragments (Roche Diagnostics), henceforth known as the antibody. A pre-detection centrifugation (16,000 x *g*) of the antibody stock solution can help to clarify the solution. The blot with this solution was incubated in the hybridisation oven (Thermo Fisher Scientific) as before, at room temperature for 30 min. The blot was transferred to a clean dish containing 100 ml Wash Buffer and was washed a further 2 times with fresh 100 ml Wash Buffer and vigorous mixing.

The blot was placed between two unsealed transparent polystyrene sheets and 1 ml of CDP-Star (Amersham, GE Healthcare Life Sciences) was added, drop-wise to the surface of the blot for every 100 cm^2 of blot. The two sheets were closed over and allowed to incubate for 5 min in the dark. Excess liquid was forced out and the two sheets were sealed using a vacuum sealer.

2.4.7. Development

The sealed blot was exposed to BioMax Light film (Kodak, c/o Sigma-Aldrich) for varying lengths of time (usually 10-20 min) in a light cassette (Kodak) and the image was developed in the dark as follows: 30 s in developer solution (Kodak), 30 s in distilled water, 30 s in fixing solution (Kodak) and 1 min in distilled water. The X-ray film was then air dried and viewed.

2.5. RNA techniques

2.5.1. RNA extraction

Two methods were used for RNA extraction. The 'rapid method' was used for RNA extractions of overnight cultures only. For other cultures, including those with hyphal and pseudohyphal morphology, the freeze-fracture method was used. Both are described below.

2.5.1.1. Rapid method

This method is an adapted version of that described in the RNeasy Mini Handbook (Qiagen, 2012). Relevant strains were grown on YEPD agar plates at 30 °C for 48 h. A single colony from this was used to inoculate 2 ml YEPD, which was incubated at 37 °C for 18 h. The cells were harvested by centrifugation at 10,000 x *g* for 5 min at 4 °C. The supernatant was discarded and the pellet was re-suspended in 600 µl of Buffer RLT (Qiagen, West Sussex, UK) containing 1% (v/v) β-mercaptoethanol (Sigma-Aldrich). The cell pellet was re-suspended by gentle vortexing. The sample was then added to a sterile 1.5 ml screw-capped tube (Sarstedt) containing 600 µl of acid-washed 420 – 600 µm glass beads (Sigma-Aldrich) and processed in a FastPrep (Thermo Fisher Scientific) for 2 rounds of 45 s. Between rounds of beating, the samples were cooled on ice for 1 min.

The centrifugation steps that follow were carried out in a bench-top microcentrifuge (Eppendorf). The beads were allowed to settle for 2 min and the lysate was removed and transferred to a new micro-centrifuge tube (Eppendorf). This lysate was centrifuged at 13,000 x *g* for 2 min and the supernatant was transferred to a new micro-centrifuge tube (Eppendorf).

One volume of 70 % (v/v) Ethanol was added to the sample and mixed by pipetting. The entire sample was transferred to an RNeasy spin column with collection tube (Qiagen) and centrifuged for 30 s at 10,000 x *g*. The flow-through

was discarded. This was repeated until all of the sample had been passed through the spin column. A 700 µl volume of Buffer RW1 (Qiagen) was added to the spin column and centrifuged at 10,000 x *g* for 30 s. The flow-through was discarded. 500 µl of Buffer RPE (Qiagen) was added to the spin column and centrifuged at 10,000 x *g* for 30 s. The flow-through was discarded. An additional 500 µl of Buffer RPE (Qiagen) was added to the spin column and centrifuged at 10,000 x *g* for 2 min. The flow-through was discarded. The RNeasy spin column was transferred to a new collection tube (Qiagen) and centrifuged at 16,000 x *g* for 1 min to ensure removal of excess ethanol.

The spin column was then transferred to a new 1.5 ml microcentrifuge tube (Eppendorf) and 50 µl of sterile Milli-Q ultrapure water (Merck-Millipore) was added directly to the column membrane. The column was incubated for 10 min at room temperature and subsequently centrifuged at 10,000 x *g* for 1 min to elute the RNA.

A 5 µl volume of TURBO DNase Buffer (Ambion, Life Technologies, USA) and 1 µl TURBO DNase (Ambion) was added to the sample and mixed. The sample was incubated in a water bath at 37 °C for 30 min. A 5 µl volume of DNase inactivation reagent (Ambion) was added to the sample followed by thorough mixing by pipetting. This mixture was incubated at room temperature for 5 min with mixing every 90 s. The samples were centrifuged at 10,000 x *g* for 1.5 min and the supernatant was transferred to a new micro-centrifuge tube (Eppendorf). This sample is the cleaned RNA.

2.5.1.2. Freeze-fracture method

Relevant strains were grown on YEPD agar plates at 30 °C for 48 h. A single colony from this was used to inoculate 2 ml YEPD, which was incubated at 37 °C for 18 h. The culture was then centrifuged for 3 min at 10,000 x *g* and washed as described before, three times with sterile PBS. The washed pellet was re-suspended in sterile PBS to a final volume of 1 ml. Cells were counted as described in Section 2.1.7. An appropriate volume of cells was added to 50 ml of the desired media in an Erlenmeyer flask (Thermo Fisher Scientific) with air-permeable rubber bung, to a final concentration of 2 X 10^6 cells per ml. The cultures were incubated at 37 °C for the desired length of time; depending on the experiment; after which they were transferred to polystyrene Falcon tubes (Greiner Bio-One) and centrifuged using a bench-top swing-bucket centrifuge

(Eppendorf) for 10 min at 2,500 x *g*. All but 1 ml of supernatant was discarded and the pellet was re-suspended in this remaining liquid. This resulting 'slurry' of cells was added dropwise to 30 ml of liquid nitrogen (Calor Gas, Dublin, Ireland) in 50 ml polystyrene Falcon tubes, with gentle mixing so as to prevent aggregation of droplets. Immediately after vaporisation of the liquid nitrogen, the frozen cell droplets were stored at -80 °C for up to 7 days.

Prior to RNA extraction, the apparatus required for mechanical breakage were soaked in RNase Away (Molecular BioProducts) for 15 min at room temperature and rinsed with sterile ultrapure water treated with 0.1 % (v/v) diethylpyrocarbonate (DEPC) (Sigma-Aldrich). Apparatus were left to air dry and then were pre-cooled in liquid nitrogen. In order to extract the RNA, the frozen pellets of cells were transferred to polytetrafluoroethylene (PTFL) vessels (Sartorius Mechatronics, Goettingen, Germany) containing a tungsten-carbide grinding ball (Sartorius Mechatronics). The PTFL vessels were then sealed and processed on a Mikro-Dismembranator S series (Sartorius Mechatronics) for 2 min at 1,500 r.p.m.. The PTFL vessels were then opened and the grinding balls removed for cleaning.

A 600 µl volume of RLT Buffer (Qiagen, West Sussex, UK) containing 1% (v/v) β-mercaptoethanol (Sigma-Aldrich) was added to the PTFL vessel containing finely ground cells and the mixture was allowed to thaw for 2 min. The resulting mixture was added to 2 ml microcentrifuge tubes (Eppendorf) and equilibrated with an equal volume of 70 % (v/v) ice-cold ethanol. Additional processing was carried out as described above in section 2.5.1.1.

2.5.2. cDNA synthesis

Prior to cDNA synthesis, the RNA template was checked for integrity by agarose gel electrophoresis as described in section 2.1.9. The RNA isolation protocols as described in 2.5.1.1. and 2.5.1.2. make use of the RNeasy cleanup column which gives sufficient purity for downstream cDNA synthesis. The RNA was treated with TURBO DNase (Ambion) as described in 2.4.1.2. to ensure purity.

First strand synthesis of cDNA was carried out using the Superscript III First strand synthesis system for RT-PCR (Life Technologies). A 100 ng quantity of RNA was used as the template and was added to a 0.2 ml thin-walled tube (Molecular BioProducts) with 50 µM Oligo dT (Promega), 10 mM of each dATP,

dTTP, dGTP, and dCTP, and sterile water up to 10 µl. This reaction was incubated in a thermal cycler (Kyratech) at 65 °C for 5 min then on ice for 2 min. 1X RT buffer (Life technologies), 25 mM $MgCl_2$ (Promega), 100 mM DTT (Life technologies), 40 U RNase OUT (Life technologies) and 200 U of Superscript III RT enzyme mix (Life technologies) was added to each tube. The reaction was incubated at 50 °C for 50 min in a thermal cycler (Kyratech) and then for 10 min at 85 °C followed immediately by incubation on ice.

cDNA was stored at 4 °C for short term storage and at -20 °C for longer-term storage.

Chapter 3

Characterisation of the *TLO* genes in *Candida dubliniensis*.

3.1 Introduction

As discussed in Chapter 1, the *TLO* genes in *Candida albicans* and *Candida dubliniensis* have remained uncharacterised until recently. In this chapter, molecular and bioinformatic techniques were utilised in order to explore the characteristics of the *TLO* genes in *C. dubliniensis* and this was performed in order to gain an insight into the functions of this important gene family and to begin to characterise the *TLO* mutant strains.

Firstly, using a combination of Polymerase Chain Reaction (PCR) and Southern immunoblotting, the presence and genotype of the *TLO* genes was explored. Likewise, after disruption and re-introduction of the *TLO* genes in *C. dubliniensis*, PCR as well as Southern immunoblotting was used in order to confirm putative deletions.

Secondly, using a number of *in silico* tools, the *TLO* genes and their respective putative proteins in *C. dubliniensis* were characterised. Homology, functional and syntenic comparisons were carried out both with each other and with other members of the *Saccharomycetaceae*, including *C. albicans* and *S. cerevisiae*. As discussed, it had been reported that the *TLO* genes showed homology to Med2 in *Saccharomyces cerevisiae*. Recent studies have suggested that the Tlos in *C. albicans* are in essence the previously un-annotated Med2 subunits of the Mediator complex that were not characterised until recently (Zhang *et al.*, 2012). This relationship was explored using bioinformatic comparisons.

In order to determine whether *TLO1* and *TLO2* were actively transcribed in *C. dubliniensis*, the expression of the mRNA of *TLO1* and *TLO2* was determined at a range of time-points using quantitative Real-Time PCR (qRT-PCR). qRT-PCR allows the user to assess levels of transcription of a gene and this technique is used widely (Bustin *et al.*, 2009; Marotta *et al.*, 2013) and relies on the PCR method with the inclusion of a non-specific fluorescent dye (SYBR Green) which intercalates with double stranded DNA amplicons as the reaction progresses (Applied Biosystems, 2011). The templates used in this study consisted of single stranded complementary DNA (cDNA), which was reverse transcribed from total RNA extracted from cells in a particular growth phase/condition. Relative expression of the *TLO*s was determined in comparison to *ACT1*, a constitutively expressed gene in *C. dubliniensis* (O'Connor, 2009).

Finally, as will be outlined later in this study (Chapter 5), disruption of *TLO*s affected gene expression on a global scale both by repression and activation. In combination with this and their likely relationship with Mediator, it was predicted that these proteins would be localised to the nuclear compartment where transcriptional regulation occurs. In past studies involving transcriptional effectors (Cassola *et al.*, 2004; Giacometti *et al.*, 2006), green fluorescent protein has been used to allow visualisation of the protein within the bounds of the cell. In this study, an improved method (Milne *et al.*, 2011) for construction of a *TLO-GFP* fusion cassette was used to allow expression and translation of a Tlo1-Gfp fusion protein. In tandem, nuclei were stained with 4'6-diamidion-2-phenylindole (DAPI), which selectively binds and fluoresces at AT-rich regions of DNA (Kapuscinski, 1995)

The analyses and experiments within this Chapter provide the basis for many future experiments to investigate the role and functions of the *TLO* genes and Tlo proteins, without which it would be difficult to infer any meaningful conclusion about their effects in *C. dubliniensis* and *C. albicans*.

3.2 Materials and Methods

3.2.1. Chemicals, buffers, solutions & oligonucleotides

All chemicals discussed in the following sections in this chapter were supplied by Sigma-Aldrich, unless otherwise stated. All solutions were filter sterilised using Steritop Vacuum-driven filtration systems with a 0.22 μM membrane (Merck-Millipore) unless noted otherwise. All plasticware and glassware were sterilised by autoclaving prior to use, as described in section 2.1.3. All oligonucleotides (primers) were manufactured by Sigma-Aldrich.

3.2.2. Bioinformatic analyses of *TLO* genes

A number of different resources were used to analyse and compare the *TLO* gene sequences. Basic information was obtained from CGD (Inglis *et al.*, 2012) and GeneDB (Logan-Klumpler *et al.*, 2012). Basic analyses were carried out using Serial Cloner (Serial Basics, France) and CLC sequence viewer (CLCBio, Qiagen). Analyses of repeat regions were performed using REPFIND (Betley *et al.*, 2002) and DNA sequence alignments utilised the Emboss NEEDLE algorithm (Rice *et al.*, 2000). GO-term analysis and assessment of synteny was performed at CGD (Inglis *et al.*, 2012).

3.2.3. Bioinformatic analyses of Tlo proteins

Protein sequences of *TLO* genes in *C. dubliniensis* and *C. albicans* were obtained from CGD (Inglis *et al.*, 2012) and aligned using t-coffee servers (Notredame *et al.*, 2000; Di Tommaso *et al.*, 2011). Multiple sequence alignments (MSA) were carried out using t-coffee-msa, clustalW-msa and muscle-msa algorithms (McWilliam *et al.*, 2013). Alignment data was saved as a fasta file and visualised using the desktop version of Jalview (Waterhouse *et al.*, 2009). Alignments were coloured based on identity and images were exported as .eps files and presented as shown in Figure 3.8.

Identification of regions of identity to other known proteins was assessed using pfam (Finn *et al.*, 2014), which identified domains that possessed homology (either inferred, curated or computational) to families of proteins across eukaryotes. Localisation patterns were predicted using LocTree3 (Goldberg *et al.*, 2014) as part of the predictprotein software suite (Kaján *et al.*, 2013).

3.2.4. Construction of Tlo-Gfp fusion proteins

Plasmid SBC153 was obtained from Milne *et al.* (2011) which contained the *GFP* orf sequence followed by an *ADH1* termination sequence. The inclusion of a nourseothricin resistance cassette allowed for selection and maintenance of strains. Oligonucleotide primers were designed with complementary sequences to both the gene of interest (*TLO*) and the *GFP-NAT* cassette so that PCR amplification would create a fusion Tlo-Gfp protein (in-frame). PCR was carried out as described in section 2.3.1, products were cleaned as described in section 2.3.2. and DNA encoding fusion proteins was transformed into Wü284 as described in section 2.2.8. using 100 μg/ml nourseothricin as a selective agent. Proper recombination of DNA sequence was confirmed by PCR (section 2.3.1) and Sanger sequencing (section 2.2.5).

3.3. Results

3.3.1. Confirming the genotypes of *C. dubliniensis TLO* mutant strains.

3.3.1.1. Using PCR to confirm genotype.

Disruption of the *TLO* genes in *C. dubliniensis* strain Wü284 was carried out previously as described (Jackson *et al.*, 2009) using the *SAT1*-flipper cassette system (Reuss *et al.*, 2004). Briefly, this involved insertion of the *SAT1*-flipper cassette successively in the place of each allele of the gene of interest by site-directed homologous recombination of gene-flanking sequences. Successful transformants were selected using nourseothricin and confirmed by PCR. The cassette was then induced to 'flip' out by expression of the flippase through growth on maltose. It was necessary to confirm the presence or absence of alleles of *TLO1* and *TLO2* in the mutant strains described in Table 2.1. prior to commencing further characterisation.

To confirm the deletion of *TLO1* in strain *Δtlo1* and the deletion of *TLO2* in strain *Δtlo2*, PCR was carried out using primers TLO1L/TLO1R and TLO2L/TLO2R (Figure 3.1) to detect intact copies of *TLO1* and TLO2 respectively. In both cases, the absence of a product in mutant strains compared to a clear amplicon (of 916 bp and 507 bp respectively) in wild-type strain Wü284, indicated the absence of the intact gene. PCR was also carried out on putative heterozygous *TLO* deletion mutants using the same primer pairs, which confirmed the presence of the *TLO1* in *Δtlo1/TLO1*. As discussed below, a *Δtlo2/TLO2* strain did not exist due to the truncation of one allele of *TLO2* in Wü284.

Primers located further up and downstream of *TLO1* and *TLO2* were also used in additional confirmatory PCR experiments. Amplification of a larger upstream and downstream region in conjunction with the coding regions of *TLO1* or *TLO2* was performed in order to determine and confirm allelic heterozygosity or homozygosity. Primer pairs CTA21KF/ CTA21SIR were used to amplify a 1783 bp region flanking and including *TLO1* (Figure 3.1). When the gene was deleted (*tlo1::FRT*), a shorter 820 bp amplicon was produced, allowing successful differentiation between a heterozygous deletion and homozygous allelic deletion. Likewise, for *TLO2*, primer pair CTA2F/CTA2R were used to amplify a 1611 bp product flanking and including the *TLO2* orf (Figure 3.1). When the orf was deleted (*tlo2::FRT*), a 537 bp product was amplified allowing confirmation of the

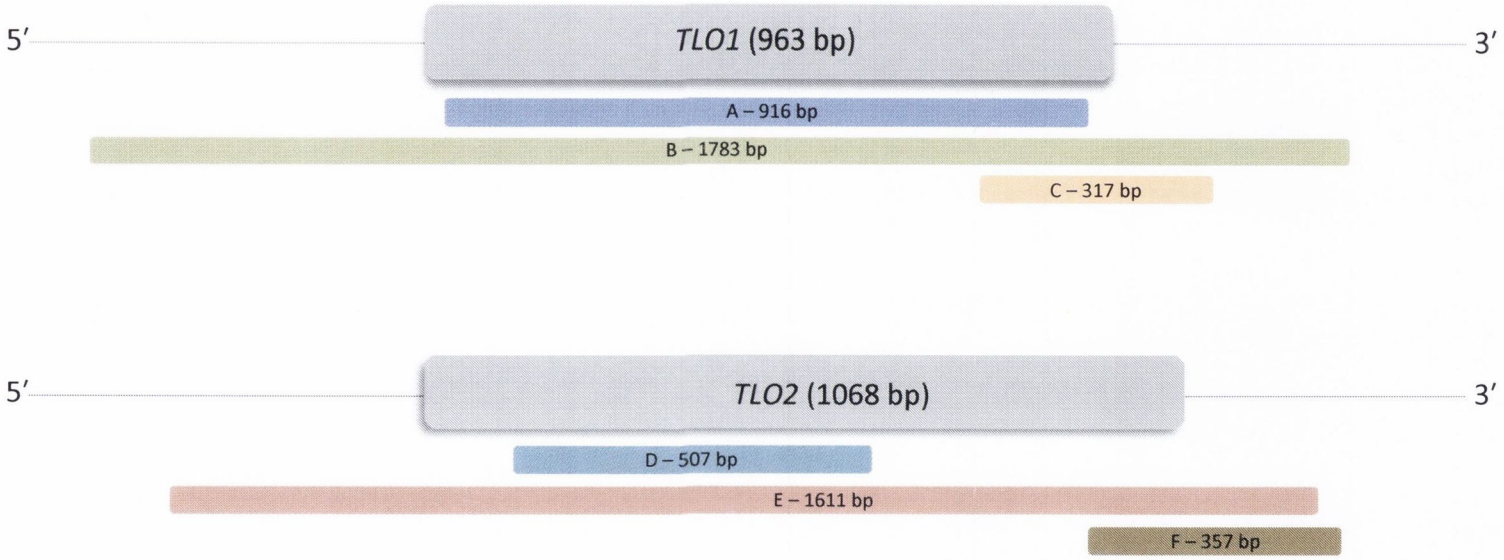

Figure 3.1. Amplification of *TLO1* and *TLO2*

Schematic diagram indicating the different amplicon sizes and locations of amplified fragments generated during reactions using primer pairs TLO1L/TLO1R (A), CTA21KF/CTA21SIR (B), TLO1BF/TLO1BR (C), TLO2L/TLO2R (D), CTA2F/CTA2R (E) and TLO2BF/TLOBR (F) as outlined in Section 3.3.1.1. Diagrams and amplicons are fully to-scale based on the *C. dubliniensis* CD36 genome sequence and the sizes of each amplicon and gene are indicated. Only one allelic copy is shown for ease of illustration.

homozygous deletion. Both deletions were confirmed to be homozygous for *tlo1::FRT* or *tlo2::FRT* in strains Δ*tlo1* and Δ*tlo2* respectively. Also, the double *TLO* mutant ΔΔ*tlo* was confirmed in the same way. Some issues with non-specific amplification were encountered leading to design of new primers TLO1BF/TLO1BR and TLO2BF/TO2BR, which amplified the 3-prime internal fragment of the gene and the downstream flanking region of *TLO1* and *TLO2*, respectively (Figure 3.1). The 3-prime region (317 bp) of *TLO1* was detected in Wü284 and strain Δ*tlo2* but not in strains Δ*tlo1* or ΔΔ*tlo*, thus confirming the deletion of *TLO1* in these strains. The 3-prime region of *TLO2* (357 bp) was detected in wild-type strain Wü284 and strain Δ*tlo1*. However, unexpectedly this 357 bp fragment of *TLO2* could also be amplified from strains Δ*tlo2* and ΔΔ*tlo*, despite predictions that this region of *TLO2* should be deleted in these strains. This finding suggests that there exists a portion of the 3-prime of *TLO2* that remains in the Δ*tlo2* and ΔΔ*tlo* mutant strains.

3.3.1.2. Using Southern immunoblotting to determine genotype.

In order to unambiguously confirm the presence or absence of the *TLO* genes in the mutant strains of *C. dubliniensis*, Southern immunoblot analysis was performed (Figure 3.2). Primers TLO1SFW and TLO1SRE were designed to amplify a 200 bp digoxigenin (DIG) - labelled probe (Figure 3.3) 100 % homologous to the 5′ region of *TLO1* and 80 % homologous to the corresponding region in the 5′ sequence of *TLO2* (the region of highest conservation). In order to differentiate *TLO1* and *TLO2* hybridising bands, the genome sequence was analysed for restriction fragment length polymorphisms that could be used for the differentiation of *TLO1* and *TLO2* by size. *Nde*I was predicted to generate a *TLO1* hybridising band of 14.07 kb and a *TLO2* hybridising fragment of 5.96 kb.

In the case of the Δ*tlo1* mutant, one band was observed at ~6 kb which correlated with the presence of the *TLO2* hybridising fragment (Figure 3.2. A). For the Δ*tlo2* mutant, one band was present at ~14 kb which was also consistent with the expected fragment size containing the *TLO1* gene (Figure 3.2. A). The sample containing DNA from Wü284 displayed a band each at 14 kb and 6 kb, with the former showing increased intensity, perhaps due to increased homology of the probe to *TLO1* (Figure 3.2. A). No bands were observed in the ΔΔ*tlo* sample (Figure 3.2. A).

Heterozygous strains were also probed for the presence of *TLO*s. Both *Δtlo1/TLO1* and *Δtlo2/TLO2* were putative heterozygous mutants for *TLO1* and *TLO2* respectively. The banding pattern for *Δtlo1/TLO1* was as expected, with both a 14.07 kb product, corresponding to the remaining allele of *TLO1* and a 5.96 kb product corresponding to *TLO2* being detected (Figure 3.2. B). However, only the 14.07 kb *TLO1* hybridising band was detected in the putative *Δtlo2/TLO2* strain (Figure 3.2. B). Our inability to detect a second intact allele of *TLO2* in the putative *Δtlo2/TLO2* mutant strain using a 5'-prime homologous probe suggests that the second allele of *TLO2* is either absent or truncated at the 5'-prime end. Interestingly, the PCR data from section 3.3.1.1, indicates the presence of a 3'-prime fragment of *TLO2* in all mutant strains, despite predictions that this region should be deleted in strains Δ*tlo2* and ΔΔ*tlo*. Taken together, the PCR data and the Southern immunoblot data indicate that strain Wü284 harbors one intact, full-length copy of *TLO2* and one truncated copy consisting of a short 3'-remnant.

3.3.2. Bioinformatic analysis of *TLO* genes

3.3.2.1. Basic analyses of the *TLO* genes in *C. dubliniensis*

TLO1 (*Cd36_72860*) is 963 nucleotides in length and is encoded (oriented with respect to the Watson strand) on chromosome 7 in *C. dubliniensis*. It is located at position 734,111 to 735,073 internally on the chromosome, which is approximately 1.022 Mbp in length (Jackson *et al.*, 2009) *TLO2* (*Cd36_35580*) is 1068 nucleotides in length and is encoded (oriented with respect to the Crick strand) on the ancestral chromosome R. It is located in the sub-telomeric region at position 2,254,730 to 2,253,663 on the chromosome, which is approximately 2.27 Mbp in length (Jackson *et al.*, 2009). *TLO1* and *TLO2* have 42.1 % and 40.9 % GC content respectively.

3.3.2.2. Comparison of *TLO* genes in *C. dubliniensis*

Jackson *et al.* (2009) provided data showing that the *TLO* genes in *C. dubliniensis* strain CD36 were more divergent from each other compared to the level of divergence observed within the *C. albicans TLO* family. To verify this in strain Wü284, it was necessary to compare the *TLO* genes of Wü284 to the annotated sequences in *C. dubliniensis* strain CD36 described by Jackson *et al.* (2009). This was carried out using small-scale Sanger sequencing (Source

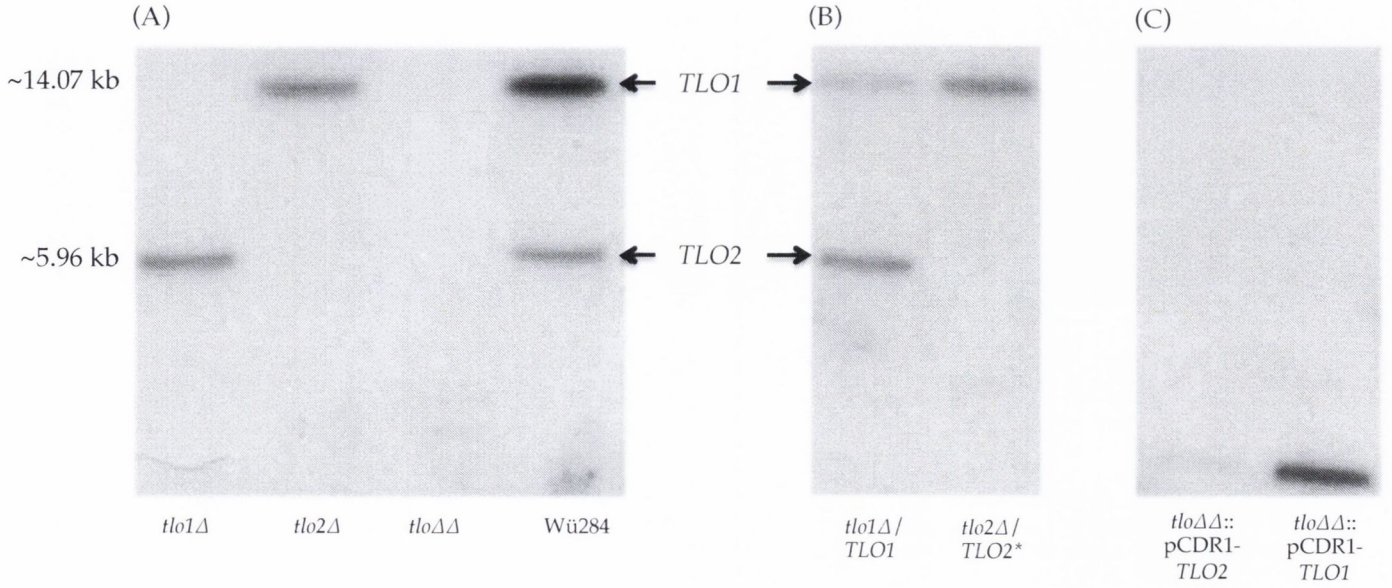

Figure 3.2. Southern immunoblot used to confirm *TLO* genotypes.

Southern hybridisation immunoblots of *Nde*I-digested genomic DNA from *Candida dubliniensis*. Fragments were detected using a digoxigenin (DIG) -labelled probe of 200 bp. Fragments in panels (A) and (B) were deduced using sequence prediction and DIG-labelled ladder (not shown) to have fragment sizes of 14.07 kb and 5.96 kb for those containing *TLO1* and *TLO2* respectively. Strains probed for and gene fragments identified are indicated.

*Putative Δ*tlo2*/*TLO2* mutant strain

A)

```
Score =   361 bits (400),  Expect = 2e-104
Identities = 200/200 (100%), Gaps = 0/200 (0%)
Strand=Plus/Plus

TLO1  51    AAAGGCCTCAGGGTACATCTTCGAAATAATCAACCATAACAAAAAGCAAAGCAATTTGAT  110
            ||||||||||||||||||||||||||||||||||||||||||||||||||||||||||||
Probe  1    AAAGGCCTCAGGGTACATCTTCGAAATAATCAACCATAACAAAAAGCAAAGCAATTTGAT  60

TLO1  111   AACTGGCCCCAACAATGAACTAATCCAACAATCGATCATACAACAACTAAGCGACCACAT  170
            ||||||||||||||||||||||||||||||||||||||||||||||||||||||||||||
Probe  61   AACTGGCCCCAACAATGAACTAATCCAACAATCGATCATACAACAACTAAGCGACCACAT  120

TLO1  171   TCAAGGGTTTAATGATATCTTAGACCAAACAGTTTCCAAATTTAATGATGCAAAGTGGTG  230
            ||||||||||||||||||||||||||||||||||||||||||||||||||||||||||||
Probe  121  TCAAGGGTTTAATGATATCTTAGACCAAACAGTTTCCAAATTTAATGATGCAAAGTGGTG  180

TLO1  231   TGTCGCCGTTATGATTGAGA  250
            ||||||||||||||||||||
Probe  181  TGTCGCCGTTATGATTGAGA  200
```

B)

```
Score =   244 bits (270),  Expect = 4e-69
Identities = 173/198 (87%), Gaps = 0/198 (0%)
Strand=Plus/Plus

TLO2  51    AAAGTCTGCAGGGTTCATGTTTGAGATAATCAACCATAACAGAGAGCAAAGCAATTTGAT  110
            |||| |  ||||||  ||| || || |||||||||||||||| | ||||||||||||||||
Probe  1    AAAGGCCTCAGGGTACATCTTCGAAATAATCAACCATAACAAAAAGCAAAGCAATTTGAT  60

TLO2  111   AGCTGGACCCAACAATGAACTCATCCAACAATCGATTGTGCAACAACTAAACGACAACAT  170
            | |||| ||||||||||||||| |||||||||||||||  | |||||||||| |||| ||||
Probe  61   AACTGGCCCCAACAATGAACTAATCCAACAATCGATCATACAACAACTAAGCGACCACAT  120

TLO2  171   TCAAAAGTTTAATGATATCTTAGACCAGACCGTTTCGAAGTTTAACGATGCAAAGTGGTG  230
            ||||  |||||||||||||||||||| || ||||| || ||||| ||||||||||||||||
Probe  121  TCAAGGGTTTAATGATATCTTAGACCAAACAGTTTCCAAATTTAATGATGCAAAGTGGTG  180

TLO2  231   TGTTGCCGTTATGATTga  248
            ||| ||||||||||||||
Probe  181  TGTCGCCGTTATGATTGA  198
```

C)

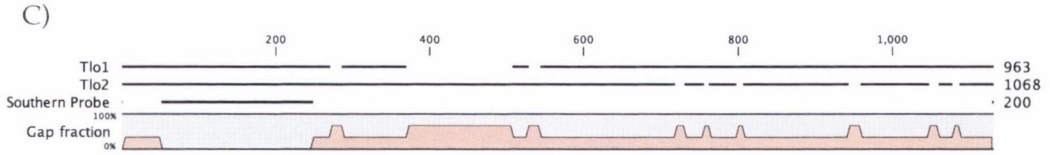

Fig 3.3. Specificity of DNA probe used in Southern immunoblotting.

Sequence comparisons were carried out in Serial Cloner using NCBI BLAST between Tlo1 (A) or Tlo2 (B) and the DNA probe sequence used for Southern immunoblotting. Overall schematic diagram for comparison purposes (C) is shown.

Biosciences). Both *TLO1* and *TLO2* from strain Wü284 were observed to be 100 % identical to their published sequences from strain CD36 (*Cd36_72860* and *Cd36_35580* respectively).

Further to this, the confirmed sequences were aligned using Emboss NEEDLE (Rice *et al.*, 2000) pairwise global alignment. *TLO1* and *TLO2* are 968 and 1063 bp in length respectively and display 65.8 % identity (Figure 3.4. A). The increased length of *TLO2* can mostly be accounted for by the insertion of highly repetitive regions of nucleotides as can be observed in the expanded alignment (Figure 3.4. B). Analysis of the repeats found within each gene was carried out using REPFIND (Betley *et al.*, 2002) which found that repeat sequences in *TLO1* are mostly composed of short clustered repeats (Figure 3.5. A), whereas *TLO2* contains longer, more distant repeat motifs alongside many short repeats (Figure 3.5. B) as found in *TLO1*. The longer repeat sequences in *TLO2* are centered around the regions with lowest homology between *TLO1* and *TLO2*, and account for most of the increased length of *TLO2*. The repeats in *TLO2* also have an effect in significantly altering the amino acid sequence, which will be explored in section 3.3.4. Sequence divergence within the *TLO* family of genes in *C. dubliniensis* is greater than that of the *C. albicans TLO* genes. In fact, the nucleotide content of the *C. dubliniensis TLO1* and *TLO2* genes is more similar to *C. albicans TLO16* and *TLO2* respectively, than each other

3.3.2.3. Synteny and homology with other species

TLO genes were analysed for synteny across other *Saccharomycetaceae* genome sequences using the *Candida* Genome Order Browser (CGOB) (Maguire *et al.*, 2013). *TLO1* is located on the same chromosome as *TLO16* in *C. albicans* strain *SC5314* but does not display a syntenic relationship (Figure 3.6). *TLO2* displayed a greater conservation of synteny among the species compared (Figure 3.7) including *TLO2* in *C. albicans SC5314*. The *TLO* genes and genes displaying homologous sequence were arranged phylogenetically using Semphy (Ninio *et al.*, 2007) at CGD (Inglis *et al.*, 2012) as outlined in Figure 3.8. Identity across other members of the *Saccharomycetaceae* was observed for *TLO2* (Figure 3.8. B).

3.3.3. Confirmation of expression of *TLO* genes

Oligonucleotide primers specific for *TLO1* and *TLO2* were designed according to MIQE guidelines and recommendations (Bustin *et al.*, 2009). Primers

specific for the 3'-prime end of *TLO1* and were chosen, however due to the repetitive nature of the *TLO2* 3'-prime end, primers specific for the 5'-prime end were chosen. Primer sequences were submitted to Primer BLAST (Ye *et al.*, 2012), ordered and tested for suitability by checking their efficiency compared to each other (efficiency values between 0.8 and 1.2). In order to quantify expression, Quantitative Real-Time PCR (qRT-PCR) was carried out on mRNA samples prepared from cultures grown in YEPD at 37 °C at various time points ranging from 30 min to 24 h. Results were compared against the endogenous control gene *ACT1* (Figure 3.9)

Expression of *TLO1* was higher overall compared to *TLO2*, but both were expressed at significantly lower rates compared to *ACT1* expression (Figure 3.9. A). Expression of *TLO1* is relatively low in the early phases of growth (5 – 23 % compared to *ACT1*). Expression appears to increase dramatically at both 8 h (21 % versus *ACT1*) and 24 h (76 % versus *ACT1*) time-points corresponding to exponential and early stationary phases, respectively. *TLO2* expression remains constitutively low (under 4 % compared to *ACT1*) until 8h, during which it begins to increase (to 10 % of *ACT1*). The expression of *TLO2* continues to lag behind the expression of *TLO1* in the wild-type background. By 24 h (stationary phase), *TLO1* is expressed at 76 % of *ACT1* levels and *TLO2* is expressed at 43 % of *ACT1* levels (Figure 3.9. A).

Disruption of *TLO2* in Wü284 (Δ*tlo2*) results in a slight decrease in expression of *TLO1* overall compared to wild-type (up to 20 %) which was particularly evident at later time-points (Figure 3.9. B). *TLO1* expression was not detected at 3 h and 5 h time-points in Δ*tlo2* (Figure 3.9. B). Disruption of *TLO1* in strain Δ*tlo1* affected expression levels of *TLO2* in a similar manner, with *TLO2* expression decreased in Δ*tlo1* by up to 75 % of that observed in wild-type cultures (Figure 3.9. C). It appeared that *TLO2* expression in the Δ*tlo1* mutant was slightly elevated compared to wild-type during the 3 h and 5 h time-points, however problems with reproducibility of these expression datasets prevented any significance being detected (Figure 3.9. C).

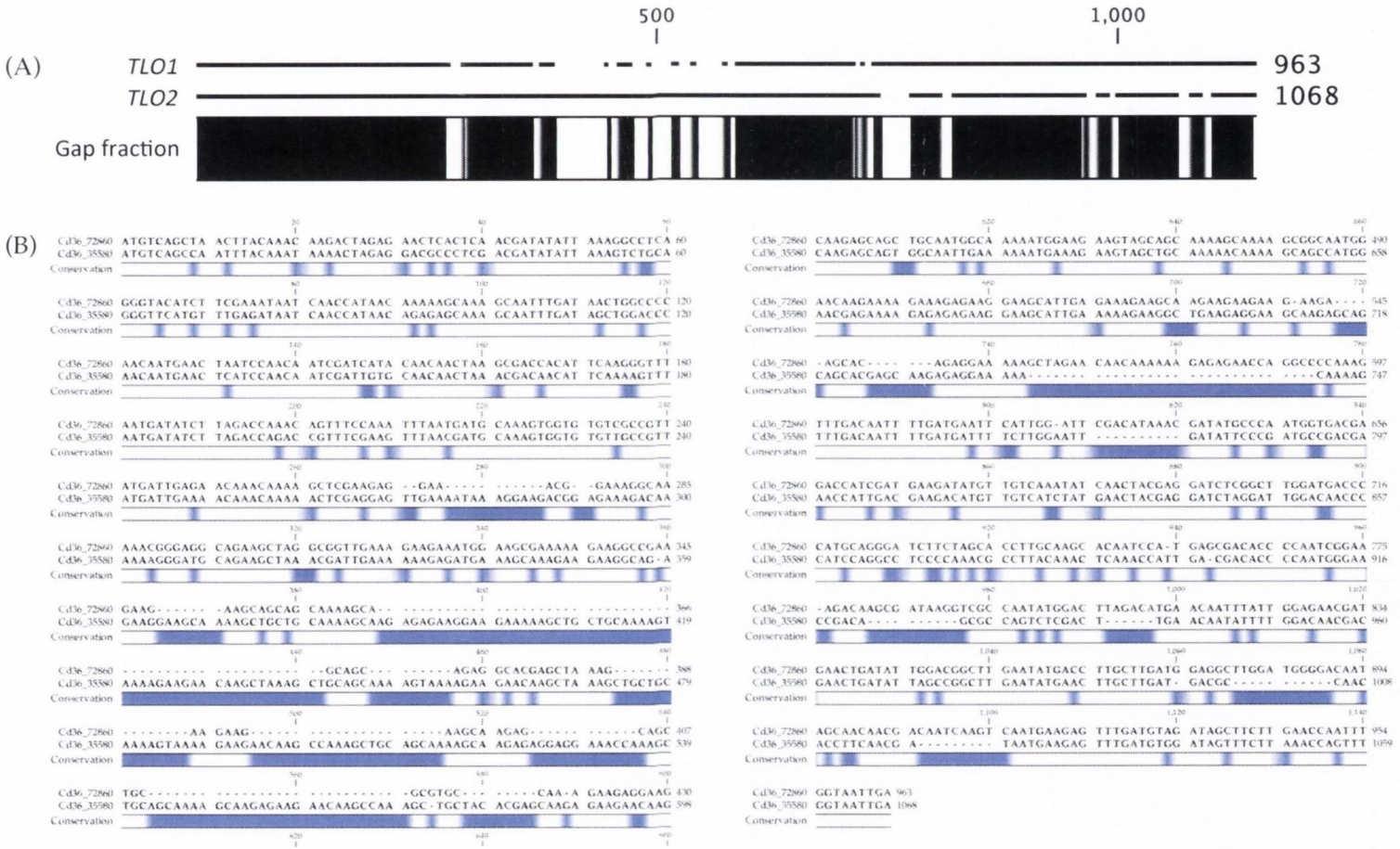

Figure 3.4. Global alignment of *C. dubliniensis TLO* genes.

The confirmed sequences of *TLO1 (Cd36_72860)* and *TLO2 (Cd36_35580)* from strain Wü284 were aligned using EMBOSS Needle (Rice, *et al.*, 2000). An overview (A) of the alignment was created using CLC Sequence Viewer (Qiagen) and a more detailed illustration of the alignment was then created (B) Regions of homology between the genes are displayed below the alignment with divergent regions highlighted in blue.

Figure 3.5. Repeat motifs found in *C. dubliniensis TLO1* and *TLO2*.

REPFIND (Betley *et al.*, 2002) was used to assess and compare the sequences of *TLO1* (A) and *TLO2* (B) for repeat regions. The 25 top scored repeat motifs are displayed, with p-values indicated (the smaller the number, the lower the probability that the repeats exist by chance). Those repeat motifs that are most significant are outlined with a red panel. Coloured boxes are used to indicate the strongest computed cluster of repeats. Each repeat sequence is indicated. Φ denotes the triplet motif discussed in section 3.3.2.2.

Fig 3.6. *C. dubliniensis TLO1* does not show synteny with regions of other genomes.

Candida Gene Order Browser (CGOB) showing the *C. dubliniensis TLO1* gene and syntenic genes in other species. Each box represents a single gene. Each species is outlined on the right of the illustration. *C. dubliniensis TLO1* is marked with a gold border and large red arrow. Homologous genes are stacked in adjacent columns and synteny is indicated by solid black connectors joining chromosomally adjacent genes. Grey connectors indicate intergenic space. Absence of connectors indicates a non-adjacent gene. Chromosomes are indicated in each box. Grey boxes indicated a lack of synteny. Arrows beneath each box indicate direction of transcription. Source: http://cgob.ucd.ie

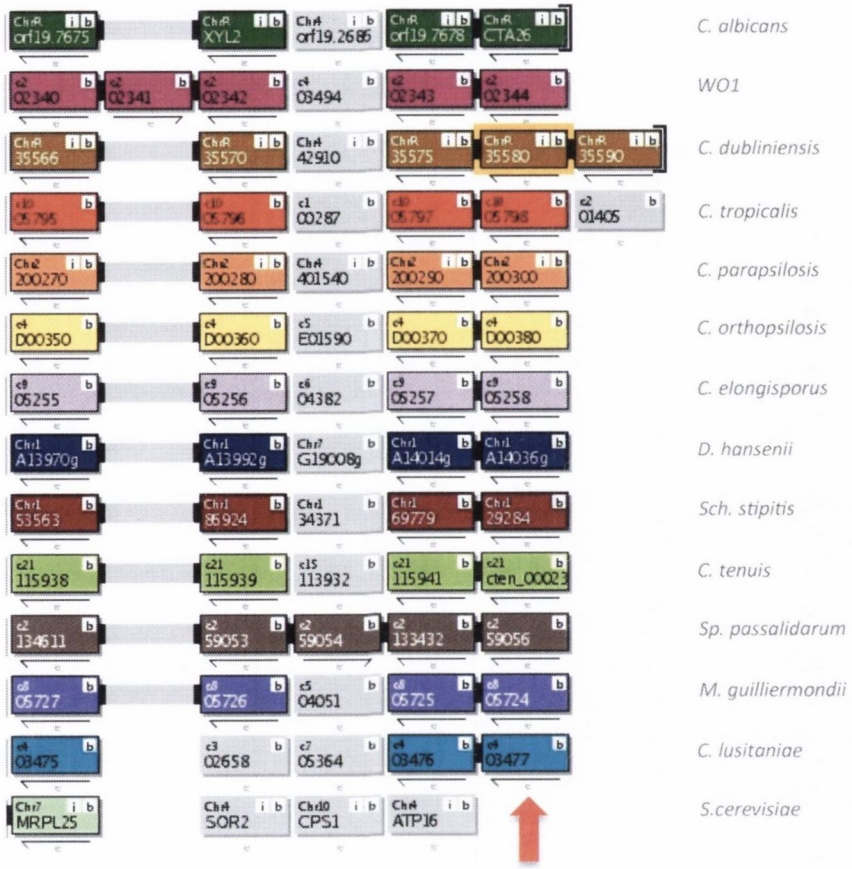

Fig 3.7. *C. dubliniensis TLO2* displays synteny with regions of other genomes.

Candida Gene Order Browser (CGOB) showing the *C. dubliniensis TLO2* gene and syntenic genes in other species. Each box represents a single gene. Each species is outlined on the right of the illustration. *C. dubliniensis TLO2* is marked with a gold border and large red arrow. Homologous genes are stacked in adjacent columns and synteny is indicated by solid black connectors joining chromosomally adjacent genes. Grey connectors indicate intergenic space. Absence of connectors indicates a non-adjacent gene. Chromosomes are indicated in each box. Grey boxes indicated a lack of synteny. Arrows beneath each box indicate direction of transcription. Source: http://cgob.ucd.ie

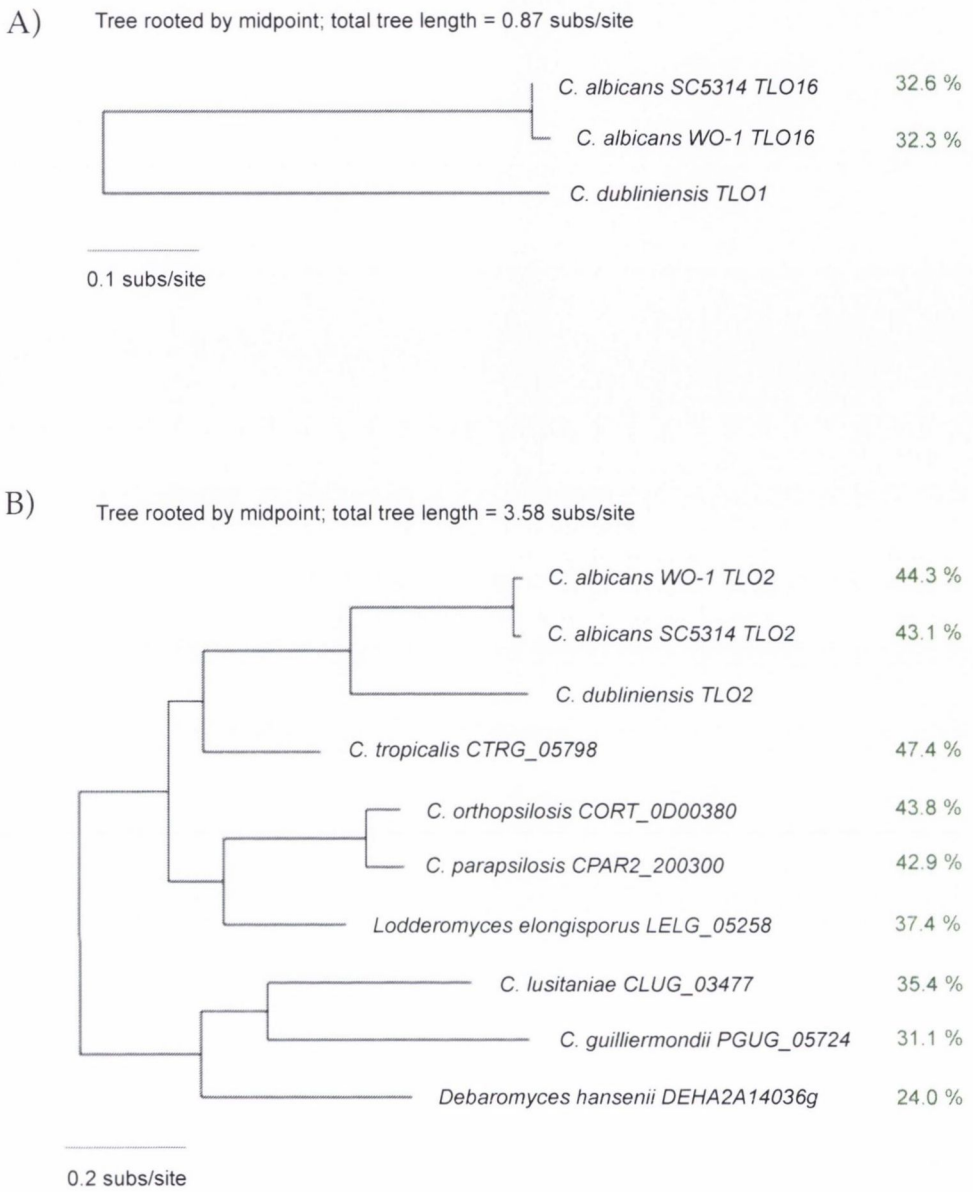

Fig 3.8. *TLO* homology across other *Saccharomycetaceae* .

Maximum likelihood trees were produced using Semphy (Ninio, Privman, Pupko, & Friedman, 2007) at *Candida* genome database (Inglis *et al.*, 2012) to display predicted relatedness of genetic sequences of the genes displaying closest homology to *TLO1* (A) and *TLO2* (B). Species names are shown along with the gene name (in italics). Percentage identity is shown in green to the right of each species.

Adapted from source: http://www.candidagenome.org

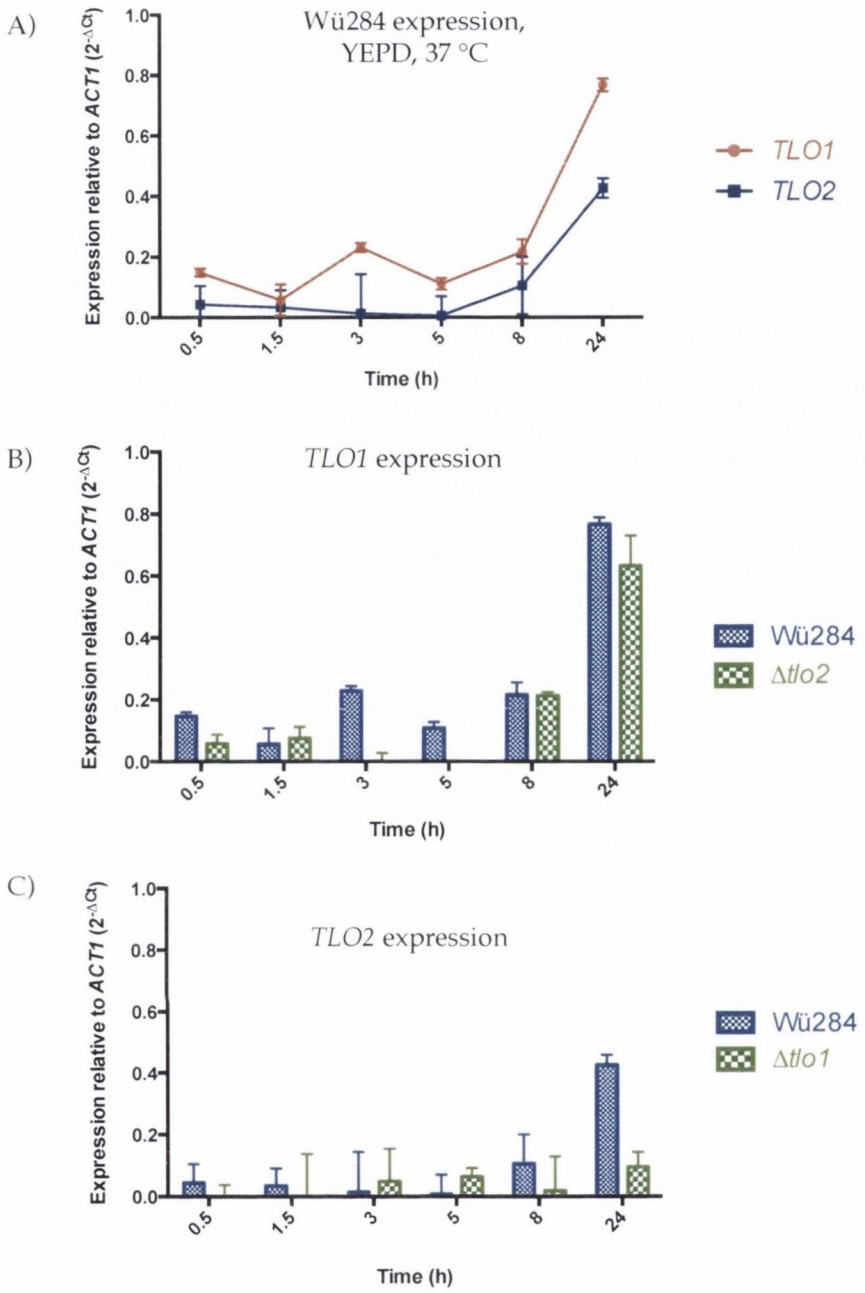

Fig 3.9. Expression of *TLO* genes in *C. dubliniensis*

Expression of *TLO1* and *TLO2* mRNA levels in *C. dubliniensis* strains during growth in YEPD at 37 °C. A) Expression of both *TLO1* and *TLO2* in Wü284, B) expression of *TLO1* in Δ*tlo2* compared to wild-type (Wü284) and C) expression of *TLO2* in Δ*tlo1* compared to in wild-type (Wü284). Time in hours is plotted along the x-axis for each graph, whilst mRNA expression of the target gene relative to mRNA expression of *ACT1* (endogenous control) are shown along the y-axis ($2^{-\Delta Ct}$). Samples were grown in YEPD at 37 °C with shaking at 200 r.p.m. and at the relevant time-point, cells were flash frozen and RNA was prepared as described in section 2.5.1.2., followed by cDNA preparation (2.5.2.). Error bars represent the calculated combined standard deviation from the mean value of at least three separate experiments.

3.3.4. Bioinformatic analysis of the Tlo proteins

3.3.4.1. Tlo proteins across the CTG clade

C. dubliniensis TLO genes encode two putative proteins; Tlo1 which is 320 amino acids in length (molecular weight = 36087.7 g/mol) and Tlo2 which is 355 amino acids in length (molecular weight = 39746.5 g/mol); which display 58 % identity (BIOSUM62 alignment) to each other. In the previous sections, it was observed that the divergence in sequence identity between *TLO1* and *TLO2* was mostly due to the presence of repeats. This is also true for the protein sequences – Tlo2 is 25 amino acids longer than Tlo1 and contains a central repeat motif KAAAKVEKEEQ encoded for by the repeat sequence described in Figure 3.5. B, (denoted by Φ). The amino acid composition of Tlo1 and Tlo2 are relatively similar with several exceptions (Figure 3.10). The amount of alanine in Tlo2 (16.6 %) is greater than in Tlo1 (11.2 %). Likewise, the amount of lysine in Tlo2 (13 %) is greater than in Tlo1 (9.1 %). These differences, predicted by ExPASy ProtParam (Walker, 2005), are primarily due to the presence of repeat sequence in Tlo2, also accounting for its longer length. These repeat sequence have a high proportion of AAA/AAG (lysine) and GCA/GCG (alanine).

As discussed in Chapter 1, there are 14 putative Tlo proteins (14 genes and 1 pseudogene) in *C. albicans*. The Tlo proteins in *C. dubliniensis* were aligned with the *C. albicans* Tlo protein sequences using tcoffee (Di Tommaso *et al.*, 2011). The protein sequence of *S. cerevisiae* Med2 (ScMed2) was included in the alignment for reference (Figure 3.11). All proteins aligned with varying success, but there was an obvious alignment observed between all proteins at two points in each sequence, near the N-terminal and near the C-terminal (Figure 3.11). The N-terminal region of homology, which consists of approximately 119/120 residues has been suggested to be the functional subunit of Med2 (Anderson *et al.*, 2012; Zhang *et al.*, 2012). At present, the biological significance of the C-terminal homology is unknown.

Using NCBI 'blastp' (Basic Local Alignment Tool – Protein), proteins from other *Candida* species with similarity/identity in protein sequence were identified. Tlo1 showed most identity to Tlo2 in *C. dubliniensis* ($e = 6 \times 10^{-116}$), identity = 56 %), CTRG_05798 in *C. tropicalis* ($e = 6 \times 10^{-81}$, identity = 55 %), *C. maltosa* G210_0130 ($e = 6 \times 10^{-71}$, identity = 51 %), *C. parapsilosis* CPAR2_200300 ($e = 2 \times 10^{-69}$, identity = 47 %), *C. albicans* Tlo1 ($e = 6 \times 10^{-60}$, identity = 45 %). Tlo2 showed

similar levels of similarity with Tlo1 in *C. dubliniensis* ($e = 6 \times 10^{-116}$, identity = 56%), *C. tropicalis* ($e = 6 \times 10^{-81}$, identity = 55 %), *C. maltosa* G210_0130 ($e = 6 \times 10^{-71}$), *C. parapsilosis* CPAR2_200300 ($e = 2 \times 10^{69}$, identity = 47 %) and *C. albicans* Tlo1 ($e = 6 \times 10^{-60}$, identity = 45 %). The proteins in *C. parapsilosis* and *C. maltosa* are noted to have inferred homology to Med2 in *S. cerevisiae* according to pfam analysis (Marchler-Bauer *et al.*, 2013) carried out on the Med2 subunit across fungi (Bourbon *et al.*, 2004; Hallberg *et al.*, 2004).

3.3.4.2. Tlo1 and Tlo2 display homology to ScMed2

Using pfam (Finn *et al.*, 2014) alignment, similarities were identified between Tlo1 in *C. dubliniensis* and ScMed2 in *S. cerevisiae*. The amino acid sequences aligned with a bit (confidence) score of 106.9 and expectation value of $e = 4.8 \times 10^{-31}$. Tlo2 in *C. dubliniensis* did not align as well as Tlo1, giving a bit score of 69.4 and $e = 2.2 \times 10^{-19}$. For comparison, alignment of ScMed2 with Tlo1 in *C. albicans* creates a bit score of 116.9 and $e = 3.6 \times 10^{-34}$. Previously published data has suggested that p/e value of $< 1 \times 10^{-5}$ is sufficient for significance (Anderson *et al.*, 2012). In addition to ScMed2 similarities, identity was found overall to the Med2 subunit family of proteins encoded by a variety of species, e.g. *Ashbya gossypii, Kluvyeromyces lactis, C. glabrata, Scherffersomyces stipites, Lodderomyces elongisporus, Meyerozyma guilliermondii* and *S. cerevisiae.* None of these species contain *TLO* genes, but do possess a Med2 ortholog.

Tlo1 and Tlo2 were analysed using LocTree3 (Goldberg *et al.*, 2014; Kaján *et al.*, 2013) in an attempt to predict localisation of the proteins within the cell. Tlo1 is predicted with 84 % predicted accuracy to localise within the cytoplasm due to homology with the Myosin family of proteins found in many eukaryotes (Hartman & Spudich, 2012). Likewise, Tlo2 is predicted to localise to the cytoplasm only with 82 % confidence.

3.3.5. Tlo proteins may encode proteins that localise to the nucleus

In order to further investigate the localisation of the Tlo proteins within the cell, *TLO-GFP* fusion cassettes were created. Primer pairs T1GFPF/T1GFPR and T2GFPF/T2GFPR contained sequences homologous to either *TLO1* or *TLO2*, respectively, as well as the 5-prime end of the *GFP* cassette in plasmid pGFP-NAT1 (Milne *et al.*, 2011). Using *CaNAT* in the cassette as a selectable marker to

Amino Acid	% of Tlo1	% of Tlo2	Codon	Occurrences in Tlo1	Occurrences in Tlo2
Alanine (Ala)	11.2 %	16.6 %	GCG	3	0
			GCA	22	30
			GCT	5	17
			GCC	6	12
Cysteine (Cys)	0.3 %	0.3 %	TGT	1	1
			TGC	0	0
Aspartic Acid (Asp)	8.4 %	8.5 %	GAT	15	13
			GAC	12	17
Glutamic Acid (Glu)	13.8 %	13 %	GAG	12	15
			GAA	32	31
Phenylalanine (Phe)	3.1 %	3.1 %	TTT	6	8
			TTC	4	3
Glycine (Gly)	4.1 %	2.3 %	GGG	3	1
			GGA	4	5
			GGT	2	1
			GGC	4	1
Histidine (His)	0.6 %	0.3 %	CAT	1	1
			CAC	1	0
Isoleucine (Ile)	5.3 %	5.4 %	ATA	6	6
			ATT	3	9
			ATC	8	4
Lysine (Lys)	9.1 %	13 %	AAG	14	15
			AAA	15	31
Leucine (Leu)	7.8 %	7 %	TTG	12	10
			TTA	5	6
			CTA	4	3
			CTT	1	2
			CTC	3	4
Methionine (Met)	4.1 %	2.8 %	ATG	13	10
Asparagine (Asn)	9.1 %	7 %	AAT	14	9
			AAC	15	16
Proline (Pro)	1.6 %	1.4 %	CCG	0	0
			CCA	2	2
			CCT	0	0
			CCC	3	3
Glutamine (Gln)	6.6 %	5.6 %	CAG	3	3
			CAA	18	17
Arginine (Arg)	3.8 %	4.2 %	AGG	3	1
			AGA	5	10
			CGG	2	0
			CGA	1	4
			CGT	1	0
			CGC	0	0
Serine (Ser)	5.3 %	3.4 %	AGT	0	2
			AGC	7	2
			TCG	1	2
			TCA	4	2
			TCT	2	2
			TCC	2	1
			CTG	1	1
Threonine (Thr)	2.8 %	2.8 %	ACG	1	0
			ACA	3	2
			ACT	1	1
			ACC	4	7
Valine (Val)	2.2 %	2.8 %	GTG	0	3
			GTA	2	4
			GTT	2	3
			GTC	3	0
Tryptophan (Trp)	0.3 %	0.3 %	TGG	1	1
Tyrosine (Tyr)	0.6 %	0.3 %	TAT	0	0
			TAC	2	1
Stop Codon	n/a	n/a	TGA	1	1
			TAG	0	0
			TAA	0	0

Figure 3.10. Amino acid composition of Tlo proteins

Amino acid composition of both Tlo1 and Tlo2 sequences derived from published sequences (Jackson, *et al.*, 2009) were determined using ExPASy ProtParam (Gasteiger, *et al.*, 2005). Amino acids are outlined in the following format: "Amino acid name" ("Amino acid three letter code"). Each codon for each amino acid was analysed for number of incidences (codon frequency) in either Tlo1 or Tlo2 and are outlined in the right-most columns.

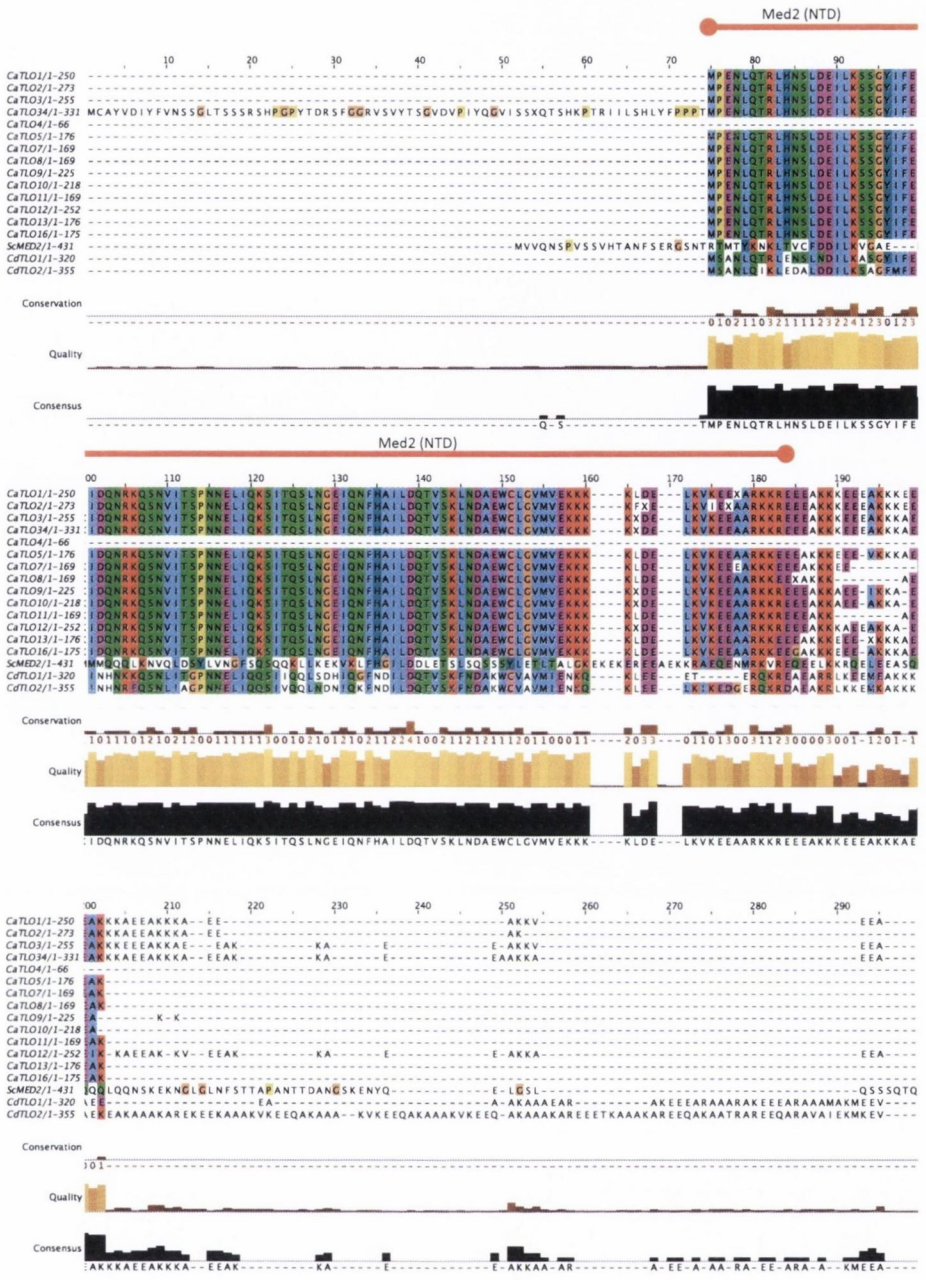

Fig 3.11. Tlo protein sequence alignment

Protein sequences for *TLO* genes in *C. albicans* and *C. dubliniensis* were aligned using tcoffee servers with tcoffee, clustalW and muscle multiple sequence alignment modes (McWilliam *et al.*, 2013). Results data file (.fasta) was visualised using Jalview (Waterhouse, *et al.*, 2009) and coloured by identity. *S. cerevisiae* Med2 (ScMed2) was included in the alignment for reference purposes. Histograms below each codon alignment indicate the conservation of the sequence, the quality of the alignment and the built consensus sequence along with confidence levels. Red line near the start of the sequence marks the N-terminal 'Med2' domain referred to in Section 3.3.4.1.

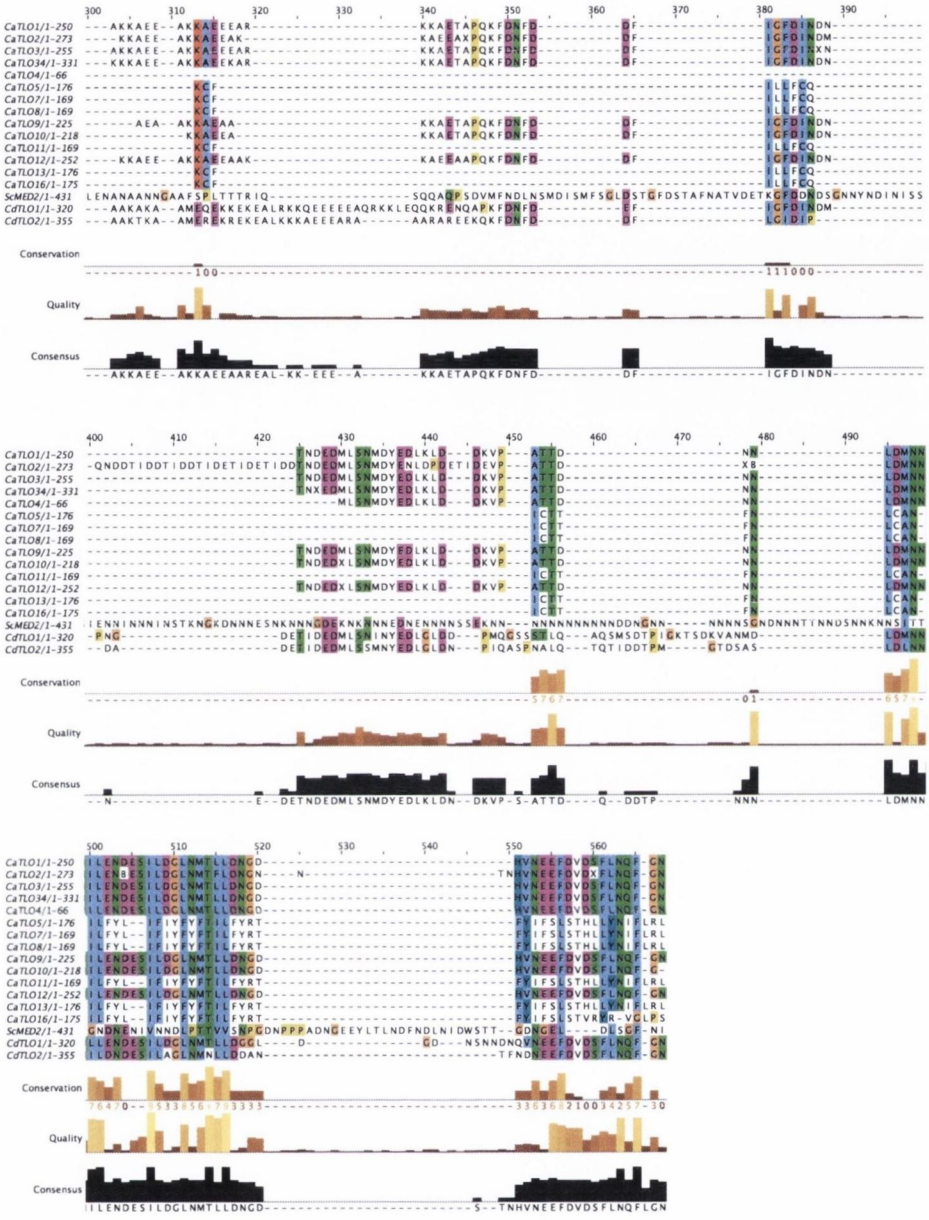

Fig 3.11. *TLO* protein sequence alignment

…continued from previous page.

confer resistance, cells were transformed (section 2.2.7.) with *TLO1-GFP* and *TLO2-GFP* to create C-terminal fusion Tlo1-Gfp and Tlo2-Gfp proteins. Presence of the correct tags was confirmed with PCR using primers TLO1-F/GFP-R and TLO2-F/GFPR.

Putative localisation of the proteins was visualised using phase-contrast microscopy with the aid of Gfp- and DAPI-optimised fluorescence filters. DAPI-staining was used in order to visualise the nuclear compartment. It had been reported by Milne, *et al.*, (2011) that carryover was not observed between the Gfp/DAPI-wavelengths using this cassette system. Under the Gfp-filter settings, Tlo1-Gfp fluorescence was observed and appeared to localise to the DAPI-stained compartment (Figure 3.12). Tlo2-Gfp localisation data was not conclusive (not pictured) as weak fluorescence was observed.

3.4 Discussion

3.4.1. *TLO* genotype

In this study, the genotypes of the deletions for *TLO1* or *TLO2* (or both) were investigated using a number of molecular techniques. PCR and Southern immunoblotting indicated correct deletion of the genes, and that *TLO1* and *TLO2* were present or absent as expected in various strains used. However, results also suggested that Wü284 only possessed only one fully intact copy of *TLO2* and that a truncated 3'-prime region of *TLO2* was detected in Wü284 and all strains derived from Wü284. This may have occurred by recombination under unknown environmental conditions. Studies have shown that locus-specific recombination resulting in allelic heterozygosity can increase with oxidative, heat and drug-induced stress and that such instances of allele recombination are higher in clinical isolates (Forche *et al.*, 2011; Rustchenko, 2007). In future studies, it would be important to determine if the allelic heterozygosity of *TLO2* is consistent across other strains. It was originally thought that the strain Δ*tlo2* (Jackson *et al.*, 2009) had two copies of *TLO2* deleted. This deletion was carried out using the *SAT1*-flipper mechanism (Reuss *et al.*, 2004). It now appears likely that only one copy was disrupted (the intact allele in Wü84) and that subsequent transformation resulted in reinsertion of the *SAT1*-flipper cassette into the same locus. The true genotype of Wü284 is most probably like that illustrated in Figure 3.13.

TLO1 in *C. dubliniensis* does not display any synteny across the *Candida* species, however *TLO2* shows synteny to *MED2*-like genes throughout most of the *Candida* species. As such, it is likely that *TLO2*, which resides on the ancestral chromosome R is the original *TLO* gene from which *TLO1* diverged from; probably through transposition events; evidence for which is discussed below.

Recent unpublished data from whole genome sequencing of *C. dubliniensis* environmental and clinical strains (McManus, 2012) has identified *TLO1* and *TLO2* in *C. dubliniensis* strains CD36, Av5, Eg3207, He30, and p7276 on chromosomes 7 and R respectively. However, in strain CD06037, *TLO2* could not be detected and in Wü284, *TLO2* was detected within contigs from chromosome 3. Further experiments will need to be performed to further clarify the presence of *TLO* genes across strains and the presence or absence of intact *TLO2* alleles. However, it is apparent from this preliminary data that the genotype of *TLO* genes may be more complex than previously suggested.

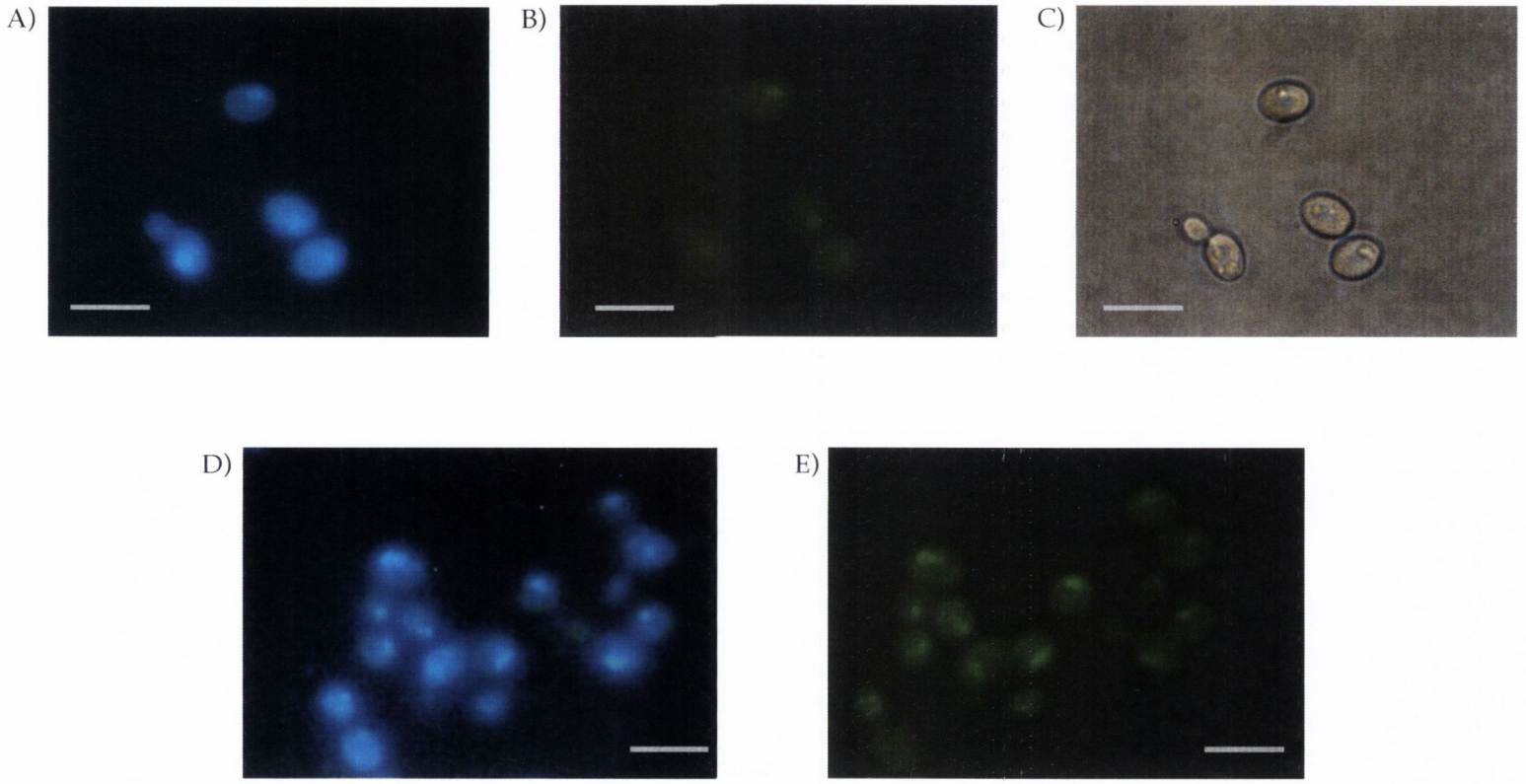

Fig 3.12. Gfp fluorescence indicates localisation of Tlos to the nuclear compartment.

Using a DAPI counterstain, Tlo1-Gfp fusion protein is shown to localise to the same area as the nucleus. Photographs of two different cultures (A) – (C) and (D) – (E) are shown. DAPI filter was applied to visualise DAPI-stained nuclei (A), (D). GFP filter was used to visualise Tlo1-Gfp fusion protein (B), (E). Phase contrast image is shown for reference (C). Scale bars indicate 15 μM length.

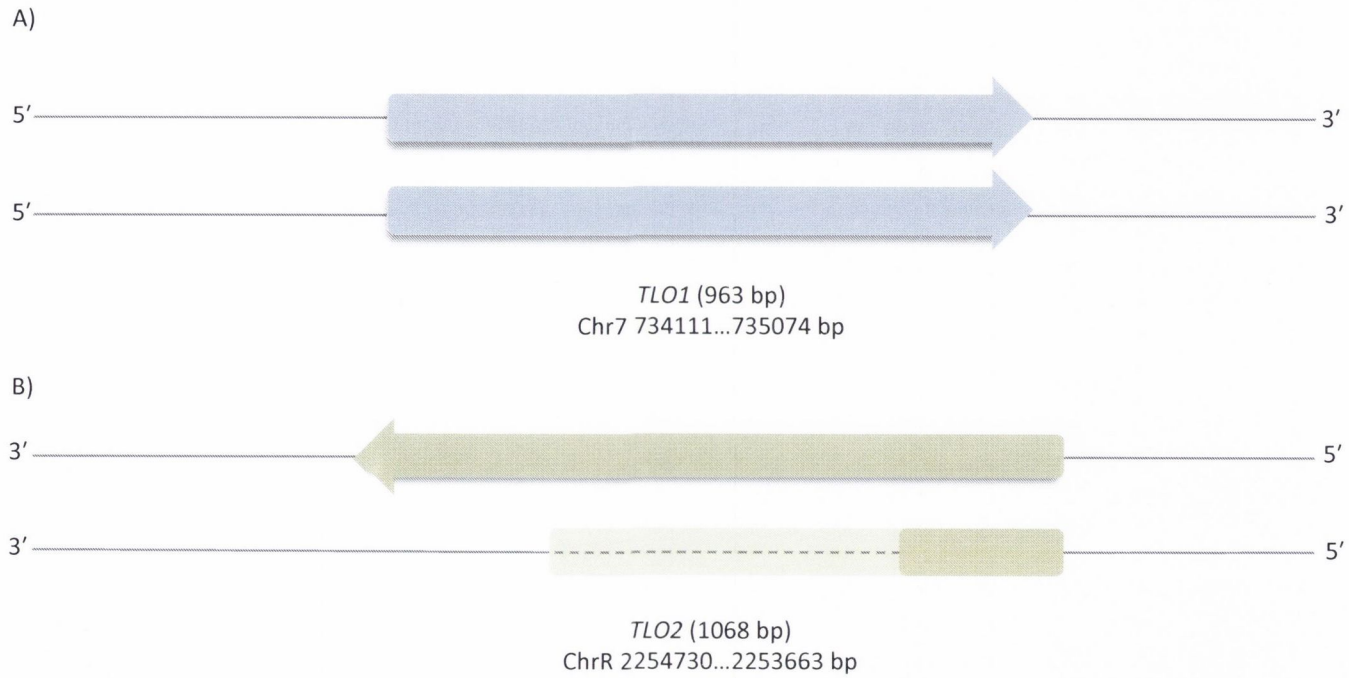

Figure 3.13. Genotype of *TLO* genes in Wü284

Schematic diagram indicating the genotype of *TLO1* and *TLO2* in Wü284. Chromosomal coordinates derived from CD36 are outlined. *TLO2* is orientated with respect to the Crick strand. For each gene, two alleles are shown. Dashed line indicates region that may not be present based on experimental results.

Analysis of expression of the *TLO* genes in *C. dubliniensis* has shown that the mRNA of *TLO1* is expressed higher (at least 2-fold) than *TLO2* in Wü284 cultured in YEPD at 37 °C. Furthermore, expression of both, particularly *TLO1* increases as cultures enter stationary phase. Expression of *TLO2* is consistently low in all strains, except during late stationary phase. qRT-PCR has shown that the expression of *TLO1* is somewhat dependent on the expression of *TLO2*, in that when *TLO2* is deleted, *TLO1* expression is decreased across all time-points in comparison, especially at 30 min, 3 h, 6 h and 24 h. Likewise, expression of *TLO2* is dependent on the expression of *TLO1* in that upon deletion of *TLO1*, *TLO2* expression is significantly lower at similar time-points as above, in particular at 24 h. The relationship in expression between these two genes may indicate that they regulate each other's expression. Also, increased expression at discrete time-points, especially during stationary phase is consistent with the roles of Mediator in mediating growth phase-specific expression (Uwamahoro *et al.*, 2012), the implications of which are discussed in Chapter 7.

3.4.2. Tlo proteins

The sequences for the putative Tlo proteins for both *C. albicans* and *C. dubliniensis* were aligned and similarities and syntenic characteristics were identified not only with each other, but also with Med2-like proteins in a variety of *Saccharomycetaceae*. Predictive analysis of the protein sequences also suggested a homology with the Med2 family of proteins (PFAM ID:PF11214). In particular, it was found that all Tlo proteins in *C. albicans* and *C. dubliniensis*, with the exception of the pseudogene Tlo34, possessed N-terminal homology to *S. cerevisiae* Med2. Med2, as described in Chapter 1 (Figure 1.2), is part of the tail region of the highly conserved Mediator complex, which is an essential complex in transcriptional regulation (Uwamahoro *et al.*, 2012). It was recently reported that Tlos represent components of the Mediator complex in *C. albicans* (Zhang *et al.*, 2012). While further evidence of this relationship will be discussed later in this study, *in silico* observations have further suggested this link. However, the same study that described Tlos as components of the Mediator complex Zhang *et al.* (2012) had noted that much of the Tlo population within the cell is not associated with the Mediator and may perform additional function(s).

In addition to N-terminal homology, a region of C-terminal homology was identified (Figure 3.11) amongst the Tlo proteins in *C. albicans* and *C. dubliniensis*.

This region may play a role in localisation or protein-protein interactions. While the function of this region has yet to be determined, Anderson, *et al.*, (2012) indicated that the *C. albicans TLO* genes can be alternatively spliced due to the presence of introns in the 3′ half of the gene and that these introns contain sequences with homology to retrotransposon LTRs. Based on the structure of these introns, they grouped the *TLO* genes into several clades. These LTR retrotransposition events have resulted in considerable divergence of the Tlo C-terminus region relative to that of ScMed2, however the function of the C-terminal region is still not known. Further evidence for such transposition events can be seen by the presence of a putative pseudogene (*TLO34*) on chromosome 1 adjacent to a coding *TLO* gene (*TLO3).* In addition, it was previously identified (Anderson *et al.*, 2012; van het Hoog *et al.*, 2007) that each *TLO* gene in *C. albicans* is flanked by LTR sequences further suggesting frequent transposition events.

Predictive analyses have suggested that the Tlos localise to the cytoplasm of the cell (LocTree3), however limited data for *Candida* species exists to allow for major comparative predictions to be carried out. The hypothesis of the Tlos' relationship with Mediator would suggest localisation to transcriptional machinery, i.e. to the nuclear compartment (Whiteside & Goodbourn, 1993). In addition, if Tlos are independent to this, acting as transcriptional activators or repressors, then localisation to the nucleus would corroborate this. In order to investigate this, experiments were carried out using Gfp-tagged Tlo proteins in *C. dubliniensis* and it appeared that localisation did occur within the nucleus for Tlo1 at least. However, ideally these experiments would be repeated with more sensitive staining procedures and using confocal microscopy to increase clarity of the images. As mentioned above, *TLO2* expression is consistently significantly lower than that of *TLO1*. Localisation of Tlo2-Gfp could not be determined, which may be as a result of this expression dichotomy.

The *TLO* genes and their encoded proteins have expanded significantly in *C. albicans* compared to *C. dubliniensis*. Bioinformatic analysis has determined that *TLO2* is the ancestral *TLO* gene in *C. dubliniensis* from which *TLO1* was derived. Further evidence for this lies in the synteny and homology of *TLO2* (significantly more than *TLO1)* to the *TLO*s in *C. albicans* and even other *Saccharomycetes*. Despite this expansion, there is much more redundancy in sequence between the *TLO* genes of *C. albicans* than *C. dubliniensis*, all of which are homologous to *ScMED2*. Then, consistent with their role as subunits of the tail region of the Mediator

complex, it is possible that *TLO* expansion has allowed a wider variety of functions that may in part account for the increased success of *C. albicans* in eliciting specific transcriptional responses. Their reduced incidence, but increased divergence in *C. dubliniensis* suggests that for whatever niche it has evolved to inhabit, two *TLO* genes are sufficient. Therefore, it is probable that there are differing functions of these two genes, which will be explored in the following chapter.

Chapter 4

Phenotypic analysis of *tlo* mutant strains of *Candida dubliniensis*

4.1. Introduction

As discussed in Chapter one, it was hoped that disruption of the *TLO* genes in *Candida dubliniensis* would allow us to characterise their function in both *C. dubliniensis* and *Candida albicans*. This in turn could provide an insight into the reason for the contrast in copy number between these closely related species. In addition, this could partly explain the dichotomy in virulence between these two species. In this section, the role(s) of the *TLO* genes in regulating common attributes of *Candida* species are explored and discussed with a view to elucidating the basic functions of this gene family. Increased understanding of the processes and functions that the *TLO* genes are involved in may illustrate their involvement in pathogenesis and contribute to our understanding of the contrasts between *C. albicans* and *C. dubliniensis*.

The differences between *C. albicans* and *C. dubliniensis* have been extensively reviewed (Moran *et al.*, 2012; Sullivan *et al.*, 2005) and are discussed in detail in Chapter One. Perhaps the most obvious difference lies in the contrasting ability to form true hyphae under a range of conditions. The formation of hyphae has been implicated as a factor in the virulence (Mayer *et al.*, 2013; Sudbery, 2011; Yang *et al.*, 2014; Yang, 2003) of *Candida* spp. and the contrasting abilities in forming hyphal cells is likely a causative factor in the differing virulence between these two species (Sullivan & Moran, 2011). As such, it is pertinent to examine the relationship between the disruption of the *TLO* genes and the formation of hyphae in *C. dubliniensis*. It has been shown previously (O'Connor *et al.*, 2010) that pre-culture in nutrient-rich YEPD at 30 °C followed by growth at 37 °C in water supplemented with 10 % foetal calf serum was a highly suitable medium for induction of hyphal formation in *C. dubliniensis*. This is due to the combination of temperature, nutrient and pH shifts afforded by this method. This medium was used for the induction of hyphae in this project.

A challenge when assessing hyphal formation is accurately differentiating between true hyphal cells and pseudohyphal cells, the biology of which have been discussed in Chapter One. For the purposes of this study, it was decided to adhere to a set of guidelines based on those in Sudbery *et al.*, (2004) in differentiating between these similar morphologies. This method allowed consistency and reduced subjectivity, thereby reducing error. Hyphae, under these criteria, are

defined as elongated germ-tubes that have no dividing walls within the cell. The presence of one or more of the following indicates that the cell is pseudohyphal:

- The presence of cross-walls or constrictions at more than one junction,
- Inconsistent cell width between cellular compartments, or
- Cell sides are not parallel

By following these guidelines and running all experiments alongside a control strain, the identification of pseudohyphae was made less subjective.

The yeast-to-hypha switch is just one of the situations in which *Candida* species can undergo morphological switching, which is reviewed in detail in Chapter One. Another major phenotypic switch observed in *Candida* is the shift between 'white' and 'opaque' cell types as outlined in Chapter One, which has been shown to be involved in a plethora of processes including mating and virulence (Soll, 2014). This study attempts to gain an insight as to whether the *TLO* genes are involved in this process.

Another known morphological change that *Candida* species can undergo is a change in cell morphology to a thick-walled, spore-like structure known as the chlamydospore. Interestingly, while relatively little is known about the reasons *Candida* form these structures, chlamydospore formation has only been observed in *C. albicans* and *C. dubliniensis* (Staib & Morschhäuser, 2007). It is widely assumed that these structures are involved in survival in harsh environments, but this is yet to be fully explored (Citiulo *et al.*, 2009). In this Chapter, the association between *TLO*s and chlamydospore formation was investigated.

An important trait of any fungus, whether environmental or pathogenic is in its ability to respond to and deal with changes in its surrounding environment. This response is most often the result of a complex genetic signaling network, induced or repressed as needed. Temperature change is perhaps one of the most fundamental of environmental factors with which all living creatures must contend. *C. albicans* and *C. dubliniensis* have adapted to grow well at temperatures ranging from ambient to body temperature (Lackey *et al.*, 2013), however *C. dubliniensis* has a slower rate of growth at 42 °C than *C. albicans* (Campanha *et al.*, 2005). This inability to efficiently handle a wider range of temperatures may be a causative factor in its inferiority as a pathogen (with elevated temperature a key part of the innate immune response in humans). The effect of *TLO* disruption on the response to this ubiquitous environmental factor is explored in this study.

The human immune response has a vast arsenal of antifungal tools other than temperature modulation in order to combat the invasion of fungal pathogens such as *Candida* spp. Activated phagocytes, as part of the innate immune system use the production of non-specific reactive oxygen species (e.g. superoxide radicals, hydrogen peroxide and hydroxyl radicals) in the defence against pathogenic organisms, exposing them to severe oxidative stress (Gantner *et al.*, 2005). *Candida* species have evolved to deal with this attack by utilising highly conserved networks of genes, which include catalases and superoxide dismutases to survive this oxidative attack. The mechanisms of these are discussed in later sections, however the ability of *tlo* mutants to grow in the presence of oxidative stress is explored in this section in order to understand the relationship between Tlos and the pathogenicity of the organism.

Resistance to antifungal therapy is a growing threat, especially in patients suffering from fungal infection (Mathé & Van Dijck, 2013; Taff *et al.*, 2013), which is made more dangerous by the shortage of new and effective antifungal therapies (Wong *et al.*, 2014). In this section, the resistance to three common antifungal drugs is tested, Amphotericin B, itraconazole and fluconazole.

Rapid growth of a fungus is important in a number of ways, e.g. it allows the organism to gain a foothold over competing organisms or even the host immune response. Similarly, growth on a range of substrates is of huge benefit to any organism, as adaptability is often tantamount to survival. Often, nutrients required for growth are simply unavailable and the ability to overcome this is a hallmark of a successful scavenger and coloniser (Potrykus *et al.*, 2014). The re-wiring of transcriptional networks to allow for utilisation of alternative nutrient sources is an important trait of *Candida* species (Brown *et al.*, 2014; Sandai *et al.*, 2012) and the role of *TLO*s in this process is explored. Previous research in this laboratory (Personal Communication, Yeomans, 2010), has suggested that growth of *C. dubliniensis tlo* mutants in galactose and succinate-based media may be retarded. As such, these sugars were used as primary carbon sources in some growth experiments outlined in this chapter.

The cell wall of *Candida* species is of major importance, having been associated with a range of processes including invasion (Gow *et al.*, 2012; Hiller *et al.*, 2011) , immunomodulation and immune recognition (Citiulo *et al.*, 2012; Lowman *et al.*, 2014; Vylkova & Lorenz, 2014), structural integrity (Free, 2013; Gow & Hube, 2012; Hall & Gow, 2013) and adhesion (de Groot *et al.*, 2013; Hiller *et*

al., 2011; Mayer *et al.*, 2013). Using cell wall disrupting chemicals, this study explores the effect of deletion of *TLO* genes on the stability and integrity of the cell wall. Strains were exposed to the detergent sodium dodecyl sulphate (SDS) which disrupts cell wall integrity (Guan *et al.*, 2012), calcoflour white which destabilises chitin synthesis and deposition (Roncero *et al.*, 1985) and congo red which interferes with the stability of glucan microfibrils (Leach *et al.*, 2012; Roncero *et al.*, 1985).

As mentioned, a major role of the cell wall is in the process of adhesion. This includes cell-cell adhesion and adhesion to other substrates, both of which are important in biofilm formation (Cuéllar-Cruz *et al.*, 2012). Biofilms are complex communities of many single or multiple organisms surrounded by an extracellular matrix and can occur on a range of surfaces (Jabra-Rizk *et al.*, 2004). The formation of biofilms has long been associated with infection (Sorgo *et al.*, 2013) and can act as a reservoir for reinfection (Coulthwaite & Verran, 2007) or as a protectant against antifungal therapies (Bonhomme & d'Enfert, 2013). The role of *TLO*s in the initiation and maintenance of biofilms is explored in this section.

In summary, this Chapter explores multiple facets of phenotypic behaviour typical in *Candida spp.* and attempts to identify what sort of role the *TLO* gene family may play in these.

4.2. Materials and Methods

4.2.1. Spot plate assay

In order to test the susceptibility of *Candida* strains and *tlo* mutant derivatives to a range of chemicals and environmental conditions, the spot plate assay was used. Strains of *Candida* spp. were plated on YEPD agar and incubated at 30 °C for 48 h in a static incubator (Gallenkamp). Colonies from these plates were then used to inoculate YEPD broth in 2 ml screw-capped Sterilin tubes (Sarstedt), which were incubated at 30 °C for 18 h with shaking at 200 r.p.m. in an orbital incubator (Gallenkamp)

Cultures were transferred to 2 ml microcentrifuge tubes (Eppendorf) and centrifuged at 6,000 x *g* for 3 min in a bench-top centrifuge (Eppendorf). They were then re-suspended in 1 ml of sterile PBS. This wash step was repeated a total of three times and the culture was finally re-suspended in sterile PBS to a final volume of 1 ml. Cells were counted as described in section 2.1.7. and a solution of cells with a concentration of 2 X 10^6 cells/ml was created using sterile PBS.

Serial dilutions were carried out resulting in cell suspension dilutions ranging from 10^0 to 10^{-4}. A 20 µl volume of each of these suspensions was pipetted onto agar plates containing various media using a multi-channel pipette (Eppendorf). Specific media, additives, supplements and conditions are outlined in the relevant results section. Plates were incubated at either 30 °C, 37 °C or 42 °C (as indicated in the relevant experiment) in a static incubator for 48 h and photographs were taken using a Flash'N'Go Automatic Colony Counter camera (IUL S.A., Barcelona, Spain) or iPhone 5 (Apple, CA, USA)

4.2.2. Antifungal susceptibility screening

Single colonies of *Candida* strains were taken from fresh YEPD plates that had been incubated for 48 h at 30 °C in a static incubator (Gallenkamp). These colonies were used to incubate 2 ml of YEPD broth in 15 ml Sterilin tubes (Sarstedt) which were incubated for 18 h at 30 °C with shaking at 200 r.p.m. in an orbital incubator (Gallenkamp) The following day, these cultures were centrifuged at 6,000 x *g* for 3 min in a swing-bucket centrifuge (Eppendorf), followed by re-suspension in sterile PBS to a final volume of 1 ml.

Using a sterile swab (Sarstedt), culture suspensions were lawned onto separate Yeast Nitrogen Base (YNB) with amino acids and ammonium sulphate

(Sigma-Aldrich) agar plates and allowed to dry for 15 – 20 min. Once dry, E-test® (BioMérieux, Basingstoke, UK) strips containing either Amphotericin, Itraconazole or Fluconazole were placed on plates (3 tests per plate) and plates were incubated at 35 °C for 48 h. After incubation, susceptibility to antifungals was interpreted by reading the point on the plate that intersects the zone of inhibition edge and the E-test strip. If there was no zone of inhibition, the MIC was interpreted as greater than the highest value on the strip. If the zone of inhibition is below the E-test strip, the MIC was recorded as less than the lowest value on the strip.

4.2.3. Induction of the white-opaque switch

In an attempt to induce strains to switch, strains were sub-cultured on Lee's medium with either 2 % (w/v) glucose (Sigma-Aldrich) or 1.25 % (w/v) N-acetylglucosamine (Sigma-Aldrich) as described by Huang *et al.*, (2010). Phloxine-B (Sigma Aldrich) was added to cooled, but still molten media to a final concentration of 5 μg/ml (Lockhart *et al.*, 2002). Inoculated media was incubated for 5 – 7 days at 25 °C and 30 °C.

4.2.4. Induction of chlamydospore formation

This method was derived from Citiulo *et al.*, (2009). Briefly, strains of *C. dubliniensis* were sub-cultured onto Pal's agar medium (50 g/l *Helianthus annuus* seeds [Sigma-Aldrich], 1 g/l glucose [Sigma-Aldrich], 1 g/l monopotassium phosphate [Sigma-Aldrich], 1 g/l creatinine [Sigma-Aldrich] and 15 g/l agar [Becton-Dickinson]). The medium was prepared as described by Khan *et al.*, (2004) and the pH was adjusted to 5.5. Strains were incubated for 48 h at 30 °C in a static incubator. Photographs of colonies were taken and samples of colonies were removed and emulsified in 50 μl of sterile PBS (Oxoid) in order to view on a light microscope (Nikon Instruments) using phase-contrast at 400 X magnification. Strains were randomised and photographs of the cellular morphology were taken at least three times at random viewpoints in order to reduce subjectivity and bias.

4.2.5. Growth rate determination

Each strain to be tested was grown on YEPD agar, cultured in YEPD broth and then washed with PBS as outlined in Section 4.2.1. Cells were re-suspended in a final volume of 1 ml of sterile PBS (Sigma-Aldrich) and were counted as described in section 2.1.7.

50 ml of YEPD in a 200 ml Erlenmeyer flask (Thermo Fisher Scientific) was inoculated with the washed and counted overnight culture to a final concentration of 2 X 10^6 cells per ml and subsequently incubated at 30 °C or 37 °C with shaking at 200 r.p.m. in an orbital incubator (Gallenkamp) for up to 12 h. Samples of 1 ml were taken from the cultures every 30 min, added to a cuvette and the relative optical density was measured using a bench-top Evolution 60S absorbance spectrophotometer (Thermo Fisher Scientific) at 600 nm wavelength. Samples taken were diluted with YEPD and re-measured if O.D. $_{600nm}$ measured at over 0.8 to maintain accuracy (due to the upper limits of detection of the instrument).

Results were recorded over a desired time-course and analysed and interpreted using either Microsoft Excel (Microsoft) or GraphPad Prism (Graphpad Software Inc.). Overall growth phenotypes of strains were compared and contrasted.

In order to determine the doubling time of each strain, the exponential phase of growth was identified and graphed separately in a new data sheet in GraphPad Prism (Graphpad Software Inc). Doubling time was calculated based on the following equation:

$$D = \frac{(t_2 - t_1) \times \ln(2)}{\ln(q_2/q_1)}$$

where, D = doubling time; t_1 and t_2 represent distinct time-points during exponential growth; q_1 and q_2 represent the O.D.$_{600nm}$ measurements at t_1 and t_2 respectively. This calculation was carried out at several different points, which were averaged to yield *D*. All units were in min.

4.2.6. Agar Invasion Experiments

Overnight cultures were setup as described in Section 4.2.1 and then counted as described in Section 2.1.7. Freshly prepared YEPD agar plates (15 ml) were allowed to solidify and immediately, 20 µl of a 2 X 10^6 cells/ml solution of each strain was added to the surface of the agar and allowed to dry. A further 15 ml of YEPD agar (cooled almost to solidification) was poured on top of the existing agar. The plates were allowed to set and were incubated at either 30 °C or 37 °C for 48 h in a static incubator (Gallenkamp).

Results were interpreted qualitatively based on the ability of each strain to penetrate the upper and lower layers of the agar.

4.2.7. Hyphal production assay

Two methods were devised to accurately determine the extent of true hyphal production. For the purposes of this study, hyphal bodies that contained cross walls or were unusually swollen were presumed to be pseudohyphae and were not counted as true hyphae (described in Chapter 1). All results were analysed and presented using either Microsoft Excel (Microsoft) or Prism (GraphPad Software Inc.).

4.2.7.1. Large-scale method

For each strain of *Candida* spp. tested, strains were grown on YEPD agar for 48 h at 30 °C in a static incubator (Gallenkamp). For each strain, a single colony was taken and used to inoculate 2 ml of YEPD broth and incubated at 30 °C for 18 h with shaking at 200 r.p.m in an orbital incubator (Gallenkamp). These cultures were centrifuged in a bench-top microcentrifuge (Eppendorf) for 3 min at 10,000 x *g* and re-suspended in 1 ml of sterile PBS (Sigma-Aldrich) to wash the cells. The samples were then subjected to additional centrifugation as before. This washing was repeated a further two times and the final supernatant was discarded.

The washed pellet of cells was re-suspended in sterile PBS up to a final volume of 1 ml. Cells were accurately counted as described in section 2.1.7. A 25 ml volume of sterile water with 10% (v/v) foetal calf serum (Sigma-Aldrich) was inoculated to a final concentration of 2 X 10^6 cells per ml of media in 200 ml Erlenmeyer flasks with rubber BugStopper® (Thermo Fisher Scientific). Cultures were incubated for 6 h at 37 °C with shaking at 200 r.p.m. and 20 µl samples were taken at 30 min intervals for the first 2 h and at 1 h intervals thereafter. These

samples were added to a clean microscopic slide (Erie Scientific Company, NH, USA) covered with a thin coverslip and viewed using light microscopy at 400 X magnification (Nikon Instruments).

A total of 300 cells were counted over random areas on the slide. The number of cells that were forming true hyphae was represented as a percentage of 300 cells. Photographs of each field of vision were taken while viewing under the phase-contrast filter in order to enable verification of counts at a later time. When counting more than one strain of *Candida* spp., samples were counted in a randomised way so that bias could be avoided as much as possible.

4.2.7.2. Small-scale method:

This method is a scaled-down, higher throughput version of the one described above in Section 4.2.7.1. Instead of 25 ml cultures, cells were added to a 2 ml volume of media in the well of a six-well tissue culture plate (with lid (Greiner Bio-One) to yield a final cell concentration of 2.5 X 10^5 cells per ml. These were incubated at 37 °C in a static incubator (Gallenkamp) with occasional agitation (every 10 min). Plates were set up in groups of seven and one plate was removed for counting at 30 min, 60 min, 90 min, 2 h, 3 h, 4h and 5 h time-points. 100 cells were counted using X 400 magnification on a light microscope (Nikon Instruments) and the proportion of true-hyphal cells was represented as a percentage of 100 cells.

4.2.8. Biofilm formation assay

4.2.8.1. Induction of biofilm formation

Strains were sub-cultured on YEPD and overnight cultures were grown and washed as described in Section 4.2.1. The $O.D._{600\ nm}$ of the cell suspension was measured using an Evolution 60S bench-top absorbance spectrophotometer (Thermo Fisher Scientific) using 1 ml of water with 10 % (v/v) foetal calf serum (Sigma-Aldrich) as a blank sample for base absorbance readings. 1.5 ml suspensions of the cells were made with 10% (v/v) foetal calf serum so that the $O.D._{600nm}$ of each suspension was 0.5. The volume of culture added was calculated using the following equation:

$$S\ (\mu l) = \frac{0.5 \times 1500 \mu l}{A}$$

where A is the true (undiluted) absorbance reading of the sample to be added and S is the total volume of washed overnight culture (in µl) to be added to a final volume of 1.5 ml 10 % (v/v) foetal calf serum (Sigma-Aldrich).

A 100 µl volume of each suspension was added to wells, in triplicate on a 96-well, flat-bottomed polystyrene plate (Greiner Bio-One) with lid. Outer wells were excluded due to the possibility of evaporation. 100 µl of sterile water with 10% (v/v) foetal calf serum (Sigma-Aldrich) was added to three wells in order to act as a control and blank measurement. Plates were then incubated for the desired length of time (up to 72 h) in a static incubator (Gallenkamp) set to 37 °C. Growth in the presence of 5% (v/v) CO_2 was carried out in a static tissue culture incubator with 5 % (v/v) relative humidity (Gallenkamp).

Once the desired incubation time had elapsed, plates were removed and the liquid was withdrawn from each well and discarded. All wells were washed 5 times with 200 µl sterile PBS (Oxoid), taking care not to disturb any adhered cells. As part of each wash, gentle rocking of the plate was performed so as to remove non-adherent cells. One of two methods was used to determine the extent of biofilm formation, as outlined below.

4.2.8.2. Quantitative measurement of biofilm formation

4.2.8.2.1. XTT Method

After the final wash, 200 µl of 200 µg/ml 2,3-Bis(2-methoxy-4-nitro-5-sulfophenyl)-2*H*-tetrazolium 5-carboxanilide inner salt (XTT) (Sigma-Aldrich) with 50 µg/ml CoEnzyme Q (Sigma-Aldrich) (kept at 37 °C) was added to each well. The plates were then incubated at 37 °C in the dark for 50 min.

Once this incubation was complete, 100 µl of the XTT/CoEnzyme Q solution was removed from each well and transferred to a fresh 96-well, flat-bottomed polystyrene plate (Greiner Bio-One). The absorbance of each well was measured at 480 nm using a Tecan Plate Reader system (Tecan AG, Switzerland). Results were analysed and graphed using Microsoft Excel for Mac (Microsoft)

4.2.8.2.2. Biomass (staining) method

This method is similar to that described above, but deviates from the outlined protocol after the final post-incubation wash step. At this point, 200 µl of 0.1 % (w/v) crystal violet (Sigma-Aldrich) solution (made with MilliQ water [Merck-Millipore]) was added to each well and the plate was incubated at room temperature for 10 min. The solution was removed and wells were washed with sterile PBS three times. 100 µl of 95 % (v/v) ethanol was added to each well and the plate was incubated at room temperature for 15 min in order to solubilise the dye. The wells were mixed by pipetting and the $O.D._{580\ nm}$ was measured using a plate absorbance reader (Tecan AG). Results were analysed and presented using Microsoft Excel for Mac (Microsoft). Welch's correction was used a post-analysis correction.

4.3. Results

4.3.1. Effect of temperature on the growth of *C. dubliniensis tlo* mutants.

Spot plate assays were carried out to investigate the ability of strains to grow at different temperatures. *C. dubliniensis* wild-type strain (Wü284) displayed normal growth on YEPD agar at 30 °C, 37 °C and reduced growth as indicated by the smaller colony size at 42 °C over 72 h (Figure 4.1) At 30 °C and 37 °C there were no detectable difference in the growth of *tlo* mutant strains. At the elevated temperature of 42 °C however, Δ*tlo2* showed reduced growth compared to wild-type and other *tlo* mutant strains (Figure 4.1).

4.3.2. Antifungal susceptibility of *C. dubliniensis tlo* mutants.

The susceptibility of *C. dubliniensis tlo* mutant strains to three antifungal drugs, Fluconazole, Itraconazole and Amphotericin B was tested using the commercially available E-test® system. At 48 h of growth, the minimum inhibitory concentrations (M.I.C.s) of the antifungals was recorded by reading the edge of the zone of inhibition against the scale on the E-test strip.

M.I.C.s are outlined in Table 4.1. In the case of fluconazole, a member of the triazole antifungal family with fungistatic activity, there was no observable difference in susceptibility between Wü284 (wild-type) and the *tlo* mutant strains. Similarly, for itraconazole, another triazole, no significant difference in susceptibility was observed (Table 4.1.)

In the presence of Amphotericin B, a polyene fungicidal drug which acts on cell membranes, there were minor differences in susceptibility between strains. However, these differences were less than two-fold and were not deemed significant (Table 4.1.)

4.3.3. Effect of *TLO* disruption on cell wall integrity

Susceptibilities of *C. dubliniensis* wild-type strain (Wü284) and *tlo* mutant derivatives were assessed using spot plates containing 10 μg/ml to 100 μg/ml Calcofluor (Brilliant) White (CFW). At 10 μg/ml (Figure 4.2), a significant growth retardation was observed for ΔΔ*tlo* with partial restoration of growth with re-introduction of either *TLO1* (ΔΔ*tlo*::*TLO1*) or *TLO2* (ΔΔ*tlo*::*TLO2*). No retardation was observed for either single *tlo* mutant Δ*tlo1* or Δ*tlo2*.

Additional spot plates were carried out on YEPD agar containing 100 μg/ml and 200 μg/ml concentrations of Congo Red. At both 100 μg/ml and 200 μg/ml (Figure 4.3), Δ*tlo1* and ΔΔ*tlo* showed severely reduced growth compared to wild-type. Both complemented strains (ΔΔ*tlo*::*TLO1* and ΔΔ*tlo*::*TLO2)* exhibited restored levels of growth. Heterozygous *tlo* mutants grew at similar levels to wild-type, as did Δ*tlo2*.

4.3.4. Effect of detergent on *tlo* mutant strains of *C. dubliniensis*.

Wild-type (Wü284) *tlo* mutant derivatives were grown in the presence of sodium dodecyl sulphate (SDS) using YEPD plates supplemented with 10 % (w/v) SDS. After incubation at 37 °C for 48 h, both the ability to grow and colony size were significantly different between strains (Figure 4.4) Wild-type and the heterozygous *tlo1* mutant (Figure 4.4. A and B) all grew to roughly the same extent with the same colony morphology. However, Δ*tlo2* and to a lesser extent, Δ*tlo1*, displayed significantly larger colony morphology along with a tendancy to grow more quickly (Figure 4.4. C and D). The double *tlo* mutant had difficulty growing under these conditions, with colony size and growth severely reduced (Figure 4.4. E)

Due to colony size being relatively small, it was decided to incubate each strain for a further 24 h, bringing the total incubation time to 72 h. This permitted better visualisation of individual colonies as shown in Figure 4.4. F, G, H, I and J. Wild-type, heterozygous *tlo1* mutant and Δ*tlo1* all displayed typical circular, convex, glistening colonies (Figure 4.4. F, G and H). However, Δ*tlo2* colonies were circular, flat, dull in appearance (Figure 4.4. I). Similarly, ΔΔ*tlo* colonies were flat and dull in appearance, but smaller than Δ*tlo2*. (Figure 4.4. J).

4.3.5. *TLO* disruption causes a defect in cell separation

In the early stages of this study, it was observed that the cellular morphology of ΔΔ*tlo* was often 'clumped' in appearance (Figure 4.5). To investigate whether this clumping was due to increased adhesion or defective cell separation (cytokinesis), a number of experiments were carried out.

Overnight cultures (YEPD, 30 °C) were stained with calcofluor white and visualised under the microscope (400 X) to assess whether mother-daughter yeast cells exhibited defective separation, indicated by the presence of a chitin ring between the cells. Cells connected due to flocculation would not exhibit these

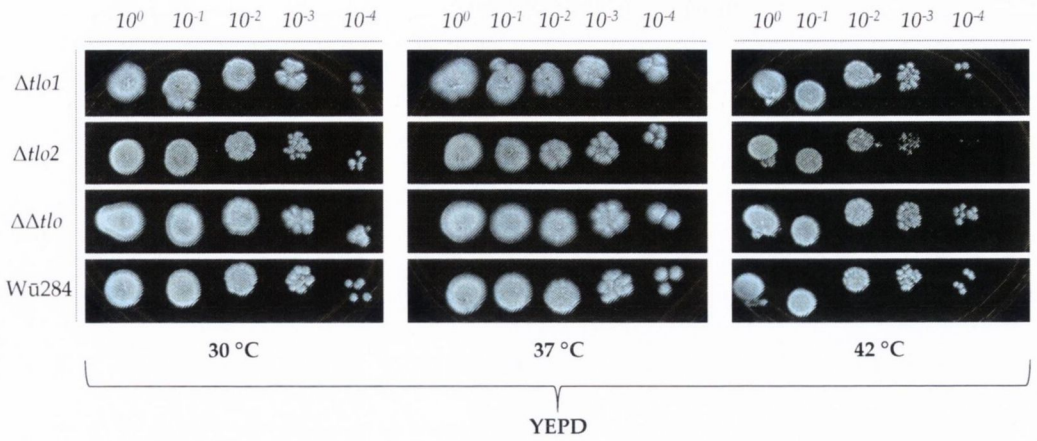

Figure 4.1. Effect of temperature on the growth of *C. dubliniensis tlo* mutants
YEPD spot plates were prepared as described in 4.2.1. and 4.3.1; serial dilutions of a 2 X 10^6 cells per ml culture were pipetted onto plates and were incubated at the indicated temperatures for 72 h. Photographs are representative of the average result from three separate experiments. Strains and conditions are indicated.

	Wü284	Δ*tlo1*	Δ*tlo2*	ΔΔ*tlo*	Mode of action
Fluconazole	0.25	0.25	0.25	0.25	Fungistatic, triazole
Itraconazole	0.006	0.004	0.004	0.004	Fungistatic, triazole
Amphotericin	0.023	0.023	0.016	0.032	Fungicidal, polyene

Table 4.1. Susceptibility of *Candida dubliniensis* to common antifungals.
Minimum inhibitory concentrations (M.I.C.s) of three antifungals are shown. All amounts are in μg/ml

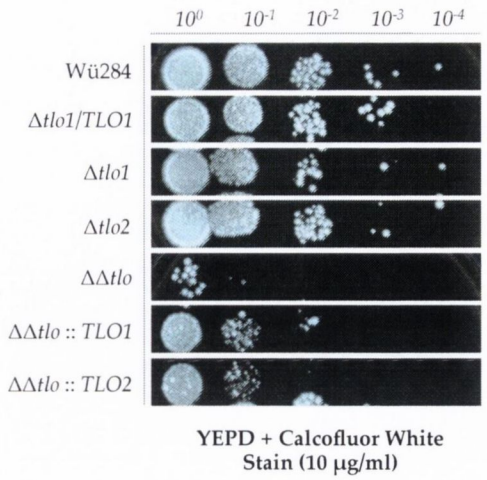

Figure 4.2. Growth of *C. dubliniensis* in the presence of Calcofluor White.
Overnight cultures of the indicated strains were serially diluted and grown on YEPD supplemented with 10 μg/ml Calcofluor White stain. Photographs are representative sample of results from at least three separate experiments.

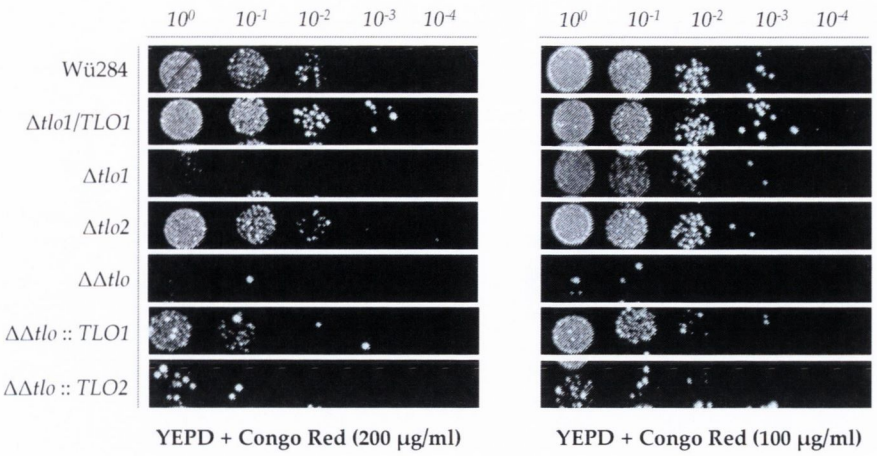

Figure 4.3. Growth of *C. dubliniensis* in the presence of Congo Red.
Overnight cultures of the indicated strains were serially diluted and grown on YEPD with either 100 μg/ml or 200 μg/ml Congo Red at 30 °C for 48 h. Photographs are representative sample of results from at least three separate experiments.

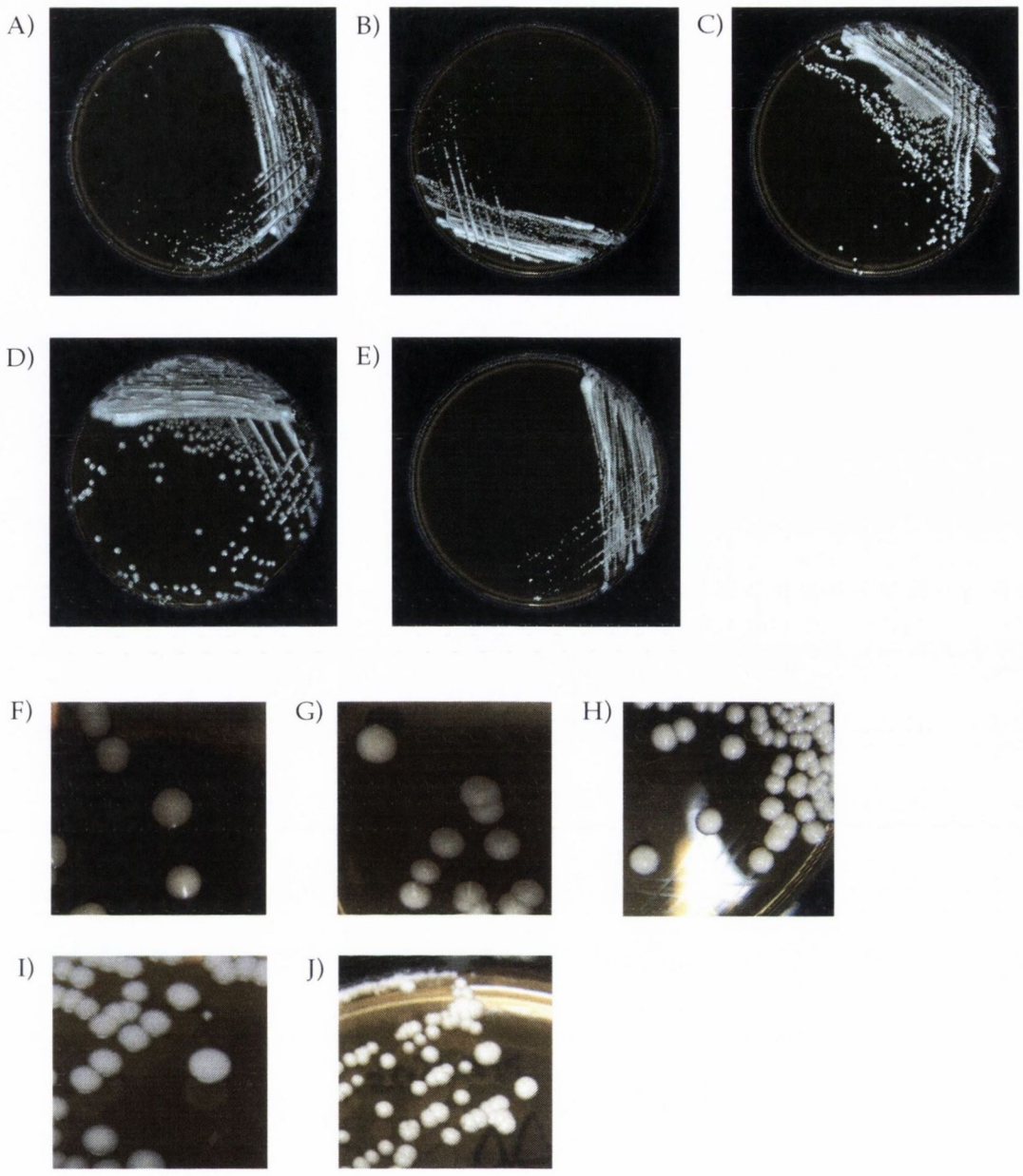

Figure 4.4. Growth of *C. dubliniensis* in the presence of SDS.

Strains of *C. dubliniensis* Wü284 (A), Δ*tlo1*/*TLO1* (B), Δ*tlo1* (C), Δ*tlo2* (D), ΔΔ*tlo* (E), were plated on YEPD supplemented with 10 % (w/v) SDS and incbuated at 30 °C for 2 days. Plates were left to incubate for a further 24 h (72 h in total) and higher magnification images were captured to illustrate varying colony topology for Wü284 (F), Δtlo1/*TLO1* (G), Δ*tlo1* (H), Δ*tlo2* (I), ΔΔ*tlo* (J) All images are scaled to be equivalent to each other and are representative of typical samples from three separate experiments.

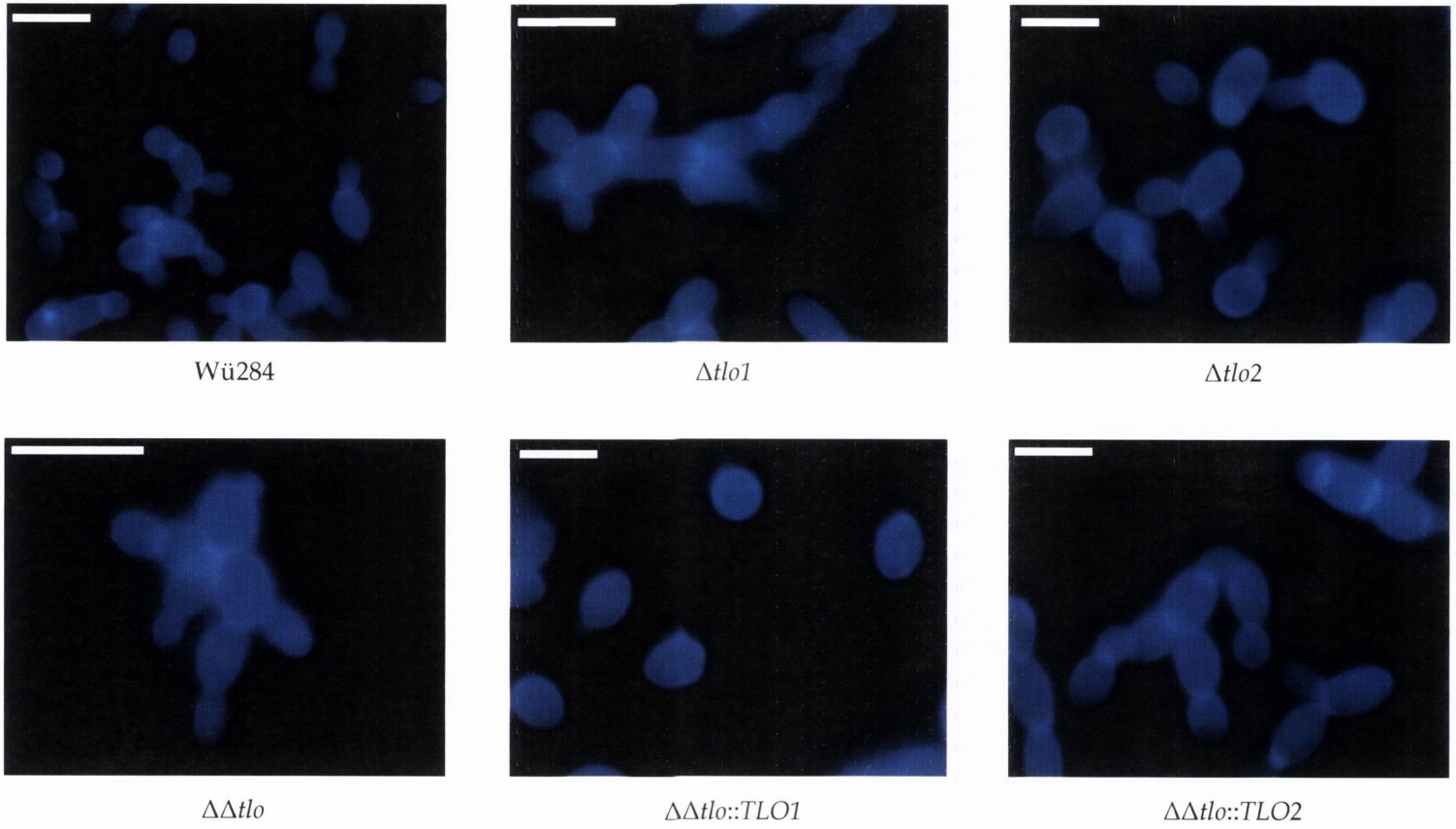

Figure 4.5. Calcofluor white-stained *C. dubliniensis tlo* mutant strains.

Strains of *C. dubliniensis* (indicated below each photograph) were cultured in YEPD at 30 °C for 18 h with shaking at 200 r.p.m and then Calcofluor white -stained as described in section 4.3.5. Scale bar is for all samples indicates 10 μM length.

chitin-rich contact points. When compared to Wü284, ΔΔ*tlo* displayed increased chitin staining around cell-cell junctions (Figure 4.5), which supports the hypothesis of defective cell separation as opposed to clumping caused by passive cell-cell adherence.

Samples from cultures of Wü284 and ΔΔ*tlo* were also visualised using scanning electron microscopy (SEM). It was observed that defective cell separation was significantly more widespread in the case of ΔΔ*tlo*, as was expected based on early observations under light microscopy. Groups of cells from ΔΔ*tlo* were compared directly to groups of cells from Wü284 and differences in the appearance of cell-cell junctions were detected (Figure 4.6). It was observed that while cells in the Wü284 culture showed evidence of normal budding and separation (e.g. typical bud scarring was widespread), (Figure 4.6. A and B), cells from ΔΔ*tlo* showed a higher incidence of atypical bud scars (Figure 4.6. C and D). In addition, fibres were visible during the separation of cells of Wü284 whereas no such examples could be found for ΔΔ*tlo*, despite extensive searches. The presence of an excess of cell wall material and atypical bud scars have been suggested by Firon, *et al.*, (2007) as good indicators of a cell separation defect (Firon *et al.*, 2007) and were observed in the ΔΔ*tlo* strain only.

Cells were treated with chitinase and subjected to treatments with detergents (e.g. SDS) in an attempt to separate cells, however these attempts were unsuccessful. In addition, cells were subjected to rounds of sonication using a sonicating waterbath, however cells either tended to remain unchanged or lyse as opposed to separate. Treatment with Zymolyase-100T was the only successful method in separating cells, which essentially spheroplasted the cells, further supporting a defect in cell separation.

4.3.6. Effect of *TLO* disruption on the response of *C. dubliniensis* to osmotic stress.

Spot plate assays using strains of *C. dubliniensis* (Wü284, Δ*tlo1*, Δ*tlo2* and ΔΔ*tlo*) were setup on YEPD agar containing a range of concentrations of calcium chloride ($CaCl_2$; 100 mM – 600 mM). Plates were incubated for a total of 48 h at 30 °C and visualised (Figure 4.7). At concentrations of 200 mM $CaCl_2$ and above, a difference in the growth of strains was observed. At 400 mM $CaCl_2$, Wü284 and Δ*tlo2* grew at similar levels. However, at this concentration, growth of Δ*tlo1* was significantly impaired between dilutions of 10^{-2} and 10^{-3}. Even more evident was the lack of growth of ΔΔ*tlo* (Figure 4.7). This trend is visibly present over the range of concentrations.

A spot plate assay was also carried out using YEPD supplemented with 500 mM to 1.6 M sodium chloride (NaCl) solution (Figure 4.8). At 1M NaCl, wild-type (Wü284) was able to grow better than all of the *tlo* mutant strains. However, there was little difference observed between the mutant strains, except for slightly reduced density of growth for Δ*tlo1* (Figure 4.8).

Further assays were carried out using sorbitol as an additive to YEPD (Figure 4.9). Unlike with previous spot plate assays, ΔΔ*tlo* and Δ*tlo1* appeared to grow slightly better than either Wü284 or Δ*tlo2* at all concentrations tested (0.5 M – 1.5 M).

4.3.7. Effect of *TLO* disruption on the response to oxidative stress.

4.3.7.1. Spot plate assay

Sensitivity of *C. dubliniensis tlo* mutants to reactive oxygen species (ROS) and superoxide radicals was determined using spot plates supplemented with a range of concentrations of hydrogen peroxide (H_2O_2), from 5 mM to 10 mM H_2O_2. Phenotypes were observed between 7 mM and 8 mM H_2O_2 (Figure 4.10). At 7 mM concentrations, growth of Δ*tlo1* but not wild-type was inhibited at the 10^{-3} dilution. Growth of Δ*tlo2* was not affected at 7 mM H_2O_2, however growth of ΔΔ*tlo* was significantly retarded with growth only apparent at the undiluted 10^0 spot. More pronounced inhibition was observed at 8 mM H_2O_2 (Figure 4.10). At this concentration the Δ*tlo1* mutant only grew to the 10^{-1} dilution whereas wild-type

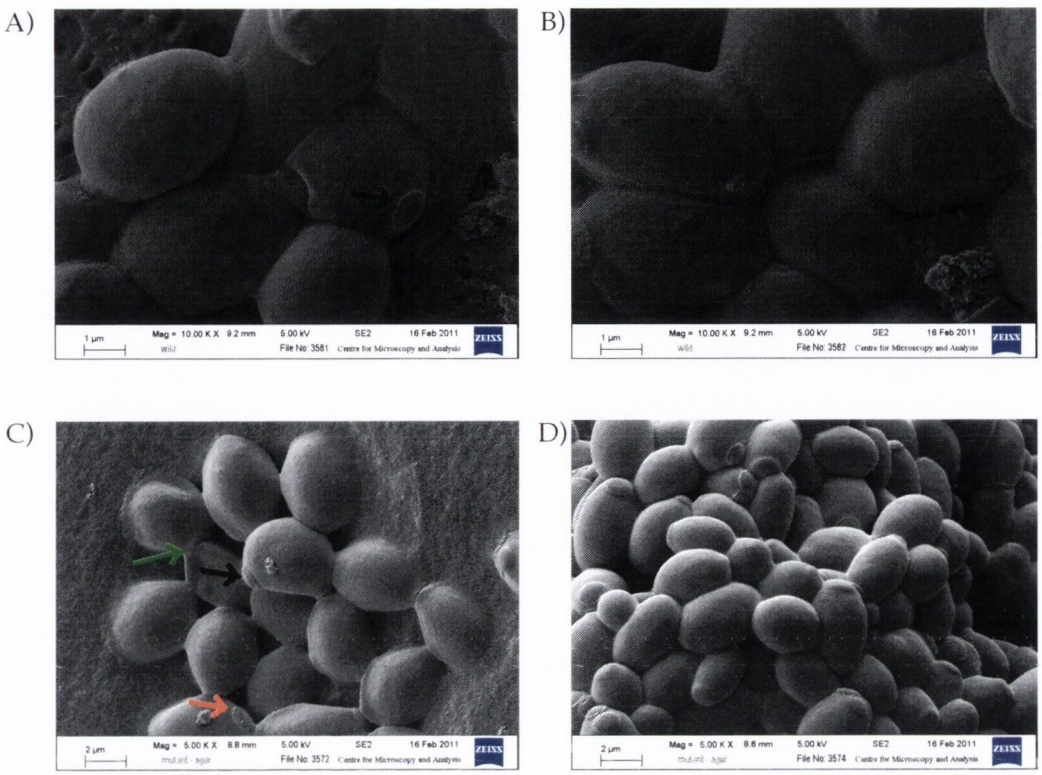

Figure 4.6. Visualisation of cell-cell contacts in wild-type *C. dubliniensis* and double *tlo* mutant.

Scanning electron microscopy was performed to visualise Wü284 (A,B) and ΔΔ*tlo* (C,D) as described in Materials and Methods. Scale bars are indicated in white panels beneath each image. Atypical bud scar in atypical location is indicated with a red arrow, whilst normal bud scars are indicated with solid black arrows. Excess of cell wall material is indicated with a green arrow.

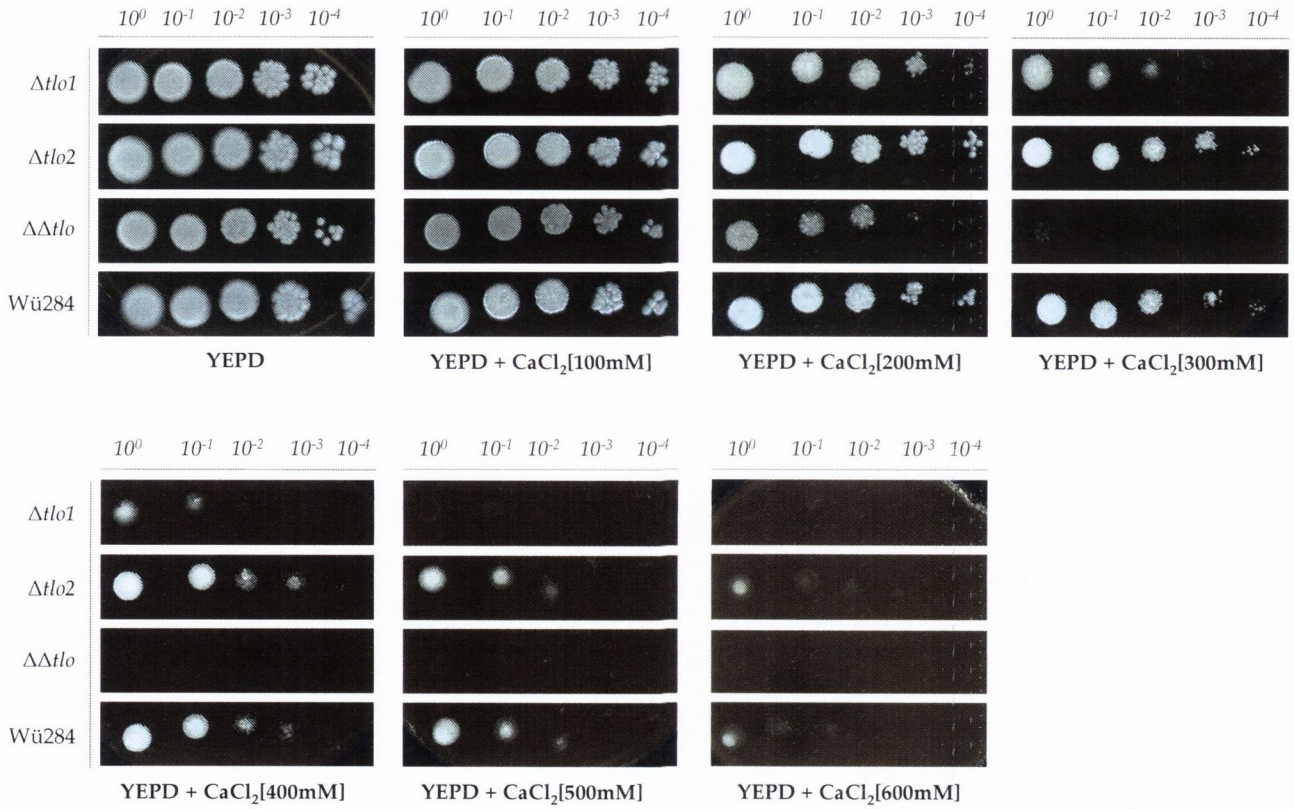

Figure 4.7. Growth of *C. dubliniensis* in the presence of calcium chloride.

Spot plate assays were used to investigate the ability of strains to grow in the presence of increasing concentrations of calcium chloride ($CaCl_2$). 10-fold dilutions of a 2 X 10^6 cells/ml culture were carried out on YEPD with varying concentrations of $CaCl_2$ added prior to solidification of the agar. Plates were then incubated at 30 °C for 48 h. Strains and dilutions are indicated, as well as concentrations of $CaCl_2$ for each plate.

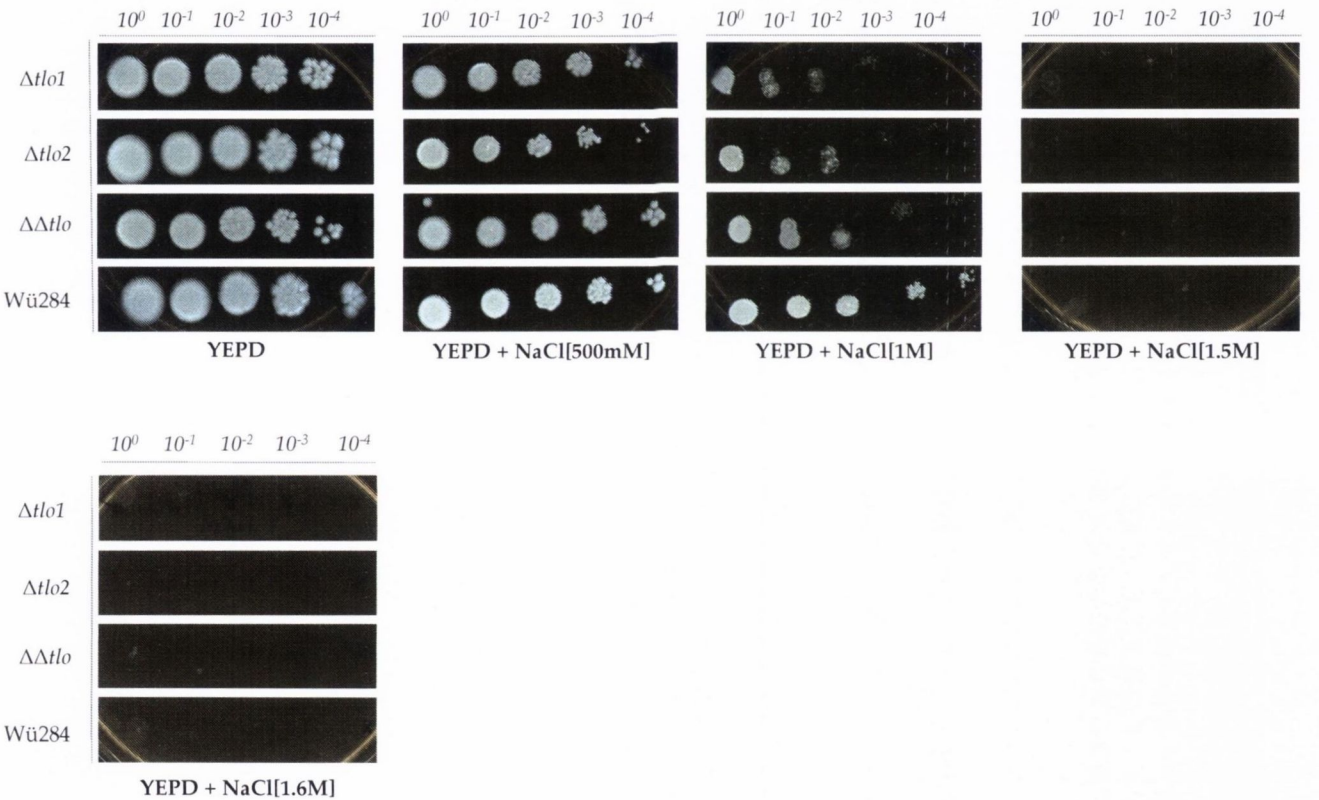

Figure 4.8. Growth of *C. dubliniensis* in the presence of Sodium Chloride.

Spot plate assays were used to investigate the ability of strains to grow in the presence of increasing concentrations of sodium chloride (NaCl). 10-fold dilutions of a 2 X 10^6 cells/ml culture were carried out on YEPD containing a range of concentrations of NaCl. Plates were then incubated at 30 °C for 48 h. Strains and dilutions are indicated, as well as concentrations of NaCl for each plate. Experiment was repeated on three separate occasions and photographs represent the typical result.

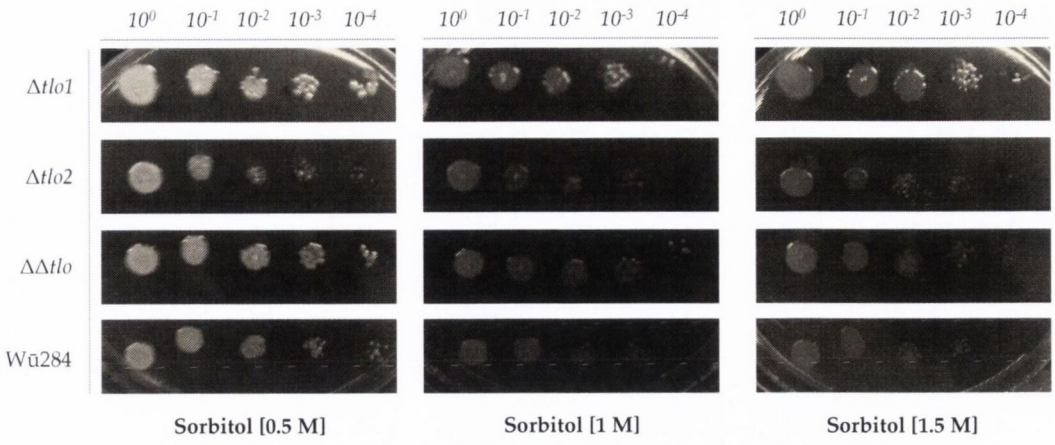

Figure 4.9. Effect of sorbitol on the growth of *C. dubliniensis tlo* mutants.
YEPD spot plates were prepared as described in section 4.2.1. and were supplemented with a range of concentrations (0.5 M – 1.5 M) of sorbitol. The plates were incubated at 30 °C for 48 h. Photographs are representative of the average result from three separate experiments. Strains and conditions are indicated in the legend.

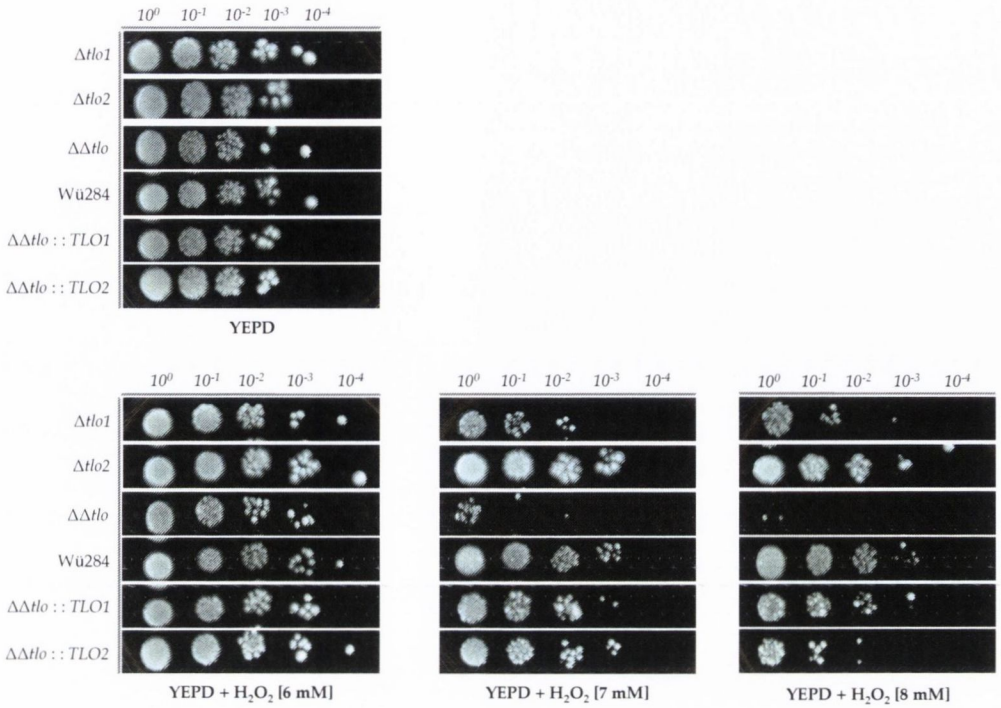

Figure 4.10. Effect of hydrogen peroxide (H_2O_2) on the growth of *C. dubliniensis tlo* mutants.

Spot plate assays were used to investigate the ability of strains to grow in the presence of increasing concentrations of hydrogen peroxide (H_2O_2). 10-fold dilutions of a 2 X 10^6 cells/ml culture were carried out on YEPD agar containing a range of concentrations (5 μM – 10 mM) of H_2O_2. Plates were then incubated at 30 °C for 48 h. Plates pictured are of the optimal concentrations required to yield a visible phenotype. Strains and dilutions are indicated, as well as concentrations of H_2O_2 for each plate. Experiment was repeated on three separate occasions and photographs represent the typical result. A plate without the addition of H_2O_2 is also included as a growth control.

Wü284 grew to the 10^{-3} dilution. In addition, ΔΔ*tlo* displayed significantly retarded growth compared to all other strains. Reintroduction of *TLO1* or *TLO2* at 7 mM H_2O_2 resulted in growth similar to Wü284. At 8 mM, *TLO1* re-introduction had the ability to restore wild-type phenotype, but *TLO2* could only partially restore the tolerance levels to H_2O_2 at this concentration (Figure 4.10.).

Sensitivity of the *tlo* mutant strains to superoxide radicals was determined by supplementing YEPD agar plates with menadione bisulphate at concentrations ranging from 5 μM to 1 mM. Phenotypes were observed at concentrations of 50 μM and 100 μM (Figure 4.11). At 50 μM menadione, strain Wü284 grew at the 10^{-3} dilution whereas the ΔΔ*tlo* mutant was inhibited at the 10^{-2} dilution (Figure 4.11). Growth of Δ*tlo1* was reduced, whereas growth of Δ*tlo2* was not affected compared to wild-type (Figure 4.11). At the higher concentration of 100 μM menadione, Δ*tlo1* exhibited reduced growth relative to that observed on the 50 μM plate, whereas the other strains exhibited similar patterns of growth (Figure 4.11). At both concentrations of menadione, restoration of *TLO1* or *TLO2* was sufficient to restore wild-type levels of growth.

4.3.7.2. Broth micro-dilution test

In order to confirm the results observed in the spot plate assays, broth micro-dilution tests were used in an attempt to identify minimum inhibitory concentrations for the chemicals used. The assay was setup using a range of H_2O_2 concentrations from 160 mM to 0.3125 mM in YEPD with each well having the same initial inoculum. After 18 h of growth, the optical density was measured and converted logarithmically relative to the positive (growth without H_2O_2) and negative (sterile, no inocula) growth controls. As expected, disruption of both *TLO* genes in *C. dubliniensis* ΔΔ*tlo* resulted in a significantly decreased growth phenotype (ANOVA $p < 0.001$) compared to Wü284 at 2.5 mM H_2O_2 ($p = 0.0126$) and at 5 mM H_2O_2 ($p = 0.0063$) (Figure 4.12. A). In the case of Δ*tlo1* or Δ*tlo2*, no significant difference in tolerance to hydrogen peroxide was detected, either compared to each other or to Wü284 (Figure 4.12. B) at any of the concentrations tested. At 2.5 mM concentrations of H_2O_2, re-introduction of *TLO1* was able to restore the growth of ΔΔ*tlo* background to wild-type levels as was observed by a significant difference ($p = 0.0246$) between ΔΔ*tlo* and ΔΔ*tlo*::*TLO1* at 2.5 mM (Figure 4.12. C). While *TLO2* appeared also to be sufficient to restore levels of

growth, the results were highly variable and could not be deemed significant ($p = 0.2387$). The re-introduction of *C. albicans TLO11* or *TLO12* to the Δ*tlo1* background was not sufficient to restore growth levels at 5 mM H_2O_2 (Figure 4.12. D).

A broth micro-dilution test was carried out using menadione, however the results were difficult to interpret due to the colour change in media caused by menadione bisulphate (yellow colour) interfering with the absorbance measurements.

4.3.8. White-opaque switching frequency in *C. dubliniensis TLO* strains

Despite several attempts using various media formulations (including GlcNAc as a carbon source), white-opaque switching could not be observed in any of the tested strains.

4.3.9. Effect of *TLO* disruption on the formation of chlamydospores in *C. dubliniensis*.

Strains of *C. dubliniensis* were sub-cultured on Pal's agar medium to induce the formation of chlamydospores. After incubation at 30 °C for 48 h, the colony morphology of each strain differed significantly and samples of the colony morphology were taken to be viewed under phase contrast light microscopy at X 400 magnification.

For wild-type *C. dubliniensis,* colonies were round, umbonate and filamentous in appearance and typical chlamydospore formation was observed microscopically (Figure 4.13. A). Colonies of Δ*tlo1* were round and umbonate, but smoother in appearance than wild-type and did not appear filamentous. No true chlamydospores were observed in Δ*tlo1* colonies, however chlamydospore-like structures were observed which were smaller in size and thinner-walled in appearance (Figure 4.13. B). Colonies of Δ*tlo2* were analogous in appearance to wild-type and chlamydospores were visible under the light microscope (Figure 4.13. C). For ΔΔ*tlo*, no chlamydospores were observed (Figure 4.13. D). Instead, the strain exhibited long chains of rod-shaped cells containing multiple structures resembling nuclei.

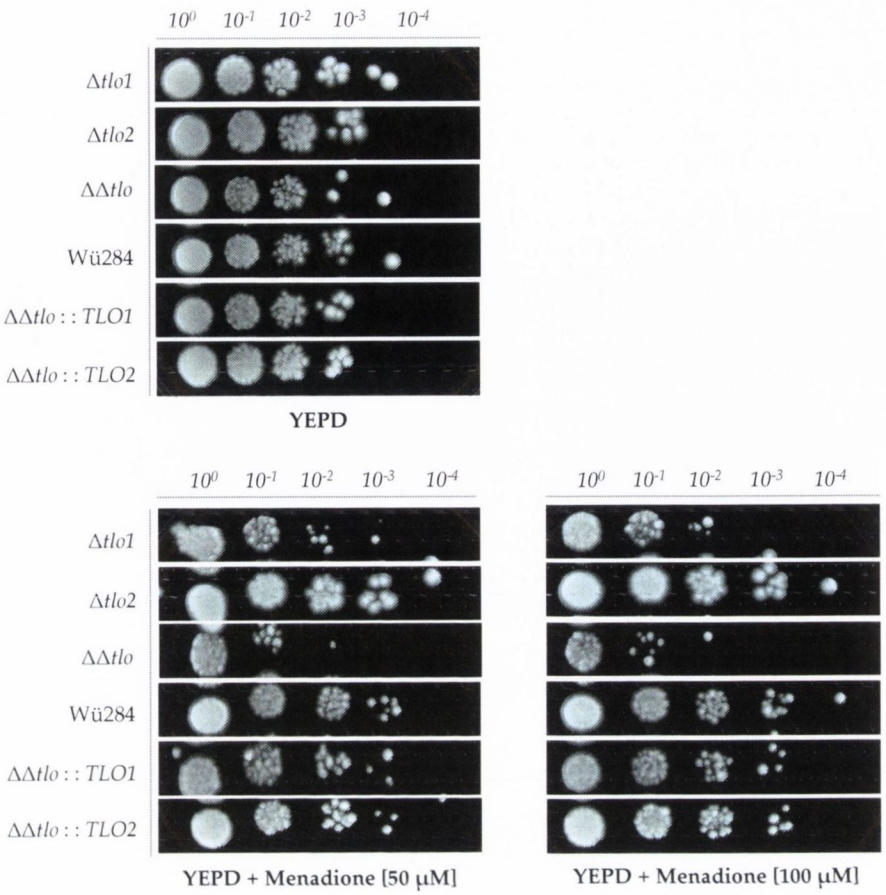

Figure 4.11. Effect of menadione on the growth of *C. dubliniensis tlo* mutants.

Spot plate assays were used to investigate the ability of strains to grow in the presence of increasing concentrations of menadione bisulphate. 10-fold dilutions of a 2 X 10^6 cells/ml culture were carried out on YEPD agar containing a range of concentrations of menadione (50 μM and 100 μM). Plates were then incubated at 30 °C for 48 h. Strains and dilutions are indicated, as well as concentrations of menadione for each plate. Experiment was repeated on three separate occasions and photographs represent the typical result. A plate without the addition of menadione is also included as a growth control.

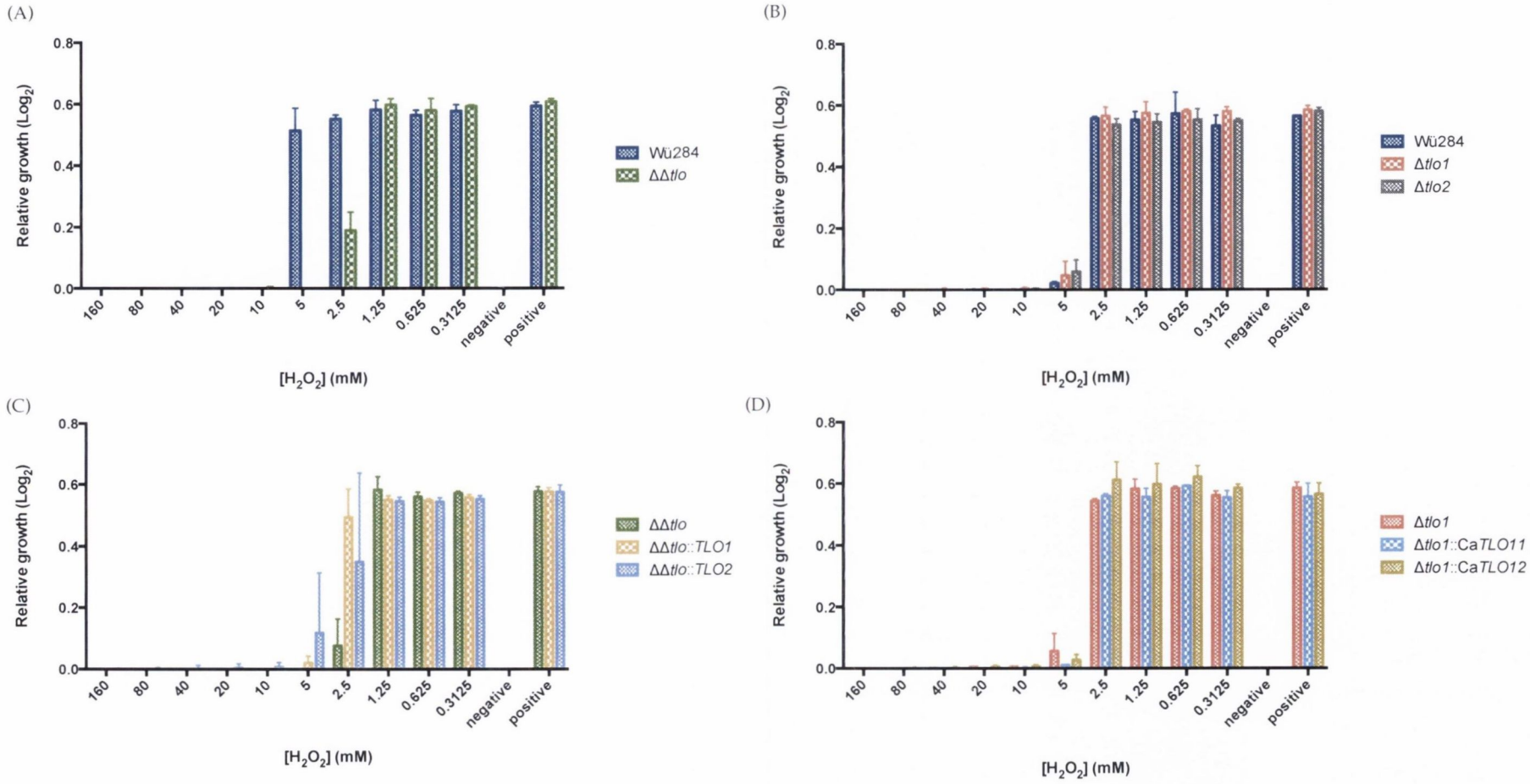

Figure 4.12. Growth of *tlo* mutants under oxidative stress.

Strains of *C. dubliniensis* were subjected to growth under varying concentrations of hydrogen peroxide (H_2O_2) in a micro-dilution test. Data is represented by the Log_2 growth relative to both positive (no H_2O_2) and negative (sterile, no inocula) controls. Strains are indicated in each legend. Error bars correspond to the standard deviation of at separate experiments (n=3).

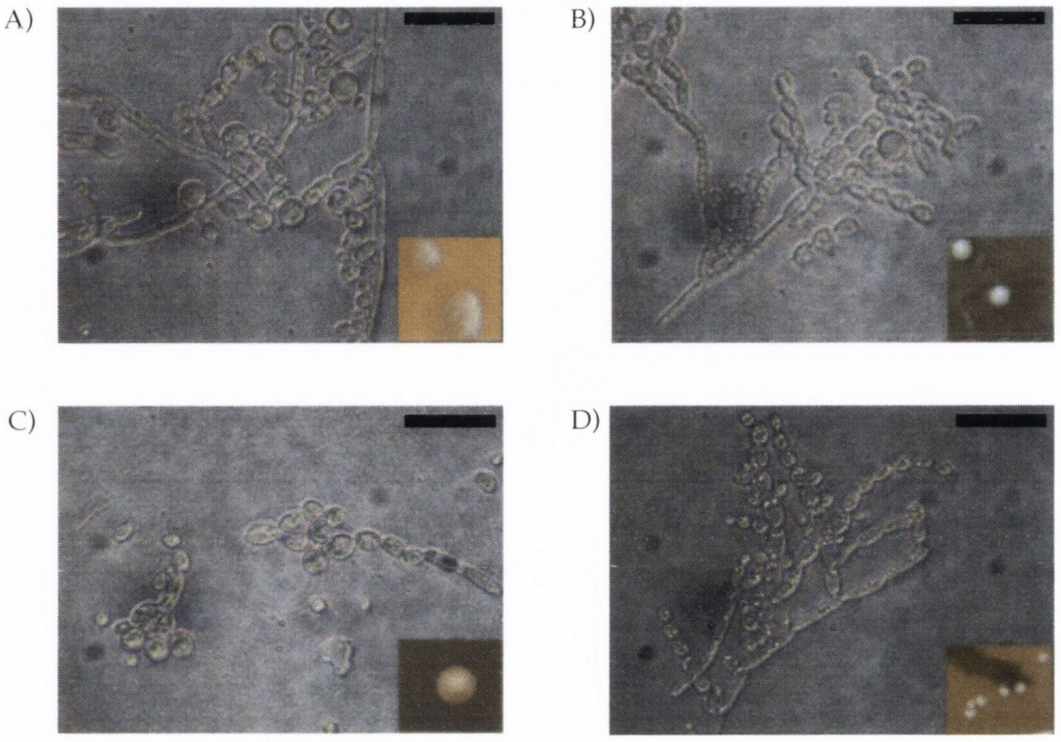

Figure 4.13. Chlamydospore formation in *C. dubliniensis tlo* mutants.

Strains of C. *dubliniensis* were cultured on Pal's agar medium and incubated for 48h at 30 °C. Colonies were removed from the plate and gently emulsified in 50 μl of sterile PBS in order to view on a light microscope using phase contrast at 400 X magnification. Photographs are representative examples from 3 separate experiments. Scale bar indicates 20 μM length. Original colony morphology is shown inset for each photograph.

Typical chlamydospore formation was observed for Wü284 (A) and Δ*tlo2* (C), chlamydospore-like structures were observed for Δ*tlo1* (B) and no chlamydospores formed in ΔΔ*tlo* (D), instead atypical opaque-like cells were observed.

4.3.10. *TLO* disruption affects growth of *C. dubliniensis*

4.3.10.1. Effect of *TLO* disruption on growth in nutrient-rich conditions

Overnight (18 h, YEPD, 30 °C) cultures were stained with Calcofluor White to increase contrast and to visualise cell-cell divisions and photographed (Figure 4.5). Both Δ*tlo1* and ΔΔ*tlo* grew as clumped pseudohyphal-like cells, compared to Wü284 and Δ*tlo2*, which grew as mainly yeast cells. This propensity for the *tlo1* and double *tlo* mutants to grow as pseudohyphal or clumped cells is reflected in their ability to filament as discussed in Section 4.3.12. In addition, restoration of *TLO1* was able to restore wild-type like phenotype, whereas *TLO2* was not.

Strains of *C. dubliniensis* were then inoculated and grown under favourable, nutrient rich conditions in YEPD at 37 °C. The growth curve of each strain over 72 h is shown in Figure 4.14.A. Both Δ*tlo1* and ΔΔ*tlo* grew at significantly slower rates than wild-type. To quantify the behaviour of each strain during growth, the doubling time was calculated from the exponential growth phase as shown in Figure 4.14.B and doubling times, along with the corresponding r-squared values are detailed in Table 4.2. Briefly, Wü284 had a doubling time in YEPD of 94.92 min. In the case of Δ*tlo1*, the doubling time is increased by almost 10 % to 104.6 min. Disruption of *TLO2* however, does not affect doubling time in YEPD which averaged at 91.72 min. Deletion of both *TLO* genes resulted in slow growth, similar to Δ*tlo1* with a doubling time of 102.9 min. All strains remained yeast-like in appearance during growth in YEPD at 37 °C

4.3.10.2. Effect of *TLO* disruption on growth in alternate carbon sources.

The glucose component in YEPD was substituted with 2 % (w/v) galactose (YEPG) and growth at 37 °C was analysed as in Section 4.3.10.1. Overall growth patterns for up to 48 h of growth are shown in Figure 4.15.A. As in YEPD, ΔΔ*tlo* displayed slower growth. Data were fit to a regression curve, as described in section 4.2.5. and the doubling times were calculated (Table 4.2). Wild-type *C. dubliniensis* (Wü284) had a doubling time of 95.17 min. Disruption of *TLO1* (Δ*tlo1*) resulted in a dramatic increase in doubling time by over 35 % to 129.2 min. Disruption of *TLO2* (Δ*tlo2*) increased doubling time by 12 % to 106.8 min. Most significantly, ΔΔ*tlo* displayed a striking retardation in growth with a 57 % increase in doubling time compared to wild-type, to 149.3 min. Re-introduction of *TLO1*

was sufficient to restore wild-type levels of growth in the ΔΔ*tlo* background. In fact, growth was slightly faster with a doubling time of 84.29 min for ΔΔ*tlo*::*TLO1*. Reintroduction of *TLO2* also improved growth in the ΔΔ*tlo* background, with ΔΔ*tlo*::*TLO2* having a doubling time of 103.1 min. During growth in YEPG, cells for all strains were yeast in appearance, with the exception of ΔΔ*tlo* which grew as a mixture of pseudohyphal cells and chains of yeast cells.

Following from this, the glucose in YEPD was replaced with 2 % (w/v) succinate (YEPS) and the same strains were incubated at 37 °C. Overall growth patterns for up to 48 h of growth are displayed in Figure 4.16.A. As outlined above, the doubling times were calculated (from Figure 4.16. B) in the exponential phase of growth and are outlined in Table 4.2. Wü284 had a doubling time in YEPS of 89.31 min. Disruption of *TLO1* resulted in a 24 % increase in doubling time compared to wild-type, at 110.8 min. However, deletion of *TLO2* did not result in any significant change in doubling time, with Δ*tlo2* averaging at 91.88 min. The most significant retardation of growth was seen in ΔΔ*tlo* with a doubling time of 132 min (48 % slower). Almost full restoration of wild-type growth rates was seen upon re-introduction of *TLO1* in ΔΔ*tlo*::*TLO1* (94.46 min) and a lesser improvement in growth rate was observed in ΔΔ*tlo*::*TLO2* (112 min). During growth in YEPS, all strains grew as yeast with the exception of ΔΔ*tlo*, which grew as a mixture of yeast cells and pseudohyphal cells.

4.3.10.3. Effect of *TLO* disruption on growth in minimal media.

Strains were grown in Lee's minimal defined media at 30 °C and the levels of growth we recorded for up to 24 h (Figure 4.17. A). As a result of slow growth in this media, it was difficult to identify differences in growth from the overall profiles shown in Figure 4.17.A. Doubling times were calculated (from Figure 4.17. B) as described in the above sections and are listed in Table 4.2. Wü284 had a doubling time of 100.6 min. Disruption of either *TLO1* or *TLO2* did not yield any significant change in growth rates, resulting in doubling times of 106.6 and 97.27 min respectively. However, deletion of both *TLO* genes resulted in a doubling time increase of 57 % to 157.6 min. Reintroduction of *TLO1* or *TLO2* to ΔΔ*tlo* background improved doubling times to 127.3 and 130.1 min respectively.

Strains of *C. dubliniensis tlo* mutants were also grown on solid Lee's medium agar (pH 4.5) at 30 °C for 7 days. Colony sizes after growth were significantly smaller than colonies on YEPD agar due to limited nutrients. The

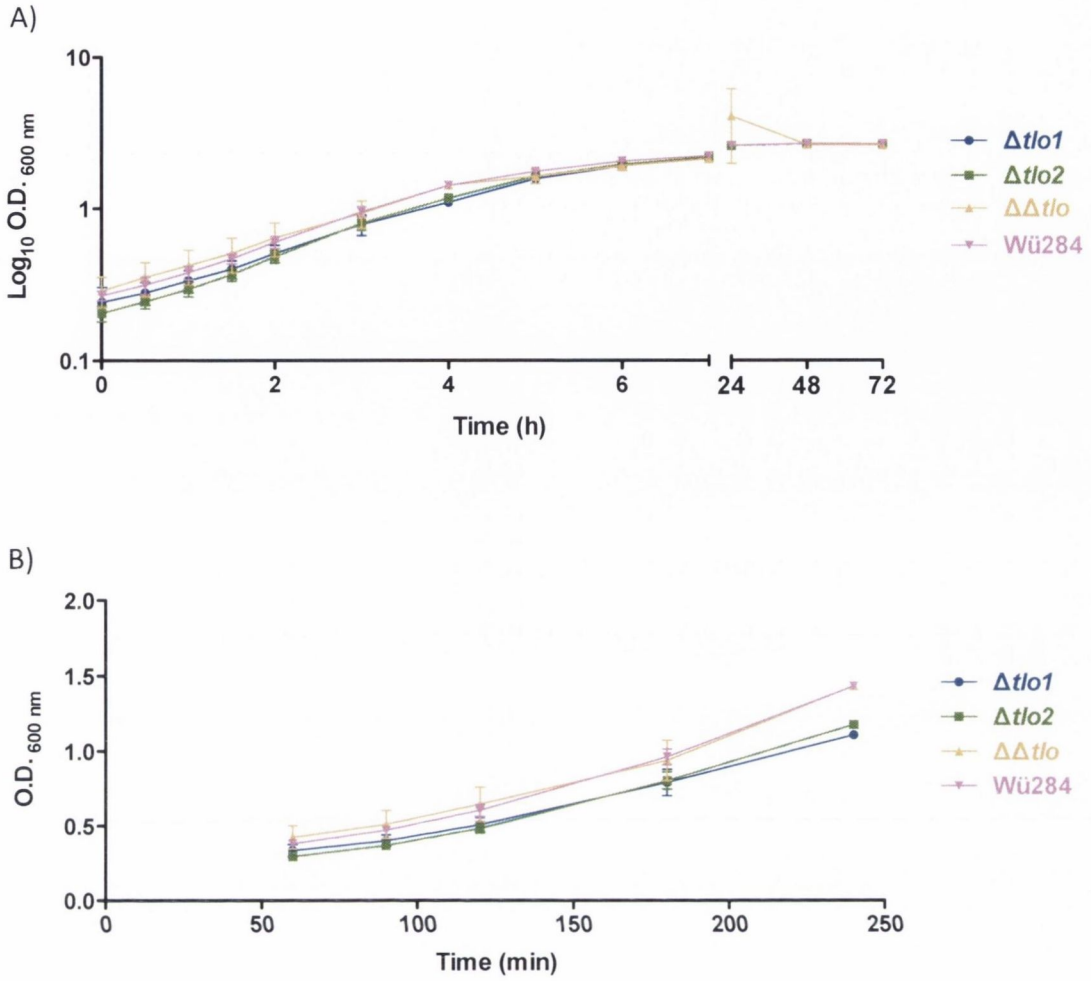

Figure 4.14. Growth behaviour of *C. dubliniensis tlo* mutants in nutrient-rich conditions. Strains were grown in YEPD at 37 °C as described in section 4.2.5.

(A) OD_{600nm} readings were recorded at various intervals over at least three separate experiments. The data were averaged and transformed logarithmically (to base 10) then visualised using GraphPad Prism software (Graphpad). Error bars are shown for each data point and represent the standard deviation, where $p < 0.05$. Legends for each data line are displayed to the right of each plot. Data points from the exponential phase only were transformed to non-log data points and visualised in a 'log growth' only plot (B) to help visualise the similarities and differences between strains and to aid in the calculation of doubling times.

Growth Media	°C	Wü284	Δ*tlo1*	Δ*tlo2*	ΔΔ*tlo*	ΔΔ*tlo*::*TLO1*	ΔΔ*tlo*::*TLO2*
YEPD	37	94.92	104.6	91.72	102.9	*nd*	*nd*
		0.9865	*0.9502*	*0.9783*	*0.9044*	*nd*	*nd*
YEP-Galactose	37	95.17	129.2	106.8	149.3	84.29	103.1
		0.9828	*0.9933*	*0.9995*	*0.9821*	*0.9916*	*0.9974*
YEP-Succinate	37	89.31	110.8	91.88	132	94.46	112
		0.9228	*0.9835*	*0.9826*	*0.9037*	*0.9707*	*0.8614*
Lee's defined medium	30	100.6	106.6	97.27	157.6	127.3	130.1
		0.978	*0.9598*	*0.9836*	*0.7243*	*0.8682*	*0.9675*
Spider medium	30	152.4	168.2	145.4	178.7	161.1	175.9
		0.9535	*0.9842*	*0.9528*	*0.966*	*0.9464*	*0.9456*

Table 4.2. Doubling times of *tlo* mutant strains.

Doubling times (min) were calculated as described in section 4.2.5. using optical density ($O.D._{600nm}$) measurements from the exponential/logarithmic phase of growth only. The coefficient of determination (R^2) value is shown italicised below each doubling time value as an indicator of confidence in the data when analysed using regression.

**nd* – not determined

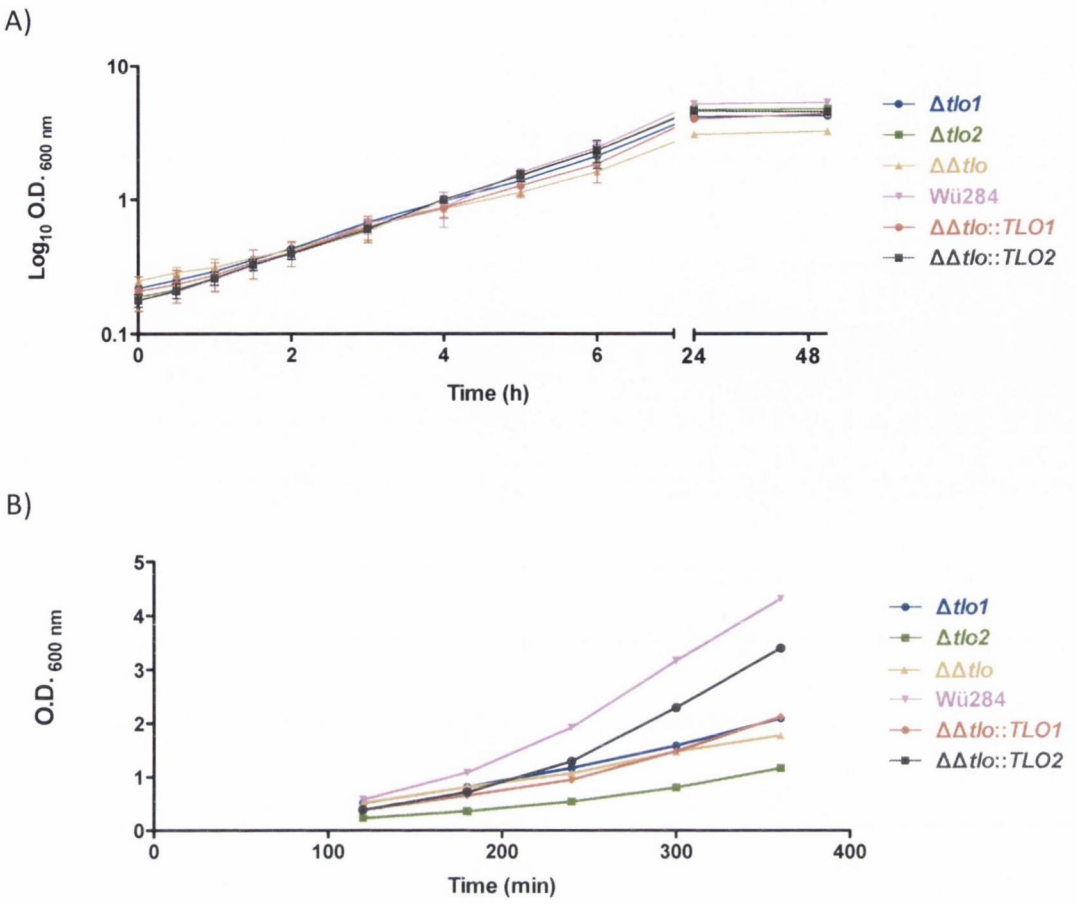

Figure 4.15. Growth behaviour of *C. dubliniensis tlo* mutants in galactose-based media. Dextrose (glucose) in YEPD was substituted with galactose and incubation was carried out at 37 °C as described in section 4.2.5.

(A) OD_{600nm} readings were recorded at various intervals over at least three separate experiments. The data were averaged and transformed logarithmically (to base 10) then visualised using GraphPad Prism software. Error bars are shown for each data point and represent the standard deviation, where $p < 0.05$. Legends for each data line are displayed to the right of each plot. Data points from the exponential phase only were transformed to non-log data points and visualised in a 'log growth' only plot (B) to help visualise the similarities and differences between strains and to aid in the calculation of doubling times

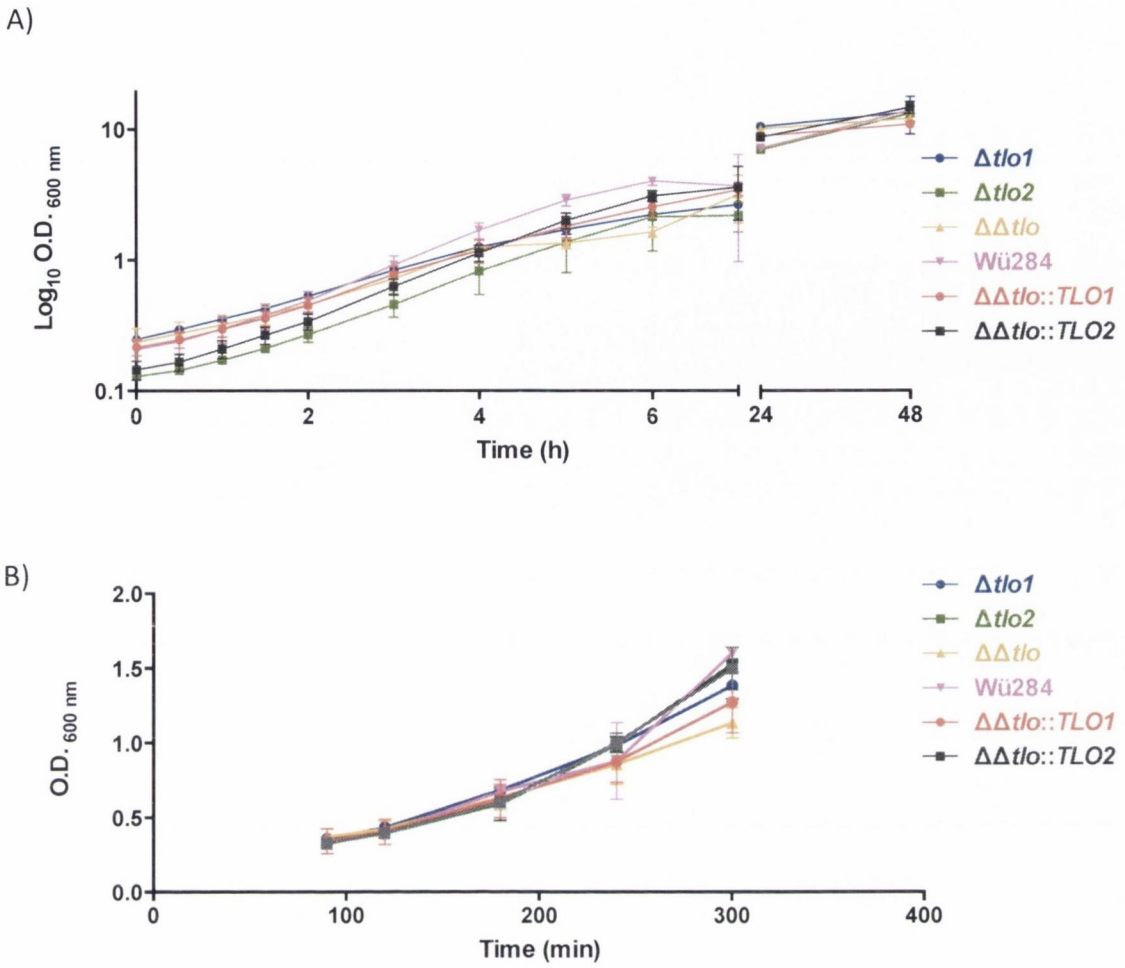

Figure 4.16. Growth behaviour of *C. dubliniensis tlo* mutants in succinate-based media. Dextrose (glucose) in YEPD was substituted with succinate and incubated at 37 °C as outlined in section 4.2.5.

(A) OD_{600nm} readings were recorded at various intervals over at least three separate experiments. The data were averaged and transformed logarithmically (to base 10) then visualised using GraphPad Prism (Graphpad) software. Error bars are shown for each data point and represent the standard deviation, where $p < 0.05$. Legends for each data line are displayed to the right of each plot. Data points from the exponential phase only were transformed to non-log data points and visualised in a 'log growth' only plot (B) to help visualise the similarities and differences between strains and to aid in the calculation of doubling times.

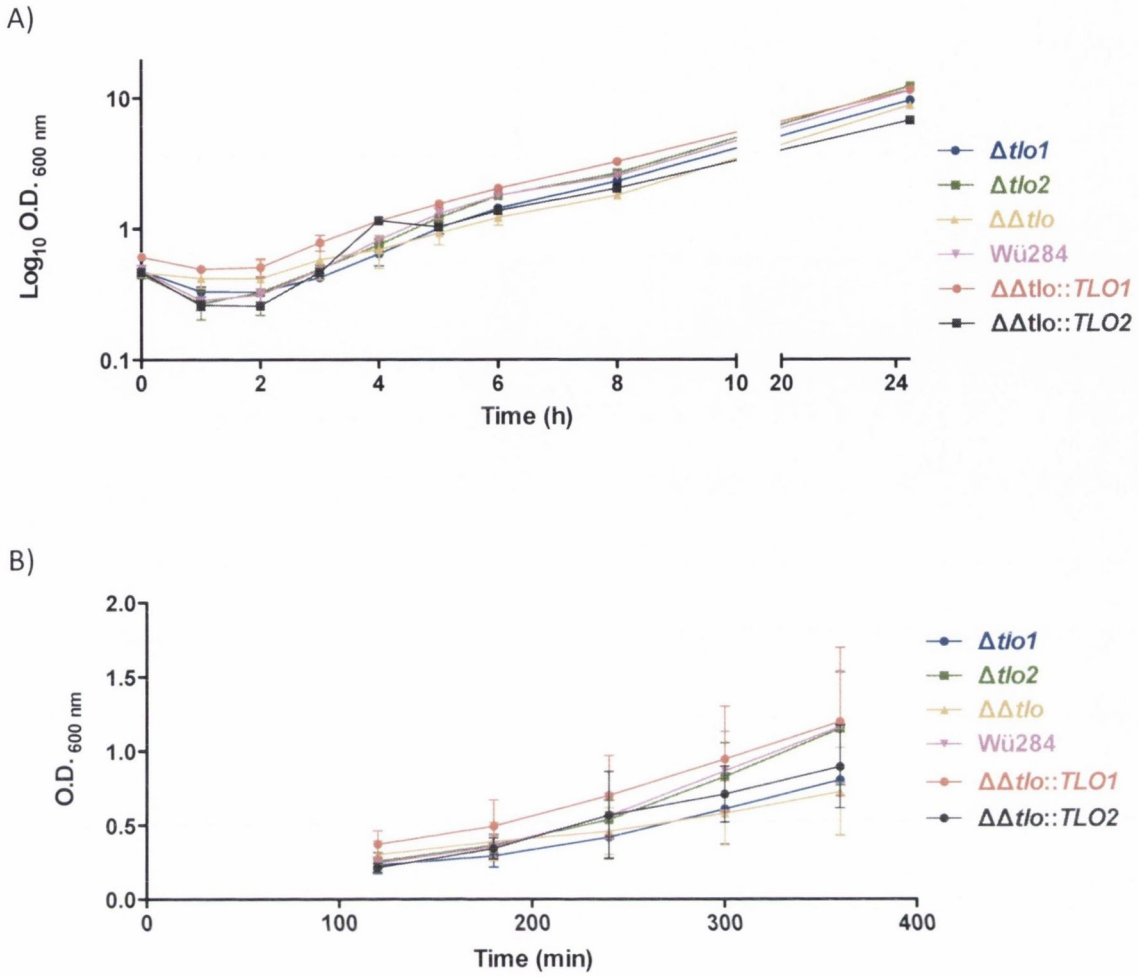

Figure 4.17. Growth behaviour of *C. dubliniensis tlo* mutants in minimal media.

Strains were incubated in Lee's defined minimal media with supplements at 30 °C as outlined in section 4.2.5.

(A) OD_{600nm} readings were recorded at various intervals over at least three separate experiments. The data were averaged and transformed logarithmically (to base 10) then visualised using GraphPad Prism (Graphpad) software. Error bars are shown for each data point and represent the standard deviation, where $p < 0.05$. Legends for each data line are displayed to the right of each plot. Data points from the exponential phase only were transformed to non-log data points and visualised in a 'log growth' only plot (B) to help visualise the similarities and differences between strains and to aid in the calculation of doubling times.

cellular morphology of Wü284 was of normal yeast-type cells (Figure 4.18. A). Heterozygous deletion of *TLO1* resulted in larger colonies with a slightly smaller cellular morphology than in wild-type (Figure 4.18 B). Both Δ*tlo1* and Δ*tlo2* grew similarly to Wü284 (Figure 4.18 C and D) and were similar in cellular morphology. ΔΔ*tlo* grew as significantly smaller colonies (Figure 4.18. E) than any of the other strains tested, however cellular morphology was not observed to be any different to the previously tested strains.

4.3.10.4. Effects of *TLO* disruption on growth in Spider Medium.

Strains were grown in Spider medium and incubated at 30 °C for up to 72 h. From the overall growth profile (Figure 4.19. A), it was not immediately clear whether there were differences in growth phenotypes between strains. Doubling times were calculated from the exponential phase of growth (Figure 4.19. B) as described in the preceding sections and are listed in Table 4.2. Wü284 had a doubling time of 152.4 min. Disruption of either *TLO1* or *TLO2* resulted in doubling times of 168.2 and 145.4 min respectively. The ΔΔ*tlo* mutant had a doubling time increase of 17 % to 178.7. Re-introduction of *TLO1* improved doubling time somewhat (161.1. min), whereas *TLO2* re-introduction had no observable effect (175.9 min).

4.3.11 Effect of *TLO* disruption on filamentous colony morphology.

Strains of *C. dubliniensis* were sub-cultured on Spider medium and incubated at 30 °C for 48 h. Differences in colony morphologies were observed between strains as is shown in Figure 4.20. Wü284 displayed the typical round glossy colonies (Figure 4.20 B), which is normal for *C. dubliniensis* which does not form wrinkled colonies on Spider Medium (Personal Communication; Moran, 2011). The heterozygous *tlo1* mutant exhibited umbonate colonies, that were smaller in size compared to wild-type (Figure 4.20. C). A homozygous *tlo1* mutant produced wrinkled colonies (Figure 4.20. D). A *tlo2* null mutant did not exhibit any difference compared to wild-type (Figure 4.20. E). The double *tlo* mutant displayed retarded growth and smaller colonies with a wrinkled morphology (Figure 4.20. F). Restoration of *C. dubliniensis TLO1* (Figure 4.20 G) was sufficient to restore wild-type colony size and shape, whereas the *TLO2* re-integrant (Figure 4.20 H) did not restore wild-type morphology. Introduction of the *C. albicans TLO*

genes *TLO11* (Figure 4.20 I) and *TLO12* (Figure 4.20. J) to the Δ*tlo1* background also restored *C. dubliniensis* wild-type colony morphology.

4.3.12. Effect of *TLO* disruption on filamentation in liquid culture

In order to assess the effect of disruption of the *TLO* genes in *C. dubliniensis* on filamentation, strains were induced to form hyphae by incubation in water supplemented with 10 % (v/v) foetal calf serum (FCS) at 37 °C. Results were reported in terms of the percentage of true hyphal cells out of the total number of cells counted in the culture (n = 300). As is typical with wild-type *C. dubliniensis*, Wü284 cultures were between 80 % and 100 % true hyphal in composition by 3 h of growth in the above conditions (Figure 4.21. A). Disruption of one copy of *TLO1* (heterozygous mutant) resulted in a moderate reduction in filamentous growth (Figure 4.21. A). Homozygous deletion of *TLO1* in *C. dubliniensis* resulted in a more significant reduction in the levels of true hyphal formation even at 1 h growth in culture (Figure 4.21. B). By 2 h in culture, true hyphal formation in Δ*tlo1* plateaued at around 30 %, showing less than half the amount of true hyphae compared to wild-type. While the rate of hyphal formation was slower, cellular morphology of Δ*tlo1* was similar to Wü284 (Figure 4.22). Deletion of *TLO2* resulted in a slight lag in true hyphal formation, but by 3 h, Δ*tlo2* had reached wild-type levels of true hyphal morphology (80 %). It appeared that after 30 min, Δ*tlo2* formed true hyphae slightly quicker than Wü284 (Figure 4.21. B), while cellular morphology was generally similar to Wü284 (Figure 4.22).

The double deletion mutant, ΔΔ*tlo* displayed the most extreme phenotype. Throughout culture, it remained unable to form any true-hyphal cells (Figure 4.21. C). Instead, the culture was composed of pseudohyphal clumps of cells (Figure 4.22). In addition, this strain was unable to revert to yeast-like cells at any stage (tested up to 24 h of growth). Reintroduction of *TLO1* was able to significantly reverse the non-hyphal phenotype of ΔΔ*tlo*, with levels of true hyphae (Figure 4.22) reaching 60 % by 3 h of culture (Figure 4.21. D). As time progressed, true hypha formation reached near wild-type levels by 5 h. Reintroduction of *TLO2* however, was only able to partially restore true hypha formation, which plateaued at under 40 % in a fashion very similar to Δ*tlo1* (Figure 4.21. D, Figure 4.22).

Introduction of *C. albicans TLO11* and *TLO12* to Δ*tlo1* background resulted in a dramatic restoration of true hyphal formation to levels above that normally seen in wild-type *C. dubliniensis* (Figure 4.21. E).

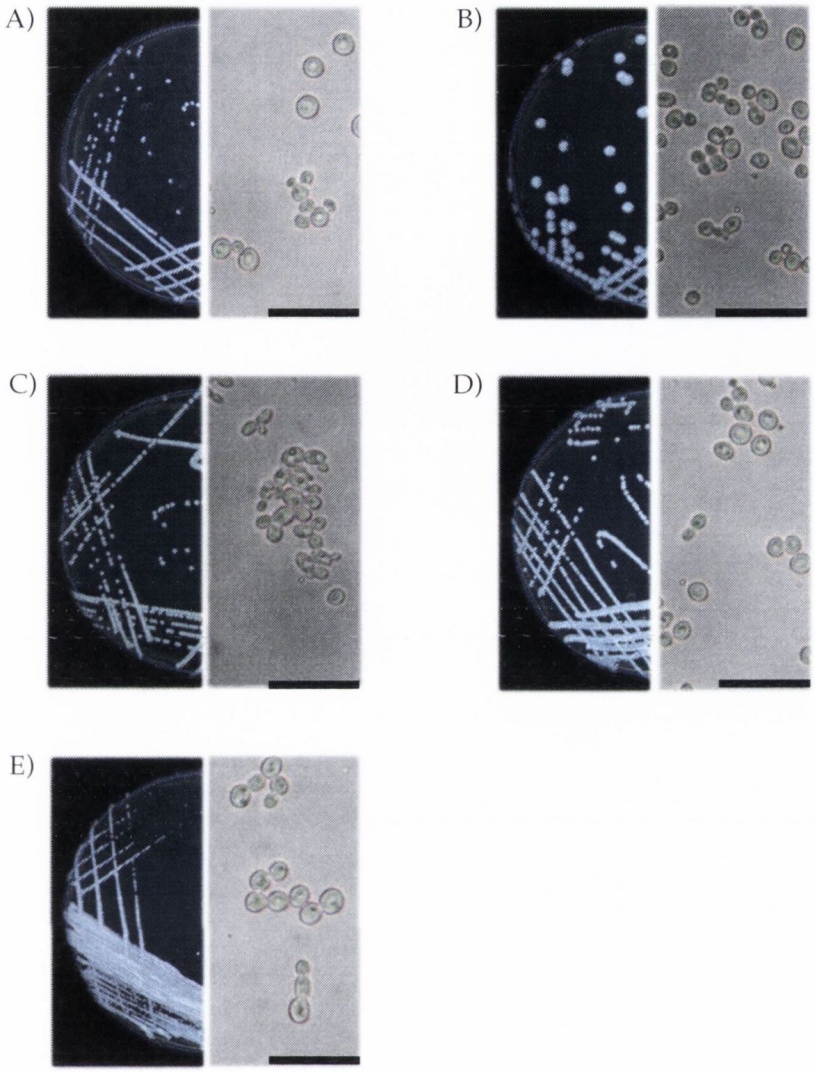

Figure 4.18. Growth of *C. dubliniensis tlo* mutants on solid minimal media.

Strains of *C. dubliniensis* [Wü284 (A), Δ*tlo1*/*TLO1*(B), Δ*tlo1* (C), Δ*tlo2* (D) and ΔΔ*tlo* (E)] were plated on Lee's medium (pH 4.5) and incubated at 30 °C for 7 days. Beside each plate image is a photograph displaying typical cellular morphology. For this, a colony was then emulsified in 50 μl of PBS for visualisation at 400 X magnification on a light microscope. Scale bar represents 15 μM. All images are scaled to be equivalent and are representative of typical samples from three separate experiments.

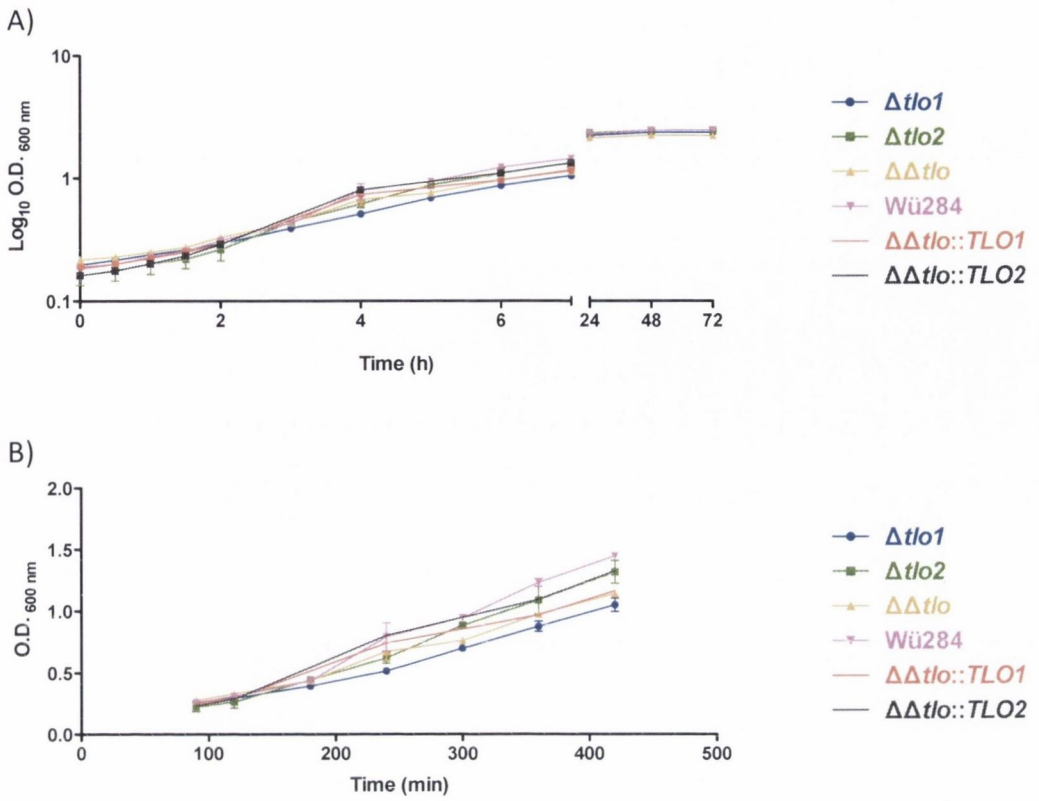

Figure 4.19. Growth of *C. dubliniensis tlo* mutants in liquid Spider medium.
Strains were incubated in Spider medium as described in section 4.2.5. at 30 °C. (A) OD_{600nm} readings were recorded at various intervals over at least three separate experiments. The data were averaged and transformed logarithmically (to base 10) then visualised using GraphPad Prism (GraphPad) software. Error bars are shown for each data point and represent the standard deviation, where $p < 0.05$. Legends for each data line are displayed to the right of each plot. Data points from the exponential phase only were transformed to non-log data points and visualised in a 'log growth' only plot (B) to help visualise the similarities and differences between strains and to aid in the calculation of doubling times.

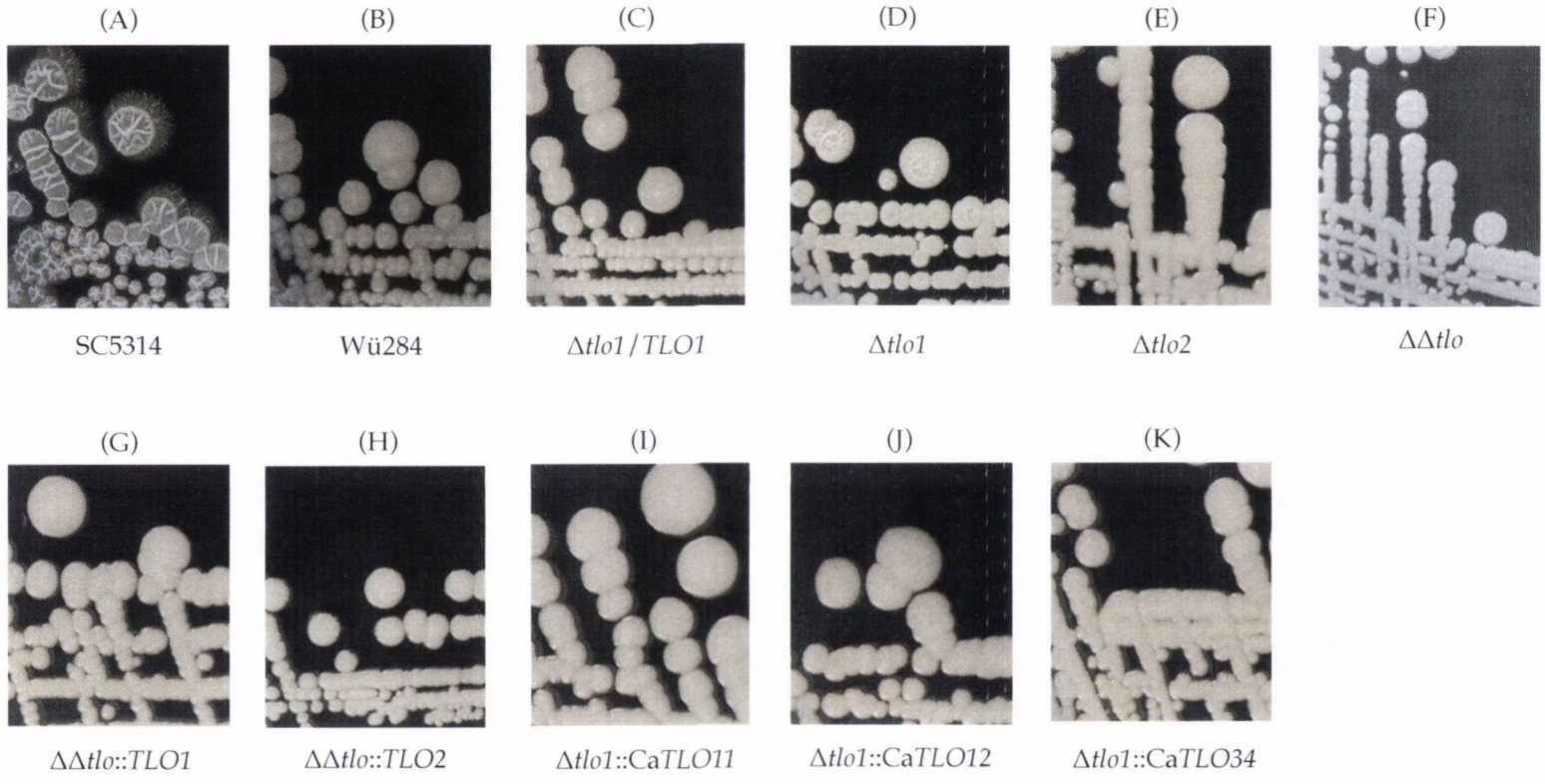

Figure 4.20. Growth of *C. dubliniensis tlo* mutant strains on solid filament-inducing medium.

Strains of *C. dubliniensis* (A-K) were sub-cultured on Spider medium and incubated at 30 °C for 48 h. Strains were then photographed at the same scale. Differences in colony morphology were noted between strains (strains indicated below each photograph) Photographs are examples representative of samples from three separate experiments. Zoom and magnification has been normalised to ensure colony sizes are directly comparable in these images.

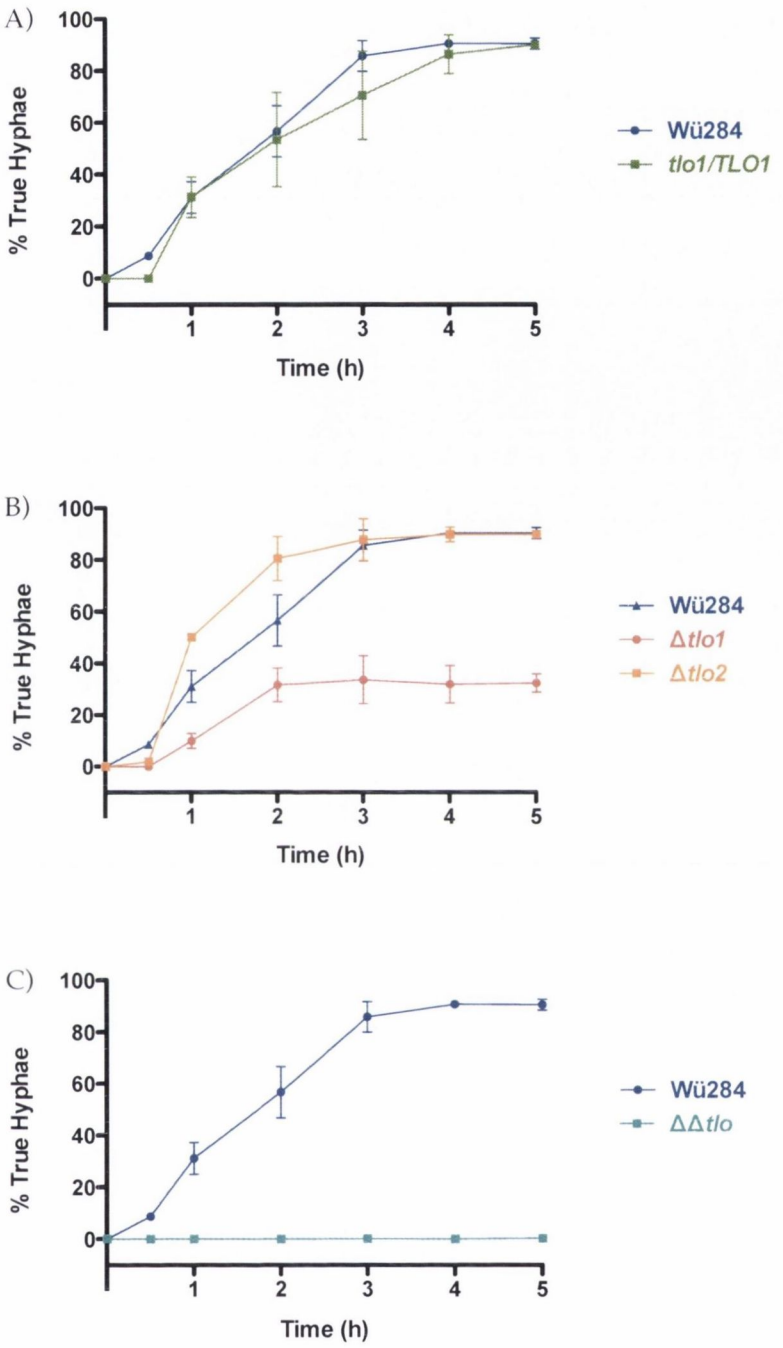

Figure 4.21. (A – C). True hyphal formation in *C. dubliniensis tlo* mutant strains. True hyphal formation for strains (A-C) of *C. dubliniensis* in water with 10% foetal calf serum is represented as the percentage of total cells (regardless of morphology) counted that were 'true hyphal' as detailed in section 4.1. Each count is an average of at least three separate experiments. Error bars shown represent the standard deviation of the average counts.

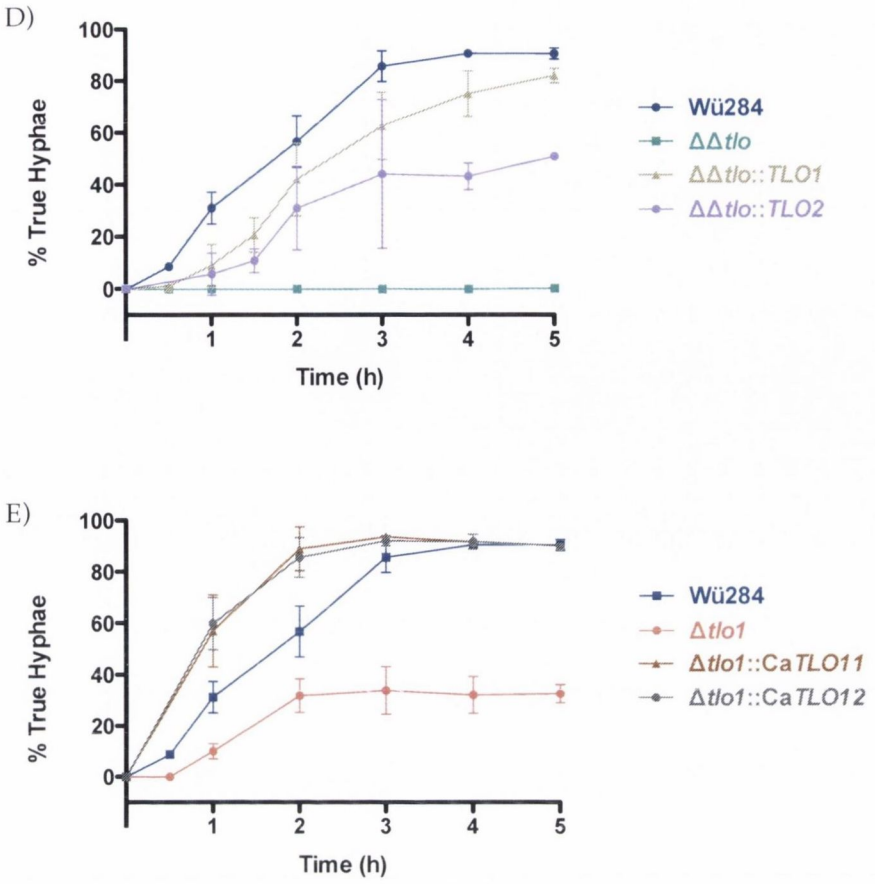

Figure 4.21 (D – E). True hyphal formation in *C. dubliniensis tlo* mutant strains.
True hyphal formation for strains (D - E) of *C. dubliniensis* in water with 10% foetal calf serum is represented as the percentage of total cells (regardless of morphology) counted that were 'true hyphal' as detailed in section 4.1. Each count is an average of at least three separate experiments. Error bars shown represent the standard deviation of the average counts.

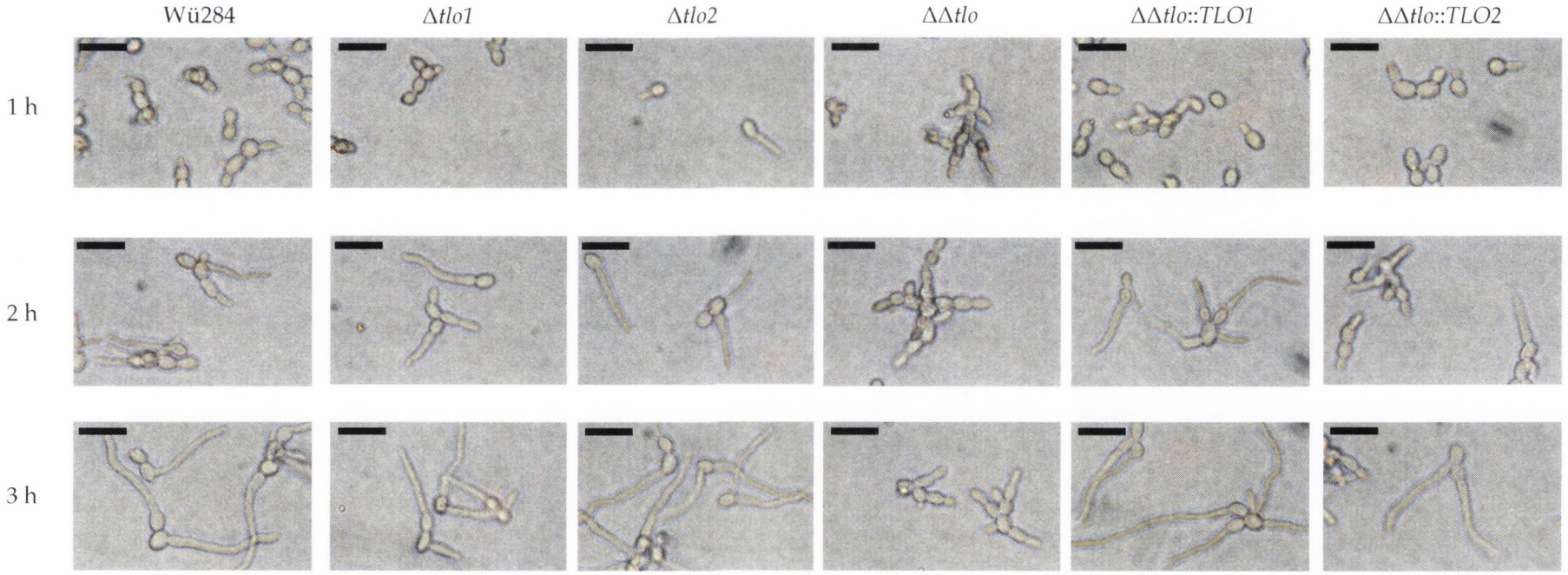

Figure 4.22. Hyphal formation in *C. dubliniensis tlo* mutants

Strains of *C. dubliniensis* (indicated) were pre-cultured in YEPD at 30 °C for 18 h with shaking at 200 r.p.m. and then incubated in water supplemented with 10% (v/v) foetal calf serum at 37 °C with shaking at 200 r.p.m. Samples were taken at hourly intervals and viewed under 400X magnification under phase contrast microscopy. Scale bar is identical for all samples and indicates 15 μM length.

4.3.13. Effect of *TLO* disruption on the ability of *C. dubliniensis* to form and maintain biofilms

In order to examine the effects of the *tlo* mutant strains of *C. dubliniensis* to form biofilms *in vitro*, each strain was seeded to 96-well polystyrene plates as described in section 4.2.8, in water with 10 % serum either in ambient air or 5 % (v/v) CO_2. After 24 h and several vigorous washing steps, the XTT assay was used to determine the amount of viable cells as a way of quantifying the initiation of a biofilm.

After 24 h of incubation, Wü284 was relatively poor at forming biofilm under normally aerated conditions (Figure 4.23. A). There was significantly higher biofilm formation for Δ*tlo1* ($p = 0.0005$) but not for Δ*tlo2* ($p = 0.1787$). Disruption of both *TLO* genes resulted in a highly significant increase in biofilm formation at 24 h in strain ΔΔ*tlo* ($p < 0.0001$). Restoration of either *TLO1* or *TLO2* into the ΔΔ*tlo* background appeared to bring biofilm formation back down to wild-type levels, with restoration of *TLO2* appearing to have a greater effect in that it is not significantly different from Wü284 ($p = 0.0934$). By 48 h, Wü284 displayed an increase in the levels of biofilm. However, all other strains displayed decreased levels of biofilm compared to the earlier time point (Figure 4.23. B). The ΔΔ*tlo* strain still displayed significantly higher biofilm formation compared to Wü284 ($p = 0.0014$). Δ*tlo1* ($p = 0.0104$) and Δ*tlo2* ($p = 0.0022$) exhibited lower levels of biofilm maintenance than Wü284. Reintroduction of either *TLO1* or *TLO2* in the ΔΔ*tlo* background was sufficient to restore lower levels of biofilm similar to Wü284.

Incubation in the presence of 5 % w/v CO_2 generated a set of results with similar trends to those seen following biofilm formation in ambient air (Figure 4.23. A). However, it increased the significance of some differences between wild-type and *tlo* mutant strains, as seen by the reduced p values generated when Δ*tlo1* ($p = 0.0001$) and ΔΔ*tlo*::*TLO1* ($p = <0.0001$) were compared to wild-type. Following 48 h incubation in the presence of 5 % (v/v) CO_2 both Δ*tlo1* ($p = 0.0913$) and ΔΔ*tlo* ($p < 0.0001$) displayed significantly more biofilm formation than Wü284.

In an attempt to confirm results at the 48-h time-point, crystal violet stain was used to visualise and quantify the amount of biomass present in each well. This method was typically less sensitive than the XTT method and did result in reproducible data (Figure 4.23. C).

4.3.14. Ability of *C. dubliniensis tlo* mutant strains to invade solid substrates

Each of Δ*tlo1*, Δ*tlo2*, ΔΔ*tlo* and Wü284 were tested as described in section 4.2.6. for the ability to invade agar surfaces. No ability to invade agar was observed for any of the *C. dubliniensis* strains tested under these conditions (data not shown).

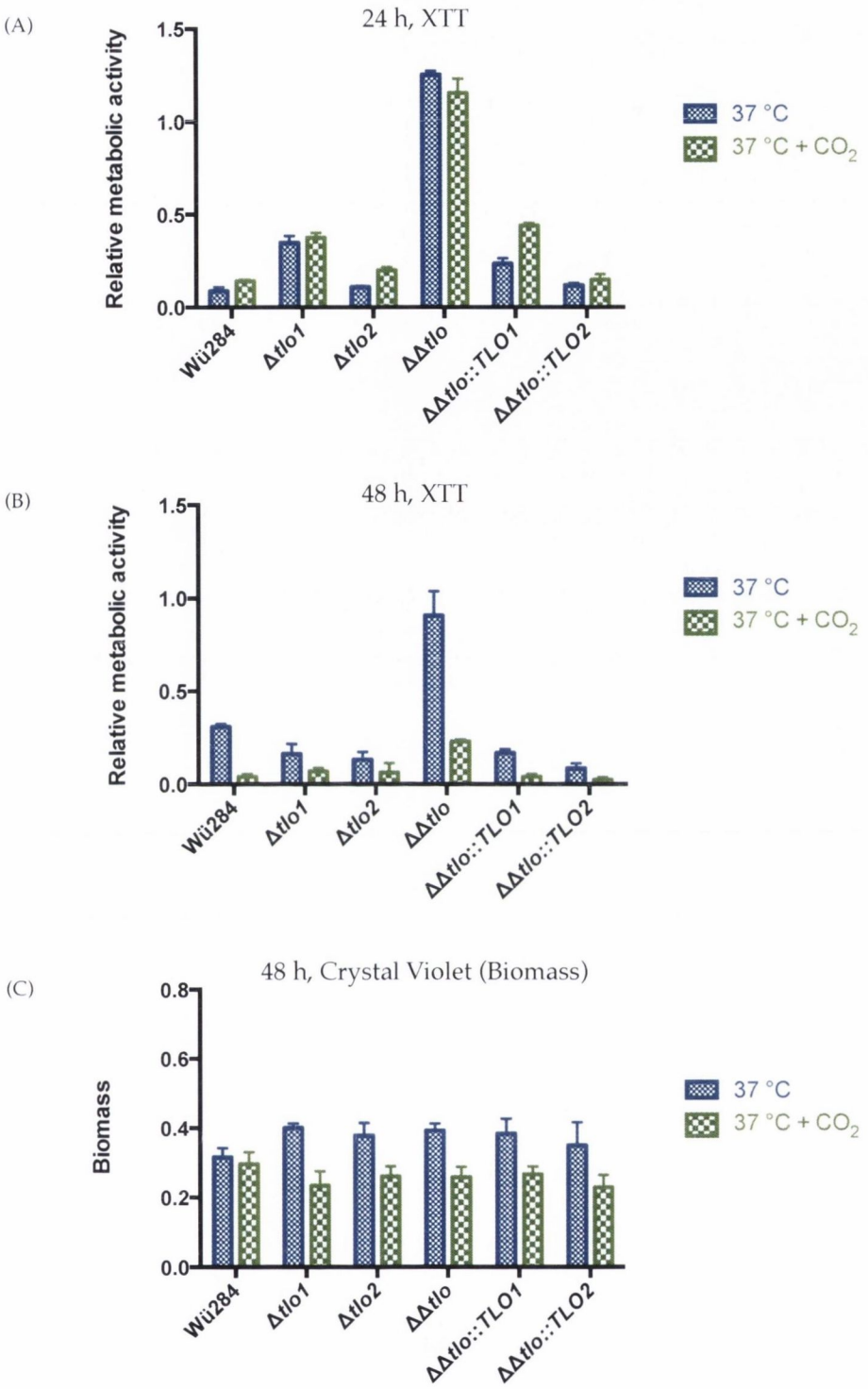

Figure 4.23. Determination of the effects of *TLO* disruption on biofilm initiation and maintenance.

Strains of *C. dubliniensis* were incubated with (Blue) and without (Green) 5 % Carbon dioxide for either 24 hours (A) or 48 hours (B) and the existing biofilm was measured using XTT. At the 48 hour timepoint, crystal violet was also used to determine results (C). Each experiment was repeated three times (n = 9) and error bars represent the standard deviation from the mean result.

4.4 Discussion

4.4.1. The *TLO*s regulate the morphological state of *C. dubliniensis*

In this study, it was observed that disruption of the *TLO* genes significantly affected the yeast-to-hypha transition. This morphological switch has been strongly implicated in the virulence of the organism (Sudbery, 2011). In the absence of *TLO1*, the rate of true hyphal formation appeared to be retarded and reach a plateau lower than wild-type, which normally is 90 % hyphal within 3 h of incubation in 10% serum (O'Connor *et al.*, 2010). A double disruption of both *TLO1* and *TLO2* completely abrogated any ability to form true hyphae under ideal inducing conditions. The Δ*Δtlo* cells appear in clumps as if unable to separate leading to a pseudohyphal appearance. This was most likely due to a cell separation defect as indicated by the calcofluor staining, SEM images and the requirement for cell wall digestion to separate cells. Of particular interest was the ability of *C. albicans TLO*s to restore filamentation to higher than wild-type levels, which supports our hypothesis that *C. albicans* and *C. dubliniensis TLO*s are functionally similar, as discussed in Chapter 3.

This inability to form true hyphae has wide-reaching knock-on phenotypic effects. For example, hyphal formation is important in the development of biofilms. Biofilms are a key facet of many successful pathogens, carrying out many vital functions associated with the initiation of infection and the persistence/maintenance of infection. These masses of cells, often multi-organism in composition, can act as reservoirs of infection on indwelling devices (Uppuluri & Chaffin, 2007) and physical barriers against attack e.g. from antifungals (Hawser & Douglas, 1995; Taff *et al.*, 2013). Interestingly, the disruption of both *TLO* genes led to a significant increase in both the initial adherence and maintenance of basic *in vitro* biofilms. It is possible that this may not accurately reflect the *in vivo* situation, however it was interesting that a strain that cannot form true hyphae was better at forming and maintaining biofilms *in vitro*. Hyphae have been implicated as an important component of the mature *Candida* biofilm aiding in increased biofilm formation, maintenance and resistance to antifungal drugs (Banerjee *et al.*, 2013; López-Ribot, 2005) and provide a structural scaffold to the developed biofilm (Paramonova *et al.*, 2009; Richard *et al.*, 2005). As such, *in vivo* experiments might show that the *tlo* mutants have biofilm maintenance defects. The increased ability to form biofilms may also be due to a change in the

transcriptional landscape of the genes encoding adhesion proteins or biofilm regulators which will be further explored in Chapter 5, many of which show altered expression in the absence of *TLO*s (e.g. *UME6*, *HWP1*). Alternatively, cell clumping, mediated by a defect in cell separation may provide more surface area for the initial adhesion stages of early biofilm formation. From these experiments, it would appear that true hyphal formation is not necessary for the formation of the biofilm in *C. dubliniensis*, nor in the maintenance up to 48 h. However, in other *Candida* species (Laffey & Butler, 2005), it has been shown that pseudohyphae are important in biofilm maturation. Further experiments are required to fully elucidate the relationship between the *TLO*s and biofilm development.

Besides hyphal and biofilm formation, the absence of both *TLO*s in *C. dubliniensis* affected the formation of chlamydospores. While these thick-walled spore-like bodies are thought to be involved in response/survival in harsh conditions (Staib & Morschhäuser, 2007), little is definitively known about their true functions, except that they are an exclusive trait to *C. dubliniensis* and *C. albicans*. (Citiulo *et al.*, 2009). Likewise, *TLO* genes are observed only in these two strains (with a more distant ortholog in *C. tropicalis*) and as such it is possible that the ability to form these structures is connected with the acquisition/expansion of the *TLO* family of genes.

The *TLO*s appear to be indispensible for normal morphological switching. This suggests that *TLO* expression is necessary to modulate the proper transcriptional signals that promote this switch. Fitting in with the relationship between the *TLO*s and Mediator, the *TLO*s could be responsible for the specific activation of gene pathways under certain environmental conditions. Moreover, the *TLO*s (in conjunction with Mediator) might be required for rapid activation of the hyphal induction process, i.e. hyphal initiation and subsequent development is intricately linked to strict control of certain regulators such as *NRG1* (Lu *et al.*, 2011), *ECE1* (Nantel *et al.*, 2002), and *UME6* (Sudbery, 2011).

4.4.2. The *TLO*s affect the tolerance of *C. dubliniensis* to environmental stress

Environmental stress is something with which all living organisms must contend and ranges from changes in temperature to active attack from systems like the human immune arsenal. High temperature is often used as a means to differentiate cultures of *C. dubliniensis* from *C. albicans*, the latter growing significantly better at higher temperatures than *C. dubliniensis*, which shows severe

growth retardation at or above 42 °C (Campanha *et al.*, 2005). Disruption of *TLO2* resulted in slightly reduced ability to grow at the higher temperature. While this difference in growth was not a large one, it is interesting as one of the only phenotypes that could be directly attributed to deletion of *TLO2* alone. The reason for this is unknown, but may suggest a difference in functions of the two *TLO* genes.

Two *tlo* mutants (Δ*tlo1* and ΔΔ*tlo*) also displayed retarded growth in the presence of cell wall stressing chemicals as well as detergent. In the presence of osmotic stress, effects appeared to be dependent on the chemical used, i.e. Δ*tlo1* and ΔΔ*tlo* showed reduced growth in the presence of calcium chloride, whereas in the presence of sorbitol Δ*tlo1* and ΔΔ*tlo* showed better growth. While the human body as a host is normally quite hospitable in terms of temperature and osmotic stress, the immune system has evolved methods to such as elevated temperature during fever and high osmotic solutions e.g. sweat to combat invading organisms (Reece *et al.*, 2010). Dealing with these stresses is also important in other (perhaps uncharacterised) environments and it appears that *TLO*s play a role in the regulation of processes designed to combat these stresses.

Oxidative stress mediated by phagocytes is one of the primary defences in the adaptive immune system, against which *Candida* species have evolved a number of methods in dealing (Miramón *et al.*, 2012). Deletion of both *TLO* genes or, to a lesser extent *TLO1*, significantly affected the organism's ability to grow in the presence of either hydrogen peroxide or menadione, which is a quinone that produces superoxide radicals by redox cycling in the cell (Mutoh *et al.*, 2005). As with other stresses, the regulatory network behind the response to oxidative stress is complex, but observations in this Chapter suggest that the absence of *TLO*s has had an effect, whether direct or downstream, on the cellular response to oxidative stress.

In this Chapter, it was detailed that *TLO* genes were important in the ability of *C. dubliniensis* to grow in a variety of media. In particular, when the carbon source is other than glucose, e.g. galactose, deletion of *TLO* genes dramatically increases the doubling time. Likewise in minimal media and filamentous media, absence of *TLO* genes reduces growth. *Candida* possesses regulatory networks that allow for tailored expression of the sets of genes needed to deal with each of the nutrient sources (Horák, 2013; Sitepu *et al.*, 2014) and it is likely that *TLO*s are

involved in this regulation, as can be seen by the ability to restore near normal growth rates with reintegration of the *TLO*s.

Dealing with any of the stresses above is vital to the success of *Candida* as a pathogen. However, it is important to note that *Candida* species are considered opportunistic pathogens (Vilela *et al.*, 2002) and are quite successful as commensal organisms. An ideal characteristic of both pathogens and commensals is the ease with which they can acquire nutrients and deal with shifts in the local environment. Lack of functional *TLOs* has affected a number of such responses. As such, it is probable that Δ*Δtlo* would be impaired in a virulence model due to its defective morphological switch and its reduced resistance to chemical stresses and changes in nutrient availability. It is interesting to note however, that *C. parapsilosis* which cannot form true hyphae and forms only yeast and pseudohyphae, is successful as a pathogen *in vivo* (Laffey & Butler, 2005), so it would be of interest to investigate *C. dubliniensis tlo* mutants and their morphological and growth defects translate to clinically-relevant defects in a virulence model.

4.4.3. *TLO1* versus *TLO2*

Interestingly, the experiments in this Chapter have highlighted that the *TLOs* are not identical in function. Deletion of *TLO1*, *TLO2* or both results in different phenotypes in several assays employed. Morphology appeared to be affected mainly by *TLO1*, with a deletion of *TLO1* causing a significant reduction in true hyphal formation. However, true hyphal growth continued, albeit to a lesser extent, in the presence of a single copy of *TLO2*. Subsequent deletion of *TLO2* resulted in a complete inability to form true hyphae or chlamydospores. Restoration was observed with introduction of either gene, although restoration of *TLO1* resulted in greater hyphal growth than *TLO2*. Like hyphal formation, *TLO1* was more important in resistance to detergents, osmotic stress and oxidative stress, shown by the fact that Δ*tlo2* was not as susceptible (if at all) compared to Δ*tlo1* or Δ*Δtlo*. In many cases, such as in hyphal formation, when *TLO1* is deleted the defect is extreme, but not as severe as when both *TLO*s are removed. As such, there must be a degree of cross-functionality between the two genes.

A similar disparity can be seen in other phenotypes examined in this chapter. Growth in the presence of calcofluor white was not affected by deletion of either *TLO1* or *TLO2*, but was reduced by deletion of both *TLO*s and interestingly,

either *TLO1* or *TLO2* could restore growth. Likewise, growth in the presence of Congo red was affected only by deletion of both *TLO*s, yet was restored by either *TLO1* or *TLO2*. These results suggest that both *TLO*s are can perform the relevant function in order to induce resistance to these stressors, but in its native state, *TLO2* does not seem to play a role. This is most likely due to a difference in expression between the wild-type *TLO2* locus and the reintegrated *TLO2* locus, which can be expressed at a significantly higher level (Boyle, H., Personal Communication, 2013).

While it can only be speculated as to the reason for this dichotomy in functional importance in cases such as hyphal formation, global transcriptional analysis may provide an insight into the possibly distinct roles of *TLO1* and *TLO2*. Different stresses induce unique sets of genes equipped to deal with the change in the environment. In the next chapter, DNA microarray analysis was carried out to explore the relationship between global transcriptional changes and the disruption of the *TLO*s, many of which correlate with the phenotypes observed in this chapter. However, it is obvious from the results presented here that the *TLO*s play important roles in virulence and metabolic processes which may be direct, or the result of a more complex interaction. While a *C. albicans tlo* null mutant proves difficult to design, the results help to predict what phenotypes the *TLO*s are involved in. Moreover, the copy number of *TLO*s in these two species are different which may suggest that increased *TLO* genes could help *C. albicans* to be better equipped to deal with these stresses. For example, as mentioned above, Tlos functioning as part of the Mediator complex might be required for induction of expression of specific sets of genes under specific circumstances/conditions. An expanded repertoire of *TLOs* might mean the ability to deal with more environmental conditions, or perhaps a larger pool of Tlos in order to mount faster transcriptional responses. The ability of *C. albicans TLO11* and *TLO12* to restore defective phenotypes brought about by *C. dubliniensis TLO* deletion such as hyphal formation, further points towards an overlap in function between the *TLO*s but also a redundancy - one which *C. albicans* has evolved by expanding the *TLO* family. If *C. albicans* has acquired additional *TLO*s compared to *C. dubliniensis*, there is surely a fitness or evolutionary advantage brought about by this expanded gene family. Deletion of *C. albicans TLO* genes would be very useful in exploring this further.

Chapter 5

Expression analysis of *tlo* mutant strains in *Candida dubliniensis*

5.1. Introduction

In Chapter 4, it was established that disruption of the *TLO* genes in *Candida dubliniensis* resulted in a number of different virulence-associated and metabolic phenotypes, ranging from changes in filamentation to changes in growth behaviour. In the most basic sense, it is generally accepted that changes in phenotype are intrinsically linked to the genetic makeup of the organism. As such, it is highly likely that the *TLO* genes are involved in regulation of the phenotypes observed in the previous Chapter. By exploring the behaviour of the genes affected by the deletion of *TLO*s, it is possible to gain a better insight into the specific regulatory effects that the *TLO* genes have and the role they play in important processes and functions in *C. dubliniensis* and by homology, in *Candida albicans*.

Methods for analysing gene expression have improved dramatically in the last few years. Historically, techniques such as the use of a reporter gene (e.g. *lacZ, GFP*) or Northern immunoblots were used to determine single gene expression. As the importance of gene expression in a global context became more apparent, techniques such as quantitative real-time PCR (qRT-PCR) and serial analysis of gene expression (SAGE) were adapted and utilised extensively which allowed for increased speed and accuracy. However, arguably the most useful technique to arise was DNA-microarray analysis. This technique was derived from Southern blot analysis, which relies on DNA-DNA hybridisation (Maskos & Southern, 1992) and began with a comparatively small number of probes, allowing determination of the presence or absence of genes. Incorporating fluorescent labeling, the technique was adapted for use with mRNA samples to determine expression instead of simply the presence of a sequence. With the advent of whole genomic sequencing (Fleischmann *et al.*, 1995) and increasingly advanced engineering, it became possible to 'print' many DNA oligonucleotide probes onto a glass substrate which allowed for the creation of the high-throughput DNA microarrays (Schena *et al.*, 1995). Eventually, further miniaturisation allowed for the first whole eukaryotic genome (*Saccharomyces cerevisiae*) printed on a DNA microarray (Lashkari *et al.*, 1997) With this technique, expression for all known coding regions within the genome of an organism could be determined and analysed allowing for an accurate and efficient snapshot of the genetic landscape of an organism at a particular time.

The DNA microarray formats used in this study were of the Agilent Technologies 4 X 44K array template. As such, there were 4 separate array tiles per slide each containing the full set unique, duplicated 60-mer probe sequences from all known coding regions in the *C. dubliniensis* genome (Moran, 2011; O'Connor *et al.*, 2010). The data were averaged over the four tiles in combination with a dye-swap implemented on two of the tiles to allow for high accuracy and precision, thereby reducing bias, false positive and false negative results.

Not only have the experimental tools for expression analysis improved vastly in recent years; the bioinformatic resources have become more advanced also. When the *C. albicans* genome sequence was initially published, gene function was based on inferred homology and orthology to *S. cerevisiae* genes. There now exists multiple resources and tools that utilise published functional analysis data from various *Candida* research groups, e.g. The *Candida* Genome Database (Arnaud *et al.*, 2005; Inglis *et al.*, 2012). Confidence in the validity of interpretations of genetic experimental data has improved greatly with the use of tools like these.

In this section, the relationship between the *TLO* genes and the genome of *C. dubliniensis* is explored using these tools and resources. By studying the gene expression patterns associated with *TLO* deletion mutants, it was hoped to elucidate specific roles played by the *TLO* genes in manipulating the genetic landscape of *C. dubliniensis* and by extension, *C. albicans*.

5.2. Materials and Methods

5.2.1. Two-colour DNA microarray analysis

Preparation of samples for two-colour DNA microarray analysis was based on a modified version of the protocol outlined in the Two-Color Microarray-Based Gene Expression Analysis handbook (Agilent Technologies, 2012). All dilutions and reactions were carried out in 1.5 ml microcentrifuge tubes (Eppendorf) unless otherwise described.

In each experiment, there were 8 samples: four experimental (Δ*Δtlo*) and four control (Wü284) each prepared as biological replicates.

5.2.1.1. Sample preparation

Firstly, 'Spike-In' mixes were prepared. Spike-In mixes contain control RNA transcript sequences designed to uniquely hybridise with control regions of the DNA microarray, allowing determination and control of background fluorescence and alignment of the tile template (Yang, 2006). Spike-In Mix A and B (Agilent Technologies) were allowed to thaw and were then mixed thoroughly and heated to 37 °C for 5 min followed by additional mixing. Dilutions of each Spike-In mix were created using sterile Milli-Q water (Millipore) resulting in final dilutions of 1:20, 1:800, 1:1,2800 and 1:25,600.

DNase-treated, total RNA samples were prepared as described in Section 2.5.1.1. In four tubes, using two of each of the experimental and control samples, 100 ng of RNA was combined with 2 µl of the 1:25,600 dilution Spike-In Mix A and made to a final volume of 3.5 µl with sterile Milli-Q water (Millipore). In four additional tubes, 2 µl of the 1:25,600 Spike-In Mix B was combined with 100 ng of RNA from the remaining biological replicates and made to a final volume of 3.5 µl with sterile Milli-Q water (Millipore). This resulted in eight tubes, four with Spike-In Mix A, four with Spike-In Mix B, with both sets divided into two experimental samples and two control samples.

5.2.1.2. Labelling & Amplification

Labelling and amplification was carried out using the Low Input Quick Amp Labeling Kit, Two-Colour (Agilent Technologies). Firstly, a 0.8 µl volume of T7 Primer (Agilent Technologies) was combined with 1 µl of nuclease-free water (Agilent Technologies) and the 1.8 µl mix was added to each RNA-Spike-In Mix.

Each 5.3 µl reaction tube was then incubated at 65 °C in a recirculating water bath (Thermo Fisher Scientific) for 10 min followed immediately by incubation on ice for 5 min. 4.7 µl of cDNA master mix, which was composed of 2 µl 5x First strand buffer (Agilent Technologies), 1 µl 0.1 M DTT (Sigma-Aldrich), 0.5 µl 10 mM dNTP mix (Agilent Technologies) and 1.2 µl Affinity Script RNase Block Mix (Agilent Technologies), was added to each of the four reaction tubes and samples were incubated at 40 °C for 2 h in a recirculating water bath (Thermo Fisher Scientific), followed by an incubation at 70 °C in a recirculating water bath (Thermo-Fisher Scientific) for 15 min. Finally, the samples were incubated on ice for 5 min.

A 6 µl volume of Transcription Master Mix containing 1x Transcription Buffer (Agilent Technologies), 10 mM DTT (Agilent Technologies), 1 µl NTP mix (Agilent Technologies), 0.21 µl T7 RNA Polymerase blend (Agilent Technologies) and 0.24 µl of either Cyanine 3-CTP or Cyanine 5-CTP per reaction volume, was added to each sample tube. Sample tubes containing Spike-In Mix A and B Cyanine-3 and Cyanine-5 mixes respectively. Samples were incubated at 42 °C in a recirculating water bath (Thermo Fisher Scientific) for 2 h.

5.2.1.3. Cleanup & Purification

Each of the eight samples was diluted with 84 µl of sterile Milli-Q water (Millipore) and processed using the RNeasy Mini Kit (Qiagen). Briefly, 350 µl of buffer RLT (containing 10% v/v β-mercaptoethanol [Sigma-Aldrich]) and 250 µl of 100 % (v/v) ethanol were added to the 100 µl samples and mixed thoroughly by pipetting. The mix was then processed in an RNeasy column as described in the RNeasy Mini Kit handbook (Section 2.5.1.), with a final elution in 30 µl of RNase-Free Water (Qiagen). From this point, all samples were kept on ice whenever possible to prevent degradation.

To assess labeling and transcription of the cRNA, 1 µl of each sample was measured on the NanoDrop Spectrophotometer (Thermo Fisher Scientific) as described in Section 2.1.8 using the RNA quantification settings within the software (Nanodrop). The success of the amplification was determined by calculating the concentration of cRNA (µg) using the formula:

$$\text{Total cRNA } (\mu g) = \frac{\text{cRNA concentration } (ng/\mu l) \times \text{Elution volume } (\mu l)}{1000}$$

Then, the success of the labeling reaction was assessed by determining the concentration of Cy-dye per μg of cRNA as follows:

$$\text{Cy3/Cy5 per ug cRNA} = \frac{\text{Cy3 or Cy5 concentration } (pmol/\mu l)}{\text{cRNA concentration } (ng/\mu l)} \times 1000$$

The result of this equation should yield a minimum of 0.825 μg of cRNA and 6 pmol of Cy-dye in each μg of cRNA. If this threshold was not met, samples were discarded and the protocol was restarted.

5.2.1.4. Hybridisation

Once the quality standards of the labelled cRNA samples had been confirmed, fragmentation mix was prepared in new tubes. 825 ng of a Cy3-labelled cRNA and 825 ng of a Cy5-labelled cRNA were combined with 1 x Gene Expression Blocking Agent (Agilent Technologies), 1 x Fragmentation Buffer (Agilent Technologies) and then nuclease–free water (Agilent Technologies) up to a final volume of 55 μl. This results in four sample mixes which are differentially labelled, i.e. the first sample would contain Cy3-labelled experimental sample and Cy5-labelled control sample, then the second contained Cy5-labelled experimental sample and Cy3-labelled control sample and so on. This alternation is referred to as 'dye-swap' and the rationale behind it is discussed in the introductory section.

Each of the four mixes were incubated at 60 °C for 30 min and then on ice for 1 min. Each sample was combined with 2 X Hi-RPM Hybridisation Buffer (Agilent Technologies) at a ratio of 1:1, up to a total of 110 μl. The samples were mixed by pipetting without excess aeration and centrifuged at 10,000 *x g* for 1 min to reduce bubbles. The 4 X 44K DNA microarray slide (Agilent Technologies) was loaded into a hybridisation chamber (Agilent Technologies) and 100 μl of each sample was loaded carefully onto one of the four array tiles. A gasket slide was then positioned in alignment with the array and the chamber sealed. The chamber was incubated at 65 °C in a hybridisation oven (Thermo Fisher Scientific) for 18 h with rotation set to 15 r.p.m.

5.2.1.5. Washing

The apparatus was carefully disassembled in Gene Expression Wash Buffer (GEWB) 1 (Agilent Technologies) at room temperature. The slide was carefully transferred to fresh GEWB 1 and incubated for 1 min at room temperature with gentle mixing. The slide was then transferred to a new dish containing GEWB 2 (Agilent Technologies) that was pre-warmed to 37 °C and incubated for 1 min with gentle mixing.

5.2.1.6. Scanning & image processing

The slide was carefully removed from the buffer and immediately inserted into the scanning chamber of a Genepix 4100A scanner (Molecular Devices, Sunnyvale, CA, USA). The microarray slides were scanned at 5 μM pixel resolution at wavelengths 635 nm and 532 nm. Combined image files were saved at .tiff images.

Array slides were aligned both automatically and manually with a *C. dubliniensis* template .GAL file using Genepix Pro software version 6.1.0.4 (Molecular Devices). Individual array spots were annotated based on signal to noise ratio (SNR) flags and background fluorescence using Genepix Pro software (Molecular Devices). Results were saved as GenePix Pro Results (GPR) files. Array spots with SNR of < 1 were excluded as background.

5.2.1.7. Analysis

Results were imported from GPR files directly into Genespring GX software version 11.0 (Agilent Technologies). The software was directed to interpret the correct arrays for dye-swap inclusion and the data imported were subjected to normalisation based on the Lowess method (Berger *et al.*, 2004). Data were transformed logarithmically to base 2 for display purposes. Data were then filtered based on the flags Present (P), Marginal (M) and Absent (A) based on SNR values and base fluorescence as described in the previous section. Data flagged as absent were excluded from further analysis. Results were subjected to a range of statistical tests, were filtered by fold-change in gene expression and were represented visually using a hierarchical organisation heat-map, e.g. by using Euclidian squared/Centroid organisational patterns. Methods of analysis are described in detail in the results section of this Chapter.

5.3. Results

5.3.1. Investigation of the effects of deletion of *TLO* genes in *C. dubliniensis* under nutrient-rich conditions.

5.3.1.1. Basic analysis

As described in sections 5.1 and 5.2.1, two-colour DNA microarrays were used to compare the gene expression profile of $\Delta\Delta tlo$ compared to the gene expression profile of Wü284 (wild-type) during exponential growth, i.e. in YEPD growth medium at 37 °C with agitation at an optical density of 0.8 $O.D._{600nm}$. The optical density measurement of 0.8 was chosen as the ideal point for 'mid-exponential' growth based on the growth phenotypes outlined in section 4.3.10. For the purposes of this study, fluorescence data of oligonucleotide probes for each open reading frame were averaged across multiple microarray slides and classed as single entities, each representing one probe sequence for an open reading frame. Statistical tests were applied as summarised in Table 5.1. After the averaging and normalisation procedures, there were 12,034 entities available for analysis which corresponded to 5,987 distinct characterised or putative open reading frames in *C. dubliniensis*, as found on the *Candida* genome database (Inglis *et al.*, 2012). The distribution of entities is illustrated in Figure 5.1. Filters were then applied to ensure stringent exclusion of weak signal close to background (noise) as described in sections 5.2.1.6 and 5.2.1.7, which reduced the number of genes for analysis to 9,579 entities or 4,963 distinct *C. dubliniensis* orfs.

Statistical analysis was carried out on these orfs by using the Student's t-test against zero on averaged biological samples ($n = 4$) with a stringent p-value cutoff of < 0.05 necessary for inclusion of the data in further downstream analysis. This reduced the data set from 9,579 to 2,951 entities corresponding to 1,918 orfs. The data were subjected to asymptotic correction using the 'Storey with bootstrapping' method (Meuwissen & Goddard, 2004) with a corrected q-value cutoff of < 0.05. This further correction reduced the dataset to 2,467 entities corresponding to 1,635 *C. dubliniensis* orfs. The dataset of entities excluded by this post-t-test correction method were manually analysed to ensure that the correction method was not overly-stringent. Unless otherwise mentioned, downstream analyses were performed on the dataset containing 1,635 orfs, which were said to show a statistically significant ($p < 0.05$, $q < 0.05$) change in expression from the

Analysis step	YEPD 37 °C, Mid-Exponential phase	WS, 1h (Early hyphal growth)	WS, 3h (Late hyphal growth)
Lowess Normalisation	12,034 5,987	12,034 5,987	12,034 5,987
Entities remaining after signal-noise ratio exclusion	9,579 4,963	10,314	9,218
Fold Change >1.5	*1,381* 1,097	2,783 *1,681*	1,839 *1,113*
Entities passed t-test, $p < 0.05$	2,951 1,918	4,251 *2,620*	3,722 *2,281*
Entities passed t-test, $p < 0.05$, Asymptotic Correction (Storey w/ bootstrapping)	2,467 1,635	5,234 3,164	4,374 2,634
Genes UP	*876*	*1,511*	*1,332*
Genes DOWN	*759*	*1,653*	*1,302*

Table 5.1. Filtering applied to DNA microarray data.

Table outlining the successive stages of analysis and quality control during interpretation of DNA microarray results from three separate conditions. At each stage, the number of array DNA probes is listed (underlined) followed by the number of orfs to which this translates (italicised)

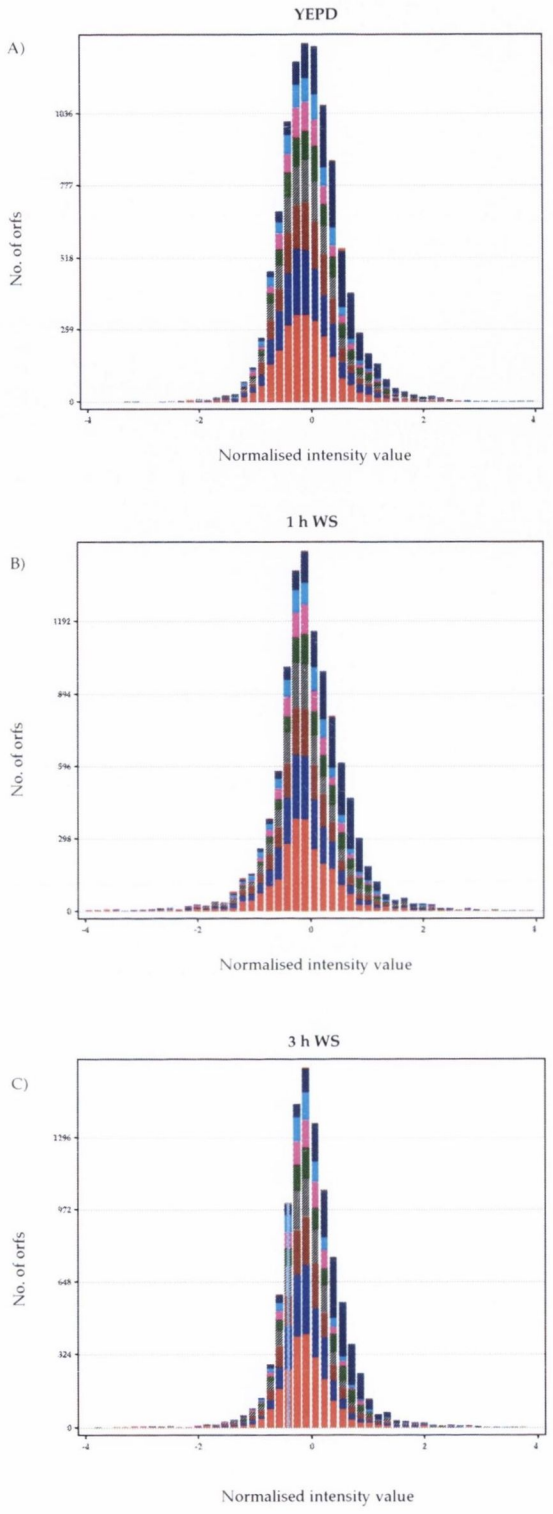

Figure 5.1. Distribution of entities on DNA microarrays.

Normalised intensity values of each entity (expression probeset) was plotted on the x-axis with the count (i.e. number of entities at that value) recorded on the y-axis. Note that y-axes are to different scales. Histograms represent data from DNA microarrays carried out on strains grown in A) YEPD (mid-exponential), B) WS 1h and C) WS 3 h. Colours are based on chromosomal frequency.

wild-type in the ΔΔ*tlo* background. A full list of genes with > 1.5-fold changes in expression is outlined in Table S.1.

5.3.1.2. Genes expressed at higher levels in the *tlo* deletion mutant

Of the 1,635 differentially expressed genes, 876 were considered to be significantly expressed at a higher level, or 'up-regulated' in the ΔΔ*tlo* background compared to in the wild-type.

Genes that were up-regulated more than 1.5 fold in ΔΔ*tlo* are outlined in Table S.1. For further analysis, this gene list was submitted to several Gene Ontology (GO) -term finder and GO-term slim mapper services (Arnaud *et al.*, 2005, 2009; Inglis *et al.*, 2012) which allowed clustering of the genes based on frequency within a gene family compared to the frequency of each gene ontology term over the entire genome. A p-value was also included to indicate significance and confidence of clustering.

Major correlations between the gene dataset and GO-terms were determined using the GO-term finder tool. Most of the genes with increased expression were associated with general metabolic processes, e.g. oxoacid metabolic processes (n = 71, p = 0.028) and organonitrogen compound catabolic processes (n = 32, p = 0.00499). The genes analysed also have roles in oxidation-reduction processes (n = 83, p = 0.01781). Functional computational analysis by gene ontology terms was carried out and two functions were attributed to the genes that were expressed at a higher level in ΔΔ*tlo* compared to Wü284. 84 genes (p = 0.00377) were associated with oxidoreductase activity, i.e. catalysis of an oxidation-reduction reaction and 188 genes were associated with ion binding functions (p = 0.00934).

A more general analysis of the dataset was carried out using GO term slim mapper to identify higher order GO-terms common in the list of genes. For this, a fold-change in expression cutoff of 1.5 (ΔΔ*tlo* versus Wü284) was used (n = 746). Many genes involved in basic metabolic processes were up-regulated. This included genes associated with vitamin metabolism (e.g. *ISA1, RIB1, THI20, THI4*), cellular respiration (e.g. *AOX1, CIT1, DLD2, KGD1, FGD2, MCT1, MDH1, SDH2*) which includes genes involved in the TCA cycle (*ACO1, FUM11*) and carbohydrate metabolism (e.g. *CHT1, INO1*) which includes genes involved in gluconeogenesis (e.g. *PCK1, FBP1*) and *N*-acetylglucosamine metabolism. Several genes involved in the cell cycle were also up-regulated under these conditions

(e.g. *BUD5, RAD35, RAD51*). Genes involved in amino acid catabolism were up-regulated (e.g. *ARO1, PUT1, PUT2, LAP3, LPD1, FDH1, UGA1, UGA2*). Up-regulation of some important genes involved in morphogenesis was observed (e.g. *TEC1, SFL1, WOR2*). Other processes whose associated genes had a higher expression in the mutant included the response to stress, transport, RNA metabolic processes, lipid metabolic processes, cell adhesion and translation.

5.3.1.3. Genes expressed at lower levels in the *tlo* deletion mutant

759 of the 1635 genes differentially expressed, were expressed at a lower level in Δ*Δtlo* compared to Wü284. Genes that were significantly down-regulated > 1.5 fold are outlined in Table S.1. The same methods as described in Section 5.3.1.2 were used to analyse the dataset. A significant amount of down-regulated genes were associated with RNA processing (n = 99, p = 7.82 X 10^{-9}) and downstream processes such as RNA modification (n = 27, p = 0.00087), rRNA processing (n = 47, p = 0.00066) and tRNA metabolism (n = 38, p = 0.00091). There was significant correlation between genes down-regulated in Δ*Δtlo* and those involved in sulphur amino acid biosynthesis (n = 13, p = 0.00327) and carbohydrate derivative metabolic processes (n = 61, p = 0.01676).

Functional analysis as carried out in section 5.3.1.2, demonstrated a correlation between ribosomal and translation-associated GO-terms and genes down-regulated in Δ*Δtlo*, e.g. genes associated with translation factor activity (n = 17, p = 0.00072), genes associated with the structural constituent of the ribosome (n = 46, p = 1.4 X 10^{-6}) and genes associated with RNA polymerase I activity (n = 7, p = 0.09332). Component analysis agreed with these predictions, identifying putative associations with components of the ribosome ($p < 0.01$).

As before, filtering of the dataset using a fold change cutoff of 1.5 allowed a more general analysis to identify correlations between specific GO-terms and genes down-regulated in the Δ*Δtlo* compared to Wü284. Genes involved in ribosome biogenesis (e.g. *KRE30, UPT21, TIF5*), glycolysis (e.g. *TYE7, PFK1, PFK2, ENO1*), filamentation (e.g. *CDC42, CDC14, TOP1, CHS2*) and translation (e.g. *GLN4, RPL18, RPS22A*) were all down-regulated. Genes involved in the utilisation of galactose (e.g. *GAL1, GAL102,* GAL7) were also down-regulated.

5.3.2. Investigation of the effects of deletion of *TLO* genes in *C. dubliniensis* under early hypha-inducing conditions

As discussed in previous chapters, growth at 37 °C in water supplemented with 10% serum (WS) is an ideal condition for inducing hyphal formation in *C. dubliniensis*. Samples were taken at 1 h growth in such conditions and DNA microarray analysis was carried out comparing the global gene expression profile of Δ*Δtlo* in comparison to Wü284. Methods of normalisation and analysis have been discussed previously (Section 5.3.1.1) and are summarised in Table 5.1. After averaging and normalisation (Lowess), there were 12,034 entities to analyse. The distribution of entities is illustrated in Figure 5.1. A quality control filter based on signal to noise ratio (Section 5.2.1.6.) excluded 1,720 entities, reducing the dataset to 10,314. An asymptotic t-test against zero was carried out with a p-value cutoff of 0.05, which resulted in 4,251 entities. However, after assessment of the test, it was decided that it was too stringent in its exclusion of data points. Subsequently, a post-correction 'Storey with bootstrapping' algorithm was applied, using a q-value cutoff of 0.05. This allowed for re-introduction of some previously excluded entities, bringing the total number of statistically significant entities to 5,234, or 3,155 orfs. A full list of genes displaying more than 1.5-fold change in expression from this dataset is outlined in Table S.2.

5.3.2.1. Genes expressed at higher levels in a *tlo* deletion mutant

Of these, 1,511 genes were expressed at a higher level in Δ*Δtlo* compared to Wü284. Genes significantly up-regulated > 1.5-fold are outlined in Table S.2. The data were analysed in the same fashion as in section 5.3.1.2. A significant number of genes up-regulated in Δ*Δtlo* were associated with proteasome assembly (n = 16, p = 0.03249), oxidation-reduction (n = 129, p = 0.0213), protein localisation to the mitochondrion (n = 30, p = 0.00216), mitochondrion organisation (n = 90, p = 0.00036) and carboxylic acid metabolism (n = 107, p = 0.03255).

Functional analysis predicted correlation between the genes expressed at a higher level in Δ*Δtlo* and oxidoreductase activity (n = 133, p = 0.00112), being a structural constituent of the ribosome (n = 59, p = 0.02472) and threonine-type (endo-)peptidase activity (n = 14, $p = 2.63 \times 10^{-7}$).

A more general analysis of the datasets was carried out using a 1.5 fold-change cutoff in expression as described in section 5.3.1.2. Genes involved in regulation of filamentation (e.g. *SFL1, HSP90, EED1*), general metabolism (e.g.

UGP1, HXK1, SOL3), response to stress (e.g. *SOD1, SOD2, SOD4, CAT1*), cell cycle (e.g. *HHT2, POL2, MUM2*) and biofilm formation (e.g. *ECE1, GCA1, GCA2*) were all up-regulated in ΔΔ*tlo* compared to Wü284.

5.3.2.2. Genes expressed at lower levels in a *tlo* deletion mutant

1,653 genes were expressed at a lower level in ΔΔ*tlo* compared to Wü284 and those with >1.5-fold change in expression are outlined in Table S.2. As before, the data were analysed using GO-term analysis (Arnaud *et al.*, 2005, 2009; Inglis *et al.*, 2012). RNA localisation (n = 97, p = 0.04347), growth (n = 219, p = 8.07×10^{-8}), filamentation (n = 212, p = 2.97×10^{-7}), regulation of transcription from RNA PolII promoter (n = 133, p = 3.13×10^{-6}), cellular response to pH (n = 42, p = 0.00025) and Golgi vesicle transport (n = 72, p = 1.72×10^{-5}) were all associated with the dataset of genes that were down-regulated in ΔΔ*tlo* compared to Wü284.

Functional analyses predicted correlations between genes lowly expressed and translation factor activity (n = 26, p = 0.00019), DNA translocase activity (n = 10, p = 0.01475) and single-stranded RNA binding (n = 11, p = 0.04432).

As before, a fold-change in expression cutoff of 1.5 was used for a more general analysis of the association of genes down-regulated in ΔΔ*tlo* compared to wild-type with specific processes (Table S.2). It was found that important genes involved in filamentation (including hyphal and pseudohyphal morphological transitions, as well as filament-associated biofilm formation) (e.g. *ACE2, ALS1, CEK1, CPH1, CLN3, CZF1, DFG16, EFG1, HWP1, OLE1, UME6, TYE7, SOD5*) were down-regulated in ΔΔ*tlo* compared to Wü284. Also, genes involved in ribosome biogenesis (e.g. *RPL10, RPS1*), the cell wall (e.g. *SUR7, DSE1*), stress response (e.g. *HOG1, SOD5, YAF9, RIM101*), transcriptional regulation (e.g. *SSN6, SWI1, TAF14*) and galactose utilisation (e.g. *GAL1, GAL7, GAL10, GAL102*) were generally down-regulated in ΔΔ*tlo*.

5.3.3. Investigation of the effects of deletion of *TLO* genes in *C. dubliniensis* under later hypha-inducing conditions

Samples were taken at 3 h growth in water supplemented with 10% (v/v) foetal calf serum (WS) (see section 5.3.2.) for DNA microarray analysis. After averaging and normalisation procedures (summarised in Table 5.1.), there were 12,034 entities available for analysis. Filtering based on SNR allowed exclusion of 2,816 entities reducing the dataset to 9,218 entities. The distribution of entities is

illustrated in Figure 5.1. A t-test against zero was carried out with a p-value cutoff of 0.05, which reduced the dataset to 3,722 entities. As with the 1 h time point in serum, it was decided that the normal t-test was overly stringent and a post-correction method 'Storey with bootstrapping' was applied using a q-value cutoff of 0.05. This allowed re-introduction of data points to bring the total number of entities for downstream analysis to 4,374 entitles or 2,633 putative orfs.

5.3.3.1. Genes expressed at higher levels in a *tlo* deletion mutant

1,332 genes were said to be significantly up-regulated based on the statistical criteria discussed above. GO-term analysis was carried out as outlined in the preceding sections. Genes in this dataset were predicted to be involved in lipid metabolic processes (n = 85, p = 0.00058) and membrane fusion (n = 28, p = 0.00315). Functional analysis predicted that several genes had hydrolase activity as a common function (n = 212, p = 0.03782) and that more than a quarter of the genes were associated with membrane structures (n = 351 p = 2.97×10^{-6}).

As before, a cutoff in fold change of expression of 1.5 was used as a more general dataset to carry out more correlations between genes up-regulated in Δ*Δtlo* compared to Wü284 based on GO-terms. Several genes involved in filamentous growth were up-regulated (e.g. *EED1, FGR2, GLN3, HST7, SFL1, TEC1*). Likewise, some genes involved in carbohydrate metabolism (e.g. *FBP1, GCA1, SOL3*), the cell cycle (e.g. *ATG15, BUD5, CDC24, YVH1*), response to stress, and biofilm formation were up-regulated in Δ*Δtlo*. A full list of genes (>1.5-fold) from this dataset is outlined in Table S.3.

5.3.3.2. Genes expressed at lower levels in a *tlo* deletion mutant

1,302 genes were said to be down-regulated in Δ*Δtlo* compared to Wü284 at the 3 h time point in WS. Analyses carried out as described in previous sections displayed a correlation between these genes and general metabolic processes (n = 749, p = 4.22×10^{-15}) with over 60 % of the genes falling into this category. The down-regulated genes were also strongly associated with RNA processing (n = 151, p = 2.58×10^{-11}), response to stress (n = 233, p = 7.58×10^{-5}), ribosome biogenesis (n = 110 p = 5.45×10^{-11}), mitotic cell cycle (n = 83, p = 0.00104) and response to hypoxia (n = 8, p = 0.03963). Functional analysis suggested an association with chromatin binding (n = 35, p = 0.00778) and anion binding (n = 170, p = 0.02248).

As with all previous arrays, the cutoff of 1.5-fold change in expression was applied to the data in order to carry out a global GO-term analysis of the relationship between genes down-regulated and specific processes. Several important genes involved in filamentation (including regulation) were down-regulated (e.g. *EFG1, ALS1, CEK1, CLN3, HOG1, SUR7, HWP1*). Also, other processes including biofilm formation (e.g. *AHR1, FOX2, DSE1, IRO1*), carbohydrate metabolism (e.g. *GAL1, GAL10, GAL7, CHT1, CHT2*), ribosome biogenesis (e.g. *NEP1, NOP1, RPS6A*), cell cycle (e.g. *DAM1, GIN4, POL30, SWI1*) and the response to stress (e.g. *ERG1, CSI2*) were associated with down-regulation in ΔΔ*tlo*. A full list of genes showing down-regulated expression (> 1.5-fold) at the 3 h time point are outlined in Table S.3.

5.3.4. Comparison of datasets

A full analysis of the datasets is discussed in section 5.4. Each condition was compared in a profile plot of genes displaying more than 1.5-fold change in expression between *tlo* mutant and Wü284 (Figure 5.2). Overlaps in datasets were detected using Venn diagrams (Figure 5.3).

5.3.5. Confirmation of select expression patterns

In order to confirm levels of expression reported in the DNA microarray experiments, qRT-PCR was carried out on the experimental samples. These confirmatory experiments were carried out on specific families of genes that related to the phenotypes observed in Chapter 4.

It had been identified in the preceding sections that genes involved in galactose utilisation were generally down-regulated in all three conditions. As such, qRT-PCR was carried out to determine the expression levels of *GAL1, GAL7* and *GAL10* in the three conditions (mid-exponential growth in YEPD, 1 h growth in WS and 3 h growth in WS). In the array data, *GAL1* expression was significantly down-regulated in ΔΔ*tlo* compared to Wü284 in all three conditions and qRT-PCR using primer pair GAL1FW/GAL1RE appeared to validate these patterns (Figure 5.4. A). The overall expression levels were relatively low which resulted in high p-values for each data set, however the overall trends correlated with the raw values in the array data. Likewise, *GAL7* expression was significantly down-regulated in ΔΔ*tlo* compared to Wü284 and this was validated by qRT-PCR using primer pair GAL7FW/GAL7RE (Figure 5.4. B). The qRT-PCR for *GAL10* using primer pair

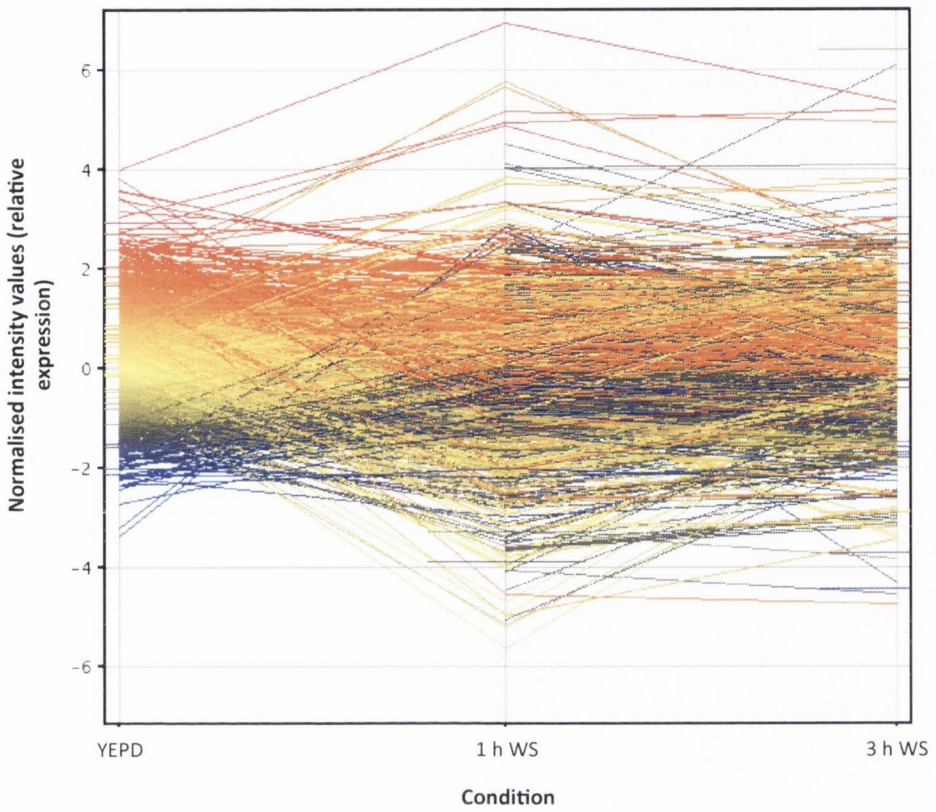

Figure 5.2. Profile plot of expression of *tlo* mutant compared to Wü284

Graph shows intensity values (normalised expression values) over three conditions – Mid exponential growth in YEPD, growth in water supplemented with 10 % foetal calf serum (WS) at 1h and at 3h. Colour scheme is based on expression values in YEPD array dataset. Red indicates higher expression in the *tlo* mutant compared to wild-type, blue indicates lower expression. Expression levels can be determined using the left y-axis values.

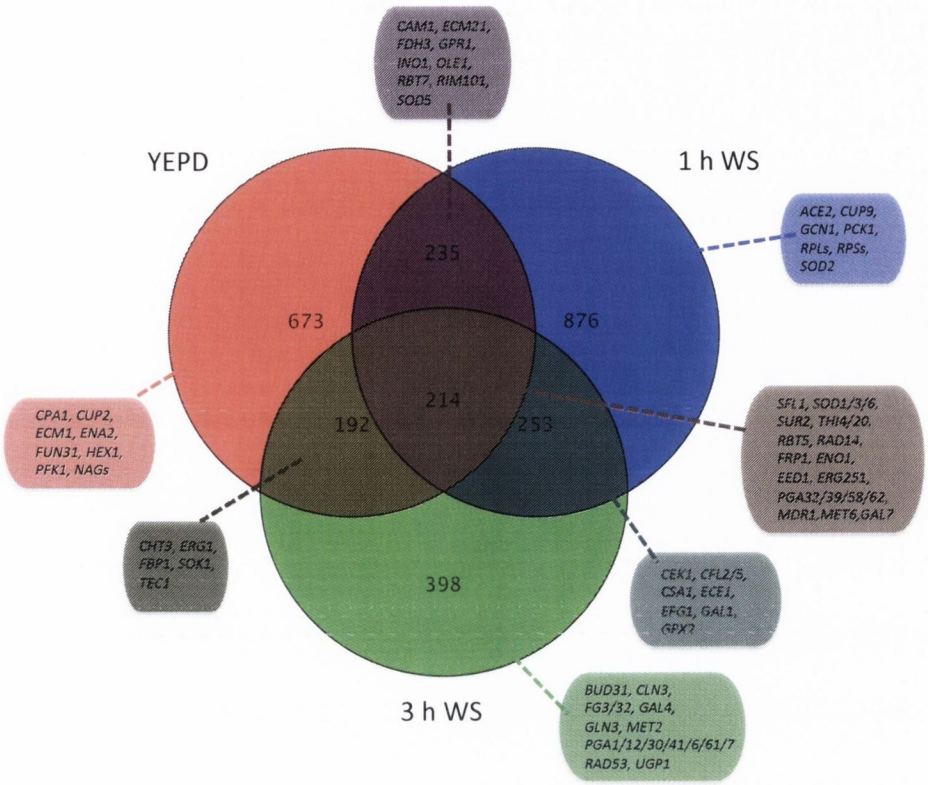

Figure 5.3. Overview of overlap in DNA microarray datasets

Venn diagram showing common number of genes with more than 1.5 fold change between each of the three DNA microarray condition datsets - Mid-exponential growth in YEPD, 1 h and 3 h growth in WS (Water supplemented with 10% foetal calf serum).

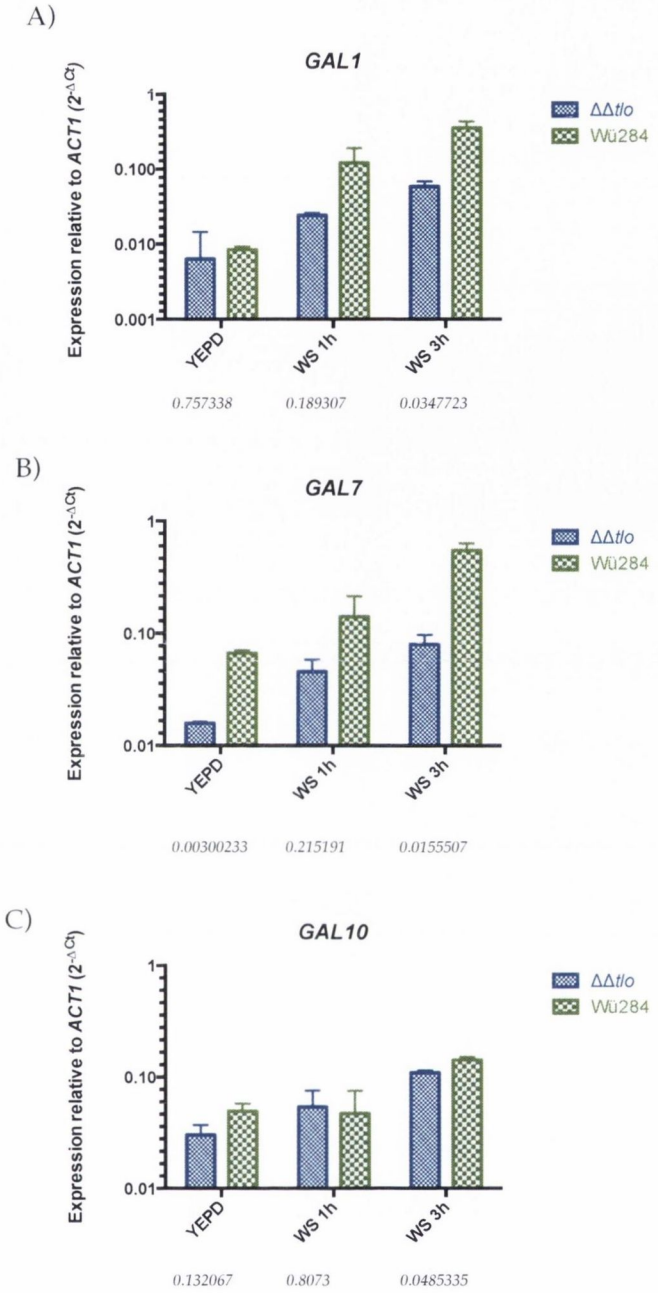

Figure 5.4. Expression patterns of genes involved in galactose metabolism upon deletion of *TLO* genes is confirmed by qRT-PCR.

Expression of selected genes *GAL1, GAL7* and *GAL10* were confirmed by qRT-PCR at identical timepoints to those in the DNA microarray studies. Expression is marked along the y-axis and is the $\log_{[10]}$ transformed expression relative to *ACT1* (endogenous control). P-values derived from a students t-test for each data set are indicated in italics below each axis.

GAL10FW/GAL10RE showed that the ΔΔ*tlo* mutant expressed lower levels of the *GAL10* mRNA in YEPD broth. However, it did not confirm the level of differential expression observed in the WS microarrays (Figure 5.4 .C)

Expression levels of the superoxide dismutase genes (*SOD*s) were also determined using qRT-PCR. The DNA microarray data had indicated that *SOD3* was expressed at higher levels in strain ΔΔ*tlo* relative to Wü284 in YEPD (2-fold), but lower in WS conditions (4-fold). Using primers SOD3FW/SOD3RE, these expression patterns were confirmed (Figure 5.5. A). QRT-PCR also showed that expression of *SOD5* was reduced in ΔΔ*tlo* relative to Wü284 in YEPD and in the early stages of hyphal development (1h WS) using primer pair SOD5FW/SOD5RE (Figure 5.5. B). These data confirm the 4–fold reduction in *SOD5* expression detected at 1 h in WS in the microarray experiments. Microarray analysis also indicted that expression of *SOD6* was lower in strain ΔΔ*tlo* relative to Wü284 in all conditions analysed and qRT-PCR using primer pair SOD6FW/SOD6RE confirmed this (Figure 5.5. C).

As will be discussed in the following section, many genes associated with filamentation and regulation of filamentation displayed significant changes in expression upon disruption of the *TLO* genes. QRT-PCR was used to confirm the expression patterns of the genes *HWP1*, *RBT5* and *ECE1*, encoding hypha-induced transcripts, and the filamentous growth regulators *UME6* and *NRG1*. Using primer pair HWP1FW/HWP1RE, *HWP1* mRNA was confirmed to be expressed at significantly lower levels during growth in WS in strain ΔΔ*tlo* relative to Wü284 (Figure 5.6. A), with little detectable mRNA expression during growth in YEPD. According to the microarray data, *RBT5* appeared to be expressed slightly higher in strain ΔΔ*tlo* in YEPD, but lower in WS medium at 1 h and 3h. These expression patterns could be confirmed in qRT-PCR experiments using primer pair RBT5FW/RBT5RE (Figure 5.6. B). *ECE1* was expressed at higher levels in strain ΔΔ*tlo* in all conditions, particularly in WS in the microarray experiments. Again, this pattern was confirmed in qRT-PCR experiments using primer pair ECE1FW/ECE1RE (Figure 5.6. C).

The patterns of expression for *UME6* and *NRG1* were partially confirmed by qRT-PCR (Figure 5.6. D, E). *UME6*, a positive regulator of filamentous growth exhibits a massive decrease in expression during the early stages of filamentous growth, represented here by the 1 h time point in WS. Microarray analysis indicated that *UME6* was expressed at lower levels (4-fold) in strain ΔΔ*tlo* relative

to wild-type. QRT-PCR using primer pair UME6FW/UME6RE confirmed this defect in expression at 1 h in WS and also indicated that expression was reduced in YEPD and at 3 h in WS. Also, microarray data indicated that the negative regulator of filamentous growth *NRG1* exhibited increased expression in YEPD (2.8-fold). This was confirmed by qRT-PCR experiments using primer pair NRG1FW/NRG1RE, which also indicated increased expression of *NRG1* in all conditions tested (Figure 5.6).

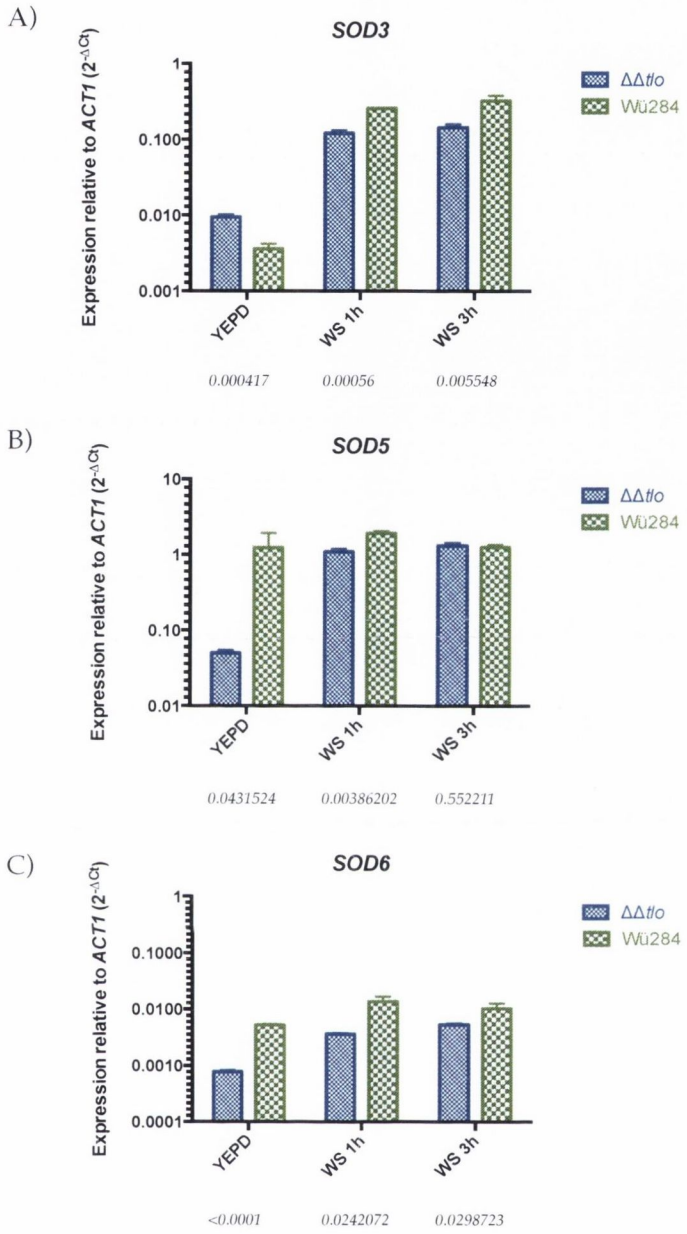

Figure 5.5. Expression patterns of *SOD* genes is confirmed by qRT-PCR. Expression of selected genes *SOD1, SOD5* and *SOD6* were confirmed by qRT-PCR at identical timepoints to those in the DNA microarray studies. Expression is marked along the y-axis and is the $\log_{[10]}$ transformed expression relative to *ACT1* (endogenous control).

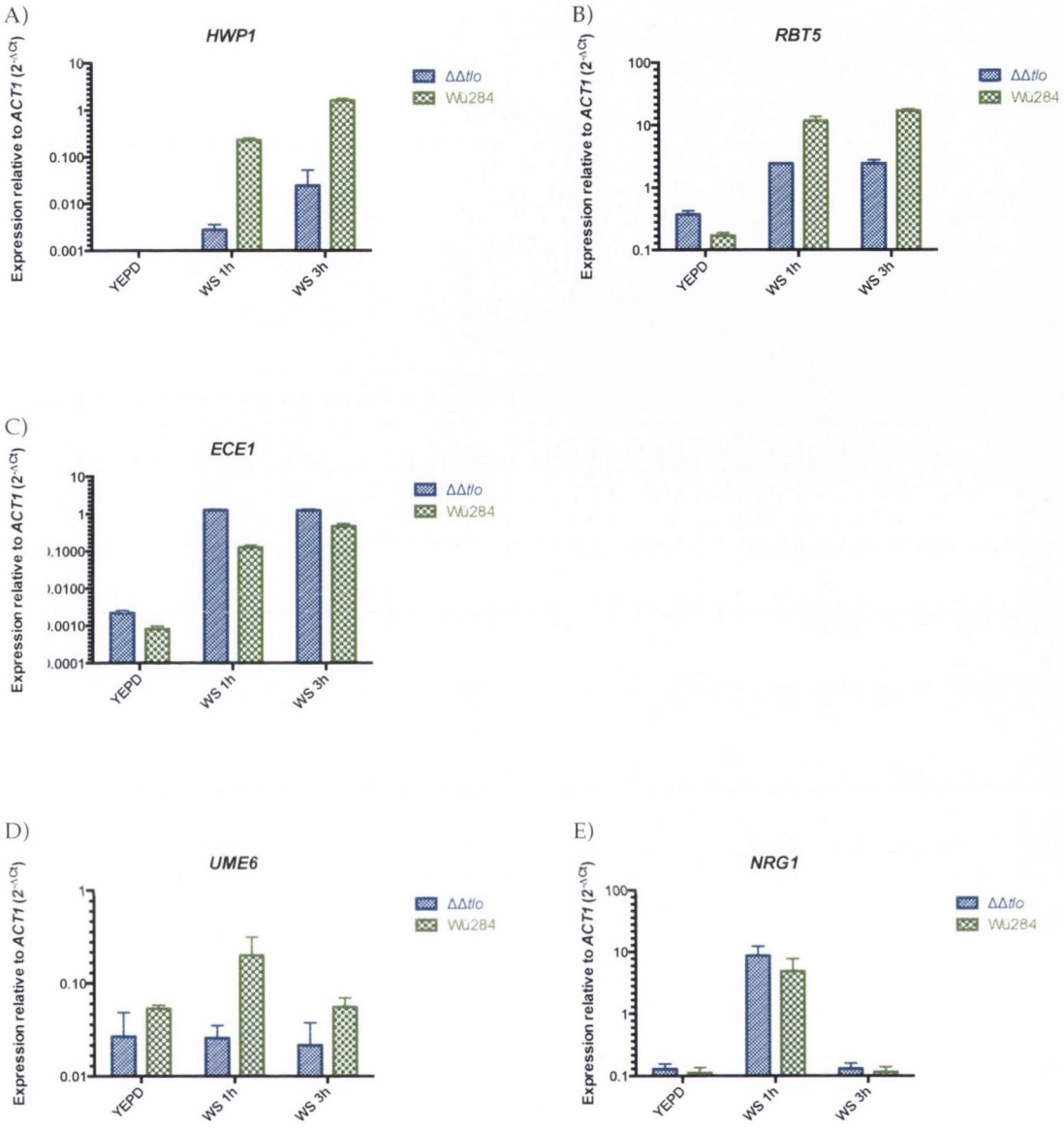

Figure 5.6. Expression patterns of genes involved in filamentation analysed by qRT-PCR. Expression of selected hyphal-associated and filamentous regulatory genes *HWP1 RBT5* and *ECE1* were confirmed by qRT-PCR. Analysis of *UME6* and *NRG1* was not in agreement with the array data. Expression was measured at identical timepoints to those in the DNA microarray studies. Expression is marked along the y-axis and is the $\log_{[10]}$ transformed expression relative to *ACT1* (endogenous control).

5.4. Discussion

This Chapter has shown that the effects of deletion of the *TLO* genes on the transcriptome in *C. dubliniensis* are extensive and result in a number of significant changes to well described transcriptional programmes, the most significant of which will be discussed in the following sections.

5.4.1. Filamentation & biofilm formation

As discussed in Chapter 4, the *TLO* genes appear to play a major role in the regulation of filamentation in *C. dubliniensis*. In the absence of both *TLO1* and *TLO2*, cells were unable to form true-hyphal cells when exposed to environmental conditions highly inducive to such a morphological transition. Cells of this mutant instead grew as clumps of pseudohyphal cells. The switch from yeast to hyphae is the result of a complex chain of regulatory signals and changes in gene expression (Sudbery, 2011). This transition is the subject of interest due to the obvious links with pathogenesis and virulence of *C. albicans* (Berman, 2006; Brand, 2012; Moran *et al.*, 2012).

The DNA microarray experiments carried out in this study have elucidated several interesting changes in gene expression of several key regulators of filamentation in Δ*Δtlo* compared to Wü284 (Figure 5.7). Figure 5.8 summarises the relationship between the expression of these regulators and hyphal formation during growth in WS at 1 h. These data show that *SFL1*, which is an important negative regulator of filamentation (Li *et al.*, 2007) was significantly up-regulated in the absence of *TLO* expression under all conditions. Additionally, *HSP90*, encoding a negative regulator of the Ras/cAMP pathway also exhibited an increase in expression. Furthermore initiation of filamentous growth may also be inhibited due to the increased expression of *NRG1* observed in YEPD broth. Several positive regulators of filamentous growth also exhibited reduced expression in the early stages of hyphal growth. *RIM101*, which is required for the induction of hyphal formation via *EFG1* in response to neutral or alkaline pH (Nobile *et al.*, 2008) is expressed noticeably higher in YEPD and significantly lower in WS at 1 h. The expression of *UME6*, which promotes hyphal extension and maintenance (Martin *et al.*, 2011) is significantly lower at 1h growth in WS. *UME6* expression is normally highly induced during the induction of filamentous growth in WS and the microarray data and qRT-PCR data together indicate a defect in

induction in WS at 1 h. As well as this, expression of the filamentous regulator *EFG1* was expressed at lower levels during filament-inducing growth. Unexpectedly, *EED1*, which has been shown to be involved in the maintenance of hyphal extension (Martin *et al.*, 2011) was up-regulated significantly in all conditions.

In addition to regulators of filamentation, several fungal cell wall-specific and hyphal-specific genes displayed altered expression patterns after deletion of the *TLO*s (Figure 5.9), some of which are associated with biofilm formation and maintenance also. Genes such as *HWP1*, *RBT1*, *RBT5* and *CSA1* encoding cell wall proteins which are all induced during filamentation were down-regulated in strain Δ*Δtlo* (Braun *et al.*, 2000; Lamarre *et al.*, 2000; Nobile *et al.*, 2006). *PGA13* was significantly up-regulated in the absence of *TLO*s in YEPD and at 3 h growth in WS. *PGA13* has recently been suggested to negatively affect hyphal formation and to be integral in cell wall integrity (Gelis *et al.*, 2012). As well as this *CLN3*, a depletion of which is known to cause hyphal abnormalities (Bachewich & Whiteway, 2005) was expressed at a lower level in 1 h and 3 h growth in WS.

These changes in the expression of important filamentous growth regulators and hypha-specific genes may largely explain the filamentation phenotype that was observed in Chapter 4. However, there were many paradoxical effects in the expression of genes such as *EED1* and *ECE1*, whose expression exhibited a strong increase in strain Δ*Δtlo*, which would be more fitting with a normally filamentous phenotype. It is clear that the regulation of filamentation by the *TLOs* is a complex process, perhaps involving several additional levels of regulation upstream and downstream, which may explain some of the unusual expression profiles.

5.4.2. Stress responses

The ability to adequately respond to stress is an important trait of any successful organism. Like all organisms, *Candida* species are exposed to both external (environmental factors) and internal (intracellular) stress. As opportunistic pathogens, *C albicans* and *C. dubliniensis* are exposed to a plethora of stresses from the moment they come into contact with the host. At this point, *Candida* cells have to be able to tolerate temperature changes, alkalinity, etc. Over millions of years the immune system has evolved intricate methods in an attempt

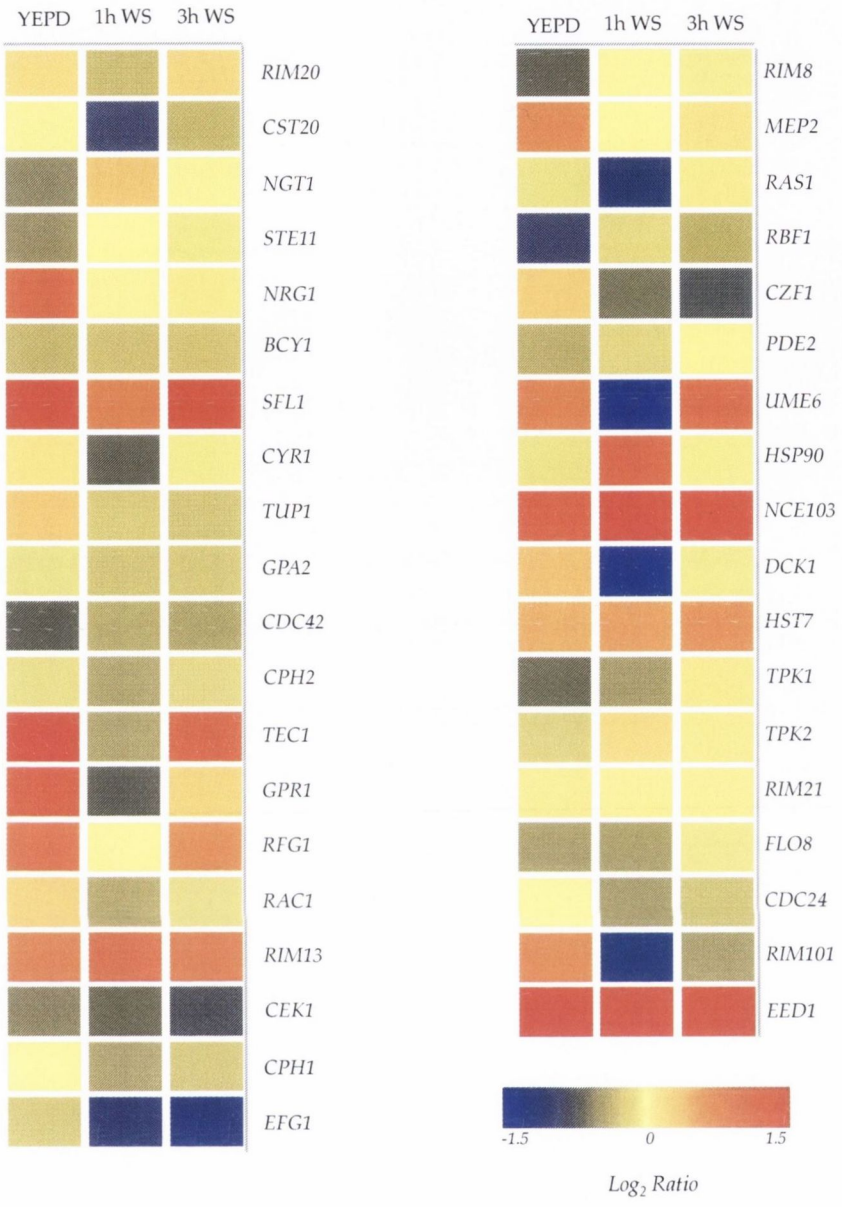

Figure 5.7 DNA microarray analysis of genes involved in the regulation of filamentation.

Two-colour DNA microarray analyses were carried out in *C. dubliniensis* strains ΔΔ*tlo* versus Wü284. Heatmaps were generated using Genespring software version 12 (Agilent Technologies) showing changes in expression of selected filamentous growth regulators, where red represents increased mRNA expression in strain ΔΔ*tlo* versus Wü284 and blue indicates decreased expression. The intensity of the colour represents the scale of differential expression, as indicated in the legend.

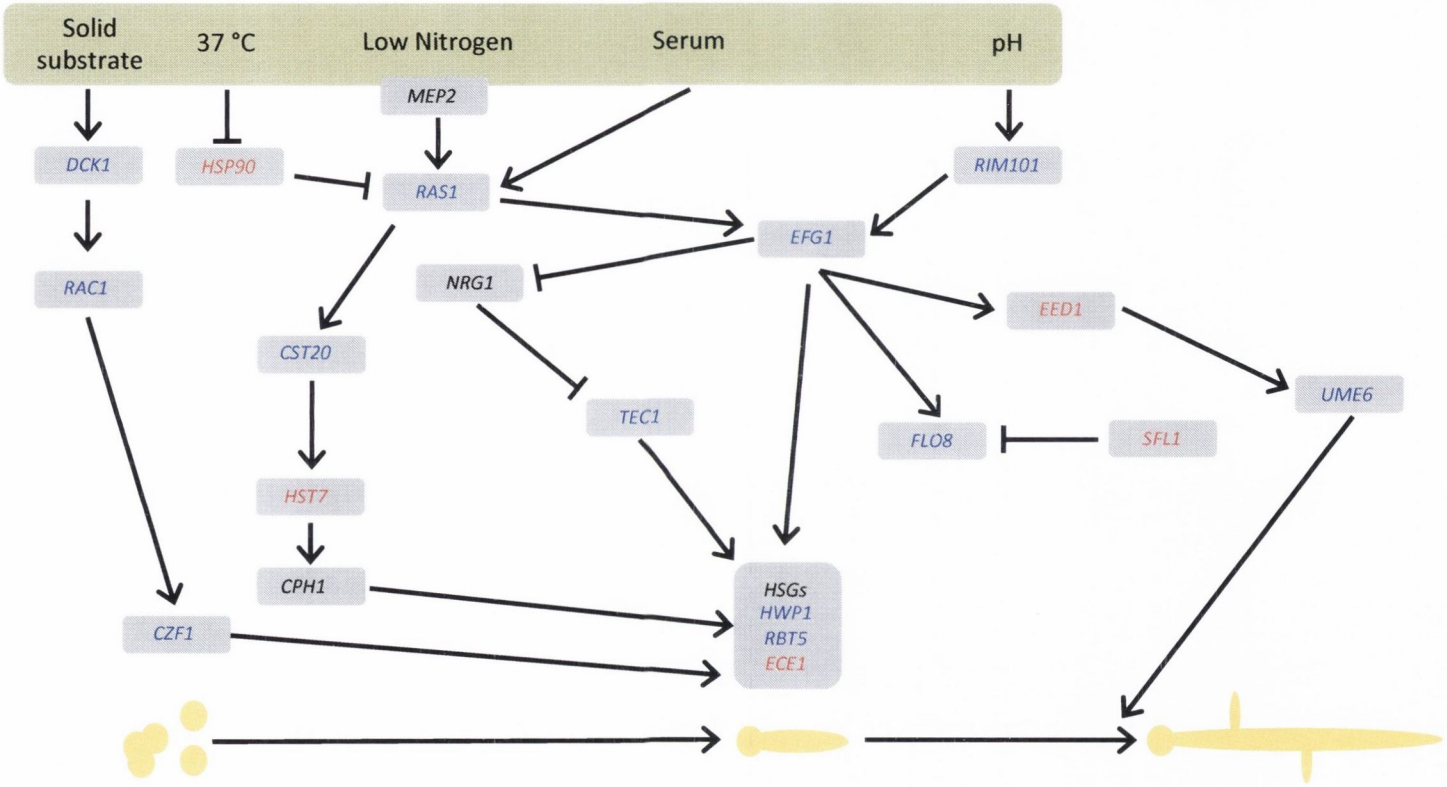

Figure 5.8. The network of regulators and transcription factors involved in hyphal formation.

Illustration adapted from Sudbery *et al* (2011), with additional data retrieved from other sources listed in the main text. Map illustrates the expression of genes in ΔΔ*tlo* compared to Wü284 during growth in 1 h WS. Text coloured in blue indicates a decrease in expression and text coloured in red indicates an increase in expression. Expression data for the *tlo* mutant was extracted from Table 3.3.

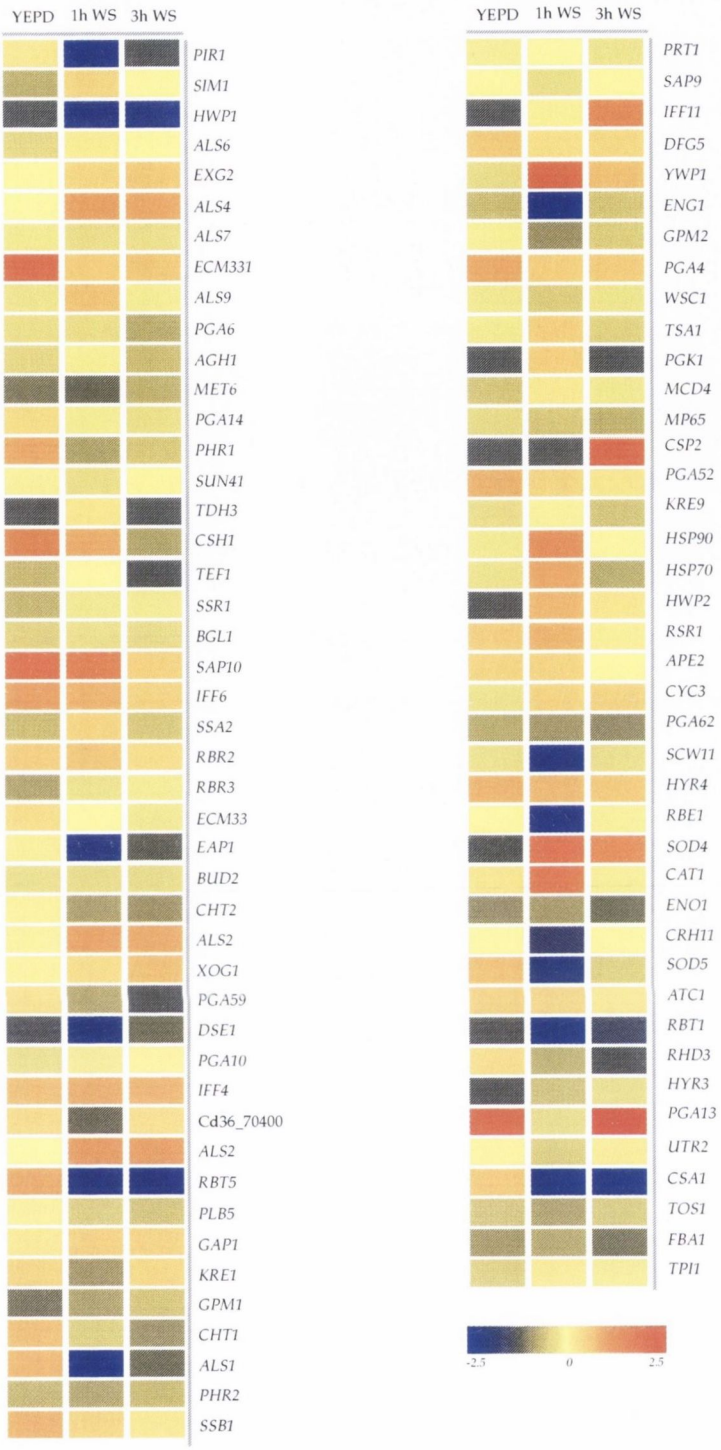

Figure 5.9. DNA microarray analysis of genes specific to the fungal cell wall.

Two-colour DNA microarray analyses were carried out in *C. dubliniensis* strains ΔΔ*tlo* versus Wü284. Heatmaps generated using Genespring software version 12 (Agilent Technologies) are shown to illustrate differences between the expression profiled in these two strains of specific genes known or predicted to be associated with the cell wall (including, but not limited to hyphal cell wall) in *C. albicans* or *C. dubliniensis*. Legend shown illustrates the colour scale corresponding to normalised expression levels used within each map.

to thwart any threat to the body (Danilova, 2008). Likewise, *Candida* species have evolved ways in which to combat these efforts (Brown *et al.*, 2014).

Perhaps one of the most important components of the innate immune system is the phagocytic cell, being one of the most conserved cell types amongst higher order eukaryotes (Janeway *et al.*, 2001; Miramón *et al.*, 2013; Seider *et al.*, 2010). Phagocytes including monocytes, macrophages, dendritic cells and polymorphonuclear neutrophils are part of the first line of defence in the immune system (Miramón *et al.*, 2013). Recognition and engulfment of *Candida* is via a complex network of immune modulatory signals, including the recognition of pathogen-associated molecular patterns (PAMPs) and pattern recognition receptors (PRRs), the mechanisms of which have been reviewed in detail by Miramón *et al.*, (2013). Once engulfed by the phagocyte, the cell activates a number of different mechanisms aimed at killing the *Candida* cell. One of the most widely studied of these is the oxidative burst during which reduced NADPH oxidase facilitates the production of superoxide radicals (O_2^-) via oxygen reduction which is then converted to H_2O_2, hydroxyl radicals (OH^-) and other damaging reactive oxygen species (ROS) (Fang, 2004).

ROS-mediated oxidative stress can originate from external sources (e.g. phagocyte attack/engulfment) and internal sources (age-dependent oxidative stress) (Miramón *et al.*, 2012, 2013). *Candida* have an arsenal of proteins and enzymes involved in dealing with both sources of oxidative stresses, such as the stress-activated (and mitogen activated) protein kinases (SAPKs) to which Hog1 is central (Smith *et al.*, 2010). *HOG1* activation mediates the induction of numerous genes involved in the response to osmo- and oxidative-stress (e.g. *AHP1, GPX1, TRX1,* etc.) both through and independent of the SAPK pathway (Vylkova *et al.*, 2007) (Cheetham *et al.*, 2011). Null mutants for *HOG1* have shown a significant reduction in virulence in a murine model (Alonso-Monge *et al.*, 1999). In addition to *HOG1*-mediated stress signaling, *Candida* possesses a number of genes that are involved in protecting the cell from oxidative stress, such as those that encode for superoxide dismutases (SODs) which catalyse the breakdown of superoxide radicals into hydrogen peroxide and oxygen (Wang *et al.*, 2006)

In this study, DNA microarrays were carried out as described in the previous sections to attempt to elucidate a role for the *TLO*s in *Candida* species. In Chapter 4, a severe retardation of growth in the presence of chemically induced oxidative stress was observed. To further study this important phenotype, the

genes introduced above and several others involved in protecting the cell from oxidative stress were analysed for unusual changes in expression in the absence of both *TLO1* and *TLO2* in *C. dubliniensis*. Although the cells of each strain were grown in YEPD at 37 °C, which is not an environment in which there are many extreme stressors, there still exists a shift in the expression of oxidative stress-associated genes in the absence of *TLO* expression under this condition. Also, in WS media, which creates a more stressful environment for growth of *Candida*, a more pronounced shift in expression is observed at both early hyphal growth (1 h) and late hyphal growth (3h). Results are summarised in Figure 5.10. Genes involved in the SAPK pathway and Hog1-mediated response to stress (Figure 5.10. A) show changes in expression. *HOG1* and *SSU81* were significantly down-regulated in Δ*Δtlo* compared to Wü284 at all three time points. *SSU81* is predicted to encode for an adapter protein involved in MAPK-signaling upstream of Hog1 and *HOG1* is a vital part of the SAPK-mediated (and non-SAPK-mediated) stress response as outlined above. Down-regulation of these genes and the resulting effectors could be in part responsible for the difficulty the Δ*Δtlo* has in dealing with oxidative stress. However, *CHK1* which is predicted to have a role in sensing oxidative stress in *C. dubliniensis* is up-regulated particularly in YEPD which is unusual and may suggest that the Δ*Δtlo* strain is under some sort of undefined, internal stress.

As mentioned above, the *SAPK* pathway is also involved in the response to osmolarity-induced stress. *CHK1* is involved in this pathway and in *C. albicans* is predicted to be part of the osmo-sensory machinery, as is *YPD1,* which were both up-regulated in Δ*Δtlo,* particularly in YEPD and 3 h WS (Smith *et al.*, 2010) (Calera *et al.*, 2000; Mavrianos *et al.*, 2014). In Chapter 4, an impaired response to growth under osmotic stress was observed, however up-regulation of these effectors is at odds with this observation which may suggest the involvement of an as yet unidentified upstream regulator, or perhaps more intriguing, a defect in induction of effectors linked with the *TLO*s.

Other genes involved in the response to oxidative stress show altered expression patterns. In particular, the family of SODs show unusual expression patterns (Figure 5.10. B). *SOD6,* which encodes for a copper/zinc-containing superoxide dismutase, shows a marked decrease in expression under all conditions. *SOD3* and *SOD5* (encoding manganese and copper/zinc SODs, respectively) show decreased expression under late and early hyphal growth

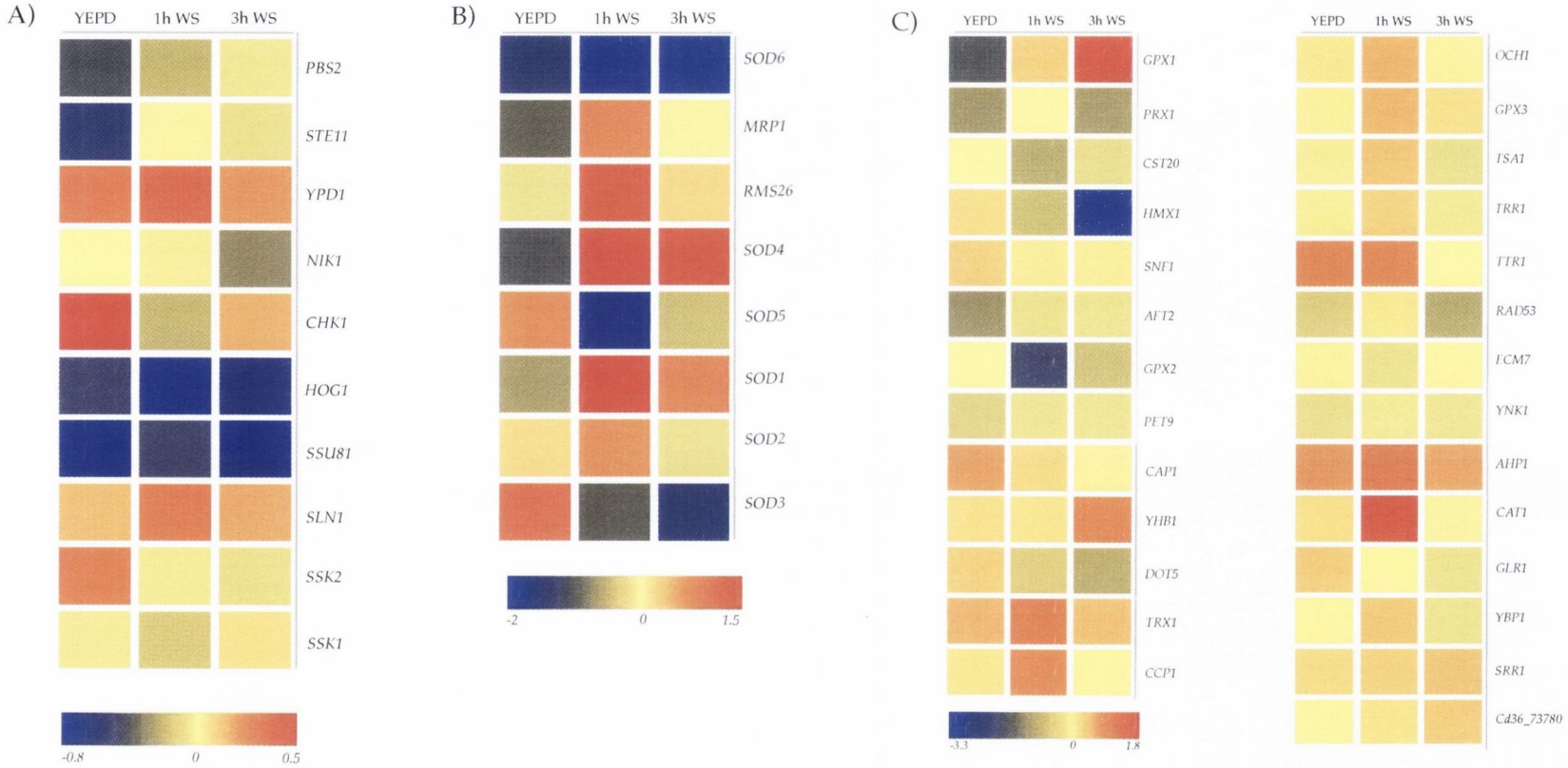

Figure 5.10. DNA microarray analysis of genes involved in the cellular response to stress.

Two-colour DNA microarray analysies were carried out in *C. dubliniensis* strains ΔΔ*tlo* versus Wü284. Heatmaps generated using Genespring software version 12 (Agilent Technologies) are shown to illustrate differences in gene expression in these two strains for genes known or predicted to be involved the response to stress (osmo- and oxidative-) in *Candida* species. The genes involved in the stress-activated protein kinase (SAPK) pathway are shown in (A), the genes encoding for superoxide dismutases are shown in (B) and non-categorised genes involved in oxidative stress response are shown in (C). The legend below each heat-map indicates the intensity of differential expression, in Log_2 values, by colour.

stages, respectively. Interestingly, these genes both showed an increase in expression under nutrient-rich growth in YEPD. *SOD1* and *SOD4* (which both encode for copper/zinc-containing superoxide dismutases) appeared to show increases in expression under both stages of hyphal growth. Altered expression of *SOD* genes has been suggested to result in increased damage to cell structure and decreases in growth (Xu *et al.*, 2013).

Additional genes involved in the response to oxidative stress are shown in Figure 5.10. C. Several genes show slightly elevated expression in WS, particularly at 3 h (e.g. *GPX1, YHB1, TRX1, AHP1*). *CAT1,* which has been implicated in the oxidative and core stress responses was unexpectedly expressed higher at 1 h growth in WS (Znaidi *et al.*, 2013). *DSE1,* which is an essential protein located in the cell wall is important for cellular response to oxidative stress is significantly down-regulated in early and later hyphal induction (11.2 fold and 2-fold respectively) and also in nutrient-rich conditions (2.5 fold down-regulation) (Daher *et al.*, 2011). *CFL1,* which is expressed at slightly lower levels under all three conditions has recently been shown to be important in the cellular response to oxidative stress (Xu *et al.*, 2014).

The decreases in expression observed in YEPD for genes such as *HOG1, SOD6* and *SSU81* directly explain the phenotypes observed in Chapter 4 where strain ΔΔ*tlo* exhibited increased susceptibility to oxidative stress. In addition, during intrinsic stress, mRNA translation is thought to be error-prone and it is thought that the cell may attempt to reduce levels of expression of genes overall in order to contend with this (Shenton *et al.*, 2006). This may, in part, explain some of the lowly-expressed genes. However, DNA microarrays under specific stresses would help to explore this further. The increased expression of some stress response genes in a mutant, which is generally more susceptible to stress, is perhaps paradoxical at first glance. However, it may suggest that these cells are responding to some constitutive internal stress, perhaps osmotic or oxidative. The marked increase of the expression of these genes (e.g. *SOD4, CHK1, YPD1, TRX1,* etc.) compared to that of wild-type cells may point to a stress, perhaps intracellular, that the absence of *TLO* expression confers. *CAP1* is also expressed at slightly higher levels (1.2-fold in WS, 1 h and 1.5-fold in YEPD) in strain *tlo*ΔΔ, which is also unusual. Cap1 is activated by H_2O_2 and has been shown to be necessary for macrophage escape mediated by filamentation (Patterson *et al.*, 2013). Targets of ROS such as *RLI1* (not pictured), is down-regulated almost 2-fold

in YEPD but slightly increased at both 1 h and 3 h in WS. These unusual observations might further add to the hypothesis that these cells are undergoing a response to an internal stress conferred by deletion of the *TLO* genes.

Another interesting aspect of the oxidative stress response its relationship with other processes such as metabolism and virulence. For example, the availability of iron is an important factor, which affects DNA damage under oxidative stress. Likewise, when iron is present in excess, it can lead to the production of ROS *in vivo* through the Fenton reaction (Xu *et al.*, 2014). In the next section, changes in the expression of metabolism-associated genes are discussed and it is important to keep in mind that like in the example of the Fenton reaction, many of these responses are linked to one another.

5.4.3. Nutrient acquisition & starvation response

The acquisition and utilisation of nutrients is vital for an organism to survive and thrive in a range of environments. Like in higher order eukaryotes, iron is an important molecule that is required for the function of numerous proteins and processes including respiration, DNA repair/synthesis and metabolism. However despite being one of the most plentiful metals it often exists in forms that are insoluble (mostly ferric hydroxide complexes) for immediate use (Ardon *et al.*, 1998). Fungi have evolved numerous methods of both utilising these sources of iron and storing their unstable byproducts (Howard, 1999).

One of the more important pathways involved in high-affinity uptake of iron consist of enzymes encoded by a group of ferric reductases, permeases and multi-copper oxidases (Liang *et al.*, 2009). Interestingly, many of these genes showed significantly altered expression upon disruption of the *TLO* genes in *C. dubliniensis* as summarised in Figure 5.11. The family of genes predicted to encode ferric reductases displayed particularly different levels of expression (Figure 5.11. A) (Almeida *et al.*, 2009). The expression of these genes has previously been shown to be regulated directly by iron availability (Bensen *et al.*, 2004). In addition, Rim101 has been described as a regulator of this family of reductive enzymes as evidenced by its direct regulation of the expression of *FRE2* and *FRP1* in *C. albicans* (Baek *et al.*, 2008; Liang *et al.*, 2009). *RIM101*, whose expression is required for growth in alkaline, nutrient-limiting conditions (Almeida *et al.*, 2009) was down-regulated in Δ*Δtlo* compared to wild-type in filament-inducing conditions.

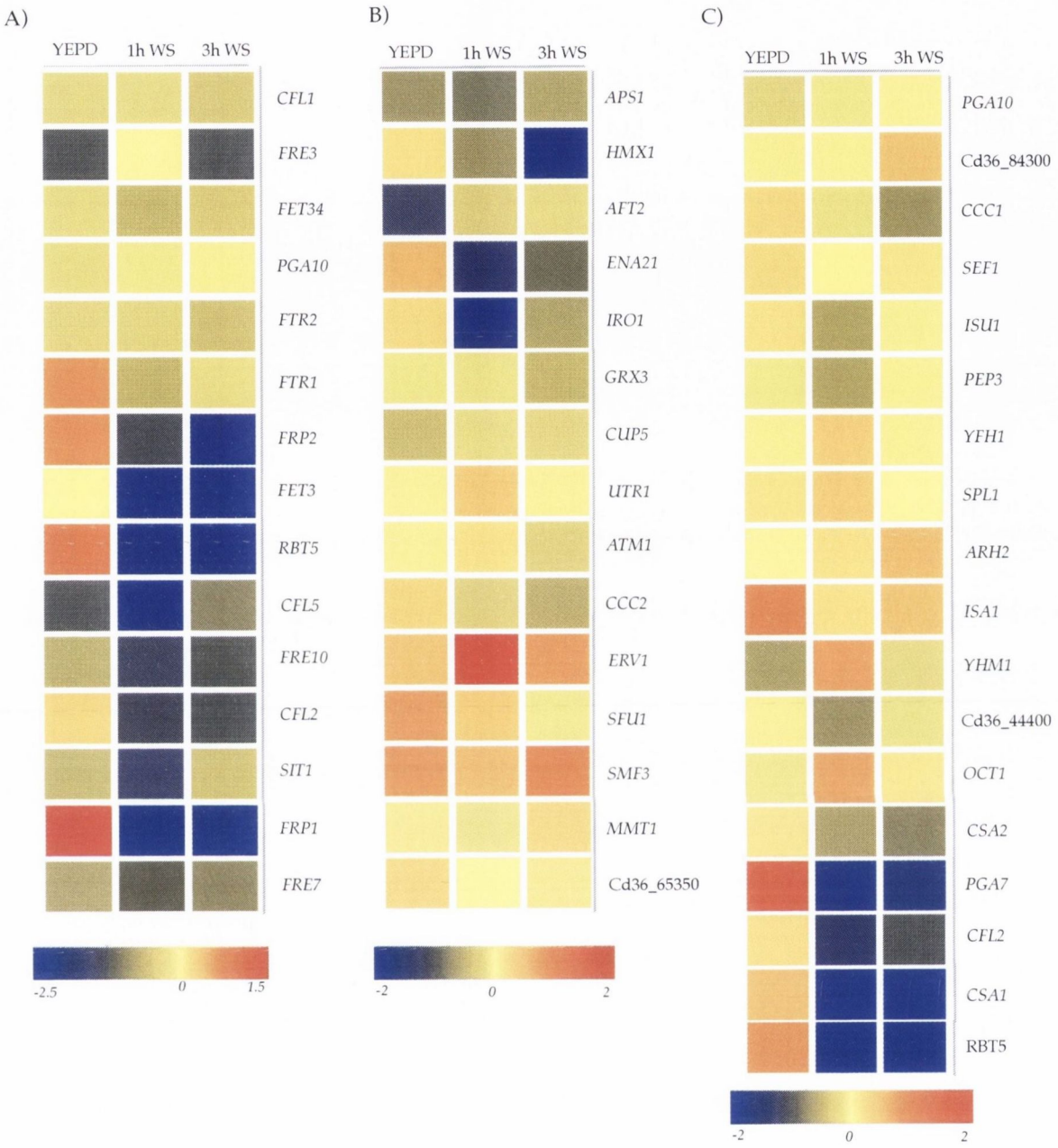

Figure 5.11. Deletion of *TLO* genes in *C. dubliniensis* alters the expression of genes involved in iron uptake and homeostasis.

Heatmaps from two-colour DNA microarray analysis of ΔΔ*tlo* versus Wü284 are shown for genes involved in iron uptake (A) and iron homeostasis (B & C). Colour scales representing normalised gene expression values are shown beneath each heatmap.

FET3 showed significant down-regulation in the mutant compared to wild-type in all conditions. *FET3* is part of the family of multi-copper oxidases (Figure 5.11. B) that encode enzymes involved in the oxidation of Fe_2^+ to the less reactive Fe_3^+ (Kosman, 2003). While not necessary for virulence, *FET3* has previously been shown to be integral to the iron uptake system in *C. albicans* through deletion experiments leading to defective uptake *in vitro* (Eck *et al.*, 1999). As well as the reductases and oxidases, the iron permeases play an important role in iron uptake in *Candida*, allowing for the sequestering and transport of Fe^{3+} inside the cell (Almeida *et al.*, 2009). When iron is depleted, *FTR1* expression is induced. *FTR1* expression was slightly induced in the YEPD dataset in ΔΔ*tlo* compared to wild-type, however it is down regulated during early hyphal growth and to a lesser extent, at the 3 h time point in WS. It has been shown in other studies that a null mutant for *FTR1* is avirulent (Ramanan & Wang, 2000).

A major source of iron for *Candida* within the human body is haemoglobin, which accounts for 66 % of the total iron content in the body (Almeida *et al.*, 2009; Evans *et al.*, 1999). One method of utilising this abundant iron source for yeast cells that have entered the circulatory system is to utilise Rbt5 which binds haemoglobin and the resulting complex is taken up into the cell through endocytic internalisation (Almeida *et al.*, 2009; Weissman *et al.*, 2008). *RBT5* is up-regulated significantly in the presence of low iron concentrations. In the experiments carried out in this study, while *RBT5* was up-regulated in YEPD in ΔΔ*tlo* compared to Wü284, it was significantly down-regulated (14-fold) during early hyphal growth and at 3 h WS (7-fold).

Once internalised, haemoglobin is degraded by a haem-oxygenase, encoded by *HMX1* for further downstream processing. *HMX1* is positively regulated by low iron and the shift from lower temperatures to body temperature. In WS, after such a temperature shift, ΔΔ*tlo* expressed *HMX1* 1.6-fold lower than wild-type at 1 h and 10-fold lower than in wild-type by 3 h.

Clearly the expression of genes involved in iron uptake, assimilation and subsequent utilisation/degradation was affected by the disruption of both *TLO* genes in *C. dubliniensis*. In most cases, genes involved in the later internalisation and degradation of iron containing molecules (e.g. *HMX1* and *RBT5*) which are normally expressed at higher levels in low iron, were down-regulated in the ΔΔ*tlo* strain compared to Wü284 in WS. Likewise, other genes encoding proteins involved in the surface reduction and transport of iron molecules (e.g. *FET3*, *FTR1*,

FRE7) which are also normally regulated by iron availability were down-regulated in Δ*Δtlo* in WS. However it has been determined that foetal calf serum contains high levels (up to 1 % [w/v]) of iron and the expression of such genes is at odds with this (Kakuta *et al.*, 1997). It is plausible that the disruption of the *TLO* genes has an effect on a global regulator (e.g. Hap43 and Sfu1 show altered expression) that is thereby affecting the expression of the genes outlined above. For example, Rim101 is known to be involved in the up-regulation of genes necessary for iron reduction, e.g. *FRP1* (Bensen *et al.*, 2004) (Almeida *et al.*, 2009; Baek *et al.*, 2008). However, *RIM101* expression was not significantly changed in WS, but was slightly up regulated in Δ*Δtlo* in YEPD compared to wild-type. Without further experiments, it is difficult to determine if the effects of *TLO* deletion are direct or act via a complex network of upstream regulators. Nonetheless, the transcriptional landscape of genes involved in iron assimilation and utilisation were altered enough to warrant discussion.

As well as iron and siderophore sequestration and uptake, *Candida* species have evolved intricate pathways to maximise their growth by developing the ability to utilise alternative nutrients when the preferred sources are not available. Glucose is the preferred carbon source for most organisms (Brown *et al.*, 2009; Reece *et al.*, 2010), however most organisms have evolved pathways to allow for uptake and assimilation of other nutrients when enough glucose is not available or accessible. Galactose is one such sugar, and the processes of galactose utilisation are well described in yeast (Brown *et al.*, 2009). A number of genes involved in galactose degradation via the Leloir pathway were affected upon deletion of the *TLO*s (Figure 5.12). *GAL10* which encodes for a dual function epimerase, *GAL7* which encodes for a galactose-1-phosphate uridylyl transferase and *GAL1* which encodes a galactokinase are all integral in the conversion of galactose into fermentable glucose (Holden *et al.*, 2003; Martchenko *et al.*, 2007; Singh *et al.*, 2007; Skrzypek *et al.*, 2010). All of these genes were expressed at lower levels during both stages of hyphal growth and in YEPD (Figure 5.12). Other genes associated with this process also show changes in expression in *tlo* mutants. For example, *UGP1* which encodes a glucose-1-phosphate uridyltransferase (Skrzypek *et al.*, 2010) showed increased expression in serum (Figure 5.10) and *GCA1* which encodes an extracellular membrane-associated glucoamylase involved in starch degradation and which is regulated by galactose concentration was expressed at much higher levels in *tlo* mutants than in Wü284.

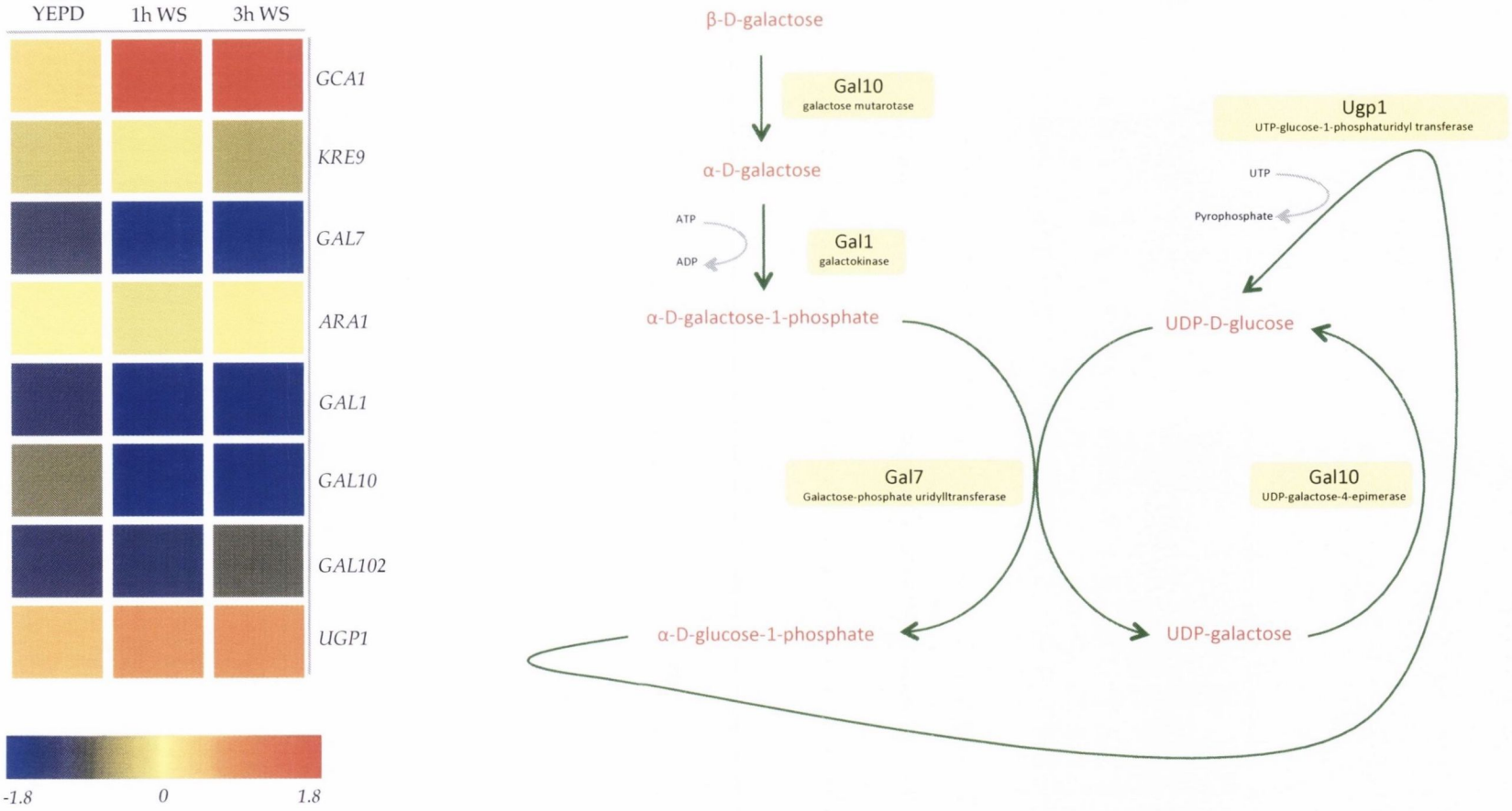

Figure 5.12. Expression of genes involved in galactose degradation is affected by the deletion of *TLO* genes in *C. dubliniensis*.

A) Heatmap representing DNA microarray analysis of ΔΔ*tlo* versus Wü284 in *C. dubliniensis* under 3 conditions (labeled at top of heatmap). Coloured scale for normalised expression levels is show below heatmap. B) Schematic diagram of the 'Leloir' pathway involved in degradation of galactose into usable by-products. Products are highlighted in red, genes and their encoded enzymes are in yellow boxes and reaction directions are indicated by arrows. Scheme adapted from (Singh, *et* al., (2007), Holden *et* al., (2003) and Skrzypek *et al.*, (2010).

The changes in the expression patterns of these genes are interesting when viewed in conjunction with the growth curve experiments in section 4.3.10. during which *tlo* mutants displayed significantly increased doubling times in galactose-based media suggesting impairment in galactose utilisation. These effects are most likely linked to other changes in the expression landscape of ΔΔ*tlo*. For instance, *GAL10* has also been linked to filamentation and response to oxidative stress (Singh *et al.*, 2007), both of which were defective in the *tlo* mutant strain.

Due to the very obvious change in expression of most of the genes associated with galactose degradation, it is likely that the *TLOs* are involved in their regulation, either directly or indirectly through other upstream effectors. In *S. cerevisiae*, the genes that encode galactose metabolising enzymes are regulated by Gal4 (encoded by *GAL4*), which serves to activate transcription of these genes. It was assumed for some times that this regulation was present across the *Saccharomycetaceae* family due to synteny of the enzyme-encoding genes. However, it was described by Martchenko *et al.* (2007) that mechanisms of regulation are distinct between *S. cerevisiae* and *C. albicans*. It was found that instead of *GAL4*-mediated activation of *GAL10*, Cph1 (a known regulator of filamentation) mediates activation of *GAL10* in *C. albicans*. Interestingly, in the same study, *GAL4* was shown to be involved in the regulation of the *TLO* genes (Martchenko *et al.*, 2007). In a *Δgal4* mutant strain, the *C. albicans TLO* genes are expressed at lower levels. Further analysis showed that the *TLO* promoter regions contained a Gal4 protein-binding site, and that in the absence of this sequence, *TLO* expression was decreased (Martchenko *et al.*, 2007). With these findings, in combination with our data in which the *GAL* genes show differential expression in ΔΔ*tlo*, it is plausible to suggest that the *TLO* genes may be involved in a regulatory circuit that may allow for indirect activation of *GAL10* expression by Gal4, via the *TLOs*.

Another important carbon source for *Candida* species is *N*-acetylglucosamine (GlcNAc). GlcNAc is an important constituent of chitin in the cell wall of *Candida* species and also plays a role in glycosylphosphatidylinositol (GPI) anchoring (Naseem *et al.*, 2011). More interestingly, it has been shown play an important role as a signaling molecule for processes such as filamentation and biofilm formation (Naseem *et al.*, 2011; Pérez-Campo & Domínguez, 2001). In fact, GlcNAc is used in the laboratory to induce hyphal formation in *Candida* species (Hyde, P., Personal Communication, 2013). GlcNAc acts by inducing increased cAMP-signaling, which promotes the switch from white to opaque cells and the

expression of virulence genes *in vitro* (Huang *et al.*, 2010). It is thought that this may resemble the *in vivo* process during infection and invasion of the mucosa. As well as this, GlcNAc also acts as a self regulating molecule in that it signals induction of GlcNAc-metabolic and catabolic genes (Huang *et al.*, 2010; Naseem *et al.*, 2011). In a *tlo* deletion mutant, many of these genes showed altered expression (Figure 5.13). *NAG1* encodes for a glucosamine 6-phosphate deaminase enzyme and is one such gene that is up-regulated in the presence of GlcNAc (Kumar *et al.*, 2000). *NAG1* was up-regulated in all three conditions in Δ*Δtlo* compared to Wü284. In addition to this, *NGT1*, a transporter of GlcNAc was up-regulated during early hyphal growth in the *tlo* mutant. *HXK1* and *DAC1*, both mediators of GlcNAc catabolism (Naseem *et al.*, 2011) were expressed at lower levels in the *tlo* mutant compared to wild-type. The consequence of up-regulation of these genes in this context of observable phenotypes is unknown, however with GlcNAc being an alternative carbon source, it is possible that this evidence of a starvation mode that deletion of *TLO*s has triggered.

Evidence for a starvation mode was observed in several other metabolic processes during growth in YEPD. For example, *FPB1*, which encodes a fructose-1,6-bisphosphatase, and *PCK1*, which encodes a phosphoenolpyruvate carboxykinase, are both integral parts of the gluconeogenesis pathway and were both up-regulated in Δ*Δtlo*. Conversely *PFK1*, which encodes 6-phosphofructokinase and *FBA1* which encodes fructose-bisphosphate aldolase are key components of the glycolytic cycle and were down-regulated in the *tlo* mutant. This down-regulation of a typical metabolic process with up-regulation of one associated with low concentrations of glucose (despite YEPD containing high glucose levels) further suggests that the mutant strain is behaving as if responding to carbon starvation. As well as this, other genes involved in ergosterol biosynthesis (*ERG* genes), amino acid metabolism (*MET* genes) or catabolism (*PUT* genes) and the TCA cycle all showed altered expression in the case of the *tlo* mutant. As such, there is strong evidence that the absence of *TLO*s creates a stressful environment with subsequent regulation of stress-associated pathways.

5.4.4. Closing remarks & additional observations

The DNA microarray, despite the advent of next-generation sequencing technology, continues to be an invaluable tool used to explore the intricacies of global gene expression. However, there are a number concerns that merit mention

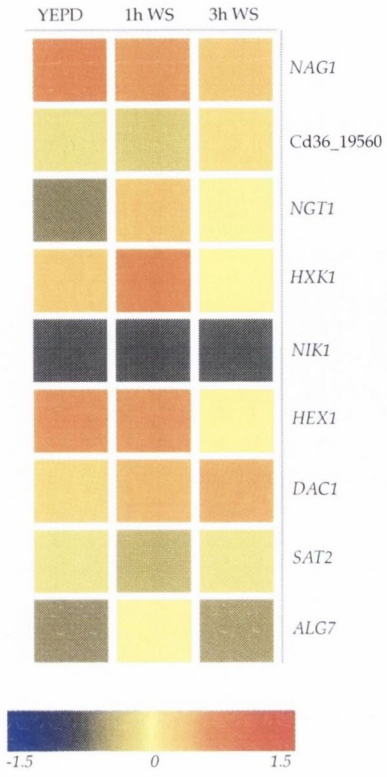

Figure 5.13. DNA microarray analysis of genes involved with N-acetylglucosamine-associated processes.

Heatmaps from two-colour DNA microarray analysis of Δ*Δtlo* versus Wü284 are shown for genes involved in N-acetylglucosamine uptake, transport, metabolism and catabolism. Colour scales representing normalised gene expression values are shown beneath each heatmap.

in this study. As mentioned in the introductory remarks, much is known about the *C. albicans* genome, thanks both to gene homology and orthology to *S. cerevisiae* genes as well as the extensive research carried out over the last few decades on various families of *C. albicans* genes. However, *C. dubliniensis* has not been as widely studied and as such, less information is available on its genome. Much of the data on the *C. dubliniensis* gene content comes from a small selection of papers (Jackson *et al.*, 2009) and predicted homology to *C. albicans* genes. As such, it has been common practice (Jackson *et al.*, 2009; Moran *et al.*, 2012) to use *C. albicans* gene names and ontology data when analysing *C. dubliniensis* gene expression as there are significantly more detailed *C. albicans* annotations and purpose-built bioinformatics tools. These homology and orthology predictions have very often been proven accurate (Jackson *et al.*, 2009; O'Connor, 2009), however it is important to remember that the two organisms are distinct and some major differences may exist. Also, many genes simply remain uncharacterised. Consequently, this creates a *caveat* during the interpretation of the results of this and other *C. dubliniensis* studies.

Although many of the changes in gene expression described reflect the phenotypic data described in Chapter 4, some of the changes in gene expression were unexpected, or paradoxical. For example, *ECE1, EED1,* and *IDH1* were expressed at high levels in YEPD, a pattern at odds with their normal expression patterns during filamentation in *Candida*. This suggests that perhaps the *TLO*s are working as both activators and repressors in a gene-specific or condition-specific manner. Therefore, *TLO*s appear to have pleotropic effects on a number of genes. As well as this, qRT-PCR results showed that during growth in WS, many genes were induced slower in the absence of *TLO* expression than in wild-type (e.g. *UME6, SOD5, GAL1* and *GAL7*), suggesting Tlos may mediate rapid transcriptional changes, a role that also fits with the role of the Mediator complex. Characterisation of the interaction between the Tlo proteins, chromatin and the Mediator complex itself, would allow us to develop a hypothesis on their function and this will be investigated in the following sections.

Chapter 6

The relationship between Tlo1 and DNA in *Candida dubliniensis*.

6.1. Introduction

6.1.1. Opening Remarks

In previous chapters, it was established that *TLO* disruption affects a wide range of phenotypes and leads to a shift in the transcriptional landscape of the cell in *Candida dubliniensis*. Such changes in expression are likely the result of disruption to regulatory pathways, in which the *TLO* genes and their encoded proteins are thought to play a major role. Interestingly, despite the huge array of regulatory networks in *Candida* spp., these generally converge on a small number of important transcription factors that are central to these transcriptional pathways and their associated phenotypes (Paul & Moye-Rowley, 2014; Saputo *et al.*, 2012; Shapiro & Cowen, 2012). In many cases where a transcriptional regulator's overall role has been elucidated, there are a multitude of possible ways in which these factors can exert control over transcription, including direct protein-DNA binding, cofactor binding and chromatin modulation (Lelli *et al.*, 2012; Slattery *et al.*, 2014). As discussed in the first chapter, the *TLO* genes were first identified through yeast one-hybrid experiments in an attempt to identify trans-activating proteins (Kaiser *et al.*, 1999). In addition, it has been hypothesised, both in recent publications (Zhang *et al.*, 2012) and in ongoing work in our laboratory (Personal Communication, Moran, 2011) that Tlo proteins form a subunit of the Mediator complex. While the activation potential of Tlos and the intricacies of their relationship with Mediator are discussed in other sections, this evidence in conjunction with expression data from this study suggest that these are a family of effectors involved in transcriptional regulation via an interaction with DNA or chromatin.

As such, it was pertinent to investigate the relationship between the Tlo proteins and the genome. Recent studies in various organisms (Ansari *et al.*, 2014; Huang *et al.*, 2014), including in *Candida albicans* (Lassak *et al.*, 2011; Lohse *et al.*, 2013) have shown Chromatin immunoprecipitation (ChIP) to be an invaluable tool in uncovering the details of the association of proteins with DNA. In this study, ChIP in conjunction with DNA-tiling microarrays (ChIP-on-chip) was used as a way of gaining an insight into the global association of Tlo1 with DNA in *C. dubliniensis*.

6.1.2. ChIP-on-chip

ChIP is a complex technique utilised by research groups around the globe since its initial publication in 1985 (Gilmour & Lis, 1985). ChIP involves the cross-linking of proteins to gDNA followed by fragmentation of the DNA and subsequent isolation of DNA fragments associated with a specific tagged protein of interest via an antibody-mediated pull down. Proteins can be tagged with a number of different epitopes, including c-myc, which is a part of the proto-oncogene *myc*, His6 which is composed of six concurrent histidine residues, green fluorescent protein (*gfp*) and haemagglutinin (HA) tag derived from the human influenza HA protein (Lavoie *et al.*, 2008). In this study, Tlo1 was tagged with 3 successive HA epitopes to allow immunoprecipitation of the protein with an anti-HA mouse monoclonal antibody 12CA5 (subtype $IgG_{2b,}{}^{K}$). The workflow for the experiment is outlined in Figure 6.1.

ChIP and ChIP-on-chip have been detailed extensively in the literature for studies using *Saccharomyces cerevisiae* and *C. albicans*, however to our knowledge there are only two instances of *C. dubliniensis*-based ChIP, none of which involved the use of strain Wü284 or carried out ChIP on a global scale. In addition, this study describes the first instance of ChIP of the Tlo proteins in *Candida* species. As such, extensive optimisation was required and was carried out for the experiments contained in this chapter. The ChIP-chip experiments were performed in collaboration with the Berman lab at the University of Minnesota. Subsequent single gene ChIP-qRT-PCR analysis was carried out in conjunction with the Fleming lab, Trinity College Dublin and the Trinity College Biosciences Institute.

ChIP of the Tlo proteins had been attempted in *C. albicans* by collaborators in the Berman Laboratory (Personal Communication, Anderson, 2012) without success and it was hypothesised that this was due to the fact that only one of 15 Tlo proteins expressed in this species was tagged, thus leading to poor recovery of Tlo-bound chromatin. In addition, a single cross-linking step (with 37 % [w/v] formaldehyde) may not have been sufficient to immunoprecipitate (IP) the Tlo-Mediator complex as discussed in other sections. To address this concern, cross-linking was carried out in *C. dubliniensis* with a secondary (2°) cross-linking agent, dimethyladipimidate (DMA) followed by primary (1°) cross-linking with 37 % (w/v) formaldehyde (formalin) for extended periods. Success has been achieved using this method of cross-linking for other species in previous studies (Kurdistani & Grunstein, 2003; McCabe & Innis, 2005).

As well as the cross-linking steps, the spheroplasting and subsequent DNA fragmentation steps proved troublesome in *C. dubliniensis*. Previous work with chromosomal DNA isolation of *C. albicans* and *C. dubliniensis* strains (unpublished) had demonstrated that the efficiency and times of spheroplasting using lyticase (Zymolyase) enzymes (including beta,1,3-glucan laminaripentaohydrolase) was subject to extreme variations dependent on strain (Rodríguez-Peña *et al.*, 2013). Sonication of DNA fragments was highly dependent on the success of the spheroplasting and lysis steps so optimisation of the sonication was required in Dublin and Minnesota. ChIP-qRT-PCR was carried out at a later date in Dublin and for this method it was decided that mechanical breakage was more desirable in terms of consistency. Also, newer systems, including the magnetic-bead based IP were utilised. Development of both of these techniques is discussed in this chapter.

Interpretation of the data obtained from these experiments also proved a novel challenge due to the lack of resources for proteomic and genomic analysis in *C. dubliniensis* backgrounds. However, despite these obstacles and challenges, the results of the study provided the first global overview of Tlo occupancy and have greatly expanded our knowledge of Tlos in *Candida* species.

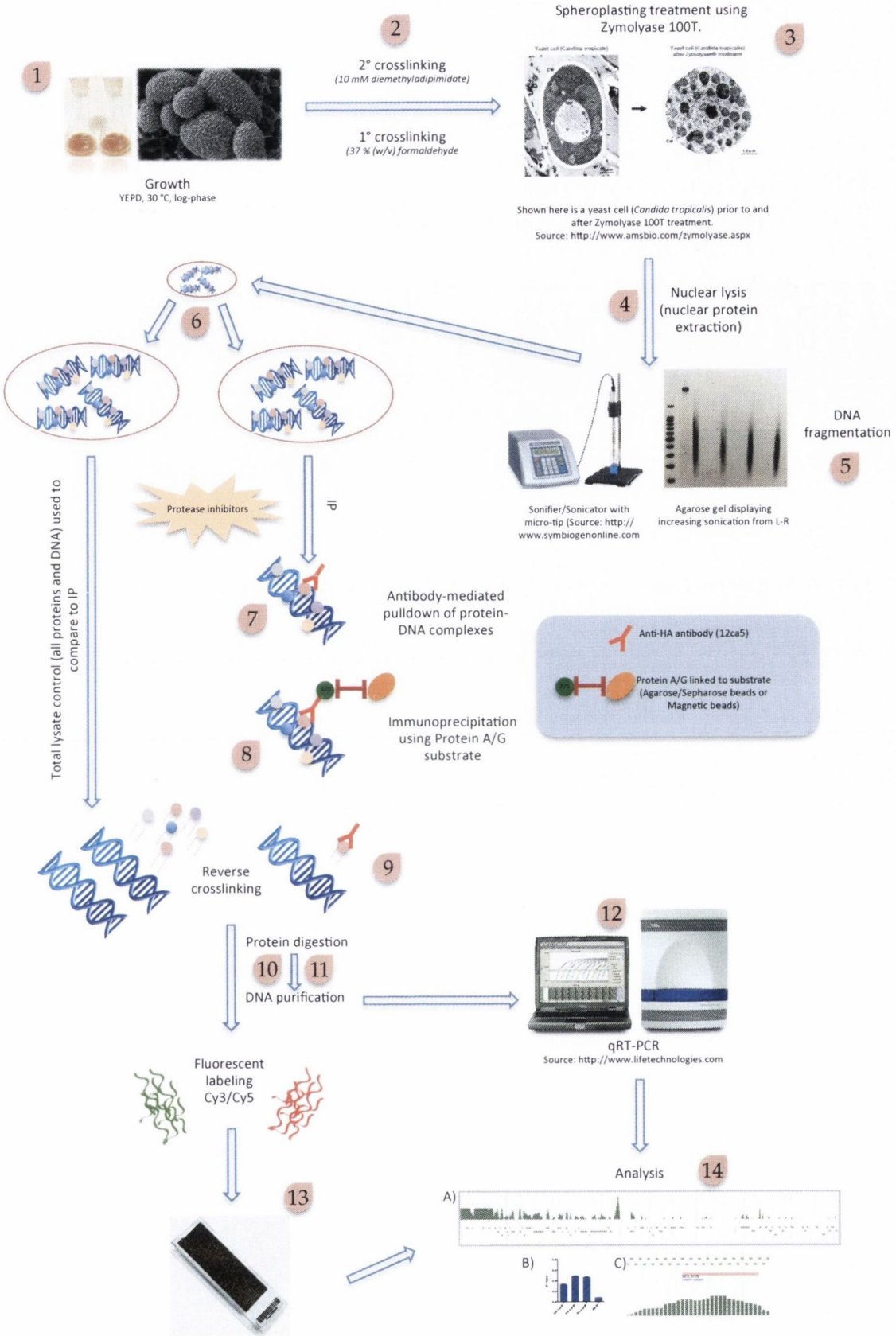

A. JBrowse snapshot of Tlo1 enrichment along chromosome 5:1-200 kb
B. qRT-PCR confirmation of Tlo1 enrichment on *PUT1*
C. *PUT1* region zoomed in to visualise enrichment for Tlo1.

Figure 6.1. Overview of Chromatin immunprecipitation (ChIP) and ChIP-on-chip methodology.

1. Yeast cells are grown to desired density/phase. Two parallel cultures are setup for each replicate – one of wild-type (Wü284) and one of the strain containing Tlo1-HA tag.
2. Cross-linking is carried out. In this study, both primary (formaldehyde) and secondary (dimethyladipimidate) crosslinking agents were used.
3. Cross-linked cell walls were digested with lytic enzymes to form sphaeroplasts.
4. Detergent-based extraction of the nuclear protein-DNA complexes
5. DNA fragmentation by sonication
6. Samples were split into two – the total cell lysate control (input) and the immunoprecipitate (IP). Protease inhibitors are used throughout the following processes to avoid degradation of protein-DNA complexes.
7. Using anti-HA, DNA-protein complexes specific for Tlo1 are pulled down.
8. Using protein A or G (both suitable for 12CA5 antibody), DNA-protein-Antibody complexes are immunoprecipitated
9. Samples are heated to reverse cross-links.
10. Proteins are enzymatically digested
11. DNA is purified. At this point input contains DNA that was bound to any/all proteins during growth. The IP contains only DNA that was specifically associated with Tlo1
12. Samples can be analysed with single-gene ChIP by qRT-PCR to estimate enrichment of Tlo1 over a specific region compared to the input.
13. Samples can also be differentially labeled and hybridised to a DNA tiling array to determine Tlo1 enrichment over the entire genome.
14. Analysis of the data is carried out resulting in enrichment peaks which can be assigned a peak score with Bioconductor software (R) or qPCR can be graphed using Prism (Graphpad).

*Specific methods are outlined in detail throughout Chapter 6.

6.2. Materials and Methods

All chemicals discussed in the following sections of this chapter were derived from stocks supplied by Sigma-Aldrich. All solutions were filter sterilised using Steritop Vacuum-driven filtration systems with a 0.22 μM membrane (Merck-Millipore). All plasticware and glassware were sterilised by autoclaving. Centrifugation steps were carried out in a bench-top bucket centrifuge (Eppendorf) for volumes of over 2 ml. For volumes equal to or less than 2 ml, centrifugation steps were carried out in a bench-top mini-centrifuge (Eppendorf). The rationale behind the various steps in the experiments carried out is discussed in section 6.3.

6.2.1. Estimating extent of cell lysis and breakage

Four identical cultures were setup and cell pellets were prepared as described in Section 6.2.4. Cell pellets were thawed on ice and re-suspended in 400 μl of Lysis Buffer (50 mM HEPES pH 7.5, 140 mM Sodium Chloride, 1 mM EDTA, 1 % (v/v) Triton X-100, 0.1 % (w/v) Sodium deoxycholate) containing 1X protease inhibitor (PI) cocktail and 2 mM phenylmethanesulfonylfluoride (PMSF). Each mixture was split into two fractions in 1.5 ml screw-capped tubes (Sarstedt), each containing 400 μl of 425-600 μm acid-washed glass beads resulting in a total of 8 identical fractions.

The tubes were then subjected to the desired number of 30 s cycles, at 6 m/s in a Fastprep Homogeniser 24 (MP Biomedical, Santa Ana, CA, USA). Tubes were placed on ice for 5 min between each cycle. The first mixture was subjected to one cycle, the second tube subjected to two cycles and this pattern was continued up to 7 cycles. The eighth mixture was not subjected to any breakage and was used as a control mixture.

After breakage was complete, tubes were pierced using a sterile 23G needle (Becton, Dickinson & Co.) and centrifugation at 2,500 x *g* at 4 °C was performed to elute the lysate from the beads into 50 ml polystyrene tubes (Greiner Bio-One) and then lysates were transferred to fresh 1.5 ml microcentrifuge tubes (Eppendorf).

The lysates were then processed in one of two ways as described below:

6.2.1.1.Visual estimation of lysis

After each time point, 20 µl of lysate was removed and transferred to a microscopic slide with coverslip and visualised using a light microscope (Nikon Instruments) under 400 X magnification. The numbers of cells present in the field of view were counted using a haemocytometer (Neubauer) as described in section 2.1.7. This was repeated for three separate areas on the slide and the average of the three counts was calculated. The average amount of intact cells present was used to assess the success of breakage.

6.2.1.2 Bradford assay

Protein standards were setup by preparing five dilutions of Bovine Serum Albumin (BSA) at 2 µg/ml, 4 µg/ml, 6 µg/ml, 8 µg/ml and 10 µg/ml in final volume of 800 µl. To each, 200 µl of pre-mixed Bradford reagent (BioRad) was added.

Each of the eight lysis samples was diluted 1:100 with Lysis Buffer (Section 6.2.4.) and 1X PI cocktail. A 100 µl volume of diluted sample was combined with 200 µl of pre-mixed Bradford reagent (BioRad) and 700 µl sterile water in a total of 1 ml to give a 1:1000 dilution of sample. To another tube, 20 µl of diluted sample was combined with 200 µl of pre-mixed Bradford reagent and 780 µl sterile water to give a 1:5000 dilution of sample.

All tubes (five standards, eight 1:1000 diluted samples and eight 1:5000 diluted samples) were allowed to incubate at room temperature for five min and then were transferred to plastic cuvettes (Sarstedt) and the absorbance of each was measured at 595 nm using an Evolution 60S absorbance spectrophotometer (Thermo Fisher Scientific).

The absorbance values of the standards were plotted on an XY graph using Excel (Microsoft), which allowed interpolation of protein concentrations in each sample, thereby indicating the success of lysis. For sensitive measurements, a blank tube containing no protein was setup as before and used as a baseline absorbance value measurement.

6.2.2. Chromatin immunoprecipitation (Berman Laboratory Method)

The following is an optimised protocol devised during a lab visit to the Berman Lab, University of Minnesota in June-August 2012 and was used for global ChIP-chip analysis.

6.2.2.1 Growth and chemical fixation

Colonies of required strains were sub-cultured onto YEPD agar and grown for 48 h at 30 °C in a static incubator (Gallenkamp). From these plates, one colony was used to inoculate 12.5 ml of YEPD in 250 ml borosilicate Erlenmeyer narrow-neck flasks (Thermo Fisher Scientific) and incubated at 30 °C with shaking at 200 r.p.m. in an orbital incubator (Gallenkamp) overnight, for 16 – 18 h.

The next day, the optical density of each overnight culture was measured at 600 nm wavelength on an absorbance spectrophotometer (Thermo Fisher Scientific). For each of the overnights, a volume (X ml) was added to YEPD in an Erlenmeyer narrow-neck flask so as to have an initial O.D. 600 nm of 0.2. The volume X was calculated as described in section 2.1.7. The cultures were then each incubated at 30 °C with shaking at 200 r.p.m. in an orbital incubator (Gallenkamp) until they had reached an O.D. $_{600\ nm}$ of 2.0. This was typically at 5.5 – 6 h of growth for strains of *C. dubliniensis*.

At this point, cells were transferred to 50 ml polystyrene tubes (Greiner Bio-One) and centrifuged at 2,000 x *g* for 5 min. Supernatants were disposed of and the cell pellets (if multiple tubes were used for single cultures) were combined and re-suspended in 10 ml sterile PBS. Cultures were then centrifuged as before and the supernatant was disposed of. Washed pellets were re-suspended in 20 ml of 10 mM DMA-PBS in the polystyrene tubes and incubated at room temperature for 45 min with mixing on a Unimax mixing tray (Heidolph).

Samples were then centrifuged as before and the supernatants were disposed of. Cells were washed in 10 ml PBS and centrifuged once again. Supernatants were disposed of and cell pellets were re-suspended in 36 ml PBS. 1 ml of 37% formaldehyde was added to each sample and then each sample (about 40 ml) was transferred to 100 ml Erlenmeyer narrow-neck flasks (Thermo Fisher Scientific) and incubated at 30 °C with shaking at 200 r.p.m. in an orbital incubator (Gallenkamp) for exactly 30 min. 2 ml of sterile 5M glycine was added to each flask to quench cross-linking reactions and samples were left to incubate for a

further 10 min. Sample were then transferred to 50 ml polystyrene tubes (Greiner Bio-One) and centrifuged as before with the supernatants being disposed of. At this point, pellets were stored on ice at 4 °C for up to 48 h prior to additional processing.

6.2.2.2 Spheroplasting

Pellets that were stored at 4 °C were re-suspended in 3 ml of pre-spheroplasting buffer (200 mM Tris pH 9.5, 10 mM Dithiothreitol [DTT], prepared immediately prior to use), taking care to avoid introducing bubbles/foaming. The suspension was then transferred to a 15 ml polystyrene tube (Greiner Bio-One) and mixed with shaking at 200 r.p.m. in an orbital incubator (Gallenkamp) at 30°C for 15 min. Suspensions were then centrifuged at 2,000 x *g* for 5 min.

The resulting pellet was washed with 5 ml spheroplasting buffer (1.2 M sorbitol, 20 mM 4-(2-hydroxyethyl)-1-piperazineethanesulfonic acid [HEPES] pH 7.4), followed by centrifugation as before. Supernatants were discarded and pellets re-suspended in 5ml spheroplasting buffer. Zymolyase 100T (AMS Biotechnology) was added to each suspension to a final concentration of 0.4 mg/ml from a pre-prepared 10 mg/ml stock solution (prepared in 1.2 M Sorbitol). 4-(2-Aminoethyl) benzenesulfonyl fluoride hydrochloride (AEBSF) was added to each suspension to a final concentration of 0.5 mM from a pre-prepared 100 mM stock solution.

Each suspension was mixed with shaking at 200 r.p.m. in an orbital incubator (Gallenkamp) at 30°C for 2.5 h, or until suspension of cells was > 50 % spheroplasts. Progress of spheroplasting was checked in 45 minute intervals by preparing a wet mount of 10 µl of the suspension and viewing on a light microscope. Number of spheroplasts was represented as a percentage of 100 randomly counted cells.

At this point, 5 ml of pre-chilled post-spheroplasting buffer (1.2 M Sorbitol, 1mM $MgCl_2$, 20 mM 1,4-Piperazinediethanesulfonic acid [PIPES] pH 6.8) was added followed by centrifugation at 2,000 x *g* for 5 min at 4°C. While keeping all samples stored in ice, the supernatant was removed and the pellet washed with 5 ml of pre-chilled PBS with the addition of 0.5 mM AEBSF. Samples were centrifuged as before and the supernatant was discarded. Cell pellets were washed with 5 ml of pre-chilled Buffer 1 (0.25 % v/v Triton X-100, 10 mM ethylenediaminetetraaceticacid [EDTA] pH 8.0, 0.5 mM ethylene glycol tetra-acetic

acid [EGTA], 10 mM HEPES pH 6.5) with the addition of 0.5 mM AEBSF. Samples were then centrifuged at 2,000 x *g* for 5 min at 4°C and the supernatants were discarded. Cell pellets were washed with 5 ml of pre-chilled Buffer 2 (200 mM NaCl, 1mM EDTA pH 8.0, 0.5 mM EGTA, 10 mM HEPES pH 6.5) with the addition of 0.5 mM AEBSF. Samples were centrifuged at 2,000 x g for 5 min at 4°C and the supernatants discarded.

6.2.2.3 DNA fragmentation

Cell pellets (kept at 4°C) were re-suspended in 1.5 ml pre-chilled Extraction Buffer (140 mM NaCl, 1mM EDTA, 1% [v/v] Triton X-100, 0.1% [w/v] Deoxycholate [DOC], 50 mM HEPES pH 7.5). Pepstatin A (solution in methanol) was added to a final concentration of 10 μg/ml. E64 (solution in water) was added to a final concentration of 10 μM. 1.5 μl of 500X Benzamidine hydrochloride hydrate and 2 μg/ml A-protinin were added to the solution.

Samples were then sonicated using a modified sonication probe (Branson Ultrasonics, Danbury, CT, USA) for 25 s at 100 % duty, power setting 2.75 followed by 120 s rest period on ice. The sonication step was carried out a total of 8 consecutive times.

6.2.2.4 Pre-binding of Antibody

The resulting solution was transferred to a 2 ml microcentrifuge tube (Eppendorf) and was then centrifuged at 16,000 x *g* for 5 min at 4 °C. The supernatant was transferred to a new 2 ml microcentrifuge tube (Eppendorf) and was subjected to an additional centrifugation step of 16,000 x *g* for 15 min at 4 °C. The supernatant (lysate) was transferred to a new 2 ml microcentrifuge tube (Eppendorf). 120 μl of this solution was transferred to a new 1.5 ml microcentrifuge tube (Eppendorf), labelled as 'input' and stored at – 20 °C. The remaining lysate was split into fractions of 600 μl in separate 2 ml microcentrifuge tubes (Eppendorf). To two of these, 900 μl of ice-cold IP dilution buffer (167 mM Tris-HCl, 167 mM NaCl, 1 mM EDTA, 1% [v/v] Triton X-100) was added. Any remaining lysate was frozen at - 20 °C. To one tube, anti-HA 12CA5 antibody (Roche Diagnostics) was added at a final concentration of 4 μg/ml. This tube was marked as 'IP.' Nothing was added to the other tube labelled 'no-Ab' (no antibody control) and both were incubated overnight at 4 °C on a rotating wheel (Thermo Fisher Scientific).

6.2.2.5. Immunoprecipitation

The next day, 70 µl of Protein A sepharose-agarose bead slurry (Santa Cruz Biotech, California, USA) was added to both tubes followed by mixing on rotating wheel (Thermo Fisher Scientific) at 4 °C for 4 h.

6.2.2.6 Washing

Tubes were then centrifuged at 16,000 x *g* for 2 min and supernatant was discarded taking care not to disturb the sepharose-agarose beads. 1 ml of ice-cold Extraction Buffer was added to each tube and briefly mixed by hand, followed by centrifugation at 16,000 x *g* for 2 min. Supernatant was discarded and 1 ml of ice-cold Extraction Buffer was added to each tube followed by mixing on a rotating wheel (Thermo Fisher Scientific) at 4 °C for 5 min. Tubes were centrifuged at 16, 000 x *g* for 2 min and supernatant was discarded.

1 ml of ice-cold High-Salt Extraction buffer (500 mM NaCl, 1 mM EDTA, 1 % [v/v] Triton X-100, 0.1% [w/v] Sodium Deoxycholate and 50 mM HEPES, pH 7.5] was added to each tube, and briefly mixed by hand, followed by centrifugation at 16,000 x *g* for 2 min. Supernatant was discarded and 1 ml of ice-cold High-Salt Extraction buffer was added to each tube followed by mixing on a rotating wheel (Thermo Fisher Scientific) at 4 °C for 5 min. Tubes were centrifuged at 16,000 x *g* for 2 min and supernatant was discarded.

1 ml of ice-cold LiCl Wash Buffer (10 mM Tris-HCl pH 8, 250 mM LiCl, 1 mM NP-40, 0.5% [w/v] Sodium Deoxycholate and 1 mM EDTA) was added to each tube, and briefly mixed by hand, followed by centrifugation at 16,000 x *g* for 2 min. Supernatant was discarded and 1 ml of ice-cold LiCl wash buffer was added to each tube followed by mixing on a rotating wheel (Thermo Fisher Scientific) at 4 °C for 5 min. Tubes were centrifuged at 16, 000 x *g* for 2 min and supernatant was discarded.

1 ml of ice-cold TE was added to each tube, and briefly mixed by hand, followed by centrifugation at 16,000 x *g* for 2 min. Supernatant was discarded and 1 ml of ice-cold TE was added to each tube followed by mixing on a rotating wheel (Thermo Fisher Scientific) at 4 °C for 5 min. Tubes were centrifuged at 16, 000 x *g* for 2 min and supernatant was discarded.

6.2.2.7 Elution

150 µl of EB1 (50 mM Tris-HCl pH 8.0 10 mM EDTA, 1 % [w/v] SDS) was added to each tube of beads. The mixtures were incubated at 65 °C in a circulating water bath (Clifton, UK) for 15 min. Tubes were centrifuged at 16,000 x *g* for 5 min and the supernatants were transferred to two new 1.5 ml microcentrifuge tubes (Eppendorf). 210 µl of EB2 (10 mM Tris pH 8.0, 1 mM EDTA, 0.67% [w/v] SDS) was added to the bead mixtures to elute any remaining protein-DNA molecules. The tubes were incubated at 65 °C in a circulating water bath (Clifton) for 5 min and centrifuged at 16,000 x *g* for 5 min and the supernatants were added to the tubes containing EB1 (i.e. supernatants for each reaction were pooled – keeping 'IP' and 'No Ab control' reactions distinct). At this point, the total lysate control was thawed on ice and diluted 1:4 with EB1.

6.2.2.8. Reverse cross-linking and cleanup

The three fractions (IP, No Ab control and input) were incubated at 65 °C in a circulating water bath (Clifton) for 18 h to reverse cross-links.

Samples were diluted with TE to bring final concentration of SDS to 0.5 % (w/v). RNaseA was added to each tube to a concentration of 50 µg/ml and tubes were incubated at 37 °C in a circulating water bath (Clifton) for 1 h. Proteinase K was added to each tube to a final concentration of 500 µg/ml and tubes were incubated at 37 °C in a circulating water bath (Clifton) for 2 h. LiCl was added to each tube to a final concentration of 0.4 M and 600 µl of PCI (24:24:1; pH 8.0) was added to both tubes. Tubes were mixed by vortexing for 1 min and centrifuged at 16,000 x *g* for 5 min. The aqueous layer was transferred to a new 1.5 ml microcentrifuge tube (Eppendorf) for each of the reactions. 600 µl of chloroform was added to each reaction and mixed vigorously by vortexing for 1 min. Mixtures were centrifuged at 16,000 x *g* for 5 min and the aqueous layers were transferred to a new 1.5 ml microcentrifuge tube (Eppendorf) for each of the reactions.

Glycogen (Roche Diagnostics) was added to each tube to a final concentration of 20 µg/ml. 900 µl of ice-cold 95 % (v/v) ethanol was added to each tube. Mixtures were incubated overnight at – 20 °C. Tubes were centrifuged at 16,000 x *g* at 4 °C for 1 h. Pelleted were washed with 500 µl of 70 % (v/v) ethanol followed by centrifugation at 16,000 x *g* for 30 min. This wash step was repeated.

The DNA pellets were then allowed to air-dry and each pellet (IP, No Ab control and input) was re-suspended in 80 µl of 10 mM Tris-HCl, pH 8.0 for either qRT-PCR (section 6.2.5.) or ChIP-chip (section 6.2.3.) to proceed.

6.2.3. ChIP-on-Chip

The following modified protocol was originally based on the Agilent yeast ChIP-on-Chip analysis protocol (Agilent Technologies, 2007).

6.2.3.1. Blunt-end DNA preparation

70 µl of 'blunting mix' (10X NEBuffer 2 [New England Biolabs], 10 mg/ml BSA [New England Biolabs], 20 mM dNTP mix [Qiagen], 3 U/µl T4 DNA Polymerase [New England Biolabs]) was added to 40 µl of each IP sample in 0.2 ml thin-walled PCR tubes (Molecular Bio Products). 11 µl of blunting mix was added to 1.5 µl of each input in 0.2 ml thin-walled PCR tubes (Molecular Bio Products). All reactions were made up to 110 µl with sterile MilliQ water (Merck-Millipore). Reactions were mixed and incubated for 20 min at 12 °C. After incubation, 11.5 µl of 3 M Sodium Acetate and 0.5 µl of 20 mg/ml Glycogen (Roche Diagnostics) was added to each tube and gently mixed. The reactions were then transferred to microcentrifuge tubes (Eppendorf) and combined with an equal volume of PCI (24:24:1) mix. Each reaction was mixed on a vortex for 1 min and centrifuged at 13,000 *x g* for 5 min. The aqueous phase was transferred to a new microcentrifuge tube (Eppendorf) and combined with 2 volumes of ice-cold 100 % (v/v) ethanol. The solution was mixed by inversion and incubated at -20 °C for 1 h. After incubation, the samples were centrifuged at 13,000 x *g* for 15 min at 4 °C to allow precipitation of a DNA pellet. The pellet was washed with 500 µl 70 % (v/v) ethanol and centrifuged at 13,000 x *g* for 5 min. All liquid was removed and the pellet was allowed to dry. The dried pellet was then re-suspended in 25 µl of sterile DNase/RNase-free water.

6.2.3.2. Blunt-end ligation

The unidirectional linker was prepared by combining 250 µl 1M Tris-HCl (pH 7.9), 150 µl of oligonucleotide oJW102 (40 µM), 150 µl of oligonucleotide oJW103 (40 µM) and denaturing the mix at 95 °C for 5 min in a heating block (Thermo Fisher Scientific). The reactions were then allowed to cool to room

temperature and then incubated for 16 h at 4 °C. A 6.7 µl volume of this mix was combined with 1X DNA ligase buffer with ATP (Invitrogen), 0.5 µl of T4 DNA ligase (New England Biolabs), 8 µl of DNase/RNase-free water and 25 µl of one of the blunt-end prepared samples from section 6.2.3.1. This reaction was mixed and incubated for 18 h at 16 °C.

6.2.3.3. Amplification

To each reaction, 6 µl of 3 M Sodium Acetate pH 5.2 was added and mixed with 130 µl ice-cold 100 (v/v) ethanol. Each reaction was mixed vigorously and incubated at 4 °C for 1 h. Each sample was centrifuged at 13,000 x *g* at 4 °C. The supernatant was discarded and the pellet was washed with 500 µl of 70 % (v/v) ice-cold ethanol. After further centrifugation, remaining liquid was discarded and the pellet was re-suspended in 25 µl DNase/RNase-free water.

In separate 0.2 ml thin-walled PCR tubes (Molecular Bio Products), each sample was combined with 1X Thermopol Buffer (New England Biolabs), 250 µM dNTP mix (Promega), 1 µM oJW102 oligonucleotide, 0.25 U Taq polymerase (Promega) and DNase/RNase free water to a final volume of 50 µl. The reaction was run on a thermal cycler (Kyratech) with the following conditions: 55 °C for 4 min, 72 °C for 3 min, 95 °C for 2 min. This was followed by 14 cycles of incubation at 95 °C for 30 s, 55 °C for 30 s and 72 °C for 1 min. The programme was completed a final incubation at 72 °C for 5 min followed by storage at 4 °C.

Each sample was diluted to a final volume of 525 µl with DNase/RNase-free water. A 5 µl volume of this diluted sample was transferred to a new 0.2 ml thin-walled PCR tube (Molecular Bio Products) along with 1 X Thermopol buffer (New England Biolabs), 250 µM dNTP mix (Promega), 1 µM JW102 oligonucleotide and 1.25 U Taq polymerase (Promega) and DNase/RNase-free water to a final volume of 50 µl. Each sample was incubated in a thermal cycler (Kyratech) at 95 °C for 2 min. This was followed by 24 cycles of: 95 °C for 30 s, 55 °C for 30 s and 72 °C for 1 min. Finally, a 72 °C hold was applied for 5 min followed by overnight hold at 4 °C.

Each sample (from the second round of amplification) was transferred to a 1.5 ml microcentrifuge tube (Eppendorf) and combined with 625 mM ammonium acetate and 75 % (v/v) ethanol. Each tube was incubated at - 80 °C for 1 h and centrifuged at 20,000 x *g* for 10 min at 4 °C. DNA pellets were washed with 500 µl

ice-cold 70 % (v/v) ethanol. Using a vacuum desiccator/Speed-Vac (Savant, Thermo Fisher Scientific), pellets were dried for 10 min, followed by immediate re-suspension in 50 µl DNase/RNase-free water (Invitrogen). Using a nanodrop (section 2.1.8.), concentrations of DNA were measured. All samples were diluted to 100 ng/µl for downstream processing.

6.2.3.4. Labelling

Each normalised sample was transferred to thin-walled 0.2 ml PCR tubes (Molecular BioProducts), and combined with 1 X random primer solution (Invitrogen), and made to a final volume of 75 µl with DNase/RNase-free water (Invitrogen). Each mix was vigorously mixed for at least 1 min and incubated at 95 °C to denature in a heat-block (Thermo Fisher Scientific) for 5 min then at 4 °C for 5 min.

Each sample was mixed thoroughly and combined with nucleotide mix containing 112 nM dATP, dGTP, dCTP and 56 nM dTTP (Invitrogen), 17 µM of either Cy3 or Cy5 (Agilent Technologies), 60 U of Klenow polymerase (Invitrogen) and DNase/RNase-free water (Invitrogen) to a final volume of 13 µl for each tube. A dye-swap was carried out so that each technical replicate was labelled alternately. Each reaction was mixed and incubated at 37 °C for 3 h in a circulating water bath (Thermo Fisher Scientific) in the dark. After incubation, 9 µl of stop buffer (Invitrogen) was added to each tube and the samples were each transferred to separate 1.5 ml microcentrifuge tubes (Eppendorf).

0.4 ml of Purelink Purification Buffer A (Invitrogen) was added to each tube and mixed for 30 s. This was then transferred to a Purelink CGH column (Invitrogen) and centrifuged at 10,000 x *g* for 1 min after which the eluent was discarded. 600 µl of Purelink Purification Buffer B (Invitrogen) was added to the column and centrifuged for 1 min at 10,000 x *g* and the eluent was discarded. A further 200 µl of Purelink Purification Buffer B was added followed by centrifugation at 10,000 x *g* for 1 min and the eluent was discarded. The purified labelled DNA was eluted by application of 50 µl of DNase/RNase-free water (Invitrogen) and incubation at room temperature for 5 min, followed by centrifugation at 10,000 x *g* for 1 min.

Using the nanodrop (Section 2.1.8.), the labeling reaction was assessed for successful dye-incorporation as described in section 5.2.1.3. The lower limits for a

successful reaction were 3.5 pmol/µl Cy3 incorporation or 2.5 pmol/µl Cy5 incorporation with a total concentration of at least 100 ng/µl.

6.2.3.5. Microarray hybridisation

Pairs of Cy3- or Cy5-labelled samples were combined with sterile water to a final volume of 39 µl in a 1.5 ml microcentrifuge tube (Eppendorf). Concentrations were calculated so that the same amount of IP and input was in each mix. To each tube, 5 µl of Human Cot-1 DNA (Agilent Technologies), 1 X Blocking Agent (Agilent Technologies) and 1 X Hybridisation Buffer (Agilent Technologies) were added and gently mixed followed by incubation at 95 °C for 3 min in a heat block (Thermo Fisher Scientific). This incubation was immediately followed by another incubation at 37 °C for 30 min in a circulating water bath (Thermo Fisher Scientific). Samples were the centrifuged at 18,000 x *g* for 1 min in a bench-top microcentrifuge and each of the three samples were loaded onto one section of a 4-section gasket slide (Agilent Technologies) which was in turn applied to a whole genome *C. dubliniensis* CGH Chip array slide (Agilent Technologies) containing replicated arrays, each consisting of 175,758 unique 60-mer DNA probe sequences spaced at 20 bp intervals. The array 'sandwich' was sealed in a gasket chamber (Agilent Technologies) and incubated at 65 °C with rotation at 20 r.p.m. for 24 h in a hybridisation oven (Thermo Fisher Scientific).

All washing dishes and equipment were rinsed with 100% (v/v) acetonitrile followed with sterile MilliQ water (Merck-Millipore). The array/gasket assembly was disassembled while immersed in Oligo aCGH /ChIP-on-chip Wash Buffer 1 (Agilent Technologies) and the array was transferred carefully to a dish containing fresh Oligo aCGH /ChIP-on-chip Wash Buffer 1 (Agilent Technologies) and was mixed for 5 min using a magnetic stirrer. The slide was then transferred to a dish containing Oligo aCGH /ChIP-on-chip Wash Buffer 2 (Agilent Technologies) which had been warmed to 31 °C and was incubated at this temperature for 5 min. The slide was immediately scanned as described in the next section.

6.2.3.6. Scanning

Scanning of the chip was carried out on an Agilent G2565B rotating multi-slide hyb-scanner (Agilent Technologies /University of Minnesota) using a 5 µm

resolution and PMT settings at 100% for both channels (Green/Red). The scan area was set to 61 X 21.6 mm.

The raw images were saved as .TIFF files and processed using Agilent Feature Extraction software suite v 10.5.1.1 (Agilent Technologies). Extraction was automatically carried out using the 'CGH automatic' programme to align and normalise fluorescent probe spots on the array assuming a linear relationship between dye signals. The file was then saved as a *txt file and analysed using several different software bundles as described below.

6.2.3.7. Analysis

Quality control and analysis of the ChIP-on-chip data was carried out by uploading the data to R programming environment (Chambers, 2014).
Specifically, the packages used for quality control and analysis were Limma (Gordon K, 2005) Ringo (Toedling *et al.*, 2007) and Bioconductor (Gentleman *et al.*, 2004). Labels were assigned to each dye channel (G and R) and an annotation file (pA) was applied. 'Nimblegen'-type processing was used to parse and analyse the data points. All replicates were combined and a 'smoothing' was carried out on the data which computed the running medians of data points based on the sliding-window method (Toedling & Huber, 2008) with a computational window size of 500. Specific areas of the genome were plotted to show enrichment using the plot function. Thresholds were applied to rule out background signal. Detailed functions and specific code used with R statistical software were constructed specifically for this study and are outlined in Figure S1

JBrowse was used as a user-friendly graphical user interface (GUI) tool to present the data and is available for viewing at:

http://bioinf.gen.tcd.ie/jbrowse1.6/cdub.html

For this, the data was processed by Karsten Hokamp (Smurfit Institute of Genetics, Trinity College Dublin) using methods identical to those described above with reconfiguration of the data files to suit upload to JBrowse.

6.2.4. Chromatin immunoprecipitation (Fleming Laboratory TCD)

The following is a revised protocol devised in collaboration with Michael Church, Conor Young, Suzanne Beggs and Alistair Fleming, Department of Microbiology, Trinity College Dublin.

For the purposes of this protocol, cultures were assigned arbitrary 'O.D. units' (ODUs). One ODU is equivalent to 1 ml of culture at an O.D. $_{600\,nm}$ of 1.0. For example, a 200 ml culture at an O.D. $_{600\,nm}$ of 2.0 is the equivalent of 400 ODUs.

6.2.4.1. Growth and chemical fixation

Growth and chemical fixation was carried out in an identical manner to that described in 6.2.2.1. However, pellets were stored at -80 °C prior to additional processing instead of 4 °C

6.2.4.2. Cell lysis

All solutions were kept on ice as much as possible from this point onwards. Cell pellets were thawed on ice and re-suspended in 400 µl of Lysis Buffer (50 mM HEPES pH 7.5, 140 mM NaCl, 1 mM EDTA, 1 % [v/v] Triton X-100, 0.1 % [w/v] Sodium deoxycholate) containing 1X protease inhibitor (PI) cocktail (Roche Diagnostics) and 2 mM phenylmethanesulfonylfluoride (PMSF). The mixture was split into two fractions in 1.5 ml screw-capped tubes (Sarstedt), each containing a 400 µl volume of 425-600 µm acid-washed glass beads. The tubes were then subjected to the desired number of 30 s cycles, at 6 m/s in the Fastprep Homogeniser 24 (MB Biotechnologies). Tubes were placed on ice for 5 min between each cycle. Lysis was checked by visualisation using microscopy (described in 6.2.1.1.). Alternatively, a Bradford assay (described in 6.2.1.2.) was also used to determine success of breakage. For *C. dubliniensis* preparations, it was determined that 6 cycles were required for optimal breakage (outlined in results section).

After breakage was complete, tubes were pierced using a sterile 23G needle (Becton, Dickinson & Co.) and centrifugation was used to elute the lysate from the beads into 50 ml polystyrene tubes (Greiner Bio-One) and then lysates were transferred to fresh 1.5 ml microcentrifuge tubes (Eppendorf). The split lysates were pooled and then made up to a final volume of 1 ml with Lysis Buffer with 1 X PI cocktail and 2 mM PMSF.

6.2.4.3. DNA fragmentation

1 ml lysates were subjected to 10 s rounds of sonication, with 120 s incubation on ice between rounds. The number of rounds of sonication required to

result in DNA fragments of ~ 500 bp was determined by sonicating identical samples for increasing numbers of rounds and pronase digesting samples (described in 6.2.4.8.) followed by processing 2.5 ODUs by agarose gel electrophoresis (section 2.1.9.) It was determined that 14 rounds was optimal for *C. dubliniensis* strains, as outlined in 6.3.2.3.

After sonication was complete, samples were centrifuged at 16,000 x *g* for 30 min at 4 °C in a refrigerated bench-top microcentrifuge (Eppendorf). The supernatants were then transferred to new 2 ml tubes and then aliquoted to 1.5 ml microcentrifuge tubes (Eppendorf) in volumes equivalent to 5 ODUs each.

6.2.4.4. Pre-binding of Antibody-protein complexes

To each tube of 5 ODUs, an appropriate amount of Lysis Buffer with 1X PI cocktail was added to bring the volume to 500 µl. 20 µl of this solution was transferred to a 0.2 ml thin-walled polystyrene PCR tube (Molecular BioProducts) and labelled 'input.' To the remaining 480 µl, an appropriate amount of 12CA5 antibody (Roche Diagnostics) was added. The optimal amount of antibody required was determined by using several different volumes as outlined in section 6.3.3. An additional tube of 5 ODUs was setup as before but omitting the antibody addition, to act as a 'no antibody control.' For positive control reactions, 2 µl of 8WG16 Anti-RNA Polymerase CTD antibody (Abcam) was added. Each tube containing antibody was incubated at 4 °C on a rotating wheel (Thermo Fisher Scientific) running at 16 r.p.m. for 18 h. The 'input samples' were treated as described below in section 6.2.4.8.

6.2.4.5. Immunoprecipitation

A 40 µl volume of Protein G magnetic beads (New England Biolabs) were pre-washed with 1 ml of Lysis Buffer with 1X PI for 5 min on a rotating wheel at room temperature. This wash step was repeated two additional times with the final re-suspension in 40 µl of Lysis buffer with 1X PI, for a total of n samples. 40 µl of the beads were added to each reaction tube and the mixtures were incubated at 4 °C on a rotating wheel (Thermo Fisher Scientific) running at 16 r.p.m. for 2 h.

6.2.4.6. Washing

The following washes were carried out using a Neodymium magnetic (New England BioLabs) rack instead of centrifugation to allow separation of beads

and liquid to facilitate removal of supernatants. Each wash involves separation of beads followed by removal of magnetic rack and thorough mixing of the solution, followed again by re-introduction of the magnetic rack to allow liquid removal. Beads were washed once with Lysis Buffer only, then twice with Wash buffer 1 (50 mM HEPES pH 7.5, 0.5 M NaCl, 1mM EDTA, 1 % [v/v] Triton X-100, 0.1 % [w/v] sodium deoxycholate), then twice with Wash buffer 2 (10 mM Tris-HCl pH 8.0, 250 mM LiCl, 1 mM EDTA, 0.5 % [v/v] NP-40, 0, 0.5 % [w/v] sodium deoxycholate) and finally once with TE (pH 7.5).

6.2.4.7. Elution

Beads in each tube were suspended in 250 µl of Elution buffer (50 mM Tris-HCl pH 7.5, 10 mM EDTA, 1 % [w/v] SDS). Samples were mixed thoroughly by vortexing and then were incubated at 65 °C in a heat block (Thermo Fisher Scientific) for 20 min, with mixing by vortexing every 5 min. Samples were then incubated at room temperature on a rotating wheel at 16 r.p.m. for 10 min. Samples were separated in a magnetic rack and the supernatants were transferred to a new 1.5 ml microcentrifuge tube (Eppendorf).

6.2.4.8. Reverse cross-linking & pronase digestion

The 20 µl 'input' sample was combined with 100 µl of Elution Buffer, 60 µl TE, 1 µl $CaCl_2$ and Pronase mix (Sigma-Aldrich) to a final concentration of 2 mg/ml. The 250 µl volume 'IP' samples that were eluted in the previous section were combined with 1.5 µl of $CaCl_2$ and Pronase mix to a final concentration of 2 mg/ml. All mixtures were transferred to 0.2 ml thin-walled polystyrene PCR tubes (Molecular BioProducts) and incubated in a thermal cycler (Kyratech) at 42 °C for 2 h followed by 65 °C for 6 h with a hold at 4°C.

6.2.4.9 DNA Cleanup

The Pronase-treated samples were processed using a Qiaex-II PCR purification kit (Qiagen) according to the manufacturer's instructions (Technologies, 2008). The DNA was eluted from the spin columns using 50 µl of sterile, DNase/RNase-free water. Samples to be used for qRT-PCR were diluted 1:2 and 1:50 for the IP and input samples respectively.

6.2.5. ChIP-qRT-PCR

qRT-PCR was carried out on IP and input samples at the concentrations described above. Oligonucleotide primers specific for the region were used and qRT-PCR was carried out using the standard curve method outlined in section 2.3.3.2., which determined relative DNA concentrations after the reactions.

Relative enrichment of a region of DNA was quantified by calculating the ratio of IP divided by Input and displayed using Graphpad Prism (Graphpad Inc.). In these experiments, a control reaction that contained no antibody (i.e. theoretically, no pull-down) was run alongside three IP reactions containing increasing volumes of antibody. In order to distinguish between enriched and non-enriched regions, the IP/input score of the antibody-containing reactions needed to be at least double that of the no-antibody control reaction. For quality control and optimisation purposes, a control IP reaction containing Anti-RNA polymerase II CTD repeat antibody 8WG16 (Abcam, Cambridge, UK) was carried out alongside the reactions to act as an experimental control.

6.2.6. Western Immunoblot

To ensure HA-tag was present and maintained in Tlo1-HA strain, lysates were made using TCA buffer as described by Fleming, *et al.* (2014). Prepared samples were processed by SDS-PAGE using 8 % - 16 % (w/v) acrylamide-Tris HEPES gel (Pierce, Thermo Fisher Scientific) followed by transfer to an Immobilon filter (Millipore-Merck). The filter was incubated with anti-HA antibody 12CA5 (Roche Diagnostics) and developed with ECL Substrate (Pierce) as previously described (Fleming *et al.*, 2014; Millar *et al.*, 1995).

6.3. Results

6.3.1. Whole genome chromatin immunoprecipitation

To determine if Tlo1 protein interacts with DNA, Chromatin Immunoprecipitation hybridised to DNA microarrays (ChIP-on-chip) was carried out. A haemagglutinin (HA)-tagged version of Tlo1 was constructed using PCR-directed insertion of a 3 X HA tag sequence downstream of the coding region of *TLO1* whilst keeping the insert in-frame. The insert was placed beginning in the place of the stop codon which was swapped out once the sequence had inserted. The Tlo1-HA strain used in this study was constructed by Lawrence Myers, Dartmouth Medical School (Personal Communication, Myers, L. 2012). The strain of *C. dubliniensis* Wü284 carrying once copy of Tlo1-HA was constructed using a *SAT1* marker (Reuss *et al.*, 2004) for ease of selection during transformation. As such, routine growth on YEPD agar containing 200 µg/ml Nourseothricin (Supplier) was used as a confirmation of the presence of the tagged copy of Tlo1.

To confirm that the tagged protein was expressed, the Tlo1-HA tagged strain was processed for Western Immunoblot analysis as described in section 6.2.6. Using Anti-HA antibody, Tlo1-HA was detected at approximately 56 kDa which correlates with the expected size of the protein expressed from the *TLO1-3xHA* fusion (Figure 6.2)

6.3.1.1. Optimisation of spheroplasting for ChIP-on-chip

While spheroplasting using Zymolyase 100T (AMS Biotechnologies) has been described (Gelis *et al.*, 2012), optimisation was required in order to properly spheroplast the cells in *C. dubliniensis*. Different concentrations of Zymolyase 100T, along with different incubation times and temperatures were used (data not shown). Cultures were grown as described and viewed every 30 min to assess spheroplasting. Reactions were stopped once 80 % of cells had spheroplasted. This analysis determined that 150 min at 30 °C with inversion using a rotating wheel (Thermo Fisher Scientific) resulted in greater than 80% spheroplast formation in *C. dubliniensis* Wü284 and Tlo-HA tagged derivatives.

6.3.1.2. Whole genome ChIP-on-chip

ChIP-on-chip was carried out as described in sections 6.2.2. and 6.2.3. In order to analyse the raw ChIP data, a customised script (Figure S.1.) was constructed using the R statistical programme with packages "Bioconductor" (Gentleman *et al.*, 2004), "limma" (Gordon K, 2005), "Ringo" (Toedling *et al.*, 2007) and "arrayQualityMetrics" (Kauffmann *et al.*, 2009). Different methods of pre-processing were investigated. Since the arrays were biological replicates, it was decided to normalise between arrays instead of within arrays. During normalisation, two methods have commonly been used in the literature, namely the variance stabilisation and normalisation (vsn) and Nimblegen methods. Normalisation using vsn depends on transformation (both additive and multiplicative) of probe intensity values so that the variances are equal, taking into account the high variance that can often be seen for lower intensity values (Beissbarth *et al.*, 2005; Huber *et al.*, 2002; Poustka, 2002). Normalisation using the Nimblegen method implements a Tukey bi-weight scaling procedure so that the data is relative to a baseline of zero (Smyth, 2005). This method of normalisation was chosen as definitive negative control regions with no Tlo1 binding were not known. After normalisation and annotation to the truncated genome of *C. dubliniensis*, data were uploaded to JBrowse v1.3 for easy visualisation (Lee *et al.*, 2013; Skinner & Holmes, 2010; Skinner *et al.*, 2009). Results can be viewed at http://bioinf.gen.tcd.ie/jbrowse1.6/cdub.html.

Enrichment for Tlo1 was observed throughout the genome, on all chromosomes. No chromosome showed any particular bias for enrichment (Figure 6.3). Chromosome 5 showed a larger distribution and this is most likely due to the inclusion of the fully intact telomeres and MRS in the array probes for this chromosome (other chromosomes were trimmed for long repeat sequences). In particular, significant areas of enrichment were found at telomeric and sub-telomeric sequences, particularly evident on chromosome 5 (Figure 6.4). It also appeared that Tlo1 was associated with the Major Repeat Sequence (MRS) on each chromosome, again particularly evident on chromosome 5 (Figure 6.4). As a result of the extensive coverage of Tlo1 over all regions, stringent thresholds of 0.8 (*y1*) and 0.9 (*y2*) were applied as the minimum values of significance instead of the automatic (*y0*) threshold, which assumes more discrete peaks and troughs in the data (Figure 6.5). The thresholds selected were chosen to identify areas of Tlo-

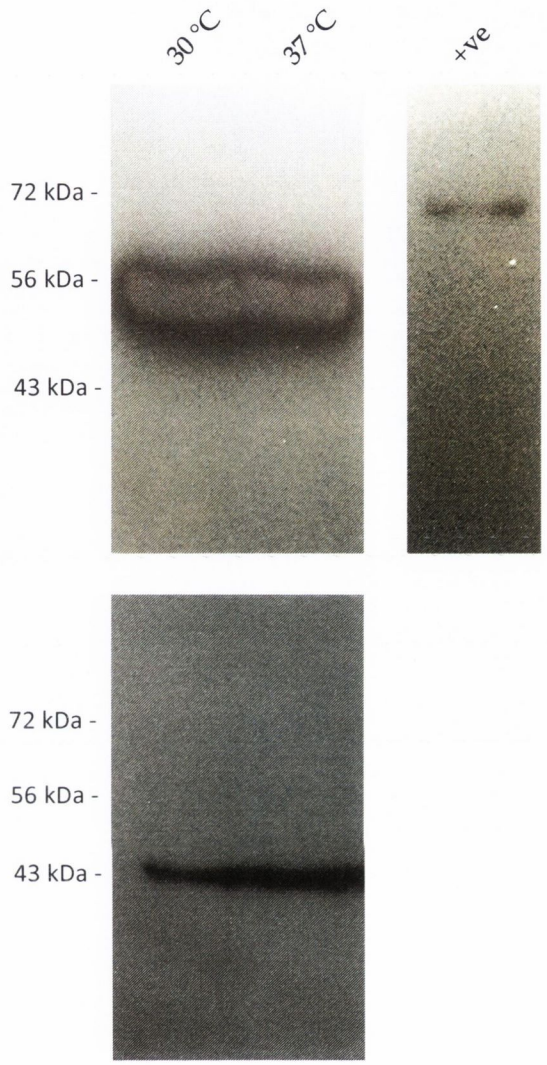

Figure 6.2. Confirmation of HA-epitope on Tlo1-HA fusion protein.

The presence of Tlo1-HA was confirmed by Western immunoblot analysis with a mouse monoclonal Anti-HA antibody 12CA5 (A). Cultures grown at 30 °C and 37 °C were tested for the presence of Tlo1 protein to rule out any major difference between growth conditions. Positive control of a purified HA-tagged protein from *S. cerevisiae* (Personal Communication. Fleming *et al,* 2013) is shown adjacent. Loading control is shown in (B).

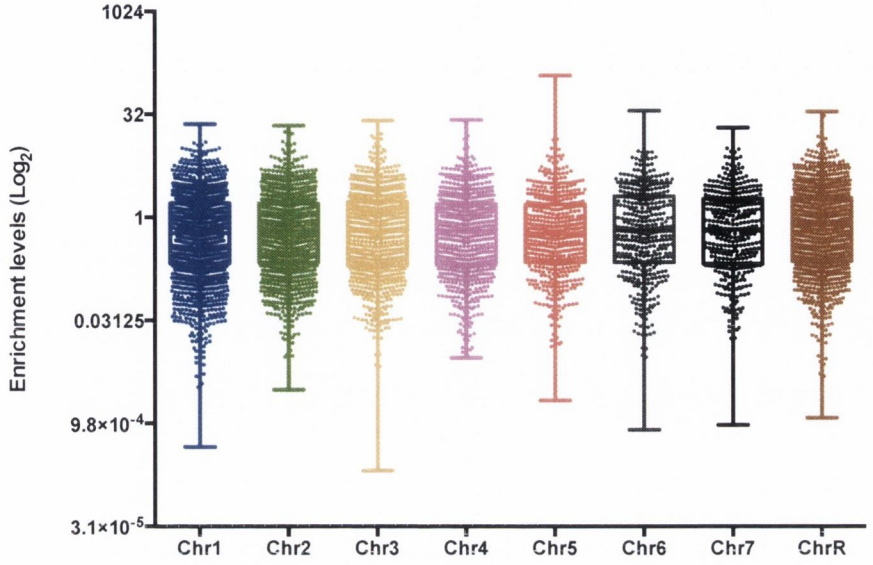

Figure 6.3. Distribution of enrichment scores over chromosomes.

Boxplot (with all points) showing the spread of enrichment scores at threshold $y1 = 0.8$. Chromosomes are along the x-axis and enrichment scores as derived from analyses carried out in section 6.3.1.2 are along the y-axis. Distribution is marked by error bars.

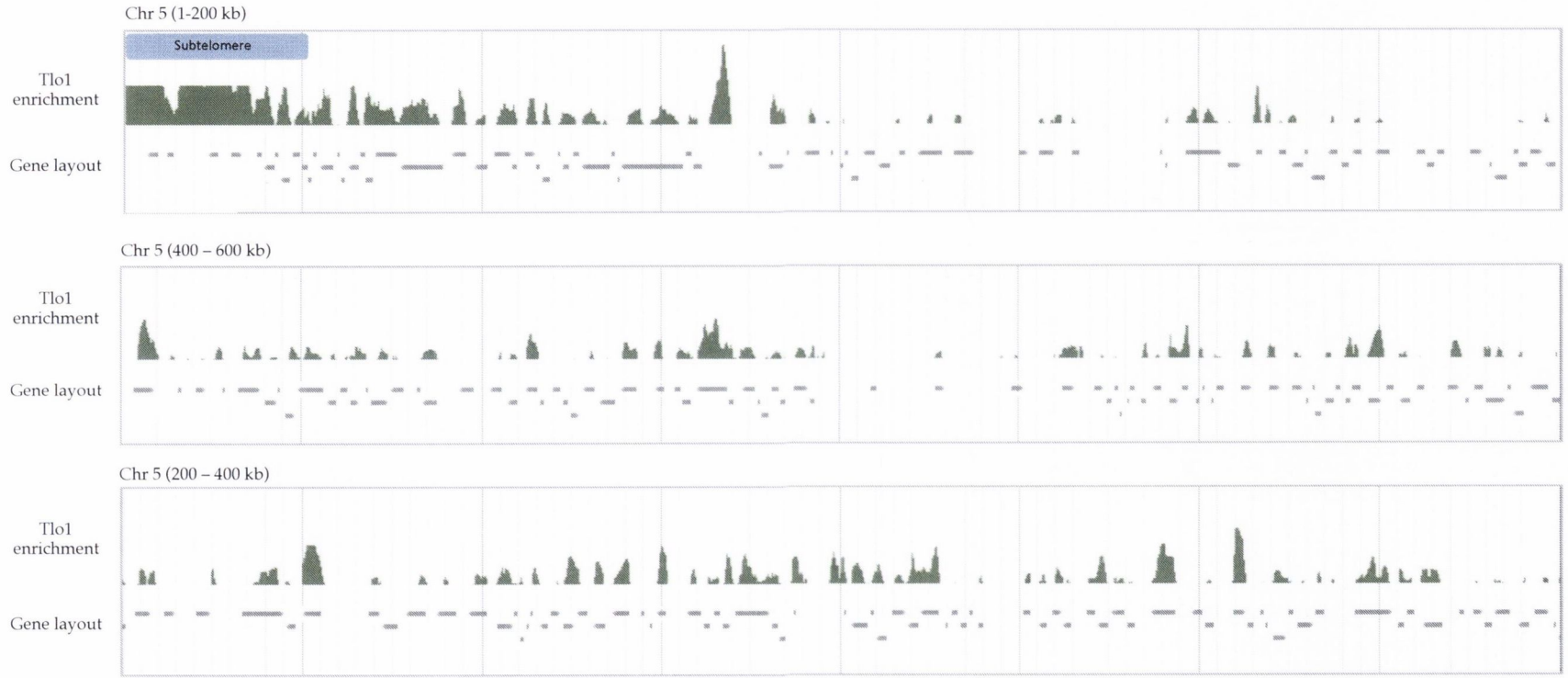

Figure 6.4. Tlo1 enrichment across chromosome 5 of *C. dubliniensis*.

Histograms detailing the enrichment of Tlo1 over chromosome 5. Data was obtained from signal ratio of labeled-immunoprecipitated DNA compared to labeled-whole cell extract DNA (IP/input). Each panel displays approximately 200 kb of the chromosome (region is noted above each panel) over which green peaks indicate the Tlo1 'enrichment' patterns that have been normalised to display only enrichment scores of > 1. Gene layout is displayed on the lower half of each panel. The Major Repeat Sequence (MRS) and subtelomeric regions are marked. (continued overleaf...)

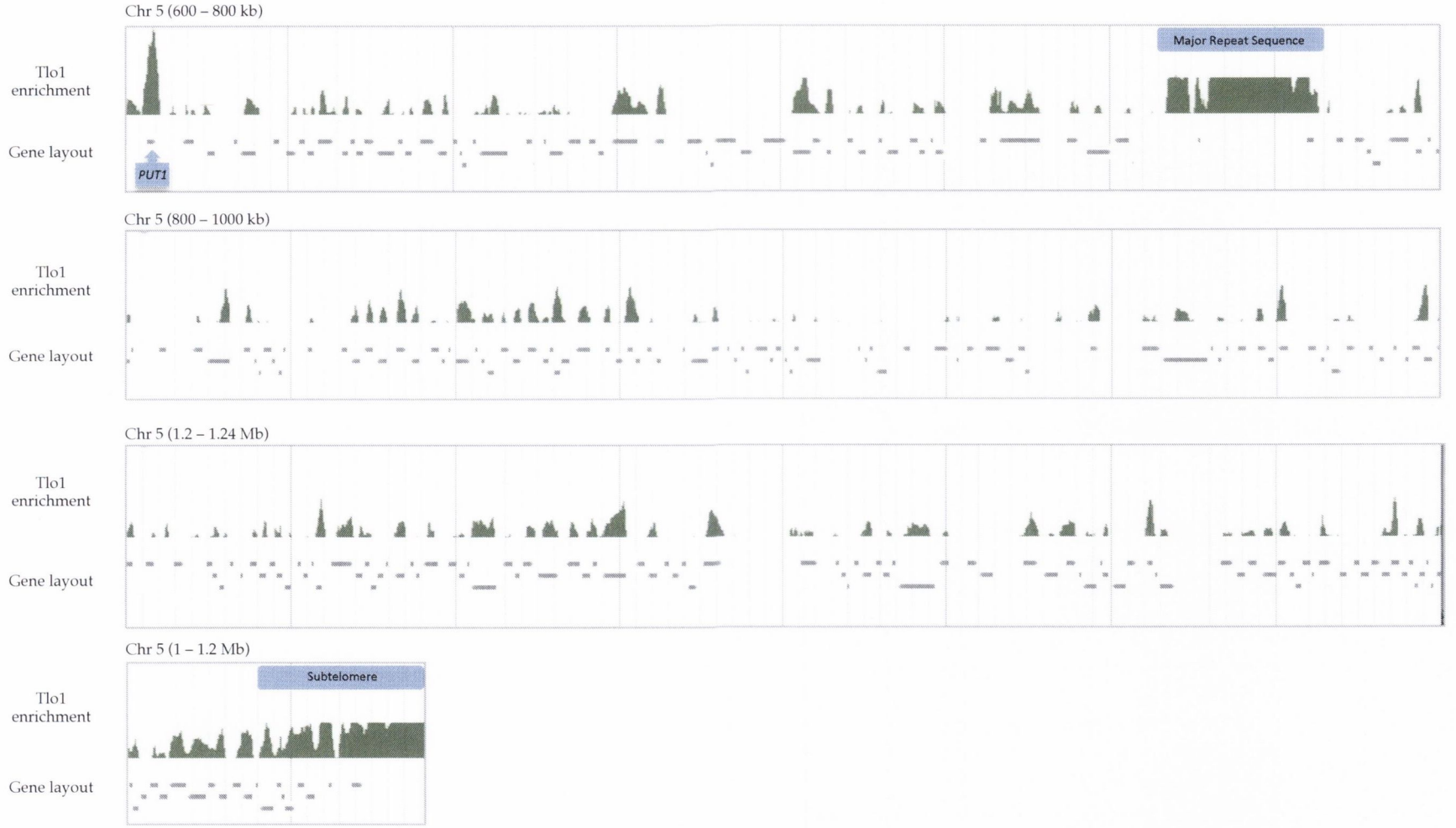

Figure 6.4. Tlo1 enrichment across chromosome 5 of *C. dubliniensis*.

...continued from previous page.

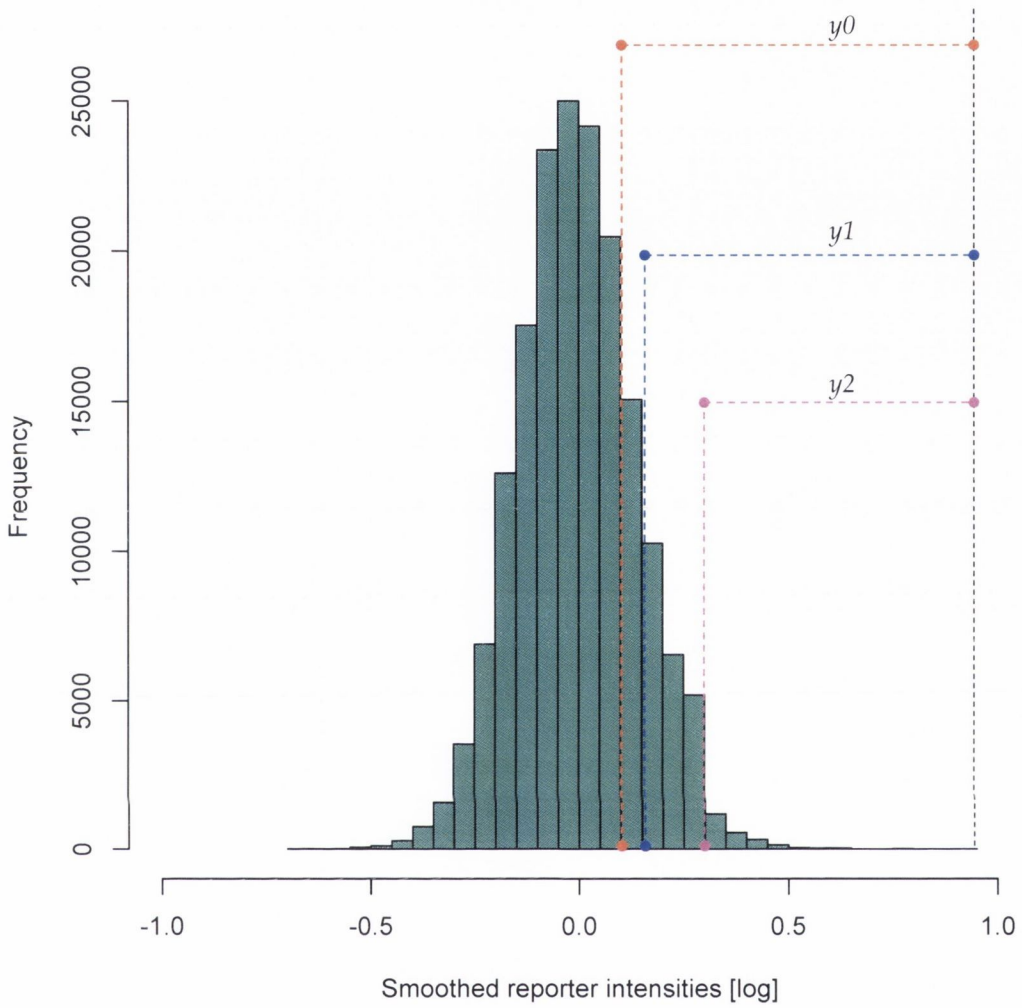

Figure 6.5. Significance of distribution of Tlo1 enriched regions is dependent on threshold.

Histogram displaying the distribution of Tlo1-enriched genes and the threshold values used in the analyses as outlined in the main text. Automatic threshold (*y0*) was estimated by Ringo package in R statistical software. Additional thresholds were based on the probability of probe intensities falling outside the symmetric null distribution of enrichment values and into the significant distribution, i.e. the minimum data value for significance. For this study, the thresholds used were 0.8 (*y1* = 80th percentile) and 0.9 (*y2* = 90th percentile). Each threshold and the data included by its application are shown using dashed lines.

enrichment (0.8 [*y1*]) and also areas considered to have high-level Tlo-enrichment (0.9 [*y2*]).

Using a threshold in the 80th percentile (*y2* > 0.8), 6,289 chromosomal enriched regions (CHERs) were identified. Using the 90th percentile threshold (*y3* = 0.9), 4110 CHERs were identified. Some CHERs consisted of multiple peaks within one region of enrichment and were combined for the purpose of analysis. Significant enrichment (*y2* > 0.8) was found along 1,617 genes or orfs which constituted approximately 27 % of all annotated *C. dubliniensis* genes. Only 45 non-coding, intergenic regions were observed with significant enrichment. Of those genes that were enriched, the region of enrichment was generally focused within the orf and radiating outwards either upstream or downstream of the gene. Most gene-specific peaks involved a short 5-prime extension which sharply decreased within 100 bp. 3-prime regions generally had a longer, more gradual extension with more gradual tapering of the enrichment than at the 3-prime. It was found however, that overall there was no observable bias for either 3-prime or 5-prime enrichment, in fact most enriched genes harboring gene-central peaks displayed some enrichment on both flanking regions (Figure 6.6. A,B). Genes whose highest enrichment peak lay outside a coding region were slightly different. Such peaks generally lay within 2 kb of the 5-prime region of the nearest gene but were generally much closer to the 3-prime region of the other nearest gene, suggesting a slight bias for 3-prime-adjacent regions as opposed to 5-prime-adjacent regions (Figure 6.6. C,D). Further analysis was carried out on genes showing significant high-level enrichment (*y2* = 0.9, n = 367) based on correlations with expression and gene ontology as outlined in the following sections.

6.3.2. Design of single-gene ChIP-qRT-PCR assay

In order to support the results in the global ChIP experiment, ChIP-qRT-PCR was carried out on a single gene basis. This was carried out in the Dept. of Microbiology, TCD. As such, many of the aspects of the global ChIP that had been successfully optimised needed to be re-investigated. The sections below describe the optimisation steps carried out.

6.3.2.1. Breakage optimisation

The method utilised for lysing cells in the single-gene ChIP experiments differed from that carried out during preparation of samples for whole-genome ChIP-on-chip. In this experiment, a bead-mill was used to mechanically break cells. As a result of the change in technique, it was necessary to ascertain the optimal levels and conditions of breakage. Cross-linked cultures were subjected to successive rounds of breakage as outlined in (sections 6.2.1. and 6.2.4.2.). Eight identical replicates were setup, each receiving one additional round of breakage in the bead mill compared to the last. Protein release has been demonstrated to be a convenient indicator of successful cell lysis/breakage (Ernst & Zor, 2010). Therefore, a Bradford assay (BioRad) was used to estimate the total protein release compared to the number of cycles of mechanical breakage (Figure 6.7).

In addition to this, after each successive round of breakage, an aliquot of the sample was visualised using traditional light microscopy. The total number of cells in a field of view were counted. This was then combined with the Bradford assay data to help to identify the optimum breakage conditions (Figure 6.8). The time at which least intact cells were visible and most protein was released/present in solution was identified as between 6 and 7 cycles on the bead mill.

6.3.2.2. Sonication optimisation

As with cell breakage, sonication of DNA fragments is highly sensitive. With the use of new equipment, optimisation was required and was carried out on samples that had been subjected to 7 cycles of mechanical breakage (determined in section 6.3.2.2. to be the optimal number of cycles). The samples were then subjected to 10 s pulses using the Branson sonicator tip. The technique is fully outlined in sections 6.2.2.3 and 6.2.4.3., but in this case, samples were subjected to 7, 10, 12, 14, 16, 18, 20 or 24 x 10 s pulses (each with 120 s rest time on ice between pulses).

All sonicated samples were treated in exactly the same way. Each was pronase treated (section 6.2.4.8.) and DNA was purified as previously described (section 2.2.2.). Using agarose (1.8 % [w/v]) gel electrophoresis (section 2.1.9.), the extent to which the DNA had had been fragmented was visualised (Figure 6.9. A). It was found that 14 pulses was the optimum treatment to allow fragmentation to an average size of 500 bp as shown in Figure (6.9. B)

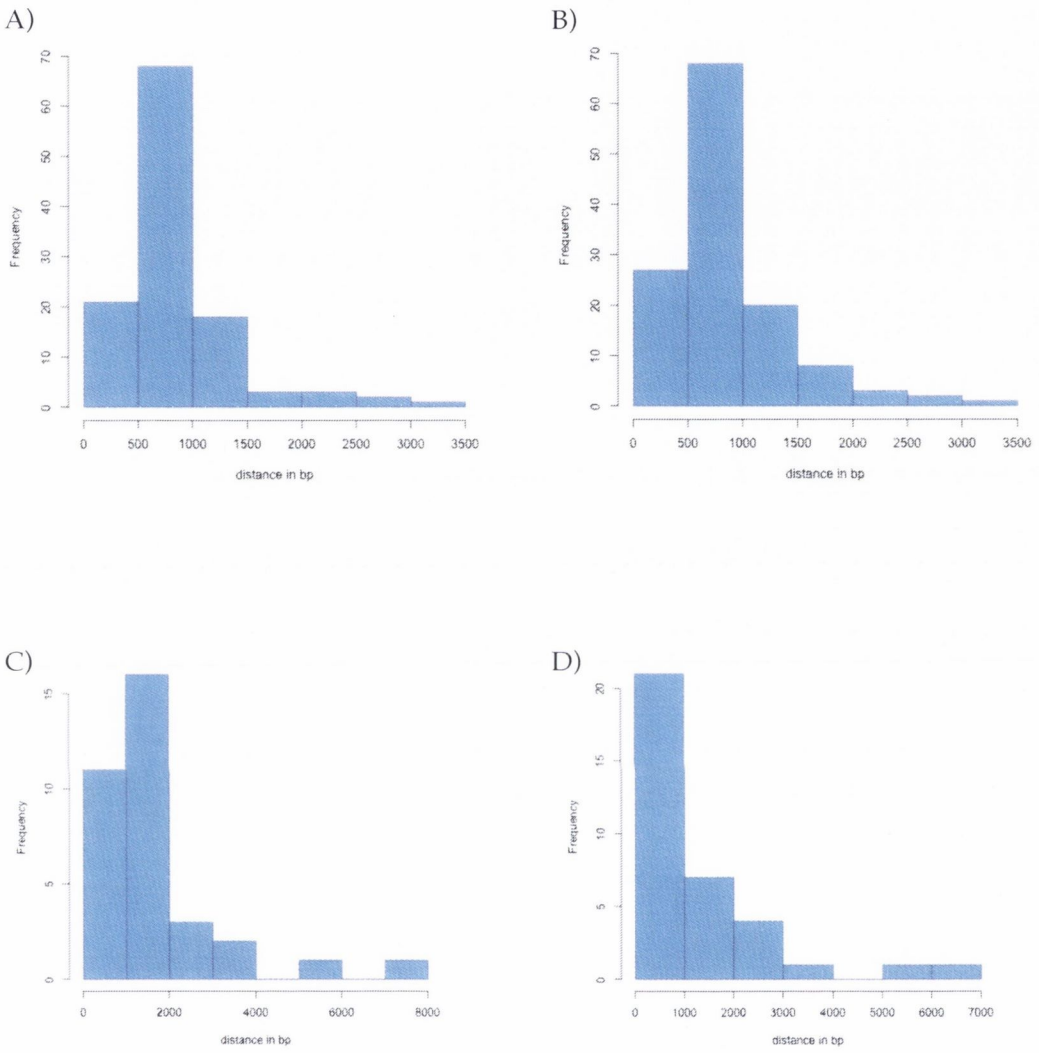

Figure 6.6. Enrichment of Tlo1 is not biased towards 5-prime or 3-prime regions of genes.

Histograms showing the frequency of distribution of 'enriched regions' whose highest enrichment lies within an orf versus the distance (in base pairs) to the (A) 5-prime or (B) 3-prime of the nearest gene. The frequency of distribution of 'enriched regions' whose highest level of enrichment lies outside an orf versus the distance to the (C) 5-prime or (D) 3-prime of the nearest gene. Data was generated using Bioconductor.

A)

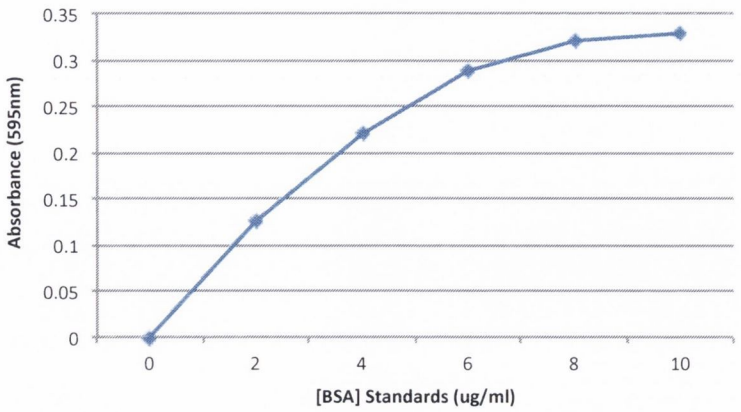

B)

# cycles	*Absorbance(595 nm)*	*Concentration**	*µg/ml sample***	*mg/ml sample*
0	0.12	1.164013608	1164.013608	1.164013608
1	0.123	1.270065941	6350.329707	6.350329707
2	0.168	2.860850939	14304.25469	14.30425469
3	0.211	4.380934381	21904.6719	21.9046719
4	0.188	3.567866493	17839.33247	17.83933247
5	0.176	3.14365716	15718.2858	15.7182858
6	0.201	4.027426603	20137.13302	20.13713302
7	0.205	4.168829714	20844.14857	20.84414857

Figure 6.7. Determination of cell lysis & breakage .

Bradford assay was used to estimate amount of protein released as a direct indicator of the success of cell breakage. Bovine Serum Albumin (BSA) at known concentrations were used as standards (A) to facilitate quantification of the amounts of protein present in experimental samples following increasing cycles of disruption (B).

* Concentration of samples was calculated by interpolation based on the standard curve of known protein standard samples.

**µg/ml of samples were calculated based on dilution measured (1:1000 or 1:5000).

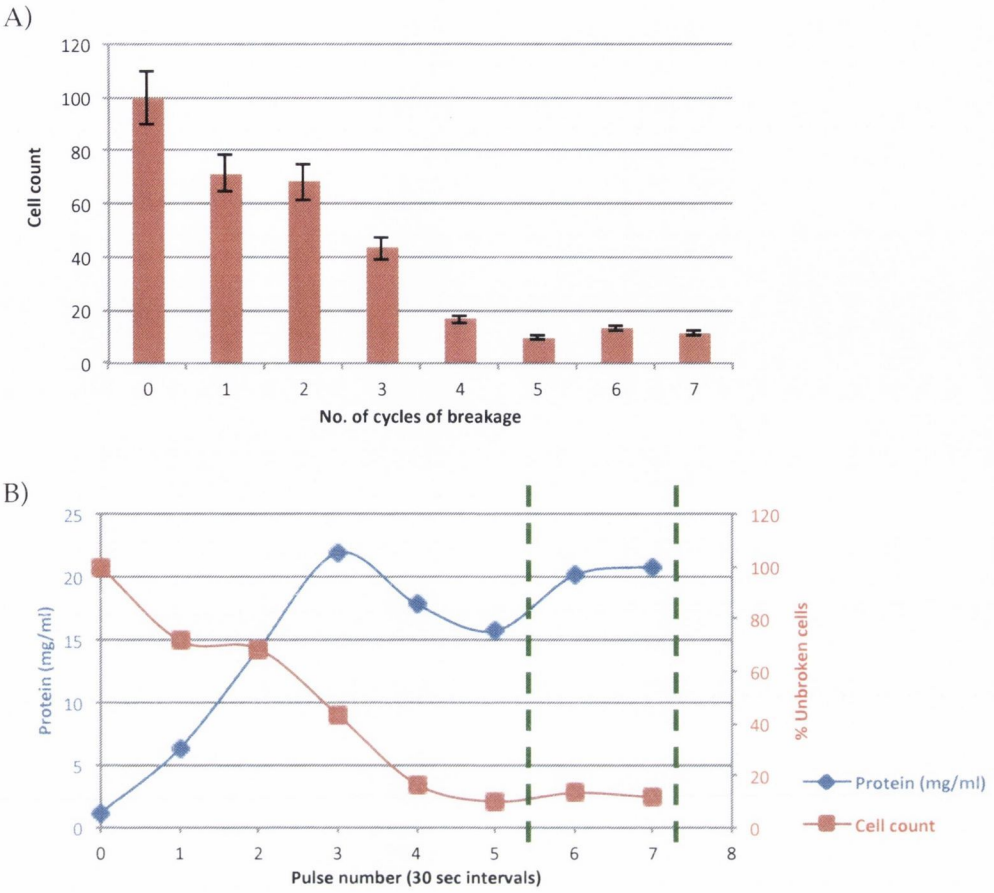

Figure 6.8. Visualisation of extent of cell breakage & lysis in experimental samples.

Light microscopy was used to estimate the number of cells present in samples after successive rounds of breakage in the 'bead beater' (Thermo Fisher Scientific). Cells in the field of view at magnification X400 were counted. Results were represented as an average of three independent counts (A). Error bars are included and represent standard deviation of counts. Number of cells present decreased over time as expected. Results were plotted (B) against protein released as measured by a Bradford assay and described in section 6.2.1.2. Dashed lines indicate region of optimal breakage/protein release as indicators of successful lysis.

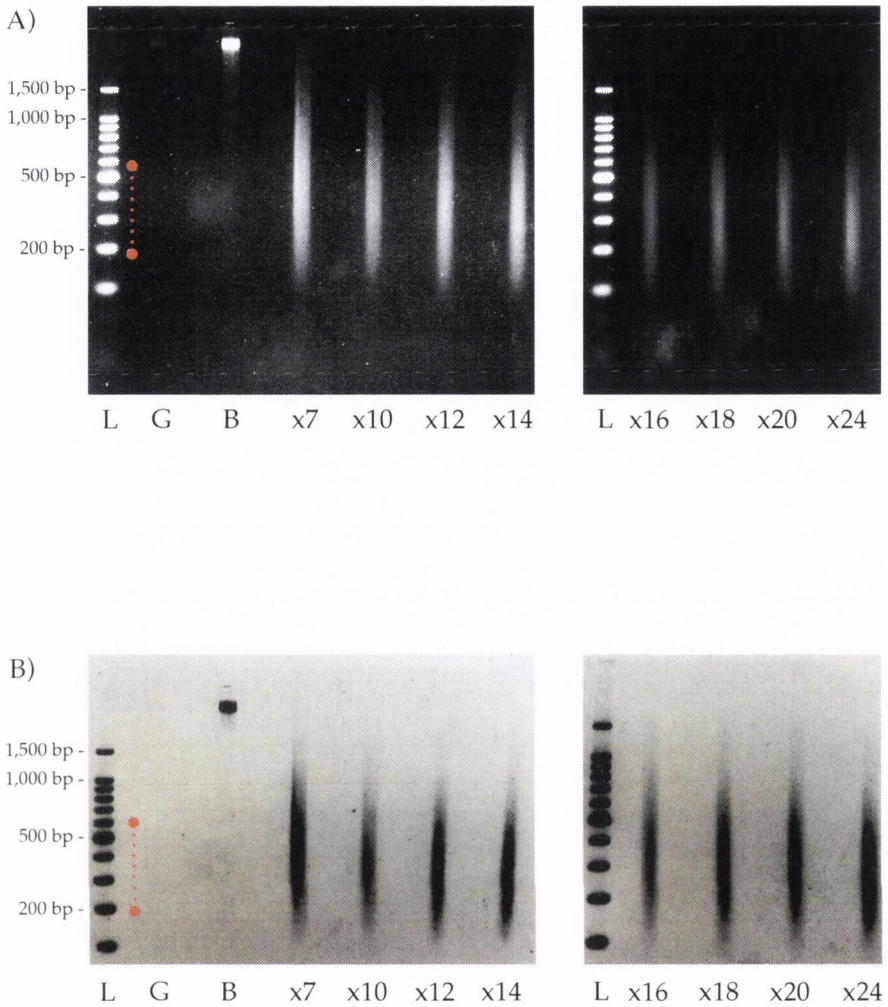

Figure 6.9. Optimisation of sonication step in Chromatin immunoprecipitation protocol. Fixed/cross-linked samples were subjected to varying rounds of sonication. Each round consisted of a pulse of 10 s duration at 9 micron amplitude on a Branson sonifier followed immediately by 120 s rest time on ice. Samples were kept on ice during all steps. 5 ODU of sonicated samples were subjected to pronase treatment and reverse crosslinking as described in 6.2.4., followed by phenol-chloroform DNA purification. Samples were subjected to agarose (1.8 % [w/v]) gel electrophoresis at 100 V for approximately 2.5 h. Optimal resolution resulting from sonication was between 600 bp and 250 bp. Visualisation was carried out by Gel Red staining for 30 min and images were viewed under a UV transilluminator as described in 2.1.9. (A). Images were also post-processed in 'negative' for ease of viewing (B). Rounds of sonication are indicated alongside other lanes: L – 100 bp ladder (Promega), G – genomic DNA purified from non-related experiment, B – DNA that has undergone breakage by glass bead disruption only (prior to sonication step).

6.3.2.3. Immunoprecipitation optimisation

Following the above optimisation steps, it was decided to use a more efficient system for immunoprecipitation (IP). The Magnetic Bead system (New England Biolabs), based on the Dynabead (Life technologies) system involved a paramagnetic particle covalently coupled to Protein G allowing immuno-magnetic purification of IgG (New England Biolabs) via Neodymium magnets (New England Biolabs)

The same antibody (12CA5) used in whole genome ChIP-chip experiments was used here. Separate IPs using 2 µl, 4 µl and 6 µl amounts were used alongside a control without antibody. In addition, an antibody against the C-terminal domain of RNA Polymerase (Covance 8WG16) was used on another IP to allow for validation of the system.

6.3.3. Confirmation of global ChIP-on-chip with single gene ChIP-qRT-PCR

We selected a number of regions of the *C. dubliniensis* genome for qRT-PCR verification of the ChIP-on-chip enrichment patterns, including orfs and intergenic regions. In these experiments, a control reaction that contained no antibody (i.e. theoretically, no pull-down) was run alongside three IP reactions containing increasing volumes of antibody. In order to distinguish between enriched and non-enriched regions, the IP/input score of the IP reaction needed to be at least double (> 200 %) that of the no-antibody control reaction.

The most significant enrichment peak in the ChIP-chip dataset was in *PUT1*, a proline oxidase involved in amino acid catabolism which is up-regulated in response to alkaline stress via Rim101 (Bensen *et al.*, 2004). qRT-PCR was used to confirm Tlo1 enrichment within the *PUT1* (*Cd36_52370*) gene (Figure 6.10). Significant enrichment was seen using ChIP-chip over the coding region and over the 5-prime and (to a lesser extent) the 3-prime flanking regions. Primer pairs PUT1AF/PUT1AR and PUT1BF/PUT1BR were designed close to the area with highest enrichment. Enrichment of Tlo1 was calculated as a proportion of DNA immunoprecipitated in the IP sample compared to the input (total lysate control) and all were compared to the control lacking antibody (no-Ab) Enrichment in the no-Ab control was low and all IP samples were significantly ($p < 0.0001$) higher in comparison, with 4 µl of antibody being more successful than with 2 µl in immunoprecipitating the DNA (Figure 6.10. A, B). The high relative enrichment correlates with the ChIP-chip enrichment patterns observed (Figure 6.10. C).

An intergenic region at which no enrichment was observed, was confirmed by qRT-PCR. Primers NEG1F and NEG1R were used to assess enrichment at an intergenic region from 521680 to 521729 bp on chromosome 5. As with *PUT1* the IP appeared more successful at higher antibody concentrations (Figure 6.11. A). However, the highest IP was significantly lower (8.3-fold, $p < 0.0001$) than in the *PUT1* (Figure 6.11. A) examples and was close enough to the no-Ab control that no enrichment could be detected (Figure 6.11. A). This correlates with the ChIP-chip enrichment patterns observed for this region (Figure 6.11. B).

CLN1 (*Cd36_51640*) which encodes a putative G1 cyclin involved in hyphal maintenance (Loeb *et al.*, 1999) displayed no enrichment in the global ChIP-chip experiments, apart from a small region at the 3' end of the ORF (Figure 6.12. B) Using qRT-PCR and primers CLN1AF/CLN1AR, enrichment was detected compared to the no-Ab control ($p < 0.0001$), but at comparatively low levels of enrichment relative to *PUT1* (Figure 6.12. A).

Cd36_52970 is a putative pseudogene in *C. dubliniensis* that shows homology to isocitrate dehydrogenases (Hernández *et al.*, 2004). This orf was selected as is it maintained as part of the highly repetitive MRS, but represents a largely non-repetitive region of this element. Using qRT-PCR and primer pairs IDH1AF/IDH1AR and IDH1BF/IDH1BR, higher enrichment was observed in all IP samples compared to the no-Ab control (Figure 6.13. A). According to the ChIP-chip data, enrichment levels were higher at the 3-prime end of the gene (Figure 6.13. B), which is validated by the qRT-PCR data in which enrichment is slightly higher for primer pairs IDH1BF/IDH1BR.

Cd36_51290 whose orthologs are involved in N-terminal amino acid acetylation (Arnaud *et al.*, 2005) showed no enrichment in the Chip-on-chip dataset (Figure 6.14. C). qRT-PCR was carried out using primer sets Cd36_51290AF/Cd36_51290AR and Cd26_51290BF/Cd36_51290BR. Results showed a 2-fold increase in enrichment compared to the no-Ab control ($p < 0.0001$), (Figure 6.14. A) however error margins were high for the second reaction and enrichment could not be concluded from this (Figure 6.14. B).

FGR6-3 (*Cd36_52975*) which is a pseudogene whose ortholog in *C. albicans* is involved in filamentation (Uhl *et al.*, 2003) is located at the end of the MRS in *C. dubliniensis* and showed moderate Tlo1 enrichment in the ChIP-on-chip experiments (Figure 6.15. C). qRT-PCR using primer pairs FGR6-3AF/FGR6-3AR

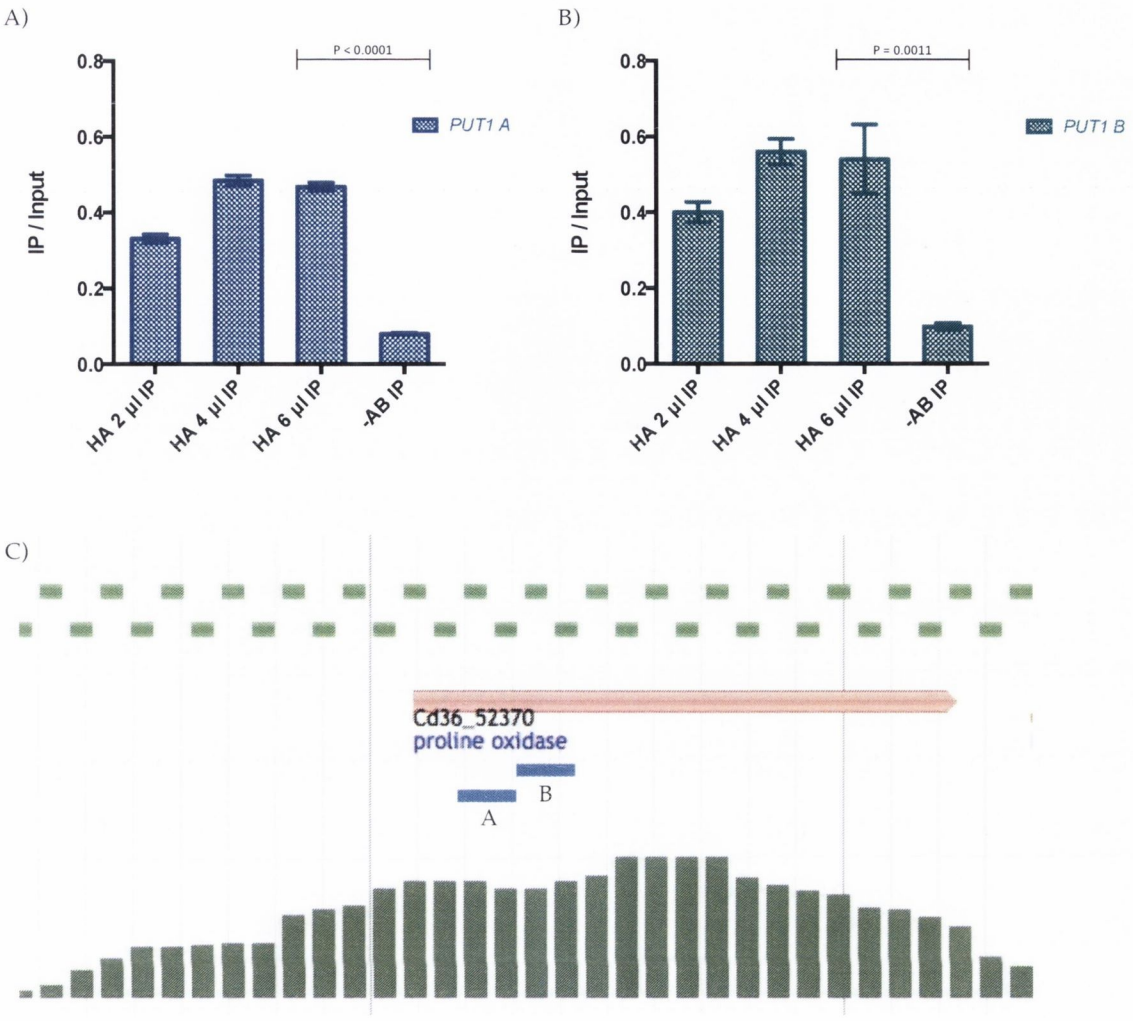

Figure 6.10. qRT-PCR was used to confirm Tlo1 enrichment at *PUT1* (*Cd36_52370*). ChIP was carried out as described followed by qRT-PCR using primer pairs PUT1AF/ PUT1AR and PUT1BF/PUT1BR. Results for each amplification (A, B) are presented using DNA concentration in the immunoprecipitated sample as a proportion of the DNA concentration in the input (whole cell extract) sample. Different titres of Anti-HA antibody were used during optimisation, the concentrations of which are shown along the x-axis. Corresponding enrichment patterns from the global ChIP experiments outlined in section 6.3.1.2. are shown in (C) with positions of primers used in (A) and (B) indicated by blue markers below the gene. p-values from compared columns (t-test) are displayed.

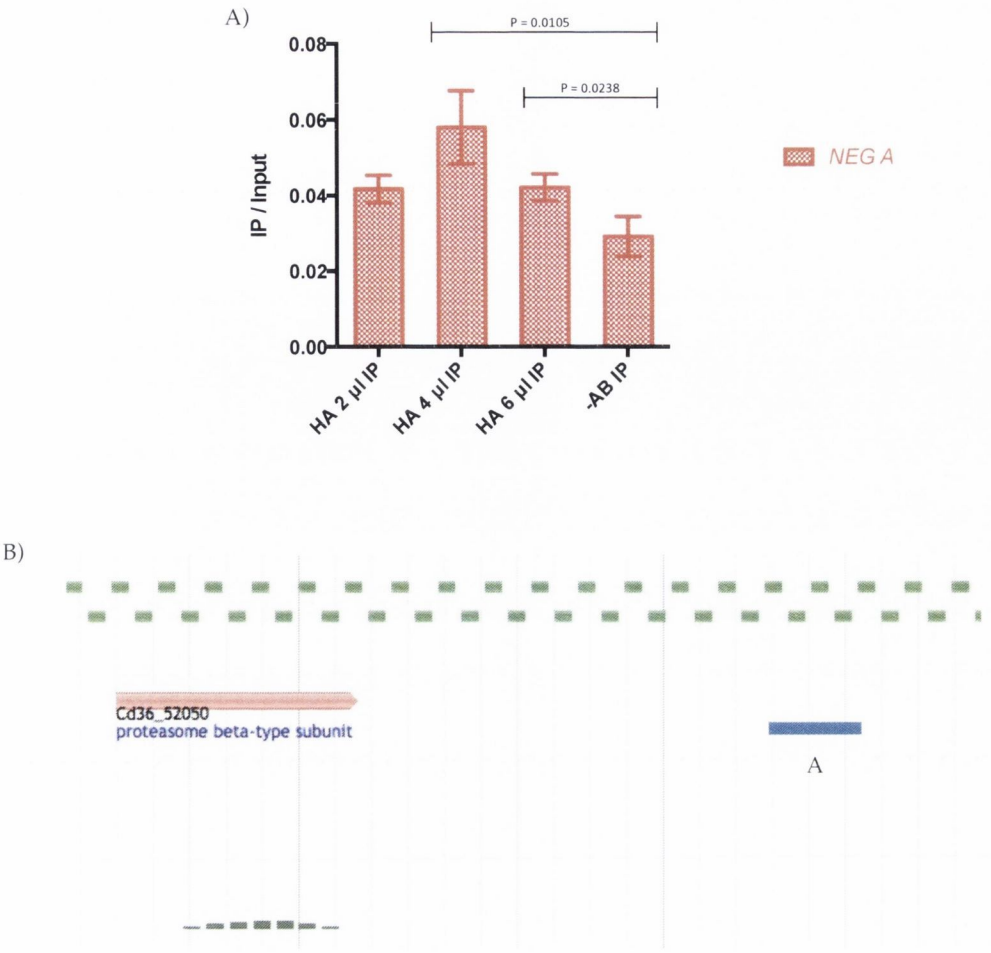

Figure 6.11. qRT-PCR was used to confirm Tlo1 enrichment patterns at an intergenic region (*NEG*).

ChIP was carried out as described followed by qRT-PCR using primer pairs NEG1F/ NEG1R. Results for each amplification (A) are presented using DNA concentration in the immunoprecipitated sample as a proportion of the DNA concentration in the input (whole cell extract) sample. Different titres of Anti-HA antibody were used during optimisation, the concentrations of which are shown along the x-axis. Corresponding enrichment patterns from the global ChIP experiments outlined in section 6.3.1.2. are shown in (B) with positions of primers used in (A) indicated by blue markers below the gene. p-values from compared columns (t-test) are displayed.

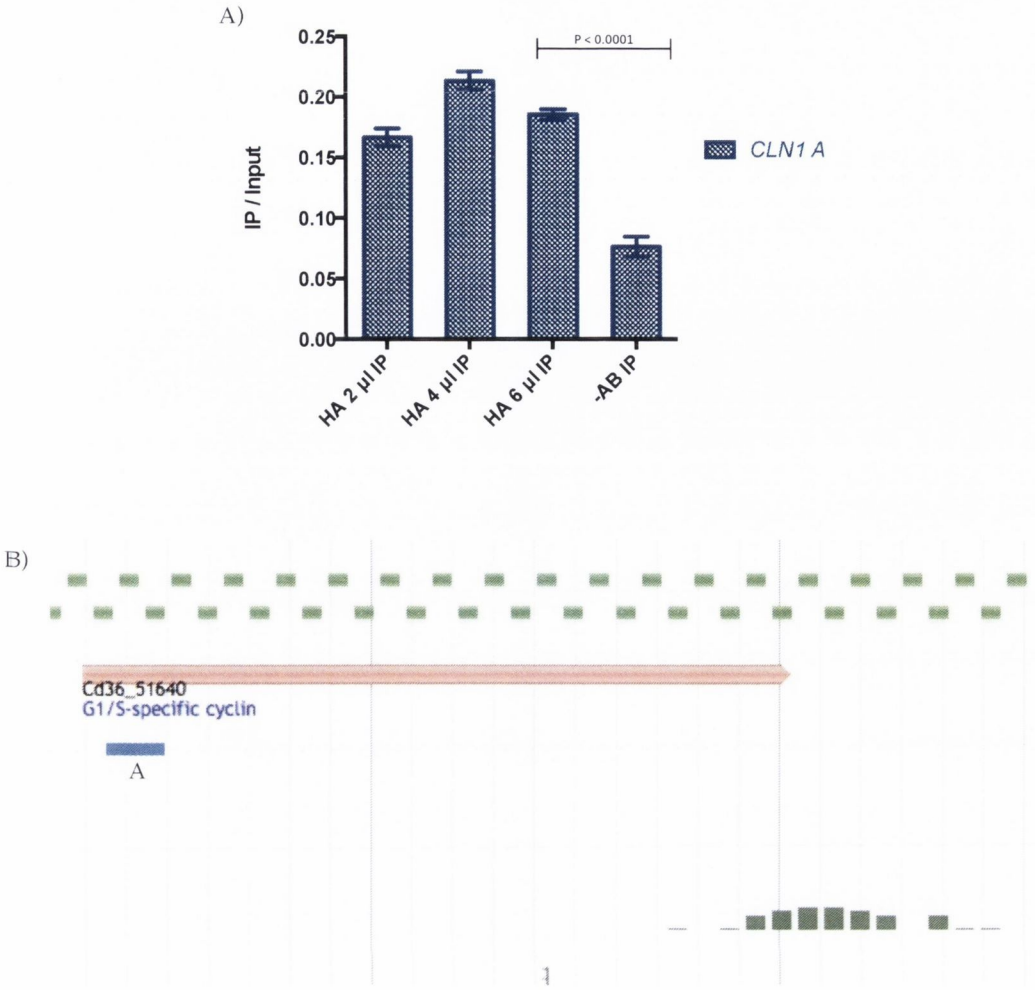

Figure 6.12. qRT-PCR was used to confirm Tlo1 enrichment at *CLN1* (*Cd36_51640*). ChIP was carried out as described followed by qRT-PCR using primer pairs CLN1AF/ CLN1AR. Results for each amplification (A) are presented using DNA concentration in the immunoprecipitated sample as a proportion of the DNA concentration in the input (whole cell extract) sample. Different titres of Anti-HA antibody were used during optimisation, the concentrations of which are shown along the x-axis. Corresponding enrichment patterns from the global ChIP experiments outlined in section 6.3.1.2. are shown in (B) with positions of primers used in (A) indicated by a blue marker below the gene. p-values from compared columns (t-test) are displayed.

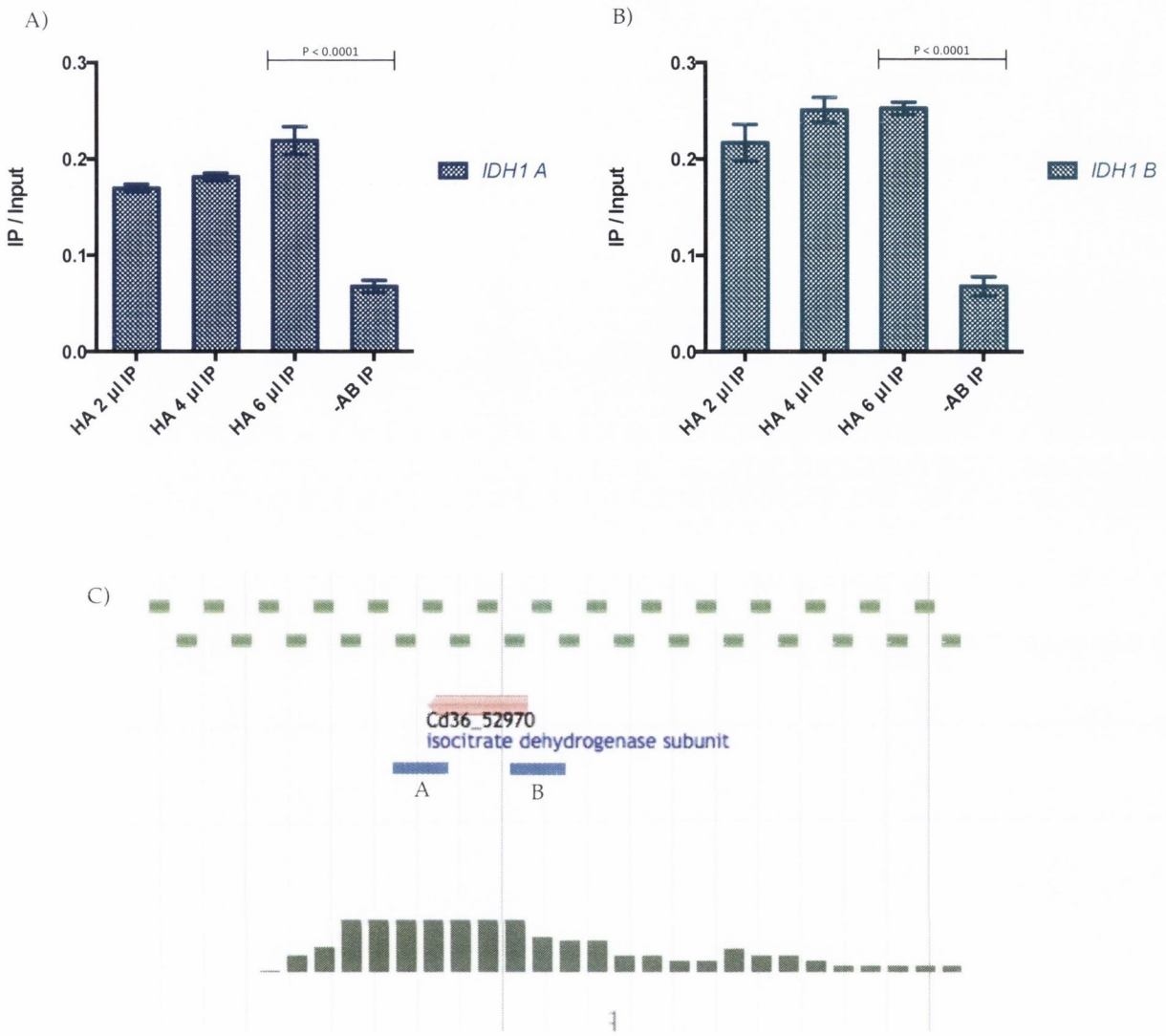

Figure 6.13. qRT-PCR was used to confirm Tlo1 enrichment at *Cd36_52970.*

ChIP was carried out as described followed by qRT-PCR using primer pairs IDH11AF/ IDH1AR and IDH1BF/IDH1BR. Results for each amplification (A, B) are presented using DNA concentration in the immunoprecipitated sample as a proportion of the DNA concentration in the input (whole cell extract) sample. Different titres of Anti-HA antibody were used during optimisation, the concentrations of which are shown along the x-axis. Corresponding enrichment patterns from the global ChIP experiments outlined in section 6.3.1.2. are shown in (C) with positions of primers used in (A) and (B) indicated by blue markers below the gene. p-values from compared columns (t-test) are displayed.

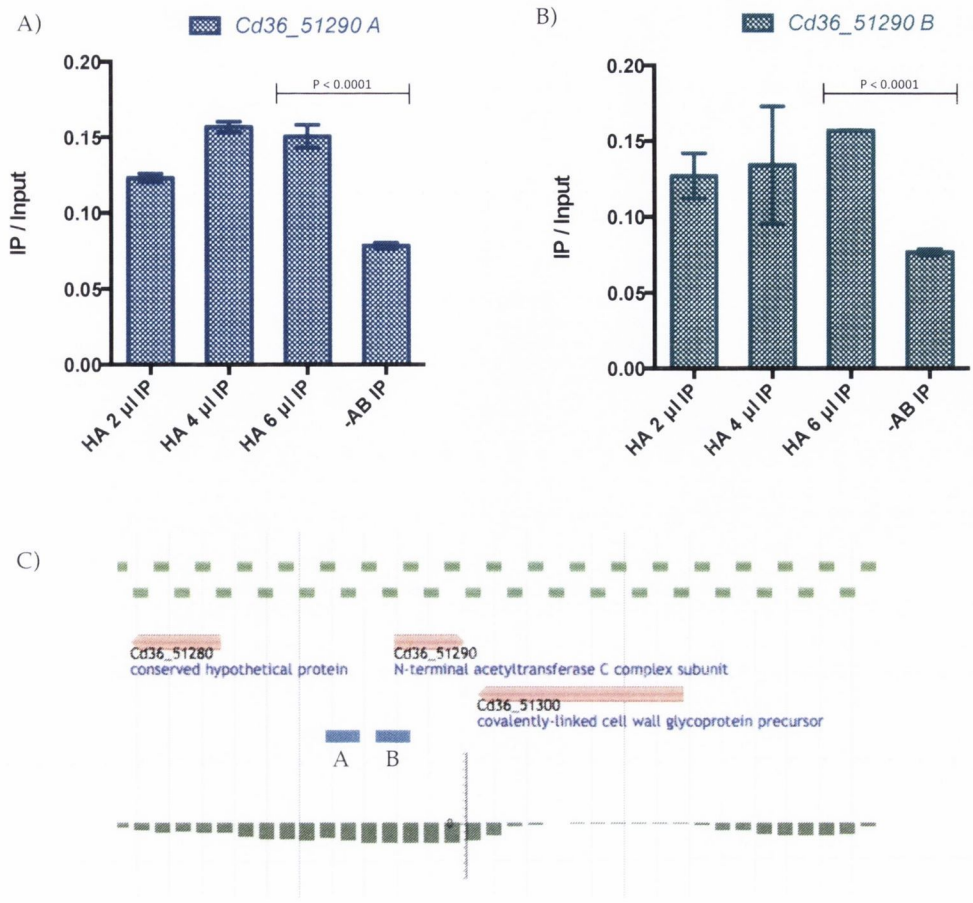

Figure 6.14. qRT-PCR was used to assess Tlo1 enrichment at *Cd36_51290*.

ChIP was carried out as described followed by qRT-PCR using primer pairs Cd36_51290AF/Cd36_51290AR and Cd36_51290BF/Cd36_51290BR. Results for each amplification (A, B) are presented using DNA concentration in the immunoprecipitated sample as a proportion of the DNA concentration in the input (whole cell extract) sample. Different titres of Anti-HA antibody were used during optimisation, the concentrations of which are shown along the x-axis. Corresponding enrichment patterns from the global ChIP experiments outlined in section 6.3.1.2. are shown in (C) with positions of primers used in (A) and (B) indicated by blue markers below the gene. p-values from compared columns (t-test) are displayed.

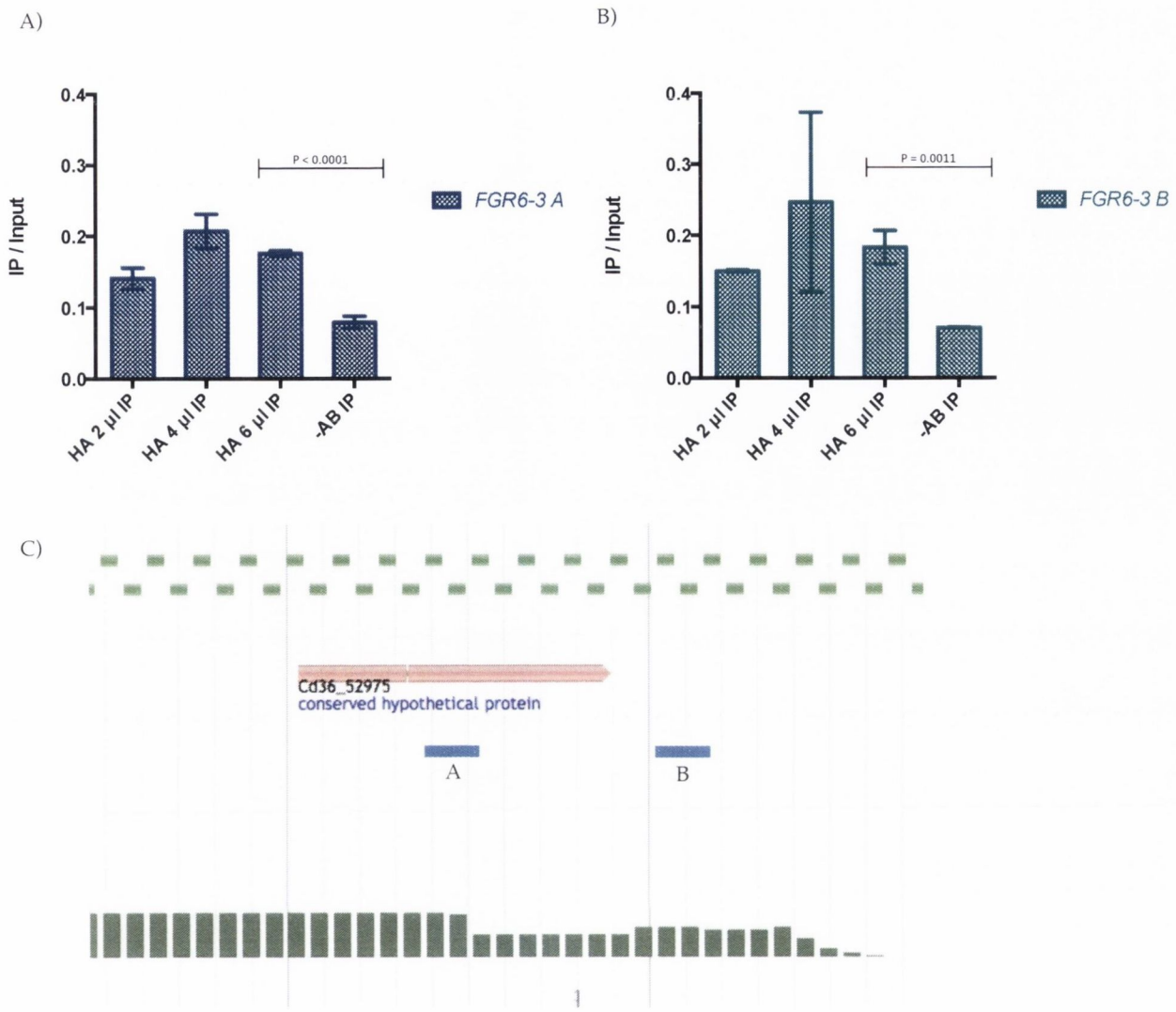

Figure 6.15. qRT-PCR was used to confirm Tlo1 enrichment at *FGR6-3* (*Cd36_52975*). ChIP was carried out as described followed by qRT-PCR using primer pairs FGR6-3AF/ FGR6-3AR and FGR6-3BF/FGR6-3BR. Results for each amplification (A, B) are presented using DNA concentration in the immunoprecipitated sample as a proportion of the DNA concentration in the input (whole cell extract) sample. Different titres of Anti-HA antibody were used during optimisation, the concentrations of which are shown along the x-axis. Corresponding enrichment patterns from the global ChIP experiments outlined in section 6.3.1.2. are shown in (C) with positions of primers used in (A) and (B) indicated by blue markers below the gene. p-values from compared columns (t-test) are displayed.

and FGR6-3BF/FGR6-3BR showed some enrichment compared to the no-Ab ($p = 0.0011$) control but the significance levels were low (Figure 6.15. A,B)

ACT1 (*Cd36_12690*) encodes for actin, a highly conserved and integral part of the cytoskeleton in *C. dubliniensis* (Donnelly *et al.*, 1999). Using primer pairs ACT1F/ACT1R, significant enrichment ($p < 0.0001$) was observed over the no-Ab control (Figure 6.16. A). This corroborates the pattern of enrichment in the global ChIP-on-chip data (Figure 6.16. B)

MTLalpha2 (*Cd36_51540*) encodes a predicted DNA-binding protein, and a putative ortholog to the mating-type gene *MATalpha2* in *C. albicans* (Pujol *et al.*, 2004). Primer pair MTLαAF/ MTLαAR were used in qRT-PCR experiments demonstrated 2-fold increase in enrichment ($p = 0.0006$) compared to the no-Ab control (Figure 6.17. A) ChIP-on-chip experiments showed no enrichment for Tlo1 at this region (Figure 6.17. B)

Finally, *Cd36_17440* encodes for a putative uroporphyrin-III c-methyltransferase involved in siroheme biosynthesis (Arnaud *et al.*, 2005). Using primer pairs Cd36_17440AF/ Cd36_17440AR, Cd36_17440BF/ Cd36_17440BR and Cd36_17440CF/ Cd36_17440CR, qRT-PCR demonstrated enrichment at the centre (Figure 6.18. A) of the gene (>2-fold higher than no-Ab) and at the 5-prime end of the gene (Figure 6.18. B). However, at the 5-prime flanking region, differences in enrichment between IP and no-Ab control were not as pronounced (Figure 6.18. C). This correlates with the pattern seen in the Chip-on-chip for this region (Figure 6.18. D).

In addition to the confirmatory ChIPs carried out, a control IP was also performed alongside and the same regions/genes outlined above were checked for IP pull-down. We observed that the three most highly enriched genes in our confirmatory datasets were the most enriched for RNA Polymerase II also (Figure 6.19. A). The other genes and regions were enriched to a lesser extent (Figure 6.19. B), but this control proved extremely useful as a check for the validity of our experiment.

6.3.4. Gene ontology (GO) analysis of chromosomal enriched regions (ChERs)

As with expression analyses carried out in Section 6.3.3., it was important to identify any links between the genes enriched and specific functional groups of genes as assigned by gene ontology (GO). 20.5 % of genes significantly enriched for Tlo1 were involved in transport processes (n = 75) e.g. *HET1, CDR1, ENA21*

and 19 % were involved in the response to stress (n = 70) e.g. *CZF1, RIM101, CAT1*. Also, 16.3 % (n = 60) of significantly enriched genes were involved in filamentous growth, e.g. *TUP1, EFG1,* and *EED1*.

Using Gene Ontology term finder (Arnaud *et al.*, 2005), a correlation between those genes significantly enriched by Tlo1 and groups of processes was identified. GO-terms identified included response to stress (n = 70, $p < 0.001$), oxidation-reduction (n = 49, $p < 0.001$), hexose transport (n = 13, $p < 0.001$), carboxylic acid catabolism (n = 16, $p < 0.001$), localisation (n = 83, $p < 0.001$), alpha amino acid metabolism (n = 21, $p < 0.001$), transport (n = 75, $p < 0.001$), pyruvate metabolism (n = 10, $p < 0.001$), tricarboxylic acid cycle (n = 8, p = 0.00014), filamentous growth (n = 60, p = 0.00018), glycolysis (n = 8, p = 0.00028), and glyoxylate cycle (n = 4, p = 0.01993). Similar analyses have also identified that the group of enriched genes are involved in oxidoreductase activity (n = 39, p = 0.00439), glucose transport (n = 7, p = 0.1655), transmembrane transport (n = 36, p = 0.00095) and RNA polymerase II transcription factor binding (n = 4, p = 0.04275). In addition, 100 % of the genes associated with the oxoglutarate dehydrogenase complex (involved in the TCA cycle) were enriched for Tlo1 (n = 3, p = 0.00363) and 5 of 9 genes part of the TCA cycle enzyme complex were enriched for Tlo1 (p = 0.00028).

6.3.5. Relationship between expression and Tlo1 enrichment

In order to ascertain if there was a correlation between the enrichment of genes by Tlo1 and the expression of those genes, the CHER dataset was compared to the single channel (Wü284) DNA microarray data from the experiments in YEPD at 30 °C discussed in Chapter 5. It was found that genes enriched for Tlo1 in the ChIP experiments (y 0.8; n = 1617) displayed on average higher levels of expression in Wü284 relative to those genes not enriched with Tlo1 ($p < 0.0001$) (Figure 6.20).

Closer inspection of the expression levels of the genes that were highly enriched for Tlo1 (y 0.9, n = 367) indicated that this group consisted of genes that display both high and low expression levels. The highly expressed, Tlo1-enriched genes included those in functional categories such as translation (n = 5), glycolysis (n = 7) and sulphur amino acid biosynthesis (n = 4). Interestingly, microarray analysis in Chapter 4 indicates that these highly expressed, Tlo1-enriched genes exhibit reduced expression in the Δ*tlo* mutant strain, suggesting that Tlo plays a

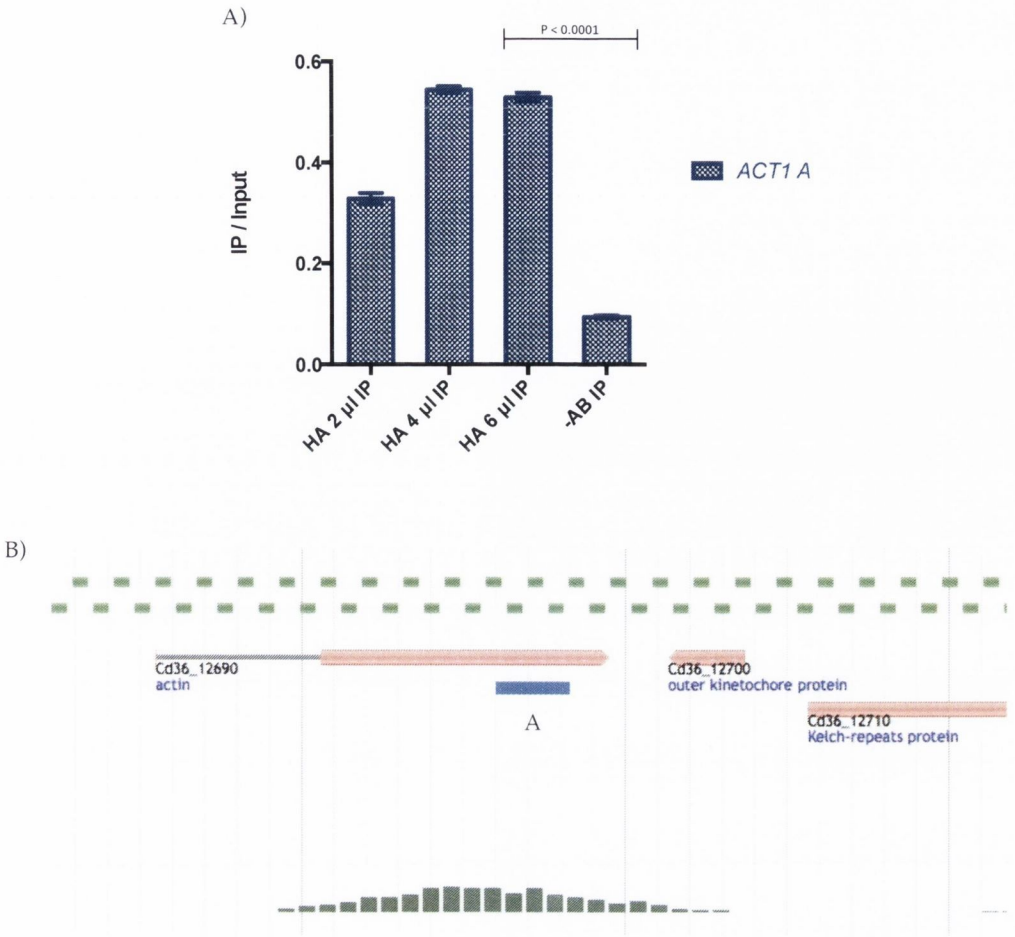

Figure 6.16. qRT-PCR was used to confirm Tlo1 enrichment at *ACT1* (*Cd36_12690*). ChIP was carried out as described followed by qRT-PCR using primer pairs ACT1F/ ACT1R. Results for each amplification (A) are presented using DNA concentration in the immunoprecipitated sample as a proportion of the DNA concentration in the input (whole cell extract) sample. Different titres of Anti-HA antibody were used during optimisation, the concentrations of which are shown along the x-axis. Corresponding enrichment patterns from the global ChIP experiments outlined in section 6.3.1.2 are shown in (B) with positions of primers used in (A) indicated by a blue marker below the gene. p-values from compared columns (t-test) are displayed.

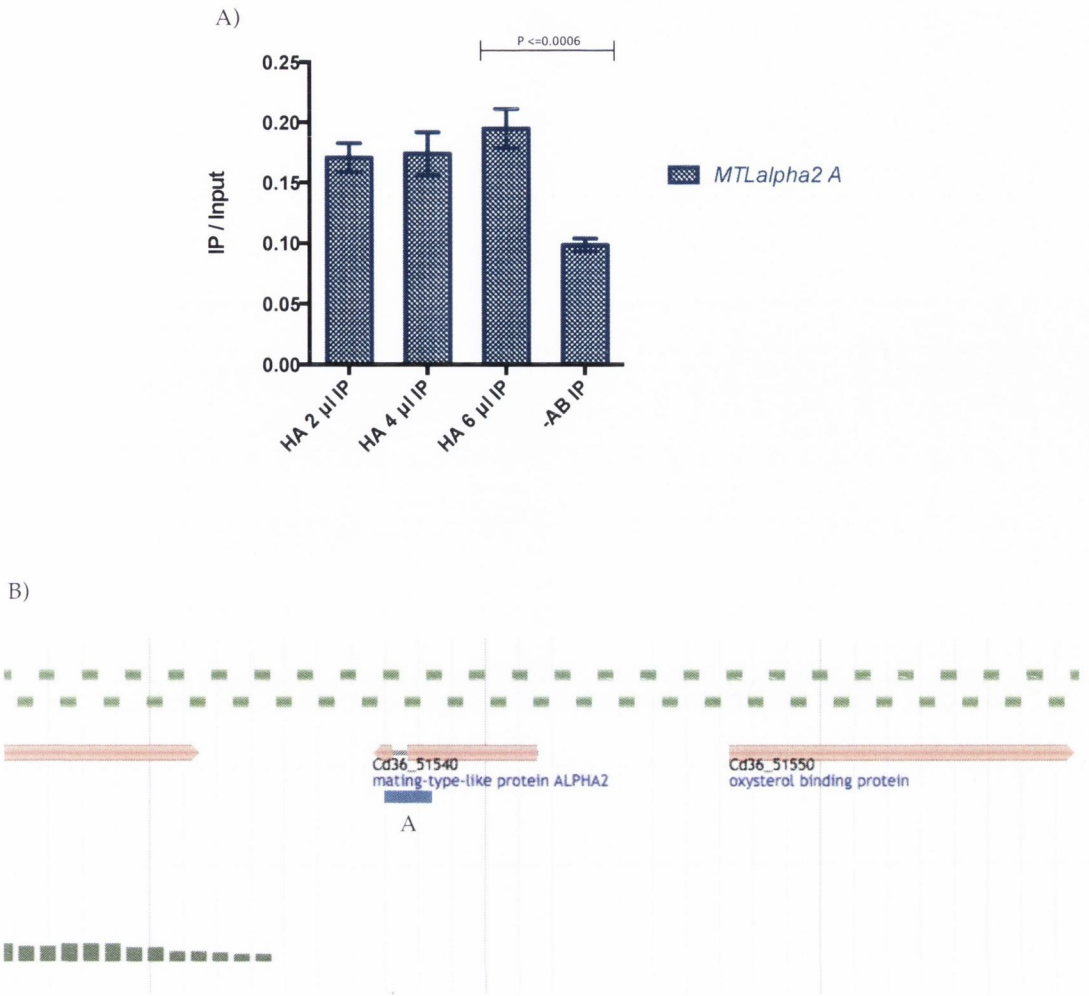

Figure 6.17. qRT-PCR was used to confirm Tlo1 enrichment at *MTLalpha2* (*Cd36_51540*). ChIP was carried out as described followed by qRT-PCR using primer pairs MTLαAF/ MTLαAR. Results for each amplification (A) are presented using DNA concentration in the immunoprecipitated sample as a proportion of the DNA concentration in the input (whole cell extract) sample. Different titres of Anti-HA antibody were used during optimisation, the concentrations of which are shown along the x-axis. Corresponding enrichment patterns from the global ChIP experiments outlined in section 6.3.1.2. are shown in (B) with positions of primers used in (A) indicated by a blue marker below the gene. p-values from compared columns (t-test) are displayed.

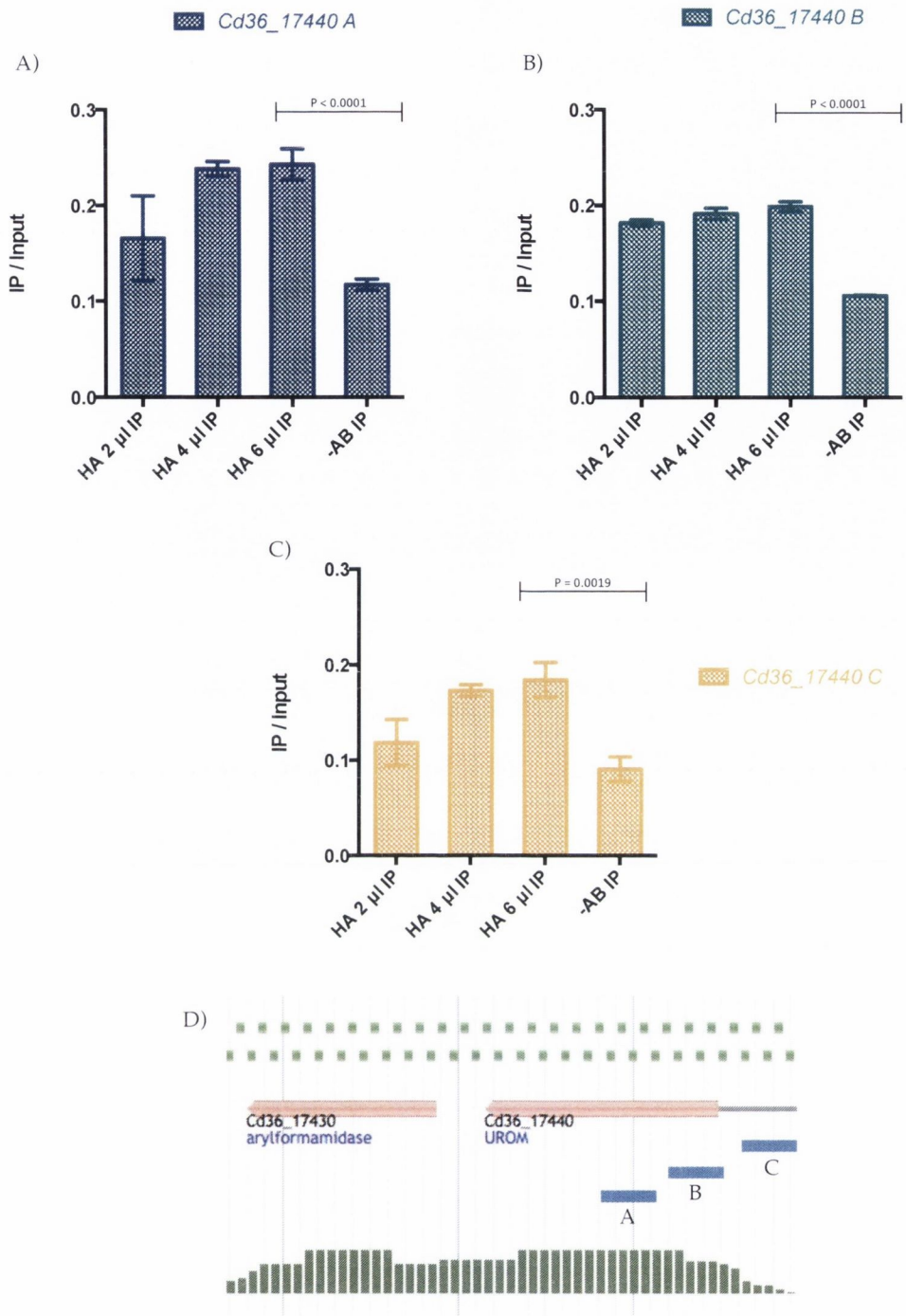

Figure 6.18. qRT-PCR was used to confirm Tlo1 enrichment at *Cd36_17440*.

ChIP was carried out as described followed by qRT-PCR using primer pairs Cd36_17440AF/Cd36_17440AR, Cd36_17440BF/Cd36_17440BR and Cd36_17440CF/Cd36_17440CR. Results for each amplification (A, B, C) are presented using DNA concentration in the immunoprecipitated sample as a proportion of the DNA concentration in the input (whole cell extract) sample. Different titres of Anti-HA antibody were used during optimisation, the concentrations of which are shown along the x-axis. Corresponding enrichment patterns from the global ChIP experiments outlined in section 6.3.1.2. are shown in (D) with positions of primers used in (A), (B) and (C) indicated by blue markers below the gene. p-values from compared columns (t-test) are displayed.

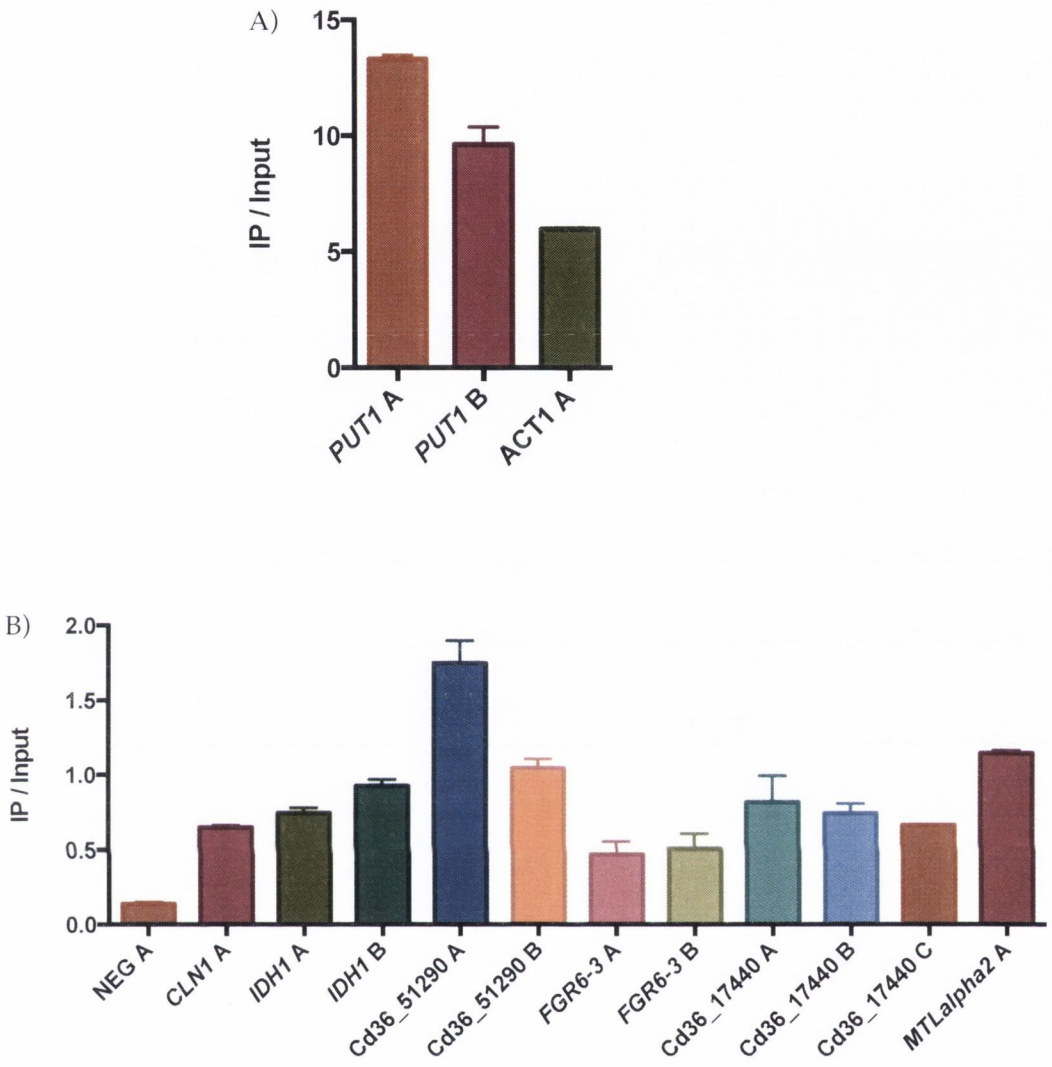

Figure 6.19. RNA Polymerase II ChIP.

Alongside the ChIP-PCR experiments used to confirm ChIP-chip results, a separate pulldown was carried out using an antibody against RNA Polymerase II CTD repeat YSPTSTS. IP/Input was calculated as in previous examples and the most enriched genes (A) were plotted separately to the other lesser enriched genes (B). qRT-PCR runs were carried out in the same manner as in the ChIP-qRT-PCR experiments from section 6.3.3.

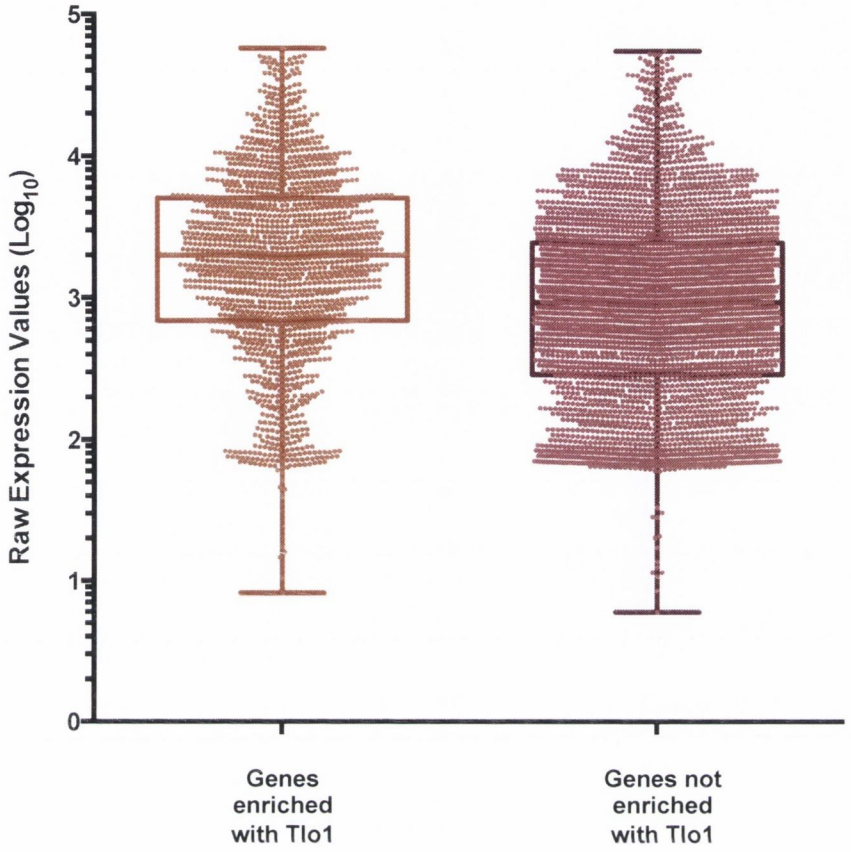

Figure 6.20. Gene-specific relationship between expression and Tlo1 enrichment.

Boxplot showing raw intensity values of Wü284 gene expression in two categories: (i) genes that are enriched for Tlo1 in the ChIP-on-chip dataset and (ii) genes with no enrichment found in the Tlo1-ChIP experiments. All individual values are displayed. Using a two-tailed student's t-test, the mean and median of two datasets are significantly different ($p < 0.0001$).

role in maintaining their expression (Figure 6.21). Conversely, genes involved in starvation responses such as gluconeogenesis (n=3), alpha-amino acid catabolism (n = 7), hexose transport (n = 5) and nitrogen scavenging (n = 5) which are normally expressed at low levels in wild-type strain Wü284 exhibited increased expression in the ΔΔ*tlo* mutant strain (Figure 6.21), suggesting that Tlo may play a role in repressing the expression of these categories of genes. The exceptions to this pattern are genes encoding enzymes of the TCA cycle (n = 8) which are normally highly expressed in wild-type cells and exhibited increased expression in the ΔΔ*tlo* mutant strain.

6.4. Discussion

6.4.1. General remarks

As mentioned in the introductory remarks, this is the first time that a ChIP-on-chip has been carried out in *C. dubliniensis* and the first instance of ChIP or ChIP-chip on the Tlo genes in either *C. albicans* or *C. dubliniensis*. As such, the successful development of the methods contained in this chapter will stand as an invaluable tool to be used to further investigate the function and behaviour of Tlo proteins and beyond, in *Candida* spp.

Many challenges were encountered during both inception and application of these experiments. One such challenge was the lack of known positive and negative controls. As the role of Tlos in the cell were poorly characterised, there were no known regions of the genome to which Tlo1 was definitively known to interact with. This led to normalisation of enrichment data being carried out in a multitude of stringent ways in order to lessen the probability of false positives, while also ensuring as best as possible, not to exclude interesting results. Normalisation experiments where comparisons were made against regions of presumptive low enrichment produced similar results (data not shown). Dye-swaps were implemented in the experimental procedure in order to decrease the probability of any bias. In addition to this, stringent minimum values (thresholds) of enrichment scores were applied to ensure reliability of the data. Different methods of processing and identifying the chromosomally enriched regions (CHERs) were explored, including vsn and Nimblegen methods in combination with the 'sliding window method', all of which are described in the Chapter. In future experiments, it will be desirable to compare the same negative regions, normalisation methods and thresholds to ensure that our approach has been as accurate as possible. It will also be useful to compare the overall datasets to each other.

Other challenges encountered during this study included the propensity for *C. dubliniensis* to be somewhat resistant to spheroplasting and subsequent lysis and sonication steps. Wü284 cell walls have been observed in our lab to be more difficult to digest than *C. albicans* strains (Personal Communication, Peter Hyde, 2013) and other *C. dubliniensis* strains (unpublished data). Despite these obstacles, useful results were obtained from this pilot study.

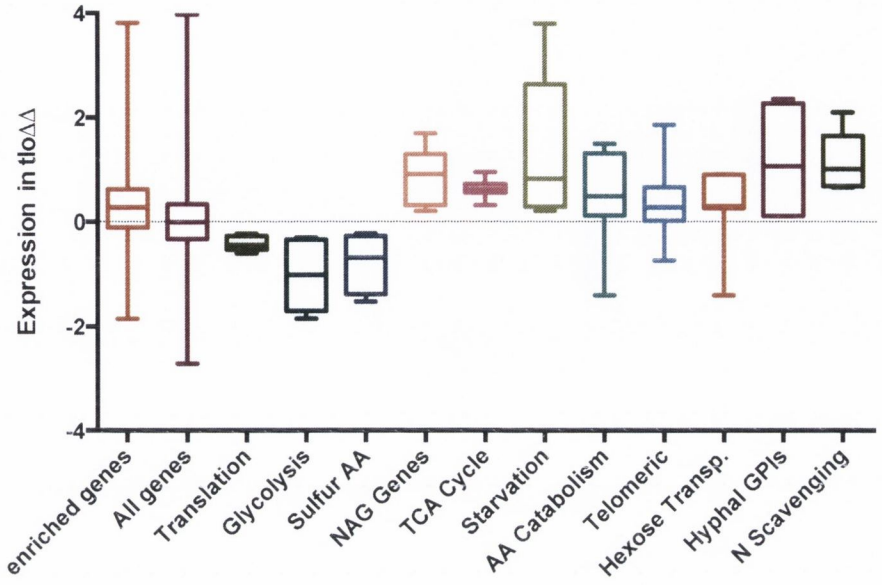

Figure 6.21. Expression of significantly enriched gene groups.

Boxplot showing the change in expression levels of different categories of Tlo1 enriched genes (y 0.9) in the *tlo* mutant relative to wild-type, as determined in DNA microarray studies from Chapter 5.

Enrichment patterns obtained through the high-throughput ChIP-chip were validated by single gene ChIP-qRT-PCR as outlined in the previous section. Unfortunately, difficulties in qRT-PCR oligonucleotide design for the highly repetitive MRS and telomeric regions prevented any meaningful confirmation of those regions and this will need to be addressed in future experiments.

6.4.2. Enrichment at repetitive regions

Telomeres are regions of tandem repetitive DNA repeats at the ends of chromosomes and are found across all eukaryotic genomes (Bianchi & Shore, 2007). In *C. dubliniensis,* the telomere repeat unit consists of 5'-[AAC TTC TGG TGT ACG GAT GTC T]-3' (Yu *et al.*, 2007). They exist as heterochromatic DNA-protein structures (Chen *et al.*, 2000; Chico *et al.*, 2011) that are often transcriptionally silenced due to the telomere position effect (TPE) (Yu, 2012). Telomeres act as a protective 'cap' to the end of the chromosome and as regulators of chromosome length maintenance (Yu, 2012). Tlo proteins may therefore be involved in chromosome maintenance and protection. One of the main observations in the experimental data has shown that the telomeres and sub-telomeres in *C. dubliniensis* Wü284 are significantly enriched for Tlo1, as is particularly evident on the chromosomal enrichment plot for chromosome 5 (Figure 6.4). On all chromosomes, most orfs (85 %) within the sub-telomeric region (within 20 kb of chromosome end) are significantly enriched. In addition, enrichment levels are particularly high at the ends of telomeres. While it is useful to note that some binding at the telomeres may be the result of an artefact associated with the repetitive nature of these regions, telomere ChIPs have been carried out in the past with few issues (Fujita *et al.*, 2013; Kitada *et al.*, 2012; Ma, 2011).

The ChIP-on-chip data have also shown significant enrichment of Tlo1 over the MRS. The MRS is present across all chromosomes in *C. dubliniensis* except for chromosome R (Jackson *et al.*, 2009) and its definitive functions remain relatively unknown. It is thought that this series of highly repetitive sequences may be involved in chromosomal translocation events, transcriptional regulation of phenotypes or insertion/deletion events within chromosomes (Chibana & Magee, 2009). Association of Tlo1 with the MRS might suggest a role for Tlos in regulating these chromosomal rearrangements.

Due to the repetitive nature of these regions, in particular of the MRS, qRT-PCR was not specific enough to accurately confirm enrichment patterns. It was possible however, to estimate enrichment at orfs flanking the regions. To properly validate enrichment at the MRS and telomeres, chromatin IP with sequencing (ChIP-seq) would be appropriate, removing the difficult step of designing primers specific for successive repeats, instead using next generation sequencing (NGS), a method with which success has been demonstrated (Day *et al.*, 2010). The association of Tlos with both telomeres and the MRS suggests that the Tlos might have a role (perhaps indirectly) in the regulation of processes involved in chromosomal maintenance, rearrangement and loss as well as chromatin remodeling (silencing at telomeres, etc.)

6.4.3. Enrichment at open reading frames (orfs)

In addition to repetitive regions, the ChIP data have indicated that many orfs (not including those associated with [sub-]telomeres and the MRS) are enriched for Tlo1. The incidence of enrichment at coding regions (n =1,617 orfs) was much higher than that found at intergenic regions, of which there were approximately 46 incidences. This enrichment pattern translates to over 25 % of all RNA Polymerase II transcribed genes.

Expression levels of these genes vary and no significant correlation between particular expression and enrichment was found (section 6.3.3.), although Tlo1-enriched genes exhibited on average 1.5-fold higher levels of expression relative to non-enriched genes. As well as this, some functional correlations were found based on GO-terms (Section 6.3.3.).

It is interesting to note that many of the genes enriched for Tlo1 in the ChIP-on-chip data showed altered expression in the absence of both *TLO* genes in DNA microarray experiments under similar conditions (Chapter 5). This suggests a functional interaction with these genes and should be explored in further studies. Interestingly, as discussed in section 6.3.3., the Tlo1-enriched genes can exhibit both high and low levels of expression. GO-analyses of the Tlo1-enriched genes were used to group these genes into functional categories, resulting in the identification of highly expressed house-keeping genes involved in glycolysis and translation as well as poorly expressed categories of genes involved in starvation responses, that are normally repressed under the conditions investigated. Microarray analysis showed that these functional categories of genes exhibited

changes in expression following deletion of both *TLO* genes, supporting a hypothesis that Tlos may be playing an active role in the regulation, either by activation or repression of specific subsets of genes. This will be discussed in Chapter 7.

In particular with the enrichment seen over orfs, there have been concerns in the past about regions with high expression resulting in false 'hyper-ChIP-ability' (Teytelman *et al.*, 2013). When the expression of telomeric genes and sub-telomeric genes are compared to Tlo1 enrichment in our data, there is a mix of expression levels and enrichment levels suggesting that this at least, is not a hyper-ChIP-able region. In addition, a stringent cutoff (Ringo Peak Score > 0.9) was applied to the data prior to any significance analyses. As well as this, other methods of reducing false positives (e.g. high background threshold, etc.) were applied so as to ensure reliable results. Such stringency may lead to exclusion of some regions of minor Tlo1 enrichment, however this was preferable to false positive discovery.

6.4.4. Other remarks

As discussed in Chapter 1, our hypothesis is that Tlos form part of the Mediator complex in *C. albicans* and *C. dubliniensis*. This hypothesis fits with the overall enrichment patterns of Tlo1 in the current ChIP dataset. Mediator is an integral part of the RNA Polymerase II-central transcriptional machinery in eukaryotes and as such, is associated with coding regions. This has been demonstrated by ChIP experiments in *S. cerevisiae* (Zhu *et al.*, 2006) and correlates to the observations in this study. In addition, a central hallmark of the ChIP data presented here is the extent of enrichment over the entire genome, including large peaks and troughs spread almost periodical in appearance over the chromosomes (Figure 6.4). A similar pattern of enrichment was observed by Zhu, *et al*, (2006), however unlike their findings, a bias for enrichment at the 5-prime end of genes could not be found in our data. Mediator was also shown to be directly associated with telomeres and is involved in the mediation of transcriptional activity in the region (Peng & Zhou, 2012; Zhu *et al.*, 2011). The enrichment patterns presented in this chapter also show association with telomeres

The pattern of Tlo1 interaction with DNA shown in this study is compatible with the pattern of Mediator-DNA interactions shown in studies in *S. cerevisiae*, further supporting the hypothesis that Tlos are components of the Mediator

complex in *C. dubliniensis*. During this project, a study by Zhang *et al* demonstrated that Tlo proteins co-purify with Mediator in *C. albicans* and are most likely part of the complex (Zhang *et al.*, 2012). Together, our data and the study of Zhang *et al.* (2012) present compelling evidence that Tlo proteins are components of Mediator that play a role in transcriptional regulation. This theory will be discussed further in Chapter 7.

Overall, ChIP has provided a significant overview of the relationship of Tlo1 with the genome in *C. dubliniensis*. Tlo1 is likely associated with Mediator and this relationship may account for many of the enrichment patterns observed in this study. The finding that Tlo1 enrichment is associated with altered expression following deletion of the *TLO* genes indicates a role for Tlos in transcriptional regulation, whether through Mediator interactions or as an independent activator/repressor. Further to this, there probably exists a population of 'Free Tlo' as described by Zhang *et al.*, (2012) which may be involved in regulation and could contribute to other enrichment patterns observed in this study.

Chapter 7

General Discussion

7.1. General Discussion

At the outset of this study, the *TLO*s presented as an intriguing family of genes, whose expansion in *Candida albicans* compared to *Candida dubliniensis* perhaps suggested a role in explaining the dichotomy in virulence between these two closely related species. As the study developed and the functions of the *TLOs* became evident, it became clear that they were involved in regulating a range of phenotypes and were part of the core transcriptional machinery of *Candida* species.

As mentioned in Chapter One, *C. albicans* possesses 14 *TLO* genes (and 1 pseudogene), whereas its close relative *C. dubliniensis* possesses only two. Previous attempts at disrupting *TLO* genes in *C. albicans* have proven difficult (Personal Communication, Anderson, 2012) and it is likely that given the high identity amongst the *C. albicans TLO*s that there may be some functional overlap, meaning that creation of a null mutant would require 15 separate diploid gene deletions. The two *TLO* gene copies in *C. dubliniensis* however presented a more manageable background in which to create a *TLO* null mutant, and are much more divergent from each other at the nucleotide sequence level than the *C. albicans* family and as such, substantial functional overlap was less likely. However, the level of similarity with the *C. albicans TLOs* is high enough that one could infer from our data on the general *TLO* functions in *C. albicans*. These aspects made *C. dubliniensis* the ideal primary candidate for studies into the *TLO* gene family.

*TLO*s affect a variety of important phenotypes and regulatory networks

Upon successful disruption and characterisation of the *TLO* genes themselves, a plethora of phenotypic assays were used to explore the effects of *TLO* deletion on *C. dubliniensis*. One of the main phenotypes of the *TLO* mutants was the defect in the morphological switch from yeast to true hyphae. This process has been repeatedly implicated in virulence, nutrient acquisition, biofilm formation and immune evasion (Sudbery, 2011). *C. dubliniensis* does not form hyphae as efficiently and robustly as *C. albicans*, but under appropriate conditions wild-type *C. dubliniensis* can form hyphae in 90 % of cells by approximately 3 h. Disruption of the *TLO*s severely affected this ability – when both *TLO*s were deleted, *C. dubliniensis* maintained solely a pseudohyphal phenotype, regardless of

condition or induction time. Upon closer examination, these cells could not be separated even by mechanical means without rupturing the cell, suggesting a major defect in morphology. These observations were further validated in the DNA microarray studies, which pointed towards a major shift in the transcriptional landscape of the cell, particularly for genes associated with regulation of such filamentous growth programmes. Reduced expression levels of major regulators of associated processes such as *EFG1* and *UME6*, which are integral to the hyphal formation process were observed. Other morphological defects brought about by the deletion of *TLO*s included an inability to form chlamydospores and decreased colony size on solid media.

As well as effects on filamentation, *C. dubliniensis tlo* mutants were defective in their ability to grow under certain oxidative and osmotic stressors. Cell wall stress also proved to affect the growth of *tlo* mutants more than in the wild-type. As with the filamentous phenotype, many of the genes involved in these responses to stress showed altered gene expression patterns in the Δ*Δtlo*. Nutrient acquisition and utilisation in *C. dubliniensis* was affected similarly. In particular, utilisation of galactose as a primary carbon source was greatly reduced in the *tlo* mutants compared to the wild-type, displaying a significantly slower growth rate. This was confirmed by the defective expression of a number of genes involved in the galactose degradation pathway.

From these observations, it is clear that the *TLO*s are involved in regulation of multiple processes. The processes mentioned are particularly relevant to virulence and general metabolism, two vital functional networks in *Candida* species. As mentioned briefly above, deletion of the *TLO* genes in *C. dubliniensis* led to significant changes in the transcriptional landscape. Of the roughly 5,800 genes annotated in *C. dubliniensis* (Jackson *et al.*, 2009), 53% of these showed a statistically significant change in expression (25 % UP, 28 % DOWN) in the *tlo* mutant compared to wild-type during early growth in water with 10 % (w/v) serum (WS). Likewise, later growth in WS was associated with a change in 44 % of all genes (22 % UP, 22 % DOWN). A total of 28 % of genes showed a change during mid-exponential growth in favourable, nutrient-rich conditions (15 % UP, 13 % DOWN). With such high numbers of positively and negatively regulated genes, it appears as if the *TLO*s are both positive and negative regulators of transcription on a global, genome-wide level. In addition to this, several key regulators of phenotypes showed paradoxical effects in expression upon *TLO*

disruption (e.g. *EED1*) which further suggests both positive and negative regulatory effects of *TLO* expression.

Interestingly, it was observed in the microarray data that many of genes that exhibited defective induction in the *tlo* mutant in response to serum did actually exhibit low levels of induction over the course of the serum exposure time-course (1-3 h). Experiments using qRT-PCR (Figures 5.5. – 5.7.) also demonstrated this phenomenon and suggest that fast/optimal induction of certain genes (e.g. *HWP1*) may be dependent on Tlo function. Further expression analysis time-courses should be carried out to fully ascertain this perceived function.

This study has provided evidence that Tlo functions may be gene-specific, as the effects of *TLO* deletions on phenotypes are not always comparable. For example, deletion of *TLO2* had no effect on hyphal formation, whereas *TLO1* deletion caused a partially disrupted phenotype. This suggested that *TLO1* was more important than *TLO2* in regulating this this process. However, following deletion of *TLO1*, the remaining *TLO2* gene was able to maintain hyphal formation, but at a reduced level, supporting the hypothesis that *TLO1* was more effective at stimulating hyphal growth. Re-introduction of *TLO1* in the *tlo* mutant was better at restoring phenotypes in this background (for example morphogenesis) than complementation with *TLO2*. This contrasting relationship between *TLO*s became clearer when global expression patterns of strains complemented with either *TLO1* or *TLO2* were compared. These experiments, which are ongoing, identified different key processes which were exclusive to one or the other of the *TLO*s (Personal Communication, Boyle, 2013). Re-introduction of *TLO1* or *TLO2* resulted in a change in expression in overlapping and distinct subsets of genes. *TLO1* was largely better at restoration to wild-type levels of expression of filamentous growth genes and galactose utilisation genes (e.g. *GAL* genes) while *TLO2* restored repression of some starvation responses and activation of *HWP1*. While there was much overlap in genes affected, the data show, in conjunction with phenotypic differences, that *TLO1* and *TLO2* can regulate distinct processes.

Despite these differences, *TLO1* was associated with more phenotypes and gene expression changes. This may be due to the functional diversity mentioned above, but also could be due to differences in the expression levels of *TLO1* and *TLO2*. qRT-PCR has demonstrated that *TLO2* mRNA is expressed at considerably lower levels than *TLO1* mRNA in most conditions tested. The only point at which

they reach almost equivalent levels is in the late stationary phase of growth. With less mRNA, a reduced abundance of Tlo2 compared to Tlo1 protein may explain the difference in function. However, re-introduction of *TLO2* on pCDRI results in higher expression levels than the *TLO2* native locus (preliminary experiments, data not shown). Interestingly, in these complementation experiments, where both *TLO1* and *TLO2* are expressed from pCDRI, both genes exhibited comparable mRNA levels, yet differed in their ability to complement the mutant phenotypes, suggesting functional differences between both proteins.

Upon closer examination of the *TLO* loci in *C. dubliniensis* Wü284, it was found that there were two allelic copies of *TLO1* but only one allele of *TLO2*. As such, the lesser effects and phenotypes (including expression) associated with *TLO2* may be due to the single effective copy in Wü284. Future experiments should be carried out amongst *C. dubliniensis* strains and isotypes to determine if this *TLO2* defect is exclusive to Wü284. If *TLO2* is intact in other strains, experiments to identify any phenotypes associated with *TLO2* should be carried out.

_TLO_s regulate through association with DNA

This study contained the first example of Tlo-ChIP in the literature. In fact, ChIP-chip of *C. dubliniensis* has not been carried out prior to this study. As such, many of the experiments contained herein were involved in establishing and optimising a protocol for later use. Secondary cross-linking with DMA was carried out in addition to formalin fixation to ensure proper fixing of complete protein complexes and chromatin structure to increase the chances of pulling down any complexes Tlo1 was associated with. Tlo1-ChIP provided proof of concept that ChIP of Tlos was possible. Tlo1 was found to be enriched along all chromosomes and mostly within genes. Due to the lack of a proper negative control (little was known about Tlo1 affinity for particular regions), stringent controls were put in place in order to reduce any false positives. Despite this, Tlo1 was found to be enriched across genes displaying a range of expression levels. Correlation of changes in expression in the *tlo* mutant compared with the enrichment patterns of Tlo1 further suggested a role for Tlos in the regulation of transcription. The high number of enriched regions might suggest that Tlo regulation is due to specific interaction with these orfs.

In addition to orfs, very significant enrichment was observed at telomeres, sub-telomeres and over the Major Repeat Sequence (MRS). The MRS remains relatively uncharacterised but is primarily thought to be a 'hotspot' for chromosomal rearrangement, loss and translocation events and may be involved in chromosomal length polymorphisms (Chibana & Magee, 2009; Lephart *et al.*, 2005). This may mean that *TLO*s are involved in regulation of one of these processes, but this is purely speculative and would need to be explored with further experiments, perhaps by in-depth longitudinal examination of karyotype changes in *tlo* mutants.

Tlo proteins are components of the Mediator complex

Of particular interest in the Tlo1-ChIP data, was the incidence of Tlo1 enrichment over the telomeres and sub-telomeric regions. These regions are important in heterochromatin maintenance and therefore global gene regulation (Peng & Zhou, 2012). Tlo1 appears to bind consistently over these regions, which is quite similar to enrichment patterns observed in Mediator-ChIP carried out in *S. cerevisiae* (Andrau *et al.*, 2006). While Tlo1 may be solely involved in these processes, it is far more likely that this binding is as a result of its association with the Mediator complex.

As described in Chapter One, early studies of the *TLO* gene family in *C. albicans*, which at the time were annotated as the *CTA* genes, described the presence of a Med2-like domain showing homology to the Med2 protein subunit of the Mediator complex of *S. cerevisiae* (Bourbon, 2008). In fact, there was no identified homolog of Med2 in either C. *albicans* or *C. dubliniensis*. Building on this in the present study, bioinformatics methods were used to confirm this homology with further evidence suggesting that the Tlo proteins in *C. dubliniensis* as well as in *C. albicans* were similar to the Med2 protein in *S. cerevisiae*. In addition, predictive analysis described similarity to other Med2 proteins across the *Saccharomycetaceae*.

Experimental evidence throughout this study has clearly shown a relationship between the *TLO*s and regulation of expression of a multitude of genes and processes. The expression of *TLO*s, in particular *TLO1*, is necessary for the proper filamentous phenotype commonly observed in *C. dubliniensis*, as well as for the response to external stresses such as oxidative stress and

uptake/utilisation of alternate nutrient sources. As such, it was hypothesised that the *TLO*s were a family of transcription factors. However, no putative DNA-binding sequence could be found *in silico,* nor could a consensus-binding motif be found based on Tlo1-ChIP enrichment patterns. Despite this, basic localisation studies with Tlo1-Gfp suggested that these proteins localise to the nucleus, a common trait of transcription factors (Li *et al.*, 2007). In essence, the *TLO*s and their encoded proteins have many hallmarks pointing towards their role as transcription factors but little or no evidence to suggest a direct binding of "free" Tlo1 to DNA. Instead, it is likely that much of the enrichment observed in the Tlo1-ChIP was a result of the association with the Mediator complex. The global enrichment of Tlo1 observed in this study was another hallmark of a Mediator ChIP and very similar to previously published Mediator pull-down experiments (Zhu *et al.*, 2006). Preliminary studies in this laboratory (unpublished) have shown that deletion of a tail subunit in Mediator (Med3) in *C. dubliniensis* gives rise to similar phenotypes as those observed in a double *tlo* mutant, further supporting a relationship between Tlos and the Mediator complex. As well as this, Tlos in *C. albicans* were reported to pull down with Mediator tail subunit (Zhang *et al.*, 2012), adding further weight to the evidence from this study that the Tlos are part of Mediator. Several virulence phenotypes associated with *Candida* spp. have been shown to be regulated by the Mediator complex, including filamentation and the formation of biofilms (Uwamahoro *et al.*, 2012), again adding further evidence to a common Tlo-Mediator function.

The evolution of *TLO*s in *C. dubliniensis*

From the data presented in this study, it is clear that the *TLO*s in *C. dubliniensis* have evolved to regulate multiple important processes such as virulence, stress response and growth, most likely through association with the Mediator complex. However, the presence of a considerably expanded family of *TLO*s in *C. albicans* compared to *C. dubliniensis* raises the question of possible evolutionary advantages of expressing *TLO*s. Evidence from this study (and ongoing work in our laboratory) points towards a functional relationship with the tail region of the Mediator (Figure 1.2). The Mediator plays a vital role in mediating rapid transcriptional changes, particularly in response to environmental signals (Uwamahoro *et al.*, 2014).

In conjunction with recently published data by (Zhang *et al.*, 2012), our bioinformatic analysis and Tlo1 enrichment patterns across all chromosomes and within orfs strongly supports the hypothesis that Tlos may exist as part of the Mediator, specifically the tail subunit (Figure 1.2). Moreover, many of the processes that Tlos are involved in regulating are those that require rapid induction under specific conditions. Expression data in this study shows that in the absence of *TLO*s, this quick induction is often not possible (*e.g. GAL* genes, *UME6*, etc.). As such, it is likely that a main function of the Tlos is to act with the Mediator to encourage rapid induction or expression of genes. Moreover, separate to this study, the tail subunit of the Mediator has been implicated in the regulation of stress response and virulence-associated phenotypes (Fan & Struhl, 2009; Miller *et al.*, 2012; Uwamahoro *et al.*, 2012).

Interestingly, (Zhang *et al.*, 2012) reported that as well as the significant amount of Tlo associated with the Mediator, this did not account for all cellular Tlo. Therefore, there must exist some 'free-Tlo', which is not associated with Mediator. It is possible that there may be an evolutionary advantage to having Tlo in excess, perhaps to ensure that there are sufficient intracellular levels of the proteins in readiness for when they are needed for adequate induction of expression. This might mean that the Tlos are required for adequate environmental adaptation, a trait that certainly fits with the phenotypic defects observed upon *TLO* disruption (reduced growth, poor stress adaptation, reduced filamentation). On the other hand, it could be that the Tlos can act as transcriptional regulators on their own. Likewise, it could be that the Tlos are

involved in heterochromatin maintenance and modeling (as evidenced by telomere and repeat binding) or in translocation events (as mediated from within the MRS). Both of these scenarios would mean that Tlos play an important role in the epigenetics of the organism, at a much higher order than direct gene activation or repression.

The true function of the *TLO* genes may include all of the above (and more that have yet to be elucidated). This allows the proposal of several possible methods by which Tlos exert an effect on the genome (Figure 7.1. A-D) – a) through activation of gene expression (e.g. *UME6, GAL* genes), (b) through repression of gene expression (e.g. glyoxylate cycle, *NAG* genes,), (c) through association with telomeres thereby exerting epigenetic control over the sub-telomeres and (d) through association with hotspots of chromosomal rearrangement (e.g. the MRS) thereby mediating karyotype variations. Expansion of 14 *TLO* genes (plus one pseudogene) across all chromosomes in *C. albicans*, compared to only 2 in *C. dubliniensis* (from the ancestral *TLO* on chromosome R) strongly suggests that acquisition of multiple *TLO*s is advantageous. Fitting with the proposed function as Mediator subunits, this would mean that more Tlos may allow the organism to rapidly effect regulation of different genes under specific conditions, as evidenced in the different abilities of *C. dubliniensis TLO*s to affect various phenotypes. It might be the case that each Tlo has overlap in function, but it may also hold true that each one has evolved a unique subset of regulatory processes to control. This type of regulation would certainly be advantageous for *C. albicans*, which is known as a superior pathogen and is better at adapting to environmental stresses than *C. dubliniensis*.

The *TLO*s have evolved to regulate important processes in *Candida* species and this study has suggested major roles for this gene family in shaping the global transcriptional response of the cell under many conditions. As such, future investigations into the *TLO* gene family may allow a better understanding of the evolution of *Candida albicans* as a flexible commensal and opportunistic pathogen relative to its less widely encountered relative *Candida dubliniensis*.

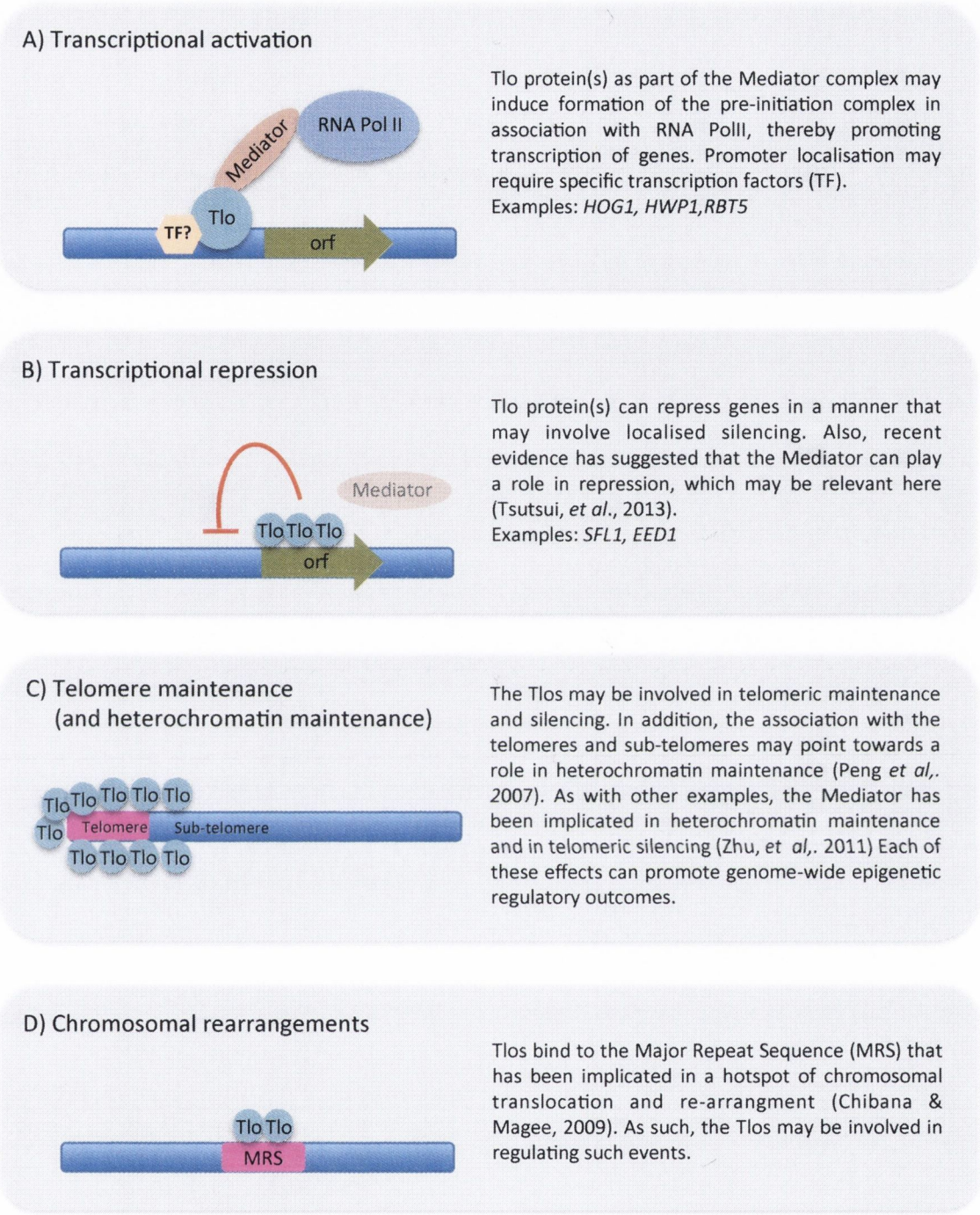

Figure 7.1. Proposed models of Tlo-mediated regulation.

Each model is further explained on the right. Illustrations are simplified representations and do not reflect true scale nor the many other effectors involved in relation of these processes.

References

Akpan, A. & Morgan, R. (2002). Oral candidiasis. *Postgrad Med J* **78**, 455–9.

Almeida, R. S., Wilson, D. & Hube, B. (2009). *Candida albicans* iron acquisition within the host. *FEMS Yeast Res* **9**, 1000–12.

Alonso-Monge, R., Navarro-García, F., Molero, G., Diez-Orejas, R., Gustin, M., Pla, J., Sánchez, M. & Nombela, C. (1999). Role of the mitogen-activated protein kinase Hog1p in morphogenesis and virulence of *Candida albicans*. *J Bacteriol* **181**, 3058–68.

Alothman, A. F., Al-Musawi, T., Al-Abdely, H. M., Salman, J. Al, Almaslamani, M., Yared, N., Butt, A. A., Raghubir, N., Morsi, W. El & Al Thaqafi, A. O. (2014). Clinical practice guidelines for the management of invasive *Candida* infections in adults in the Middle East region: Expert panel recommendations. *J Infect Public Health* **7**, 6–19. Elsevier.

Anderson, M. Z. (2012). Personal Communication. Minneapolis, MN.

Anderson, M. Z., Baller, J. A., Dulmage, K., Wigen, L. & Berman, J. (2012). The three clades of the telomere-associated TLO gene family of *Candida albicans* have different splicing, localization, and expression features. *Eukaryot Cell* **11**, 1268–75.

Andrau, J.-C., van de Pasch, L., Lijnzaad, P., Bijma, T., Koerkamp, M. G., van de Peppel, J., Werner, M. & Holstege, F. C. P. (2006). Genome-wide location of the coactivator mediator: Binding without activation and transient Cdk8 interaction on DNA. *Mol Cell* **22**, 179–92.

Ansari, S. A. & Morse, R. H. (2013). Mechanisms of Mediator complex action in transcriptional activation. *Cell Mol Life Sci* **70**, 2743–56.

Ansari, S. A., Ganapathi, M., Benschop, J. J., Holstege, F. C. P., Wade, J. T. & Morse, R. H. (2012). Distinct role of Mediator tail module in regulation of SAGA-dependent, TATA-containing genes in yeast. *EMBO J* **31**, 44–57.

Ansari, S. A., Paul, E., Sommer, S., Lieleg, C., He, Q., Daly, A. Z., Rode, K. A., Barber, W. T., Ellis, L. C. & other authors. (2014). Mediator, TATA-binding protein, and RNA polymerase II contribute to low histone occupancy at active gene promoters in yeast. *J Biol Chem* **289**, 14981–95.

Ardon, O., Nudelman, R., Caris, C., Libman, J., Shanzer, A., Chen, Y. & Hadar, Y. (1998). Iron Uptake in Ustilago maydis: Tracking the Iron Path. *J Bacteriol* **180**, 2021–2026.

Arnaud, M. B., Costanzo, M. C., Skrzypek, M. S., Binkley, G., Lane, C., Miyasato, S. R. & Sherlock, G. (2005). The *Candida* Genome Database (CGD), a community resource for *Candida albicans* gene and protein information. *Nucleic Acids Res* **33**.

Arnaud, M. B., Costanzo, M. C., Shah, P., Skrzypek, M. S. & Sherlock, G. (2009). Gene Ontology and the annotation of pathogen genomes: the case of *Candida albicans*. *Trends Microbiol*.

Asmundsdóttir, L. R., Erlendsdóttir, H., Agnarsson, B. A. & Gottfredsson, M. (2009). The importance of strain variation in virulence of *Candida dubliniensis* and *Candida albicans*: results of a blinded histopathological study of invasive candidiasis. *Clin Microbiol Infect* **15**, 576–85.

Bachewich, C. & Whiteway, M. (2005). Cyclin Cln3p links G1 progression to hyphal and pseudohyphal development in *Candida albicans*. *Eukaryot Cell* **4**, 95–102.

Baek, Y.-U., Li, M. & Davis, D. A. (2008). *Candida albicans* ferric reductases are differentially regulated in response to distinct forms of iron limitation by the Rim101 and CBF transcription factors. *Eukaryot Cell* **7**, 1168–79.

Bagshaw, H. (2010). *Personal Communication*. Dublin, Ireland.

Banerjee, M., Uppuluri, P., Zhao, X. R., Carlisle, P. L., Vipulanandan, G., Villar, C. C., López-Ribot, J. L. & Kadosh, D. (2013). Expression of UME6, a key regulator of *Candida albicans* hyphal development, enhances biofilm formation via Hgc1- and Sun41-dependent mechanisms. *Eukaryot Cell* **12**, 224–32.

Bassetti, M., Righi, E., Costa, A., Fasce, R., Molinari, M. P., Rosso, R., Pallavicini, F. B. & Viscoli, C. (2006). Epidemiological trends in nosocomial candidemia in intensive care. *BMC Infect Dis* **6**, 21.

Beissbarth, T., Ruschhaupt, M., Jackson, D., Lawerenz, C. & Mansmann, U. (2005). Recommendations for normalization of microarray data. *Natl Genome Res Newtork Recomm*.

Bensadoun, R.-J., Patton, L. L., Lalla, R. V & Epstein, J. B. (2011). Oropharyngeal candidiasis in head and neck cancer patients treated with radiation: update 2011. *Support Care Cancer* **19**, 737–44.

Bensen, E. S., Martin, S. J., Li, M., Berman, J. & Davis, D. A. (2004). Transcriptional profiling in *Candida albicans* reveals new adaptive responses to extracellular pH and functions for Rim101p. *Mol Microbiol* **54**, 1335–51.

Berger, J. A., Hautaniemi, S., Järvinen, A.-K., Edgren, H., Mitra, S. K. & Astola, J. (2004). Optimized LOWESS normalization parameter selection for DNA microarray data. *BMC Bioinformatics* **5**, 194.

Berman, J. (2006). Morphogenesis and cell cycle progression in *Candida albicans*. *Curr Opin Microbiol* **9**, 595–601.

Berman, J. & Sudbery, P. E. (2002). *Candida* Albicans: a molecular revolution built on lessons from budding yeast. *Nat Rev Genet* **3**, 918–30.

Betley, J. N., Frith, M. C., Graber, J. H., Choo, S. & Deshler, J. O. (2002). A ubiquitous and conserved signal for RNA localization in chordates. *Curr Biol* **12**, 1756–61.

Bianchi, A. & Shore, D. (2007). Early replication of short telomeres in budding yeast. *Cell* **128**, 1051–62.

Biosystems, A. (2011). *SYBR® Green Handbook*. Carslbad, California.

Bondaryk, M., Kurzątkowski, W. & Staniszewska, M. (2013). Antifungal agents commonly used in the superficial and mucosal candidiasis treatment: mode of action and resistance development. *Postępy dermatologii i Alergol* **30**, 293–301.

Bonhomme, J. & d'Enfert, C. (2013). *Candida albicans* biofilms: building a heterogeneous, drug-tolerant environment. *Curr Opin Microbiol* **16**, 398–403.

Bourbon, H.-M. (2008). Comparative genomics supports a deep evolutionary origin for the large, four-module transcriptional mediator complex. *Nucleic Acids Res* **36**, 3993–4008.

Bourbon, H.-M., Aguilera, A., Ansari, A. Z., Asturias, F. J., Berk, A. J., Bjorklund, S., Blackwell, T. K., Borggrefe, T., Carey, M. & other authors. (2004). A unified nomenclature for protein subunits of mediator complexes linking transcriptional regulators to RNA polymerase II. *Mol Cell* **14**, 553–7.

Boyle, H. (2013). *Personal Communication*. Dublin, Ireland.

Brand, A. (2012). Hyphal growth in human fungal pathogens and its role in virulence. *Int J Microbiol* **2012**, 517529.

Braun, B. R., Head, W. S., Wang, M. X. & Johnson, A. D. (2000). Identification and characterization of TUP1-regulated genes in *Candida albicans*. *Genetics* **156**, 31–44.

Brown, A. J. P., Budge, S., Kaloriti, D., Tillmann, A., Jacobsen, M. D., Yin, Z., Ene, I. V, Bohovych, I., Sandai, D. & other authors. (2014). Stress adaptation in a pathogenic fungus. *J Exp Biol* **217**, 144–55.

Brown, V., Sabina, J. & Johnston, M. (2009). Specialized sugar sensing in diverse fungi. *Curr Biol* **19**, 436–41.

Bustin, S. A., Benes, V., Garson, J. A., Hellemans, J., Huggett, J., Kubista, M., Mueller, R., Nolan, T., Pfaffl, M. W. & other authors. (2009). The MIQE guidelines: minimum information for publication of quantitative real-time PCR experiments. *Clin Chem* **55**, 611–22.

Calderone, R. A. & Fonzi, W. A. (2001). Virulence factors of *Candida albicans*. *Trends Microbiol* **9**, 327–35.

Calera, J. A., Herman, D. & Calderone, R. (2000). Identification of YPD1, a gene of *Candida albicans* which encodes a two-component phosphohistidine intermediate protein. *Yeast* **16**, 1053–9.

Campanha, N. H., Neppelenbroek, K. H., Spolidorio, D. M. P., Spolidorio, L. C. & Pavarina, A. C. (2005). Phenotypic methods and commercial systems for the discrimination between C. *albicans* and C. *dubliniensis*. *Oral Dis* **11**, 392–8.

Cannon, R. D., Lamping, E., Holmes, A. R., Niimi, K., Baret, P. V, Keniya, M. V, Tanabe, K., Niimi, M., Goffeau, A. & Monk, B. C. (2009). Efflux-mediated antifungal drug resistance. *Clin Microbiol Rev* **22**, 291–321, Table of Contents.

Cassola, A., Parrot, M., Silberstein, S., Magee, B. B., Passeron, S., Giasson, L. & Cantore, M. L. (2004). *Candida albicans* lacking the gene encoding the regulatory subunit of protein kinase A displays a defect in hyphal formation and an altered localization of the catalytic subunit. *Eukaryot Cell* **3**, 190–9.

Cassone, A. (2014). Vulvovaginal *Candida albicans* infections: pathogenesis, immunity and vaccine prospects. *BJOG*.

Cassone, A. & Cauda, R. (2012). *Candida* and candidiasis in HIV-infected patients: where commensalism, opportunistic behavior and frank pathogenicity lose their borders. *AIDS* **26**, 1457–72.

Chambers, J. M. (2014). Object-Oriented Programming, Functional Programming and R. *Stat Sci* **29**, 167–180. Institute of Mathematical Statistics.

Charlier, C., Hart, E., Lefort, A., Ribaud, P., Dromer, F., Denning, D. W. & Lortholary, O. (2006). Fluconazole for the management of invasive candidiasis: where do we stand after 15 years? *J Antimicrob Chemother* **57**, 384–410.

Cheetham, J., MacCallum, D. M., Doris, K. S., da Silva Dantas, A., Scorfield, S., Odds, F., Smith, D. A. & Quinn, J. (2011). MAPKKK-independent regulation of the Hog1 stress-activated protein kinase in *Candida albicans*. *J Biol Chem* **286**, 42002–16.

Chen, J. L., Blasco, M. A. & Greider, C. W. (2000). Secondary structure of vertebrate telomerase RNA. *Cell* **100**, 503–14.

Chibana, H. & Magee, P. T. (2009). The enigma of the major repeat sequence of *Candida albicans*. *Future Microbiol* **4**, 171–9. Future Medicine London, UK.

Chico, L., Ciudad, T., Hsu, M., Lue, N. F. & Larriba, G. (2011). The *Candida albicans* Ku70 modulates telomere length and structure by regulating both telomerase and recombination. *PLoS One* **6**, e23732 (D. T. Kirkpatrick, Ed.). Public Library of Science.

Citiulo, F., Moran, G. P., Coleman, D. C. & Sullivan, D. J. (2009). Purification and germination of *Candida albicans* and *Candida dubliniensis* chlamydospores cultured in liquid media. *FEMS Yeast Res* **9**, 1051–60.

Citiulo, F., Jacobsen, I. D., Miramón, P., Schild, L., Brunke, S., Zipfel, P., Brock, M., Hube, B. & Wilson, D. (2012). *Candida albicans* scavenges host zinc via Pra1 during endothelial invasion. *PLoS Pathog* **8**, e1002777 (A. P. Mitchell, Ed.). Public Library of Science.

Coronado-Castellote, L. & Jiménez-Soriano, Y. (2013). Clinical and microbiological diagnosis of oral candidiasis. *J Clin Exp Dent* **5**, e279–e286.

Coulthwaite, L. & Verran, J. (2007). Potential pathogenic aspects of denture plaque. *Br J Biomed Sci* **64**, 180–9.

Cuéllar-Cruz, M., López-Romero, E., Villagómez-Castro, J. C. & Ruiz-Baca, E. (2012). *Candida* species: new insights into biofilm formation. *Future Microbiol* **7**, 755–71.

Daher, J. Y., Koussa, J., Younes, S. & Khalaf, R. A. (2011). The *Candida albicans* Dse1 Protein Is Essential and Plays a Role in Cell Wall Rigidity, Biofilm Formation, and Virulence. *Interdiscip Perspect Infect Dis* **2011**, 504280.

Danilova, N. (2008). Evolution of the Human Immune System. In *Encylopedia life Sci*. Chichester, UK: John Wiley & Sons, Ltd.

Day, D. S., Luquette, L. J., Park, P. J. & Kharchenko, P. V. (2010). Estimating enrichment of repetitive elements from high-throughput sequence data. *Genome Biol* **11**, R69.

Delaloye, J. & Calandra, T. (2014). Invasive candidiasis as a cause of sepsis in the critically ill patient. *Virulence* **5**, 161–9.

Dixon, D. M. & Walsh, T. J. (1996). Antifungal Agents. In *Med Microbiol 4th Ed*, 4th edn. Edited by S. Baron. Galveston, TX: University of Texas Medical Branch at Galveston.

Donnelly, S. M., Sullivan, D. J., Shanley, D. B. & Coleman, D. C. (1999). Phylogenetic analysis and rapid identification of *Candida dubliniensis* based on analysis of ACT1 intron and exon sequences. *Microbiology* **145 (Pt 8**, 1871–82.

Dorko, E., Baranová, Z., Jenča, A., Kizek, P., Pilipčinec, E. & Tkáčiková, L. (2005). Diabetes mellitus and candidiases. *Folia Microbiol (Praha)* **50**, 255–261.

Eck, R., Hundt, S., Härtl, A., Roemer, E. & Künkel, W. (1999). A multicopper oxidase gene from *Candida albicans*: cloning, characterization and disruption. *Microbiology* **145 (Pt 9**, 2415–22.

Ernst, O. & Zor, T. (2010). Linearization of the bradford protein assay. *J Vis Exp*.

Evans, D. M., Frazer, I. H. & Martin, N. G. (1999). Genetic and environmental causes of variation in basal levels of blood cells. *Twin Res* **2**, 250–7.

Falagas, M. E., Roussos, N. & Vardakas, K. Z. (2010). Relative frequency of *albicans* and the various non-*albicans Candida* spp among candidemia isolates from inpatients in various parts of the world: a systematic review. *Int J Infect Dis* **14**, e954–66.

Fan, X. & Struhl, K. (2009). Where does mediator bind in vivo? *PLoS One* **4**, e5029.

Fang, F. C. (2004). Antimicrobial reactive oxygen and nitrogen species: concepts and controversies. *Nat Rev Microbiol* **2**, 820–32.

Fanning, S. & Mitchell, A. P. (2012). Fungal biofilms. *PLoS Pathog* **8**, e1002585 (J. Heitman, Ed.). Public Library of Science.

Farah, C. S., Lynch, N. & McCullough, M. J. (2010). Oral fungal infections: an update for the general practitioner. *Aust Dent J* **55 Suppl 1**, 48–54.

Fathilah, A. R., Himratul-Aznita, W. H., Fatheen, A. R. N. & Suriani, K. R. (2012). The antifungal properties of chlorhexidine digluconate and cetylpyrinidinium chloride on oral *Candida*. *J Dent* **40**, 609–15.

Finn, R. D., Bateman, A., Clements, J., Coggill, P., Eberhardt, R. Y., Eddy, S. R., Heger, A., Hetherington, K., Holm, L. & other authors. (2014). Pfam: the protein families database. *Nucleic Acids Res* **42**, D222–30.

Firon, A., Aubert, S., Iraqui, I., Guadagnini, S., Goyard, S., Prévost, M.-C., Janbon, G. & d'Enfert, C. (2007). The SUN41 and SUN42 genes are essential for cell separation in *Candida albicans*. *Mol Microbiol* **66**, 1256–75.

Fischer, G. (2012). Chronic vulvovaginal candidiasis: what we know and what we have yet to learn. *Australas J Dermatol* **53**, 247–54.

Fleischmann, R., Adams, M., White, O., Clayton, R., Kirkness, E., Kerlavage, A., Bult, C., Tomb, J., Dougherty, B. & other authors. (1995). Whole-genome random sequencing and assembly of Haemophilus influenzae Rd. *Science (80-)* **269**, 496–512.

Fleming, A. B., Beggs, S., Church, M., Tsukihashi, Y. & Pennings, S. (2014). The yeast Cyc8-Tup1 complex cooperates with Hda1p and Rpd3p histone deacetylases to robustly repress transcription of the subtelomeric FLO1 gene. *Biochim Biophys Acta*.

Forche, A., Abbey, D., Pisithkul, T., Weinzierl, M. A., Ringstrom, T., Bruck, D., Petersen, K. & Berman, J. (2011). Stress alters rates and types of loss of heterozygosity in *Candida albicans*. *MBio* **2**, e00129–11–.

Free, S. J. (2013). Fungal cell wall organization and biosynthesis. *Adv Genet* **81**, 33–82.

Fujita, T., Asano, Y., Ohtsuka, J., Takada, Y., Saito, K., Ohki, R. & Fujii, H. (2013). Identification of telomere-associated molecules by engineered DNA-binding molecule-mediated chromatin immunoprecipitation (enChIP). *Sci Rep* **3**, 3171.

Gantner, B. N., Simmons, R. M. & Underhill, D. M. (2005). Dectin-1 mediates macrophage recognition of *Candida albicans* yeast but not filaments. *EMBO J* **24**, 1277–86.

Geiger, J., Wessels, D., Lockhart, S. R. & Soll, D. R. (2004). Release of a potent polymorphonuclear leukocyte chemoattractant is regulated by white-opaque switching in *Candida albicans*. *Infect Immun* **72**, 667–77.

Gelis, S., de Groot, P. W. J., Castillo, L., Moragues, M.-D., Sentandreu, R., Gómez, M.-M. & Valentín, E. (2012). Pga13 in *Candida albicans* is localized in the cell wall and influences cell surface properties, morphogenesis and virulence. *Fungal Genet Biol* **49**, 322–31.

Gentleman, R. C., Carey, V. J., Bates, D. M., Bolstad, B., Dettling, M., Dudoit, S., Ellis, B., Gautier, L., Ge, Y. & other authors. (2004). Bioconductor: open software development for computational biology and bioinformatics. *Genome Biol* **5**, R80.

Giacometti, R., Souto, G., Silberstein, S., Giasson, L., Cantore, M. L. & Passeron, S. (2006). Expression levels and subcellular localization of Bcy1p in *Candida albicans* mutant strains devoid of one BCY1 allele results in a defective morphogenetic behavior. *Biochim Biophys Acta* **1763**, 64–72.

Gilfillan, G. D., Sullivan, D. J., Haynes, K., Parkinson, T., Coleman, D. C. & Gow, N. A. (1998). *Candida dubliniensis*: phylogeny and putative virulence factors. *Microbiology* **144 (Pt 4**, 829–38.

Gilmour, D. S. & Lis, J. T. (1985). In vivo interactions of RNA polymerase II with genes of Drosophila melanogaster. *Mol Cell Biol* **5**, 2009–18.

Goldberg, T., Hecht, M., Hamp, T., Karl, T., Yachdav, G., Ahmed, N., Altermann, U., Angerer, P., Ansorge, S. & other authors. (2014). LocTree3 prediction of localization. *Nucleic Acids Res* **42**, W350–5.

Gordon K, S. (2005). Bioinformatics and Computational Biology Solutions Using R and Bioconductor. In *Bioinforma Comput Biol Solut Using R Bioconductor*, Statistics for Biology and Health, pp. 397–420. Edited by R. Gentleman, V. J. Carey, W. Huber, R. A. Irizarry & S. Dudoit. New York, NY: Springer New York.

Gow, N. A. R. & Hube, B. (2012). Importance of the *Candida albicans* cell wall during commensalism and infection. *Curr Opin Microbiol* **15**, 406–12.

Gow, N. A. R., van de Veerdonk, F. L., Brown, A. J. P. & Netea, M. G. (2012). *Candida albicans* morphogenesis and host defence: discriminating invasion from colonization. *Nat Rev Microbiol* **10**, 112–22.

De Groot, P. W. J., Bader, O., de Boer, A. D., Weig, M. & Chauhan, N. (2013). Adhesins in human fungal pathogens: glue with plenty of stick. *Eukaryot Cell* **12**, 470–81.

Guan, B., Lei, J., Su, S., Chen, F., Duan, Z., Chen, Y., Gong, X., Li, H. & Jin, J. (2012). Absence of Yps7p, a putative glycosylphosphatidylinositol-linked aspartyl protease in Pichia pastoris, results in aberrant cell wall composition and increased osmotic stress resistance. *FEMS Yeast Res* **12**, 969–79.

Hall, R. A. & Gow, N. A. R. (2013). Mannosylation in *Candida albicans*: role in cell wall function and immune recognition. *Mol Microbiol* **90**, 1147–61.

Hallberg, M., Polozkov, G. V, Hu, G.-Z., Beve, J., Gustafsson, C. M., Ronne, H. & Björklund, S. (2004). Site-specific Srb10-dependent phosphorylation of the yeast Mediator subunit Med2 regulates gene expression from the 2-microm plasmid. *Proc Natl Acad Sci U S A* **101**, 3370–5.

Hartman, M. A. & Spudich, J. A. (2012). The myosin superfamily at a glance. *J Cell Sci* **125**, 1627–32.

Hawser, S. P. & Douglas, L. J. (1995). Resistance of *Candida albicans* biofilms to antifungal agents in vitro. *Antimicrob Agents Chemother* **39**, 2128–31.

Hernández, R., Nombela, C., Diez-Orejas, R. & Gil, C. (2004). Two-dimensional reference map of *Candida albicans* hyphal forms. *Proteomics* **4**, 374–82.

Hidalgo, J. A. & Vasquez, J. A. (2014). Candidiasis Treatment & Management.

Hiller, E., Zavrel, M., Hauser, N., Sohn, K., Burger-Kentischer, A., Lemuth, K. & Rupp, S. (2011). Adaptation, adhesion and invasion during interaction of *Candida albicans* with the host--focus on the function of cell wall proteins. *Int J Med Microbiol* **301**, 384–9.

Hohmann, S. (2002). Osmotic stress signaling and osmoadaptation in yeasts. *Microbiol Mol Biol Rev* **66**, 300–72.

Holden, H. M., Rayment, I. & Thoden, J. B. (2003). Structure and function of enzymes of the Leloir pathway for galactose metabolism. *J Biol Chem* **278**, 43885–8.

Van het Hoog, M., Rast, T. J., Martchenko, M., Grindle, S., Dignard, D., Hogues, H., Cuomo, C., Berriman, M., Scherer, S. & other authors. (2007). Assembly of the *Candida albicans* genome into sixteen supercontigs aligned on the eight chromosomes. *Genome Biol* **8**, R52.

Horák, J. (2013). Regulations of sugar transporters: insights from yeast. *Curr Genet* **59**, 1–31.

Howard, D. H. (1999). Acquisition, transport, and storage of iron by pathogenic fungi. *Clin Microbiol Rev* **12**, 394–404.

Huang, G., Yi, S., Sahni, N., Daniels, K. J., Srikantha, T. & Soll, D. R. (2010). N-acetylglucosamine induces white to opaque switching, a mating prerequisite in *Candida albicans*. *PLoS Pathog* **6**, e1000806 (C. M. Hull, Ed.). Public Library of Science.

Huang, S.-C., Burne, R. A. & Chen, Y.-Y. M. (2014). The pH-Dependent Expression of the Urease Operon in Streptococcus salivarius Is Mediated by CodY. *Appl Environ Microbiol* **80**, 5386–93.

Hube, B. (2004). From commensal to pathogen: stage- and tissue-specific gene expression of *Candida albicans*. *Curr Opin Microbiol* **7**, 336–41.

Huber, W., von Heydebreck, A., Sultmann, H., Poustka, A. & Vingron, M. (2002). Variance stabilization applied to microarray data calibration and to the quantification of differential expression. *Bioinformatics* **18**, S96–S104.

Inglis, D. O., Arnaud, M. B., Binkley, J., Shah, P., Skrzypek, M. S., Wymore, F., Binkley, G., Miyasato, S. R., Simison, M. & Sherlock, G. (2012). The *Candida* genome database incorporates multiple *Candida* species: multispecies search and analysis tools with curated gene and protein information for *Candida albicans* and *Candida* glabrata. *Nucleic Acids Res* **40**, D667–74.

Jabra-Rizk, M. A., Falkler, W. A. & Meiller, T. F. (2004). Fungal biofilms and drug resistance. *Emerg Infect Dis* **10**, 14–9.

Jackson, A. P., Gamble, J. A., Yeomans, T., Moran, G. P., Saunders, D., Harris, D., Aslett, M., Barrell, J. F., Butler, G. & other authors. (2009). Comparative genomics of the fungal pathogens *Candida dubliniensis* and *Candida albicans*. *Genome Res* **19**, 2231–44.

Janeway, C. A., Travers, P., Walport, M. & Shlomchik, M. (2001). Evolution of the innate immune system. In *Immunobiol 5 immunes Syst Heal Dis*, 5th edn. Garland Science.

Kaiser, B., Munder, T., Saluz, H. P., Kunkel, W. & Eck, R. (1999). Identification of a gene encoding the pyruvate decarboxylase gene regulator CaPdc2p from *Candida albicans*. *Yeast* **15**, 585–591.

Kaján, L., Yachdav, G., Vicedo, E., Steinegger, M., Mirdita, M., Angermüller, C., Böhm, A., Domke, S., Ertl, J. & other authors. (2013). Cloud prediction of protein structure and function with PredictProtein for Debian. *Biomed Res Int* **2013**, 398968.

Kakuta, K., Orino, K., Yamamoto, S. & Watanabe, K. (1997). High levels of ferritin and its iron in fetal bovine serum. *Comp Biochem Physiol A Physiol* **118**, 165–9.

Kapuscinski, J. (1995). DAPI: a DNA-specific fluorescent probe. *Biotech Histochem* **70**, 220–33.

Kauffmann, A., Gentleman, R. & Huber, W. (2009). arrayQualityMetrics--a bioconductor package for quality assessment of microarray data. *Bioinformatics* **25**, 415–6.

Khan, Z. U., Ahmad, S., Mokaddas, E. & Chandy, R. (2004). Simplified sunflower (Helianthus annuus) seed agar for differentiation of *Candida dubliniensis* from *Candida albicans*. *Clin Microbiol Infect* **10**, 590–2.

Kibbler, C. ., Seaton, S., Barnes, R. ., Gransden, W. ., Holliman, R. ., Johnson, E. ., Perry, J. ., Sullivan, D. . & Wilson, J. . (2003). Management and outcome of bloodstream infections due to *Candida* species in England and Wales. *J Hosp Infect* **54**, 18–24. Elsevier.

Kim, J. & Sudbery, P. (2011). *Candida albicans*, a major human fungal pathogen. *J Microbiol* **49**, 171–7.

Kitada, T., Kuryan, B. G., Tran, N. N. H., Song, C., Xue, Y., Carey, M. & Grunstein, M. (2012). Mechanism for epigenetic variegation of gene expression at yeast telomeric heterochromatin. *Genes Dev* **26**, 2443–55.

Klein, R. S., Harris, C. A., Small, C. B., Moll, B., Lesser, M. & Friedland, G. H. (1984). Oral candidiasis in high-risk patients as the initial manifestation of the acquired immunodeficiency syndrome. *N Engl J Med* **311**, 354–358.

Koehler, P., Tacke, D. & Cornely, O. A. (2014). Our 2014 approach to candidaemia. *Mycoses* **57**, 581–3.

Kolecka, A., Zavrel, M., Hernandez-Barbado, R., Rupp, S. & Bujdakova, H. (2011). Biofilm formation and adhesive/invasive properties of *Candida dubliniensis* in comparison with *Candida albicans*. *Cent Eur J Biol* **6**, 893–901.

Kosman, D. J. (2003). Molecular mechanisms of iron uptake in fungi. *Mol Microbiol* **47**, 1185–97.

Kumar, M. J., Jamaluddin, M. S., Natarajan, K., Kaur, D. & Datta, A. (2000). The inducible N-acetylglucosamine catabolic pathway gene cluster in *Candida albicans*: discrete N-acetylglucosamine-inducible factors interact at the promoter of NAG1. *Proc Natl Acad Sci U S A* **97**, 14218–23.

Kurdistani, S. K. & Grunstein, M. (2003). In vivo protein-protein and protein-DNA crosslinking for genomewide binding microarray. *Methods* **31**, 90–5.

Lackey, E., Vipulanandan, G., Childers, D. S. & Kadosh, D. (2013). Comparative evolution of morphological regulatory functions in *Candida* species. *Eukaryot Cell* **12**, 1356–68.

Laffey, S. F. & Butler, G. (2005). Phenotype switching affects biofilm formation by *Candida* parapsilosis. *Microbiology* **151**, 1073–81.

Lamarre, C., Deslauriers, N. & Bourbonnais, Y. (2000). Expression cloning of the *Candida albicans* CSA1 gene encoding a mycelial surface antigen by sorting of *Saccharomyces cerevisiae* transformants with monoclonal antibody-coated magnetic beads. *Mol Microbiol* **35**, 444–53.

Lashkari, D. A., DeRisi, J. L., McCusker, J. H., Namath, A. F., Gentile, C., Hwang, S. Y., Brown, P. O. & Davis, R. W. (1997). Yeast microarrays for genome wide parallel genetic and gene expression analysis. *Proc Natl Acad Sci U S A* **94**, 13057–62.

Lassak, T., Schneider, E., Bussmann, M., Kurtz, D., Manak, J. R., Srikantha, T., Soll, D. R. & Ernst, J. F. (2011). Target specificity of the *Candida albicans* Efg1 regulator. *Mol Microbiol* **82**, 602–18.

Lavoie, H., Sellam, A., Askew, C., Nantel, A. & Whiteway, M. (2008). A toolbox for epitope-tagging and genome-wide location analysis in *Candida albicans*. *BMC Genomics* **9**, 578.

Leach, M. D., Budge, S., Walker, L., Munro, C., Cowen, L. E. & Brown, A. J. P. (2012). Hsp90 orchestrates transcriptional regulation by Hsf1 and cell wall remodelling by MAPK signalling during thermal adaptation in a pathogenic yeast. *PLoS Pathog* **8**, e1003069.

Lee, E., Helt, G. A., Reese, J. T., Munoz-Torres, M. C., Childers, C. P., Buels, R. M., Stein, L., Holmes, I. H., Elsik, C. G. & Lewis, S. E. (2013). Web Apollo: a web-based genomic annotation editing platform. *Genome Biol* **14**, R93.

Lelli, K. M., Slattery, M. & Mann, R. S. (2012). Disentangling the many layers of eukaryotic transcriptional regulation. *Annu Rev Genet* **46**, 43–68. Annual Reviews.

De Leon, E., Jacober, S., Sobel, J. & Foxman, B. (2002). Prevalence and risk factors for vaginal *Candida* colonization in women with type 1 and type 2 diabetes. *BMC Infect Dis* **2**, 1.

Lephart, P. R., Chibana, H. & Magee, P. T. (2005). Effect of the major repeat sequence on chromosome loss in *Candida albicans*. *Eukaryot Cell* **4**, 733–41.

Leroux, S. & Ullmann, A. J. (2013). Management and diagnostic guidelines for fungal diseases in infectious diseases and clinical microbiology: critical appraisal. *Clin Microbiol Infect* **19**, 1115–21.

Li, Y., Su, C., Mao, X., Cao, F. & Chen, J. (2007). Roles of *Candida albicans* Sfl1 in hyphal development. *Eukaryot Cell* **6**, 2112–21.

Liang, Y., Gui, L., Wei, D.-S., Zheng, W., Xing, L.-J. & Li, M.-C. (2009). *Candida albicans* ferric reductase FRP1 is regulated by direct interaction with Rim101p transcription factor. *FEMS Yeast Res* **9**, 270–7.

Life Technologies Corporation. (2010). *Qubit® 2.0 Fluorometer.*

Lim, C. S.-Y., Rosli, R., Seow, H. F. & Chong, P. P. (2012). *Candida* and invasive candidiasis: back to basics. *Eur J Clin Microbiol Infect Dis* **31**, 21–31.

Lockhart, S. R., Pujol, C., Daniels, K. J., Miller, M. G., Johnson, A. D., Pfaller, M. A. & Soll, D. R. (2002). In *Candida albicans*, white-opaque switchers are homozygous for mating type. *Genetics* **162**, 737–45.

Lodi, G., Sardella, A., Bez, C., Demarosi, F. & Carrassi, A. (2006). Interventions for treating oral leukoplakia. *Cochrane database Syst Rev* CD001829.

Loeb, J. D. J., Sepulveda-Becerra, M., Hazan, I. & Liu, H. (1999). A G1 Cyclin Is Necessary for Maintenance of Filamentous Growth in *Candida albicans*. *Mol Cell Biol* **19**, 4019–4027.

Logan-Klumpler, F. J., De Silva, N., Boehme, U., Rogers, M. B., Velarde, G., McQuillan, J. A., Carver, T., Aslett, M., Olsen, C. & other authors. (2012). GeneDB--an annotation database for pathogens. *Nucleic Acids Res* **40**, D98–108.

Lohse, M. B., Hernday, A. D., Fordyce, P. M., Noiman, L., Sorrells, T. R., Hanson-Smith, V., Nobile, C. J., DeRisi, J. L. & Johnson, A. D. (2013). Identification and characterization of a previously undescribed family of sequence-specific DNA-binding domains. *Proc Natl Acad Sci U S A* **110**, 7660–5.

López-Ribot, J. L. (2005). *Candida albicans* biofilms: more than filamentation. *Curr Biol* **15**, R453–5.

Loreto, E. S., Scheid, L. A., Nogueira, C. W., Zeni, G., Santurio, J. M. & Alves, S. H. (2010). *Candida dubliniensis*: epidemiology and phenotypic methods for identification. *Mycopathologia* **169**, 431–43.

Lowman, D. W., Greene, R. R., Bearden, D. W., Kruppa, M. D., Pottier, M., Monteiro, M. A., Soldatov, D. V, Ensley, H. E., Cheng, S.-C. & other authors. (2014). Novel structural features in *Candida albicans* hyphal glucan provide a basis for differential innate immune recognition of hyphae versus yeast. *J Biol Chem* **289**, 3432–43.

Lu, Y., Su, C., Wang, A. & Liu, H. (2011). Correction: Hyphal Development in *Candida albicans* Requires Two Temporally Linked Changes in Promoter Chromatin for Initiation and Maintenance. *PLoS Biol* **9**, e1001105 (J. Heitman, Ed.). Public Library of Science.

Ma, W. (2011). Analysis of telomere proteins by Chromatin Immunoprecipitation (ChIP). *Methods Mol Biol* **735**, 151–9.

Maguire, S. L., ÓhÉigeartaigh, S. S., Byrne, K. P., Schröder, M. S., O'Gaora, P., Wolfe, K. H. & Butler, G. (2013). Comparative genome analysis and gene finding in *Candida* species using CGOB. *Mol Biol Evol* **30**, 1281–91.

Marchler-Bauer, A., Zheng, C., Chitsaz, F., Derbyshire, M. K., Geer, L. Y., Geer, R. C., Gonzales, N. R., Gwadz, M., Hurwitz, D. I. & other authors. (2013). CDD: conserved domains and protein three-dimensional structure. *Nucleic Acids Res* **41**, D348–52.

Marotta, D. H., Nantel, A., Sukala, L., Teubl, J. R. & Rauceo, J. M. (2013). Genome-wide transcriptional profiling and enrichment mapping reveal divergent and conserved roles of Sko1 in the *Candida albicans* osmotic stress response. *Genomics* **102**, 363–71.

Martchenko, M., Levitin, A., Hogues, H., Nantel, A. & Whiteway, M. (2007). Transcriptional rewiring of fungal galactose-metabolism circuitry. *Curr Biol* **17**, 1007–13.

Martin, R., Moran, G. P., Jacobsen, I. D., Heyken, A., Domey, J., Sullivan, D. J., Kurzai, O. & Hube, B. (2011). The *Candida albicans*-specific gene EED1 encodes a key regulator of hyphal extension. *PLoS One* **6**, e18394 (C. A. Munro, Ed.). Public Library of Science.

Maskos, U. & Southern, E. M. (1992). Oligonucleotide hybridisations on glass supports: a novel linker for oligonucleotide synthesis and hybridisation properties of oligonucleotides synthesised in situ. *Nucleic Acids Res* **20**, 1679–1684.

Mathé, L. & Van Dijck, P. (2013). Recent insights into *Candida albicans* biofilm resistance mechanisms. *Curr Genet* **59**, 251–64.

Mavrianos, J., Desai, C. & Chauhan, N. (2014). Two-component histidine phosphotransfer protein Ypd1 is not essential for viability in *Candida albicans*. *Eukaryot Cell* **13**, 452–60.

Mayer, F. L., Wilson, D. & Hube, B. (2013). *Candida albicans* pathogenicity mechanisms. *Virulence* **4**, 119–28.

McCabe, C. D. & Innis, J. W. (2005). A genomic approach to the identification and characterization of HOXA13 functional binding elements. *Nucleic Acids Res* **33**, 6782–94.

McCullough, M. J. & Savage, N. W. (2005). Oral candidosis and the therapeutic use of antifungal agents in dentistry. *Aust Dent J* **50**, S36–9.

McManus, B. A. (2012). *Personal Communication*. Dublin, Ireland.

McManus, B. A. & Coleman, D. C. (2014). Molecular epidemiology, phylogeny and evolution of *Candida albicans*. *Infect Genet Evol* **21**, 166–78.

McWilliam, H., Li, W., Uludag, M., Squizzato, S., Park, Y. M., Buso, N., Cowley, A. P. & Lopez, R. (2013). Analysis Tool Web Services from the EMBL-EBI. *Nucleic Acids Res* **41**, W597–600.

Méan, M., Marchetti, O. & Calandra, T. (2008). Bench-to-bedside review: *Candida* infections in the intensive care unit. *Crit Care* **12**, 204.

Meuwissen, T. H. E. & Goddard, M. E. (2004). Bootstrapping of gene-expression data improves and controls the false discovery rate of differentially expressed genes. *Genet Sel Evol* **36**, 191–205.

Millar, J. B., Buck, V. & Wilkinson, M. G. (1995). Pyp1 and Pyp2 PTPases dephosphorylate an osmosensing MAP kinase controlling cell size at division in fission yeast. *Genes Dev* **9**, 2117–30.

Miller, C., Matic, I., Maier, K. C., Schwalb, B., Roether, S., Strässer, K., Tresch, A., Mann, M. & Cramer, P. (2012). Mediator phosphorylation prevents stress response transcription during non-stress conditions. *J Biol Chem* **287**, 44017–26.

Milne, S. W., Cheetham, J., Lloyd, D., Aves, S. & Bates, S. (2011). Cassettes for PCR-mediated gene tagging in *Candida albicans* utilizing nourseothricin resistance. *Yeast* **3**, 833–841.

Miramón, P., Dunker, C., Windecker, H., Bohovych, I. M., Brown, A. J. P., Kurzai, O. & Hube, B. (2012). Cellular responses of *Candida albicans* to phagocytosis and the extracellular activities of neutrophils are critical to counteract carbohydrate starvation, oxidative and nitrosative stress. *PLoS One* **7**, e52850 (O. Zaragoza, Ed.). Public Library of Science.

Miramón, P., Kasper, L. & Hube, B. (2013). Thriving within the host: *Candida* spp. interactions with phagocytic cells. *Med Microbiol Immunol* **202**, 183–95.

Mishra, P. K., Baum, M. & Carbon, J. (2007). Centromere size and position in *Candida albicans* are evolutionarily conserved independent of DNA sequence heterogeneity. *Mol Genet Genomics* **278**, 455–65.

Moran, G., Stokes, C., Thewes, S., Hube, B., Coleman, D. C. & Sullivan, D. (2004). Comparative genomics using *Candida albicans* DNA microarrays reveals absence and divergence of virulence-associated genes in *Candida dubliniensis*. *Microbiology* **150**, 3363–82.

Moran, G. P. (2011). *Personal Communication*.

Moran, G. P., MacCallum, D. M., Spiering, M. J., Coleman, D. C. & Sullivan, D. J. (2007). Differential regulation of the transcriptional repressor NRG1 accounts for altered host-cell interactions in *Candida albicans* and *Candida dubliniensis*. *Mol Microbiol* **66**, 915–29.

Moran, G. P., Coleman, D. C. & Sullivan, D. J. (2012). *Candida albicans* versus *Candida dubliniensis*: Why Is C. *albicans* More Pathogenic? *Int J Microbiol* **2012**, 205921.

Morrow, B., Srikantha, T. & Soll, D. R. (1992). Transcription of the gene for a pepsinogen, PEP1, is regulated by white-opaque switching in *Candida albicans*. *Mol Cell Biol* **12**, 2997–3005.

Mutoh, N., Kawabata, M. & Kitajima, S. (2005). Effects of four oxidants, menadione, 1-chloro-2,4-dinitrobenzene, hydrogen peroxide and cumene hydroperoxide, on fission yeast Schizosaccharmoyces pombe. *J Biochem* **138**, 797–804.

Myers, R. S. (2006). Immunizing and Antimicrobial Agents.

Nantel, A., Dignard, D., Bachewich, C., Harcus, D., Marcil, A., Bouin, A.-P., Sensen, C. W., Hogues, H., van het Hoog, M. & other authors. (2002). Transcription profiling of *Candida albicans* cells undergoing the yeast-to-hyphal transition. *Mol Biol Cell* **13**, 3452–65.

Naseem, S., Gunasekera, A., Araya, E. & Konopka, J. B. (2011). N-acetylglucosamine (GlcNAc) induction of hyphal morphogenesis and transcriptional responses in *Candida albicans* are not dependent on its metabolism. *J Biol Chem* **286**, 28671–80.

Ninio, M., Privman, E., Pupko, T. & Friedman, N. (2007). Phylogeny reconstruction: increasing the accuracy of pairwise distance estimation using Bayesian inference of evolutionary rates. *Bioinformatics* **23**, e136–41.

Nobile, C. J., Nett, J. E., Andes, D. R. & Mitchell, A. P. (2006). Function of *Candida albicans* adhesin Hwp1 in biofilm formation. *Eukaryot Cell* **5**, 1604–10.

Nobile, C. J., Solis, N., Myers, C. L., Fay, A. J., Deneault, J.-S., Nantel, A., Mitchell, A. P. & Filler, S. G. (2008). *Candida albicans* transcription factor Rim101 mediates pathogenic interactions through cell wall functions. *Cell Microbiol* **10**, 2180–96.

Notredame, C., Higgins, D. G. & Heringa, J. (2000). T-Coffee: A novel method for fast and accurate multiple sequence alignment. *J Mol Biol* **302**, 205–17.

O'Connor, L. (2009). *Comparative Analysis of Stress Responses in C. albicans and C. dubliniensis*. University of Dublin, Trinity College.

O'Connor, L., Caplice, N., Coleman, D. C., Sullivan, D. J. & Moran, G. P. (2010). Differential filamentation of *Candida albicans* and *Candida dubliniensis* Is governed by nutrient regulation of UME6 expression. *Eukaryot Cell* **9**, 1383–97.

Odds, F. C. & Bernaerts, R. (1994). CHROMagar *Candida*, a new differential isolation medium for presumptive identification of clinically important *Candida* species. *J Clin Microbiol* **32**, 1923–1929.

Odds, F. C., Hanson, M. F., Davidson, A. D., Jacobsen, M. D., Wright, P., Whyte, J. A., Gow, N. A. R. & Jones, B. L. (2007). One year prospective survey of *Candida* bloodstream infections in Scotland. *J Med Microbiol* **56**, 1066–75.

Palige, K., Linde, J., Martin, R., Böttcher, B., Citiulo, F., Sullivan, D. J., Weber, J., Staib, C., Rupp, S. & other authors. (2013). Global transcriptome sequencing identifies chlamydospore specific markers in *Candida albicans* and *Candida dubliniensis*. *PLoS One* **8**, e61940 (N. Chauhan, Ed.). Public Library of Science.

Pappas, P. G., Kauffman, C. A., Andes, D., Benjamin, D. K., Calandra, T. F., Edwards, J. E., Filler, S. G., Fisher, J. F., Kullberg, B.-J. & other authors. (2009). Clinical practice guidelines for the management of candidiasis: 2009 update by the Infectious Diseases Society of America. *Clin Infect Dis* **48**, 503–35.

Paramonova, E., Krom, B. P., van der Mei, H. C., Busscher, H. J. & Sharma, P. K. (2009). Hyphal content determines the compression strength of *Candida albicans* biofilms. *Microbiology* **155**, 1997–2003.

Patterson, M. J., McKenzie, C. G., Smith, D. A., da Silva Dantas, A., Sherston, S., Veal, E. A., Morgan, B. A., MacCallum, D. M., Erwig, L.-P. & Quinn, J. (2013). Ybp1 and Gpx3 signaling in *Candida albicans* govern hydrogen peroxide-induced oxidation of the Cap1 transcription factor and macrophage escape. *Antioxid Redox Signal* **19**, 2244–60.

Paul, S. & Moye-Rowley, W. S. (2014). Multidrug resistance in fungi: regulation of transporter-encoding gene expression. *Front Physiol* **5**, 143.

Peng, J. & Zhou, J.-Q. (2012). The tail-module of yeast Mediator complex is required for telomere heterochromatin maintenance. *Nucleic Acids Res* **40**, 581–93.

Van de Peppel, J., Kettelarij, N., van Bakel, H., Kockelkorn, T. T. J. P., van Leenen, D. & Holstege, F. C. P. (2005). Mediator expression profiling epistasis reveals a signal transduction pathway with antagonistic submodules and highly specific downstream targets. *Mol Cell* **19**, 511–22.

Pérez-Campo, F. M. & Domínguez, A. (2001). Factors affecting the morphogenetic switch in Yarrowia lipolytica. *Curr Microbiol* **43**, 429–33.

Pfaller, M. A. & Diekema, D. J. (2010). Epidemiology of invasive mycoses in North America. *Crit Rev Microbiol* **36**, 1–53. Informa UK Ltd London, UK.

Poss, Z. C., Ebmeier, C. C. & Taatjes, D. J. (2013). The Mediator complex and transcription regulation. *Crit Rev Biochem Mol Biol* **48**, 575–608.

Potrykus, J., Ballou, E. R., Childers, D. S. & Brown, A. J. P. (2014). Conflicting interests in the pathogen-host tug of war: fungal micronutrient scavenging versus mammalian nutritional immunity. *PLoS Pathog* **10**, e1003910 (J. Heitman, Ed.). Public Library of Science.

Poustka, A. (2002). Variance Stabilization and Normalization using the vsn package in R **1**.

Promega Corporation. (2009). *PureYieldTM Plasmid Miniprep System.*

Promega Corporation. (2010). Wizard® SV Gel and PCR Clean-Up System.

Pujol, C., Daniels, K. J., Lockhart, S. R., Srikantha, T., Radke, J. B., Geiger, J. & Soll, D. R. (2004). The closely related species *Candida albicans* and *Candida dubliniensis* can mate. *Eukaryot Cell* **3**, 1015–27.

Qiagen. (2012). *RNeasy® Mini Handbook.*

Ramage, G., Jose, A., Coco, B., Rajendran, R., Rautemaa, R., Murray, C., Lappin, D. F. & Bagg, J. (2011). Commercial mouthwashes are more effective than azole antifungals against *Candida albicans* biofilms in vitro. *Oral Surg Oral Med Oral Pathol Oral Radiol Endod* **111**, 456–60.

Ramanan, N. & Wang, Y. (2000). A high-affinity iron permease essential for *Candida albicans* virulence. *Science* **288**, 1062–4.

Reece, J. B., Urry, L. A., Cain, M. L., Wasserman, S. A., Minorsky, P. V. & Jackson, R. B. (2010). *Campbell Biology. Campbell Biol.*

Reuss, O., Vik, A., Kolter, R. & Morschhäuser, J. (2004). The SAT1 flipper, an optimized tool for gene disruption in *Candida albicans*. *Gene* **341**, 119–127.

Rice, P., Longden, I. & Bleasby, A. (2000). EMBOSS: the European Molecular Biology Open Software Suite. *Trends Genet* **16**, 276–7.

Richard, M. L., Nobile, C. J., Bruno, V. M. & Mitchell, A. P. (2005). *Candida albicans* biofilm-defective mutants. *Eukaryot Cell* **4**, 1493–502.

Robbins, N., Uppuluri, P., Nett, J., Rajendran, R., Ramage, G., Lopez-Ribot, J. L., Andes, D. & Cowen, L. E. (2011). Hsp90 governs dispersion and drug resistance of fungal biofilms. *PLoS Pathog* **7**, e1002257 (R. C. May, Ed.). Public Library of Science.

Rodríguez-Peña, J. M., Díez-Muñiz, S., Bermejo, C., Nombela, C. & Arroyo, J. (2013). Activation of the yeast cell wall integrity MAPK pathway by zymolyase depends on protease and glucanase activities and requires the mucin-like protein Hkr1 but not Msb2. *FEBS Lett* **587**, 3675–80.

Roncero, C., Duran, A. & Durán, A. (1985). Effect of Calcofluor white and Congo red on fungal cell wall morphogenesis: in vivo activation of chitin polymerization. *J Bacteriol* **163**, 1180–5.

Rubin, A. I., Bagheri, B. & Scher, R. K. (2002). Six novel antimycotics. *Am J Clin Dermatol* **3**, 71–81.

Rustchenko, E. (2007). Chromosome instability in *Candida albicans*. *FEMS Yeast Res* **7**, 2–11.

Sandai, D., Yin, Z., Selway, L., Stead, D., Walker, J., Leach, M. D., Bohovych, I., Ene, I. V, Kastora, S. & other authors. (2012). The evolutionary rewiring of ubiquitination targets has reprogrammed the regulation of carbon assimilation in the pathogenic yeast *Candida albicans*. *MBio* **3**.

Sanglard, D. & Odds, F. C. (2002). Resistance of *Candida* species to antifungal agents: molecular mechanisms and clinical consequences. *Lancet Infect Dis* **2**, 73–85.

Santos, M. A. S., Gomes, A. C., Santos, M. C., Carreto, L. C. & Moura, G. R. (2011). The genetic code of the fungal CTG clade. *C R Biol* **334**, 607–11.

Saputo, S., Chabrier-Rosello, Y., Luca, F. C., Kumar, A. & Krysan, D. J. (2012). The RAM network in pathogenic fungi. *Eukaryot Cell* **11**, 708–17.

Saville, S. P., Lazzell, A. L., Monteagudo, C. & Lopez-Ribot, J. L. (2003). Engineered control of cell morphology in vivo reveals distinct roles for yeast and filamentous forms of *Candida albicans* during infection. *Eukaryot Cell* **2**, 1053–60.

Schena, M., Shalon, D., Davis, R. W. & Brown, P. O. (1995). Quantitative monitoring of gene expression patterns with a complementary DNA microarray. *Science* **270**, 467–70.

Seider, K., Heyken, A., Lüttich, A., Miramón, P. & Hube, B. (2010). Interaction of pathogenic yeasts with phagocytes: survival, persistence and escape. *Curr Opin Microbiol* **13**, 392–400.

Shapiro, R. S. & Cowen, L. E. (2012). Uncovering cellular circuitry controlling temperature-dependent fungal morphogenesis. *Virulence* **3**, 400–4.

Shenton, D., Smirnova, J. B., Selley, J. N., Carroll, K., Hubbard, S. J., Pavitt, G. D., Ashe, M. P. & Grant, C. M. (2006). Global translational responses to oxidative stress impact upon multiple levels of protein synthesis. *J Biol Chem* **281**, 29011–21.

Sievert, D. M., Ricks, P., Edwards, J. R., Schneider, A., Patel, J., Srinivasan, A., Kallen, A., Limbago, B. & Fridkin, S. (2012). Antimicrobial-Resistant Pathogens Associated with Healthcare-Associated Infections: Summary of Data Reported to the National Healthcare Safety Network at the Centers for Disease Control and Prevention, 2009–2010. University of Chicago PressChicago, IL.

Sigma-Aldrich. (2012). *GenEluteTM PCR Clean-Up Kit - Technical Bulletin*. St. Louis, MO.

Singh, V., Satheesh, S. V, Raghavendra, M. L. & Sadhale, P. P. (2007). The key enzyme in galactose metabolism, UDP-galactose-4-epimerase, affects cell-wall integrity and morphology in *Candida albicans* even in the absence of galactose. *Fungal Genet Biol* **44**, 563–74.

Sitepu, I., Selby, T., Lin, T., Zhu, S. & Boundy-Mills, K. (2014). Carbon source utilization and inhibitor tolerance of 45 oleaginous yeast species. *J Ind Microbiol Biotechnol* **41**, 1061–70.

Sitheeque, M. A. M. & Samaranayake, L. P. (2003). CHRONIC HYPERPLASTIC CANDIDOSIS/CANDIDIASIS (CANDIDAL LEUKOPLAKIA). *Crit Rev Oral Biol Med* **14**, 253–267.

Skinner, M. E. & Holmes, I. H. (2010). Setting up the JBrowse genome browser. *Curr Protoc Bioinformatics* **Chapter 9**, Unit 9.13.

Skinner, M. E., Uzilov, A. V, Stein, L. D., Mungall, C. J. & Holmes, I. H. (2009). JBrowse: a next-generation genome browser. *Genome Res* **19**, 1630–8.

Skrzypek, M. S., Arnaud, M. B., Costanzo, M. C., Inglis, D. O., Shah, P., Binkley, G., Miyasato, S. R. & Sherlock, G. (2010). New tools at the *Candida* Genome Database: biochemical pathways and full-text literature search. *Nucleic Acids Res* **38**, D428–32.

Slattery, M., Zhou, T., Yang, L., Dantas Machado, A. C., Gordân, R. & Rohs, R. (2014). Absence of a simple code: how transcription factors read the genome. *Trends Biochem Sci* **39**, 381–399. Elsevier.

Smeekens, S. P., van de Veerdonk, F. L., Kullberg, B. J. & Netea, M. G. (2013). Genetic susceptibility to *Candida* infections. *EMBO Mol Med* **5**, 805–13.

Smith, D. A., Morgan, B. A. & Quinn, J. (2010). Stress signalling to fungal stress-activated protein kinase pathways. *FEMS Microbiol Lett* **306**, 1–8.

Smyth, G. (2005). Limma: linnear models for microarray data. In *Bioinforma Comput Biol Solut Using R Bioconductor*, pp. 397–420. Edited by R. Gentleman, V. J. Carey, S. Dudoit, R. Irizarry & W. Huber. New York, NY: Springer New York.

Soll, D. R. (2014). The role of phenotypic switching in the basic biology and pathogenesis of *Candida albicans*. *J Oral Microbiol* **6**.

Soll, D. R. (2007). Mating and Switching in *Candida*. In *Candida Comp Funct Genomics*, pp. 27–50. Edited by C. d'Enfert & B. Hube. Caister Academic Press.

Sorgo, A. G., Heilmann, C. J., Brul, S., de Koster, C. G. & Klis, F. M. (2013). Beyond the wall: *Candida albicans* secret(e)s to survive. *FEMS Microbiol Lett* **338**, 10–7.

Spiering, M. J., Moran, G. P., Chauvel, M., Maccallum, D. M., Higgins, J., Hokamp, K., Yeomans, T., d'Enfert, C., Coleman, D. C. & Sullivan, D. J. (2010). Comparative transcript profiling of *Candida albicans* and *Candida dubliniensis* identifies SFL2, a C. *albicans* gene required for virulence in a reconstituted epithelial infection model. *Eukaryot Cell* **9**, 251–65.

Staib, P. & Morschhäuser, J. (2007). Chlamydospore formation in *Candida albicans* and *Candida dubliniensis*--an enigmatic developmental programme. *Mycoses* **50**, 1–12.

Staniszewska, M., Bondaryk, M., Swoboda-Kopec, E., Siennicka, K., Sygitowicz, G. & Kurzatkowski, W. (2013). *Candida albicans* morphologies revealed by scanning electron microscopy analysis. *Braz J Microbiol* **44**, 813–21.

Stokes, C., Moran, G. P., Spiering, M. J., Cole, G. T., Coleman, D. C. & Sullivan, D. J. (2007). Lower filamentation rates of *Candida dubliniensis* contribute to its lower virulence in comparison with *Candida albicans*. *Fungal Genet Biol* **44**, 920–31.

Sudbery, P., Gow, N. & Berman, J. (2004). The distinct morphogenic states of *Candida albicans*. *Trends Microbiol* **12**, 317–24.

Sudbery, P. E. (2011). Growth of *Candida albicans* hyphae. *Nat Rev Microbiol* **9**, 737–48. Nature Publishing Group, a division of Macmillan Publishers Limited. All Rights Reserved.

Sullivan, D. J., Westerneng, T. J., Haynes, K. A., Bennett, D. E. & Coleman, D. C. (1995). *Candida dubliniensis* sp. nov.: phenotypic and molecular characterization of a novel species associated with oral candidosis in HIV-infected individuals. *Microbiology* **141 (Pt 7**, 1507–21.

Sullivan, D. & Coleman, D. (1998). *Candida dubliniensis*: Characteristics and Identification. *J Clin Microbiol* **36**, 329–334.

Sullivan, D. J. & Moran, G. P. (2011). Differential virulence of *Candida albicans* and C. *dubliniensis*: A role for Tor1 kinase? *Virulence* **2**, 77–81.

Sullivan, D. J., Moran, G. P. & Coleman, D. C. (2005). *Candida dubliniensis*: ten years on. *FEMS Microbiol Lett* **253**, 9–17.

Sundstrom, P., Balish, E. & Allen, C. M. (2002). Essential role of the *Candida albicans* transglutaminase substrate, hyphal wall protein 1, in lethal oroesophageal candidiasis in immunodeficient mice. *J Infect Dis* **185**, 521–30.

Taff, H. T., Mitchell, K. F., Edward, J. A. & Andes, D. R. (2013). Mechanisms of *Candida* biofilm drug resistance. *Future Microbiol* **8**, 1325–37.

Technologies, A. (2007). *Yeast ChIP-on-chip analysis*.

Technologies, A. (2012). Two-Color Microarray-Based Gene Expression Analysis (Low Input Quick Amp Labeling).

Technologies, A. (2008). October 2008 QIAEX II ® Handbook For DNA extraction from agarose and polyacrylamide gels and for desalting Sample & Assay Technologies QIAGEN Sample and Assay Technologies.

Teytelman, L., Thurtle, D. M., Rine, J. & van Oudenaarden, A. (2013). Highly expressed loci are vulnerable to misleading ChIP localization of multiple unrelated proteins. *Proc Natl Acad Sci U S A* **110**, 18602–7.

Toedling, J. & Huber, W. (2008). Analyzing ChIP-chip data using bioconductor. *PLoS Comput Biol* **4**, e1000227 (F. Lewitter, Ed.). Public Library of Science.

Toedling, J., Skylar, O., Sklyar, O., Krueger, T., Fischer, J. J., Sperling, S. & Huber, W. (2007). Ringo--an R/Bioconductor package for analyzing ChIP-chip readouts. *BMC Bioinformatics* **8**, 221.

Di Tommaso, P., Moretti, S., Xenarios, I., Orobitg, M., Montanyola, A., Chang, J.-M., Taly, J.-F. & Notredame, C. (2011). T-Coffee: a web server for the multiple sequence alignment of protein and RNA sequences using structural information and homology extension. *Nucleic Acids Res* **39**, W13–7.

Tsutsui, T., Fukasawa, R., Shinmyouzu, K., Nakagawa, R., Tobe, K., Tanaka, A. & Ohkuma, Y. (2013). Mediator complex recruits epigenetic regulators via its two cyclin-dependent kinase subunits to repress transcription of immune response genes. *J Biol Chem* **288**, 20955–65.

Tumbarello, M., Fiori, B., Trecarichi, E. M., Posteraro, P., Losito, A. R., De Luca, A., Sanguinetti, M., Fadda, G., Cauda, R. & Posteraro, B. (2012). Risk factors and outcomes of candidemia caused by biofilm-forming isolates in a tertiary care hospital. *PLoS One* **7**, e33705 (F. L. Wormley, Ed.). Public Library of Science.

Uhl, M. A., Biery, M., Craig, N. & Johnson, A. D. (2003). Haploinsufficiency-based large-scale forward genetic analysis of filamentous growth in the diploid human fungal pathogen *C.albicans*. *EMBO J* **22**, 2668–78.

Uppuluri, P. & Chaffin, W. L. (2007). Defining *Candida albicans* stationary phase by cellular and DNA replication, gene expression and regulation. *Mol Microbiol* **64**, 1572–86.

Uwamahoro, N., Qu, Y., Jelicic, B., Lo, T. L., Beaurepaire, C., Bantun, F., Quenault, T., Boag, P. R., Ramm, G. & other authors. (2012). The functions of Mediator in *Candida albicans* support a role in shaping species-specific gene expression. *PLoS Genet* **8**, e1002613 (R. Morse, Ed.). Public Library of Science.

Uwamahoro, N., Verma-Gaur, J., Shen, H.-H., Qu, Y., Lewis, R., Lu, J., Bambery, K., Masters, S. L., Vince, J. E. & other authors. (2014). The pathogen *Candida albicans* hijacks pyroptosis for escape from macrophages. *MBio* **5**, e00003–14.

Vilela, M. M. S., Kamei, K., Sano, A., Tanaka, R., Uno, J., Takahashi, I., Ito, J., Yarita, K. & Miyaji, M. (2002). Pathogenicity and virulence of *Candida dubliniensis* : comparison with C. *albicans*. *Med Mycol* **40**, 249–257. Oxford University Press.

Vylkova, S. & Lorenz, M. C. (2014). Modulation of phagosomal pH by *Candida albicans* promotes hyphal morphogenesis and requires Stp2p, a regulator of amino acid transport. *PLoS Pathog* **10**, e1003995.

Vylkova, S., Jang, W. S., Li, W., Nayyar, N. & Edgerton, M. (2007). Histatin 5 initiates osmotic stress response in *Candida albicans* via activation of the Hog1 mitogen-activated protein kinase pathway. *Eukaryot Cell* **6**, 1876–88.

Walker, J. M. (Ed.). (2005). *The Proteomics Protocols Handbook*. Totowa, NJ: Humana Press.

Wang, W., Yao, X., Huang, Y., Hu, X., Liu, R., Hou, D., Chen, R. & Wang, G. (n.d.). Mediator MED23 regulates basal transcription in vivo via an interaction with P-TEFb. *Transcription* **4**, 39–51.

Wang, Y., Cao, Y.-Y., Jia, X.-M., Cao, Y.-B., Gao, P.-H., Fu, X.-P., Ying, K., Chen, W.-S. & Jiang, Y.-Y. (2006). Cap1p is involved in multiple pathways of oxidative stress response in *Candida albicans*. *Free Radic Biol Med* **40**, 1201–9.

Waterhouse, A. M., Procter, J. B., Martin, D. M. A., Clamp, M. & Barton, G. J. (2009). Jalview Version 2--a multiple sequence alignment editor and analysis workbench. *Bioinformatics* **25**, 1189–91.

Weissman, Z., Shemer, R., Conibear, E. & Kornitzer, D. (2008). An endocytic mechanism for haemoglobin-iron acquisition in *Candida albicans*. *Mol Microbiol* **69**, 201–17.

White, T. C. & Agabian, N. (1995). *Candida albicans* secreted aspartyl proteinases: isoenzyme pattern is determined by cell type, and levels are determined by environmental factors. *J Bacteriol* **177**, 5215–21.

Whiteside, S. T. & Goodbourn, S. (1993). Signal transduction and nuclear targeting: regulation of transcription factor activity by subcellular localisation. *J Cell Sci* **104 (Pt 4**, 949–55.

Williams, D. W., Jordan, R. P. C., Wei, X.-Q., Alves, C. T., Wise, M. P., Wilson, M. J. & Lewis, M. A. O. (2013). Interactions of *Candida albicans* with host epithelial surfaces. *J Oral Microbiol* **5**.

Wisplinghoff, H., Bischoff, T., Tallent, S. M., Seifert, H., Wenzel, R. P. & Edmond, M. B. (2004). Nosocomial bloodstream infections in US hospitals: analysis of 24,179 cases from a prospective nationwide surveillance study. *Clin Infect Dis* **39**, 309–17.

Wong, S. S. W., Samaranayake, L. P. & Seneviratne, C. J. (2014). In pursuit of the ideal antifungal agent for *Candida* infections: high-throughput screening of small molecules. *Drug Discov Today*.

Xu, N., Cheng, X., Yu, Q., Qian, K., Ding, X., Liu, R., Zhang, B., Xing, L. & Li, M. (2013). Aft2, a novel transcription regulator, is required for iron metabolism, oxidative stress, surface adhesion and hyphal development in *Candida albicans*. *PLoS One* **8**, e62367.

Xu, N., Qian, K., Dong, Y., Chen, Y., Yu, Q., Zhang, B., Xing, L. & Li, M. (2014). Novel role of the *Candida albicans* ferric reductase gene CFL1 in iron acquisition, oxidative stress tolerance, morphogenesis and virulence. *Res Microbiol* **165**, 252–61.

Yang, I. V. (2006). Use of external controls in microarray experiments. *Methods Enzymol* **411**, 50–63.

Yang, W., Yan, L., Wu, C., Zhao, X. & Tang, J. (2014). Fungal invasion of epithelial cells. *Microbiol Res*.

Yang, Y.-L. (2003). Virulence factors of *Candida* species. *J Microbiol Immunol Infect* **36**, 223–8.

Yapar, N. (2014). Epidemiology and risk factors for invasive candidiasis. *Ther Clin Risk Manag* **10**, 95–105.

Ye, J., Coulouris, G., Zaretskaya, I., Cutcutache, I., Rozen, S. & Madden, T. L. (2012). Primer-BLAST: a tool to design target-specific primers for polymerase chain reaction. *BMC Bioinformatics* **13**, 134.

Yeomans, T. (2010). Personal Communication.

Yu, E. Y. (2012). Telomeres and telomerase in *Candida albicans*. *Mycoses* **55**, e48–59.

Yu, E. Y., Steinberg-Neifach, O., Dandjinou, A. T., Kang, F., Morrison, A. J., Shen, X. & Lue, N. F. (2007). Regulation of telomere structure and functions by subunits of the INO80 chromatin remodeling complex. *Mol Cell Biol* **27**, 5639–49.

Zakikhany, K., Naglik, J. R., Schmidt-Westhausen, A., Holland, G., Schaller, M. & Hube, B. (2007). In vivo transcript profiling of *Candida albicans* identifies a gene essential for interepithelial dissemination. *Cell Microbiol* **9**, 2938–54.

Zhang, A., Petrov, K. O., Hyun, E. R., Liu, Z., Gerber, S. A. & Myers, L. C. (2012). The Tlo proteins are stoichiometric components of *Candida albicans* mediator anchored via the Med3 subunit. *Eukaryot Cell* **11**, 874–84.

Zhang, A., Liu, Z. & Myers, L. C. (2013). Differential Regulation of White-Opaque Switching by Individual Subunits of *Candida albicans* Mediator. *Eukaryot Cell* **12**, 1293–304.

Zhu, X., Wirén, M., Sinha, I., Rasmussen, N. N., Linder, T., Holmberg, S., Ekwall, K. & Gustafsson, C. M. (2006). Genome-wide occupancy profile of mediator and the Srb8-11 module reveals interactions with coding regions. *Mol Cell* **22**, 169–78.

Zhu, X., Liu, B., Carlsten, J. O. P., Beve, J., Nyström, T., Myers, L. C. & Gustafsson, C. M. (2011). Mediator influences telomeric silencing and cellular life span. *Mol Cell Biol* **31**, 2413–21.

Znaidi, S., Nesseir, A., Chauvel, M., Rossignol, T. & d'Enfert, C. (2013). A Comprehensive Functional Portrait of Two Heat Shock Factor-Type Transcriptional Regulators Involved in *Candida albicans* Morphogenesis and Virulence. *PLoS Pathog* **9**, e1003519. Public Library of Science.

Appendices

Figure S.1.

Sample script used in R/Bioconductor to process ChIP-on-chip data. Commands preceded by # are not functional.

```
rm(list=ls())
graphics.off()
ls()

setwd("/Users/John/Documents/Lab/Chromatin IP/R/workingdir")
getwd()


library(base)
library(datasets)
library(grDevices)
library(graphics)
library(grid)
library(methods)
library(utils)
library(stats)
library(Biobase)
library(BiocGenerics)
library(Matrix)
library(RColorBrewer)
library(Ringo)
library(lattice)
library(limma)
library(mclust)
library(AnnotationDbi)
library(IRanges)
library(KernSmooth)
library(RSQLite)
library(annotate)
library(genefilter)
library(splines)
library(stats4)
library(survival)
library(tools)
library(xtable)
library("arrayQualityMetrics")

targets <- readTargets()
RG <- read.maimages(targets, source="agilent")

spottypes <- readSpotTypes()

RG$genes$Status <- controlStatus(spottypes, RG)
ex
show(RG)


#changing replicates for between array normalisation
temp <- RG$G[,2]  # G corresponds to Cy3
RG$G[,2] <- RG$R[,2]
RG$R[,2] <- temp

pA <- posToProbeAnno("C.dubliniensis.pos")
```

```
#X1 preprocessed with nimblegen method; X2 with vsn for comparison
X1 <- preprocess(RG[RG$genes$ControlType==0,], method="nimblegen",
 idColumn="ProbeName",ChIPChannel = "R", inputChannel= "G")
sampleNames(X1)

X2 <- preprocess(RG[RG$genes$ControlType==0,], method="vsn",
 idColumn="ProbeName",ChIPChannel = "R",)
sampleNames(X2)

sampleNames(X1) <- X1$SlideNumber

sampleNames(X2) <- X2$SlideNumber

probeDists <- diff(pA["1.start"])
br <- c(0, 50, 60, 70, 75, 80, 85, 90, 95, 100, 200, 300, 500, 1000, 10000,
 max(probeDists))
table(cut(probeDists, br))

smoothX1 <- computeRunningMedians(X1, modColumn="Cy5", winHalfSize=500, min.probes=3,
 probeAnno=pA, combineReplicates=FALSE)

plot(smoothX1, pA, chr="1", coord=10000+c(0, 50000))

graphics.off()

smoothX2 <- computeRunningMedians(X1, modColumn="Cy5", winHalfSize=500, min.probes=3,
 probeAnno=pA, combineReplicates=TRUE)

plot(smoothX1, pA, chr="1", coord=10000+c(0, 50000))

graphics.off()

#replicates are averaged and now smoothed reporter intensities will be transposed onto
 individual intensity values

combX1 <-combine(X1, smoothX1)
plot(smoothX1, pA, chr="1")

#stringent threshold is applied

(y0 <- apply(exprs(smoothX1),2,upperBoundNull))
chersX1 <- findChersOnSmoothed(smoothX1, probeAnno=pA, thresholds=y0, allChr="1",
 distCutOff=600, cellType="Candida")

#maybe not needed?
chersX1 <- relateChers()

chersX1D <-as.data.frame.cherList(chersX1)
chersX1D[order(chersX1D$maxLevel, decreasing=TRUE),]

write.table(chersX1D[order(chersX1D$maxLevel, decreasing=TRUE),])

#y1 for threshold of 0.8, y2 for threshold of 0.9
#smoothX2 is the list with nimblegen, combined datasets
y1 <- apply(exprs(smoothX2),2,upperBoundNull, prob = 0.8)
y2 <- apply(exprs(smoothX2),2,upperBoundNull, prob = 0.9)

chersX2A1 <- findChersOnSmoothed(smoothX2, probeAnno=pA, thresholds=y2, distCutOff=600,
 cellType="Candida")
```

```
chersX2A1 <- relateChers()
chersX2A1P <-as.data.frame.cherList(chersX2A1)
chersX2A1P[order(chersX2A1P$maxLevel, decreasing=TRUE),]
write.csv(chersX2A1P[order(chersX2A1P$maxLevel, decreasing=TRUE),], file =
 "allchromosomesnew0.9.csv")

chersX2A1 <- findChersOnSmoothed(smoothX2, probeAnno=pA, thresholds=y1, distCutOff=600,
 cellType="Candida")
chersX2A1 <- relateChers()
chersX2A1P <-as.data.frame.cherList(chersX2A1)
chersX2A1P[order(chersX2A1P$maxLevel, decreasing=TRUE),]
write.csv(chersX2A1P[order(chersX2A1P$maxLevel, decreasing=TRUE),], file =
 "allchromosomesnew0.8.csv")

#finding out about thresholds for smoothX2:
#y0 or suggested threshold:
hist(exprs(smoothX2)[, 1], n = 25, xlab = "Smoothed reporter intensities [log]", xlim =
 c(-1, 1), main = NA, col = brewer.pal(8, "Set2")[1])
abline(v = y0, col = "550", font = "2", ) #pink
abline(v = y1, col = "562", font = "2") #red
abline(v = y2, col = "561", font = "2") #brown
```

Table S.1. Changes in gene expression greater than 1.5-fold in ΔΔ*tlo* compared to Wü284 during mid-exponential growth in YEPD

Gene Name	*C. dubliniensis* Cd36 identifier	*C. albicans* orf19 identifier	C'some	Fold change expression	Normalised Expression	*S. cerevisiae* ortholog	Description
RNR22	Cd36_21850	orf19.1868	2	-6.532708	-2.7076812	*RNR2*	Protein described as ribonucleoside diphosphate reductase
SUL2	Cd36_42530	orf19.2738	4	-5.3880253	-2.4297566	*SUL1*	Protein described as a sulfate transporter
CHA1	Cd36_16150	orf19.1996	2	-5.1045127	-2.3517733	*CHA1*	Protein similar to serine/threonine dehydratases, catabolic
	Cd36_12860		1	-5.0748887	-2.3433762		
	Cd36_05260	orf19.411	1	-4.635633	-2.2127664	*SRP40*	Similar to GTPase regulators
OPT7	Cd36_40500	orf19.5673	4	-3.926569	-1.9732692	*OPT2*	Putative oligopeptide transporter
ECM17	Cd36_20560	orf19.4099	2	-3.6024437	-1.8489759	*ECM17*	Predicted enzyme of sulfur amino acid biosynthesis
HEM13	Cd36_83990	orf19.2803	3	-3.555565	-1.8300788	*HEM13*	Homolog of S. cerevisiae coproporphyrinogen III oxidase
RNR21	Cd36_17780	orf19.5801	2	-3.4303007	-1.7783351	*RNR2*	Protein described as similar to ribonucleoside-diphosphate reductase
MET14	Cd36_50440	orf19.946	5	-3.4173064	-1.7728596	*MET14*	Predicted ORF in Assemblies 19, 20 and 21
TYE7	Cd36_12210	orf19.4941	1	-3.3881898	-1.7605147	*TYE7*	Putative bHLH (basic region, helix-loop-helix) transcription factor
PFK2	Cd36_71630	orf19.6540	7	-3.3582175	-1.7476957	*PFK2*	Beta subunit of phosphofructokinase (PFK), which is a heteromultimer of Pfk1p and Pfk2p
	Cd36_01980		1	-3.3496215	-1.743998		
ERG1	Cd36_08100	orf19.406	1	-3.2098064	-1.6824863	*ERG1*	Squalene epoxidase, catalyzes epoxidation of squalene to 2,3(S)-oxidosqualene in the ergosterol biosynthetic pathway
FET3	Cd36_60410	orf19.4211	6	-3.1994686	-1.6778324	*FET3*	Multicopper oxidase
	Cd36_50410	orf19.951	5	-3.183007	-1.6703904		Predicted ORF in Assemblies 19, 20 and 21
SEO1	Cd36_32190	orf19.700	R	-3.1499999	-1.6553518	*SEO1*	Similar to permeases
	Cd36_22660	orf19.3625	2	-3.106515	-1.635297	*YNG1*	Predicted ORF in Assemblies 19, 20 and 21
GPD2	Cd36_62130	orf19.691	6	-3.092066	-1.6285712	*GPD1*	Similar to glycerol 3-P dehydrogenases
GCV2	Cd36_07910	orf19.385	1	-3.0584953	-1.612822	*GCV2*	Putative protein of glycine catabolism
FCY23	Cd36_09940	orf19.1832	1	-3.0037198	-1.5867503	*TPN1*	Putative transporter
RHR2	Cd36_80290	orf19.5437	3	-2.9038079	-1.537946	*RHR2*	Putative glycerol 3-phosphatase
MET1	Cd36_17440	orf19.5811	2	-2.8875368	-1.5298393	*MET1*	Putative uroporphyrin-3 C-methyltransferase
CHT3	Cd36_35130	orf19.7586	R	-2.8779984	-1.5250658	*CTS1*	Chitinase, major
	Cd36_17710			-2.8305266	-1.5010705		
ERG9	Cd36_22740	orf19.3616	2	-2.8257482	-1.4986329	*ERG9*	Putative farnesyl-diphosphate farnesyl transferase (squalene synthase) involved in the sterol biosynthesis pathway
	Cd36_86670	orf19.7459	3	-2.799785	-1.485316	*RMD9*	Predicted ORF in Assemblies 19, 20 and 21
SOD6	Cd36_15220	orf19.2108	2	-2.766028	-1.4678158		Copper- and zinc-containing superoxide dismutase
	Cd36_24430		2	-2.7393134	-1.4538143		
	Cd36_04690	orf19.50	1	-2.7136474	-1.4402332	*UFO1*	Predicted ORF in Assemblies 19, 20 and 21
HGT6	Cd36_15940	orf19.2020	2	-2.6747704	-1.419415	*HXT6|HXT7*	Putative glucose transporter of major facilitator superfamily
	Cd36_64490	orf19.5775	6	-2.6386957	-1.399825	*YIL169C*	Predicted ORF in Assemblies 19, 20 and 21
CRK1	Cd36_19450	orf19.3523	2	-2.6360538	-1.3983798	*SGV1*	Protein kinase of the Cdc2 kinase subfamily involved in hyphal development and virulence
	Cd36_72320	orf19.3701	7	-2.6302266	-1.3951871		Protein not essential for viability
	Cd36_19250	orf19.150	2	-2.6298337	-1.3949716	*TIM17*	Predicted ORF in Assemblies 19, 20 and 21
	Cd36_29850	orf19.541	R	-2.620541	-1.3898647		Predicted ORF in Assemblies 19, 20 and 21
	Cd36_43670	orf19.1208	4	-2.611728	-1.3850046		Predicted ORF in Assemblies 19, 20 and 21
FGR6-3	Cd36_72390	orf19.4712	7	-2.595184	-1.3758368	*AGA1*	Protein lacking an ortholog in S. cerevisiae
	Cd36_34360	orf19.7279	R	-2.5804513	-1.3676233	*NIT2*	Predicted ORF in Assemblies 19, 20 and 21
CDC21	Cd36_19690	orf19.3549	2	-2.5596812	-1.3559642	*CDC21*	Predicted ORF in Assemblies 19, 20 and 21
SUR2	Cd36_17510	orf19.5818	2	-2.5305166	-1.339432	*SUR2*	Protein described as similar to ceramide hydroxylase
	Cd36_53910	orf19.3905	5	-2.4955287	-1.3193455		Predicted ORF in Assemblies 19, 20 and 21
ERG251	Cd36_41530	orf19.4631	4	-2.4811802	-1.3110266	*ERG25*	Predicted ORF in Assemblies 19, 20 and 21
DSE1	Cd36_22620	orf19.3629	2	-2.4743793	-1.3070667	*DSE1*	Predicted cell wall protein
	Cd36_41990	orf19.4581	4	-2.4636028	-1.3007697	*GPI14*	Predicted ORF in Assemblies 19, 20 and 21
FGR6-4	Cd36_24200	orf19.3490	2	-2.4621842	-1.2999387	*YIL169C*	Protein lacking an ortholog in S. cerevisiae
	Cd36_52980			-2.4565465	-1.2966316		
MET15	Cd36_40270	orf19.5645	4	-2.4547791	-1.2955933	*MET17*	O-acetylhomoserine O-acetylserine sulfhydrylase
RPS3	Cd36_30190	orf19.6312	R	-2.4468489	-1.290925	*RPS3*	Putative ribosomal protein
SAM2	Cd36_10740	orf19.657	1	-2.4376209	-1.2854738	*SAM2*	S-adenosylmethionine synthetase, localizes to surface of hyphal cells, but not yeast-form cells
	Cd36_72380	orf19.3695	7	-2.4279728	-1.2797523	*EPT1*	Predicted ORF in Assemblies 19, 20 and 21
	Cd36_23170	orf19.206	2	-2.4166956	-1.2730358	*MUC1*	Predicted ORF in Assemblies 19, 20 and 21
AGP2	Cd36_41090	orf19.4679	4	-2.4166257	-1.272994	*AGP2*	Protein described as an amino acid permease
GPH1	Cd36_70860	orf19.7021	7	-2.4002035	-1.2631567	*GPH1*	Putative glycogen phosphorylase
	Cd36_12400	orf19.4963	1	-2.390346	-1.2572196	*YDR161W*	Predicted ORF in Assemblies 19, 20 and 21
MET10	Cd36_23290	orf19.4076	2	-2.387818	-1.255693	*MET10*	Predicted enzyme of sulfur amino acid metabolism
	Cd36_09590	orf19.4889	1	-2.3838296	-1.2532811	*HOL1*	Predicted ORF in Assemblies 19, 20 and 21
FGR6-10	Cd36_45130	orf19.1234	4	-2.372911	-1.246658	*AGA1*	Protein lacking an ortholog in S. cerevisiae
	Cd36_22420	orf19.1354	2	-2.3664756	-1.24274	*YER067W*	Transcriptionally regulated by iron or by yeast-hyphal switch
	Cd36_63370	orf19.5550	6	-2.3658223	-1.2423418	*MRT4*	Predicted ORF in Assemblies 19, 20 and 21
	Cd36_07460	orf19.5065	1	-2.3521025	-1.233951	*ERD1*	Predicted ORF in Assemblies 19, 20 and 21
	Cd36_70700	orf19.1208	7	-2.3503864	-1.232898		Predicted ORF in Assemblies 19, 20 and 21
RPS4A	Cd36_01510	orf19.5341	1	-2.3456218	-1.2299705	*RPS4A*	Predicted ribosomal protein
OP4	Cd36_12150	orf19.4934	1	-2.318589	-1.2132471		Ala- Leu- and Ser-rich protein
DUR3	Cd36_53230	orf19.6656	5	-2.313643	-1.2101662	*DUR3*	Alkaline downregulated
	Cd36_02020	orf19.3674	1	-2.307288	-1.2061981	*GAL10*	Predicted ORF in Assemblies 19, 20 and 21

Gene Name	*C. dubliniensis* Cd36 identifier	*C. albicans* orf19 identifier	C'some	Fold change expression	Normalised Expression	*S. cerevisiae* ortholog	Description
ZRT2	Cd36_17380	orf19.1585	2	-2.3048415	-1.2046676	*ZRT2*	Protein described as predicted zinc transporter
	Cd36_17140	orf19.1569	2	-2.3045974	-1.2045147	*UTP22*	Predicted ORF in Assemblies 19, 20 and 21
	Cd36_08680	orf19.4778	1	-2.303235	-1.2036617	*LYS14*	Putative transcription factor with zinc cluster DNA-binding motif
	Cd36_21440	orf19.2272	2	-2.3004794	-1.2019346	*AFT2*	Predicted ORF in Assemblies 19, 20 and 21
	Cd36_72660	orf19.5161	7	-2.2999902	-1.2016277	*MRPL49*	Predicted ORF in Assemblies 19, 20 and 21
	Cd36_86820	orf19.6816	3	-2.2872941	-1.1936419	*YJR096W*	Predicted ORF in Assemblies 19, 20 and 21
AAF1	Cd36_86430	orf19.7436	3	-2.261612	-1.1773515	*DEF1*	Possible regulatory protein
	Cd36_72490	orf19.5180	7	-2.2583108	-1.1752441	*PRX1*	Protein described as a putative cysteine peroxidase
CIP1	Cd36_61180	orf19.113	6	-2.2559292	-1.1737218		Protein with slight similarity to plant isoflavone reductase
	Cd36_43440	orf19.1308	4	-2.2509248	-1.1705179	*VBA1*	Predicted ORF in Assemblies 19, 20 and 21
	Cd36_43860	orf19.5312	4	-2.2469058	-1.1679397	*MET4*	Predicted ORF in Assemblies 19, 20 and 21
ERF1	Cd36_19610	orf19.3541	2	-2.217005	-1.148612	*SUP45*	Putative translation release factor 1, which interacts with stop codons and promotes release of nascent peptides from ribosomes
	Cd36_53190	orf19.2639	5	-2.204864	-1.1406896		Predicted ORF in Assemblies 19, 20 and 21
	Cd36_62630	orf19.3483	6	-2.2043512	-1.1403542	*YPL206C*	Predicted ORF in Assemblies 19, 20 and 21
IMH3	Cd36_20770	orf19.18	2	-2.204298	-1.1403193	*IMD4*	Inosine monophosphate (IMP) dehydrogenase
	Cd36_63060	orf19.5576	6	-2.2039425	-1.1400867	*YDR531W*	Protein similar to S. cerevisiae Ydr531wp
MET16	Cd36_46500	orf19.3106	4	-2.1956835	-1.13467	*MET16*	Putative 3'-phosphoadenylsulfate reductase
ADE4	Cd36_07230	orf19.1233	1	-2.1898234	-1.1308146	*ADE4*	Predicted ORF in Assemblies 19, 20 and 21
ZPR1	Cd36_01050	orf19.3300	1	-2.1822221	-1.125798	*ZPR1*	Protein with putative zinc finger
DBP2	Cd36_27480	orf19.171	R	-2.1722023	-1.1191585	*DBP2*	Predicted ORF in Assemblies 19, 20 and 21
DIM1	Cd36_12720	orf19.5010	1	-2.1709747	-1.1183429	*DIM1*	Protein likely to be essential for growth, based on an insertional mutagenesis strategy
	Cd36_18430	orf19.846	2	-2.16743	-1.1159854	*YKL171W*	Predicted ORF in Assemblies 19, 20 and 21
	Cd36_52430	orf19.4283	5	-2.165985	-1.1150234		Predicted ORF in Assemblies 19, 20 and 21
NIP7	Cd36_62570	orf19.3478	6	-2.1589496	-1.1103295	*NIP7*	Protein described as a nucleolar protein with role in ribosomal assembly
	Cd36_61280	orf19.124	6	-2.1477523	-1.1028275	*CIC1*	Predicted ORF in Assemblies 19, 20 and 21
	Cd36_22260	orf19.2178	2	-2.1472402	-1.1024835	*MRS3|MRS4*	Predicted ORF in Assemblies 19, 20 and 21
GAL1	Cd36_01990	orf19.3670	1	-2.1420393	-1.098985	*GAL3*	Galactokinase
PGA54	Cd36_42920	orf19.2685	4	-2.1335351	-1.0932459	*DAN4*	Putative GPI-anchored protein
PDR16	Cd36_03560	orf19.1027	1	-2.1333654	-1.0931311	*PDR16*	Phosphatidylinositol transfer protein
	Cd36_22340	orf19.2168.3	2	-2.1249013	-1.0873959	*YOP1*	ORF Predicted by Annotation Working Group
NUP	Cd36_71390	orf19.6570	7	-2.1162703	-1.0815239		Nucleoside permease
GAL7	Cd36_02030	orf19.3675	1	-2.1098485	-1.0771394	*GAL7*	Predicted ORF in Assemblies 19, 20 and 21
	Cd36_51460	orf19.585	5	-2.1066625	-1.0749593	*MRPL17*	Predicted ORF in Assemblies 19, 20 and 21
	Cd36_03530	orf19.1030	1	-2.1036892	-1.0729215	*FPR3*	Predicted ORF in Assemblies 19, 20 and 21
HXK2	Cd36_29870	orf19.542	R	-2.102386	-1.0720276	*HXK2*	Protein described as hexokinase II
	Cd36_00780	orf19.6023	1	-2.1016786	-1.071542	*YDR338C*	Predicted ORF in Assemblies 19, 20 and 21
CDC5	Cd36_00900	orf19.6010	1	-2.0956361	-1.0673883	*CDC5*	Polo-like kinase
	Cd36_19020	orf19.4517	2	-2.0887175	-1.0626173		Predicted ORF in Assemblies 19, 20 and 21
	Cd36_11970	orf19.6343	1	-2.0848777	-1.0599627	*FEN1*	Predicted ORF in Assemblies 19, 20 and 21
	Cd36_19030	orf19.4516	2	-2.0796764	-1.056359	*MET7*	Predicted ORF in Assemblies 19, 20 and 21
GPM1	Cd36_18020	orf19.903	2	-2.0706525	-1.0500854	*GPM1*	Protein described as phosphoglycerate mutase
FAL1	Cd36_05320	orf19.2488	1	-2.0665715	-1.0472393	*FAL1*	Predicted ORF in Assemblies 19, 20 and 21
RIM2	Cd36_19110	orf19.4499	2	-2.0649261	-1.0460902	*RIM2*	Protein similar to S. cerevisiae Rim2p
MET6	Cd36_26580	orf19.2551	R	-2.0588415	-1.0418327	*MET6*	5-methyltetrahydropteroyltriglutamate-homocysteine methyltransferase (cobalamin-independent methionine synthase)
	Cd36_61820	orf19.3414	6	-2.0582767	-1.0414369	*SUR7*	Predicted ORF in Assemblies 19, 20 and 21
	Cd36_40860	orf19.4160	4	-2.0567024	-1.040333	*QRI7*	Predicted ORF in Assemblies 19, 20 and 21
GPD1	Cd36_24300	orf19.1756	2	-2.056565	-1.0402367	*GPD1*	Protein similar to S. cerevisiae glycerol-3-phosphate dehydrogenase (enzyme of glycerol biosynthesis)
AAT1	Cd36_19740	orf19.3554	2	-2.055343	-1.0393791	*AAT1*	Protein described as aspartate aminotransferase
CAS5	Cd36_41190	orf19.4670	4	-2.0445564	-1.0317879	*MIG1*	Putative transcription factor: regulates cell wall damage response
CUP2	Cd36_12620	orf19.5001	1	-2.0399559	-1.028538	*HAA1*	Protein not essential for viability
	Cd36_00060		1	-2.035176	-1.0251536		
	Cd36_64570	orf19.1214	6	-2.0347292	-1.0248368	*MAP2*	Predicted ORF in Assemblies 19, 20 and 21
	Cd36_86390	orf19.7427	3	-2.033232	-1.0237749	*YML018C*	Predicted ORF in Assemblies 19, 20 and 21
RPL32	Cd36_61795	orf19.3415.1	6	-2.0320458	-1.022933	*RPL32*	Predicted ribosomal protein
PGA45	Cd36_05620	orf19.2451	1	-2.0254924	-1.0182726	*PLB2*	Putative GPI-anchored protein of unknown function
	Cd36_21250	orf19.2250	2	-2.0248387	-1.017807	*SPE3*	Predicted ORF in Assemblies 19, 20 and 21
	Cd36_73060	orf19.1334	7	-2.024136	-1.0173063		Predicted ORF in Assemblies 19, 20 and 21
DOT4	Cd36_43230	orf19.3370	4	-2.0203857	-1.0146308	*UBP10*	Protein similar to ubiquitin C-terminal hydrolase
	Cd36_61660	orf19.3430	6	-2.0185025	-1.0132854		Predicted ORF in Assemblies 19, 20 and 21
RBF1	Cd36_63270	orf19.5558	6	-2.0179005	-1.012855	*DEF1*	Transcription factor
	Cd36_62600	orf19.3481	6	-2.0158772	-1.0114079	*MRH4*	Predicted ORF in Assemblies 19, 20 and 21
CAM1	Cd36_85940	orf19.7382	3	-2.0153477	-1.0110288	*CAM1*	Putative translation elongation factor eEF1 gamma
	Cd36_83220	orf19.326	3	-2.014745	-1.0105972		Predicted ORF in Assemblies 19, 20 and 21
	Cd36_44550	orf19.3788	4	-2.01324	-1.0095192		Predicted ORF in Assemblies 19, 20 and 21
GDB1	Cd36_44790	orf19.744	4	-2.0128534	-1.009242	*GDB1*	Putative glycogen debranching enzyme
	Cd36_52320	orf19.4268	5	-2.0083299	-1.0059962	*UTP13*	Predicted ORF in Assemblies 19, 20 and 21
	Cd36_85890	orf19.7377	3	-1.991375	-0.9937649	*ASE1*	Predicted ORF in Assemblies 19, 20 and 21
	Cd36_42540	orf19.2739	4	-1.9871291	-0.9906856	*RLF2*	Predicted ORF in Assemblies 19, 20 and 21
MIT1	Cd36_23310	orf19.4077	2	-1.985832	-0.9897436	*SUR1|CSH1*	Protein involved in sphingolipid biosynthesis
CHL4	Cd36_04310	orf19.6851	1	-1.9826789	-0.9874511	*CHL4*	Protein described as having role in chromosome segregation

Gene Name	*C. dubliniensis* Cd36 identifier	*C. albicans* orf19 identifier	C'some	Fold change expression	Normalised Expression	*S. cerevisiae* ortholog	Description
	Cd36_84450	orf19.5905	3	-1.9753239	-0.9820893	*YBL028C*	Predicted ORF in Assemblies 19, 20 and 21
	Cd36_10970		1	-1.9680064	-0.9767349		
SER33	Cd36_11260	orf19.5263	1	-1.962125	-0.9724169	*SER3*	Predicted enzyme of amino acid biosynthesis
	Cd36_63900	orf19.5602	6	-1.9586377	-0.96985054		Predicted ORF in Assemblies 19, 20 and 21
WHI3	Cd36_72010	orf19.6494	7	-1.9571097	-0.9687246	*WHI3*	Predicted ORF in Assemblies 19, 20 and 21
NOP1	Cd36_46180	orf19.3138	4	-1.9545041	-0.9668026	*NOP1*	Nucleolar protein
	Cd36_85960	orf19.7384	3	-1.9525551	-0.96536326	*NOG1*	Predicted ORF in Assemblies 19, 20 and 21
	Cd36_19140	orf19.4496	2	-1.9521459	-0.96506095	*GDT1*	Predicted ORF in Assemblies 19, 20 and 21
	Cd36_18720	orf19.813	2	-1.9515618	-0.9646292	*NAB3*	Predicted ORF in Assemblies 19, 20 and 21
	Cd36_17560	orf19.5825	2	-1.9514096	-0.96451664	*NCB2*	Predicted ORF in Assemblies 19, 20 and 21
	Cd36_08530	orf19.4760	1	-1.950951	-0.9641775	*YIL110W*	Predicted ORF in Assemblies 19, 20 and 21
MRPL3	Cd36_07440	orf19.5064	1	-1.9480228	-0.9620106	*MRPL3*	Predicted ORF in Assemblies 19, 20 and 21
	Cd36_06990	orf19.2795	1	-1.9465934	-0.96095157	*LHP1*	Predicted ORF in Assemblies 19, 20 and 21
FUR1	Cd36_53170	orf19.2640	5	-1.9428313	-0.95816064	*FUR1*	Uracil phosphoribosyltransferase
	Cd36_73460	orf19.7202	7	-1.9422688	-0.9577429	*RER1*	Predicted ORF in Assemblies 19, 20 and 21
CYS3	Cd36_33930	orf19.6402	R	-1.9400024	-0.9560585	*CYS3*	Predicted enzyme of sulfur amino acid biosynthesis
	Cd36_87200	orf19.6769	3	-1.9346303	-0.95205784	*YHL029C*	Predicted ORF in Assemblies 19, 20 and 21
	Cd36_15980	orf19.2017	2	-1.9340906	-0.9516554	*RPA49*	Predicted ORF in Assemblies 19, 20 and 21
	Cd36_51270	orf19.1967	5	-1.93013	-0.94869804	*IMG1*	Predicted ORF in Assemblies 19, 20 and 21
	Cd36_11790	orf19.3755	1	-1.929326	-0.948097	*MRPL15*	Predicted ORF in Assemblies 19, 20 and 21
	Cd36_82930	orf19.288	3	-1.9291252	-0.9479468	*MET13*	Predicted ORF in Assemblies 19, 20 and 21
	Cd36_09430	orf19.4870	1	-1.9287223	-0.9476454	*DBP3*	Predicted ORF in Assemblies 19, 20 and 21
	Cd36_84230	orf19.5871	3	-1.9283863	-0.94739413	*SNF5*	Predicted ORF in Assemblies 19, 20 and 21
VRG4	Cd36_07220	orf19.1232	1	-1.9264364	-0.94593453	*VRG4*	GDP-mannose transporter
NIP1	Cd36_41490	orf19.4635	4	-1.9175422	-0.93925834	*NIP1*	Putative translation initiation factor
	Cd36_16910	orf19.1528	2	-1.9096012	-0.9332714	*MTF1*	Predicted ORF in Assemblies 19, 20 and 21
	Cd36_81440	orf19.1697	3	-1.9094462	-0.93315434	*TMA46*	Predicted ORF in Assemblies 19, 20 and 21
	Cd36_21040	orf19.3148	2	-1.9091192	-0.9329072	*IXR1*	Predicted ORF in Assemblies 19, 20 and 21
SSC1	Cd36_21650	orf19.1896	2	-1.9062464	-0.93073463	*SSC1*	Heat shock protein
ENO1	Cd36_08010	orf19.395	1	-1.9057811	-0.9303825	*ENO1*	Enolase (2-phospho-D-glycerate-hydrolyase), enzyme of glycolysis and gluconeogenesis
	Cd36_30340	orf19.1806	R	-1.905159	-0.9299114	*DEF1*	Predicted ORF in Assemblies 19, 20 and 21
CAM1-1	Cd36_53070	orf19.2651	5	-1.9050953	-0.9298632	*CAM1*	Putative translation elongation factor
NDH51	Cd36_19150	orf19.4495	2	-1.9038757	-0.92893934		Subunit of nicotinamide adenine dinucleotide dehydrogenase complex I, of the mitochondrial electron transport chain
ECM1	Cd36_43760	orf19.5299	4	-1.903793	-0.92887664	*ECM1*	Decreased mRNA abundance observed in cyr1 homozygous mutant hyphae
	Cd36_82490	orf19.242.2	3	-1.8994484	-0.9255805	*YSY6*	ORF Predicted by Annotation Working Group
	Cd36_81730	orf19.1662	3	-1.894019	-0.92145085	*MRP1*	Predicted ORF in Assemblies 19, 20 and 21
	Cd36_27740	orf19.2830	R	-1.8894644	-0.91797733	*RRP9*	Predicted ORF in Assemblies 19, 20 and 21
	Cd36_50020		5	-1.8892505	-0.917814		
	Cd36_85820	orf19.7369	3	-1.8873389	-0.91635346	*TRM12*	Predicted ORF in Assemblies 19, 20 and 21
RPN6	Cd36_43530	orf19.1299	4	-1.8866746	-0.91584563	*RPN6*	Predicted ORF in Assemblies 19, 20 and 21
	Cd36_40710	orf19.4176	4	-1.8815383	-0.9119127	*MRPS17*	Predicted ORF in Assemblies 19, 20 and 21
	Cd36_63330	orf19.5553	6	-1.8813946	-0.91180253	*YKL069W*	Predicted ORF in Assemblies 19, 20 and 21
	Cd36_11130	orf19.5279	1	-1.8794003	-0.91027236	*MRPL51*	Predicted ORF in Assemblies 19, 20 and 21
	Cd36_50750	orf19.6297	5	-1.8779541	-0.9091618	*DEG1*	Predicted ORF in Assemblies 19, 20 and 21
ASC1	Cd36_71100	orf19.6906	7	-1.8776816	-0.9089524	*ASC1*	Protein described as part of 40S ribosomal subunit
	Cd36_73330	orf19.6693	7	-1.8764874	-0.90803456	*YOL098C*	Predicted ORF in Assemblies 19, 20 and 21
NEP1	Cd36_10670	orf19.665	1	-1.8756803	-0.90741396	*EMG1*	Protein of unknown function
ILV2	Cd36_82300	orf19.1613	3	-1.8724073	-0.90489435	*ILV2*	Protein described as acetolactate synthase
PHO87	Cd36_05600	orf19.2454	1	-1.8693345	-0.9025247	*PHO87*	Protein similar to phosphate permeases
	Cd36_70850	orf19.7022	7	-1.8685464	-0.9019163		Predicted ORF in Assemblies 19, 20 and 21
	Cd36_84920	orf19.5964	3	-1.8668878	-0.90063524	*ARF2*	Predicted ORF in Assemblies 19, 20 and 21
CNT	Cd36_20440	orf19.4118	2	-1.8656372	-0.89966846		Cation-coupled nucleoside transporter (H(+)/nucleoside symporter)
	Cd36_04320		1	-1.8585275	-0.89416003		
	Cd36_19820	orf19.3564	2	-1.8519354	-0.8890338	*RPC40*	Predicted ORF in Assemblies 19, 20 and 21
YCK2	Cd36_85620	orf19.7001	3	-1.8517727	-0.88890696	*YCK2*	Protein similar to S. cerevisiae Yck2p, which is a plasma membrane-bound casein kinase I isoform
CSI2	Cd36_11540	orf19.5232	1	-1.8515488	-0.88873255	*BRX1*	Protein essential for growth
	Cd36_81570	orf19.1675	3	-1.8510582	-0.88835025	*YDL133W*	Predicted ORF in Assemblies 19, 20 and 21
	Cd36_62990	orf19.5541	6	-1.8503892	-0.8878288	*YPL184C*	Predicted ORF in Assemblies 19, 20 and 21
	Cd36_09150	orf19.4835	1	-1.847725	-0.88575006	*UTP7*	Predicted ORF in Assemblies 19, 20 and 21
TUB4	Cd36_45170	orf19.1238	4	-1.846548	-0.8848307	*TUB4*	Putative gamma-tubulin
GAR1	Cd36_10840	orf19.1164	1	-1.845146	-0.88373494	*GAR1*	Predicted ORF in Assemblies 19, 20 and 21
NOP15	Cd36_70640	orf19.7050	7	-1.8444575	-0.8831966	*NOP15*	Protein described as a nucleolar ribosome biogenesis factor
	Cd36_72540	orf19.5175	7	-1.8441783	-0.8829782	*SSM4*	Predicted ORF in Assemblies 19, 20 and 21
	Cd36_05190	orf19.417	1	-1.8429177	-0.8819916	*MTM1*	Predicted ORF in Assemblies 19, 20 and 21
	Cd36_86880	orf19.6809	3	-1.8417288	-0.8810606	*PMU1*	Predicted ORF in Assemblies 19, 20 and 21
	Cd36_07000	orf19.2794	1	-1.8400811	-0.8797693	*YBL036C*	Protein regulated by Gcn4p
YML6	Cd36_70880	orf19.7019	7	-1.8382887	-0.8783634	*YML6*	Protein described as a mitochondrial ribosomal protein
ERG11	Cd36_50660	orf19.922	5	-1.8356407	-0.87628365	*ERG11*	Lanosterol 14-alpha-demethylase, member of cytochrome P450 family that functions in ergosterol biosynthesis
	Cd36_02910		1	-1.8345225	-0.8754046		
SHM2	Cd36_64270	orf19.5750	6	-1.8344231	-0.8753264	*SHM2*	Cytoplasmic serine hydroxymethyltransferase
GCV1	Cd36_62730	orf19.5519	6	-1.8332415	-0.8743968	*GCV1*	Protein described as T subunit of glycine decarboxylase
SPE2	Cd36_50700	orf19.568	5	-1.8330787	-0.8742688	*SPE2*	Predicted ORF in Assemblies 19, 20 and 21
	Cd36_41500	orf19.4634	4	-1.8297166	-0.8716202	*NCS6*	Predicted ORF in Assemblies 19, 20 and 21

Gene Name	*C. dubliniensis* Cd36 identifier	*C. albicans* orf19 identifier	C'some	Fold change expression	Normalised Expression	*S. cerevisiae* ortholog	Description
	Cd36_86030	orf19.7392	3	-1.8276217	-0.86996746	*DBP1*	Predicted ORF in Assemblies 19, 20 and 21
MAM33	Cd36_73610	orf19.7187	7	-1.8254948	-0.86828756	*MAM33*	Predicted ORF in Assemblies 19, 20 and 21
	Cd36_20750	orf19.5500	2	-1.8229226	-0.86625326	*MAK16*	Predicted ORF in Assemblies 19, 20 and 21
ABP140	Cd36_02040	orf19.3676	1	-1.8228434	-0.8661907	*ABP140*	Protein similar to S. cerevisiae actin-binding protein Abp140p
	Cd36_04680	orf19.48	1	-1.8218954	-0.86544013	*RPM2*	Predicted ORF in Assemblies 19, 20 and 21
	Cd36_63520	orf19.5704	6	-1.8211206	-0.86482644	*YGR150C*	Predicted ORF in Assemblies 19, 20 and 21
	Cd36_21320	orf19.2259	2	-1.8191928	-0.8632984		Predicted ORF in Assemblies 19, 20 and 21
GLC3	Cd36_63660	orf19.5622	6	-1.8171483	-0.8616762	*GLC3*	Protein described as similar to 1,4-glucan branching enzyme
RIM11	Cd36_18940	orf19.791	2	-1.815651	-0.860487	*RIM11*	Protein not essential for viability
	Cd36_01010	orf19.3295	1	-1.8151186	-0.8600638		Predicted ORF in Assemblies 19, 20 and 21
	Cd36_73310	orf19.6696	7	-1.8149395	-0.85992146	*TIM9*	Predicted ORF in Assemblies 19, 20 and 21
	Cd36_06070	orf19.6264.3	1	-1.8145418	-0.8596053	*YIP3*	ORF Predicted by Annotation Working Group
TRP4	Cd36_46560	orf19.3099	4	-1.8114624	-0.85715485	*TRP4*	Predicted enzyme of amino acid biosynthesis
	Cd36_41660	orf19.4617	4	-1.8107641	-0.8565986	*MAK3*	Predicted ORF in Assemblies 19, 20 and 21
CYS4	Cd36_01710	orf19.4536	1	-1.8097898	-0.8558221	*CYS4*	Predicted enzyme of sulfur amino acid biosynthesis
PRO2	Cd36_87140	orf19.6779	3	-1.80936	-0.8554795	*PRO2*	Predicted ORF in Assemblies 19, 20 and 21
	Cd36_02370	orf19.2940	1	-1.8082783	-0.85461676	*BOS1*	Predicted ORF in Assemblies 19, 20 and 21
GAL10	Cd36_02000	orf19.3672	1	-1.8081751	-0.8545344	*GAL10*	UDP-glucose 4-epimerase, required for galactose utilization
	Cd36_42750	orf19.2708	4	-1.8073963	-0.85391283	*SDO1*	Predicted ORF in Assemblies 19, 20 and 21
	Cd36_11100	orf19.5282	1	-1.8040314	-0.8512244		Predicted ORF in Assemblies 19, 20 and 21
MED8	Cd36_19130	orf19.4497	2	-1.802679	-0.8501425	*MED8*	Protein not essential for viability
PMT5	Cd36_34920	orf19.7549	R	-1.8009912	-0.8487911	*PMT1*	Protein mannosyltransferase with an unknown role, expressed at extremely low levels
	Cd36_62440	orf19.3466	6	-1.800828	-0.84866035	*MRM2*	Predicted ORF in Assemblies 19, 20 and 21
SSU81	Cd36_08610	orf19.4772	1	-1.7968029	-0.84543216	*SHO1*	Predicted adaptor protein involved in activation of MAP kinase-dependent signaling pathways
PFK1	Cd36_54420	orf19.3967	5	-1.7933719	-0.84267473	*PFK1*	Alpha subunit of phosphofructokinase (PFK), which is Pfk1p, Pfk2p heteromultimer
HPT1	Cd36_17630	orf19.5832	2	-1.7921025	-0.8416531	*HPT1*	Protein abundance is affected by URA3 expression in the CAI-4 strain background
FBA1	Cd36_41650	orf19.4618	4	-1.7913848	-0.84107524	*FBA1*	Putative fructose-bisphosphate aldolase
PGA32	Cd36_87090	orf19.6784	3	-1.7906678	-0.84049773	*DAN4*	Putative GPI-anchored protein of unknown function
MSS51	Cd36_35080	orf19.7577	R	-1.7906033	-0.84044576	*MSS51*	Putative mRNA maturation factor
	Cd36_17900	orf19.5783	2	-1.7878064	-0.83819056	*YOR021C*	Predicted ORF in Assemblies 19, 20 and 21
	Cd36_03570	orf19.1026	1	-1.786768	-0.8373523	*CSL4*	Predicted ORF in Assemblies 19, 20 and 21
YTM1	Cd36_08970	orf19.4815	1	-1.7852441	-0.8361213	*YTM1*	Protein similar to S. cerevisiae Ytm1p, which is involved in biogenesis of the large ribosomal subunit
	Cd36_45760	orf19.10431	4	-1.783677	-0.83485436		0
	Cd36_18390	orf19.850	2	-1.78308	-0.83437145	*NTA1*	Predicted ORF in Assemblies 19, 20 and 21
ARO4	Cd36_04870	orf19.4060	1	-1.7813842	-0.83299875	*ARO4*	3-Deoxy-D-arabinoheptulosonate-7-phosphate synthase
DPM1	Cd36_07530	orf19.5073	1	-1.7794753	-0.8314519	*DPM1*	Protein with similarity to S. cerevisiae Dpm1p, which is dolichol phosphate mannose synthase
KTR2	Cd36_19160	orf19.4494	2	-1.7773172	-0.8297012	*KTR2*	Protein with similarity to S. cerevisiae Ktr2p, which is a mannosyltransferase
	Cd36_81400	orf19.1701	3	-1.7726767	-0.8259294	*RKI1*	Predicted ORF in Assemblies 19, 20 and 21
	Cd36_16100	orf19.2002	2	-1.7720942	-0.82545537	*NIC96*	Predicted ORF in Assemblies 19, 20 and 21
	Cd36_18500	orf19.839	2	-1.770303	-0.8239963	*YLR143W*	Predicted ORF in Assemblies 19, 20 and 21
	Cd36_42000	orf19.4580	4	-1.768514	-0.82253766		Predicted ORF in Assemblies 19, 20 and 21
	Cd36_70590	orf19.7082	7	-1.7685082	-0.8225329	*PET8*	Predicted ORF in Assemblies 19, 20 and 21
	Cd36_80760	orf19.6155	3	-1.7684509	-0.82248616	*CDC9*	Predicted ORF in Assemblies 19, 20 and 21
DPB2	Cd36_35000	orf19.7564	R	-1.7675791	-0.8217747	*DPB2*	Probable subunit of DNA polymerase II (DNA polymerase epsilon), similar to S. cerevisiae Dpb2p
	Cd36_44670	orf19.3774	4	-1.7675289	-0.82173383	*PPG1*	Predicted ORF in Assemblies 19, 20 and 21
	Cd36_20080	orf19.6874	2	-1.7661234	-0.8205862	*BAS1*	Predicted ORF in Assemblies 19, 20 and 21
	Cd36_04460	orf19.773	1	-1.7651551	-0.8197949	*RSA3*	Putative ortholog of S. cerevisiae Rsa3p, which is a nucleolar protein involved in maturation of pre-60S ribosomal particles that interacts with Dbp6p
	Cd36_29080	orf19.4355	R	-1.7647487	-0.8194628		Predicted ORF in Assemblies 19, 20 and 21
	Cd36_82110	orf19.1633	3	-1.7638547	-0.8187318	*UTP4*	Predicted ORF in Assemblies 19, 20 and 21
	Cd36_87380	orf19.6741	3	-1.7634878	-0.8184316		Predicted ORF in Assemblies 19, 20 and 21
	Cd36_10280		1	-1.7614315	-0.8167484		
	Cd36_42890	orf19.2688	4	-1.7596486	-0.81528735	*NAN1*	Predicted ORF in Assemblies 19, 20 and 21
ERG20	Cd36_19180	orf19.4491	2	-1.7594768	-0.81514645	*ERG20*	Putative farnesyl pyrophosphate synthetase involved in isoprenoid and sterol biosynthesis, based on similarity to S. cerevisiae Erg20p
	Cd36_08300	orf19.4738	1	-1.7594192	-0.81509924	*SLP1*	Predicted ORF in Assemblies 19, 20 and 21
MRP20	Cd36_01470	orf19.3350	1	-1.7593988	-0.81508255	*MRP20*	Protein described as component of mitochondrial ribosome
	Cd36_07050	orf19.2788	1	-1.7583947	-0.81425893	*RIB2*	Predicted ORF in Assemblies 19, 20 and 21
PTR2	Cd36_83780	orf19.6937	3	-1.7577049	-0.8136928	*PTR2*	Putative oligopeptide transporter
	Cd36_02110	orf19.3683	1	-1.754201	-0.81081414	*GCS1*	Putative transcription factor with zinc finger DNA-binding motif
	Cd36_52360	orf19.4273	5	-1.7535698	-0.81029487		Predicted ORF in Assemblies 19, 20 and 21
	Cd36_43470	orf19.1305	4	-1.7510967	-0.8082588	*TRM5*	Predicted ORF in Assemblies 19, 20 and 21
	Cd36_51210	orf19.1959	5	-1.750335	-0.807631	*OTU2*	Predicted ORF in Assemblies 19, 20 and 21
RPS7A	Cd36_81410	orf19.1700	3	-1.7486537	-0.8062446	*RPS7A*	Predicted ribosomal protein
RXT3	Cd36_19850	orf19.3568	2	-1.7481259	-0.80580914	*SCD5*	Predicted ORF in Assemblies 19, 20 and 21
	Cd36_07330	orf19.5051	1	-1.7478684	-0.8055966		Predicted ORF in Assemblies 19, 20 and 21
SLP2	Cd36_23330	orf19.4079	2	-1.7478621	-0.80559134		Predicted ORF in Assemblies 19, 20 and 21
	Cd36_20920	orf19.35	2	-1.7470602	-0.80492926	*SKY1*	Predicted ORF in Assemblies 19, 20 and 21

Gene Name	*C. dubliniensis* Cd36 identifier	*C. albicans* orf19 identifier	C'some	Fold change expression	Normalised Expression	*S. cerevisiae* ortholog	Description
	Cd36_70940	orf19.7013	7	**-1.7468765**	-0.8047776		Predicted ORF in Assemblies 19, 20 and 21
TEM1	Cd36_02880	orf19.3001	1	**-1.7453154**	-0.8034878	*TEM1*	Protein similar to S. cerevisiae Tem1p, which is a GTPase involved in termination of the M phase of the cell cycle
IDI1	Cd36_42170	orf19.2775	4	**-1.7422875**	-0.8009827	*IDI1*	Predicted ORF in Assemblies 19, 20 and 21
RPL18	Cd36_85070	orf19.5982	3	**-1.7405944**	-0.7995801	*RPL18A|RPL18E*	Predicted ribosomal protein
	Cd36_73450	orf19.7203	7	**-1.7382476**	-0.79763365	*MRP7*	Predicted ORF in Assemblies 19, 20 and 21
FRE7	Cd36_32920	orf19.6139	R	**-1.7382433**	-0.7976301	*FRE3*	Protein similar to ferric reductase Fre10p
	Cd36_09860	orf19.989	1	**-1.736872**	-0.7964914	*MRPS5*	Predicted ORF in Assemblies 19, 20 and 21
	Cd36_09930		1	**-1.7354686**	-0.7953253		
SIM1	Cd36_12920	orf19.5032	1	**-1.7351758**	-0.79508185	*UTH1*	Protein described as a DNA replication regulatory protein
	Cd36_01700	orf19.4537	1	**-1.7347248**	-0.7947068	*DST1*	Predicted ORF in Assemblies 19, 20 and 21
MCD1	Cd36_35370	orf19.7634	R	**-1.7341249**	-0.7942078	*MCD1*	Protein similar to S. cerevisiae Mcd1p
	Cd36_82730	orf19.264	3	**-1.732248**	-0.79264545		Predicted ORF in Assemblies 19, 20 and 21
	Cd36_72620	orf19.5165	7	**-1.7319912**	-0.7924316	*YNR029C*	Predicted ORF in Assemblies 19, 20 and 21
	Cd36_16990	orf19.1536	2	**-1.7316502**	-0.7921475	*ZRC1*	Predicted ORF in Assemblies 19, 20 and 21
	Cd36_07680	orf19.5092	1	**-1.7298187**	-0.7906208		Predicted ORF in Assemblies 19, 20 and 21
FAD3	Cd36_12140	orf19.4933	1	**-1.7289358**	-0.7898843		Omega-3 fatty acid desaturase, involved in production of alpha-linolenic acid, which is a major component of membranes
	Cd36_60700	orf19.3649	6	**-1.7287315**	-0.78971386	*FES1*	Predicted ORF in Assemblies 19, 20 and 21
	Cd36_44460	orf19.3797	4	**-1.7284244**	-0.78945756	*MRPL11*	Predicted ORF in Assemblies 19, 20 and 21
	Cd36_03170	orf19.3037	1	**-1.7284162**	-0.78945065	*PAB1*	Protein described as poly(A)-binding protein
RBR3	Cd36_72940	orf19.5124	7	**-1.7268592**	-0.7881504	*YMR317W*	Cell wall protein
KTR4	Cd36_03720	orf19.4475	1	**-1.7261025**	-0.78751814	*KTR4*	Protein with similarity to mannosyltransferases
PCL7	Cd36_06410	orf19.6225	1	**-1.7258267**	-0.7872876	*PCL6*	Protein described as cyclin-like, possible Pho85p cyclin
	Cd36_16760	orf19.1507	2	**-1.7257979**	-0.7872635	*AMN1*	Predicted ORF in Assemblies 19, 20 and 21
MNN3	Cd36_09470	orf19.4874	1	**-1.7248882**	-0.78650284	*MNN2*	Predicted Golgi alpha-1,2-mannosyltransferase
	Cd36_05400		1	**-1.7246706**	-0.7863209		
TAF14	Cd36_18850	orf19.798	2	**-1.7238315**	-0.7856188	*TAF14*	Putative DNA-binding transcription factor
	Cd36_10530	orf19.680	1	**-1.7222959**	-0.784333	*TIM50*	Predicted ORF in Assemblies 19, 20 and 21
	Cd36_19590	orf19.3539	2	**-1.7220812**	-0.78415316	*YBR141C*	Predicted ORF in Assemblies 19, 20 and 21
MNT1	Cd36_81700	orf19.1665	3	**-1.7216021**	-0.7837517	*KTR1*	Alpha-1,2-mannosyl transferase
	Cd36_11850	orf19.6356	1	**-1.7206064**	-0.78291714	*PRP6*	Predicted ORF in Assemblies 19, 20 and 21
TOM70	Cd36_72330	orf19.3700	7	**-1.719281**	-0.7818053	*TOM70*	Protein described as mitochondrial import receptor
RPO41	Cd36_00570	orf19.6041	1	**-1.7183663**	-0.78103757	*RPO41*	Predicted ORF in Assemblies 19, 20 and 21
RNR1	Cd36_17930	orf19.5779	2	**-1.7179613**	-0.7806976	*RNR1*	Protein similar S. cerevisiae Rnr1p, large subunit of ribonucleotide reductase
	Cd36_53210	orf19.2637	5	**-1.711759**	-0.77547956	*PER1*	Predicted ORF in Assemblies 19, 20 and 21
	Cd36_11860	orf19.6355	1	**-1.7116076**	-0.775352	*RRB1*	Predicted ORF in Assemblies 19, 20 and 21
	Cd36_50370	orf19.955	5	**-1.7101464**	-0.77411985		Predicted ORF in Assemblies 19, 20 and 21
ERG26	Cd36_45790	orf19.2909	4	**-1.7060243**	-0.7706382	*ERG26*	C-3 sterol dehydrogenase, catalyzes the second of three steps required to remove two C-4 methyl groups from an intermediate in ergosterol biosynthesis
RPS12	Cd36_87080	orf19.6785	3	**-1.7039193**	-0.768857	*RPS12*	Protein described as acidic ribosomal protein S12
RLI1	Cd36_03150	orf19.3034	1	**-1.7037554**	-0.76871824	*RLI1*	Member of RNase L inhibitor (RLI) subfamily of ABC family
	Cd36_23950		2	**-1.7030469**	-0.76811814		
	Cd36_72830	orf19.5136	7	**-1.7029343**	-0.7680228	*YGR017W*	Predicted ORF in Assemblies 19, 20 and 21
	Cd36_22840	orf19.3609	2	**-1.7028949**	-0.7679894	*UTP15*	Predicted ORF in Assemblies 19, 20 and 21
	Cd36_86730	orf19.6828	3	**-1.7016988**	-0.76697564	*RRP1*	Predicted ORF in Assemblies 19, 20 and 21
	Cd36_17060	orf19.1578	2	**-1.7011971**	-0.7665503	*RRP5*	Predicted ORF in Assemblies 19, 20 and 21
	Cd36_29400	orf19.494	R	**-1.6997995**	-0.76536465	*NAF1*	Predicted ORF in Assemblies 19, 20 and 21
	Cd36_43520	orf19.1300	4	**-1.699517**	-0.7651248	*OMS1*	Predicted ORF in Assemblies 19, 20 and 21
	Cd36_17160	orf19.1566	2	**-1.6977353**	-0.76361156	*UTP21*	Predicted ORF in Assemblies 19, 20 and 21
	Cd36_87620	orf19.6710	3	**-1.6955236**	-0.7617309		Predicted ORF in Assemblies 19, 20 and 21
	Cd36_04950	orf19.445	1	**-1.6954662**	-0.76168203		Predicted ORF in Assemblies 19, 20 and 21
	Cd36_34650	orf19.7326	R	**-1.695109**	-0.76137805	*RKM1*	Predicted ORF in Assemblies 19, 20 and 21
	Cd36_10230	orf19.2326	1	**-1.6945533**	-0.760905	*ESC2*	Predicted ORF in Assemblies 19, 20 and 21
	Cd36_87110	orf19.6782	3	**-1.6944948**	-0.7608552		Predicted ORF in Assemblies 19, 20 and 21
	Cd36_18830	orf19.801	2	**-1.6926601**	-0.75929224	*TBF1*	Predicted ORF in Assemblies 19, 20 and 21
	Cd36_18600	orf19.828	2	**-1.6921604**	-0.7588663	*MRPL24*	Predicted ORF in Assemblies 19, 20 and 21
	Cd36_63850	orf19.5608	6	**-1.6916026**	-0.75839067	*RPC34*	Predicted ORF in Assemblies 19, 20 and 21
MRPL10	Cd36_19520	orf19.3532	2	**-1.6911833**	-0.75803304	*MRPL10*	Predicted ORF in Assemblies 19, 20 and 21
	Cd36_82700	orf19.261	3	**-1.6901096**	-0.7571168	*SEC59*	Predicted ORF in Assemblies 19, 20 and 21
GIN4	Cd36_10690	orf19.663	1	**-1.688342**	-0.7556071	*GIN4*	Kinase involved in pseudohyphal-to-hyphal switch
	Cd36_62100	orf19.688	6	**-1.6880652**	-0.7553706	*MRPS18*	Predicted ORF in Assemblies 19, 20 and 21
	Cd36_85110	orf19.5987	3	**-1.687542**	-0.75492334	*TRM11*	Predicted ORF in Assemblies 19, 20 and 21
	Cd36_82100	orf19.1634	3	**-1.686703**	-0.75420594	*ACB1*	Predicted ORF in Assemblies 19, 20 and 21
	Cd36_17880	orf19.5785	2	**-1.6865034**	-0.75403523		Predicted ORF in Assemblies 19, 20 and 21
CDC14	Cd36_60580	orf19.4192	6	**-1.6826886**	-0.7507682	*CDC14*	Protein involved in exit from mitosis and morphogenesis
RPL15A	Cd36_29390	orf19.493	R	**-1.682333**	-0.75046325	*RPL15B|RPL15A*	Putative ribosomal protein
HGH1	Cd36_41940	orf19.4587	4	**-1.6821039**	-0.7502668	*HGH1*	Transcription is regulated by Mig1p
	Cd36_73050	orf19.1335	7	**-1.6820945**	-0.7502587	*MTR4*	Predicted ORF in Assemblies 19, 20 and 21
FRE10	Cd36_43990	orf19.1415	4	**-1.6818552**	-0.7500535	*FRE4*	Major cell-surface ferric reductase under low-iron conditions
	Cd36_86540	orf19.7445	3	**-1.6816981**	-0.7499187	*VID24*	Predicted ORF in Assemblies 19, 20 and 21
HTA2	Cd36_03930	orf19.1051	1	**-1.6798543**	-0.7483361	*HTA1*	Protein described as histone H2A
	Cd36_12410	orf19.4964	1	**-1.678905**	-0.74752057	*BUD13*	Predicted ORF in Assemblies 19, 20 and 21
	Cd36_17680	orf19.5838	2	**-1.678856**	-0.7474785	*SER2*	Predicted ORF in Assemblies 19, 20 and 21
RPA12	Cd36_21570	orf19.2287	2	**-1.67802**	-0.7467599	*RPA12*	Protein described as DNA-directed RNA polymerase I
	Cd36_86280	orf19.7413	3	**-1.6778958**	-0.7466531	*MMS21*	Predicted ORF in Assemblies 19, 20 and 21

Gene Name	*C. dubliniensis* Cd36 identifier	*C. albicans* orf19 identifier	C'some	Fold change expression	Normalised Expression	*S. cerevisiae* ortholog	Description
	Cd36_84700	orf19.5934	3	**-1.6763536**	-0.7453265	*TOP3*	Predicted ORF in Assemblies 19, 20 and 21
GUA1	Cd36_08950	orf19.4813	1	**-1.6722245**	-0.7417686	*GUA1*	Predicted ORF in Assemblies 19, 20 and 21
	Cd36_12510	orf19.4982	1	**-1.671676**	-0.74129534	*TGL1*	Predicted ORF in Assemblies 19, 20 and 21
	Cd36_44640	orf19.3778	4	**-1.670553**	-0.7403257	*RSA4*	Predicted ORF in Assemblies 19, 20 and 21
	Cd36_71010	orf19.6898	7	**-1.6704944**	-0.74027514		Predicted ORF in Assemblies 19, 20 and 21
	Cd36_21390	orf19.2266	2	**-1.6704754**	-0.7402587	*IOC3*	Predicted ORF in Assemblies 19, 20 and 21
URA3	Cd36_81280	orf19.1716	3	**-1.6695246**	-0.73943734	*URA3*	Orotidine-5'-phosphate decarboxylase, enzyme of pyrimidine biosynthesis
	Cd36_28490	orf19.2389	R	**-1.6694494**	-0.73937243	*SLD2*	Predicted ORF in Assemblies 19, 20 and 21
LYS4	Cd36_44080	orf19.3846	4	**-1.6687232**	-0.73874474	*LYS4*	Protein described as homoaconitase
GUK1	Cd36_53520	orf19.1115	5	**-1.668396**	-0.73846173	*GUK1*	Putative guanylate kinase
KRE30	Cd36_22210	orf19.2183	2	**-1.6678218**	-0.7379651	*ARB1*	YEF3-subfamily ABC family protein, predicted not to be a transporter
NDE1	Cd36_83390	orf19.339	3	**-1.6666491**	-0.7369504	*NDE1*	Putative NADH dehydrogenase that could act alternatively to complex I in respiration
SOD1	Cd36_42210	orf19.2770.1	4	**-1.6664908**	-0.7368133	*SOD1*	Cytosolic copper- and zinc-containing superoxide dismutase, involved in protection from oxidative stress and required for full virulence
ARF3	Cd36_81390	orf19.1702	3	**-1.6654159**	-0.7358825	*ARF3*	Transcription is filament induced
	Cd36_73870	orf19.7153	7	**-1.6645737**	-0.7351527	*LOS1*	Predicted ORF in Assemblies 19, 20 and 21
NAM7	Cd36_50510	orf19.939	5	**-1.6642711**	-0.73489046	*NAM7*	Putative role in nonsense-mediated mRNA decay
	Cd36_09390	orf19.4865	1	**-1.6638067**	-0.7344878	*SAC1*	Predicted ORF in Assemblies 19, 20 and 21
	Cd36_40790	orf19.4168	4	**-1.663341**	-0.734084	*POP7*	Predicted ORF in Assemblies 19, 20 and 21
	Cd36_09900	orf19.997	1	**-1.6599641**	-0.73115206		Predicted ORF in Assemblies 19, 20 and 21
	Cd36_73860	orf19.7154	7	**-1.6568935**	-0.7284808	*UTP18*	Predicted ORF in Assemblies 19, 20 and 21
	Cd36_60600	orf19.3660	6	**-1.6551018**	-0.7269199		Predicted ORF in Assemblies 19, 20 and 21
IFE1	Cd36_04500	orf19.769	1	**-1.6541605**	-0.7260992	*BDH2*	Protein not essential for viability
	Cd36_81050	orf19.158	3	**-1.6537751**	-0.7257631	*APD1*	Predicted ORF in Assemblies 19, 20 and 21
	Cd36_84320	orf19.5885	3	**-1.6536527**	-0.7256563	*SNU13*	Predicted ORF in Assemblies 19, 20 and 21
UPC2	Cd36_07970	orf19.391	1	**-1.6526233**	-0.7247579	*UPC2*	Transcription factor involved in regulation of ergosterol biosynthetic genes and sterol uptake
	Cd36_40870	orf19.4159	4	**-1.6497573**	-0.7222538	*YMR166C*	Predicted ORF in Assemblies 19, 20 and 21
MXR1	Cd36_15900	orf19.2028	2	**-1.6480411**	-0.72075224	*MXR1*	Protein described as a methionine sulfoxide reductase
DIP2	Cd36_07810	orf19.5106	1	**-1.6479232**	-0.720649	*DIP2*	Protein similar to S. cerevisiae Dip2p, of small ribonucleoprotein complex
	Cd36_52390	orf19.4278	5	**-1.6468383**	-0.7196989	*BYE1*	Predicted ORF in Assemblies 19, 20 and 21
SPO7	Cd36_20180	orf19.6885	2	**-1.6462377**	-0.7191727	*SPO7*	Protein similar to S. cerevisiae Spo7p
LAS1	Cd36_20420	orf19.4120	2	**-1.6459924**	-0.71895766	*LAS1*	Predicted ORF in Assemblies 19, 20 and 21
DFG16	Cd36_18150	orf19.881	2	**-1.6452906**	-0.7183425	*DFG16*	Protein of the Rim101p pathway that regulates filamentation in response to alkaline pH
	Cd36_46320	orf19.3124	4	**-1.644747**	-0.7178657	*MAP1*	Predicted ORF in Assemblies 19, 20 and 21
	Cd36_22430	orf19.1352	2	**-1.6444005**	-0.7175617	*TIM22*	Predicted ORF in Assemblies 19, 20 and 21
AAT22	Cd36_41200	orf19.4669	4	**-1.6438063**	-0.7170403	*AAT2*	Protein not essential for viability
	Cd36_00170	orf19.6090	1	**-1.6434875**	-0.7167604	*NSR1*	Predicted ORF in Assemblies 19, 20 and 21
	Cd36_20070	orf19.6873.1	2	**-1.6434499**	-0.7167275	*KTI11*	ORF Predicted by Annotation Working Group
FUN31	Cd36_86600	orf19.7451	3	**-1.6421907**	-0.7156217	*PSK2*	Protein not essential for viability
BUD7	Cd36_53550	orf19.1112	5	**-1.6420743**	-0.7155194	*BCH1*	Predicted ORF in Assemblies 19, 20 and 21
SUB2	Cd36_40290	orf19.5647	4	**-1.6413491**	-0.71488214	*SUB2*	Transcription is regulated by Mig1p
	Cd36_42010	orf19.4579	4	**-1.6411481**	-0.71470547	*ERV29*	Predicted ORF in Assemblies 19, 20 and 21
	Cd36_19510	orf19.3531	2	**-1.6410657**	-0.714633		Predicted ORF in Assemblies 19, 20 and 21
RPB7	Cd36_01440	orf19.3347	1	**-1.640804**	-0.7144029	*RPB7*	Functional homolog of S. cerevisiae Rpb7p, an essential subunit of RNA Polymerase II
HOF1	Cd36_40430	orf19.5664	4	**-1.6403426**	-0.7139971		Protein not essential for viability
ILV5	Cd36_60880	orf19.88	6	**-1.6403322**	-0.71398807	*ILV5*	Protein described as ketol-acid reductoisomerase
BEM3	Cd36_42200	orf19.2771	4	**-1.6402754**	-0.713938	*BEM3*	Putative GTPase-activating protein (GAP) for Rho-type GTPase Cdc42p
ZWF1	Cd36_08460	orf19.4754	1	**-1.6399891**	-0.7136862	*ZWF1*	Putative glucose-6-phosphate dehydrogenase
PGA62	Cd36_42270	orf19.2765	4	**-1.6369324**	-0.7109947	*FLO1*	Putative GPI-anchored protein
USO5	Cd36_83070	orf19.306	3	**-1.6368963**	-0.7109629	*MYO1*	Protein of unknown function
	Cd36_44560	orf19.3787	4	**-1.6363622**	-0.71049213	*KAE1*	Predicted ORF in Assemblies 19, 20 and 21
	Cd36_71940	orf19.6503	7	**-1.6362059**	-0.7103543	*MRP49*	Predicted ORF in Assemblies 19, 20 and 21
RMT2	Cd36_50680	orf19.920	5	**-1.6348387**	-0.7091483	*RMT2*	Minor protein arginine methyltransferases (PRMT) involved in methylation of arginine residues
	Cd36_84830	orf19.5953	3	**-1.6341782**	-0.70856524	*SFP1*	Predicted ORF in Assemblies 19, 20 and 21
MSI3	Cd36_05770	orf19.2435	1	**-1.6320733**	-0.7067058	*SSE1*	Protein of the HSP70 family
	Cd36_24180	orf19.1767	2	**-1.631202**	-0.7059355	*UBP8*	Predicted ORF in Assemblies 19, 20 and 21
	Cd36_24770		2	**-1.6309317**	-0.7056964		
	Cd36_40280	orf19.5646	4	**-1.6303507**	-0.7051823	*YPL034W*	Predicted ORF in Assemblies 19, 20 and 21
	Cd36_04640	orf19.753	1	**-1.6302179**	-0.7050648	*MNT4|MNT2*	Predicted ORF in Assemblies 19, 20 and 21
CDC42	Cd36_07960	orf19.390	1	**-1.629796**	-0.7046914	*CDC42*	Rho-type GTPase
	Cd36_19730	orf19.3553	2	**-1.6290927**	-0.70406866	*RPF2*	Predicted ORF in Assemblies 19, 20 and 21
	Cd36_86260	orf19.7411	3	**-1.6278412**	-0.70296	*OAC1*	Predicted ORF in Assemblies 19, 20 and 21
RPS1	Cd36_02890	orf19.3002	1	**-1.6277207**	-0.7028532	*RPS1A*	Probable ortholog of S. cerevisiae ribosomal protein Rp10 (Rps1Ap and Rps1Bp), elicits a host antibody response during infection
RPL17B	Cd36_19200	orf19.4490	2	**-1.6273246**	-0.702502	*RPL17B*	Predicted ribosomal protein
	Cd36_16180	orf19.1993	2	**-1.6269736**	-0.7021909	*RPN9*	Predicted ORF in Assemblies 19, 20 and 21
NOP5	Cd36_60320	orf19.1199	6	**-1.6267841**	-0.7020228	*NOP58*	Protein similar to S. cerevisiae Nop5p protein of small nucleolar ribonucleoprotein complex

Gene Name	*C. dubliniensis* Cd36 identifier	*C. albicans* orf19 identifier	C'some	Fold change expression	Normalised Expression	*S. cerevisiae* ortholog	Description
NMD5	Cd36_40600	orf19.4188	4	**-1.624728**	-0.7001982	*NMD5*	Protein not essential for viability
FLU1	Cd36_71360	orf19.6577	7	**-1.6239747**	-0.6995292	*TPO1*	Multidrug efflux pump of the plasma membrane
RPL20B	Cd36_41520	orf19.4632	4	**-1.6229324**	-0.6986029	*RPL20B|RPL20A*	Predicted ribosomal protein
DAP2	Cd36_52730	orf19.4322	5	**-1.62255**	-0.69826293	*DAP2*	Protein described as dipeptidyl aminopeptidase
	Cd36_00470	orf19.6054	1	**-1.6218433**	-0.69763446	*BUL2*	Predicted ORF in Assemblies 19, 20 and 21
GCD7	Cd36_18640	orf19.825	2	**-1.6216828**	-0.69749165	*GCD7*	Protein described as a translation initiator
RPL35	Cd36_84940	orf19.5964.2	3	**-1.6192298**	-0.69530773	*RPL35A|RPL35E*	Protein described as a ribosomal protein
	Cd36_20970	orf19.1223	2	**-1.6186756**	-0.6948139	*DBF2*	Predicted ORF in Assemblies 19, 20 and 21
	Cd36_06310	orf19.6236	1	**-1.617906**	-0.6941278	*NOP6*	Predicted ORF in Assemblies 19, 20 and 21
ARG11	Cd36_84620	orf19.5926	3	**-1.6167065**	-0.6930578	*ORT1*	Protein induced during the mating process
	Cd36_50340	orf19.962	5	**-1.6163913**	-0.69277644	*CBF5*	Predicted ORF in Assemblies 19, 20 and 21
	Cd36_15760	orf19.2042	2	**-1.6143461**	-0.6909499	*MSS1*	Predicted ORF in Assemblies 19, 20 and 21
RIM8	Cd36_00160	orf19.6091	1	**-1.613041**	-0.6897831	*RIM8*	Protein involved in the pH response pathway
	Cd36_64240	orf19.5747	6	**-1.6128274**	-0.6895921	*MRP4*	Predicted ORF in Assemblies 19, 20 and 21
	Cd36_62020	orf19.3393	6	**-1.6115835**	-0.68847895	*DBP9*	Putative DEAD-box helicase
	Cd36_10720	orf19.660	1	**-1.6113856**	-0.6883018		Predicted ORF in Assemblies 19, 20 and 21
	Cd36_81460	orf19.1691	3	**-1.6091942**	-0.6863384	*YNR018W*	Predicted ORF in Assemblies 19, 20 and 21
RPL82	Cd36_10350	orf19.2311	1	**-1.6086498**	-0.6858504	*RPL8B*	Predicted ribosomal protein
	Cd36_11520	orf19.5235	1	**-1.6078311**	-0.68511593		Protein not essential for viability
	Cd36_08790	orf19.4792	1	**-1.607763**	-0.6850548	*AGA1*	Predicted ORF in Assemblies 19, 20 and 21
	Cd36_21960	orf19.2214	2	**-1.6077298**	-0.685025	*MRPL7*	Predicted ORF in Assemblies 19, 20 and 21
	Cd36_10210	orf19.2330	1	**-1.6071624**	-0.6845157	*UTP6*	Predicted ORF in Assemblies 19, 20 and 21
	Cd36_04720	orf19.53	1	**-1.6065081**	-0.68392825	*MNN4*	Predicted ORF in Assemblies 19, 20 and 21
SSZ1	Cd36_44350	orf19.3812	4	**-1.6051873**	-0.68274164	*SSZ1*	Protein described as an HSP70 chaperone
	Cd36_23820	orf19.1376	2	**-1.6046609**	-0.6822684	*SSO2*	Predicted ORF in Assemblies 19, 20 and 21
	Cd36_02840	orf19.2995	1	**-1.604197**	-0.6818514	*LOT5*	Predicted ORF in Assemblies 19, 20 and 21
DAK2	Cd36_08670	orf19.4777	1	**-1.6030334**	-0.6808045	*DAK2*	Protein described as similar to dihydroxyacetone kinase
CRP1	Cd36_08730	orf19.4784	1	**-1.6020056**	-0.6798792	*CCC2*	Copper transporter of the plasma membrane
	Cd36_86770	orf19.6822	3	**-1.601995**	-0.67986965	*DCN1*	Predicted ORF in Assemblies 19, 20 and 21
	Cd36_64660	orf19.1090	6	**-1.601968**	-0.67984533		Predicted ORF in Assemblies 19, 20 and 21
	Cd36_12320	orf19.4954	1	**-1.6018213**	-0.67971325	*PPA1*	Predicted ORF in Assemblies 19, 20 and 21
	Cd36_10390	orf19.2308	1	**-1.6017523**	-0.679651	*PFK26*	Predicted ORF in Assemblies 19, 20 and 21
SSR1	Cd36_70800	orf19.7030	7	**-1.6007377**	-0.6787369	*CCW14*	Beta-glucan associated cell-wall protein with role in cell wall structure
	Cd36_23980	orf19.1361	2	**-1.5999186**	-0.67799854	*TIM23*	Predicted ORF in Assemblies 19, 20 and 21
CYB5	Cd36_70650	orf19.7049	7	**-1.5996611**	-0.6777663	*CYB5*	Cytochrome b(5)
TIF5	Cd36_52270	orf19.4261	5	**-1.5988765**	-0.67705846	*TIF5*	Putative translation initiation factor
	Cd36_82720	orf19.263.1	3	**-1.5988289**	-0.67701554	*YBR056W-A*	Predicted ORF in Assembly 20 and 21
	Cd36_73540	orf19.7197	7	**-1.59793**	-0.6762042	*NOC3*	Predicted ORF in Assemblies 19, 20 and 21
	Cd36_02460	orf19.2953	1	**-1.5970007**	-0.675365	*TOM20*	Predicted ORF in Assemblies 19, 20 and 21
	Cd36_07430	orf19.5063	1	**-1.5964915**	-0.6749048		Predicted ORF in Assemblies 19, 20 and 21
	Cd36_86900	orf19.6804	3	**-1.5961483**	-0.67459464	*SRP68*	Predicted ORF in Assemblies 19, 20 and 21
TOP1	Cd36_60990	orf19.96	6	**-1.595851**	-0.67432594	*TOP1*	DNA topoisomerase I
	Cd36_03080	orf19.3022	1	**-1.5956455**	-0.6741402	*RSM24*	Predicted ORF in Assemblies 19, 20 and 21
	Cd36_01400	orf19.3341	1	**-1.5953827**	-0.6739025	*YDR341C*	Putative tRNA-Arg synthetase
RPS21	Cd36_01360	orf19.3334	1	**-1.5948784**	-0.6734464	*RPS2*	Predicted ribosomal protein
	Cd36_42440	orf19.2746	4	**-1.5946362**	-0.6732273	*EMP70*	Predicted ORF in Assemblies 19, 20 and 21
SUV3	Cd36_19000	orf19.4519	2	**-1.5939265**	-0.6725851	*SUV3*	Protein required for chlamydospore formation, for embedded hyphal growth, and for wild-type respiratory growth
HTA3	Cd36_83230	orf19.327	3	**-1.5936693**	-0.6723523	*HTZ1*	Protein described as histone H2A
	Cd36_01060	orf19.3301	1	**-1.592692**	-0.6714673	*MET30*	Predicted ORF in Assemblies 19, 20 and 21
SVF1	Cd36_00330	orf19.6068	1	**-1.5922725**	-0.67108727	*SVF1*	Predicted ORF in Assemblies 19, 20 and 21
ALG7	Cd36_22170	orf19.2187	2	**-1.5919155**	-0.67076373	*ALG7*	Protein involved in cell wall mannan biosynthesis
SAS10	Cd36_42660	orf19.2717	4	**-1.5918897**	-0.67074037	*SAS10*	Predicted ORF in Assemblies 19, 20 and 21
SNQ2	Cd36_64350	orf19.5759	6	**-1.5914946**	-0.67038226	*SNQ2*	Protein similar to S. cerevisiae Snq2p transporter
RAT1	Cd36_41070	orf19.4681	4	**-1.5914623**	-0.67035294	*RAT1*	5'-->3' exoribonuclease
	Cd36_21560	orf19.2286	2	**-1.5906734**	-0.6696377	*LIA1*	Predicted ORF in Assemblies 19, 20 and 21
LYS22	Cd36_19070	orf19.4506	2	**-1.5902884**	-0.6692884	*LYS21*	Putative homocitrate synthase
	Cd36_07160	orf19.1231	1	**-1.5895277**	-0.6685982		Predicted ORF from Assembly 19
	Cd36_52560	orf19.4301	5	**-1.589312**	-0.6684023	*SPT21*	Predicted ORF in Assemblies 19, 20 and 21
RPS22A	Cd36_03380	orf19.6265	1	**-1.5887034**	-0.6678498	*RPS22A*	Predicted ribosomal protein
FCY21	Cd36_24020	orf19.1357	2	**-1.5879925**	-0.66720414	*FCY2*	High affinity, high capacity, hypoxanthine-adenine-guanine-cytosine/ H+ symporter
	Cd36_17700	orf19.5840	2	**-1.587861**	-0.6670846	*YER071C*	Predicted ORF in Assemblies 19, 20 and 21
	Cd36_72990	orf19.1341	7	**-1.5875642**	-0.6668149	*PRR2*	Predicted ORF in Assemblies 19, 20 and 21
HCR1	Cd36_35285	orf19.7613	R	**-1.5864751**	-0.6658249	*HCR1*	Putative translation initiation factor
PPT1	Cd36_81590	orf19.1673	3	**-1.5863136**	-0.665678	*PPT1*	Protein described as serine/threonine phosphatase
	Cd36_02860	orf19.2998	1	**-1.5856305**	-0.6650567	*TSR2*	Predicted ORF in Assemblies 19, 20 and 21
	Cd36_27170	orf19.3751	R	**-1.5845441**	-0.66406775	*KIN4*	Predicted ORF in Assemblies 19, 20 and 21
	Cd36_51320	orf19.1971	5	**-1.5840042**	-0.6635761		Predicted ORF in Assemblies 19, 20 and 21
	Cd36_43900	orf19.1427	4	**-1.5837654**	-0.6633587	*THI73*	Putative transporter
	Cd36_00490	orf19.6052	1	**-1.5823554**	-0.6620736	*CNS1*	Predicted ORF in Assemblies 19, 20 and 21
	Cd36_19480	orf19.3528	2	**-1.5818734**	-0.6616342	*YKR074W*	Predicted ORF in Assemblies 19, 20 and 21
	Cd36_82470	orf19.240	3	**-1.5808307**	-0.6606829	*PAM17*	Predicted ORF in Assemblies 19, 20 and 21
PET9	Cd36_50590	orf19.930	5	**-1.5802155**	-0.66012126	*PET9*	Protein involved in ATP biosynthesis
	Cd36_12090	orf19.4929	1	**-1.5795115**	-0.6594784	*PET309*	Predicted ORF in Assemblies 19, 20 and 21
ECM21	Cd36_09570	orf19.4887	1	**-1.5791396**	-0.6591387	*ECM21*	Protein not essential for viability

Gene Name	*C. dubliniensis* Cd36 identifier	*C. albicans* orf19 identifier	C'some	Fold change expression	Normalised Expression	*S. cerevisiae* ortholog	Description
HRT1	Cd36_82410	orf19.233.1	3	**-1.5791153**	-0.6591165	*HRT1*	Protein similar to S. cerevisiae Hrt1p, which is a component of a nuclear ubiquitin-protein ligase complex involved in cell cycle control
	Cd36_34817	orf19.6599.1	R	**-1.5770802**	-0.6572561	*TMA7*	ORF Predicted by Annotation Working Group
	Cd36_45120	orf19.1802	4	**-1.5765797**	-0.6567981	*TPA1*	Predicted ORF in Assemblies 19, 20 and 21
GUT2	Cd36_46220	orf19.3133	4	**-1.5763977**	-0.65663147	*GUT2*	Predicted ORF in Assemblies 19, 20 and 21
	Cd36_01950	orf19.3666	1	**-1.575452**	-0.6557658	*YGR093W*	Predicted ORF in Assemblies 19, 20 and 21
HUT1	Cd36_86910	orf19.6803	3	**-1.5740331**	-0.6544659	*HUT1*	Predicted ORF in Assemblies 19, 20 and 21
NPL3	Cd36_13250	orf19.7238	1	**-1.5728791**	-0.6534078	*NPL3*	Putative RNA-binding protein, ortholog of S. cerevisiae Npl3p
	Cd36_10220	orf19.2328	1	**-1.5726686**	-0.6532147		Predicted ORF in Assemblies 19, 20 and 21
SNZ1	Cd36_02410	orf19.2947	1	**-1.5709654**	-0.6516514	*SNZ1*	Similar to stationary-phase-related proteins
TIF34	Cd36_02590	orf19.2967	1	**-1.5705916**	-0.65130806	*TIF34*	Putative translation initiation factor
	Cd36_44070		4	**-1.5703691**	-0.65110373		
	Cd36_82450	orf19.239	3	**-1.5692694**	-0.6500931	*STH1*	Predicted ORF in Assemblies 19, 20 and 21
	Cd36_44920	orf19.2631	4	**-1.5684973**	-0.64938307	*IKI3*	Predicted ORF in Assemblies 19, 20 and 21
	Cd36_20630		2	**-1.5684328**	-0.6493237		
APT1	Cd36_16300	orf19.1448	2	**-1.568394**	-0.64928794	*APT1*	Predicted ORF in Assemblies 19, 20 and 21
CHS2	Cd36_34480	orf19.7298	R	**-1.5674567**	-0.6484256	*CHS1*	Chitin synthase
	Cd36_85480	orf19.6986	3	**-1.5657326**	-0.64683783	*MSB3*	Predicted ORF in Assemblies 19, 20 and 21
ADE5,7	Cd36_07420	orf19.5061	1	**-1.5655258**	-0.6466472	*ADE5,7*	Enzyme of adenine biosynthesis
	Cd36_85280	orf19.6966	3	**-1.5648985**	-0.64606905	*CKI1*	Predicted ORF in Assemblies 19, 20 and 21
PUS7	Cd36_24330	orf19.1753	2	**-1.5642794**	-0.6454983	*PUS7*	Protein similar to S. cerevisiae tRNA modification protein
	Cd36_02730	orf19.2984	1	**-1.5642128**	-0.64543676	*MST1*	Predicted ORF in Assemblies 19, 20 and 21
AXL2	Cd36_43700	orf19.5292	4	**-1.5641121**	-0.6453439	*AXL2*	Protein not essential for viability
TPK1	Cd36_09610	orf19.4892	1	**-1.563453**	-0.6447358	*TPK2*	Catalytic subunit of cAMP-dependent protein kinase (PKA), isoform of Tpk2p
FGR51	Cd36_19290	orf19.156	2	**-1.5631304**	-0.6444381		Protein lacking an ortholog in S. cerevisiae
PPH21	Cd36_81510	orf19.1683	3	**-1.5627906**	-0.6441245	*PPH21*	Predicted ORF in Assemblies 19, 20 and 21
	Cd36_07470	orf19.5066	1	**-1.562389**	-0.64375377	*YDR412W*	Predicted ORF in Assemblies 19, 20 and 21
PGA39	Cd36_30290	orf19.6302	R	**-1.5619138**	-0.64331484	*AGA1*	Putative GPI-anchored protein of unknown function
HBR3	Cd36_83650	orf19.6955	3	**-1.5612255**	-0.642679	*NOB1*	Essential, uncharacterized protein
	Cd36_21380	orf19.2265	2	**-1.561168**	-0.6426258	*SNF12*	Predicted ORF in Assemblies 19, 20 and 21
	Cd36_70200	orf19.7076	7	**-1.5600258**	-0.64156985	*GBP2*	Predicted ORF in Assemblies 19, 20 and 21
	Cd36_21630	orf19.1900	2	**-1.5599773**	-0.64152503	*TGS1*	Predicted ORF in Assemblies 19, 20 and 21
RIB3	Cd36_11580	orf19.5228	1	**-1.5599544**	-0.6415038	*RIB3*	3,4-Dihydroxy-2-butanone 4-phosphate synthase
	Cd36_02650	orf19.2973	1	**-1.5592479**	-0.6408503	*VTS1*	Predicted ORF in Assemblies 19, 20 and 21
	Cd36_65180	orf19.2128	6	**-1.5586667**	-0.64031243	*YLF2*	Predicted ORF in Assemblies 19, 20 and 21
	Cd36_44990	orf19.1791	4	**-1.5584455**	-0.64010763	*MAK11*	Predicted ORF in Assemblies 19, 20 and 21
	Cd36_41570	orf19.4627	4	**-1.5579057**	-0.6396079		Predicted ORF in Assemblies 19, 20 and 21
CPA1	Cd36_41540	orf19.4630	4	**-1.55639**	-0.6382036	*CPA1*	Alkaline downregulated
	Cd36_04520		1	**-1.5563103**	-0.6381297		
HIP1	Cd36_51530	orf19.3195	5	**-1.5561403**	-0.6379721	*GAP1*	Alkaline upregulated
PIL1	Cd36_04430	orf19.778	1	**-1.5560446**	-0.6378834	*PIL1*	Echinocandin-binding protein
	Cd36_87250	orf19.6757	3	**-1.5555491**	-0.637424	*GCY1*	Predicted ORF in Assemblies 19, 20 and 21
URK1	Cd36_84170	orf19.5864	3	**-1.5555209**	-0.63739777	*URK1*	Protein described as similar to uridine kinase
	Cd36_61420	orf19.139	6	**-1.5552615**	-0.6371572	*TRA1*	Predicted ORF in Assemblies 19, 20 and 21
	Cd36_17570	orf19.5825.1	2	**-1.5549845**	-0.6369002	*YOS1*	ORF Predicted by Annotation Working Group
	Cd36_01530	orf19.3356	1	**-1.5547773**	-0.6367079	*ESP1*	Predicted ORF in Assemblies 19, 20 and 21
	Cd36_87570	orf19.6718	3	**-1.5546798**	-0.6366174		Predicted ORF in Assemblies 19, 20 and 21
	Cd36_51360	orf19.1975	5	**-1.5544089**	-0.6363661	*DIB1*	Predicted ORF in Assemblies 19, 20 and 21
	Cd36_82400	orf19.232	3	**-1.5543461**	-0.6363077	*MED7*	Predicted ORF in Assemblies 19, 20 and 21
	Cd36_70840	orf19.7023	7	**-1.5534259**	-0.63545346	*IOC4*	Predicted ORF in Assemblies 19, 20 and 21
	Cd36_06030	orf19.6266	1	**-1.5534118**	-0.63544035		Predicted ORF in Assemblies 19, 20 and 21
SNU114	Cd36_19220	orf19.144	2	**-1.5516989**	-0.63384867	*SNU114*	Protein likely to be essential for growth, based on an insertional mutagenesis strategy
CGT1	Cd36_45420	orf19.1261	4	**-1.5500641**	-0.6323279	*CEG1*	mRNA 5' guanylyltransferase
	Cd36_01540	orf19.3357	1	**-1.5494353**	-0.6317425	*FYV4*	Predicted ORF in Assemblies 19, 20 and 21
RDI1	Cd36_84970	orf19.5968	3	**-1.5489672**	-0.63130665	*RDI1*	Protein similar to S. cerevisiae Rdi1p, which is an inhibitor of Rho-GDP dissociation
RHD1	Cd36_04730	orf19.54	1	**-1.5487285**	-0.6310842		Putative transmembrane protein with hydrophobic N and C termini and a Ser-Gly rich region
	Cd36_64640	orf19.1089	6	**-1.5484616**	-0.63083553	*PEX11*	Predicted ORF in Assemblies 19, 20 and 21
BRE1	Cd36_50240	orf19.976	5	**-1.5483096**	-0.6306939	*BRE1*	Putative transcription factor with C3HC4 zinc finger DNA-binding motif
THR1	Cd36_50650	orf19.923	5	**-1.5466961**	-0.6291897	*THR1*	Putative homoserine kinase
	Cd36_18760	orf19.809	2	**-1.5454385**	-0.62801623	*NOP12*	Predicted ORF in Assemblies 19, 20 and 21
SWI4	Cd36_01630	orf19.4545	1	**-1.5451956**	-0.6277895	*SWI4*	Predicted ORF in Assemblies 19, 20 and 21
	Cd36_07950	orf19.389	1	**-1.5441756**	-0.6268369		Predicted ORF in Assemblies 19, 20 and 21
	Cd36_60920	orf19.91	6	**-1.5432535**	-0.62597513	*YGR053C*	Predicted ORF in Assemblies 19, 20 and 21
	Cd36_34900	orf19.7546	R	**-1.5431367**	-0.62586594	*RRP3*	Predicted ORF in Assemblies 19, 20 and 21
	Cd36_87070	orf19.6786	3	**-1.542652**	-0.6254127		Predicted ORF in Assemblies 19, 20 and 21
	Cd36_00640		1	**-1.5420429**	-0.6248429		
DOG1	Cd36_62030	orf19.3392	6	**-1.5414122**	-0.6242528	*DOG2*	Putative 2-deoxyglucose-6-phosphatase
RCF3	Cd36_53720	orf19.3211	5	**-1.5405488**	-0.6234444	*RFC3*	Transcription is induced upon filamentous growth
YHM1	Cd36_62060	orf19.685	6	**-1.5404904**	-0.6233897	*GGC1*	Putative mitochondrial carrier protein
	Cd36_19210	orf19.4488	2	**-1.5397376**	-0.6226845	*SWI3*	Predicted ORF in Assemblies 19, 20 and 21
	Cd36_80560	orf19.5397	3	**-1.5388923**	-0.6218922	*COG7*	Predicted ORF in Assemblies 19, 20 and 21
	Cd36_63650	orf19.5623	6	**-1.5385227**	-0.6215458	*ARP4*	Predicted ORF in Assemblies 19, 20 and 21

Gene Name	*C. dubliniensis* Cd36 identifier	*C. albicans* orf19 identifier	C'some	Fold change expression	Normalised Expression	*S. cerevisiae* ortholog	Description
OLE1	Cd36_07870	orf19.5117	1	**-1.5379902**	-0.6210463	*OLE1*	Fatty acid desaturase (stearoyl-CoA desaturase), essential protein involved in oleic acid synthesis
TEA1	Cd36_85470	orf19.6985	3	**-1.5378041**	-0.6208718	*TEA1*	Putative transcription factor with zinc cluster DNA-binding motif
	Cd36_51000	orf19.1934	5	**-1.5376651**	-0.62074137	*HST3*	Predicted ORF in Assemblies 19, 20 and 21
	Cd36_87330	orf19.6748	3	**-1.5367923**	-0.61992216		Predicted ORF in Assemblies 19, 20 and 21
AIP2	Cd36_83020	orf19.300	3	**-1.5363007**	-0.6194606	*DLD2*	Protein described as an actin interacting protein
GIS2	Cd36_51760	orf19.3182	5	**-1.5353867**	-0.61860204	*GIS2*	Transcriptionally regulated by iron
	Cd36_34420	orf19.7291	R	**-1.5337353**	-0.61704946	*GCD14*	Protein not essential for viability
	Cd36_22680	orf19.3624	2	**-1.5335325**	-0.6168587	*DSS1*	Predicted ORF in Assemblies 19, 20 and 21
AFG3	Cd36_81650	orf19.1669	3	**-1.5332302**	-0.6165743	*AFG3*	Protein likely to be essential for growth, based on an insertional mutagenesis strategy
	Cd36_00220		1	**-1.5321342**	-0.61554265		
CPR6	Cd36_35470	orf19.7654	R	**-1.5314882**	-0.6149342	*CPR6*	Predicted ORF in Assemblies 19, 20 and 21
SBP1	Cd36_84020	orf19.5854	3	**-1.5313145**	-0.61477065	*SBP1*	Protein described as similar to RNA binding proteins
	Cd36_53570	orf19.1110	5	**-1.5312356**	-0.61469626	*THI80*	Predicted ORF in Assemblies 19, 20 and 21
RPL9B	Cd36_82430	orf19.236	3	**-1.5302607**	-0.6137774	*RPL9B*	Predicted ribosomal protein
	Cd36_46550	orf19.3100	4	**-1.5301096**	-0.61363506	*SPC110*	Predicted ORF in Assemblies 19, 20 and 21
	Cd36_07130	orf19.2778	1	**-1.5300264**	-0.6135566	*URB1*	Predicted ORF in Assemblies 19, 20 and 21
	Cd36_50040		5	**-1.5284958**	-0.6121125		
MRPS9	Cd36_11560	orf19.5230	1	**-1.5276303**	-0.61129546	*MRPS9*	Mitochondrial ribosomal protein S9
CDC39	Cd36_64860	orf19.1084	6	**-1.5269814**	-0.6106825	*CDC39*	Protein similar to S. cerevisiae Cdc39p, which is part of the CCR4-NOT transcription regulatory complex
	Cd36_64840	orf19.1085	6	**-1.5268476**	-0.6105561	*UBC1*	Predicted ORF in Assemblies 19, 20 and 21
	Cd36_85740	orf19.7361	3	**-1.5266998**	-0.6104164	*SEN54*	Predicted ORF in Assemblies 19, 20 and 21
	Cd36_81870		3	**-1.525498**	-0.6092803		
	Cd36_53660	orf19.3218	5	**-1.5253178**	-0.6091099	*YJR124C*	Putative multidrug resistance protein
FLO8	Cd36_64710	orf19.1093	6	**-1.524416**	-0.6082566	*SNF5*	Transcription factor
PTH1	Cd36_52070	orf19.4232	5	**-1.5243676**	-0.6082108	*TAM41*	Putative gluconate transport protein
	Cd36_17370	orf19.1584	2	**-1.5235713**	-0.6074569	*MCH4*	Predicted ORF in Assemblies 19, 20 and 21
	Cd36_35522	orf19.7663	R	**-1.5234314**	-0.6073246	*CSM1*	Predicted ORF in Assemblies 19, 20 and 21
	Cd36_43580	orf19.5039	4	**-1.5226763**	-0.60660934	*RRP42*	Predicted ORF in Assemblies 19, 20 and 21
	Cd36_22230	orf19.2181	2	**-1.5215207**	-0.60551405		ORF Predicted by Annotation Working Group
	Cd36_00110	orf19.6100	1	**-1.5213747**	-0.6053755	*CRD1*	Protein not essential for viability
	Cd36_82160	orf19.1626	3	**-1.5211303**	-0.6051438	*DYS1*	Predicted ORF in Assemblies 19, 20 and 21
	Cd36_44240	orf19.3827	4	**-1.5208861**	-0.60491204	*OMA1*	Predicted ORF in Assemblies 19, 20 and 21
GLN4	Cd36_70110	orf19.7064	7	**-1.5205226**	-0.6045673	*GLN4*	Putative tRNA-Gln synthetase
	Cd36_19700	orf19.3550	2	**-1.5200326**	-0.60410225	*SGO1*	Predicted ORF in Assemblies 19, 20 and 21
	Cd36_12810	orf19.5020	1	**-1.5195681**	-0.6036613	*DEF1*	Predicted ORF in Assemblies 19, 20 and 21
	Cd36_21970	orf19.2213	2	**-1.5193299**	-0.60343516	*YGR042W*	Predicted ORF in Assemblies 19, 20 and 21
RPL19A	Cd36_84440	orf19.5904	3	**-1.519049**	-0.6031685	*RPL19A|RPL19E*	Predicted ribosomal protein
	Cd36_21830	orf19.1872	2	**-1.5188342**	-0.6029644		Predicted ORF in Assemblies 19, 20 and 21
	Cd36_43020	orf19.2673	4	**-1.518093**	-0.6022601		Predicted ORF in Assemblies 19, 20 and 21
	Cd36_52520	orf19.4294	5	**-1.517187**	-0.60139894	*CYC2*	Predicted ORF in Assemblies 19, 20 and 21
PWP1	Cd36_41460	orf19.4640	4	**-1.5169722**	-0.6011946	*PWP1*	Predicted ORF in Assemblies 19, 20 and 21
	Cd36_08310	orf19.4739	1	**-1.5162749**	-0.60053134	*MSS116*	Predicted ORF in Assemblies 19, 20 and 21
	Cd36_18530	orf19.836	2	**-1.5159945**	-0.60026455		Protein likely to be essential for growth, based on an insertional mutagenesis strategy
CDC47	Cd36_23200	orf19.201	2	**-1.5158558**	-0.60013247		Protein described as having role in control of cell division
	Cd36_81000	orf19.2512	3	**-1.5148528**	-0.5991776		Predicted ORF in Assemblies 19, 20 and 21
	Cd36_08820	orf19.4796	1	**-1.5147731**	-0.5991018	*CAF20*	Predicted ORF in Assemblies 19, 20 and 21
	Cd36_43540	orf19.1298	4	**-1.5140256**	-0.5983896	*NUP84*	Predicted ORF in Assemblies 19, 20 and 21
	Cd36_23415		2	**-1.5138855**	-0.5982561		
	Cd36_18770	orf19.808	2	**-1.5134571**	-0.5978477	*DEP1*	Predicted ORF in Assemblies 19, 20 and 21
HOG1	Cd36_18080	orf19.895	2	**-1.5125626**	-0.5969949	*HOG1*	MAP kinase of osmotic-, heavy metal-, and core stress response
NMT1	Cd36_41450	orf19.4641	4	**-1.5121585**	-0.59660935	*NMT1*	Myristoyl-CoA:protein N-myristoyltransferase
	Cd36_20490	orf19.4110	2	**-1.511145**	-0.5956421	*TPM1*	Predicted ORF in Assemblies 19, 20 and 21
COX6	Cd36_18220	orf19.873.1	2	**-1.5111197**	-0.595618	*COX6*	Flucytosine induced
	Cd36_23680	orf19.1394	2	**-1.5105605**	-0.59508395	*YCR090C*	Protein not essential for viability
	Cd36_50770	orf19.4153	5	**-1.5090597**	-0.59364986	*ULA1*	Predicted ORF in Assemblies 19, 20 and 21
	Cd36_04940	orf19.446	1	**-1.5089318**	-0.5935276		Predicted ORF in Assemblies 19, 20 and 21
	Cd36_80340	orf19.5430	3	**-1.5088817**	-0.59347963	*BUD21*	Predicted ORF in Assemblies 19, 20 and 21
	Cd36_22190	orf19.2185	2	**-1.5087947**	-0.5933964	*NSA1*	Predicted ORF in Assemblies 19, 20 and 21
	Cd36_82020	orf19.1643	3	**-1.5073391**	-0.59200406	*PCP1*	Predicted ORF in Assemblies 19, 20 and 21
	Cd36_05290	orf19.2494	1	**-1.506773**	-0.59146214	*PET112*	Predicted ORF in Assemblies 19, 20 and 21
	Cd36_60890	orf19.89	6	**-1.5066897**	-0.59138227	*PEX7*	Predicted ORF in Assemblies 19, 20 and 21
	Cd36_21610	orf19.1902	2	**-1.5066426**	-0.5913372	*NOC4*	Predicted ORF in Assemblies 19, 20 and 21
	Cd36_08800	orf19.4793	1	**-1.5061089**	-0.59082603	*TMA16*	Predicted ORF in Assemblies 19, 20 and 21
	Cd36_40420	orf19.5663	4	**-1.5058726**	-0.5905998	*YMR034C*	Predicted ORF in Assemblies 19, 20 and 21
	Cd36_03030	orf19.3015	1	**-1.5056196**	-0.5903573	*ARX1*	Predicted ORF in Assemblies 19, 20 and 21
RSP5	Cd36_22630	orf19.3628	2	**-1.504891**	-0.589659	*RSP5*	Predicted ORF in Assemblies 19, 20 and 21
	Cd36_10290	orf19.2319	1	**-1.50453**	-0.58931285	*ESF1*	Predicted ORF in Assemblies 19, 20 and 21
	Cd36_80670	orf19.5381	3	**-1.5045176**	-0.589301	*PUF4*	Predicted ORF in Assemblies 19, 20 and 21
SIT1	Cd36_22250	orf19.2179	2	**-1.5041329**	-0.58893204	*ARN1*	Transporter of ferrichrome siderophores, but not ferrioxamine B
	Cd36_51240	orf19.1963	5	**-1.5040832**	-0.58888435	*GDS1*	Predicted ORF in Assemblies 19, 20 and 21
HLJ1	Cd36_73720	orf19.7175	7	**-1.5037118**	-0.58852816	*HLJ1*	Protein repressed during the mating process

Gene Name	*C. dubliniensis* Cd36 identifier	*C. albicans* orf19 identifier	C'some	Fold change expression	Normalised Expression	*S. cerevisiae* ortholog	Description
ERG13	Cd36_34550	orf19.7312	R	**-1.5036982**	-0.58851504	*ERG13*	Protein similar to S. cerevisiae Erg13p, which is involved in ergosterol biosynthesis
	Cd36_16600	orf19.1485	2	**-1.5026646**	-0.587523	*MRPL31*	Predicted ORF in Assemblies 19, 20 and 21
	Cd36_82180	orf19.1624	3	**-1.5025178**	-0.5873821	*MAK10*	Predicted ORF in Assemblies 19, 20 and 21
	Cd36_62500	orf19.3473	6	**-1.501796**	-0.5866889	*SGF73*	Predicted ORF in Assemblies 19, 20 and 21
	Cd36_12120	orf19.4931.1	1	**-1.5012103**	-0.5861261	*RPL14A|RPL14E*	ORF Predicted by Annotation Working Group
RPL11	Cd36_21110	orf19.2232	2	**-1.5008085**	-0.58573985	*RPL11A|RPL11E*	Predicted ribosomal protein
	Cd36_54240	orf19.3946	5	**1.5003296**	0.58527946	*COX18*	Predicted ORF in Assemblies 19, 20 and 21
	Cd36_18300	orf19.862	2	**1.5032068**	0.5880435		Predicted ORF in Assemblies 19, 20 and 21
	Cd36_28360	orf19.2400	R	**1.5032182**	0.5880544	*SQS1*	Predicted ORF in Assemblies 19, 20 and 21
	Cd36_33690	orf19.590	R	**1.5032922**	0.58812547		Predicted ORF in Assemblies 19, 20 and 21
	Cd36_44960	orf19.1290	4	**1.5034852**	0.5883107	*XKS1*	Predicted ORF in Assemblies 19, 20 and 21
MDL1	Cd36_27070	orf19.2615	R	**1.5035869**	0.58840823	*MDL1*	Putative mitochondrial, half-size MDR-subfamily ABC transporter
	Cd36_18240	orf19.871	2	**1.5046908**	0.58946705	*LST4*	Predicted ORF in Assemblies 19, 20 and 21
	Cd36_29730	orf19.528	R	**1.5053071**	0.59005785	*SEC26*	Predicted ORF in Assemblies 19, 20 and 21
YRB1	Cd36_25680	orf19.7477	R	**1.5067703**	0.5914595	*YRB1*	Functional homolog of S. cerevisiae Yrb1p, which regulates Gsp1p GTPase activity and thereby affects nucleocytoplasmic transport and cytoskeletal dynamics
	Cd36_40950	orf19.4699	4	**1.5077382**	0.592386	*TGL3*	Putative phospholipase of patatin family
	Cd36_54620	orf19.3994	5	**1.5088971**	0.5934944	*OST3*	Predicted ORF in Assemblies 19, 20 and 21
HGT14	Cd36_33400	orf19.2633	R	**1.5095501**	0.5941186	*HXT4*	Putative glucose transporter of the major facilitator superfamily
ITR1	Cd36_19460	orf19.3526	2	**1.5116912**	0.5961635	*ITR2*	Inositol transporter required for uptake of exogenous inositol
	Cd36_26150	orf19.3239	R	**1.5116994**	0.5961714	*CTF18*	Predicted ORF in Assemblies 19, 20 and 21
	Cd36_43120	orf19.3362	4	**1.5120671**	0.5965221	*AIF1*	Predicted ORF in Assemblies 19, 20 and 21
PRP8	Cd36_34250	orf19.6442	R	**1.5124325**	0.59687066	*PRP8*	Protein similar to S. cerevisiae Prp8p
	Cd36_19570	orf19.3537	2	**1.5129209**	0.59733653	*SRX1*	Predicted ORF in Assemblies 19, 20 and 21
	Cd36_52710		5	**1.5135156**	0.59790355		
	Cd36_54730	orf19.4005	5	**1.5142215**	0.5985763	*YDR196C*	Protein likely to be essential for growth, based on an insertional mutagenesis strategy
	Cd36_64470	orf19.5772	6	**1.5156686**	0.59995437	*SWC5*	Predicted ORF in Assemblies 19, 20 and 21
	Cd36_73000	orf19.1340	7	**1.5172572**	0.6014657	*YDL124W*	Predicted ORF in Assemblies 19, 20 and 21
	Cd36_82890	orf19.284	3	**1.5185554**	0.6026995		Predicted ORF in Assemblies 19, 20 and 21
YVC1	Cd36_22010	orf19.2209	2	**1.5188209**	0.60295177	*YVC1*	Protein similar to S. cerevisiae Yvc1p
DAO1	Cd36_03420	orf19.3065	1	**1.5192229**	0.6033335		Putative D-amino acid oxidase
	Cd36_64080	orf19.5720	6	**1.5203748**	0.60442704	*MCH4*	Predicted ORF in Assemblies 19, 20 and 21
HTA1	Cd36_83890	orf19.6924	3	**1.5206532**	0.60469127	*HTA1*	Putative histone H2A
HEX1	Cd36_53360	orf19.6673	5	**1.5214695**	0.6054654		Beta-N-acetylhexosaminidase (beta-N-acetylglucosaminidase/chitobiase), highly glycosylated enzyme that is secreted to the periplasm and to the culture medium
	Cd36_74020	orf19.8197	7	**1.5220059**	0.60597396		0
GAP6	Cd36_53250	orf19.6659	5	**1.5222164**	0.6061735	*GAP1*	Putative general amino acid permease
SRP54	Cd36_26110	orf19.3243	R	**1.5223027**	0.6062553	*SRP54*	Predicted ORF in Assemblies 19, 20 and 21
	Cd36_54300	orf19.3954	5	**1.5229223**	0.6068423	*PSD2*	Predicted ORF in Assemblies 19, 20 and 21
WOR2	Cd36_85150	orf19.5992	3	**1.5235367**	0.60742426	*AGA1*	Transcriptional regulator of white-opaque switching
	Cd36_20860	orf19.27	2	**1.524084**	0.60794234		Predicted ORF in Assemblies 19, 20 and 21
HBR2	Cd36_64910	orf19.1078	6	**1.5266572**	0.6103761	*AGX1*	Uncharacterized protein, regulated by Gcn4p and hemoglobin
	Cd36_15500	orf19.2073	2	**1.5280651**	0.611706	*YDR338C*	Predicted ORF in Assemblies 19, 20 and 21
CIT1	Cd36_28700	orf19.4393	R	**1.5288284**	0.6124265	*CIT1*	Protein described as citrate synthase
	Cd36_08280	orf19.4736	1	**1.5290488**	0.6126344	*PHO8*	Predicted ORF in Assemblies 19, 20 and 21
PMA1	Cd36_80660	orf19.5383	3	**1.5298834**	0.6134217	*PMA1*	Plasma membrane H(+)-ATPase
	Cd36_31020	orf19.6648	R	**1.5316365**	0.6150739	*SDA1*	Predicted ORF in Assemblies 19, 20 and 21
HGT5	Cd36_85250	orf19.6005	3	**1.5324365**	0.6158273	*STL1*	Putative glucose transporter of the major facilitator superfamily
	Cd36_24690	orf19.5345	2	**1.533121**	0.6164715	*DSK2*	Predicted ORF in Assemblies 19, 20 and 21
	Cd36_32980	orf19.6134	R	**1.534977**	0.618217	*SEC39*	Predicted ORF in Assemblies 19, 20 and 21
FTR1	Cd36_13100	orf19.7219	1	**1.536164**	0.6193323	*FTR1*	High-affinity iron permease (ferric citrate, ferrioxamines E or B, transferrin)
	Cd36_25830	orf19.3281	R	**1.5370373**	0.6201521	*JHD1*	Predicted ORF in Assemblies 19, 20 and 21
	Cd36_87280	orf19.6754	3	**1.5374202**	0.62051153		Predicted ORF in Assemblies 19, 20 and 21
NAG6	Cd36_65490	orf19.2151	6	**1.537452**	0.62054133	*SEY1*	Protein required for wild-type mouse virulence and wiild-type cycloheximide resistance
	Cd36_02900	orf19.3003	1	**1.5377971**	0.6208651	*TCB3*	Predicted ORF in Assemblies 19, 20 and 21
	Cd36_12870	orf19.5026	1	**1.5384691**	0.6214955	*YML081W*	Putative transcription factor with zinc finger DNA-binding motif
	Cd36_15250	orf19.2106	2	**1.5393096**	0.62228346	*YLR326W*	Predicted ORF in Assemblies 19, 20 and 21
	Cd36_28150	orf19.2423	R	**1.5393724**	0.62234235	*YBR239C*	Putative DNA-binding transcription factor
	Cd36_03120	orf19.3029	1	**1.5401338**	0.6230557	*EHD3*	Predicted ORF in Assemblies 19, 20 and 21
	Cd36_09320	orf19.4857	1	**1.5401796**	0.6230986		Predicted ORF in Assemblies 19, 20 and 21
ALK8	Cd36_32710	orf19.10	R	**1.5403287**	0.6232383	*DIT2*	Alkane-inducible cytochrome P450
	Cd36_73090	orf19.8911	7	**1.5409765**	0.62384486		0
	Cd36_26120	orf19.3242	R	**1.5413183**	0.6241648	*TAF10*	Predicted ORF in Assemblies 19, 20 and 21
	Cd36_10760		1	**1.541714**	0.6245351		
	Cd36_27040	orf19.2612	R	**1.5418915**	0.62470126	*SWI5*	Putative transcription factor with zinc finger DNA-binding motif
NCR1	Cd36_13270	orf19.7242	1	**1.5427015**	0.62545896	*NCR1*	Transcription is regulated by Nrg1p and Mig1p
	Cd36_26710	orf19.2565	R	**1.5429336**	0.6256759	*MDM1*	Predicted ORF in Assemblies 19, 20 and 21

Gene Name	*C. dubliniensis* Cd36 identifier	*C. albicans* orf19 identifier	C'some	Fold change expression	Normalised Expression	*S. cerevisiae* ortholog	Description
KNS1	Cd36_12480	orf19.4979	1	**1.5433986**	0.62611073	*KNS1*	Protein not essential for viability
	Cd36_30260	orf19.6306	R	**1.5445538**	0.6271901	*ALD4*	Predicted ORF in Assemblies 19, 20 and 21
RPN4	Cd36_04080	orf19.1069	1	**1.547179**	0.6296401	*RPN4*	DNA binding protein with Cys2-His2 zinc-finger
	Cd36_30590	orf19.557	R	**1.5476581**	0.6300868		Predicted ORF in Assemblies 19, 20 and 21
	Cd36_21680	orf19.1890	2	**1.5480698**	0.6304705	*YMR210W*	Predicted ORF in Assemblies 19, 20 and 21
RPN5	Cd36_54980	orf19.4032	5	**1.5483103**	0.6306946	*RPN5*	Predicted ORF in Assemblies 19, 20 and 21
TPS1	Cd36_31110	orf19.6640	R	**1.5492506**	0.6315706	*TPS1*	Trehalose-6-phosphate synthase
FGR13	Cd36_29130	orf19.562	R	**1.5492954**	0.6316123		Protein lacking an ortholog in S. cerevisiae
POR1	Cd36_03860	orf19.1042	1	**1.5495626**	0.631861	*POR1*	Protein described as similar to mitochondrial outer membrane porin
	Cd36_61200	orf19.117	6	**1.5498503**	0.63212895	*SEC9*	Predicted ORF in Assemblies 19, 20 and 21
	Cd36_72680	orf19.5159	7	**1.5501808**	0.6324365	*DUG3*	Predicted ORF in Assemblies 19, 20 and 21
KSR1	Cd36_33010	orf19.6131	R	**1.550985**	0.6331847	*TSC10*	3-ketosphinganine reductase, catalyzes the second step in phytosphingosine synthesis
GAD1	Cd36_10950	orf19.1153	1	**1.5518858**	0.6340225	*GAD1*	Protein described as glutamate decarboxylase
IDP2	Cd36_27320	orf19.3733	R	**1.5525154**	0.63460755	*IDP2*	Putative isocitrate dehydrogenase
	Cd36_35415	orf19.7644	R	**1.5528458**	0.63491464	*APC11*	Predicted ORF in Assemblies 19, 20 and 21
HGT18	Cd36_28130	orf19.2425	R	**1.5528574**	0.63492537	*YBR241C*	Putative glucose transporter of the major facilitator superfamily
	Cd36_63870	orf19.5605	6	**1.5535725**	0.6355896	*ALY2*	Predicted ORF in Assemblies 19, 20 and 21
	Cd36_25510	orf19.7497	R	**1.5538622**	0.63585854	*CDC53*	Predicted ORF in Assemblies 19, 20 and 21
YHB4	Cd36_35380	orf19.7637	R	**1.5547363**	0.6366699	*YHB1*	Protein related to flavohemoglobins
	Cd36_31420	orf19.3848	R	**1.5552864**	0.6371803		Predicted ORF in Assemblies 19, 20 and 21
ASR3	Cd36_18460	orf19.842	2	**1.5556016**	0.6374726		Gene regulated by cAMP and by osmotic stress
PAN1	Cd36_18130	orf19.886	2	**1.556444**	0.6382537	*PAN1*	Essential protein involved in endocytosis and polarized growth
CRD2	Cd36_41140	orf19.4674.1	4	**1.5564555**	0.6382643		Metallothionein
	Cd36_34410	orf19.7288	R	**1.5565504**	0.6383523		Predicted ORF in Assemblies 19, 20 and 21
	Cd36_80570	orf19.5394.1	3	**1.5567209**	0.6385102	*PET191*	ORF Predicted by Annotation Working Group
	Cd36_28640	orf19.4399	R	**1.5577757**	0.6394875	*NCS2*	Predicted ORF in Assemblies 19, 20 and 21
	Cd36_04800		1	**1.558472**	0.64013225		
	Cd36_13030	orf19.7213	1	**1.5593935**	0.640985	*YDR291W*	Putative ATP-dependent RNA helicase
ACO1	Cd36_33840	orf19.6385	R	**1.5593935**	0.640985	*ACO1*	Protein described as aconitase
MUQ1	Cd36_15240	orf19.2107	2	**1.5597221**	0.641289	*MUQ1*	Protein described as choline phosphate cytidylyltransferase/phosphoethanolamine cytidylyltransferase
CAP1	Cd36_82190	orf19.1623	3	**1.5599946**	0.641541	*YAP1*	Transcription factor, AP-1 family
	Cd36_25790	orf19.3286	R	**1.5606484**	0.64214563	*GTB1*	Predicted ORF in Assemblies 19, 20 and 21
TPM2	Cd36_34050	orf19.6414.3	R	**1.5613308**	0.64277625	*TPM1*	Protein described as tropomyosin isoform 2
FOX3	Cd36_81380	orf19.1704	3	**1.5614322**	0.64286995	*POT1*	Putative peroxisomal 3-oxoacyl CoA thiolase
	Cd36_25780	orf19.3287	R	**1.5614418**	0.6428788	*BUD22*	Predicted ORF in Assemblies 19, 20 and 21
	Cd36_25770	orf19.7460	R	**1.5622027**	0.6435816	*TRM13*	Predicted ORF in Assemblies 19, 20 and 21
THI20	Cd36_18120	orf19.889	2	**1.5626892**	0.6440308	*THI20*	Putative phosphomethylpyrimidine kinase
YMX6	Cd36_63450	orf19.5713	6	**1.5630902**	0.6444011	*NDE1*	Protein described as NADH dehydrogenase
HAC1	Cd36_05800	orf19.2432	1	**1.5634075**	0.64469385	*HAC1*	Putative transcription factor with bZIP DNA-binding motif
	Cd36_25120	orf19.7529	R	**1.5637989**	0.64505506	*EPL1*	Predicted ORF in Assemblies 19, 20 and 21
	Cd36_31170	orf19.6635	R	**1.5644017**	0.64561105		Predicted ORF in Assemblies 19, 20 and 21
	Cd36_31490	orf19.3854	R	**1.5647857**	0.6459651	*SAT4*	Protein similar to S. cerevisiae Sat4p
	Cd36_62150	orf19.692	6	**1.565163**	0.64631295	*ENT2*	Predicted ORF in Assemblies 19, 20 and 21
	Cd36_33130	orf19.2621	R	**1.5664479**	0.6474967	*SMB1*	Predicted ORF in Assemblies 19, 20 and 21
CDR11	Cd36_84000	orf19.918	3	**1.5666974**	0.64772654	*PDR5*	Putative transporter of PDR subfamily of ABC family
	Cd36_03280	orf19.3051	1	**1.5673989**	0.6483724	*YJR116W*	Predicted ORF in Assemblies 19, 20 and 21
ATP3	Cd36_26320	orf19.3223	R	**1.5688126**	0.649673	*ATP3*	Predicted ORF in Assemblies 19, 20 and 21
SOK1	Cd36_31410	orf19.451	R	**1.5731844**	0.6536877	*SOK1*	Transcription is induced in response to alpha pheromone in SpiderM medium
	Cd36_70230	orf19.7124	7	**1.573521**	0.65399647	*RVS161*	Predicted ORF in Assemblies 19, 20 and 21
	Cd36_50670	orf19.921	5	**1.5736048**	0.65407324	*PUF2*	Predicted ORF in Assemblies 19, 20 and 21
	Cd36_22890	orf19.3604	2	**1.5747427**	0.6551161	*IES2*	Predicted ORF in Assemblies 19, 20 and 21
	Cd36_26950	orf19.2605	R	**1.5757569**	0.65604496	*PRK1*	Predicted ORF in Assemblies 19, 20 and 21
RAD16	Cd36_02610	orf19.2969	1	**1.5757629**	0.65605044	*RAD16*	Protein similar to S. cerevisiae Rad16p
	Cd36_33820	orf19.6379	R	**1.5767845**	0.6569855		Predicted ORF in Assemblies 19, 20 and 21
	Cd36_02050	orf19.3677	1	**1.5769556**	0.657142	*ATG5*	Predicted ORF in Assemblies 19, 20 and 21
ARG3	Cd36_63830	orf19.5610	6	**1.5772636**	0.65742373	*ARG3*	Alkaline downregulated
ENA21	Cd36_72570	orf19.5170	7	**1.5785848**	0.6586318	*ENA2*	Predicted ORF in Assemblies 19, 20 and 21
	Cd36_10870	orf19.1162	1	**1.5796224**	0.65957975		Predicted ORF in Assemblies 19, 20 and 21
MDH1-3	Cd36_24490	orf19.5323	2	**1.5796423**	0.6595979	*MDH1*	Predicted malate dehydrogenase
UGT51C1	Cd36_27080	orf19.2616	R	**1.5797386**	0.65968585	*ATG26*	UDP-glucose:sterol glucosyltransferase
	Cd36_33670	orf19.592	R	**1.5800976**	0.6600137	*YNL092W*	Predicted ORF in Assemblies 19, 20 and 21
	Cd36_32450	orf19.1841	R	**1.5802047**	0.6601114		Predicted ORF in Assemblies 19, 20 and 21
	Cd36_12200	orf19.4940	1	**1.5802224**	0.66012764	*HIP1*	Putative histidine permease
	Cd36_71750	orf19.6527	7	**1.5806314**	0.660501	*PRM10*	Predicted ORF in Assemblies 19, 20 and 21
	Cd36_31520	orf19.3858	R	**1.5814824**	0.66127753		Predicted ORF in Assemblies 19, 20 and 21
FMP45	Cd36_72040	orf19.6489	7	**1.5828546**	0.66252875	*FMP45*	Protein induced during the mating process
	Cd36_54140	orf19.3936	5	**1.5834658**	0.6630857	*GDE1*	Predicted ORF in Assemblies 19, 20 and 21
	Cd36_27020	orf19.2610	R	**1.5844163**	0.6639514	*ARC1*	Predicted ORF in Assemblies 19, 20 and 21
	Cd36_54870	orf19.4021	5	**1.5853665**	0.6648164		Predicted ORF in Assemblies 19, 20 and 21
MEP2	Cd36_40490	orf19.5672	4	**1.5860962**	0.66548026	*MEP2*	Ammonium permease and regulator of nitrogen starvation-induced filamentation
	Cd36_30100	orf19.6318	R	**1.5879852**	0.66719747	*YJR085C*	Predicted ORF in Assemblies 19, 20 and 21

Gene Name	*C. dubliniensis* Cd36 identifier	*C. albicans* orf19 identifier	C'some	Fold change expression	Normalised Expression	*S. cerevisiae* ortholog	Description
	Cd36_33070	orf19.6121	R	**1.5898734**	0.66891193	*YER130C*	Similar to S. cerevisiae Yer130cp
	Cd36_28890	orf19.4368	R	**1.5914104**	0.67030597	*YLL029W*	Predicted ORF in Assemblies 19, 20 and 21
VRP1	Cd36_22160	orf19.2190	2	**1.5933565**	0.6720691	*VRP1*	Protein described as verprolin
	Cd36_30690	orf19.5287	R	**1.5941316**	0.67277074	*YEL077C*	Predicted ORF in Assemblies 19, 20 and 21
	Cd36_26090	orf19.3245	R	**1.5947126**	0.67329645		Predicted ORF in Assemblies 19, 20 and 21
ARC40	Cd36_31710	orf19.3873	R	**1.5948073**	0.67338204	*ARC40*	Protein similar to S. cerevisiae Arc40p, which is involved in actin filament organization in S. cerevisiae
PRP22	Cd36_54970	orf19.4033	5	**1.5963277**	0.67475677	*PRP22*	Protein described as an RNA-dependent ATPase
	Cd36_03070	orf19.3021	1	**1.5965767**	0.67498183	*YMR114C*	Predicted ORF in Assemblies 19, 20 and 21
	Cd36_33760	orf19.6373	R	**1.5972668**	0.6756053	*DCP2*	Predicted ORF in Assemblies 19, 20 and 21
	Cd36_45930	orf19.2890	4	**1.5979406**	0.67621374	*YMD8*	Predicted ORF in Assemblies 19, 20 and 21
	Cd36_65610		6	**1.5998806**	0.6779642		
	Cd36_34310	orf19.6449	R	**1.5999523**	0.6780289		Predicted ORF in Assemblies 19, 20 and 21
RPP2A	Cd36_33950	orf19.6403.1	R	**1.601302**	0.6792455	*RPP2B*	Conserved acidic ribosomal protein, likely to be involved in regulation of translation elongation
PIF1	Cd36_32990	orf19.6133	R	**1.6023259**	0.6801677	*PIF1*	Decreased transcription is observed upon fluphenazine treatment
ERG4	Cd36_80690	orf19.5379	3	**1.6027105**	0.68051386	*ERG4*	Protein described as similar to sterol C-24 reductase
	Cd36_19420	orf19.4125	2	**1.6028885**	0.6806741	*PZF1*	Putative transcription factor with zinc finger DNA-binding motif
APG7	Cd36_32270	orf19.707	R	**1.6029637**	0.6807418	*ATG7*	Protein not essential for viability
BRF1	Cd36_31000	orf19.6649	R	**1.6049435**	0.68252254	*BRF1*	Component of the general transcription factor for RNA polymerase III (TFIIIB)
HIS3	Cd36_19370	orf19.183	2	**1.6075718**	0.68488324	*HIS3*	Imidazoleglycerol-phosphate dehydratase, enzyme of histidine biosynthesis
CTR2	Cd36_08130	orf19.4720	1	**1.611717**	0.6885984	*CTR2*	Predicted ORF in Assemblies 19, 20 and 21
	Cd36_10810	orf19.1168	1	**1.6130847**	0.6898222		Predicted zinc-finger protein of unknown function
	Cd36_27710	orf19.2828	R	**1.6133702**	0.69007754	*ALF1*	Predicted ORF in Assemblies 19, 20 and 21
	Cd36_85520	orf19.6990	3	**1.613507**	0.69019985	*CPR5*	Predicted ORF in Assemblies 19, 20 and 21
	Cd36_30920	orf19.5845	R	**1.6142615**	0.6908743	*RNR1*	Protein described as large subunit of ribonucleotide reductase
	Cd36_83710	orf19.6947	3	**1.6155294**	0.69200706	*GTT1*	Predicted ORF in Assemblies 19, 20 and 21
DCG1	Cd36_82510	orf19.244	3	**1.615875**	0.6923156	*DCG1*	Transcription is regulated by Nrg1p and Mig1p
	Cd36_11170	orf19.5275	1	**1.6163408**	0.6927314	*VTA1*	Predicted ORF in Assemblies 19, 20 and 21
	Cd36_28090	orf19.2863	R	**1.6188086**	0.69493246		Predicted ORF in Assemblies 19, 20 and 21
	Cd36_65640		6	**1.6210097**	0.69689274		
	Cd36_65270	orf19.7078	6	**1.6229258**	0.69859695	*YCL012C*	Predicted ORF in Assemblies 19, 20 and 21
	Cd36_44940	orf19.2629	4	**1.6233994**	0.699018	*USO1*	Predicted ORF in Assemblies 19, 20 and 21
RPT4	Cd36_29280	orf19.482	R	**1.6236111**	0.6992061	*RPT4*	Predicted ORF in Assemblies 19, 20 and 21
	Cd36_09640	orf19.4894	1	**1.6244994**	0.6999953	*YER010C*	Protein of unknown function, has similarity to S. cerevisiae Yer010cp, which is a protein of unknown function belonging to the prokaryotic RraA family
	Cd36_00720		1	**1.626397**	0.70167947		
	Cd36_54520	orf19.3980	5	**1.6265093**	0.7017791	*SLH1*	Predicted ORF in Assemblies 19, 20 and 21
	Cd36_25700	orf19.7473	R	**1.6312472**	0.7059754		Predicted ORF in Assemblies 19, 20 and 21
	Cd36_34210	orf19.6436	R	**1.6326351**	0.70720243		Predicted ORF in Assemblies 19, 20 and 21
	Cd36_70980	orf19.7009	7	**1.6328627**	0.7074035	*YDR541C*	Predicted ORF in Assemblies 19, 20 and 21
	Cd36_26470	orf19.2533.1	R	**1.6332061**	0.7077069	*SBH2*	ORF Predicted by Annotation Working Group
PNC1	Cd36_73170	orf19.6684	7	**1.6341746**	0.70856214	*PNC1*	Predicted ORF in Assemblies 19, 20 and 21
RAD14	Cd36_71840	orf19.6517	7	**1.6388355**	0.71267104	*RAD14*	Transcription is regulated upon yeast-hyphal switch
MEP2	Cd36_40200	orf19.5672	4	**1.6394277**	0.7131922	*MEP2*	Ammonium permease and regulator of nitrogen starvation-induced filamentation
	Cd36_28180	orf19.2419	R	**1.6396111**	0.71335363	*DOM34*	Predicted ORF in Assemblies 19, 20 and 21
	Cd36_22030	orf19.2204.2	2	**1.6396116**	0.7133541	*RHO2*	ORF Predicted by Annotation Working Group (see Locus History Note for Assembly 19 correction)
	Cd36_73360	orf19.6690	7	**1.6397967**	0.713517		Predicted ORF in Assemblies 19, 20 and 21
	Cd36_83730		3	**1.6399251**	0.71362996		
	Cd36_15710	orf19.2047	2	**1.6399983**	0.71369433	*YOR289W*	Predicted ORF in Assemblies 19, 20 and 21
ATP17	Cd36_25290	orf19.7509.1	R	**1.6410269**	0.7145989	*ATP17*	Protein described as a component of mitochondrial ATPase complex
ARO10	Cd36_32400	orf19.1847	R	**1.6412646**	0.7148078	*ARO10*	Protein described as pyruvate decarboxylase
	Cd36_26290	orf19.3226	R	**1.6417688**	0.71525097	*NPC2*	Predicted ORF in Assemblies 19, 20 and 21
	Cd36_60930	orf19.92	6	**1.6422253**	0.715652	*YFR016C*	Predicted ORF in Assemblies 19, 20 and 21
	Cd36_31270	orf19.6624	R	**1.642808**	0.7161639		Predicted ORF in Assemblies 19, 20 and 21
KGD2	Cd36_33050	orf19.6126	R	**1.643369**	0.71665645	*KGD2*	Protein described as dihydrolipoamide S-succinyltransferase
	Cd36_31530	orf19.3859	R	**1.6462666**	0.719198	*YBR159W*	Predicted ORF in Assemblies 19, 20 and 21
	Cd36_02630	orf19.2971	1	**1.6466742**	0.71955514		Predicted ORF in Assemblies 19, 20 and 21
	Cd36_51130		5	**1.6475049**	0.7202828		
	Cd36_28240	orf19.2414	R	**1.648407**	0.72107244	*MPM1*	Predicted ORF in Assemblies 19, 20 and 21
DQD1	Cd36_21530	orf19.2283	2	**1.6496717**	0.72217894		Predicted ORF in Assemblies 19, 20 and 21
	Cd36_33940	orf19.6403	R	**1.6497257**	0.72222614	*SIL1*	Predicted ORF in Assemblies 19, 20 and 21
	Cd36_09850	orf19.988	1	**1.6511155**	0.7234411	*YGR149W*	Predicted ORF in Assemblies 19, 20 and 21
PHO15	Cd36_06770	orf19.4444	1	**1.6515471**	0.72381806	*PHO13*	Protein described as 4-nitrophenyl phosphatase
IFF4	Cd36_25710	orf19.7472	R	**1.652034**	0.72424346	*MUC1*	Putative GPI-anchored protein
	Cd36_28730	orf19.4391	R	**1.6527135**	0.72483665		Predicted ORF in Assemblies 19, 20 and 21
EST1	Cd36_55060	orf19.4045	5	**1.653512**	0.7255335	*EBS1*	Telomerase subunit
RPO21	Cd36_35480	orf19.7655	R	**1.6550676**	0.7268901	*RPO21*	Protein similar to S. cerevisiae Rpo21p, RNA polymerase II
	Cd36_61950	orf19.3402	6	**1.6555594**	0.72731876		Predicted ORF in Assemblies 19, 20 and 21
SFU1	Cd36_09420	orf19.4869	1	**1.6557802**	0.72751117	*GLN3*	Transcriptional regulator of iron-responsive genes
	Cd36_26420	orf19.2527	R	**1.6565217**	0.72815704	*YNL035C*	Predicted ORF in Assemblies 19, 20 and 21

Gene Name	*C. dubliniensis* Cd36 identifier	*C. albicans* orf19 identifier	C'some	Fold change expression	Normalised Expression	*S. cerevisiae* ortholog	Description
SSY1	Cd36_18710	orf19.814	2	**1.6574631**	0.7289767	*SSY1*	Amino acid sensor, required for wild-type hyphal growth on solid serum or Lees media, but not for hyphal growth under all conditions
	Cd36_12830	orf19.5022	1	**1.657711**	0.7291925	*SMF2*	Predicted ORF in Assemblies 19, 20 and 21
ARO9	Cd36_45160	orf19.1237	4	**1.657802**	0.72927165	*ARO9*	Predicted ORF in Assemblies 19, 20 and 21
KGD1	Cd36_80800	orf19.6165	3	**1.6584722**	0.7298548	*KGD1*	Protein described as 2-oxoglutarate dehydrogenase
	Cd36_45060	orf19.1797	4	**1.6606457**	0.7317443		Predicted ORF in Assemblies 19, 20 and 21
	Cd36_02770	orf19.2988	1	**1.6610659**	0.7321093		Predicted ORF in Assemblies 19, 20 and 21
HHT2	Cd36_32350	orf19.1853	R	**1.6614772**	0.73246646	*HHT2|HHT1*	Protein described as histone H3
	Cd36_54150	orf19.3937	5	**1.6640799**	0.73472476	*TIP41*	Predicted ORF in Assemblies 19, 20 and 21
	Cd36_06760	orf19.4445	1	**1.6641718**	0.7348044		Predicted ORF in Assemblies 19, 20 and 21
SYS3	Cd36_28270	orf19.2410	R	**1.6667733**	0.7370579	*IMH1*	Protein similar to S. cerevisiae Sys3p
	Cd36_87030	orf19.6790	3	**1.6668054**	0.73708564	*NGR1*	Predicted ORF in Assemblies 19, 20 and 21
MOH1	Cd36_43220	orf19.3369	4	**1.6671503**	0.73738414	*MOH1*	Protein similar to S. cerevisiae Moh1p
YVH1	Cd36_28620	orf19.4401	R	**1.66728**	0.7374964	*YVH1*	Putative dual specificity phosphatase (phosphoserine/threonine and phosphotyrosine phosphatase)
	Cd36_07570	orf19.5078	1	**1.669265**	0.739213		Predicted ORF in Assemblies 19, 20 and 21
	Cd36_54950	orf19.4030	5	**1.6697036**	0.7395921	*PRI1*	Predicted ORF in Assemblies 19, 20 and 21
	Cd36_35575	orf19.7678	R	**1.6722641**	0.7418027	*ATP16*	Predicted ORF in Assemblies 19, 20 and 21
RIM101	Cd36_13310	orf19.7247	1	**1.6724548**	0.7419672	*RIM101*	Transcription factor involved in alkaline pH response
	Cd36_87770	orf19.6189	3	**1.6724697**	0.7419801	*YHR198C*	Predicted ORF in Assemblies 19, 20 and 21
	Cd36_09200	orf19.4842	1	**1.6726385**	0.74212575		Predicted ORF in Assemblies 19, 20 and 21
PDA1	Cd36_46580	orf19.3097	4	**1.6730552**	0.74248505	*PDA1*	Protein described as similar to alpha chain of pyruvate dehydrogenase
	Cd36_33800	orf19.6377	R	**1.673103**	0.7425263	*PPM1*	Predicted ORF in Assemblies 19, 20 and 21
	Cd36_82910	orf19.286	3	**1.6733129**	0.74270725		Decreased transcription is observed upon fluphenazine treatment
	Cd36_27370	orf19.3724	R	**1.6751842**	0.7443198	*UTP23*	Predicted ORF in Assemblies 19, 20 and 21
SOD5	Cd36_15620	orf19.2060	2	**1.6754615**	0.7445586		Copper- and zinc-containing superoxide dismutase, protective role against oxidative stress
	Cd36_54640	orf19.3996	5	**1.6758351**	0.7448802	*GPI10*	Putative mannosyltransferase
HGT8	Cd36_15930	orf19.2021	2	**1.6761788**	0.7451761	*HXT6*	Putative glucose transporter of the major facilitator superfamily
	Cd36_60110	orf19.6323	6	**1.6769775**	0.7458633	*HPA3*	Predicted ORF in Assemblies 19, 20 and 21
PRE6	Cd36_29910	orf19.544.1	R	**1.6787525**	0.74738955	*PRE6*	Protein described as alpha-4 subunit of proteasome
PST3	Cd36_30720	orf19.5285	R	**1.6787764**	0.74741006	*PST2*	Putative flavodoxin
ALS1	Cd36_64210	orf19.5741	6	**1.6789187**	0.74753237	*FLO9*	Adhesin
	Cd36_22040	orf19.2204	2	**1.6806468**	0.7490165	*YPL264C*	Predicted ORF in Assemblies 19, 20 and 21
	Cd36_83960	orf19.2808	3	**1.6824328**	0.75054884	*CAT8*	Predicted zinc-finger protein of unknown function, not essential for viability
	Cd36_28740	orf19.4390	R	**1.6825254**	0.75062823		Predicted ORF in Assemblies 19, 20 and 21
	Cd36_30810	orf19.3517	R	**1.6833191**	0.7513087	*YOR223W*	Predicted ORF in Assemblies 19, 20 and 21
SMF3	Cd36_15540	orf19.2069	2	**1.6840487**	0.7519338	*SMF3*	Protein described as vacuolar iron transporter
	Cd36_27240	orf19.3742	R	**1.6843398**	0.7521832		Predicted ORF in Assemblies 19, 20 and 21
	Cd36_61920	orf19.3405	6	**1.6852249**	0.75294113	*LYS14*	Putative transcription factor with zinc finger DNA-binding motif
	Cd36_33750	orf19.6371	R	**1.685543**	0.7532134		Predicted ORF in Assemblies 19, 20 and 21
	Cd36_18260	orf19.867	2	**1.6868987**	0.7543733	*YGL160W*	Predicted ORF in Assemblies 19, 20 and 21
	Cd36_50570	orf19.932	5	**1.6869522**	0.7544191	*DNF1*	Predicted ORF in Assemblies 19, 20 and 21
	Cd36_13410		1	**1.6873333**	0.754745		
	Cd36_64400	orf19.5763	6	**1.6884611**	0.75570893	*YMR226C*	Predicted ORF in Assemblies 19, 20 and 21
MAC1	Cd36_70140	orf19.7068	7	**1.6885736**	0.755805	*MAC1*	Transcriptional regulator of CTR1, which encodes a copper transporter
	Cd36_72800	orf19.5139	7	**1.6892763**	0.75640535		Predicted ORF in Assemblies 19, 20 and 21
SKN7	Cd36_50270	orf19.971	5	**1.6894107**	0.75652003	*SKN7*	Putative homolog of S. cerevisiae Skn7p, which is predicted to be a response regulator protein in a phosphorelay signal transduction pathway
	Cd36_72160	orf19.6474	7	**1.6897186**	0.756783	*CBK1*	Predicted ORF in Assemblies 19, 20 and 21
	Cd36_33880	orf19.6393	R	**1.6912873**	0.7581217	*GTS1*	Predicted ORF in Assemblies 19, 20 and 21
UBI4	Cd36_87180	orf19.6771	3	**1.6921654**	0.7588706	*UBI4*	Ubiquitin precursor (polyubiquitin), contains three tandem repeats of the ubiquitin peptide that are processed to individual units
	Cd36_53970	orf19.3915	5	**1.6923522**	0.75902987	*DUG1*	Predicted ORF in Assemblies 19, 20 and 21
CHT1	Cd36_25200	orf19.7517	R	**1.6937714**	0.7602391	*CTS1*	Chitinase
NOT4	Cd36_28580	orf19.2379	R	**1.697358**	0.7632909	*MOT2*	Putative E3 ubiquitin-protein ligase
	Cd36_30130	orf19.6316	R	**1.6974063**	0.7633319	*YMR221C*	Predicted ORF in Assemblies 19, 20 and 21
CWH8	Cd36_02100	orf19.3682	1	**1.6977855**	0.76365423	*CAX4*	Putative dolichyl pyrophosphate (Dol-P-P) phosphatase
	Cd36_26300	orf19.3225	R	**1.6983622**	0.7641442	*CWH43*	Predicted ORF in Assemblies 19, 20 and 21
IFU5	Cd36_26730	orf19.2568	R	**1.6985301**	0.76428676	*WWM1*	Predicted membrane protein
	Cd36_84850	orf19.5956	3	**1.6989225**	0.76462007	*PIN3*	Predicted ORF in Assemblies 19, 20 and 21
SSB1	Cd36_33730	orf19.6367	R	**1.6989778**	0.76466703	*SSB2|SSB1*	Putative heat shock protein
SPT14	Cd36_29330	orf19.487	R	**1.6992241**	0.7648761	*SPT14*	Putative DNA-binding transcription factor
HYR4	Cd36_25840	orf19.3279	R	**1.6995054**	0.765115	*DAN4*	Putative GPI-anchored protein of unknown function
	Cd36_86200	orf19.7404	3	**1.6998563**	0.7654128	*CHA1*	Predicted ORF in Assemblies 19, 20 and 21
NAG1	Cd36_65540	orf19.2156	6	**1.7010906**	0.76645994		Glucosamine-6-phosphate deaminase
	Cd36_07150	orf19.1228	1	**1.701126**	0.76649	*HAP2*	Predicted ORF in Assemblies 19, 20 and 21
	Cd36_52750	orf19.4324	5	**1.701719**	0.76699287		Predicted ORF in Assemblies 19, 20 and 21
STP4	Cd36_17970	orf19.909	2	**1.7027965**	0.76790595	*STP3*	Putative transcription factor with zinc finger DNA-binding motif

Gene Name	*C. dubliniensis* Cd36 identifier	*C. albicans* orf19 identifier	C'some	Fold change expression	Normalised Expression	*S. cerevisiae* ortholog	Description
PHO81	Cd36_25690	orf19.7475	R	**1.7049482**	0.76972795	*PHO81*	Predicted ORF in Assemblies 19, 20 and 21
	Cd36_21700	orf19.1888	2	**1.7055905**	0.7702713	*URH1*	Predicted ORF in Assemblies 19, 20 and 21
	Cd36_03960	orf19.1054	1	**1.7065003**	0.7710407	*YLL023C*	Predicted ORF in Assemblies 19, 20 and 21
	Cd36_29650	orf19.519	R	**1.7075827**	0.7719555	*RRN10*	Predicted ORF in Assemblies 19, 20 and 21
	Cd36_21350	orf19.2262	2	**1.7076945**	0.7720499	*ZTA1*	Predicted ORF in Assemblies 19, 20 and 21
CSC25	Cd36_83870	orf19.6926	3	**1.7093697**	0.77346444	*CDC25*	Guanyl-nucleotide exchange factor
MDH1-1	Cd36_41790	orf19.4602	4	**1.7115544**	0.7753072	*MDH1*	Predicted malate dehydrogenase
	Cd36_35190	orf19.7596	R	**1.7123212**	0.7759533	*PMU1*	Predicted ORF in Assemblies 19, 20 and 21
UGA1	Cd36_18820	orf19.802	2	**1.7138762**	0.7772629	*UGA1*	Protein described as GABA transaminase
	Cd36_09990		1	**1.7139323**	0.77731013		
	Cd36_28840	orf19.4362	R	**1.716684**	0.77962446	*MSP1*	Predicted ORF in Assemblies 19, 20 and 21
	Cd36_28660	orf19.4396	R	**1.7191929**	0.78173137	*YKR016W*	Predicted ORF in Assemblies 19, 20 and 21
	Cd36_05100	orf19.428	1	**1.7200747**	0.7824712	*IKS1*	Predicted ORF in Assemblies 19, 20 and 21
	Cd36_54560	orf19.3984	5	**1.7216343**	0.78377867	*YGR237C*	Predicted ORF in Assemblies 19, 20 and 21
	Cd36_33320	orf19.6282	R	**1.7230124**	0.7849331	*NSR1*	Predicted ORF in Assemblies 19, 20 and 21
PGA52	Cd36_15090	orf19.1911	2	**1.7246889**	0.7863362	*YJL171C*	Putative GPI-anchored protein of unknown function
	Cd36_50060		5	**1.7270905**	0.78834367		
SEC65	Cd36_26630	orf19.2557	R	**1.7276171**	0.78878355	*SEC65*	Functional homolog of S. cerevisiae Sec65p, which is a component of the protein-targeting Signal Recognition Particle (SRP)
	Cd36_35075	orf19.7576	R	**1.7288542**	0.78981614		Protein not essential for viability
	Cd36_00030		1	**1.7294039**	0.79027486		
	Cd36_52940	orf19.4347	5	**1.7295442**	0.7903918	*PRR1*	Predicted ORF in Assemblies 19, 20 and 21
	Cd36_42060	orf19.4574	4	**1.7295697**	0.79041314	*YOR059C*	Predicted ORF in Assemblies 19, 20 and 21
ACC1	Cd36_25740	orf19.7466	R	**1.7301778**	0.79092026	*ACC1*	Protein with similarity to acetyl-coenzyme-A carboxylases
ASR1	Cd36_10070	orf19.2344	1	**1.7302103**	0.79094744	*HPF1*	Protein described as similar to heat shock proteins
OPT8	Cd36_64450	orf19.5770	6	**1.7308581**	0.79148746	*YGL114W*	Possible oligopeptide transporter
SIS1	Cd36_31550	orf19.3861	R	**1.730978**	0.79158735	*SIS1*	Predicted ORF in Assemblies 19, 20 and 21
GSL2	Cd36_25900	orf19.3269	R	**1.7330629**	0.793324	*GSC2*	Protein similar to beta-1,3-glucan synthase
PRC2	Cd36_50900	orf19.4135	5	**1.7346935**	0.79468083	*PRC1*	Protein described as a carboxypeptidase
	Cd36_83680	orf19.6951	3	**1.7349126**	0.794863	*DPL1*	Predicted ORF in Assemblies 19, 20 and 21
	Cd36_34160	orf19.6425	R	**1.7375402**	0.7970464	*SKI2*	Predicted ORF in Assemblies 19, 20 and 21
YCP4	Cd36_30710	orf19.5286	R	**1.7381015**	0.7975123	*YCP4*	Putative flavodoxin
	Cd36_31570	orf19.3862	R	**1.7388654**	0.79814625	*LST8*	Predicted ORF in Assemblies 19, 20 and 21
PGI1	Cd36_31840	orf19.3888	R	**1.7414018**	0.8002491	*PGI1*	Protein described as glucose-6-phosphate isomerase, enzyme of glycolysis
LAP3	Cd36_29830	orf19.539	R	**1.7426472**	0.8012805	*LAP3*	Protein described as an aminopeptidase
	Cd36_29750	orf19.529	R	**1.742693**	0.8013184	*MUC1*	Predicted ORF in Assemblies 19, 20 and 21
	Cd36_31240	orf19.6627	R	**1.7427155**	0.801337		Predicted ORF in Assemblies 19, 20 and 21
	Cd36_29840	orf19.540	R	**1.7431086**	0.80166245		Predicted ORF in Assemblies 19, 20 and 21
	Cd36_28460	orf19.2392	R	**1.7434961**	0.8019831		Protein not essential for viability
	Cd36_30360	orf19.633	R	**1.7438045**	0.8022382		Protein described as a putative methyltransferase
	Cd36_80370	orf19.5426	3	**1.7438436**	0.80227065	*TGL4*	Putative patatin-like phospholipase
YDC1	Cd36_46520	orf19.3104	4	**1.7441047**	0.80248666	*YDC1*	Predicted ORF in Assemblies 19, 20 and 21
	Cd36_54860	orf19.4019	5	**1.7462156**	0.80423164	*PSY4*	Predicted ORF in Assemblies 19, 20 and 21
	Cd36_33550	orf19.612	R	**1.7469952**	0.8048756	*YML050W*	Predicted ORF in Assemblies 19, 20 and 21
RIM13	Cd36_54630	orf19.3995	5	**1.7474817**	0.80527735	*RIM13*	Probable protease involved in the pH response pathway, likely to mediate activation of the transcription factor Rim101p via C-terminal cleavage
	Cd36_54380	orf19.3963	5	**1.7481345**	0.8058162	*YER182W*	Predicted ORF in Assemblies 19, 20 and 21
MCT1	Cd36_31050	orf19.6643	R	**1.7482425**	0.80590534	*MCT1*	Putative malonyl-CoA acyl carrier protein acyltransferase
	Cd36_15700	orf19.2048	2	**1.752495**	0.80941033		Transcription is positively regulated by Sfu1p
	Cd36_26440	orf19.2529	R	**1.7556602**	0.8120136		Predicted ORF in Assemblies 19, 20 and 21
RIB1	Cd36_28080	orf19.2862	R	**1.7571155**	0.81320906	*RIB1*	Putative GTP cyclohydrolase II
	Cd36_01760	orf19.4531	1	**1.7595294**	0.8151896	*YOL075C*	Putative PDR-subfamily ABC transporter
	Cd36_28750	orf19.4388	R	**1.7598033**	0.8154142	*TAF3*	Predicted ORF in Assemblies 19, 20 and 21
	Cd36_28630	orf19.4400	R	**1.7606912**	0.81614184		Predicted ORF in Assemblies 19, 20 and 21
HTB1	Cd36_83880	orf19.6925	3	**1.7632014**	0.81819725	*HTB1*	Putative histone H2B
	Cd36_81310		3	**1.763935**	0.81879735		
	Cd36_73950	orf19.7139	7	**1.7691606**	0.82306504		Predicted ORF in Assemblies 19, 20 and 21
	Cd36_54470	orf19.3973	5	**1.7713946**	0.8248856	*HUA1*	Predicted ORF in Assemblies 19, 20 and 21
ACS2	Cd36_04040	orf19.1064	1	**1.7727358**	0.82597756	*ACS2*	Probable acetyl-CoA synthetase, similar to known fungal acetyl-CoA synthetases
ICL1	Cd36_04240	orf19.6844	1	**1.774945**	0.82777435	*ICL1*	Isocitrate lyase
	Cd36_28940	orf19.4372	R	**1.7758871**	0.82853985	*YDL206W*	Predicted ORF in Assemblies 19, 20 and 21
	Cd36_30790	orf19.3515	R	**1.7759488**	0.8285899	*BNA1*	Predicted ORF in Assemblies 19, 20 and 21
	Cd36_23130	orf19.211	2	**1.7778215**	0.83011055		Predicted ORF in Assemblies 19, 20 and 21
ADP1	Cd36_31330	orf19.459	R	**1.7783026**	0.83050084	*ADP1*	Putative PDR-subfamily ABC transporter
	Cd36_11310	orf19.5257	1	**1.7783605**	0.8305478	*LCB4*	Predicted ORF in Assemblies 19, 20 and 21
SLU7	Cd36_86740	orf19.6827	3	**1.778413**	0.8305904	*SLU7*	Protein similar to S. cerevisiae Slu7p
	Cd36_54830	orf19.4016	5	**1.7784569**	0.830626	*COR1*	Predicted ORF in Assemblies 19, 20 and 21
	Cd36_25460		R	**1.7791398**	0.83117986		
	Cd36_70560	orf19.7085	7	**1.7800721**	0.83193564	*FUN12*	Predicted ORF in Assemblies 19, 20 and 21
	Cd36_08620		1	**1.7807509**	0.8324857		
PGA37	Cd36_54030	orf19.3923	5	**1.7815388**	0.8331239		Putative GPI-anchored protein of unknown function
	Cd36_25910	orf19.3268	R	**1.7819929**	0.8334916	*TMA19*	Ortholog of S. cerevisiae Tma19p (Ykl065cp)
	Cd36_26160	orf19.3237	R	**1.7854594**	0.83629537	*UFD4*	Predicted ORF in Assemblies 19, 20 and 21
RAD32	Cd36_18270	orf19.866	2	**1.7870886**	0.8376112	*RAD30*	Protein similar to S. cerevisiae protein with role in nucleotide excision repair

Gene Name	*C. dubliniensis* Cd36 identifier	*C. albicans* orf19 identifier	C'some	Fold change expression	Normalised Expression	*S. cerevisiae* ortholog	Description
	Cd36_73880	orf19.7152	7	**1.7898282**	0.8398211	*YGR012W*	Protein similar to Aspergillus CYSK O-acetylserine sulfhydrylase, suggesting that C. albicans uses an O-acetyl-serine (OAS) pathway of sulfur assimilation
	Cd36_21540	orf19.2284	2	**1.7908258**	0.84062505		Predicted ORF in Assemblies 19, 20 and 21
	Cd36_26360	orf19.2518	R	**1.7917553**	0.8413737	*SEC17*	Predicted ORF in Assemblies 19, 20 and 21
	Cd36_31080	orf19.6641	R	**1.7932656**	0.84258914		Predicted ORF in Assemblies 19, 20 and 21
	Cd36_10860		1	**1.7963245**	0.84504795		
THI4	Cd36_85100	orf19.5986	3	**1.7977353**	0.8461807	*THI4*	Protein repressed during the mating process
	Cd36_55030	orf19.4043	5	**1.797932**	0.8463385	*ASK10*	Predicted ORF in Assemblies 19, 20 and 21
	Cd36_29810	orf19.537	R	**1.7980063**	0.8463981	*YBR197C*	Predicted ORF in Assemblies 19, 20 and 21
	Cd36_26250	orf19.3230	R	**1.7981056**	0.84647775	*BOI2*	Predicted ORF in Assemblies 19, 20 and 21
	Cd36_11510	orf19.5236	1	**1.7990938**	0.8472705	*SRT1*	Predicted ORF in Assemblies 19, 20 and 21
	Cd36_26790	orf19.2574	R	**1.8009742**	0.84877753	*YFL034W*	Predicted ORF in Assemblies 19, 20 and 21
	Cd36_04200	orf19.6838	1	**1.8010105**	0.8488066	*SPS19*	Predicted ORF in Assemblies 19, 20 and 21
RAD51	Cd36_27150	orf19.3752	R	**1.8026125**	0.8500893	*RAD51*	Predicted ORF in Assemblies 19, 20 and 21
	Cd36_54930	orf19.4028	5	**1.8031572**	0.85052514	*RER2*	Predicted ORF in Assemblies 19, 20 and 21
	Cd36_65140	orf19.2127	6	**1.8036559**	0.85092413		Predicted ORF in Assemblies 19, 20 and 21
	Cd36_29920	orf19.547	R	**1.805242**	0.85219216	*RAD27*	Predicted ORF in Assemblies 19, 20 and 21
	Cd36_13020	orf19.7212	1	**1.8067524**	0.8533988	*APL1*	Predicted ORF in Assemblies 19, 20 and 21
	Cd36_53700	orf19.3213	5	**1.8069927**	0.8535906	*JIP4*	Predicted ORF in Assemblies 19, 20 and 21
	Cd36_08810	orf19.4795	1	**1.8089366**	0.8551419		Predicted ORF in Assemblies 19, 20 and 21
	Cd36_13000	orf19.7209	1	**1.8100945**	0.85606503	*RDI1*	Predicted ORF in Assemblies 19, 20 and 21
	Cd36_04900	orf19.449	1	**1.8125604**	0.8580291	*YKR070W*	Predicted ORF in Assemblies 19, 20 and 21
	Cd36_45010	orf19.1793	4	**1.8146033**	0.85965425	*HSV2*	Protein not essential for viability
PHO84	Cd36_10770	orf19.655	1	**1.8185883**	0.86281896	*PHO84*	Protein similar to high-affinity phosphate transporters
	Cd36_22410	orf19.2660	2	**1.8197113**	0.86370957	*EAF3*	Predicted ORF in Assemblies 19, 20 and 21
	Cd36_82540	orf19.247	3	**1.8201953**	0.8640933	*YGL079W*	Predicted ORF in Assemblies 19, 20 and 21
	Cd36_34000	orf19.6407	R	**1.8205254**	0.86435485	*REH1*	Predicted ORF in Assemblies 19, 20 and 21
PGA4	Cd36_54990	orf19.4035	5	**1.8209544**	0.86469483	*GAS5*	Putative cell-surface protein, predicted to carry a glycosylphosphatidylinositol (GPI) lipid anchor
	Cd36_26130	orf19.3241	R	**1.8212675**	0.8649428	*YDR128W*	Predicted ORF in Assemblies 19, 20 and 21
	Cd36_32930	orf19.6138	R	**1.8216659**	0.86525834	*FRE4*	Predicted ORF in Assemblies 19, 20 and 21
	Cd36_33090	orf19.6118	R	**1.8276875**	0.87001944	*DSS4*	Predicted ORF in Assemblies 19, 20 and 21
	Cd36_42570	orf19.2730	4	**1.8304348**	0.8721864	*RPH1*	Predicted ORF in Assemblies 19, 20 and 21
	Cd36_15680	orf19.2050	2	**1.8346816**	0.87552977	*TGL1*	Predicted ORF in Assemblies 19, 20 and 21
HST2	Cd36_26820	orf19.2580	R	**1.8350058**	0.87578464	*HST2*	Predicted ORF in Assemblies 19, 20 and 21
PGA23	Cd36_27260	orf19.3740	R	**1.837691**	0.87789416	*YFL067W*	Putative GPI-anchored protein of unknown function
	Cd36_84880	orf19.5960	3	**1.8382386**	0.87832403	*NCE102*	Predicted ORF in Assemblies 19, 20 and 21
	Cd36_31820	orf19.3886	R	**1.8393948**	0.8792312		Predicted ORF in Assemblies 19, 20 and 21
WSC4	Cd36_13330	orf19.7251	1	**1.8411695**	0.8806224	*WSC4*	Transcription is specific to white cell type
LIP3	Cd36_09310	orf19.4856	1	**1.8416518**	0.8810003		Secreted lipase, member of a lipase gene family whose members are expressed differentially in response to carbon source and during infection
	Cd36_20390	orf19.5217	2	**1.8436676**	0.8825786	*TES1*	Predicted ORF in Assemblies 19, 20 and 21
	Cd36_00980	orf19.3292	1	**1.843722**	0.88262117	*YCL033C*	Predicted ORF in Assemblies 19, 20 and 21
	Cd36_30160	orf19.6313.2	R	**1.8481128**	0.88605285		ORF Predicted by Annotation Working Group
SDS24	Cd36_07880	orf19.5118	1	**1.8519225**	0.8890238	*SDS24*	Protein described as similar to S. cerevisiae Ybr214wp
SDS22	Cd36_18670	orf19.820	2	**1.8523198**	0.88933325	*SDS22*	Predicted ORF in Assemblies 19, 20 and 21
	Cd36_33580	orf19.606	R	**1.8542181**	0.89081097	*YLR352W*	Predicted ORF in Assemblies 19, 20 and 21
IFG3	Cd36_50460	orf19.944	5	**1.8549767**	0.89140105		Putative D-amino acid oxidase
MEP1	Cd36_82290	orf19.1614	3	**1.8595865**	0.89498186	*MEP3*	Ammonium permease
	Cd36_80010		3	**1.8641292**	0.8985019		
	Cd36_43620	orf19.5045	4	**1.8649498**	0.8991368	*PTP2*	Predicted ORF in Assemblies 19, 20 and 21
ARO2	Cd36_33360	orf19.1986	R	**1.8669826**	0.90070844	*ARO2*	Putative chorismate synthase
	Cd36_27340	orf19.3730	R	**1.8698233**	0.902902	*KRE27*	Protein similar to S. cerevisiae Kre27p, which has a role in resistance to killer toxin
	Cd36_31960	orf19.719	R	**1.8717642**	0.9043987	*HRD1*	Predicted ORF in Assemblies 19, 20 and 21
	Cd36_25190	orf19.7518	R	**1.8721951**	0.9047308		Putative transcription factor with zinc cluster DNA-binding motif
UBC15	Cd36_24750	orf19.5337	2	**1.8722227**	0.904752	*UBC13*	Predicted ORF in Assemblies 19, 20 and 21
	Cd36_27400	orf19.3720	R	**1.8730799**	0.90541244	*BCY1*	Predicted ORF in Assemblies 19, 20 and 21
PTP1	Cd36_33710	orf19.6365	R	**1.8740917**	0.9061916	*PTP1*	Protein not essential for viability
	Cd36_25300	orf19.7510	R	**1.8773931**	0.90873075	*KIN2*	Predicted ORF in Assemblies 19, 20 and 21
HXT5	Cd36_28610	orf19.4384	R	**1.8779309**	0.9091439	*ITR1*	Protein described as a sugar transporter
	Cd36_34140	orf19.6423	R	**1.8785839**	0.90964556	*FBP26*	Predicted ORF in Assemblies 19, 20 and 21
	Cd36_84360	orf19.5892	3	**1.8800554**	0.9107752	*HUL4*	Predicted ORF in Assemblies 19, 20 and 21
	Cd36_26680	orf19.2563	R	**1.8802251**	0.91090536	*PRP24*	Predicted ORF in Assemblies 19, 20 and 21
	Cd36_25880	orf19.3273	R	**1.8802974**	0.9109609	*YIH1*	Predicted ORF in Assemblies 19, 20 and 21
	Cd36_27350	orf19.3728	R	**1.8828664**	0.9129306	*DAN4*	Predicted ORF in Assemblies 19, 20 and 21
HXT5	Cd36_28770	orf19.4384	R	**1.88417**	0.9139292	*ITR1*	Protein described as a sugar transporter
TPO4	Cd36_29200	orf19.473	R	**1.8848493**	0.9144492	*TPO4*	Putative sperimidine transporter
	Cd36_33330	orf19.3487	R	**1.885657**	0.9150672		Predicted ORF in Assemblies 19, 20 and 21
	Cd36_28250	orf19.2412	R	**1.894423**	0.92175853	*VPS55*	Predicted ORF in Assemblies 19, 20 and 21
	Cd36_34270	orf19.6444	R	**1.8947275**	0.9219904	*RMD11*	Predicted ORF in Assemblies 19, 20 and 21
	Cd36_16520	orf19.1477	2	**1.8959391**	0.9229126	*YGL010W*	Predicted ORF in Assemblies 19, 20 and 21
RBT7	Cd36_42950	orf19.2681	4	**1.897723**	0.9242694	*RNY1*	Protein with similarity to RNase T2 enzymes, has putative secretion signal
SFT1	Cd36_26180	orf19.3234.1	R	**1.8979987**	0.924479	*SFT1*	ORF Predicted by Annotation Working Group
	Cd36_28480	orf19.2391	R	**1.898149**	0.9245932	*YKR023W*	Predicted ORF in Assemblies 19, 20 and 21

Gene Name	*C. dubliniensis* Cd36 identifier	*C. albicans* orf19 identifier	C'some	Fold change expression	Normalised Expression	*S. cerevisiae* ortholog	Description
	Cd36_17080	orf19.1576	2	**1.8985707**	0.9249137	*YHL010C*	Predicted ORF in Assemblies 19, 20 and 21
	Cd36_42460	orf19.2730	4	**1.8995347**	0.92564607	*RPH1*	Predicted ORF in Assemblies 19, 20 and 21
	Cd36_26430	orf19.2528	R	**1.9014245**	0.92708063	*BDP1*	Predicted ORF in Assemblies 19, 20 and 21
LPI9	Cd36_71610	orf19.6544	7	**1.9038321**	0.9289062	*GIP3*	Predicted ORF in Assemblies 19, 20 and 21
	Cd36_52170	orf19.4246	5	**1.9039632**	0.9290056	*YKR070W*	Predicted ORF in Assemblies 19, 20 and 21
	Cd36_06620	orf19.6196	1	**1.9045011**	0.9294131		Predicted ORF in Assemblies 19, 20 and 21
	Cd36_21710	orf19.1887	2	**1.9048281**	0.9296608	*YEH1*	Predicted ORF in Assemblies 19, 20 and 21
	Cd36_85920	orf19.7380	3	**1.9052167**	0.9299551	*WSC3*	Predicted ORF in Assemblies 19, 20 and 21
YME1	Cd36_45280	orf19.1252	4	**1.9100497**	0.9336102	*YME1*	Protein not essential for viability
	Cd36_53750	orf19.1285	5	**1.9107541**	0.9341421	*YPR091C*	Predicted ORF in Assemblies 19, 20 and 21
TTR1	Cd36_00420	orf19.6059	1	**1.9118893**	0.934999	*GRX2*	Putative glutaredoxin
INO2	Cd36_25070	orf19.7539	R	**1.9143777**	0.93687546		Transcriptional activator that may be involved in regulation of ribosomal protein genes
	Cd36_22000	orf19.2210	2	**1.9180312**	0.9396262		Predicted ORF in Assemblies 19, 20 and 21
	Cd36_32850	orf19.6148	R	**1.9196438**	0.9408386	*USO1*	Predicted ORF in Assemblies 19, 20 and 21
	Cd36_00670	orf19.6031	1	**1.9202098**	0.9412639	*VPS27*	Predicted ORF in Assemblies 19, 20 and 21
	Cd36_28650	orf19.4398	R	**1.9202739**	0.9413121	*YPR147C*	Predicted ORF in Assemblies 19, 20 and 21
ACF2	Cd36_61790	orf19.3417	6	**1.921323**	0.94210005	*ACF2*	Putative endo-1,3-beta-glucanase
	Cd36_61780	orf19.3418	6	**1.9219381**	0.94256186		Predicted ORF in Assemblies 19, 20 and 21
	Cd36_25980	orf19.3260	R	**1.9245958**	0.9445555	*YKL088W*	Predicted ORF in Assemblies 19, 20 and 21
PHR1	Cd36_44230	orf19.3829	4	**1.9252069**	0.9450135	*GAS1*	Glycosidase of hyphal cell surface
	Cd36_60970	orf19.94	6	**1.9267834**	0.9461944		Predicted ORF in Assemblies 19, 20 and 21
SDH2	Cd36_30410	orf19.637	R	**1.9291494**	0.9479649	*SDH2*	Succinate dehydrogenase, Fe-S subunit
	Cd36_55050	orf19.4046	5	**1.933587**	0.95127964		Predicted ORF in Assemblies 19, 20 and 21
	Cd36_73970	orf19.7131	7	**1.9351488**	0.95244455	*YHL021C*	Predicted ORF in Assemblies 19, 20 and 21
	Cd36_28040	orf19.2853	R	**1.9352355**	0.95250916		Predicted ORF in Assemblies 19, 20 and 21
SRV2	Cd36_29500	orf19.505	R	**1.9402151**	0.9562166	*SRV2*	Adenylate cyclase-associated protein that regulates adenylate cyclase activity
	Cd36_81820		3	**1.9439194**	0.9589684		
	Cd36_87630	orf19.6709	3	**1.9467324**	0.96105456		Predicted ORF in Assemblies 19, 20 and 21
	Cd36_29890	orf19.543	R	**1.946855**	0.9611454	*FUM1*	Protein described as fumarate hydratase
	Cd36_13160	orf19.7227	1	**1.9480255**	0.9620125	*YPI1*	Predicted ORF in Assemblies 19, 20 and 21
ACS1	Cd36_24410	orf19.1743	2	**1.9514793**	0.96456814	*ACS1*	Putative acetyl-CoA synthetase, similar to S. cerevisiae Acs2p
LSC1	Cd36_01550	orf19.3358	1	**1.952196**	0.9650979	*LSC1*	Protein described as succinate-CoA ligase subunit
	Cd36_31770	orf19.3879	R	**1.9611669**	0.9717123		Predicted ORF in Assemblies 19, 20 and 21
	Cd36_60080	orf19.1178	6	**1.9621466**	0.97243285		Putative transcription factor with bZIP DNA-binding motif
AHP1	Cd36_42290	orf19.2762	4	**1.9633539**	0.97332025	*AHP1*	Putative alkyl hydroperoxide reductase
MDH1	Cd36_25650	orf19.7481	R	**1.9665478**	0.97566533	*MDH1*	Protein described as malate dehydrogenase, mitochondrial
SFC1	Cd36_54090	orf19.3931	5	**1.9665487**	0.9756659	*SFC1*	Alkaline upregulated
ISA1	Cd36_62750	orf19.5521	6	**1.9707714**	0.9787605	*ISA1*	Reported to have possible role in iron-sulfur cluster biogenesis or cytoplasm-to-mitochondrion iron transport
RFG1	Cd36_27640	orf19.2823	R	**1.9721289**	0.97975385	*ROX1*	Transcriptional regulator of filamentous growth and hyphal genes
GAC1	Cd36_70020	orf19.7053	7	**1.9728266**	0.9802642	*GAC1*	Protein described as similar to regulatory subunit of serine/threonine phosphoprotein phosphatase 1
TAL1	Cd36_28930	orf19.4371	R	**1.9779068**	0.98397446	*TAL1*	Predicted ORF in Assemblies 19, 20 and 21
	Cd36_25130	orf19.7527	R	**1.9859208**	0.9898081		Predicted ORF in Assemblies 19, 20 and 21
	Cd36_33430	orf19.3705	R	**1.9866679**	0.9903507	*PTC6*	Predicted ORF in Assemblies 19, 20 and 21
	Cd36_21920	orf19.1861	2	**1.9946122**	0.9961083		Predicted ORF in Assemblies 19, 20 and 21
	Cd36_20540	orf19.4104	2	**1.9948174**	0.9962567		Predicted ORF in Assemblies 19, 20 and 21
	Cd36_51150	orf19.1950	5	**1.9963455**	0.9973614	*POA1*	Predicted ORF in Assemblies 19, 20 and 21
	Cd36_22200	orf19.2184	2	**2.0003319**	1.0002394	*YNL168C*	Predicted ORF in Assemblies 19, 20 and 21
	Cd36_61100	orf19.100	6	**2.0044005**	1.0031708	*YJR107W*	Predicted ORF in Assemblies 19, 20 and 21
	Cd36_25150	orf19.7522	R	**2.0051236**	1.0036912	*BNA3*	Predicted ORF in Assemblies 19, 20 and 21
	Cd36_50800	orf19.4150	5	**2.0055847**	1.0040228	*GRX7*	Predicted ORF in Assemblies 19, 20 and 21
	Cd36_10510	orf19.2296	1	**2.008331**	1.0059972	*HPF1*	Predicted ORF in Assemblies 19, 20 and 21
SOD3	Cd36_70320	orf19.7111.1	7	**2.0085702**	1.0061688	*SOD2*	Cytosolic manganese-containing superoxide dismutase, involved in protection against oxidative stress
IFF6	Cd36_23280	orf19.4072	2	**2.010437**	1.0075091	*YBL113C*	Putative GPI-anchored protein of unknown function
	Cd36_27600	orf19.2821	R	**2.0184455**	1.0132446		Predicted ORF in Assemblies 19, 20 and 21
BCR1	Cd36_31890	orf19.723	R	**2.0205894**	1.0147762	*USV1*	Transcription factor required for wild-type biofilm formation
	Cd36_19410	orf19.4127	2	**2.0242934**	1.0174184	*YSC84*	Predicted ORF in Assemblies 19, 20 and 21
	Cd36_01500	orf19.3353	1	**2.026743**	1.0191631		Protein described as similar to a mitochondrial complex I intermediate-associated protein
HTS1	Cd36_55080	orf19.4051	5	**2.0275886**	1.0197649	*HTS1*	Putative tRNA-His synthetase
	Cd36_15880	orf19.2030	2	**2.032891**	1.0235329	*SNA4*	Predicted ORF in Assemblies 19, 20 and 21
	Cd36_01100	orf19.3305	1	**2.0332682**	1.0238006	*UPC2*	Putative transcription factor with zinc cluster DNA-binding motif
	Cd36_12610		1	**2.0350883**	1.0250914		
POT1-2	Cd36_15720	orf19.2046	2	**2.0382633**	1.0273404	*POT1*	Putative peroxisomal 3-ketoacyl CoA thiolase
	Cd36_27590		R	**2.0385818**	1.0275658		
	Cd36_87550	orf19.6720	3	**2.0395005**	1.0282159	*YDR090C*	Predicted ORF in Assemblies 19, 20 and 21
NAG3	Cd36_65570	orf19.2158	6	**2.0443847**	1.0316668	*TPO3*	Putative transporter of the major facilitator superfamily (MFS)
LPD1	Cd36_33030	orf19.6127	R	**2.0455906**	1.0325174	*LPD1*	Putative dihydrolipoamide dehydrogenase
IFC3	Cd36_27190	orf19.3749	R	**2.046295**	1.033014	*OPT2*	Oligopeptide transporter
	Cd36_26200	orf19.3233	R	**2.0467525**	1.0333366	*HSE1*	Predicted ORF in Assemblies 19, 20 and 21
PRB1	Cd36_21180	orf19.2242	2	**2.048043**	1.034246	*PRB1*	Putative endoprotease B
RGD3	Cd36_33170	orf19.729.1	R	**2.0580788**	1.0412982	*RGD2*	Putative Rho GTPase activating protein
PRC3	Cd36_05440	orf19.2474	1	**2.0588064**	1.0418081	*YBR139W*	Transcription is regulated by Nrg1p and Mig1p

Gene Name	*C. dubliniensis* Cd36 identifier	*C. albicans* orf19 identifier	C'some	Fold change expression	Normalised Expression	*S. cerevisiae* ortholog	Description
HSP78	Cd36_18140	orf19.882	2	**2.0621934**	1.0441797	*HSP78*	Protein described as a heat-shock protein
	Cd36_73140	orf19.6705	7	**2.0644016**	1.0457237	*YEL1*	Protein described as a putative guanyl nucleotide exchange factor with Sec7 domain
GIT1	Cd36_51400	orf19.1979	5	**2.0661187**	1.0469232	*GIT1*	Putative glycerophosphoinositol permease
	Cd36_23960	orf19.1363	2	**2.0695484**	1.0493159	*YOR338W*	Predicted ORF in Assemblies 19, 20 and 21
	Cd36_27280	orf19.3737	R	**2.0704193**	1.049923	*MUK1*	Predicted ORF in Assemblies 19, 20 and 21
	Cd36_29140	orf19.4358	R	**2.072431**	1.0513241	*YDL157C*	Predicted ORF in Assemblies 19, 20 and 21
	Cd36_41930	orf19.4589	4	**2.0759928**	1.0538015	*FMS1*	Predicted ORF in Assemblies 19, 20 and 21
PUT2	Cd36_54480	orf19.3974	5	**2.0765746**	1.0542057	*PUT2*	Alkaline upregulated
	Cd36_30800	orf19.3516	R	**2.0768852**	1.0544214		Predicted ORF in Assemblies 19, 20 and 21
	Cd36_83400	orf19.340	3	**2.0784426**	1.0555029		Predicted ORF in Assemblies 19, 20 and 21
	Cd36_09800	orf19.4911	1	**2.0820465**	1.0580022		Predicted ORF in Assemblies 19, 20 and 21
	Cd36_45200	orf19.1240	4	**2.0824556**	1.0582857	*YPR117W*	Predicted ORF in Assemblies 19, 20 and 21
	Cd36_25520	orf19.7495	R	**2.082891**	1.0585873	*OYE3*	Predicted ORF in Assemblies 19, 20 and 21
	Cd36_53240		5	**2.0853653**	1.0603001		
INO1	Cd36_35120	orf19.7585	R	**2.0890346**	1.0628363	*INO1*	Inositol-1-phosphate synthase
FAS1	Cd36_50220	orf19.979	5	**2.0902855**	1.0637	*FAS1*	Beta subunit of fatty-acid synthase
	Cd36_15560	orf19.2067	2	**2.0909204**	1.0641382	*NFU1*	Predicted ORF in Assemblies 19, 20 and 21
YIM1	Cd36_18420	orf19.847	2	**2.091498**	1.0645366	*YIM1*	Protein similar to protease of mitochondrial inner membrane
	Cd36_43850	orf19.5311	4	**2.0929961**	1.0655696	*MUC1*	Predicted ORF in Assemblies 19, 20 and 21
	Cd36_32810	orf19.730	R	**2.1058004**	1.0743687	*RGD2*	Predicted ORF in Assembly 20 and 21 (see Locus History)
	Cd36_32320	orf19.1857	R	**2.107862**	1.0757804	*SPT10*	Protein not essential for viability
MKC1	Cd36_25140	orf19.7523	R	**2.1119392**	1.0785682	*SLT2*	MAP kinase
RBT5	Cd36_40190	orf19.5636	4	**2.1196585**	1.0838318		GPI-anchored cell wall protein
MSB2	Cd36_16640	orf19.1490	2	**2.1268206**	1.0886984	*MSB2*	Protein of unknown function
	Cd36_83380	orf19.338	3	**2.127002**	1.0888214	*YMR196W*	Predicted ORF in Assemblies 19, 20 and 21
	Cd36_06720	orf19.4449	1	**2.1282017**	1.0896349	*CCS1*	Predicted ORF in Assemblies 19, 20 and 21
ADH5	Cd36_27000	orf19.2608	R	**2.1307428**	1.0913565	*ADH5*	Putative alcohol dehydrogenase
HNT2	Cd36_86320	orf19.7419	3	**2.1376243**	1.0960083	*HNT2*	Predicted ORF in Assemblies 19, 20 and 21
IFR1	Cd36_24240	orf19.1763	2	**2.1440957**	1.1003692	*YNL134C*	Predicted ORF in Assemblies 19, 20 and 21
	Cd36_25410		R	**2.1486328**	1.103419		
	Cd36_18010	orf19.904	2	**2.1527128**	1.1061559		Predicted ORF in Assemblies 19, 20 and 21
	Cd36_21550	orf19.2285	2	**2.1533518**	1.1065841		Increased transcription is observed upon benomyl treatment
	Cd36_33100	orf19.6117	R	**2.1642556**	1.1138709	*YBR287W*	Predicted ORF in Assemblies 19, 20 and 21
	Cd36_29420	orf19.496	R	**2.1646445**	1.11413	*MSH1*	Predicted ORF in Assemblies 19, 20 and 21
	Cd36_28430	orf19.2395	R	**2.1657789**	1.1148859	*IME2*	Predicted ORF in Assemblies 19, 20 and 21
	Cd36_85930	orf19.7381	3	**2.1670477**	1.115731	*LYS14*	Predicted zinc-finger protein of unknown function
	Cd36_02780	orf19.2989	1	**2.1706727**	1.1181421	*GOR1*	Predicted ORF in Assemblies 19, 20 and 21
	Cd36_71830	orf19.6518	7	**2.1732109**	1.1198282	*HFD1*	Predicted ORF in Assemblies 19, 20 and 21
	Cd36_10590	orf19.673	1	**2.173688**	1.1201448	*OYE3*	Predicted ORF in Assemblies 19, 20 and 21
OSM2	Cd36_12650	orf19.5005	1	**2.1739972**	1.1203501	*OSM1*	Protein described as mitochondrial fumarate reductase
ILV3	Cd36_55010	orf19.4040	5	**2.1751592**	1.1211209	*ILV3*	Putative dihydroxyacid dehydratase
	Cd36_26810	orf19.2579	R	**2.1752245**	1.1211643	*MSH4*	Predicted ORF in Assemblies 19, 20 and 21
MDR1	Cd36_63890	orf19.5604	6	**2.1769204**	1.1222887	*FLR1*	Multidrug efflux pump of plasma membrane
	Cd36_20210	orf19.6888	2	**2.1789036**	1.1236024	*LYS14*	Protein with Gal4p-like DNA-binding domain
	Cd36_32360	orf19.1852	R	**2.1806211**	1.1247392	*YIL087C*	Predicted ORF in Assemblies 19, 20 and 21
VID21	Cd36_46690	orf19.3077	4	**2.1811438**	1.1250849	*EAF1*	Predicted ORF in Assemblies 19, 20 and 21
HAP31	Cd36_29630	orf19.517	R	**2.186689**	1.1287479	*HAP3*	Protein described as a transcription factor that regulates CYC1
PGA15	Cd36_65070	orf19.2878	6	**2.1866975**	1.1287537		Putative GPI-anchored protein of unknown function
	Cd36_81770	orf19.1656	3	**2.1900642**	1.1309731	*PIB2*	Predicted ORF in Assemblies 19, 20 and 21
	Cd36_72930	orf19.5125	7	**2.1919081**	1.1321874	*YLR149C*	Predicted ORF in Assemblies 19, 20 and 21
	Cd36_32430	orf19.1842	R	**2.2044656**	1.140429	*BUD5*	Predicted ORF in Assemblies 19, 20 and 21
	Cd36_25250	orf19.7513	R	**2.204863**	1.1406891	*DIT2*	Predicted ORF in Assemblies 19, 20 and 21
	Cd36_25810	orf19.3283	R	**2.2081273**	1.1428233	*OAR1*	Predicted ORF in Assemblies 19, 20 and 21
	Cd36_32750	orf19.733	R	**2.2121093**	1.1454227	*YBR287W*	Predicted ORF in Assemblies 19, 20 and 21
PGA31	Cd36_43780	orf19.5302	4	**2.2143834**	1.146905	*MUC1*	Putative GPI-anchored protein
ARF1	Cd36_34290	orf19.6447	R	**2.2158945**	1.1478891	*ARF1*	ADP-ribosylation factor, probable GTPase involved in intracellular transport
	Cd36_18660	orf19.822	2	**2.217701**	1.1490648		Predicted ORF in Assemblies 19, 20 and 21
VPS4	Cd36_52880	orf19.4339	5	**2.219786**	1.1504205	*VPS4*	Protein involved in transport from multivesicular body (MVB) to the vacuole
	Cd36_09700	orf19.4900	1	**2.2205904**	1.1509433	*MNT4/MNT2*	Predicted ORF in Assemblies 19, 20 and 21
	Cd36_00010		1	**2.2218578**	1.1517665		
	Cd36_25260	orf19.7512	R	**2.2222316**	1.1520091	*DIT2*	Predicted ORF in Assemblies 19, 20 and 21
	Cd36_46480	orf19.3108	4	**2.2239177**	1.1531034	*MGT1*	Predicted ORF in Assemblies 19, 20 and 21
CTA8	Cd36_08650	orf19.4775	1	**2.2358584**	1.1608288	*HSF1*	Predicted ORF in Assemblies 19, 20 and 21
	Cd36_87600	orf19.6713	3	**2.2379162**	1.1621561	*DEF1*	Predicted ORF in Assemblies 19, 20 and 21
	Cd36_23100	orf19.215	2	**2.2403367**	1.1637156	*AVO2*	Predicted ORF in Assemblies 19, 20 and 21
	Cd36_33890	orf19.6396	R	**2.2431133**	1.1655025	*NTE1*	Putative patatin-like phospholipase
	Cd36_63800	orf19.5611	6	**2.2437408**	1.165906	*GRE2*	Predicted ORF in Assemblies 19, 20 and 21
HNT2	Cd36_86130	orf19.7419	3	**2.2522645**	1.1713762	*HNT2*	Predicted ORF in Assemblies 19, 20 and 21
ATG15	Cd36_61830	orf19.3412	6	**2.2540271**	1.1725049	*ATG15*	Putative lipase
	Cd36_29560	orf19.511	R	**2.256277**	1.1739442	*NRK1*	Predicted ORF in Assemblies 19, 20 and 21
	Cd36_27980	orf19.2848	R	**2.258173**	1.175156	*ATG13*	Predicted ORF in Assemblies 19, 20 and 21
	Cd36_53740	orf19.1287	5	**2.259954**	1.1762934		Predicted ORF in Assemblies 19, 20 and 21
	Cd36_87270	orf19.6755	3	**2.2613113**	1.1771595	*DLD1*	Predicted ORF in Assemblies 19, 20 and 21
	Cd36_34300	orf19.6448	R	**2.262851**	1.1781416		Predicted ORF in Assemblies 19, 20 and 21
	Cd36_27310	orf19.3734	R	**2.2660735**	1.1801946	*GEF1*	Predicted ORF in Assemblies 19, 20 and 21
	Cd36_34240	orf19.6440	R	**2.2678874**	1.181349	*ASI1*	Predicted ORF in Assemblies 19, 20 and 21

Gene Name	*C. dubliniensis* Cd36 identifier	*C. albicans* orf19 identifier	C'some	Fold change expression	Normalised Expression	*S. cerevisiae* ortholog	Description
MNT4	Cd36_30170	orf19.6313	R	2.2707508	1.1831694	*MNT4*	Transcriptionally regulated by iron
	Cd36_50010		5	2.276377	1.1867394		
	Cd36_42870	orf19.2691	4	2.2778788	1.187691		Predicted ORF in Assemblies 19, 20 and 21
	Cd36_64040			2.284354	1.1917863		
	Cd36_01140	orf19.3310	1	2.2882152	1.1942227		Predicted ORF in Assemblies 19, 20 and 21
	Cd36_30910	orf19.5846	R	2.2925463	1.1969509	*TFB2*	Predicted ORF in Assemblies 19, 20 and 21
AFG1	Cd36_08350	orf19.4743	1	2.2966335	1.1995206	*AFG1*	Protein not essential for viability
FLC2	Cd36_32680	orf19.1813	R	2.2968254	1.1996412	*FLC2*	Protein involved in heme uptake
DAL1	Cd36_80170	orf19.5454	3	2.2989452	1.2009721	*DAL1*	Predicted ORF in Assemblies 19, 20 and 21
	Cd36_20800	orf19.22	2	2.30071	1.202079	*SYM1*	Transcription is positively regulated by Sfu1p
	Cd36_60240	orf19.1189	6	2.3068855	1.2059463		Predicted ORF in Assemblies 19, 20 and 21
CWT1	Cd36_30880	orf19.5849	R	2.315841	1.2115362	*RDS2*	Putative transcription factor
FDH3	Cd36_35225	orf19.7600	R	2.3168097	1.2121395	*SFA1*	Putative protein of glycine catabolism
	Cd36_42040	orf19.4577	4	2.3180435	1.2129076	*GPB1*	Predicted ORF in Assemblies 19, 20 and 21
DES1	Cd36_55070	orf19.4048	5	2.3204608	1.2144113		Putative delta-4 sphingolipid desaturase
	Cd36_29490	orf19.504	R	2.3225029	1.2156804	*ARP5*	Predicted ORF in Assemblies 19, 20 and 21
SUA72	Cd36_30830	orf19.3519	R	2.3229632	1.2159663	*SUA7*	Predicted transcriptional regulator
	Cd36_72450	orf19.2669	7	2.3267405	1.2183104	*R161W-B|YFL0C*	Predicted ORF in Assemblies 19, 20 and 21
	Cd36_46730		4	2.327689	1.2188983		
	Cd36_44300		4	2.3300421	1.220356		
	Cd36_29460	orf19.499	R	2.3328881	1.2221172	*MTQ1*	Predicted ORF in Assemblies 19, 20 and 21
	Cd36_52830		5	2.3355308	1.2237505		
BNR1	Cd36_25090	orf19.7537	R	2.3383746	1.2255061	*BNI1*	Formin
	Cd36_35230	orf19.7601	R	2.3416536	1.2275276	*MRM2*	Predicted ORF in Assemblies 19, 20 and 21
	Cd36_34200	orf19.6435	R	2.3430939	1.2284148	*YGR243W*	Predicted ORF in Assemblies 19, 20 and 21
	Cd36_20300	orf19.5210	2	2.343219	1.2284918	*XBP1*	Predicted ORF in Assemblies 19, 20 and 21
PRN2	Cd36_05520	orf19.2463	1	2.3496134	1.2324234		Predicted ORF in Assemblies 19, 20 and 21
CSR1	Cd36_44490	orf19.3794	4	2.351678	1.2336905	*ZAP1*	Putative DNA-binding transcription factor
SAP7	Cd36_04610	orf19.756	1	2.3528519	1.2344105	*YPS3*	Member of the secreted aspartyl proteinase family
SOL3	Cd36_32240	orf19.704	R	2.3604631	1.2390699	*SOL3*	Predicted ORF in Assemblies 19, 20 and 21
NCE103	Cd36_81230	orf19.1721	3	2.3615162	1.2397134	*NCE103*	Carbonic anhydrase involved in the conversion of carbon dioxide to bicarbonate
	Cd36_34340		R	2.36482	1.2417303		
	Cd36_29160	orf19.467	R	2.3710303	1.2455142	*SNF5*	Predicted ORF in Assemblies 19, 20 and 21
	Cd36_00020		1	2.3773336	1.2493443		
WH11	Cd36_19680	orf19.3548.1	2	2.3847618	1.2538452	*HSP12*	Cytoplasmic protein expressed specifically in white phase yeast-form cells
	Cd36_40480	orf19.5671	4	2.3935578	1.2591567	*SYP1*	Predicted ORF in Assemblies 19, 20 and 21
	Cd36_25940		R	2.396713	1.2610571		
	Cd36_51180	orf19.1955	5	2.4011753	1.2637407	*SHR5*	Predicted ORF in Assemblies 19, 20 and 21
GDH2	Cd36_22140	orf19.2192	2	2.4039228	1.2653906	*GDH2*	Putative NAD-specific glutamate dehydrogenase
	Cd36_61900	orf19.3406	6	2.4107995	1.2695117	*YHL008C*	Predicted ORF in Assemblies 19, 20 and 21
AQY1	Cd36_27990	orf19.2849	R	2.4124105	1.2704754	*AQY1*	Aquaporin water channel
DDR48	Cd36_23350	orf19.4082	2	2.4213111	1.2757885	*DDR48*	Immunogenic stress-associated protein
GPR1	Cd36_51080	orf19.1944	5	2.4237237	1.2772253	*GPR1*	Putative G-protein-coupled receptor of plasma membrane
	Cd36_27450	orf19.173	R	2.4259334	1.2785399	*AZF1*	Putative transcription factor with zinc finger DNA-binding motif
	Cd36_41920	orf19.4590	4	2.426971	1.2791568	*MTL1*	Predicted ORF in Assemblies 19, 20 and 21
	Cd36_01680	orf19.4539	1	2.428639	1.280148	*RDI1*	Predicted ORF in Assemblies 19, 20 and 21
	Cd36_80020		3	2.4314988	1.2818458		
	Cd36_11420	orf19.5245	1	2.4377265	1.2855363	*BUL2*	Predicted ORF in Assemblies 19, 20 and 21
CSH1	Cd36_03770	orf19.4477	1	2.4623208	1.3000188	*YPL088W*	Member of aldo-keto reductase family, similar to aryl alcohol dehydrogenases
	Cd36_51480	orf19.583	5	2.4684832	1.3036249	*BNA2*	Putative indoleamine 2,3-dioxygenase (IDO)
	Cd36_16950	orf19.1533	2	2.4715865	1.3054374	*YKL077W*	Predicted ORF in Assemblies 19, 20 and 21
RME1	Cd36_06830	orf19.4438	1	2.4742963	1.3070183	*RME1*	Protein similar to S. cerevisiae meiotic regulator Rme1p
HGT10	Cd36_64300	orf19.5753	6	2.4747987	1.3073112	*STL1*	Putative glucose transporter of the major facilitator superfamily
	Cd36_25010		R	2.478797	1.3096402		
	Cd36_34260	orf19.6443	R	2.4828188	1.311979	*ECI1*	Predicted ORF in Assemblies 19, 20 and 21
SUC1	Cd36_34590	orf19.7319	R	2.4880362	1.3150074	*YPR196W*	Putative transcriptional regulator with N-terminal zinc finger
	Cd36_71520	orf19.6556	7	2.4886863	1.3153844	*AGA1*	Predicted ORF in Assemblies 19, 20 and 21
PRN3	Cd36_05530	orf19.2462	1	2.4888334	1.3154697		Predicted ORF in Assemblies 19, 20 and 21
XYL2	Cd36_35570	orf19.7676	R	2.489431	1.3158159	*SOR2*	Protein described as similar to D-xylulose reductase
	Cd36_84810	orf19.5952	3	2.4921598	1.3173966		Predicted ORF in Assemblies 19, 20 and 21
	Cd36_84590	orf19.5924	3	2.49351	1.3181779	*VRP1*	Predicted zinc-finger protein of unknown function
	Cd36_11910	orf19.6349	1	2.5017583	1.3229424	*RVS161*	Predicted ORF in Assemblies 19, 20 and 21
	Cd36_31650		R	2.5038323	1.3241379		
	Cd36_34010	orf19.6408	R	2.5060792	1.325432	*YDJ1*	Predicted ORF in Assemblies 19, 20 and 21
NAG4	Cd36_65590	orf19.2160	6	2.5071282	1.3260357	*TPO3*	Putative transporter
	Cd36_54110	orf19.3932	5	2.5073934	1.3261883		Predicted ORF in Assemblies 19, 20 and 21
	Cd36_54960	orf19.4031	5	2.5088935	1.3270512	*YIR007W*	Predicted ORF in Assemblies 19, 20 and 21
	Cd36_50130		5	2.5179071	1.3322251		
CSP37	Cd36_26450	orf19.2531	R	2.51978	1.3332977		Plasma membrane, hyphal cell wall protein
	Cd36_84150	orf19.5862	3	2.5227857	1.3350177	*CAR1*	Protein described as related to arginases
UGA2	Cd36_01650	orf19.4543	1	2.5236366	1.3355042	*UGA2*	Protein not essential for viability
	Cd36_35440	orf19.7648	R	2.523689	1.3355341	*YDR338C*	Predicted ORF in Assemblies 19, 20 and 21
PRP13	Cd36_29040	orf19.4379	R	2.542078	1.3460083	*YME2*	Predicted ORF in Assemblies 19, 20 and 21
	Cd36_34460	orf19.7296	R	2.5424871	1.3462405		Predicted ORF in Assemblies 19, 20 and 21

Gene Name	*C. dubliniensis* Cd36 identifier	*C. albicans* orf19 identifier	C'some	Fold change expression	Normalised Expression	*S. cerevisiae* ortholog	Description
GAT2	Cd36_04890	orf19.4056	1	2.556954	1.3544261	*GAT2*	Putative DNA-binding transcription factor
	Cd36_01570	orf19.3360	1	2.5606668	1.3565196		0
LSC2	Cd36_32310	orf19.1860	R	2.5688713	1.3611345	*LSC2*	Protein described as beta subunit of succinate-CoA ligase
ECI1	Cd36_34280	orf19.6445	R	2.5725307	1.3631883	*ECI1*	Protein similar to S. cerevisiae Eci1p, which is involved in fatty acid oxidation
	Cd36_28820	orf19.4380.1	R	2.5747244	1.364418	*YME2*	Predicted ORF in Assembly 20 and 21 (see Locus History)
RHO1	Cd36_27930	orf19.2843	R	2.5756428	1.3649325	*RHO1*	Small GTPase of Rho family
EXO70	Cd36_71870	orf19.6512	7	2.5880818	1.3718833	*EXO70*	Predicted ORF in Assemblies 19, 20 and 21
	Cd36_52870	orf19.4337	5	2.5996516	1.3783183	*ESBP6*	Predicted ORF in Assemblies 19, 20 and 21
	Cd36_26190	orf19.3234	R	2.6118715	1.3850839	*OYE3*	Predicted ORF in Assemblies 19, 20 and 21
	Cd36_54020	orf19.3922	5	2.6232226	1.3913403	*SDT1*	Predicted ORF in Assemblies 19, 20 and 21
	Cd36_40980	orf19.4698	4	2.6246672	1.3921345		Predicted ORF in Assemblies 19, 20 and 21
	Cd36_32460	orf19.178	R	2.6284819	1.3942298		Predicted ORF in Assemblies 19, 20 and 21
	Cd36_53200	orf19.2638	5	2.6521719	1.4071742		Predicted ORF in Assemblies 19, 20 and 21
	Cd36_22120	orf19.2194	2	2.6529682	1.4076073	*APM4*	Predicted ORF in Assemblies 19, 20 and 21
	Cd36_23040	orf19.223	2	2.6533413	1.4078102	*YNR047W*	Predicted ORF in Assemblies 19, 20 and 21
	Cd36_55020	orf19.4041	5	2.6627274	1.4129047	*PEX4*	Predicted ORF in Assemblies 19, 20 and 21
	Cd36_52410	orf19.4280	5	2.666893	1.41516		Predicted ORF in Assemblies 19, 20 and 21
EBP1	Cd36_61290	orf19.125	6	2.6748557	1.419461	*OYE2*	NADPH oxidoreductase
LEU1	Cd36_25490	orf19.7498	R	2.7046018	1.4354162	*LEU1*	Protein described as 3-isopropylmalate dehydratase
ALG5	Cd36_27860	orf19.2837	R	2.720354	1.4437945	*ALG5*	Putative glucosyltransferase involved in cell wall mannan biosynthesis
	Cd36_34040	orf19.6414	R	2.7248435	1.4461734		Predicted ORF in Assemblies 19, 20 and 21
SMF12	Cd36_21430	orf19.2270	2	2.739033	1.4536667	*SMF1*	Protein not essential for viability
	Cd36_80330	orf19.5431	3	2.745261	1.4569433		Predicted ORF in Assemblies 19, 20 and 21
CDG1	Cd36_34565	orf19.7314	R	2.7610474	1.4652157		Protein described as similar to cysteine dioxygenases
	Cd36_21190	orf19.2244	2	2.7614706	1.4654367	*YJR096W*	Similar to oxidoreductases and to S. cerevisiae Yjr096wp
	Cd36_84270	orf19.5876	3	2.7686615	1.4691887		Predicted ORF in Assemblies 19, 20 and 21
PUT1	Cd36_52370	orf19.4274	5	2.7725418	1.4712092	*PUT1*	Alkaline upregulated by Rim101p
GLK1	Cd36_32740	orf19.734	R	2.7879224	1.4791903	*GLK1*	Putative glucokinase
	Cd36_28380	orf19.2398	R	2.7910054	1.4807849		Predicted ORF in Assemblies 19, 20 and 21
	Cd36_15590	orf19.2064	2	2.802876	1.486908		Putative transcription factor with zinc finger DNA-binding motif
	Cd36_32890	orf19.6143	R	2.8062186	1.4886274		Predicted ORF in Assemblies 19, 20 and 21
CAR1	Cd36_54130	orf19.3934	5	2.8295875	1.5005918	*CAR1*	Transcription is regulated by Nrg1p, Mig1p, and Tup1p
NRG1	Cd36_73890	orf19.7150	7	2.8326166	1.5021353	*NRG2*	Transcriptional repressor
YHB5	Cd36_33470	orf19.3710	R	2.8467746	1.5093282	*YHB1*	Protein related to flavohemoglobins
FBP1	Cd36_87700	orf19.6178	3	2.853257	1.5126097	*FBP1*	Fructose-1,6-bisphosphatase, a key enzyme of gluconeogenesis
	Cd36_08270	orf19.4735	1	2.8630953	1.5175757	*YGL159W*	Predicted ORF in Assemblies 19, 20 and 21
FLC1	Cd36_80900	orf19.2501	3	2.8656197	1.5188471	*FLC3*	Protein involved in heme uptake
	Cd36_33440	orf19.3706	R	2.8723443	1.5222287	*AST2*	Predicted ORF in Assemblies 19, 20 and 21
SKN1	Cd36_85750	orf19.7362	3	2.8725302	1.522322	*KRE6*	Protein with predicted role in beta-1,6-glucan synthesis
	Cd36_30890	orf19.5848	R	2.8774133	1.5247724		Predicted ORF in Assemblies 19, 20 and 21
	Cd36_45920	orf19.2891	4	2.8782067	1.5251702	*AFG1*	Predicted ORF in Assemblies 19, 20 and 21
	Cd36_62000	orf19.3395	6	2.9002454	1.536175	*YHK8*	Predicted ORF in Assemblies 19, 20 and 21
	Cd36_08490	orf19.4756	1	2.933281	1.5525153	*YTP1*	Predicted ORF in Assemblies 19, 20 and 21
GLK4	Cd36_33110	orf19.6116	R	2.9349072	1.5533149	*GLK1*	Protein described as a glucokinase
	Cd36_70520	orf19.7091	7	2.9443703	1.5579591		Predicted ORF in Assemblies 19, 20 and 21
	Cd36_31600	orf19.3865	R	2.9822679	1.5764098	*RFX1*	Predicted ORF in Assemblies 19, 20 and 21
	Cd36_17200	orf19.1562	2	3.045132	1.6065047		Predicted ORF in Assemblies 19, 20 and 21
	Cd36_25400		R	3.0667057	1.6166897		
ARD	Cd36_60100	orf19.6322	6	3.0671456	1.6168966	*SPS19*	D-arabitol dehydrogenase, NAD-dependent (ArDH)
OYE2	Cd36_61520	orf19.3443	6	3.0896657	1.6274507	*OYE2*	Putative NAPDH dehydrogenase
	Cd36_29880	orf19.542.2	R	3.1042037	1.6342232	*MIM1*	ORF Predicted by Annotation Working Group
	Cd36_04210	orf19.6840	1	3.106563	1.6353194		Predicted ORF in Assemblies 19, 20 and 21
IFD3	Cd36_01150	orf19.3311	1	3.1348906	1.6484151	*YPL088W*	Transcription is regulated by Mig1p
	Cd36_54050	orf19.3926	5	3.147499	1.6542059	*RNY1*	Predicted ORF in Assemblies 19, 20 and 21
HSP104	Cd36_33850	orf19.6387	R	3.1615105	1.660614	*HSP104*	Functional homolog of S. cerevisiae Hsp104p
MUM2	Cd36_55040	orf19.4044	5	3.179421	1.668764	*MUM2*	Protein similar to S. cerevisiae Mum2p
RTA3	Cd36_20820	orf19.23	2	3.221869	1.6878978	*RSB1*	Similar to S. cerevisiae Rta1p (role in 7-aminocholesterol resistance) and Rsb1p (flippase)
FRP1	Cd36_40170	orf19.5634	4	3.2399054	1.6959517	*FRE5*	Protein similar to ferric reductases
	Cd36_32760	orf19.732	R	3.3047664	1.7245483	*SPS19*	Predicted ORF in Assemblies 19, 20 and 21
	Cd36_42230	orf19.2769	4	3.312348	1.7278543	*PBI2*	Predicted ORF in Assemblies 19, 20 and 21
	Cd36_32230	orf19.703	R	3.3260403	1.7338057	*CPD1*	Predicted ORF in Assemblies 19, 20 and 21
	Cd36_04190	orf19.6837	1	3.345355	1.7421594	*YIR035C*	Predicted ORF in Assemblies 19, 20 and 21
ENA2	Cd36_00320	orf19.6070	1	3.3776605	1.7560244	*ENA2*	Described as sodium transporter
ARR3	Cd36_46360	orf19.3122	4	3.3831992	1.7583882	*ARR3*	Protein not essential for viability
PGA7	Cd36_40180	orf19.5635	4	3.408393	1.7690916	*TIR1*	Protein described as a putative precursor of a hyphal surface antigen
	Cd36_51940	orf19.4216	5	3.4177616	1.7730517	*HSP12*	Predicted ORF in Assemblies 19, 20 and 21
CAN3	Cd36_60830	orf19.84	6	3.4220371	1.7748554	*CAN1*	Predicted ORF in Assemblies 19, 20 and 21
	Cd36_07510	orf19.5070	1	3.4663405	1.7934134	*AGA1*	Predicted ORF in Assemblies 19, 20 and 21
	Cd36_31150	orf19.6637	R	3.5064557	1.8100135		Predicted ORF in Assemblies 19, 20 and 21
RNH1	Cd36_63220	orf19.5563	6	3.5135689	1.8129371	*RNH1*	Protein described as Ribonuclease H (RNAse H)
	Cd36_11500	orf19.5237	1	3.5459983	1.8261919	*VPH2*	Predicted ORF in Assemblies 19, 20 and 21
ECM331	Cd36_52240	orf19.4255	5	3.5533917	1.8291967	*ECM33*	Putative GPI-anchored protein
	Cd36_81850	orf19.1653	3	3.5640528	1.8335187		Predicted ORF in Assemblies 19, 20 and 21

Gene Name	*C. dubliniensis* Cd36 identifier	*C. albicans* orf19 identifier	C'some	Fold change expression	Normalised Expression	*S. cerevisiae* ortholog	Description
	Cd36_25110	orf19.7531	R	3.5643263	1.8336294	*YMR090W*	Predicted ORF in Assemblies 19, 20 and 21
	Cd36_81170		3	3.609477	1.8517898		
	Cd36_42090	orf19.4570	4	3.6282098	1.8592579		Predicted ORF in Assemblies 19, 20 and 21
	Cd36_40140	orf19.376	4	3.6383185	1.8632718		Predicted ORF in Assemblies 19, 20 and 21
	Cd36_15160	orf19.2114	2	3.645116	1.8659648		Predicted ORF in Assemblies 19, 20 and 21
	Cd36_04480		1	3.6780949	1.8789587		
	Cd36_85200			3.6808705	1.880047		
	Cd36_61530	orf19.3442	6	3.828262	1.9366896	*OYE2*	Predicted ORF in Assemblies 19, 20 and 21
OPT4	Cd36_27420	orf19.176	R	3.8399835	1.9411001	*OPT2*	Oligopeptide transporter
	Cd36_42220	orf19.2770	4	3.8556314	1.9469671		Predicted ORF in Assemblies 19, 20 and 21
SAP10	Cd36_44180	orf19.3839	4	3.8669188	1.9511845	*MKC7*	Secreted aspartyl proteinase
PGA13	Cd36_34100	orf19.6420	R	3.947398	1.980902	*DAN4*	Putative GPI-anchored protein
HSP30	Cd36_01850	orf19.4526	1	4.0286417	2.0102935	*HSP30*	Protein described as similar to heat shock protein
	Cd36_18690	orf19.816	2	4.066034	2.0236223	*YLR422W*	Predicted ORF in Assemblies 19, 20 and 21
SFL1	Cd36_31370	orf19.454	R	4.066362	2.0237386	*SFL1*	Protein involved in negative regulation of flocculation and filamentous growth
	Cd36_86630	orf19.7455	3	4.2752547	2.0960104		Predicted ORF in Assemblies 19, 20 and 21
GST3	Cd36_31940	orf19.720	R	4.3845205	2.132419		Expression is regulated upon white-opaque switching
DEF1	Cd36_34980	orf19.7561	R	4.3942046	2.135602	*DEF1*	Transcription is induced upon filamentous growth
	Cd36_41750	orf19.4607	4	4.4150157	2.1424186		Predicted ORF in Assemblies 19, 20 and 21
GDH3	Cd36_45660	orf19.4716	4	4.4358835	2.1492214	*GDH3*	Protein described as similar to NADP-glutamate dehydrogenase
	Cd36_40970		4	4.4526787	2.1546736		
	Cd36_25350	orf19.7502	R	4.4772406	2.1626098		Predicted ORF in Assemblies 19, 20 and 21
	Cd36_50140	orf19.5686	5	4.48461	2.1649826		Predicted ORF in Assemblies 19, 20 and 21
FDH1	Cd36_30420	orf19.638	R	4.518934	2.1759825	*FDH1*	Putative formate dehydrogenase, oxidizes formate to produce CO2
	Cd36_11660	orf19.69	1	4.524558	2.1777768		Predicted ORF in Assemblies 19, 20 and 21
FRP6	Cd36_61540	orf19.3441	6	4.668993	2.2231114	*ATO2*	Transcription is regulated by Nrg1p and Tup1p
TEC1	Cd36_84480	orf19.5908	3	4.6848483	2.2280023	*TEC1*	TEA/ATTS transcription factor involved in regulation of hypha-specific genes
	Cd36_23670	orf19.1395	2	4.9001184	2.2928166	*PIC2*	Predicted ORF in Assemblies 19, 20 and 21
CIRT4B	Cd36_27870	orf19.2839	R	5.146689	2.3636446		Decreased transcription is observed in an azole-resistant strain that overexpresses CDR1 and CDR2
	Cd36_70450	orf19.7098	7	5.2207103	2.384246	*YKL070W*	Predicted ORF in Assemblies 19, 20 and 21
PSA2	Cd36_12220	orf19.4943	1	5.256388	2.3940718	*PSA1*	Predicted ORF in Assemblies 19, 20 and 21
	Cd36_43280	orf19.3378	4	5.2574472	2.3943624		Predicted ORF in Assemblies 19, 20 and 21
	Cd36_46100	orf19.2870	4	5.2767596	2.3996522		Predicted ORF in Assemblies 19, 20 and 21
	Cd36_05580	orf19.2457	1	5.4241905	2.4394078		Predicted ORF in Assemblies 19, 20 and 21
CUP1	Cd36_54185	orf19.3940.1	5	5.4504	2.446362		Metallothionein, involved in copper resistance
PGA58	Cd36_52810	orf19.4334	5	5.8264556	2.5426185	*CCW12*	Putative GPI-anchored protein of unknown function
	Cd36_29990	orf19.552	R	5.896918	2.559961	*ATG22*	Predicted ORF in Assemblies 19, 20 and 21
IHD1	Cd36_64370	orf19.5760	6	5.9275227	2.5674293	*SRP40*	Putative GPI-anchored protein of unknown function
	Cd36_02600	orf19.2968	1	5.9925256	2.5831642		Predicted ORF in Assemblies 19, 20 and 21
	Cd36_29540	orf19.510	R	6.015095	2.5885875	*DEF1*	Predicted ORF in Assemblies 19, 20 and 21
AOX1	Cd36_08640	orf19.4774	1	6.4761186	2.6951294		Alternative oxidase
	Cd36_16490	orf19.1473	2	6.9014273	2.7868948	*YPL113C*	Predicted ORF in Assemblies 19, 20 and 21
	Cd36_27950	orf19.2846	R	7.693277	2.9435983		Predicted ORF in Assemblies 19, 20 and 21
	Cd36_53500	orf19.1117	5	8.913903	3.1560574	*FDH1*	Predicted ORF in Assemblies 19, 20 and 21
	Cd36_73750	orf19.7167	7	10.617019	3.4083068		Predicted ORF in Assemblies 19, 20 and 21
PCK1	Cd36_25230	orf19.7514	R	14.120391	3.819708	*PCK1*	Phosphoenolpyruvate carboxykinase
CTA26	Cd36_35580	orf19.7680	R	15.781859	3.9801953		Putative transcriptional activator

Table S.2. Changes in gene expression greater than 1.5-fold in ΔΔ*tlo* compared to Wü284 at 1 h growth in WS

Gene Name	*C. dubliniensis* Cd36 identifier	*C. albicans* orf19 identifier	C'some	Fold change expression	Normalised Expression	*S. cerevisiae* ortholog	Description
FGR41	Cd36_09790	orf19.4910	1	-49.264175	-5.622467	*DSE2*	Putative GPI-anchored protein
	Cd36_87380	orf19.6741	3	-35.001965	-5.129364		Predicted ORF in Assemblies 19, 20 and 21
RBT1	Cd36_43400	orf19.1327	4	-33.31862	-5.0582566	*MUC1*	Putative cell wall protein with similarity to Hwp1p, required for virulence
RBT5	Cd36_40190	orf19.5636	4	-31.305935	-4.9683642		GPI-anchored cell wall protein
SCW11	Cd36_53810	orf19.3893	5	-25.84859	-4.6920137	*SCW11*	Cell wall protein
HWP1	Cd36_43360	orf19.1321	4	-23.427813	-4.5501504	*MUC1*	Hyphal cell wall protein
	Cd36_62260	orf19.3499	6	-17.091953	-4.0952454		Predicted ORF in Assemblies 19, 20 and 21
EAP1	Cd36_23630	orf19.1401	2	-16.148401	-4.0133195	*YDL038C*	Cell wall adhesin required for cell-cell adhesion and biofilm formation
PIR1	Cd36_23050	orf19.220	2	-15.706213	-3.9732635	*PIR1*	Structural protein of cell wall
RBE1	Cd36_13090	orf19.7218	1	-15.267681	-3.932409	*PRY1*	Putative cell wall protein
HGC1	Cd36_00690	orf19.6028	1	-14.887004	-3.8959816	*CLN2*	Hypha-specific G1 cyclin-related protein involved in regulation of hyphal morphogenesis
PGA38	Cd36_42320	orf19.2758	4	-14.036012	-3.8110611	*AGA1*	Putative GPI-anchored protein of unknown function
GAL10	Cd36_02000	orf19.3672	1	-12.743785	-3.671722	*GAL10*	UDP-glucose 4-epimerase, required for galactose utilization
	Cd36_05550	orf19.2460	1	-12.598385	-3.6551669		Predicted ORF in Assemblies 19, 20 and 21
	Cd36_17020	orf19.1541	2	-12.416954	-3.6342394	*AGA1*	Protein not essential for viability
PGA25	Cd36_60170	orf19.6336	6	-12.372017	-3.6290088	*MUC1*	Putative GPI-anchored protein of unknown function
PRY1	Cd36_07060	orf19.2787	1	-11.513912	-3.5253062	*PRY1*	Transcription is opaque specific
DSE1	Cd36_22620	orf19.3629	2	-11.222578	-3.4883323	*DSE1*	Predicted cell wall protein
ALS1	Cd36_64210	orf19.5741	6	-10.45701	-3.3863986	*FLO9*	Adhesin
CFL5	Cd36_50970	orf19.1930	5	-10.285842	-3.362588	*FRE3*	Protein similar to ferric reductase Fre10p
	Cd36_44050		4	-9.640675	-3.269134		
	Cd36_53920	orf19.3908	5	-9.524694	-3.2516727		Predicted ORF in Assemblies 19, 20 and 21
ASH1	Cd36_24700	orf19.5343	2	-8.978174	-3.1664221	*ASH1*	GATA-like transcription factor
FET3	Cd36_60410	orf19.4211	6	-8.91749	-3.1566377	*FET3*	Multicopper oxidase
CSA1	Cd36_70300	orf19.7114	7	-8.890885	-3.152327	*MUC1*	Surface antigen on elongating hyphae and buds
SCW4	Cd36_02380	orf19.2941	1	-7.810352	-2.9653876	*SCW4*	Putative cell wall protein
SIT1	Cd36_22250	orf19.2179	2	-7.5215054	-2.9110215	*ARN1*	Transporter of ferrichrome siderophores, but not ferrioxamine B
	Cd36_70210	orf19.7077	7	-7.4795017	-2.9029422	*FRE7*	Protein of unknown function
PHO89	Cd36_41830	orf19.4599	4	-7.1426744	-2.8364644	*PHO89*	Putative phosphate permease
SOD6	Cd36_15220	orf19.2108	2	-7.0204244	-2.8115582		Copper- and zinc-containing superoxide dismutase
	Cd36_10620		1	-6.656631	-2.7347922		
	Cd36_01980		1	-6.175807	-2.6266277		
GAL1	Cd36_01990	orf19.3670	1	-6.1612225	-2.6232166	*GAL3*	Galactokinase
TNA1	Cd36_52840	orf19.4335	5	-6.124245	-2.614532	*TNA1*	Putative nicotinic acid transporter
FRP1	Cd36_40170	orf19.5634	4	-6.1197753	-2.6134787	*FRE5*	Protein similar to ferric reductases
	Cd36_83450	orf19.344	3	-6.0186906	-2.5894496	*AGA1*	Predicted ORF in Assemblies 19, 20 and 21
GAL7	Cd36_02030	orf19.3675	1	-5.7512383	-2.5238726	*GAL7*	Predicted ORF in Assemblies 19, 20 and 21
ENG1	Cd36_03430	orf19.3066	1	-5.5941277	-2.4839132	*DSE4*	Endo-1,3-beta-glucanase required for cell separation after division, orthologous to S. cerevisiae Dse4p
PGA7	Cd36_40180	orf19.5635	4	-5.5653334	-2.476468	*TIR1*	Protein described as a putative precursor of a hyphal surface antigen
	Cd36_34490	orf19.7300	R	-5.177767	-2.37233		Predicted ORF in Assemblies 19, 20 and 21
RPS3	Cd36_30190	orf19.6312	R	-5.17356	-2.3711574	*RPS3*	Putative ribosomal protein
PGA44	Cd36_81300	orf19.1714	3	-5.0326552	-2.3313198	*AGA1*	Putative GPI-anchored protein of unknown function
	Cd36_23070	orf19.217	2	-4.8578696	-2.2803237	*YPR013C*	Predicted ORF in Assemblies 19, 20 and 21
	Cd36_42600	orf19.2726	4	-4.7337856	-2.2429943	*SFK1*	Predicted ORF in Assemblies 19, 20 and 21
	Cd36_81000	orf19.2512	3	-4.6741614	-2.2247076		Predicted ORF in Assemblies 19, 20 and 21
	Cd36_60240	orf19.1189	6	-4.6545935	-2.218655		Predicted ORF in Assemblies 19, 20 and 21
PGA17	Cd36_18100	orf19.893	2	-4.556911	-2.1880562		Putative GPI-anchored protein of unknown function
	Cd36_16610	orf19.1486	2	-4.536165	-2.1814733		Predicted ORF in Assemblies 19, 20 and 21
	Cd36_16490	orf19.1473	2	-4.530483	-2.1796649	*YPL113C*	Predicted ORF in Assemblies 19, 20 and 21
	Cd36_52920	orf19.4342	5	-4.4405684	-2.1507444	*SUT1*	Predicted ORF in Assemblies 19, 20 and 21
CLN3	Cd36_51220	orf19.1960	5	-4.354108	-2.1223772	*CLN3*	G1 cyclin
	Cd36_32180	orf19.699	R	-4.352412	-2.1218152		Predicted ORF in Assemblies 19, 20 and 21
	Cd36_61580	orf19.3437	6	-4.3192234	-2.110772		Predicted ORF in Assemblies 19, 20 and 21
SOD5	Cd36_15620	orf19.2060	2	-4.308607	-2.1072216		Copper- and zinc-containing superoxide dismutase, protective role against oxidative stress
STB3	Cd36_23190	orf19.203	2	-4.3044	-2.105812	*STB3*	Predicted ORF in Assemblies 19, 20 and 21
	Cd36_16850	orf19.1522	2	-4.213579	-2.0750463		Predicted ORF in Assemblies 19, 20 and 21
	Cd36_05880	orf19.1822	1	-4.205036	-2.0721183	*UME6*	Putative transcription factor with zinc cluster DNA-binding motif
GPX2	Cd36_60850	orf19.85	6	-4.127397	-2.0452323	*HYR1*	Similar to glutathione peroxidase
	Cd36_60160	orf19.6329	6	-4.100503	-2.035801	*HPF1*	Predicted ORF in Assemblies 19, 20 and 21
	Cd36_16760	orf19.1507	2	-4.090139	-2.0321498	*AMN1*	Predicted ORF in Assemblies 19, 20 and 21
	Cd36_11230	orf19.5267	1	-4.077119	-2.02755		Putative cell wall protein
OP4	Cd36_12150	orf19.4934	1	-3.9975853	-1.9991288		Ala- Leu- and Ser-rich protein
IRO1	Cd36_81290	orf19.1715	3	-3.952989	-1.982944	*YJL225C*	Putative transcription factor
	Cd36_06060	orf19.6264.4	1	-3.9154143	-1.969165	*RPL39*	ORF Predicted by Annotation Working Group

Gene Name	*C. dubliniensis* Cd36 identifier	*C. albicans* orf19 identifier	C'some	Fold change expression	Normalised Expression	*S. cerevisiae* ortholog	Description
SMI1	Cd36_07390	orf19.5058	1	-3.8940604	-1.9612752	*SMI1*	Decreased mRNA abundance observed in cyr1 homozygous null mutant hyphal cells
CTR1	Cd36_60740	orf19.3646	6	-3.843739	-1.9425104	*CTR1*	Copper transporter
	Cd36_63900	orf19.5602	6	-3.8396428	-1.9409721		Predicted ORF in Assemblies 19, 20 and 21
	Cd36_08690	orf19.4779	1	-3.7977545	-1.9251467	*YKR105C*	Putative transporter
GPT1	Cd36_04840	orf19.4063	1	-3.773727	-1.91599	*UGA4*	GABA/polyamine transporter
ARG3	Cd36_63830	orf19.5610	6	-3.7241297	-1.8969033	*ARG3*	Alkaline downregulated
	Cd36_85930	orf19.7381	3	-3.6482966	-1.867223	*LYS14*	Predicted zinc-finger protein of unknown function
	Cd36_44750		4	-3.6482441	-1.8672023		
	Cd36_53890	orf19.3902	5	-3.5981486	-1.8472548		Predicted ORF in Assemblies 19, 20 and 21
TYE7	Cd36_12210	orf19.4941	1	-3.5514443	-1.8284059	*TYE7*	Putative bHLH (basic region, helix-loop-helix) transcription factor
CFL2	Cd36_45400	orf19.1264	4	-3.5194604	-1.8153542	*FRE4*	Iron utilization protein
	Cd36_02060	orf19.3678	1	-3.467534	-1.79391		Protein not essential for viability
	Cd36_42610	orf19.2726	4	-3.4444892	-1.7842901	*SFK1*	Predicted ORF in Assemblies 19, 20 and 21
	Cd36_05920	orf19.6277	1	-3.4320326	-1.7790632	*WSC4*	Predicted ORF in Assemblies 19, 20 and 21
YHB4	Cd36_35380	orf19.7637	R	-3.3766499	-1.7555926	*YHB1*	Protein related to flavohemoglobins
PGA31	Cd36_43780	orf19.5302	4	-3.3553102	-1.7464461	*MUC1*	Putative GPI-anchored protein
	Cd36_70850	orf19.7022	7	-3.3475537	-1.7431072		Predicted ORF in Assemblies 19, 20 and 21
	Cd36_22420	orf19.1354	2	-3.322135	-1.7321107	*YER067W*	Transcriptionally regulated by iron or by yeast-hyphal switch
	Cd36_21660	orf19.1893	2	-3.3092432	-1.7265013	*YPL158C*	Predicted ORF in Assemblies 19, 20 and 21
	Cd36_85020	orf19.5975	3	-3.2042484	-1.679986	*ADR1*	Putative transcription factor with zinc finger DNA-binding motif
	Cd36_53910	orf19.3905	5	-3.1976123	-1.676995		Predicted ORF in Assemblies 19, 20 and 21
HIT1	Cd36_42620	orf19.2723	4	-3.1893923	-1.6732816	*HIT1*	Protein not essential for viability
	Cd36_63630	orf19.5626	6	-3.1825612	-1.6701882	*RLM1*	Predicted ORF in Assemblies 19, 20 and 21
ERG251	Cd36_41530	orf19.4631	4	-3.1807177	-1.6693523	*ERG25*	Predicted ORF in Assemblies 19, 20 and 21
PGA57	Cd36_41010	orf19.4689	4	-3.1777205	-1.6679922	*HPF1*	Putative GPI-anchored protein of unknown function
HGT6	Cd36_15940	orf19.2020	2	-3.1709201	-1.6649015	*HXT6/HXT7*	Putative glucose transporter of major facilitator superfamily
	Cd36_09800	orf19.4911	1	-3.1677256	-1.6634474		Predicted ORF in Assemblies 19, 20 and 21
CRH11	Cd36_42770	orf19.2706	4	-3.1429014	-1.652097	*CRH1*	Putative ortholog of S. cerevisiae Crh1p
HOF1	Cd36_40430	orf19.5664	4	-3.14038	-1.6509391		Protein not essential for viability
	Cd36_73140	orf19.6705	7	-3.1314669	-1.6468387	*YEL1*	Protein described as a putative guanyl nucleotide exchange factor with Sec7 domain
FRP3	Cd36_20980	orf19.1224	2	-3.1302443	-1.6462753	*ATO2*	Upregulated in the presence of human neutrophils
	Cd36_08720	orf19.4783	1	-3.1229196	-1.6428955		Predicted ORF in Assemblies 19, 20 and 21
RPL27A	Cd36_11610	orf19.5225.2	1	-3.109806	-1.6368246	*RPL27A*	Predicted ribosomal protein
FRE10	Cd36_43990	orf19.1415	4	-3.0655236	-1.6161336	*FRE4*	Major cell-surface ferric reductase under low-iron conditions
SGA1	Cd36_81250	orf19.1719	3	-3.0365617	-1.6024387	*SGA1*	Putative glucoamylase
	Cd36_50040		5	-3.0337954	-1.6011238		
RPL35	Cd36_84940	orf19.5964.2	3	-3.0223808	-1.5956855	*RPL35A/RPL35E*	Protein described as a ribosomal protein
	Cd36_44110			-3.0014377	-1.5856537		
CPH1	Cd36_06880	orf19.4433	1	-2.9739938	-1.5724016	*STE12*	Transcription factor required for mating and wild-type hyphal growth on solid media
	Cd36_43680	orf19.5290	4	-2.9389975	-1.5553241		Transcription is negatively regulated by Sfu1p
	Cd36_18700	orf19.815	2	-2.9070704	-1.539566	*YLR422W*	Predicted ORF in Assemblies 19, 20 and 21
	Cd36_44740		4	-2.8945036	-1.5333159		
	Cd36_70940	orf19.7013	7	-2.8615499	-1.5167967		Predicted ORF in Assemblies 19, 20 and 21
	Cd36_62390	orf19.3460	6	-2.8421724	-1.506994		Transcription is regulated upon yeast-hyphal switch
DAG7	Cd36_41020	orf19.4688	4	-2.8203025	-1.4958498	*WSC2*	Predicted ORF in Assemblies 19, 20 and 21
	Cd36_82590	rf19.254; orf19.25	3	-2.8155723	-1.4934282		
	Cd36_44070		4	-2.7964213	-1.4835818		
	Cd36_12280	orf19.4951	1	-2.791223	-1.4808974		Predicted ORF in Assemblies 19, 20 and 21
STF2	Cd36_15230	orf19.2107.1	2	-2.7676291	-1.4686506	*TMA10*	Protein involved in ATP biosynthesis
MAF1	Cd36_22300	orf19.2173	2	-2.765344	-1.467459	*MAF1*	Protein described as affecting nucleocytoplasmic transport and synthesis of RNA Polymerase III
	Cd36_65060		6	-2.7637842	-1.466645		
	Cd36_62530	orf19.3475	6	-2.750021	-1.4594426	*DEF1*	Described as a Gag-related protein
	Cd36_21060	orf19.2227	2	-2.735707	-1.4519137		Predicted ORF in Assemblies 19, 20 and 21
	Cd36_83330	orf19.334	3	-2.7314198	-1.449651		Predicted ORF in Assemblies 19, 20 and 21
	Cd36_62200	orf19.3505	6	-2.7002168	-1.4330752	*SLM2*	Predicted ORF in Assemblies 19, 20 and 21
ENA21	Cd36_72570	orf19.5170	7	-2.6902947	-1.4277642	*ENA2*	Predicted ORF in Assemblies 19, 20 and 21
	Cd36_43870	orf19.1430	4	-2.6882257	-1.4266543		Predicted ORF in Assemblies 19, 20 and 21
BUL1	Cd36_07700	orf19.5094	1	-2.6833014	-1.4240091	*BSC5*	Protein not essential for viability
RPL39	Cd36_18610	orf19.827.1	2	-2.6824934	-1.4235747	*RPL36A*	Ribosomal protein L39
LIP1	Cd36_09020	orf19.4821	1	-2.6447802	-1.4031478		Secreted lipase, member of a lipase gene family whose members are expressed differentially in response to carbon source and during infection
RPS4A	Cd36_01510	orf19.5341	1	-2.6390169	-1.4000006	*RPS4A*	Predicted ribosomal protein
GUT2	Cd36_46220	orf19.3133	4	-2.637266	-1.3990431	*GUT2*	Predicted ORF in Assemblies 19, 20 and 21
	Cd36_41040	orf19.4684.2	4	-2.6193974	-1.389235	*RPL40B*	ORF Predicted by Annotation Working Group
YST1	Cd36_85350	orf19.6975	3	-2.6133063	-1.3858762	*RPS0A*	Ribosome-associated protein
PGA23	Cd36_27260	orf19.3740	R	-2.5942826	-1.3753357	*YFL067W*	Putative GPI-anchored protein of unknown function
	Cd36_61660	orf19.3430	6	-2.5891454	-1.372476		Predicted ORF in Assemblies 19, 20 and 21
RPS7A	Cd36_81410	orf19.1700	3	-2.5880458	-1.3718631	*RPS7A*	Predicted ribosomal protein
	Cd36_25060		R	-2.5875747	-1.3716005		
FRE7	Cd36_32920	orf19.6139	R	-2.5682497	-1.3607855	*FRE3*	Protein similar to ferric reductase Fre10p
	Cd36_02020	orf19.3674	1	-2.566187	-1.3596263	*GAL10*	Predicted ORF in Assemblies 19, 20 and 21

Gene Name	*C. dubliniensis* Cd36 identifier	*C. albicans* orf19 identifier	C'some	Fold change expression	Normalised Expression	*S. cerevisiae* ortholog	Description
YCK2	Cd36_85620	orf19.7001	3	-2.564522	-1.35869	*YCK2*	Protein similar to S. cerevisiae Yck2p, which is a plasma membrane-bound casein kinase I isoform
	Cd36_23960	orf19.1363	2	-2.5599897	-1.356138	*YOR338W*	Predicted ORF in Assemblies 19, 20 and 21
PGA32	Cd36_87090	orf19.6784	3	-2.5599594	-1.356121	*DAN4*	Putative GPI-anchored protein of unknown function
	Cd36_12290	orf19.4952	1	-2.556354	-1.3540877		Predicted ORF in Assemblies 19, 20 and 21
MIG1	Cd36_52720	orf19.4318	5	-2.55297	-1.3521765	*MIG1*	Transcriptional repressor
	Cd36_83590	orf19.356	3	-2.5412607	-1.3455445	*GTT1*	Predicted ORF in Assemblies 19, 20 and 21
	Cd36_16630	orf19.1488	2	-2.5329208	-1.340802		Predicted ORF in Assemblies 19, 20 and 21
	Cd36_04900	orf19.449	1	-2.531284	-1.3398695	*YKR070W*	Predicted ORF in Assemblies 19, 20 and 21
	Cd36_21280	orf19.2253	2	-2.5225313	-1.3348721		Predicted ORF in Assemblies 19, 20 and 21
DPP3	Cd36_72240	orf19.6459	7	-2.5097837	-1.327563	*DPP1*	Protein similar to S. cerevisiae pyrophosphate phosphatase Dpp1p
	Cd36_28370	orf19.2399	R	-2.4984152	-1.3210133	*JJJ1*	Putative transcription factor with zinc finger DNA-binding motif
PCK1	Cd36_25230	orf19.7514	R	-2.4968088	-1.3200853	*PCK1*	Phosphoenolpyruvate carboxykinase
CDR3	Cd36_43320	orf19.1313	4	-2.4962327	-1.3197525	*PDR5*	Transporter of the Pdrp/Cdrp family of the ATP-binding cassette (ABC) superfamily
	Cd36_81800	orf19.1654	3	-2.4874108	-1.3146448		Predicted ORF in Assemblies 19, 20 and 21
RPS6A	Cd36_41260	orf19.4660	4	-2.4821653	-1.3115993	*RPS6A|RPS6B*	Predicted ribosomal protein
RPS22A	Cd36_06050	orf19.6265	1	-2.4764252	-1.308259	*RPS22A*	Predicted ribosomal protein
	Cd36_61820	orf19.3414	6	-2.465569	-1.3019207	*SUR7*	Predicted ORF in Assemblies 19, 20 and 21
	Cd36_17200	orf19.1562	2	-2.4639227	-1.300957		Predicted ORF in Assemblies 19, 20 and 21
RTA2	Cd36_20830	orf19.24	2	-2.462104	-1.2998917	*RSB1*	Stress-associated protein
	Cd36_64020		6	-2.461649	-1.299625		
FRP2	Cd36_70310	orf19.7112	7	-2.4596846	-1.2984734	*FRE4*	Protein described as ferric reductase
	Cd36_11100	orf19.5282	1	-2.4549432	-1.2956897		Predicted ORF in Assemblies 19, 20 and 21
SNG3	Cd36_73070	orf19.1333	7	-2.4531677	-1.2946458	*SNG1*	Predicted ORF in Assemblies 19, 20 and 21
	Cd36_34510	orf19.7305	R	-2.452799	-1.2944291		Predicted ORF in Assemblies 19, 20 and 21
	Cd36_61710	orf19.3425	6	-2.4508092	-1.2932582	*MED2*	Predicted ORF in Assemblies 19, 20 and 21
	Cd36_23060		2	-2.4503615	-1.2929946		
PFK2	Cd36_71630	orf19.6540	7	-2.4377084	-1.2855256	*PFK2*	Beta subunit of phosphofructokinase (PFK), which is a heteromultimer of Pfk1p and Pfk2p
	Cd36_65030		6	-2.4362705	-1.2846743		
	Cd36_08680	orf19.4778	1	-2.4353557	-1.2841325	*LYS14*	Putative transcription factor with zinc cluster DNA-binding motif
RPS24	Cd36_80110	orf19.5466	3	-2.424643	-1.2777724	*RPS24B|RPS24A*	Predicted ribosomal protein
RPL19A	Cd36_84440	orf19.5904	3	-2.4192958	-1.2745872	*RPL19A|RPL19B*	Predicted ribosomal protein
	Cd36_03460	orf19.1037	1	-2.412458	-1.2705038		Predicted ORF in Assemblies 19, 20 and 21
RIM101	Cd36_13310	orf19.7247	1	-2.4074202	-1.267488	*RIM101*	Transcription factor involved in alkaline pH response
FGR6-3	Cd36_07280	orf19.4712	1	-2.4032974	-1.2650152	*AGA1*	Protein lacking an ortholog in S. cerevisiae
GCN4	Cd36_24010	orf19.1358	2	-2.4010508	-1.2636659	*GCN4*	Transcriptional activator of general amino acid control response
RPL32	Cd36_61795	orf19.3415.1	6	-2.4000273	-1.2630508	*RPL32*	Predicted ribosomal protein
RPS19A	Cd36_85180	orf19.5996.1	3	-2.3998528	-1.2629459	*RPS19A*	Putative ribosomal protein
RPL11	Cd36_21110	orf19.2232	2	-2.3903415	-1.2572167	*RPL11A|RPL11B*	Predicted ribosomal protein
	Cd36_73120	orf19.6641	7	-2.381597	-1.2519293		Predicted ORF in Assemblies 19, 20 and 21
RPS1	Cd36_02890	orf19.3002	1	-2.3775423	-1.249471	*RPS1A*	Probable ortholog of S. cerevisiae ribosomal protein Rp10 (Rps1Ap and Rps1Bp), elicits a host antibody response during infection
RNR22	Cd36_21850	orf19.1868	2	-2.3764257	-1.2487934	*RNR2*	Protein described as ribonucleoside diphosphate reductase
	Cd36_61560	orf19.3439	6	-2.365257	-1.241997		Predicted ORF in Assemblies 19, 20 and 21
	Cd36_81690	orf19.1666	3	-2.3649592	-1.2418153	*YPR022C*	Predicted ORF in Assemblies 19, 20 and 21
RPL17B	Cd36_19200	orf19.4490	2	-2.3539834	-1.2351041	*RPL17B*	Predicted ribosomal protein
	Cd36_07460	orf19.5065	1	-2.3526683	-1.2342979	*ERD1*	Predicted ORF in Assemblies 19, 20 and 21
	Cd36_85440	orf19.6983	3	-2.3520572	-1.2339232	*REG1*	Predicted ORF in Assemblies 19, 20 and 21
	Cd36_11000	orf19.1150	1	-2.3511295	-1.233354	*GLN3*	Predicted ORF in Assemblies 19, 20 and 21
	Cd36_82720	orf19.263.1	3	-2.3470838	-1.2308693	*YBR056W-A*	Predicted ORF in Assembly 20 and 21
MET6	Cd36_26580	orf19.2551	R	-2.3449776	-1.2295742	*MET6*	5-methyltetrahydropteroyltriglutamate-homocysteine methyltransferase (cobalamin-independent methionine synthase)
	Cd36_05910	orf19.177	1	-2.3442	-1.2290956	*BEM1*	Predicted ORF in Assemblies 19, 20 and 21
	Cd36_73060	orf19.1334	7	-2.3424156	-1.2279971		Predicted ORF in Assemblies 19, 20 and 21
	Cd36_02180		1	-2.3337855	-1.222672		
RPL18	Cd36_85070	orf19.5982	3	-2.3292701	-1.219878	*RPL18A|RPL18B*	Predicted ribosomal protein
KIP2	Cd36_24370	orf19.1747	2	-2.314866	-1.2109288	*KIP2*	Protein similar to S. cerevisiae Kip2p
PHO84	Cd36_10770	orf19.655	1	-2.3127086	-1.2095835	*PHO84*	Protein similar to high-affinity phosphate transporters
	Cd36_20250	orf19.5204	2	-2.3106601	-1.208305	*SNF5*	Predicted ORF in Assemblies 19, 20 and 21
	Cd36_50410	orf19.951	5	-2.3082848	-1.2068212		Predicted ORF in Assemblies 19, 20 and 21
	Cd36_22230	orf19.2181	2	-2.308222	-1.206782		ORF Predicted by Annotation Working Group
PMA1	Cd36_80660	orf19.5383	3	-2.3052144	-1.204901	*PMA1*	Plasma membrane H(+)-ATPase
	Cd36_22790		2	-2.304843	-1.2046685		
	Cd36_11490	orf19.5238	1	-2.304193	-1.2042615		Predicted ORF in Assemblies 19, 20 and 21
	Cd36_04320		1	-2.30192	-1.2028376		
PGA30	Cd36_43790	orf19.5303	4	-2.29763	-1.2001466	*DAN4*	Putative GPI-anchored protein of unknown function
	Cd36_85580	orf19.6996	3	-2.2940829	-1.1979175	*MNT4*	Predicted ORF in Assemblies 19, 20 and 21
CDR4	Cd36_07580	orf19.5079	1	-2.289657	-1.1951315	*PDR5*	Putative transporter of ATP-binding cassette (ABC) superfamily
	Cd36_06070	orf19.6264.3	1	-2.2864902	-1.1931348	*YIP3*	ORF Predicted by Annotation Working Group
LDG3	Cd36_72070	orf19.6486	7	-2.284878	-1.1921171		Predicted ORF in Assemblies 19, 20 and 21

Gene Name	*C. dubliniensis* Cd36 identifier	*C. albicans* orf19 identifier	C'some	Fold change expression	Normalised Expression	*S. cerevisiae* ortholog	Description
	Cd36_22030	orf19.2204.2	2	-2.2828023	-1.1908059	*RHO2*	ORF Predicted by Annotation Working Group (see Locus History Note for Assembly 19 correction)
CSE4	Cd36_80790	orf19.6163	3	-2.2816885	-1.1901017	*CSE4*	Centromere-associated protein
RPS5	Cd36_52860	orf19.4336	5	-2.2813349	-1.1898782	*RPS5*	Predicted ribosomal protein
IFI3	Cd36_03820	orf19.4482	1	-2.2778945	-1.187701		Predicted ORF in Assemblies 19, 20 and 21
	Cd36_52940	orf19.4347	5	-2.2667549	-1.1806284	*PRR1*	Predicted ORF in Assemblies 19, 20 and 21
HAK1	Cd36_06200	orf19.6249	1	-2.2601058	-1.1763903		Putative potassium transporter
SOL1	Cd36_83830	orf19.6930	3	-2.2518785	-1.171129		Cell cycle regulator
	Cd36_83900		3	-2.2454598	-1.1670109		
RPL24A	Cd36_44530	orf19.3789	4	-2.234751	-1.160114	*RPL24B*	Predicted ribosomal protein
RAS1	Cd36_24270	orf19.1760	2	-2.2345626	-1.1599925	*RAS1|RAS2*	RAS signal transduction GTPase
ABP2	Cd36_19490	orf19.3529	2	-2.2342002	-1.1597584		Protein of unknown function
	Cd36_44730	orf19.8359	4	-2.2335174	-1.1593175		
	Cd36_23170	orf19.206	2	-2.233424	-1.1592572	*MUC1*	Predicted ORF in Assemblies 19, 20 and 21
FGR6-10	Cd36_45130	orf19.1234	4	-2.2322547	-1.1585017	*AGA1*	Protein lacking an ortholog in S. cerevisiae
RPL13	Cd36_02820	orf19.2994	1	-2.230216	-1.1571834	*RPL13A*	Protein described as ribosomal subunit
	Cd36_12120	orf19.4931.1	1	-2.229438	-1.1566801	*RPL14A|RPL14E*	ORF Predicted by Annotation Working Group
FLC1	Cd36_80900	orf19.2501	3	-2.2291338	-1.1564833	*FLC3*	Protein involved in heme uptake
	Cd36_20970	orf19.1223	2	-2.2290423	-1.156424	*DBF2*	Predicted ORF in Assemblies 19, 20 and 21
	Cd36_18380	orf19.851	2	-2.2285376	-1.1560973	*MNN4*	Protein of unknown function
	Cd36_80940	orf19.2506	3	-2.2219248	-1.15181		Predicted ORF in Assemblies 19, 20 and 21
	Cd36_62350	orf19.3456	6	-2.2206147	-1.150959	*KIC1*	Predicted ORF in Assemblies 19, 20 and 21
RPL5	Cd36_71620	orf19.6541	7	-2.2153695	-1.1475472	*RPL5*	Predicted ribosomal protein
	Cd36_09910	orf19.998	1	-2.2153203	-1.1475153	*BSP1*	Protein not essential for viability
	Cd36_81870		3	-2.2118022	-1.1452224		
CDC5	Cd36_00900	orf19.6010	1	-2.2103245	-1.1442583	*CDC5*	Polo-like kinase
	Cd36_12600	orf19.4998	1	-2.209718	-1.1438622	*TEA1*	Predicted ORF in Assemblies 19, 20 and 21
	Cd36_63060	orf19.5576	6	-2.2037215	-1.1399419	*YDR531W*	Protein similar to S. cerevisiae Ydr531wp
	Cd36_50810	orf19.4149.1	5	-2.2021787	-1.1389315	*RPS11A|RPS11E*	ORF Predicted by Annotation Working Group
	Cd36_21050	orf19.3147	2	-2.1964161	-1.1351514		Predicted ORF in Assemblies 19, 20 and 21
PDR16	Cd36_03560	orf19.1027	1	-2.1894946	-1.1305978	*PDR16*	Phosphatidylinositol transfer protein
	Cd36_61200	orf19.117	6	-2.1854804	-1.1279504	*SEC9*	Predicted ORF in Assemblies 19, 20 and 21
	Cd36_15750	orf19.2043	2	-2.1834564	-1.1266137	*NBP35*	Predicted ORF in Assemblies 19, 20 and 21
PMC1	Cd36_81200	orf19.1727	3	-2.1832862	-1.1265013	*PMC1*	Vacuolar calcium P-type ATPase
GSY1	Cd36_25850	orf19.3278	R	-2.1828098	-1.1261864	*GSY1*	Protein described as glycogen synthase
	Cd36_23040	orf19.223	2	-2.1762567	-1.1218487	*YNR047W*	Predicted ORF in Assemblies 19, 20 and 21
HGT2	Cd36_01970	orf19.3668	1	-2.1745737	-1.1207325	*RGT2*	Putative glucose transporter of the major facilitator superfamily
	Cd36_50310	orf19.967	5	-2.1742444	-1.1205142	*NUC1*	Predicted ORF in Assemblies 19, 20 and 21
	Cd36_87100	orf19.6783	3	-2.171416	-1.1186361	*MRS6*	Predicted ORF in Assemblies 19, 20 and 21
	Cd36_05400		1	-2.1677012	-1.1161659		
RPL8B	Cd36_85230	orf19.6002	3	-2.1548653	-1.1075976	*RPL8B*	Predicted ribosomal protein
EFG1	Cd36_33560	orf19.610	R	-2.1537685	-1.1068633	*SOK2*	Transcriptional repressor
ASC1	Cd36_71100	orf19.6906	7	-2.1519296	-1.1056309	*ASC1*	Protein described as part of 40S ribosomal subunit
	Cd36_16780	orf19.1510	2	-2.1515203	-1.1053565	*YOL019W*	Protein not essential for viability
	Cd36_70400	orf19.7104	7	-2.1386895	-1.0967271	*DAN4*	Predicted ORF in Assemblies 19, 20 and 21
	Cd36_71540	orf19.6554	7	-2.1340525	-1.0935957	*YOR220W*	Predicted ORF in Assemblies 19, 20 and 21
	Cd36_86820	orf19.6816	3	-2.1309855	-1.0915208	*YJR096W*	Predicted ORF in Assemblies 19, 20 and 21
RPP1A	Cd36_02810	orf19.2992	1	-2.1306217	-1.0912745	*RPP1A*	Conserved acidic ribosomal protein, likely to be involved in regulation of translation elongation
TPS2	Cd36_03180	orf19.3038	1	-2.1292078	-1.0903168	*TPS2*	Trehalose-6-phosphate (Tre6P) phosphatase
RIM11	Cd36_18940	orf19.791	2	-2.1278367	-1.0893874	*RIM11*	Protein not essential for viability
	Cd36_72030	orf19.6492	7	-2.1255672	-1.0878478	*KIN4*	Predicted ORF in Assemblies 19, 20 and 21
	Cd36_09460	orf19.4873	1	-2.122556	-1.0858027		Predicted ORF in Assemblies 19, 20 and 21
SLC1	Cd36_82560	orf19.250	3	-2.122192	-1.0855552	*SLC1*	Protein repressed during the mating process
	Cd36_00060		1	-2.115952	-1.0813069		
	Cd36_81080	orf19.3156	3	-2.1136434	-1.079732	*SRP40*	Predicted ORF in Assemblies 19, 20 and 21
	Cd36_07000	orf19.2794	1	-2.1131349	-1.0793849	*YBL036C*	Protein regulated by Gcn4p
DOG1	Cd36_62030	orf19.3392	6	-2.1130724	-1.0793421	*DOG2*	Putative 2-deoxyglucose-6-phosphatase
	Cd36_80160	orf19.5455	3	-2.1105163	-1.077596	*VTC1*	Predicted ORF in Assemblies 19, 20 and 21
AOX2	Cd36_08630	orf19.4773	1	-2.1095695	-1.0769486		Alternative oxidase
	Cd36_43670	orf19.1208	4	-2.1070719	-1.0752395		Predicted ORF in Assemblies 19, 20 and 21
GCV2	Cd36_07910	orf19.385	1	-2.1014087	-1.0713568	*GCV2*	Putative protein of glycine catabolism
CHS4	Cd36_85640	orf19.7349	3	-2.0982203	-1.0691662	*SKT5*	Activator of Chs3p chitin synthase
RPL38	Cd36_15190	orf19.2111.2	2	-2.0968642	-1.0682335	*RPL38*	Predicted ribosomal protein
	Cd36_45480	orf19.1277	4	-2.0930314	-1.065594	*MUC1*	Predicted ORF in Assemblies 19, 20 and 21
	Cd36_02830		1	-2.087526	-1.0617943		
	Cd36_21300	orf19.2257	2	-2.0866945	-1.0612193	*YNR021W*	Predicted ORF in Assemblies 19, 20 and 21
	Cd36_32700	orf19.9	R	-2.0823302	-1.0581989	*LAS17*	Predicted ORF in Assemblies 19, 20 and 21
	Cd36_09780		1	-2.077857	-1.0550964		
	Cd36_73080	orf19.1332	7	-2.0771587	-1.0546393	*SNG1*	Predicted ORF in Assemblies 19, 20 and 21
	Cd36_85270	orf19.6008	3	-2.0738993	-1.0523459	*YLL032C*	Predicted ORF in Assemblies 19, 20 and 21
	Cd36_20260	orf19.5205	2	-2.0701513	-1.0497363		Predicted ORF in Assemblies 19, 20 and 21
AGA1	Cd36_50540	orf19.935	5	-2.0687685	-1.0487722	*MUC1*	Protein with some similarity to agglutinin subunit
PGA22	Cd36_27270	orf19.3738	R	-2.0680568	-1.0482758	*MUC1*	Putative GPI-anchored protein of unknown function
	Cd36_10570	orf19.675	1	-2.0630903	-1.044807	*SRP40*	Similar to cell wall proteins
	Cd36_70560	orf19.7085	7	-2.062218	-1.0441968	*FUN12*	Predicted ORF in Assemblies 19, 20 and 21
	Cd36_22470	orf19.1349	2	-2.061039	-1.0433718	*RCR1*	Predicted ORF in Assemblies 19, 20 and 21
RPL3	Cd36_23540	orf19.1601	2	-2.0589564	-1.0419133	*RPL3*	Putative ribosomal protein

Gene Name	*C. dubliniensis* Cd36 identifier	*C. albicans* orf19 identifier	C'some	Fold change expression	Normalised Expression	*S. cerevisiae* ortholog	Description
	Cd36_16730	orf19.1502	2	-2.0578768	-1.0411566		Predicted ORF in Assemblies 19, 20 and 21
	Cd36_72160	orf19.6474	7	-2.0441031	-1.0314679	*CBK1*	Predicted ORF in Assemblies 19, 20 and 21
HOL1	Cd36_02800	orf19.2991	1	-2.0440037	-1.0313978	*HOL1*	Predicted ORF in Assemblies 19, 20 and 21
	Cd36_17965		2	-2.0398035	-1.0284302		
	Cd36_72280	orf19.6456	7	-2.0389752	-1.0278442	*BOI1*	Predicted ORF in Assemblies 19, 20 and 21
	Cd36_02750	orf19.2986	1	-2.0381866	-1.027286		Predicted ORF in Assemblies 19, 20 and 21
BCR1	Cd36_31890	orf19.723	R	-2.0320919	-1.0229656	*USV1*	Transcription factor required for wild-type biofilm formation
	Cd36_23180	orf19.204	2	-2.0270746	-1.0193992		Predicted ORF in Assemblies 19, 20 and 21
	Cd36_02690	orf19.2978	1	-2.0201762	-1.0144811		Predicted ORF in Assemblies 19, 20 and 21
SOD3	Cd36_70320	orf19.7111.1	7	-2.0186718	-1.0134063	*SOD2*	Cytosolic manganese-containing superoxide dismutase, involved in protection against oxidative stress
	Cd36_81400	orf19.1701	3	-2.0132868	-1.0095527	*RKI1*	Predicted ORF in Assemblies 19, 20 and 21
	Cd36_03690	orf19.4471	1	-2.0110998	-1.0079846	*VPS64*	Predicted ORF in Assemblies 19, 20 and 21
	Cd36_86710	orf19.6829	3	-2.0072138	-1.0051943		Predicted ORF in Assemblies 19, 20 and 21
	Cd36_81820		3	-2.0040042	-1.0028856		
ECM21	Cd36_09570	orf19.4887	1	-2.002758	-1.0019882	*ECM21*	Protein not essential for viability
FGR6-4	Cd36_24200	orf19.3490	2	-1.9986305	-0.99901175	*YIL169C*	Protein lacking an ortholog in S. cerevisiae
CHS1	Cd36_72420	orf19.5188	7	-1.9969777	-0.99781823	*CHS2*	Chitin synthase
ATP1	Cd36_04360	orf19.6854	1	-1.9964178	-0.99741364	*ATP1*	Protein similar to alpha subunit of ATP synthase
RPS21	Cd36_01360	orf19.3334	1	-1.9944191	-0.9959686	*RPS2*	Predicted ribosomal protein
NDH51	Cd36_19150	orf19.4495	2	-1.9942938	-0.995878		Subunit of nicotinamide adenine dinucleotide dehydrogenase complex I, of the mitochondrial electron transport chain
	Cd36_82490	orf19.242.2	3	-1.9942236	-0.9958272	*YSY6*	ORF Predicted by Annotation Working Group
	Cd36_21250	orf19.2250	2	-1.992344	-0.9944668	*SPE3*	Predicted ORF in Assemblies 19, 20 and 21
JEN2	Cd36_43830	orf19.5307	4	-1.987569	-0.99100494	*JEN1*	Protein described as carboxylic acid transporter
TCC1	Cd36_87440	orf19.6734	3	-1.9858202	-0.989735	*CYC8*	Protein involved in regulation of filamentous growth and virulence
	Cd36_15630	orf19.2059	2	-1.9808408	-0.98611295		Predicted ORF in Assemblies 19, 20 and 21
GAP2	Cd36_85550	orf19.6993	3	-1.9785012	-0.9844079	*GAP1*	Protein similar to amino acid permeases
MET28	Cd36_70670	orf19.7046	7	-1.977697	-0.9838214	*MET4*	Protein induced during the mating process
CDC20	Cd36_61260	orf19.122	6	-1.9717312	-0.97946286	*CDC20*	Protein similar to S. cerevisiae Cdc20p, which is a cell-cycle regulated activator of the anaphase promoting complex
SAC7	Cd36_70290	orf19.7115	7	-1.9716876	-0.9794309	*BAG7*	Protein described as a GTPase activating protein (GAP) for RHO1
	Cd36_44100		4	-1.9716831	-0.9794277		
FMP27	Cd36_61740	orf19.3422	6	-1.9714979	-0.97929215	*YLR454W*	Predicted ORF in Assemblies 19, 20 and 21
BUB2	Cd36_17590	orf19.5827	2	-1.9714886	-0.97928536	*BUB2*	Predicted ORF in Assemblies 19, 20 and 21
	Cd36_40910	orf19.4706	4	-1.9677724	-0.97656333	*PIN2*	Predicted ORF in Assemblies 19, 20 and 21
CHS8	Cd36_80650	orf19.5384	3	-1.9674184	-0.9763038	*CHS1*	Chitin synthase
	Cd36_71350	orf19.6578	7	-1.9664855	-0.97561955		Predicted ORF in Assemblies 19, 20 and 21
PDC11	Cd36_46050	orf19.2877	4	-1.9606491	-0.97133136	*PDC1*	Protein similar to pyruvate decarboxylase
	Cd36_81940		3	-1.9601719	-0.97098017		
	Cd36_19050	orf19.4513	2	-1.9596865	-0.9706229		Protein not essential for viability
	Cd36_19890	orf19.3572.3	2	-1.9583839	-0.9696636	*RPL31B|RPL31A*	ORF Predicted by Annotation Working Group
	Cd36_02390		1	-1.9564815	-0.9682615		
CPA1	Cd36_41540	orf19.4630	4	-1.9561191	-0.9679942	*CPA1*	Alkaline downregulated
RPS26A	Cd36_16470	orf19.1470	2	-1.9545293	-0.9668212	*RPS26A*	Predicted ribosomal protein
	Cd36_22540	orf19.1433	2	-1.9533	-0.96591353	*LPX1*	Predicted ORF in Assemblies 19, 20 and 21
	Cd36_64885	orf19.1082.1	6	-1.9521251	-0.96504545	*COX12*	ORF Predicted by Annotation Working Group
	Cd36_00050		1	-1.9473702	-0.9615271		
RPP2B	Cd36_84640	orf19.5928	3	-1.947113	-0.9613366	*RPP2B*	Conserved acidic ribosomal protein, likely to be involved in regulation of translation elongation
PGA56	Cd36_53620	orf19.1105.2	5	-1.9468881	-0.96116996		Regulator of sorbose utilization
	Cd36_43170	orf19.3366.1	4	-1.9427186	-0.95807695		ORF Predicted by Annotation Working Group
GAR1	Cd36_10840	orf19.1164	1	-1.9418753	-0.9574506	*GAR1*	Predicted ORF in Assemblies 19, 20 and 21
ACE2	Cd36_33060	orf19.6124	R	-1.9413476	-0.9570584	*ACE2*	Putative transcription factor involved in regulation of morphogenesis
	Cd36_19240	orf19.147	2	-1.9405932	-0.9564978	*YAK1*	Predicted ORF in Assemblies 19, 20 and 21
	Cd36_03170	orf19.3037	1	-1.9389204	-0.9552536	*PAB1*	Protein described as poly(A)-binding protein
KIP1	Cd36_32050	orf19.712	R	-1.9365281	-0.95347244	*CIN8*	Non-essential kinesin from the bipolar (Kinesis-5) family
	Cd36_34785	orf19.6607	R	-1.9343926	-0.9518806		Predicted ORF in Assemblies 19, 20 and 21
MAE1	Cd36_61770	orf19.3419	6	-1.9342498	-0.9517741	*MAE1*	Malic enzyme, mitochondrial
	Cd36_07450		1	-1.932343	-0.95035124		
FTR1	Cd36_13100	orf19.7219	1	-1.9275521	-0.94676983	*FTR1*	High-affinity iron permease (ferric citrate, ferrioxamines E or B, transferrin)
	Cd36_70590	orf19.7082	7	-1.923735	-0.9439101	*PET8*	Predicted ORF in Assemblies 19, 20 and 21
	Cd36_08780	orf19.4791	1	-1.9223872	-0.942899		Predicted ORF in Assemblies 19, 20 and 21
RPL82	Cd36_10350	orf19.2311	1	-1.9194385	-0.9406843	*RPL8B*	Predicted ribosomal protein
ARG8	Cd36_44690	orf19.3770	4	-1.9170274	-0.9388709	*ARG8*	Predicted ORF in Assemblies 19, 20 and 21
RPS25B	Cd36_53290	orf19.6663	5	-1.916352	-0.9383626	*RPS25B|RPS25A*	Predicted ribosomal protein
	Cd36_43880	orf19.1429	4	-1.9163256	-0.9383427	*SOH1*	Predicted ORF in Assemblies 19, 20 and 21
	Cd36_52910	orf19.4341	5	-1.9155748	-0.93777734	*GAB1*	Predicted ORF in Assemblies 19, 20 and 21
RPL9B	Cd36_82430	orf19.236	3	-1.9153079	-0.9375763	*RPL9B*	Predicted ribosomal protein
CHA1	Cd36_16150	orf19.1996	2	-1.9125422	-0.93549156	*CHA1*	Protein similar to serine/threonine dehydratases, catabolic
	Cd36_02910		1	-1.9114616	-0.9346762		
TRP5	Cd36_45650	orf19.4718	4	-1.9114243	-0.93464804	*TRP5*	Predicted tryptophan synthase
SAM2	Cd36_10740	orf19.657	1	-1.911157	-0.93444633	*SAM2*	S-adenosylmethionine synthetase, localizes to surface of hyphal cells, but not yeast-form cells

Gene Name	*C. dubliniensis* Cd36 identifier	*C. albicans* orf19 identifier	C'some	Fold change expression	Normalised Expression	*S. cerevisiae* ortholog	Description
LSP1	Cd36_21030	orf19.3149	2	-1.9093295	-0.9330661	*PIL1*	Predicted ORF in Assemblies 19, 20 and 21
RPS10	Cd36_22240	orf19.2179.2	2	-1.9092525	-0.93300796	*RPS10A*	Predicted ribosomal protein
MDN1	Cd36_40990	orf19.4697	4	-1.9079064	-0.9319904	*MDN1*	Protein induced during the mating process
	Cd36_86520	orf19.7444	3	-1.907887	-0.9319757	*YOR352W*	Predicted ORF in Assemblies 19, 20 and 21
	Cd36_71020	orf19.6898.1	7	-1.9076775	-0.9318173		ORF Predicted by Annotation Working Group
PTR2	Cd36_83780	orf19.6937	3	-1.9066806	-0.9310632	*PTR2*	Putative oligopeptide transporter
	Cd36_22900	orf19.3603	2	-1.9056369	-0.93027323	*YDL233W*	Predicted ORF in Assemblies 19, 20 and 21
	Cd36_06990	orf19.2795	1	-1.9049871	-0.9297812	*LHP1*	Predicted ORF in Assemblies 19, 20 and 21
RPP1B	Cd36_73600	orf19.7188	7	-1.8985757	-0.92491746	*RPP1B*	Conserved acidic ribosomal protein, likely to be involved in regulation of translation elongation
RBD1	Cd36_11530	orf19.5234	1	-1.8983161	-0.9247203		Rhomboid-like protein
PGA39	Cd36_30290	orf19.6302	R	-1.898111	-0.92456436	*AGA1*	Putative GPI-anchored protein of unknown function
	Cd36_01130	orf19.3308	1	-1.8976337	-0.9242015	*STB5*	Putative transcription factor with zinc cluster DNA-binding motif
PHO87	Cd36_05600	orf19.2454	1	-1.8971981	-0.9238703	*PHO87*	Protein similar to phosphate permeases
CEF3	Cd36_50780	orf19.4152	5	-1.8963107	-0.92319536	*HEF3*	Translation elongation factor 3 (EF-3)
PGA54	Cd36_42920	orf19.2685	4	-1.8962599	-0.92315674	*DAN4*	Putative GPI-anchored protein
RPS18	Cd36_70890	orf19.7018	7	-1.8955117	-0.9225874	*RPS18B|RPS18A*	Predicted ribosomal protein
	Cd36_10200		1	-1.8944952	-0.9218135		
	Cd36_73400	orf19.5504	7	-1.8936629	-0.92117953	*YMR317W*	Predicted ORF in Assemblies 19, 20 and 21
WOR2	Cd36_85150	orf19.5992	3	-1.8920298	-0.91993475	*AGA1*	Transcriptional regulator of white-opaque switching
	Cd36_40980	orf19.4698	4	-1.8916152	-0.9196186		Predicted ORF in Assemblies 19, 20 and 21
CST20	Cd36_52140	orf19.4242	5	-1.8915577	-0.91957474	*STE20*	Protein kinase of Ste20p/p65PAK family, required for wild-type mating efficiency and virulence in a mouse model
	Cd36_52960	orf19.4349	5	-1.8914828	-0.91951764	*NBA1*	Predicted ORF in Assemblies 19, 20 and 21
	Cd36_08790	orf19.4792	1	-1.8905985	-0.91884303	*AGA1*	Predicted ORF in Assemblies 19, 20 and 21
TAF14	Cd36_18850	orf19.798	2	-1.8875984	-0.9165518	*TAF14*	Putative DNA-binding transcription factor
	Cd36_30140	orf19.6315	R	-1.8873318	-0.9163481		Predicted ORF in Assemblies 19, 20 and 21
TRS33	Cd36_72000	orf19.6496	7	-1.8868114	-0.9159502	*TRS33*	Predicted ORF in Assemblies 19, 20 and 21
GFA1	Cd36_82250	orf19.1618	3	-1.8864932	-0.9157069	*GFA1*	Glucosamine-6-phosphate synthase
PCL2	Cd36_08080	orf19.403	1	-1.8828467	-0.9129156	*PCL2*	Cyclin homolog
	Cd36_11500	orf19.5237	1	-1.8808317	-0.91137075	*VPH2*	Predicted ORF in Assemblies 19, 20 and 21
GPH1	Cd36_70860	orf19.7021	7	-1.880062	-0.9107802	*GPH1*	Putative glycogen phosphorylase
	Cd36_80840	orf19.6169	3	-1.8771316	-0.90852976	*ADY2*	Predicted ORF in Assemblies 19, 20 and 21
	Cd36_70410	orf19.7103	7	-1.8737762	-0.90594864	*GFD2*	Predicted ORF in Assemblies 19, 20 and 21
	Cd36_40810	orf19.4166	4	-1.8718004	-0.9044266	*MUC1*	Predicted zinc-finger protein of unknown function
GPM2	Cd36_04070	orf19.1067	1	-1.8705387	-0.9034538	*GPM1*	Protein described as phosphoglycerate mutase
COX9	Cd36_20350	orf19.5213.2	2	-1.8693962	-0.9025724	*COX9*	Putative subunit VIIa of cytochrome c oxidase
	Cd36_05260	orf19.411	1	-1.8687748	-0.9020927	*SRP40*	Similar to GTPase regulators
MNN7	Cd36_73340	orf19.6692	7	-1.8620411	-0.8968849	*MNN2*	Protein described as mannosyltransferase
RPS14B	Cd36_06040	orf19.6265.1	1	-1.8602018	-0.8954592	*RPS14B|RPS14A*	Putative ribosomal protein
RAD32	Cd36_18270	orf19.866	2	-1.857219	-0.8931439	*RAD30*	Protein similar to S. cerevisiae protein with role in nucleotide excision repair
	Cd36_06610	orf19.6197	1	-1.8565862	-0.89265233	*DHH1*	Predicted ORF in Assemblies 19, 20 and 21
CAN2	Cd36_61160	orf19.111	6	-1.8550845	-0.891485	*CAN1*	Putative amino acid permease
	Cd36_06270	orf19.6240	1	-1.8550545	-0.8914616	*CYK3*	Predicted ORF in Assemblies 19, 20 and 21
	Cd36_50020		5	-1.852679	-0.8896129		
	Cd36_18740	orf19.811	2	-1.8523612	-0.88936543	*YLR283W*	Protein not essential for viability
PCL7	Cd36_06410	orf19.6225	1	-1.850986	-0.888294	*PCL6*	Protein described as cyclin-like, possible Pho85p cyclin
FGR29	Cd36_24440	orf19.5316	2	-1.8509313	-0.8882513		Protein lacking an ortholog in S. cerevisiae
	Cd36_70700	orf19.1208	7	-1.8505086	-0.8879218		Predicted ORF in Assemblies 19, 20 and 21
	Cd36_03800	orf19.4479	1	-1.8503841	-0.88782483	*NOP9*	Predicted ORF in Assemblies 19, 20 and 21
	Cd36_04100	orf19.5203	1	-1.8496897	-0.8872833	*CCW14*	Predicted ORF in Assemblies 19, 20 and 21
	Cd36_24680	orf19.5346	2	-1.8493799	-0.88704157	*TAF8*	Predicted ORF in Assemblies 19, 20 and 21
IPK1	Cd36_43100	orf19.1439	4	-1.8483965	-0.88627434	*IPK1*	Predicted ORF in Assemblies 19, 20 and 21
HAC1	Cd36_05800	orf19.2432	1	-1.8465766	-0.8848531	*HAC1*	Putative transcription factor with bZIP DNA-binding motif
	Cd36_83090	orf19.308	3	-1.8456019	-0.8840914	*SNG1*	Predicted ORF in Assemblies 19, 20 and 21
	Cd36_50820	orf19.4148	5	-1.8455064	-0.88401675	*RTS1*	Predicted ORF in Assemblies 19, 20 and 21
	Cd36_10990		1	-1.8448759	-0.8835238		
	Cd36_72250	orf19.6458.1	7	-1.8443214	-0.88309	*LSM4*	ORF Predicted by Annotation Working Group
	Cd36_71450	orf19.6563	7	-1.8419452	-0.8812301	*YJR054W*	Predicted ORF in Assemblies 19, 20 and 21
	Cd36_00870	orf19.6012	1	-1.8412672	-0.88069904	*YOR296W*	Predicted ORF in Assemblies 19, 20 and 21
	Cd36_51130		5	-1.8399107	-0.8796358		
	Cd36_24770		2	-1.8349943	-0.8757756		
	Cd36_45640	orf19.4719	4	-1.8338456	-0.8748722	*CWH41*	Processing alpha glucosidase I, involved in N-linked protein glycosylation and assembly of cell wall beta 1,6 glucan
SIN3	Cd36_00880	orf19.6011	1	-1.8317759	-0.873243	*SIN3*	Protein similar to S. cerevisiae Sin3p (transcriptional corepressor involved in histone deacetylase recruitment)
RPL16A	Cd36_00190	orf19.6085	1	-1.8312799	-0.8728523	*RPL16A*	Protein similar to S. cerevisiae ribosomal protein Rpl16Ap
KRE1	Cd36_29000	orf19.4377	R	-1.8308778	-0.87253547	*KRE1*	Predicted GPI-anchor, role in 1,6-beta-D-glucan biosynthesis
RPS8A	Cd36_20060	orf19.6873	2	-1.8307889	-0.8724654	*RPS8B|RPS8A*	Putative ribosomal protein
QCR9	Cd36_42760	orf19.2707.1	4	-1.8292521	-0.87125397	*QCR9*	ORF Predicted by Annotation Working Group
	Cd36_05930	orf19.6276	1	-1.8269954	-0.869473	*MUC1*	Predicted ORF in Assemblies 19, 20 and 21
	Cd36_42900	orf19.2687.1	4	-1.8247353	-0.8676872	*RPB10*	ORF Predicted by Annotation Working Group
MNT1	Cd36_81700	orf19.1665	3	-1.8245614	-0.86754966	*KTR1*	Alpha-1,2-mannosyl transferase
	Cd36_81770	orf19.1656	3	-1.8228971	-0.8662331	*PIB2*	Predicted ORF in Assemblies 19, 20 and 21
	Cd36_11660	orf19.69	1	-1.8212365	-0.86491823		Predicted ORF in Assemblies 19, 20 and 21
ATP14	Cd36_20680	orf19.5491.1	2	-1.8200266	-0.86395955	*ATP14*	ORF Predicted by Annotation Working Group
	Cd36_09750	orf19.4906	1	-1.8197322	-0.86372614	*MUC1*	Predicted ORF in Assemblies 19, 20 and 21

Gene Name	*C. dubliniensis* Cd36 identifier	*C. albicans* orf19 identifier	C'some	Fold change expression	Normalised Expression	*S. cerevisiae* ortholog	Description
	Cd36_21470	orf19.2276	2	-1.8190296	-0.86316895	*RPB9*	Predicted ORF in Assemblies 19, 20 and 21
	Cd36_06520	orf19.6211	1	-1.8185098	-0.8627567		Predicted ORF in Assemblies 19, 20 and 21
	Cd36_63930		6	-1.817851	-0.8622339		
	Cd36_72830	orf19.5136	7	-1.815189	-0.8601198	*YGR017W*	Predicted ORF in Assemblies 19, 20 and 21
ATP4	Cd36_19960	orf19.3579	2	-1.8140534	-0.8592169	*ATP4*	Predicted ORF in Assemblies 19, 20 and 21
RGT1	Cd36_42430	orf19.2747	4	-1.81295	-0.8583392	*RGT1*	Transcriptional repressor involved in the regulation of glucose transporter genes
	Cd36_51360	orf19.1975	5	-1.8127716	-0.8581971	*DIB1*	Predicted ORF in Assemblies 19, 20 and 21
	Cd36_33080	orf19.6119	R	-1.8114214	-0.8571222		Predicted ORF in Assemblies 19, 20 and 21
	Cd36_81760	orf19.1658	3	-1.8095633	-0.8556416	*YDR348C*	Predicted ORF in Assemblies 19, 20 and 21
	Cd36_01570	orf19.3360	1	-1.808181	-0.85453916		
	Cd36_23100	orf19.215	2	-1.808044	-0.8544297	*AVO2*	Predicted ORF in Assemblies 19, 20 and 21
RPL20B	Cd36_41520	orf19.4632	4	-1.8056077	-0.85248446	*RPL20B|RPL20A*	Predicted ribosomal protein
UGA11	Cd36_18350	orf19.854	2	-1.804608	-0.8516855	*UGA1*	Predicted ORF in Assemblies 19, 20 and 21
MET18	Cd36_81370	orf19.1706	3	-1.8045915	-0.8516723	*MET18*	Predicted ORF in Assemblies 19, 20 and 21
	Cd36_86930	orf19.6801	3	-1.8040203	-0.8512156	*RPD3*	Putative ortholog of S. cerevisiae RPD3, which encodes a histone deacetylase
	Cd36_70750	orf19.7036	7	-1.7972481	-0.84578955	*WHI2*	Predicted ORF in Assemblies 19, 20 and 21
TRP4	Cd36_46560	orf19.3099	4	-1.7963767	-0.8450899	*TRP4*	Predicted enzyme of amino acid biosynthesis
	Cd36_00240	orf19.6080	1	-1.7954656	-0.84435797	*BFA1*	Predicted ORF in Assemblies 19, 20 and 21
RPS4A	Cd36_24720	orf19.5341	2	-1.7943509	-0.843462	*RPS4A*	Predicted ribosomal protein
	Cd36_22760	orf19.3613	2	-1.7938074	-0.843025	*PAF1*	Predicted ORF in Assemblies 19, 20 and 21
	Cd36_00380		1	-1.7937715	-0.8429961		
	Cd36_41290	orf19.4657	4	-1.7931713	-0.8425133	*NEM1*	Predicted ORF in Assemblies 19, 20 and 21
	Cd36_51250	orf19.1964	5	-1.7916888	-0.84132004		Decreased transcription is observed upon fluphenazine treatment
	Cd36_50570	orf19.932	5	-1.7905595	-0.84041053	*DNF1*	Predicted ORF in Assemblies 19, 20 and 21
	Cd36_62910	orf19.5533	6	-1.7894425	-0.8395102	*VPS9*	Predicted ORF in Assemblies 19, 20 and 21
ISU1	Cd36_71600	orf19.6548	7	-1.784709	-0.8356888	*ISU1*	Similar to NifU
	Cd36_44600	orf19.3782.2	4	-1.784699	-0.8356807	*YCL057C-A*	ORF Predicted by Annotation Working Group
	Cd36_10040	orf19.2350	1	-1.7844571	-0.8354852	*YOR378W*	Protein similar to S. cerevisiae Yor0378wp
	Cd36_62770		6	-1.783466	-0.83468366		
PGA62	Cd36_42270	orf19.2765	4	-1.7824692	-0.8338771	*FLO1*	Putative GPI-anchored protein
COX6	Cd36_18220	orf19.873.1	2	-1.7822809	-0.83372474	*COX6*	Flucytosine induced
BUD2	Cd36_50500	orf19.940	5	-1.7783358	-0.8305278	*BUD2*	GTPase activating protein (GAP) for Rsr1p
	Cd36_72740	orf19.5147	7	-1.7744068	-0.8273368	*YLL007C*	Predicted ORF in Assemblies 19, 20 and 21
KEL1	Cd36_00150	orf19.6092	1	-1.7713337	-0.824836	*KEL2*	Protein containing a Kelch repeat domain, similar to S. cerevisiae Kel1p
PGA61	Cd36_64390	orf19.5762	6	-1.7708989	-0.82448184	*CCW14*	Putative GPI-anchored protein of unknown function
CHT2	Cd36_53830	orf19.3895	5	-1.7667505	-0.8210983	*CTS1*	Chitinase
VAC7	Cd36_44040	orf19.1409	4	-1.7643579	-0.8191433	*VAC7*	Protein not essential for viability
ENO1	Cd36_08010	orf19.395	1	-1.7627667	-0.81784153	*ENO1*	Enolase (2-phospho-D-glycerate-hydrolyase), enzyme of glycolysis and gluconeogenesis
REG1	Cd36_16080	orf19.2005	2	-1.7627387	-0.81781864	*REG1*	Predicted ORF in Assemblies 19, 20 and 21
	Cd36_82260	orf19.1617	3	-1.7617686	-0.81702447	*YDR282C*	Protein similar to S. cerevisiae Ydr282cp
	Cd36_63730	orf19.5617	6	-1.7614567	-0.816769	*CTI6*	Predicted ORF in Assemblies 19, 20 and 21
	Cd36_18930	orf19.792	2	-1.7608128	-0.8162415	*NST1*	Predicted ORF in Assemblies 19, 20 and 21
LYS22	Cd36_19070	orf19.4506	2	-1.7604232	-0.81592226	*LYS21*	Putative homocitrate synthase
RPL25	Cd36_62095	orf19.687.1	6	-1.7580575	-0.81398225	*RPL25*	ORF Predicted by Annotation Working Group
	Cd36_00790	orf19.6022	1	-1.7572018	-0.81327987	*YBL113C*	Predicted ORF in Assemblies 19, 20 and 21
	Cd36_20150	orf19.6882.1	2	-1.7568473	-0.81298876	*RPL33A*	ORF Predicted by Annotation Working Group
WSC4	Cd36_13330	orf19.7251	1	-1.7554958	-0.8118785	*WSC4*	Transcription is specific to white cell type
	Cd36_81160		3	-1.7545773	-0.8111235		
	Cd36_85360	orf19.6976	3	-1.7537379	-0.81043315	*YJL163C*	Predicted ORF in Assemblies 19, 20 and 21
RPP2A	Cd36_33950	orf19.6403.1	R	-1.7535658	-0.8102915	*RPP2B*	Conserved acidic ribosomal protein, likely to be involved in regulation of translation elongation
MNN3	Cd36_09470	orf19.4874	1	-1.7521882	-0.8091577	*MNN2*	Predicted Golgi alpha-1,2-mannosyltransferase
	Cd36_84920	orf19.5964	3	-1.7510611	-0.80822945	*ARF2*	Predicted ORF in Assemblies 19, 20 and 21
SUR2	Cd36_17510	orf19.5818	2	-1.7506653	-0.8079033	*SUR2*	Protein described as similar to ceramide hydroxylase
FGR44	Cd36_84960	orf19.5967	3	-1.7501545	-0.80748224	*RBS1*	Protein lacking an ortholog in S. cerevisiae
PHR1	Cd36_44230	orf19.3829	4	-1.7494903	-0.8069346	*GAS1*	Glycosidase of hyphal cell surface
RTS1	Cd36_20780	orf19.20	2	-1.7476354	-0.8054042	*RTS1*	Transcription is regulated upon yeast-hyphal switch
	Cd36_35524	orf19.7664	R	-1.7445184	-0.8028288	*YCR087C-A*	Predicted ORF in Assemblies 19, 20 and 21
	Cd36_10370	orf19.2309.2	1	-1.7442402	-0.8025987	*RPL2A|RPL2B*	ORF Predicted by Annotation Working Group
CAM1	Cd36_85940	orf19.7382	3	-1.743933	-0.80234456	*CAM1*	Putative translation elongation factor eEF1 gamma
	Cd36_04680	orf19.48	1	-1.7427667	-0.80137944	*RPM2*	Predicted ORF in Assemblies 19, 20 and 21
	Cd36_12800	orf19.5019	1	-1.7419245	-0.80068207		Predicted ORF in Assemblies 19, 20 and 21
PAN1	Cd36_18130	orf19.886	2	-1.7408727	-0.79981077	*PAN1*	Essential protein involved in endocytosis and polarized growth
TYS1	Cd36_42850	orf19.2694	4	-1.7403392	-0.7993685	*TYS1*	Putative tRNA-Tyr synthetase
RHD1	Cd36_04730	orf19.54	1	-1.7391659	-0.7983955		Putative transmembrane protein with hydrophobic N and C termini and a Ser-Gly rich region
	Cd36_71670	orf19.6536	7	-1.7385498	-0.79788446	*IQG1*	Predicted ORF in Assemblies 19, 20 and 21
	Cd36_86070	orf19.7396	3	-1.7372928	-0.7968409		Predicted ORF in Assemblies 19, 20 and 21
RHD3	Cd36_43810	orf19.5305	4	-1.735793	-0.79559493		Putative GPI-anchored protein that localizes to the cell wall
BEM2	Cd36_71380	orf19.6573	7	-1.7353591	-0.7952342	*BEM2*	Putative Rho1p GTPase activating protein (GAP)
MOB1	Cd36_62840	orf19.5528	6	-1.7340277	-0.794127	*MOB1*	Predicted ORF in Assemblies 19, 20 and 21
	Cd36_44120			-1.7339274	-0.7940434		
AAT1	Cd36_19740	orf19.3554	2	-1.7296525	-0.7904823	*AAT1*	Protein described as aspartate aminotransferase

Gene Name	*C. dubliniensis* Cd36 identifier	*C. albicans* orf19 identifier	C'some	Fold change expression	Normalised Expression	*S. cerevisiae* ortholog	Description
	Cd36_82930	orf19.288	3	-1.7257099	-0.78718996	*MET13*	Predicted ORF in Assemblies 19, 20 and 21
ARG11	Cd36_84620	orf19.5926	3	-1.7241937	-0.7859218	*ORT1*	Protein induced during the mating process
	Cd36_11030	orf19.1146	1	-1.7198657	-0.78229594		Predicted ORF in Assemblies 19, 20 and 21
	Cd36_02170	orf19.3690	1	-1.7192347	-0.78176653		Predicted ORF from Assembly 19
	Cd36_22020	orf19.2208	2	-1.7187792	-0.7813842	*NST1*	Predicted ORF in Assemblies 19, 20 and 21
ADE2	Cd36_84460	orf19.5906	3	-1.7172784	-0.78012395	*ADE2*	Phosphoribosylaminoimadazole carboxylase
	Cd36_06760	orf19.4445	1	-1.7165966	-0.779551		Predicted ORF in Assemblies 19, 20 and 21
	Cd36_22480		2	-1.7161918	-0.7792108		
IFE1	Cd36_04500	orf19.769	1	-1.7154219	-0.7785635	*BDH2*	Protein not essential for viability
	Cd36_08540	orf19.4761	1	-1.714413	-0.7777147	*HST1*	Predicted ORF in Assemblies 19, 20 and 21
ARG1	Cd36_25720	orf19.7469	R	-1.7133105	-0.77678657	*ARG1*	Similar to argininosuccinate synthase
CRZ1	Cd36_85720	orf19.7359	3	-1.7130826	-0.77659464	*CRZ1*	Putative transcription factor
STP2	Cd36_12380	orf19.4961	1	-1.7120489	-0.77572393	*STP2*	Transcription factor
RPS22A	Cd36_03380	orf19.6265	1	-1.7099398	-0.77394557	*RPS22A*	Predicted ribosomal protein
	Cd36_64320	orf19.5755	6	-1.709616	-0.7736722	*PHO80*	Predicted ORF in Assemblies 19, 20 and 21
HAP43	Cd36_10520	orf19.681	1	-1.7094866	-0.77356315	*YAP3*	Similar to transcription factor AP-1
TOS1	Cd36_81470	orf19.1690	3	-1.7086139	-0.77282643	*TOS1*	Protein described as similar to alpha agglutinin anchor subunit
RPL21A	Cd36_18480	orf19.840	2	-1.7080106	-0.77231693	*RPL21A*	Putative ribosomal protein
RNR21	Cd36_17780	orf19.5801	2	-1.7063534	-0.77091646	*RNR2*	Protein described as similar to ribonucleoside-diphosphate reductase
	Cd36_81850	orf19.1653	3	-1.7038509	-0.76879907		Predicted ORF in Assemblies 19, 20 and 21
	Cd36_26210		R	-1.7037033	-0.7686741		
MSN5	Cd36_43070	orf19.2665	4	-1.7031065	-0.7681687	*MSN5*	Predicted ORF in Assemblies 19, 20 and 21
PXA2	Cd36_11330	orf19.5255	1	-1.7021954	-0.7673967	*PXA2*	Putative peroxisomal, half-size adrenoleukodystrophy protein (ALD or ALDp) subfamily ABC transporter
GPM1	Cd36_18020	orf19.903	2	-1.7016059	-0.76689696	*GPM1*	Protein described as phosphoglycerate mutase
	Cd36_85200			-1.7012038	-0.766556		
	Cd36_12660	orf19.5006	1	-1.7007223	-0.7661476	*GCV3*	Predicted ORF in Assemblies 19, 20 and 21
	Cd36_07110	orf19.2782	1	-1.7006203	-0.76606107	*GRX5*	Predicted ORF in Assemblies 19, 20 and 21
	Cd36_54430	orf19.3969	5	-1.7000672	-0.76559174	*SFL1*	Predicted ORF in Assemblies 19, 20 and 21
	Cd36_23010	orf19.3585	2	-1.700044	-0.7655721	*TRM112*	Predicted ORF in Assemblies 19, 20 and 21
	Cd36_01270		1	-1.6989455	-0.7646396		
	Cd36_72910	orf19.5129	7	-1.6971619	-0.7631242		Predicted ORF in Assemblies 19, 20 and 21
BEM1	Cd36_41420	orf19.4645	4	-1.6959202	-0.7620683	*BEM1*	Protein required for wild-type budding, hyphal growth, and virulence in a mouse systemic infection
	Cd36_05730	orf19.2439	1	-1.6951716	-0.76143134	*ACP1*	Predicted ORF in Assemblies 19, 20 and 21
	Cd36_86590	orf19.7450	3	-1.6931897	-0.7597437	*BNI5*	Predicted ORF in Assemblies 19, 20 and 21
RPL15A	Cd36_29390	orf19.493	R	-1.6910992	-0.7579613	*RPL15B|RPL15A*	Putative ribosomal protein
	Cd36_09930		1	-1.6905657	-0.75750613		
COX5	Cd36_08520	orf19.4759	1	-1.6904185	-0.7573805	*COX5A*	Protein described as cytochrome oxidase subunit V
	Cd36_05150	orf19.423	1	-1.6903155	-0.7572925	*DCP1*	Predicted ORF in Assemblies 19, 20 and 21
VPS24	Cd36_15870	orf19.2031	2	-1.6898252	-0.75687397	*VPS24*	Protein similar to S. cerevisiae Vps24p, which is a member of the ESCRT III protein sorting complex
	Cd36_00220		1	-1.6874446	-0.75484014		
	Cd36_04830		1	-1.6872838	-0.75470257		
TLG2	Cd36_17000	orf19.1538	2	-1.6865094	-0.75404036	*TLG2*	Predicted ORF in Assemblies 19, 20 and 21
RPS15	Cd36_84630	orf19.5927	3	-1.6850929	-0.7528281	*RPS15*	Putative ribosomal protein
	Cd36_52980			-1.6849208	-0.7526808		
	Cd36_31880	orf19.725	R	-1.6834531	-0.7514235		Predicted ORF in Assemblies 19, 20 and 21
HAP5	Cd36_51340	orf19.1973	5	-1.6815488	-0.74979067	*HAP5*	Component of CCAAT-binding transcription factor
FGR6-3	Cd36_72390	orf19.4712	7	-1.6801533	-0.74859285	*AGA1*	Protein lacking an ortholog in S. cerevisiae
SSN6	Cd36_86950	orf19.6798	3	-1.6800569	-0.7485101	*CYC8*	Functional homolog of S. cerevisiae Cyc8p/Ssn6p
PTC7	Cd36_40400	orf19.5661	4	-1.6784282	-0.74711084	*PTC7*	Protein phosphatase, type 2C
	Cd36_87600	orf19.6713	3	-1.677937	-0.7466886	*DEF1*	Predicted ORF in Assemblies 19, 20 and 21
	Cd36_84530	orf19.5915	3	-1.6773067	-0.74614644	*DUR3*	Predicted ORF in Assemblies 19, 20 and 21
	Cd36_53700	orf19.3213	5	-1.6745871	-0.7438054	*JIP4*	Predicted ORF in Assemblies 19, 20 and 21
	Cd36_20920	orf19.35	2	-1.6744299	-0.74367	*SKY1*	Predicted ORF in Assemblies 19, 20 and 21
	Cd36_44370	orf19.3810	4	-1.6732184	-0.7426257	*MTD1*	Predicted ORF in Assemblies 19, 20 and 21
TEM1	Cd36_02880	orf19.3001	1	-1.6729352	-0.7423816	*TEM1*	Protein similar to S. cerevisiae Tem1p, which is a GTPase involved in termination of the M phase of the cell cycle
VAN1	Cd36_87410	orf19.6738	3	-1.6721939	-0.74174213	*VAN1*	Member of Mnn9p family
	Cd36_80120	orf19.5465	3	-1.6701692	-0.7399943	*YJU2*	Predicted ORF in Assemblies 19, 20 and 21
	Cd36_87550	orf19.6720	3	-1.6696618	-0.73955584	*YDR090C*	Predicted ORF in Assemblies 19, 20 and 21
	Cd36_04110		1	-1.6687368	-0.7387564		
	Cd36_40390	orf19.5660.1	4	-1.6682435	-0.7383299	*TIM11*	ORF Predicted by Annotation Working Group
	Cd36_85890	orf19.7377	3	-1.6680852	-0.73819304	*ASE1*	Predicted ORF in Assemblies 19, 20 and 21
	Cd36_85390	orf19.6979	3	-1.667747	-0.7379005	*MAM3*	Predicted ORF in Assemblies 19, 20 and 21
RPL4B	Cd36_13080	orf19.7217	1	-1.6675315	-0.73771405	*RPL4B*	Putative ribosomal protein
ABC1	Cd36_01330	orf19.3331	1	-1.6668639	-0.73713636	*ABC1*	Protein described as ubiquinol-cytochrome-c reductase
	Cd36_24430		2	-1.66628	-0.7366309		
	Cd36_08840	orf19.4799	1	-1.6657302	-0.7361548	*CEF1*	Predicted ORF in Assemblies 19, 20 and 21
PGA59	Cd36_42250	orf19.2767	4	-1.6656356	-0.7360728	*YDR134C*	Putative GPI-anchored protein of unknown function
RPS27	Cd36_33250	orf19.6286.2	R	-1.6655378	-0.73598814	*RPS27B*	Putative ribosomal protein
UBI3	Cd36_46640	orf19.3087	4	-1.6653088	-0.7357898	*RPS31*	Fusion of ubiquitin with the S34 protein of the small ribosomal subunit
ADE5,7	Cd36_07420	orf19.5061	1	-1.665231	-0.7357223	*ADE5,7*	Enzyme of adenine biosynthesis
	Cd36_44870	orf19.6860	4	-1.6649036	-0.73543864	*PIS1*	Predicted ORF in Assemblies 19, 20 and 21
	Cd36_25040		R	-1.6644878	-0.73507833		

Gene Name	*C. dubliniensis* Cd36 identifier	*C. albicans* orf19 identifier	C'some	Fold change expression	Normalised Expression	*S. cerevisiae* ortholog	Description
	Cd36_18500	orf19.839	2	-1.6639597	-0.7346206	*YLR143W*	Predicted ORF in Assemblies 19, 20 and 21
	Cd36_11920	orf19.6348	1	-1.6637836	-0.73446774		Protein not essential for viability
SMI1B	Cd36_85330	orf19.6972	3	-1.6633492	-0.73409104	*SMI1*	Protein of unknown function
PMR1	Cd36_70530	orf19.7089	7	-1.6625293	-0.73337984	*PMR1*	Putative secretory pathway P-type Ca2+/Mn2+-ATPase, required for protein glycosylation and cell wall maintenance
FBA1	Cd36_41650	orf19.4618	4	-1.6613991	-0.73239875	*FBA1*	Putative fructose-bisphosphate aldolase
GPR1	Cd36_51080	orf19.1944	5	-1.6595689	-0.7308085	*GPR1*	Putative G-protein-coupled receptor of plasma membrane
	Cd36_00170	orf19.6090	1	-1.656569	-0.7281983	*NSR1*	Predicted ORF in Assemblies 19, 20 and 21
	Cd36_07590		1	-1.6563532	-0.7280104		
CHS2	Cd36_34480	orf19.7298	R	-1.6560391	-0.7277367	*CHS1*	Chitin synthase
	Cd36_13050	orf19.7215	1	-1.651281	-0.7235856	*UTP10*	Predicted ORF in Assemblies 19, 20 and 21
	Cd36_40160	orf19.5633	4	-1.6508275	-0.72318935		Predicted ORF in Assemblies 19, 20 and 21
CTA9	Cd36_01180	orf19.3315	1	-1.6491867	-0.7217548		Protein induced during the mating process
	Cd36_40120	orf19.372	4	-1.6485842	-0.72122765	*YER163C*	Predicted ORF in Assemblies 19, 20 and 21
	Cd36_73820	orf19.7159	7	-1.6485448	-0.7211931	*YMR185W*	Predicted ORF in Assemblies 19, 20 and 21
UTR2	Cd36_81610	orf19.1671	3	-1.6483312	-0.72100616	*UTR2*	Putative cell-surface glycosidase, role in adhesion
	Cd36_20040	orf19.6871	2	-1.6478853	-0.72061586	*YMR124W*	Predicted ORF in Assemblies 19, 20 and 21
	Cd36_17140	orf19.1569	2	-1.6465982	-0.7194886	*UTP22*	Predicted ORF in Assemblies 19, 20 and 21
VMA8	Cd36_45890	orf19.2895	4	-1.6453888	-0.7184286	*VMA8*	Protein similar to the S. cerevisiae Vma8p subunit of vacuolar H+-ATPase
SSU81	Cd36_08610	orf19.4772	1	-1.644939	-0.718034	*SHO1*	Predicted adaptor protein involved in activation of MAP kinase-dependent signaling pathways
IPL1	Cd36_62510	orf19.3474	6	-1.6439614	-0.71717644	*IPL1*	Predicted ORF in Assemblies 19, 20 and 21
	Cd36_00750		1	-1.643438	-0.716717		
	Cd36_43890	orf19.1428	4	-1.6434005	-0.7166841		Predicted ORF in Assemblies 19, 20 and 21
	Cd36_60570	orf19.4193	6	-1.6405418	-0.71417236	*YDR063W*	Predicted ORF in Assemblies 19, 20 and 21
ATP20	Cd36_11770	orf19.3757	1	-1.6394767	-0.7132354	*ATP20*	Predicted ORF in Assemblies 19, 20 and 21
MET8	Cd36_87130	orf19.6780	3	-1.6392133	-0.71300364	*MET8*	Predicted ORF in Assemblies 19, 20 and 21
MLP1	Cd36_41050	orf19.4683	4	-1.6383901	-0.71227884	*MLP1*	Protein similar to S. cerevisiae Mlp1p, which is a myosin-like protein
	Cd36_45450	orf19.1258	4	-1.6378733	-0.7118237	*CRH1*	Predicted ORF in Assemblies 19, 20 and 21
CDC19	Cd36_19920	orf19.3575	2	-1.6373767	-0.7113862	*CDC19*	Putative pyruvate kinase
HGT19	Cd36_80200	orf19.5447	3	-1.637118	-0.7111583	*HXT3*	Putative glucose/myo-inositol transporter of major facilitator superfamily
YTH1	Cd36_20130	orf19.6881	2	-1.636792	-0.710871	*YTH1*	Protein described as an mRNA cleavage and polyadenylation specificity factor
ILV2	Cd36_82300	orf19.1613	3	-1.6364815	-0.7105973	*ILV2*	Protein described as acetolactate synthase
HMX1	Cd36_00290	orf19.6073	1	-1.636472	-0.71058893	*HMX1*	Heme oxygenase
	Cd36_45000	orf19.1792	4	-1.6364198	-0.7105429	*CDC16*	Predicted ORF in Assemblies 19, 20 and 21
RAD57	Cd36_22290	orf19.2174	2	-1.6362549	-0.7103975	*RAD57*	Essential protein
ARF3	Cd36_81390	orf19.1702	3	-1.6330528	-0.7075715	*ARF3*	Transcription is filament induced
	Cd36_40640	orf19.4184	4	-1.632537	-0.70711565	*YAP1801*	Predicted ORF in Assemblies 19, 20 and 21
	Cd36_09010	orf19.4820	1	-1.6319731	-0.70661736		Predicted ORF in Assemblies 19, 20 and 21
ADE4	Cd36_07230	orf19.1233	1	-1.6317081	-0.706383	*ADE4*	Predicted ORF in Assemblies 19, 20 and 21
	Cd36_10390	orf19.2308	1	-1.626011	-0.701337	*PFK26*	Predicted ORF in Assemblies 19, 20 and 21
UBC8	Cd36_01670	orf19.4540	1	-1.6255891	-0.70096266	*UBC8*	Protein similar to S. cerevisiae Ubc8p
	Cd36_44400	orf19.3804	4	-1.6250172	-0.70045495	*YMR134W*	Predicted ORF in Assemblies 19, 20 and 21
URA1	Cd36_09160	orf19.4836	1	-1.6249175	-0.7003665	*URA1*	Dihydroorotate dehydrogenase (DHODH)
	Cd36_22780	orf19.3611	2	-1.6245419	-0.70003295		Predicted ORF in Assemblies 19, 20 and 21
HOG1	Cd36_18080	orf19.895	2	-1.623877	-0.6994424	*HOG1*	MAP kinase of osmotic-, heavy metal-, and core stress response
THR1	Cd36_50650	orf19.923	5	-1.6236188	-0.699213	*THR1*	Putative homoserine kinase
	Cd36_22870	orf19.3606	2	-1.6234921	-0.6991004	*SNA4*	Predicted ORF in Assemblies 19, 20 and 21
RIB3	Cd36_11580	orf19.5228	1	-1.622638	-0.69834113	*RIB3*	3,4-Dihydroxy-2-butanone 4-phosphate synthase
GPD2	Cd36_62130	orf19.691	6	-1.6223154	-0.6980543	*GPD1*	Similar to glycerol 3-P dehydrogenases
STE23	Cd36_63260	orf19.5559	6	-1.6221997	-0.69795144	*RAV2*	Protein similar to S. cerevisiae Ste23p, which is involved in maturation of pheromone
AAF1	Cd36_86430	orf19.7436	3	-1.6213645	-0.6972084	*DEF1*	Possible regulatory protein
	Cd36_06240	orf19.6245	1	-1.6206489	-0.6965716		Predicted ORF in Assemblies 19, 20 and 21
	Cd36_40680	orf19.4180	4	-1.6186228	-0.69476676	*SEC72*	Protein described as component of ER protein-translocation complex
	Cd36_05290	orf19.2494	1	-1.618412	-0.6945789	*PET112*	Predicted ORF in Assemblies 19, 20 and 21
	Cd36_52620	orf19.4307	5	-1.6181872	-0.6943785	*DID2*	Predicted ORF in Assemblies 19, 20 and 21
	Cd36_42490	orf19.2734	4	-1.6180522	-0.6942582	*YOR246C*	Protein not essential for viability
MET14	Cd36_50440	orf19.946	5	-1.6179849	-0.69419813	*MET14*	Predicted ORF in Assemblies 19, 20 and 21
	Cd36_17570	orf19.5825.1	2	-1.61759	-0.693846	*YOS1*	ORF Predicted by Annotation Working Group
GSP1	Cd36_20700	orf19.5493	2	-1.6165246	-0.6928954	*GSP2*	Small RAN G-protein
	Cd36_71330	orf19.6580	7	-1.614571	-0.6911509		Predicted ORF in Assemblies 19, 20 and 21
	Cd36_02550	orf19.2964	1	-1.6139315	-0.6905794	*RSC2|RSC1*	Predicted ORF in Assemblies 19, 20 and 21
HGT1	Cd36_01840	orf19.4527	1	-1.6137105	-0.69038177	*HXT11*	High-affinity glucose transporter, member of major facilitator superfamily
	Cd36_82450	orf19.239	3	-1.6130463	-0.68978786	*STH1*	Predicted ORF in Assemblies 19, 20 and 21
SEC12	Cd36_61860	orf19.3409	6	-1.6125454	-0.68933976	*SED4*	Protein described as a guanyl-nucleotide exchange factor
	Cd36_86630	orf19.7455	3	-1.6119902	-0.688843		Predicted ORF in Assemblies 19, 20 and 21
	Cd36_50550		5	-1.6114701	-0.6883774		
	Cd36_72730	orf19.5151	7	-1.6108084	-0.6877849		Predicted ORF from Assembly 19
	Cd36_64740		6	-1.6100254	-0.6870835		
	Cd36_22580	orf19.3635	2	-1.6090474	-0.6862068	*MUC1*	Predicted ORF in Assemblies 19, 20 and 21
	Cd36_86540	orf19.7445	3	-1.6089448	-0.6861148	*VID24*	Predicted ORF in Assemblies 19, 20 and 21

Gene Name	*C. dubliniensis* Cd36 identifier	*C. albicans* orf19 identifier	C'some	Fold change expression	Normalised Expression	*S. cerevisiae* ortholog	Description
	Cd36_09520	orf19.4882	1	-1.6079099	-0.6851866	*TFA2*	Predicted ORF in Assemblies 19, 20 and 21
IRA2	Cd36_11650	orf19.5219	1	-1.6079038	-0.68518114	*IRA2*	Predicted ORF in Assemblies 19, 20 and 21
	Cd36_52760	orf19.4325	5	-1.6075871	-0.68489695	*MUC1*	Predicted ORF in Assemblies 19, 20 and 21
HOS2	Cd36_80710	orf19.5377	3	-1.6072998	-0.6846391	*HOS2*	Histone deacetylase
CRL1	Cd36_01310	orf19.3330	1	-1.6070487	-0.6844137	*RHO4*	Predicted GTPase of RHO family
	Cd36_00140	orf19.6094	1	-1.6064287	-0.68385696	*VPS53*	Predicted ORF in Assemblies 19, 20 and 21
PIKA	Cd36_51560	orf19.3199	5	-1.6062835	-0.68372655	*PIK1*	Putative phosphatidylinositol kinase
	Cd36_71660	orf19.6537	7	-1.6048487	-0.6824373	*NSL1*	Predicted ORF in Assemblies 19, 20 and 21
	Cd36_40760	orf19.4171	4	-1.6027558	-0.6805546		Predicted ORF in Assemblies 19, 20 and 21
	Cd36_70770	orf19.7034	7	-1.6027087	-0.6805122	*PAN1*	Predicted ORF in Assemblies 19, 20 and 21
	Cd36_07690	orf19.5093	1	-1.6022693	-0.68011665	*SFH1*	Predicted ORF in Assemblies 19, 20 and 21
	Cd36_61380	orf19.136	6	-1.6012762	-0.6792221	*QDR3*	Predicted ORF in Assemblies 19, 20 and 21
PTK2	Cd36_61800	orf19.3415	6	-1.6011391	-0.6790986	*PTK2*	Putative protein kinase of polyamine import
GIT4	Cd36_51390	orf19.1980	5	-1.6007351	-0.67873454	*GIT1*	Putative glycerophosphoinositol permease
	Cd36_31120	orf19.6639	R	-1.6004492	-0.6784769		Predicted ORF in Assemblies 19, 20 and 21
	Cd36_42280	orf19.2763	4	-1.6004195	-0.6784501		Protein not essential for viability
	Cd36_87790		3	-1.5997555	-0.67785144		
HEM13	Cd36_83990	orf19.2803	3	-1.5993209	-0.6774595	*HEM13*	Homolog of S. cerevisiae coproporphyrinogen III oxidase
	Cd36_81120		3	-1.5983489	-0.67658234		
GNP1	Cd36_60280	orf19.1193	6	-1.5978758	-0.6761553	*AGP1*	Protein described as similar to asparagine and glutamine permease
	Cd36_81900		3	-1.5975621	-0.67587197		
URA2	Cd36_32590	orf19.2360	R	-1.5966673	-0.6750637	*URA2*	Predicted ORF in Assemblies 19, 20 and 21
BRO1	Cd36_81640	orf19.1670	3	-1.5966593	-0.67505646	*BRO1*	Protein involved in transport from multivesicular body to vacuole
	Cd36_84750	orf19.5942	3	-1.5934579	-0.672161	*ITT1*	Protein described as a zinc finger protein similar to S. cerevisiae Itt1p
	Cd36_64490	orf19.5775	6	-1.5923704	-0.67117596	*YIL169C*	Predicted ORF in Assemblies 19, 20 and 21
	Cd36_12360	orf19.4959	1	-1.592275	-0.67108953	*CYC8*	Predicted ORF in Assemblies 19, 20 and 21
	Cd36_06440		1	-1.591705	-0.670573		
RPL10	Cd36_02320	orf19.2935	1	-1.5909708	-0.66990733	*RPL10*	Putative ribosomal protein
NOP1	Cd36_46180	orf19.3138	4	-1.5907714	-0.6697266	*NOP1*	Nucleolar protein
	Cd36_64030		6	-1.5897341	-0.66878545		
OLE1	Cd36_07870	orf19.5117	1	-1.588502	-0.6676669	*OLE1*	Fatty acid desaturase (stearoyl-CoA desaturase), essential protein involved in oleic acid synthesis
CAN1	Cd36_61010	orf19.97	6	-1.5881046	-0.66730595	*CAN1*	Amino acid permease, transports basic amino acids
DFG16	Cd36_18150	orf19.881	2	-1.5857636	-0.6651777	*DFG16*	Protein of the Rim101p pathway that regulates filamentation in response to alkaline pH
	Cd36_52010		5	-1.5853608	-0.66481113		
	Cd36_12970	orf19.7206	1	-1.5832459	-0.6628853	*YDR067C*	Predicted ORF in Assemblies 19, 20 and 21
SSN8	Cd36_85680	orf19.7355	3	-1.5825776	-0.66227627	*SSN8*	Protein not essential for viability
	Cd36_62450	orf19.3467	6	-1.582575	-0.6622739	*SEC27*	Predicted ORF in Assemblies 19, 20 and 21
CUP9	Cd36_71860	orf19.6514	7	-1.5819893	-0.6617398	*CUP9*	Transcription reduced upon yeast-hyphal switch
	Cd36_02470		1	-1.581949	-0.6617031		
	Cd36_45050	orf19.1796	4	-1.5816221	-0.66140497	*YPL113C*	Predicted ORF in Assemblies 19, 20 and 21
POS5	Cd36_86940	orf19.6800	3	-1.5816008	-0.66138554	*POS5*	Protein likely to be essential for growth, based on an insertional mutagenesis strategy
	Cd36_17710			-1.5814981	-0.66129184		
ATP5	Cd36_80420	orf19.5419	3	-1.5801662	-0.6600764	*ATP5*	Predicted ORF in Assemblies 19, 20 and 21
PHM7	Cd36_22320	orf19.2170	2	-1.5793186	-0.65930223	*PHM7*	Putative transporter
RDI1	Cd36_84970	orf19.5968	3	-1.5788627	-0.6588857	*RDI1*	Protein similar to S. cerevisiae Rdi1p, which is an inhibitor of Rho-GDP dissociation
	Cd36_17650	orf19.5834	2	-1.5782844	-0.65835714	*SXM1*	Predicted ORF in Assemblies 19, 20 and 21
PSY2	Cd36_02130	orf19.3685	1	-1.5778434	-0.6579541	*PSY2*	Predicted ORF in Assemblies 19, 20 and 21
	Cd36_24640	orf19.5352	2	-1.5776157	-0.65774584		Protein not essential for viability
	Cd36_16750	orf19.1505	2	-1.5775015	-0.6576414		Predicted ORF in Assemblies 19, 20 and 21
	Cd36_17270	orf19.1549	2	-1.5746354	-0.65501785		Predicted ORF in Assemblies 19, 20 and 21
	Cd36_06600		1	-1.5736942	-0.65415525		
	Cd36_18750	orf19.810	2	-1.5732812	-0.6537765	*HFM1*	Predicted ORF in Assemblies 19, 20 and 21
	Cd36_23820	orf19.1376	2	-1.5731318	-0.65363955	*SSO2*	Predicted ORF in Assemblies 19, 20 and 21
	Cd36_41750	orf19.4607	4	-1.573065	-0.6535783		Predicted ORF in Assemblies 19, 20 and 21
RPP0	Cd36_70930	orf19.7015	7	-1.5723659	-0.65293694	*RPP0*	Putative ribosomal protein
	Cd36_21830	orf19.1872	2	-1.5709976	-0.65168095		Predicted ORF in Assemblies 19, 20 and 21
ERG1	Cd36_08100	orf19.406	1	-1.5709857	-0.65167	*ERG1*	Squalene epoxidase, catalyzes epoxidation of squalene to 2,3(S)-oxidosqualene in the ergosterol biosynthetic pathway
CEK1	Cd36_45970	orf19.2886	4	-1.5706118	-0.65132666	*FUS3*	ERK-family protein kinase, required for wild-type yeast-hyphal switching, mating efficiency, and virulence in a mouse model
WAL1	Cd36_34820	orf19.6598	R	-1.5705837	-0.6513008	*LAS17*	Protein required for hyphal growth and for wild-type cell morphology, polarized budding, endocytosis, vacuole morphology
	Cd36_86640	orf19.7456	3	-1.5703847	-0.65111804		Predicted ORF in Assemblies 19, 20 and 21
	Cd36_71060	orf19.6902	7	-1.5702754	-0.65101767	*DBP7*	Predicted ORF in Assemblies 19, 20 and 21
	Cd36_20010	orf19.6867	2	-1.5685916	-0.64946973	*DAP1*	Predicted ORF in Assemblies 19, 20 and 21
	Cd36_63980	orf19.5592	6	-1.56833	-0.6492292		Predicted ORF in Assemblies 19, 20 and 21
	Cd36_53090	orf19.2650	5	-1.5679741	-0.6489017	*MED2*	Predicted ORF in Assemblies 19, 20 and 21
	Cd36_21380	orf19.2265	2	-1.5673833	-0.648358	*SNF12*	Predicted ORF in Assemblies 19, 20 and 21
	Cd36_00950	orf19.3289	1	-1.5666974	-0.64772654	*ORC6*	Predicted ORF in Assemblies 19, 20 and 21
	Cd36_40260	orf19.5644	4	-1.5656363	-0.64674914	*SMA2*	Predicted ORF in Assemblies 19, 20 and 21

Gene Name	*C. dubliniensis* Cd36 identifier	*C. albicans* orf19 identifier	C'some	Fold change expression	Normalised Expression	*S. cerevisiae* ortholog	Description
	Cd36_42160	orf19.4560	4	-1.5656003	-0.6467159	*BFR1*	Predicted ORF in Assemblies 19, 20 and 21
	Cd36_01120	orf19.3307	1	-1.5642792	-0.64549804	*FMO1*	Predicted ORF in Assemblies 19, 20 and 21
RPS12	Cd36_87080	orf19.6785	3	-1.5634459	-0.6447294	*RPS12*	Protein described as acidic ribosomal protein S12
	Cd36_72670	orf19.5160	7	-1.5632253	-0.64452565	*SAP190*	Predicted ORF in Assemblies 19, 20 and 21
	Cd36_51755	orf19.3181.1	5	-1.5631703	-0.644475	*NCE101*	ORF Predicted by Annotation Working Group
OSM1	Cd36_20140	orf19.6882	2	-1.5630975	-0.64440775	*OSM1*	Putative flavoprotein subunit of fumarate reductase
	Cd36_46190	orf19.3136	4	-1.5619507	-0.64334893	*IMP2*	Predicted ORF in Assemblies 19, 20 and 21
EIF4E	Cd36_35334	orf19.7626	R	-1.5618942	-0.6432967	*CDC33*	Putative translation initiation factor eIF4E
	Cd36_22370	orf19.2166	2	-1.5615166	-0.6429479	*VMA5*	Predicted ORF in Assemblies 19, 20 and 21
	Cd36_43750	orf19.5297	4	-1.5609913	-0.64246243	*TFB1*	Predicted ORF in Assemblies 19, 20 and 21
CHL4	Cd36_04310	orf19.6851	1	-1.5604409	-0.6419537	*CHL4*	Protein described as having role in chromosome segregation
RTA4	Cd36_34850	orf19.6595	R	-1.5597452	-0.64131033	*RSB1*	Predicted ORF in Assemblies 19, 20 and 21
RPL12	Cd36_82090	orf19.1635	3	-1.5590459	-0.6406634	*RPL12B|RPL12A*	Predicted ribosomal protein
	Cd36_20490	orf19.4110	2	-1.5588804	-0.6405103	*TPM1*	Predicted ORF in Assemblies 19, 20 and 21
RPG1A	Cd36_11950	orf19.6345	1	-1.5585724	-0.6402252	*RPG1*	Putative translation initiation factor
HAP42	Cd36_16560	orf19.1481	2	-1.5583717	-0.6400393	*MUC1*	Predicted ORF in Assemblies 19, 20 and 21
	Cd36_53470	orf19.1121	5	-1.5582616	-0.6399375		Predicted ORF in Assemblies 19, 20 and 21
	Cd36_11380	orf19.5249	1	-1.5582108	-0.63989043		Predicted ORF in Assemblies 19, 20 and 21
CAM1-1	Cd36_53070	orf19.2651	5	-1.5580417	-0.6397338	*CAM1*	Putative translation elongation factor
NUP49	Cd36_12540	orf19.4987	1	-1.5576555	-0.63937616	*NUP49*	Nuclear pore protein
	Cd36_84010		3	-1.5575147	-0.63924575		
	Cd36_61455	orf19.3449.2	6	-1.5574743	-0.6392083	*YHR100C*	ORF Predicted by Annotation Working Group
	Cd36_42790		4	-1.5570397	-0.63880575		
GPD1	Cd36_24300	orf19.1756	2	-1.5567595	-0.6385461	*GPD1*	Protein similar to S. cerevisiae glycerol-3-phosphate dehydrogenase (enzyme of glycerol biosynthesis)
	Cd36_02920	orf19.3004	1	-1.5551927	-0.6370933	*YDR262W*	Predicted ORF in Assemblies 19, 20 and 21
GCN1	Cd36_24780	orf19.5328	2	-1.5548488	-0.6367743	*GCN1*	Protein not essential for viability
ILV5	Cd36_60880	orf19.88	6	-1.5534313	-0.63545847	*ILV5*	Protein described as ketol-acid reductoisomerase
DFR1	Cd36_72780	orf19.5142	7	-1.55325	-0.63529	*DFR1*	Dihydrofolate reductase
	Cd36_41370	orf19.4702	4	-1.5523589	-0.6344621		Predicted ORF in Assemblies 19, 20 and 21
	Cd36_19750	orf19.3555	2	-1.5488224	-0.6311717	*BUD14*	Predicted ORF in Assemblies 19, 20 and 21
RPS20	Cd36_33780	orf19.6375	R	-1.5467651	-0.6292541	*RPS20*	Putative ribosomal protein
	Cd36_42940	orf19.2682	4	-1.546494	-0.62900126	*TOA1*	Predicted ORF in Assemblies 19, 20 and 21
	Cd36_18620	orf19.827	2	-1.5463239	-0.6288426		Predicted ORF in Assemblies 19, 20 and 21
	Cd36_42570	orf19.2730	4	-1.5446154	-0.6272477	*RPH1*	Predicted ORF in Assemblies 19, 20 and 21
	Cd36_20080	orf19.6874	2	-1.5442278	-0.62688565	*BAS1*	Predicted ORF in Assemblies 19, 20 and 21
	Cd36_52280	f19.4262; orf19.42	5	-1.5439309	-0.62660813		
VRG4	Cd36_07220	orf19.1232	1	-1.5435928	-0.6262922	*VRG4*	GDP-mannose transporter
ADE8	Cd36_17860	orf19.5789	2	-1.543085	-0.62581754	*ADE8*	Predicted enzyme of amino acid biosynthesis
END3	Cd36_81330	orf19.1711	3	-1.5424665	-0.62523913	*END3*	Regulated by Gcn4p
	Cd36_81830		3	-1.5408844	-0.6237586		
FESUR1	Cd36_86990	orf19.6794	3	-1.5400918	-0.62301636		Protein described as ubiquinone reductase
CZF1	Cd36_46280	orf19.3127	4	-1.540016	-0.6229454	*UME6*	Transcriptional regulator of white-opaque switching
	Cd36_83970	orf19.2805	3	-1.5397956	-0.62273884		Predicted ORF in Assemblies 19, 20 and 21
	Cd36_19810	orf19.3563	2	-1.5393059	-0.62228	*DAN4*	Protein not essential for viability
	Cd36_28350	orf19.2401	R	-1.5385324	-0.62155485	*ATG4*	Predicted ORF in Assemblies 19, 20 and 21
	Cd36_05570	orf19.2458	1	-1.538322	-0.62135744	*SIP5*	Putative transcription factor with zinc finger DNA-binding motif
OPT6	Cd36_41310	orf19.4655	4	-1.538039	-0.6210921	*OPT2*	Putative oligopeptide transporter
	Cd36_65180	orf19.2128	6	-1.538018	-0.6210724	*YLF2*	Predicted ORF in Assemblies 19, 20 and 21
	Cd36_18300	orf19.862	2	-1.5379611	-0.621019		Predicted ORF in Assemblies 19, 20 and 21
LTE1	Cd36_21160	orf19.2238	2	-1.5366038	-0.61974525	*LTE1*	Protein similar to S. cerevisiae Lte1p
	Cd36_83050	orf19.304	3	-1.536122	-0.61929274	*YOR378W*	Putative transporter similar to MDR proteins
FGR51	Cd36_19290	orf19.156	2	-1.5359361	-0.6191182		Protein lacking an ortholog in S. cerevisiae
	Cd36_41850	orf19.4596	4	-1.5340899	-0.617383	*YHR159W*	Predicted ORF in Assemblies 19, 20 and 21
	Cd36_00210	orf19.6082	1	-1.5318896	-0.61531234	*GSF2*	Predicted ORF in Assemblies 19, 20 and 21
FZO1	Cd36_43930	orf19.1422	4	-1.5316975	-0.6151314	*FZO1*	Putative mitochondrial biogenesis protein
COX4	Cd36_16480	orf19.1471	2	-1.5316886	-0.61512303	*COX4*	Protein described as subunit IV of cytochrome c oxidase
	Cd36_62440	orf19.3466	6	-1.5315359	-0.61497915	*MRM2*	Predicted ORF in Assemblies 19, 20 and 21
	Cd36_27780	orf19.2832	R	-1.5314995	-0.61494493	*YNL152W*	Predicted ORF in Assemblies 19, 20 and 21
	Cd36_04580	orf19.759	1	-1.5311418	-0.6146078	*SEC21*	Predicted ORF in Assemblies 19, 20 and 21
	Cd36_81860	orf19.5773	3	-1.5310397	-0.6145117	*YOL057W*	Predicted ORF in Assemblies 19, 20 and 21
CSI2	Cd36_11540	orf19.5232	1	-1.530236	-0.61375415	*BRX1*	Protein essential for growth
	Cd36_86800	orf19.6818	3	-1.5299215	-0.6134577	*YLR419W*	Predicted ORF in Assemblies 19, 20 and 21
	Cd36_09210	orf19.4843	1	-1.5299026	-0.6134398	*FRE8*	Predicted ORF in Assemblies 19, 20 and 21
FTH1	Cd36_08870	orf19.4802	1	-1.527691	-0.6113528	*FTH1*	Protein not essential for viability
	Cd36_45570	orf19.4412	4	-1.5264584	-0.61018825	*REV1*	Predicted ORF in Assemblies 19, 20 and 21
CSA2	Cd36_46390	orf19.3117	4	-1.5263239	-0.61006117		Predicted ORF in Assemblies 19, 20 and 21
	Cd36_15565		2	-1.5257517	-0.6095202		
CAN3	Cd36_60830	orf19.84	6	-1.5248077	-0.6086273	*CAN1*	Predicted ORF in Assemblies 19, 20 and 21
	Cd36_61570	orf19.3438	6	-1.5245756	-0.60840774	*SCJ1*	Predicted ORF in Assemblies 19, 20 and 21
GEA2	Cd36_81320	orf19.1712	3	-1.5244327	-0.60827243	*GEA2*	Protein described as an ARF GTP/GDP exchange factor
	Cd36_03120	orf19.3029	1	-1.5234964	-0.6073861	*EHD3*	Predicted ORF in Assemblies 19, 20 and 21
	Cd36_62990	orf19.5541	6	-1.5227125	-0.60664356	*YPL184C*	Predicted ORF in Assemblies 19, 20 and 21
	Cd36_22280	orf19.2175	2	-1.5224253	-0.6063714	*AIF1*	Predicted ORF in Assemblies 19, 20 and 21
	Cd36_71000	orf19.7006	7	-1.5218716	-0.60584664	*MSC3*	Predicted ORF in Assemblies 19, 20 and 21
	Cd36_17160	orf19.1566	2	-1.5216845	-0.60566926	*UTP21*	Predicted ORF in Assemblies 19, 20 and 21
	Cd36_87330	orf19.6748	3	-1.5212485	-0.60525584		Predicted ORF in Assemblies 19, 20 and 21
	Cd36_11170	orf19.5275	1	-1.5207044	-0.6047398	*VTA1*	Predicted ORF in Assemblies 19, 20 and 21

Gene Name	*C. dubliniensis* Cd36 identifier	*C. albicans* orf19 identifier	C'some	Fold change expression	Normalised Expression	*S. cerevisiae* ortholog	Description
	Cd36_16840	orf19.1519	2	-1.5203105	-0.60436606	*MUC1*	Predicted ORF in Assemblies 19, 20 and 21
	Cd36_42340	orf19.2756	4	-1.519774	-0.6038568	*ERD2*	Predicted ORF in Assemblies 19, 20 and 21
	Cd36_62710	orf19.5517	6	-1.5196385	-0.6037282	*ADH7*	Similar to alcohol dehydrogenases
CYT1	Cd36_19470	orf19.3527	2	-1.5192193	-0.60333014	*CYT1*	Protein described as cytochrome c1
GAT2	Cd36_04890	orf19.4056	1	-1.5185616	-0.6027055	*GAT2*	Putative DNA-binding transcription factor
RPS13	Cd36_60560	orf19.4193.1	6	-1.5182515	-0.6024108	*RPS13*	Putative ribosomal protein
	Cd36_15880	orf19.2030	2	-1.5166708	-0.60090804	*SNA4*	Predicted ORF in Assemblies 19, 20 and 21
	Cd36_24705		2	-1.5161624	-0.6004243		
KRS1	Cd36_87320	orf19.6749	3	-1.5158112	-0.60009	*KRS1*	Putative tRNA-Lys synthetase
	Cd36_06190	orf19.6250	1	-1.5153531	-0.59965396	*SCD6*	Predicted ORF in Assemblies 19, 20 and 21
SSZ1	Cd36_44350	orf19.3812	4	-1.5151718	-0.59948134	*SSZ1*	Protein described as an HSP70 chaperone
	Cd36_04170	orf19.5195	1	-1.5145569	-0.5988958	*URA6*	Predicted ORF in Assemblies 19, 20 and 21
SWI1	Cd36_40360	orf19.5657	4	-1.5132364	-0.5976374	*SWI1*	Protein involved in transcription regulation
	Cd36_11670	orf19.68.2	1	-1.512717	-0.5971421		ORF Predicted by Annotation Working Group
HOL4	Cd36_01620	orf19.4546	1	-1.5113436	-0.59583163	*HOL1*	Protein described as an ion transporter
	Cd36_70510	orf19.7092	7	-1.511296	-0.59578633	*YLR290C*	Predicted ORF in Assemblies 19, 20 and 21
	Cd36_11510	orf19.5236	1	-1.5106046	-0.59512615	*SRT1*	Predicted ORF in Assemblies 19, 20 and 21
DAP2	Cd36_52730	orf19.4322	5	-1.5105275	-0.5950525	*DAP2*	Protein described as dipeptidyl aminopeptidase
FUS1	Cd36_10920	orf19.1156	1	-1.5103278	-0.59486175	*WSC4*	Probable ortholog of S. cerevisiae Fus1p, which is a membrane protein required for mating
	Cd36_81570	orf19.1675	3	-1.5100957	-0.59464	*YDL133W*	Predicted ORF in Assemblies 19, 20 and 21
	Cd36_22730	orf19.3617	2	-1.5097337	-0.5942941	*GTR1*	Predicted ORF in Assemblies 19, 20 and 21 (see Locus History Note for Assembly 19 correction)
YAF9	Cd36_73430	orf19.5501	7	-1.5091343	-0.59372115	*YAF9*	Predicted ORF in Assemblies 19, 20 and 21
	Cd36_08560	orf19.4764	1	-1.5088208	-0.59342146	*PAN2*	Predicted ORF in Assemblies 19, 20 and 21
UTP20	Cd36_81100	orf19.3159	3	-1.507972	-0.59260964	*UTP20*	Protein likely to be essential for growth, based on an insertional mutagenesis strategy
CDC68	Cd36_45990	orf19.2884	4	-1.5075716	-0.5922265	*SPT16*	Functional homolog of S. cerevisiae Cdc68p, which is a transcription elongation factor
DRG1	Cd36_07620	orf19.5083	1	-1.507179	-0.59185076	*RBG1*	Member of the DRG family of GTP-binding proteins
	Cd36_01490	orf19.3352	1	-1.5070847	-0.5917605	*YOR246C*	Predicted ORF in Assemblies 19, 20 and 21
	Cd36_80060		3	-1.5070535	-0.5917306		
	Cd36_45920	orf19.2891	4	-1.5062678	-0.59097826	*AFG1*	Predicted ORF in Assemblies 19, 20 and 21
NPL3	Cd36_13250	orf19.7238	1	-1.5062406	-0.5909523	*NPL3*	Putative RNA-binding protein, ortholog of S. cerevisiae Npl3p
	Cd36_08190	orf19.4726	1	-1.5056574	-0.59039354	*FRQ1*	Predicted ORF in Assemblies 19, 20 and 21
ADK1	Cd36_62040	orf19.3391	6	-1.5052862	-0.5900378	*ADK1*	Protein described as adenylate kinase
SUB2	Cd36_40290	orf19.5647	4	-1.5040909	-0.58889174	*SUB2*	Transcription is regulated by Mig1p
	Cd36_43550	orf19.1297	4	-1.5037115	-0.5885278	*ATG20*	Predicted ORF in Assemblies 19, 20 and 21
AXL2	Cd36_43700	orf19.5292	4	-1.502738	-0.58759356	*AXL2*	Protein not essential for viability
	Cd36_16410	orf19.1464	2	-1.5022844	-0.58715796		Predicted ORF in Assemblies 19, 20 and 21
CLB2	Cd36_16270	orf19.1446	2	-1.5008163	-0.5857475	*CLB2*	B-type mitotic cyclin (cyclin-dependent protein kinase regulatory subunit)
	Cd36_18810	orf19.804	2	-1.5005151	-0.5854578	*YPR011C*	Predicted ORF in Assemblies 19, 20 and 21
HCH1	Cd36_61990	orf19.3396	6	1.5002483	0.58520126	*HCH1*	Protein not essential for viability
PRE3	Cd36_85530	orf19.6991	3	1.5005726	0.5855131	*PRE3*	Protein described as beta-1 subunit of proteasome
HST2	Cd36_26820	orf19.2580	R	1.5005755	0.585516	*HST2*	Predicted ORF in Assemblies 19, 20 and 21
	Cd36_63520	orf19.5704	6	1.5012429	0.58615744	*YGR150C*	Predicted ORF in Assemblies 19, 20 and 21
	Cd36_03920	orf19.1050	1	1.5018518	0.5867424		Predicted ORF in Assemblies 19, 20 and 21
DAO2	Cd36_43150	orf19.3365	4	1.5022862	0.58715963		Putative D-amino acid oxidase
	Cd36_26240	orf19.3231	R	1.503364	0.5881944	*CDC27*	Predicted ORF in Assemblies 19, 20 and 21
RPL7	Cd36_31630	orf19.3867	R	1.5036103	0.58843064	*RLP7*	Putative ribosomal-related protein
	Cd36_31270	orf19.6624	R	1.5036364	0.5884557		Predicted ORF in Assemblies 19, 20 and 21
HTS1	Cd36_55080	orf19.4051	5	1.5036465	0.58846545	*HTS1*	Putative tRNA-His synthetase
PGA4	Cd36_54990	orf19.4035	5	1.5039995	0.588804	*GAS5*	Putative cell-surface protein, predicted to carry a glycosylphosphatidylinositol (GPI) lipid anchor
CDC48	Cd36_10120	orf19.2340	1	1.5045474	0.5893295	*CDC48*	Protein described as microsomal ATPase
	Cd36_00030		1	1.5045934	0.5893736		
	Cd36_29490	orf19.504	R	1.505543	0.5902839	*ARP5*	Predicted ORF in Assemblies 19, 20 and 21
	Cd36_41100	orf19.4678	4	1.5057259	0.5904591	*YJR107W*	Predicted ORF in Assemblies 19, 20 and 21
ADR1	Cd36_42380	orf19.2752	4	1.5057609	0.5904927	*ADR1*	Putative transcription factor with zinc finger DNA-binding motif
	Cd36_26090	orf19.3245	R	1.5072243	0.59189415		Predicted ORF in Assemblies 19, 20 and 21
	Cd36_54680	orf19.4000	5	1.5074811	0.59213996	*PHO2*	Predicted ORF in Assemblies 19, 20 and 21
	Cd36_84590	orf19.5924	3	1.507972	0.59260964	*VRP1*	Predicted zinc-finger protein of unknown function
SHE3	Cd36_33180	orf19.729	R	1.5081676	0.5927968		Protein similar to S. cerevisiae She3p
	Cd36_53750	orf19.1285	5	1.5082759	0.5929003	*YPR091C*	Predicted ORF in Assemblies 19, 20 and 21
ATP3	Cd36_26320	orf19.3223	R	1.508278	0.5929024	*ATP3*	Predicted ORF in Assemblies 19, 20 and 21
	Cd36_01080	orf19.3303	1	1.5085855	0.5931964	*PPM2*	Predicted ORF in Assemblies 19, 20 and 21
	Cd36_70250	orf19.7121	7	1.5090514	0.593642		Predicted ORF in Assemblies 19, 20 and 21
	Cd36_71750	orf19.6527	7	1.5096499	0.59421396	*PRM10*	Predicted ORF in Assemblies 19, 20 and 21
	Cd36_09960	orf19.1834	1	1.5106086	0.59512985		Predicted ORF in Assemblies 19, 20 and 21
	Cd36_29320	orf19.486	R	1.5114057	0.595891	*NIP100*	Predicted ORF in Assemblies 19, 20 and 21
	Cd36_40610	orf19.4187	4	1.5118244	0.5962906	*MMM1*	Predicted ORF in Assemblies 19, 20 and 21
SDH2	Cd36_30410	orf19.637	R	1.5119793	0.5964384	*SDH2*	Succinate dehydrogenase, Fe-S subunit
	Cd36_41730	orf19.4609	4	1.5124227	0.59686136	*YAL049C*	Protein abundance is affected by URA3 expression in the CAI-4 strain background
	Cd36_26100	orf19.3244	R	1.5128701	0.59728813	*COX23*	Predicted ORF in Assemblies 19, 20 and 21
	Cd36_25560	orf19.7490	R	1.5136126	0.597996	*BSC6*	Predicted ORF in Assemblies 19, 20 and 21

Gene Name	*C. dubliniensis* Cd36 identifier	*C. albicans* orf19 identifier	C'some	Fold change expression	Normalised Expression	*S. cerevisiae* ortholog	Description
	Cd36_80680	orf19.5380	3	**1.5136904**	0.59807014	*LYS14*	Putative transcription factor with zinc cluster DNA-binding motif
	Cd36_30530	orf19.649	R	**1.5137985**	0.59817314		Predicted ORF in Assemblies 19, 20 and 21
	Cd36_28840	orf19.4362	R	**1.5139791**	0.5983453	*MSP1*	Predicted ORF in Assemblies 19, 20 and 21
	Cd36_09890	orf19.993	1	**1.5142844**	0.59863615		Predicted ORF in Assemblies 19, 20 and 21
PRE2	Cd36_21120	orf19.2233	2	**1.5149269**	0.5992482	*PRE2*	Protein described as beta-5 subunit of proteasome
	Cd36_29060	orf19.4354	R	**1.5160123**	0.6002815	*MCM2*	Predicted ORF in Assemblies 19, 20 and 21
	Cd36_25820	orf19.3282	R	**1.5172279**	0.6014378		Predicted ORF in Assemblies 19, 20 and 21
MDL1	Cd36_27070	orf19.2615	R	**1.5181571**	0.60232115	*MDL1*	Putative mitochondrial, half-size MDR-subfamily ABC transporter
	Cd36_06090	orf19.6263	1	**1.5183458**	0.60250044	*MCH4*	Predicted ORF in Assemblies 19, 20 and 21
ICL1	Cd36_04240	orf19.6844	1	**1.5185311**	0.6026764	*ICL1*	Isocitrate lyase
	Cd36_00780	orf19.6023	1	**1.5194197**	0.6035204	*YDR338C*	Predicted ORF in Assemblies 19, 20 and 21
	Cd36_53570	orf19.1110	5	**1.5204849**	0.6045315	*THI80*	Predicted ORF in Assemblies 19, 20 and 21
	Cd36_53820	orf19.3894	5	**1.5214039**	0.6054032		Predicted ORF in Assemblies 19, 20 and 21
GRP2	Cd36_52640	orf19.4309	5	**1.5241474**	0.6080024	*GRE2*	Similar to S. cerevisiae Gre2p (methylglyoxal reductase)
	Cd36_09740	orf19.4905	1	**1.5263526**	0.61008835		Predicted ORF in Assemblies 19, 20 and 21
RPN6	Cd36_43530	orf19.1299	4	**1.5266075**	0.61032915	*RPN6*	Predicted ORF in Assemblies 19, 20 and 21
MNT4	Cd36_30170	orf19.6313	R	**1.5266511**	0.6103704	*MNT4*	Transcriptionally regulated by iron
	Cd36_20790	orf19.21	2	**1.5267628**	0.610476	*SYM1*	Predicted ORF in Assemblies 19, 20 and 21
	Cd36_04200	orf19.6838	1	**1.5275495**	0.61121917	*SPS19*	Predicted ORF in Assemblies 19, 20 and 21
	Cd36_73570	orf19.7194	7	**1.5275657**	0.6112344		Protein not essential for viability
	Cd36_17230	orf19.1557	2	**1.5286026**	0.6122134	*YLR137W*	Predicted ORF in Assemblies 19, 20 and 21
	Cd36_01880	orf19.4523	1	**1.5295572**	0.6131141	*FAU1*	Predicted ORF in Assemblies 19, 20 and 21
35520	Cd36_21670	orf19.1891	2	**1.5295856**	0.6131408	*PEP4*	Vacuolar aspartic proteinase
	Cd36_32810	orf19.730	R	**1.5299582**	0.61349225	*RGD2*	Predicted ORF in Assembly 20 and 21 (see Locus History)
	Cd36_34270	orf19.6444	R	**1.531273**	0.61473155	*RMD11*	Predicted ORF in Assemblies 19, 20 and 21
	Cd36_53580	orf19.1109	5	**1.5321709**	0.6155772		Predicted ORF in Assemblies 19, 20 and 21
	Cd36_41640	orf19.4620	4	**1.5326592**	0.6160369	*MRS5*	Predicted ORF in Assemblies 19, 20 and 21
HST7	Cd36_29180	orf19.469	R	**1.5329373**	0.6162987	*STE7*	MAP kinase kinase, involved in signal transduction pathways for mating and hyphal growth
	Cd36_34840	orf19.6596	R	**1.5339862**	0.6172855	*YJL068C*	Gene is possibly transcriptionally regulated by Tac1p
SMC1	Cd36_28880	orf19.4367	R	**1.5344129**	0.61768675	*SMC1*	Protein described as similar to chromosomal ATPases
UGT51C1	Cd36_27080	orf19.2616	R	**1.5350571**	0.61829233	*ATG26*	UDP-glucose:sterol glucosyltransferase
LSC1	Cd36_01550	orf19.3358	1	**1.5354364**	0.61864877	*LSC1*	Protein described as succinate-CoA ligase subunit
MAS1	Cd36_03100	orf19.3026	1	**1.5356727**	0.61887074	*MAS1*	Predicted ORF in Assemblies 19, 20 and 21
GPX1	Cd36_60870	orf19.87	6	**1.5357754**	0.6189673	*HYR1*	Predicted ORF in Assemblies 19, 20 and 21
	Cd36_53660	orf19.3218	5	**1.5358894**	0.61907434	*YJR124C*	Putative multidrug resistance protein
	Cd36_46160	orf19.3140.1	4	**1.5364279**	0.61958003	*UMP1*	ORF Predicted by Annotation Working Group
DBP2	Cd36_27480	orf19.171	R	**1.5409508**	0.6238208	*DBP2*	Predicted ORF in Assemblies 19, 20 and 21
HNT2	Cd36_86320	orf19.7419	3	**1.5411052**	0.62396526	*HNT2*	Predicted ORF in Assemblies 19, 20 and 21
	Cd36_51380	orf19.1977	5	**1.5416582**	0.62448287	*URA4*	Predicted ORF in Assemblies 19, 20 and 21
	Cd36_11370	orf19.5250	1	**1.54185**	0.6246624		Predicted ORF in Assemblies 19, 20 and 21
	Cd36_29360	orf19.490	R	**1.5419644**	0.62476945	*NAT5*	Predicted ORF in Assemblies 19, 20 and 21
RNH1	Cd36_63220	orf19.5563	6	**1.5419976**	0.62480044	*RNH1*	Protein described as Ribonuclease H (RNAse H)
	Cd36_42220	orf19.2770	4	**1.5427023**	0.6254597		Predicted ORF in Assemblies 19, 20 and 21
VID27	Cd36_60120	orf19.6324	6	**1.5428076**	0.62555814	*VID27*	Protein similar to S. cerevisiae Vid27p
URA7	Cd36_54190	orf19.3941	5	**1.5435892**	0.6262889	*URA7*	Predicted ORF in Assemblies 19, 20 and 21
	Cd36_40140	orf19.376	4	**1.5450695**	0.6276717		Predicted ORF in Assemblies 19, 20 and 21
PGA12	Cd36_35200	orf19.7597	R	**1.5451251**	0.6277237	*PMU1*	Putative GPI-anchored protein of unknown function
	Cd36_08530	orf19.4760	1	**1.5453538**	0.6279372	*YIL110W*	Predicted ORF in Assemblies 19, 20 and 21
	Cd36_21460	orf19.2275	2	**1.5459698**	0.62851214	*MNP1*	Predicted ORF in Assemblies 19, 20 and 21
SOD2	Cd36_01390	orf19.3340	1	**1.5459889**	0.62853	*SOD2*	Mitochondrial manganese-containing superoxide dismutase
ABP1	Cd36_42810	orf19.2699	4	**1.5464637**	0.628973	*ABP1*	Protein similar to S. cerevisiae Abp1p, which is an actin-binding protein of the cortical actin cytoskeleton
	Cd36_61530	orf19.3442	6	**1.5470172**	0.6294893	*OYE2*	Predicted ORF in Assemblies 19, 20 and 21
	Cd36_54620	orf19.3994	5	**1.5471915**	0.6296518	*OST3*	Predicted ORF in Assemblies 19, 20 and 21
MRPL37	Cd36_04620	orf19.755	1	**1.5476763**	0.6301038	*MRPL37*	Predicted ORF in Assemblies 19, 20 and 21
SPT14	Cd36_29330	orf19.487	R	**1.5483779**	0.6307576	*SPT14*	Putative DNA-binding transcription factor
SRP54	Cd36_26110	orf19.3243	R	**1.5495633**	0.6318617	*SRP54*	Predicted ORF in Assemblies 19, 20 and 21
RDH54	Cd36_24530	orf19.5367	2	**1.5499074**	0.6321821	*RDH54*	Protein described as having role in DNA recombination, repair
OYE32	Cd36_46240	orf19.3131	4	**1.5502264**	0.63247895	*OYE3*	Protein of NAD(P)H oxidoreductase family
	Cd36_25770	orf19.7460	R	**1.5503858**	0.63262725	*TRM13*	Predicted ORF in Assemblies 19, 20 and 21
CDR2	Cd36_84860	orf19.5958	3	**1.5515734**	0.63373196	*PDR5*	Multidrug transporter, ATP-binding cassette (ABC) superfamily
TRM1	Cd36_25950	orf19.3265	R	**1.5549706**	0.6368873	*TRM1*	Protein described as an N2,N2-dimethylguanine tRNA methyltransferase
	Cd36_26680	orf19.2563	R	**1.5558361**	0.63769007	*PRP24*	Predicted ORF in Assemblies 19, 20 and 21
FAA2-3	Cd36_73850	orf19.7156	7	**1.5560201**	0.6378608	*FAA2*	Predicted acyl CoA synthetase
HHF1	Cd36_04000	orf19.1059	1	**1.5563077**	0.6381273	*HHF2|HHF1*	Putative histone H4
	Cd36_16860	orf19.1523	2	**1.5563201**	0.6381388		Predicted ORF in Assemblies 19, 20 and 21
	Cd36_25100	orf19.7534	R	**1.5564167**	0.6382284	*MIS1*	Predicted ORF in Assemblies 19, 20 and 21
HGT3	Cd36_29090	orf19.4356	R	**1.556828**	0.6386095	*YDL199C*	Putative glucose transporter of the major facilitator superfamily
	Cd36_60960	orf19.93	6	**1.5574199**	0.639158	*MIC17*	Predicted ORF in Assemblies 19, 20 and 21
	Cd36_16140	orf19.1998	2	**1.5578038**	0.6395135		Predicted ORF in Assemblies 19, 20 and 21
	Cd36_44220	orf19.3831	4	**1.5578532**	0.63955927	*PXR1*	Predicted ORF in Assemblies 19, 20 and 21
	Cd36_26940	orf19.2604	R	**1.5585096**	0.640167	*YNL022C*	Predicted ORF in Assemblies 19, 20 and 21

Gene Name	*C. dubliniensis* Cd36 identifier	*C. albicans* orf19 identifier	C'some	Fold change expression	Normalised Expression	*S. cerevisiae* ortholog	Description
	Cd36_44500	orf19.3793	4	**1.5591649**	0.64077353		Predicted ORF in Assemblies 19, 20 and 21
TKL1	Cd36_07840	orf19.5112	1	**1.5597152**	0.64128256	*TKL1*	Putative transketolase
	Cd36_27340	orf19.3730	R	**1.5601498**	0.64168453	*KRE27*	Protein similar to S. cerevisiae Kre27p, which has a role in resistance to killer toxin
	Cd36_27580	orf19.2820	R	**1.5603795**	0.64189696	*NUP57*	Predicted ORF in Assemblies 19, 20 and 21
BNR1	Cd36_25090	orf19.7537	R	**1.5617375**	0.643152	*BNI1*	Formin
	Cd36_08980	orf19.4816	1	**1.5623263**	0.64369583	*YMR209C*	Predicted ORF in Assemblies 19, 20 and 21
	Cd36_12610		1	**1.5624359**	0.6437969		
	Cd36_15040	orf19.1920	2	**1.5637602**	0.6450193	*YJL160C*	Predicted ORF in Assemblies 19, 20 and 21
	Cd36_26250	orf19.3230	R	**1.5643646**	0.6455767	*BOI2*	Predicted ORF in Assemblies 19, 20 and 21
	Cd36_25510	orf19.7497	R	**1.5646355**	0.6458266	*CDC53*	Predicted ORF in Assemblies 19, 20 and 21
RPN1	Cd36_12340	orf19.4956	1	**1.5650133**	0.6461749	*RPN1*	Predicted ORF in Assemblies 19, 20 and 21
	Cd36_17880	orf19.5785	2	**1.5669088**	0.6479212		Predicted ORF in Assemblies 19, 20 and 21
	Cd36_54060	orf19.3928	5	**1.5696222**	0.6504173	*AZF1*	Putative transcription factor with zinc finger DNA-binding motif
	Cd36_50340	orf19.962	5	**1.5696495**	0.65044236	*CBF5*	Predicted ORF in Assemblies 19, 20 and 21
IFD3	Cd36_01150	orf19.3311	1	**1.5710155**	0.6516974	*YPL088W*	Transcription is regulated by Mig1p
	Cd36_32840	orf19.6151	R	**1.5712214**	0.65188646	*ARC15*	Predicted ORF in Assemblies 19, 20 and 21
	Cd36_26800	orf19.2575	R	**1.5718125**	0.6524291	*YLR063W*	Predicted ORF in Assemblies 19, 20 and 21
MEX67	Cd36_29340	orf19.488	R	**1.5721198**	0.65271115	*MEX67*	Nuclear export protein
	Cd36_25520	orf19.7495	R	**1.5721625**	0.6527504	*OYE3*	Predicted ORF in Assemblies 19, 20 and 21
	Cd36_32230	orf19.703	R	**1.5731884**	0.65369153	*CPD1*	Predicted ORF in Assemblies 19, 20 and 21
HXK1	Cd36_65510	orf19.2154	6	**1.5743968**	0.6547992	*HXK1*	N-acetylglucosamine (GlcNAc) kinase
	Cd36_52130	orf19.4240	5	**1.574966**	0.65532064	*PER1*	Predicted ORF in Assemblies 19, 20 and 21
	Cd36_01160	orf19.3312	1	**1.5753429**	0.6556659	*YER080W*	Predicted ORF in Assemblies 19, 20 and 21
	Cd36_33870	orf19.6392	R	**1.576166**	0.6564195		Predicted ORF in Assemblies 19, 20 and 21
	Cd36_32830	orf19.6152	R	**1.5764067**	0.6566398		Predicted ORF in Assemblies 19, 20 and 21
	Cd36_20030	orf19.6869	2	**1.5783585**	0.658425	*AST2*	Predicted ORF in Assemblies 19, 20 and 21
PHO15	Cd36_06770	orf19.4444	1	**1.5792419**	0.65923214	*PHO13*	Protein described as 4-nitrophenyl phosphatase
FOX2	Cd36_80740	orf19.1288	3	**1.5811098**	0.66093755	*FOX2*	Predicted 3-hydroxyacyl-CoA epimerase, required for fatty acid beta-oxidation
	Cd36_54470	orf19.3973	5	**1.581878**	0.66163826	*HUA1*	Predicted ORF in Assemblies 19, 20 and 21
MSK1	Cd36_71690	orf19.6533	7	**1.582558**	0.6622584	*MSK1*	Predicted ORF in Assemblies 19, 20 and 21
ARC40	Cd36_31710	orf19.3873	R	**1.5826093**	0.6623051	*ARC40*	Protein similar to S. cerevisiae Arc40p, which is involved in actin filament organization in S. cerevisiae
MCT1	Cd36_31050	orf19.6643	R	**1.5841773**	0.6637337	*MCT1*	Putative malonyl-CoA acyl carrier protein acyltransferase
COX11	Cd36_43980	orf19.1416	4	**1.5855685**	0.6650002	*COX11*	Protein repressed during the mating process
	Cd36_34230	orf19.6438	R	**1.5857726**	0.6651859	*LCB1*	Predicted ORF in Assemblies 19, 20 and 21
RPD3	Cd36_27810	orf19.2834	R	**1.5864601**	0.6658113	*RPD3*	Histone deacetylase
	Cd36_09710	f19.4902; orf19.49	1	**1.5879165**	0.667135		
	Cd36_03600	orf19.4459	1	**1.5883886**	0.6675639	*YNL234W*	Predicted ORF in Assemblies 19, 20 and 21
	Cd36_42910	orf19.2686	4	**1.5901039**	0.669121	*CPS1*	Predicted ORF in Assemblies 19, 20 and 21
DBP8	Cd36_30970	orf19.6652	R	**1.5904132**	0.66940165	*DBP8*	Protein likely to be essential for growth, based on insertional mutagenesis
	Cd36_25940		R	**1.5914638**	0.67035437		
RPN10	Cd36_20550	orf19.4102	2	**1.5916308**	0.67050576	*RPN10*	Predicted ORF in Assemblies 19, 20 and 21
	Cd36_41510	orf19.4633	4	**1.5925441**	0.6713333	*YMR226C*	Predicted ORF in Assemblies 19, 20 and 21
ADA2	Cd36_10190	orf19.2331	1	**1.5929288**	0.6716817	*ADA2*	Putative transcriptional coactivator
	Cd36_03280	orf19.3051	1	**1.5935229**	0.67221975	*YJR116W*	Predicted ORF in Assemblies 19, 20 and 21
ALS9	Cd36_64220	orf19.5742	6	**1.5959616**	0.67442596	*FLO1*	ALS family protein
	Cd36_83150	orf19.318	3	**1.596043**	0.6744995	*IBA57*	Predicted ORF in Assemblies 19, 20 and 21
	Cd36_60190	orf19.1182	6	**1.5971214**	0.675474	*VAM7*	Predicted ORF in Assemblies 19, 20 and 21
	Cd36_31730	orf19.3876	R	**1.5984671**	0.676689		Predicted zinc-finger protein of unknown function
FGR2	Cd36_70160	orf19.7071	7	**1.5994333**	0.6775608		Protein similar to phosphate transporters
	Cd36_43610	orf19.5043	4	**1.5995739**	0.67768764		Predicted ORF in Assemblies 19, 20 and 21
	Cd36_54940	orf19.4029	5	**1.600082**	0.6781459	*SQT1*	Predicted ORF in Assemblies 19, 20 and 21
	Cd36_09380	orf19.4864	1	**1.6001333**	0.67819214	*YJU3*	Predicted ORF in Assemblies 19, 20 and 21
	Cd36_16950	orf19.1533	2	**1.6013817**	0.67931724	*YKL077W*	Predicted ORF in Assemblies 19, 20 and 21
	Cd36_80020		3	**1.6015469**	0.679466		
	Cd36_60290	orf19.1195	6	**1.6021591**	0.6800175	*35703*	Predicted ORF in Assemblies 19, 20 and 21
	Cd36_04350	orf19.6853	1	**1.6022751**	0.6801219		Predicted ORF in Assemblies 19, 20 and 21
	Cd36_33410	orf19.3704	R	**1.6027428**	0.68054295	*DBP6*	Predicted ORF in Assemblies 19, 20 and 21
	Cd36_25260	orf19.7512	R	**1.6027901**	0.6805855	*DIT2*	Predicted ORF in Assemblies 19, 20 and 21
	Cd36_54010	orf19.3921	5	**1.6029879**	0.6807635	*FSH3*	Predicted ORF in Assemblies 19, 20 and 21
	Cd36_33610	orf19.603	R	**1.6030557**	0.6808245	*IMP4*	Predicted ORF in Assemblies 19, 20 and 21
	Cd36_29110	orf19.4357	R	**1.6033113**	0.6810546	*YMR115W*	Predicted ORF in Assemblies 19, 20 and 21
	Cd36_85280	orf19.6966	3	**1.6037995**	0.68149376	*CKI1*	Predicted ORF in Assemblies 19, 20 and 21
	Cd36_04960	orf19.444	1	**1.6038675**	0.68155503	*PUB1*	Predicted ORF in Assemblies 19, 20 and 21
	Cd36_28480	orf19.2391	R	**1.6042655**	0.6819129	*YKR023W*	Predicted ORF in Assemblies 19, 20 and 21
	Cd36_33690	orf19.590	R	**1.6046301**	0.6822407		Predicted ORF in Assemblies 19, 20 and 21
	Cd36_25790	orf19.3286	R	**1.605395**	0.6829283	*GTB1*	Predicted ORF in Assemblies 19, 20 and 21
	Cd36_19350	orf19.185	2	**1.6069741**	0.6843467	*MRP51*	Predicted ORF in Assemblies 19, 20 and 21
	Cd36_54440	orf19.3970	5	**1.6069999**	0.6843698	*YGR251W*	Predicted ORF in Assemblies 19, 20 and 21
	Cd36_73030	orf19.1336.2	7	**1.6074541**	0.6847775	*YBL059C-A*	ORF Predicted by Annotation Working Group
	Cd36_26440	orf19.2529	R	**1.6074941**	0.6848135		Predicted ORF in Assemblies 19, 20 and 21
	Cd36_25160	orf19.7521	R	**1.6084734**	0.6856921		Predicted ORF in Assemblies 19, 20 and 21
MRPS9	Cd36_11560	orf19.5230	1	**1.6098969**	0.6869683	*MRPS9*	Mitochondrial ribosomal protein S9
	Cd36_00560	orf19.6043	1	**1.6100215**	0.6870799	*DLD1*	Predicted ORF in Assemblies 19, 20 and 21
	Cd36_28150	orf19.2423	R	**1.6109471**	0.6879091	*YBR239C*	Putative DNA-binding transcription factor

Gene Name	*C. dubliniensis* Cd36 identifier	*C. albicans* orf19 identifier	C'some	Fold change expression	Normalised Expression	*S. cerevisiae* ortholog	Description
	Cd36_33890	orf19.6396	R	**1.6109953**	0.6879523	*NTE1*	Putative patatin-like phospholipase
	Cd36_35190	orf19.7596	R	**1.6112016**	0.68813705	*PMU1*	Predicted ORF in Assemblies 19, 20 and 21
	Cd36_08810	orf19.4795	1	**1.6123147**	0.6891334		Predicted ORF in Assemblies 19, 20 and 21
POR1	Cd36_03860	orf19.1042	1	**1.6125265**	0.68932295	*POR1*	Protein described as similar to mitochondrial outer membrane porin
	Cd36_12630	orf19.5003	1	**1.6128494**	0.6896117	*YRB30*	Predicted ORF in Assemblies 19, 20 and 21
AMS1	Cd36_42240	orf19.2768	4	**1.6134758**	0.69017196	*AMS1*	Putative alpha-mannosidase
CHO2	Cd36_27490	orf19.169	R	**1.6135638**	0.69025064	*CHO2*	Putative phosphatidyl-ethanolamine N-methyltransferase
	Cd36_20840	orf19.25	2	**1.6151197**	0.6916411	*TRM10*	Predicted ORF in Assemblies 19, 20 and 21
	Cd36_25410		R	**1.615567**	0.69204056		
	Cd36_26050	orf19.3250	R	**1.615718**	0.6921754	*PRP40*	Predicted ORF in Assemblies 19, 20 and 21
	Cd36_27980	orf19.2848	R	**1.6171972**	0.6934956	*ATG13*	Predicted ORF in Assemblies 19, 20 and 21
	Cd36_87450	orf19.6732	3	**1.6172209**	0.69351673	*YCR015C*	Predicted ORF in Assemblies 19, 20 and 21
	Cd36_30480	orf19.643	R	**1.6175234**	0.6937866	*INO80*	Predicted ORF in Assemblies 19, 20 and 21
	Cd36_30580	orf19.556	R	**1.6175994**	0.69385433		Predicted ORF in Assemblies 19, 20 and 21
SSU72	Cd36_28340	orf19.2402	R	**1.6176956**	0.69394016	*SSU72*	Predicted ORF in Assemblies 19, 20 and 21
	Cd36_54520	orf19.3980	5	**1.6190786**	0.695173	*SLH1*	Predicted ORF in Assemblies 19, 20 and 21
	Cd36_09700	orf19.4900	1	**1.6196827**	0.69571114	*MNT4/MNT2*	Predicted ORF in Assemblies 19, 20 and 21
	Cd36_25150	orf19.7522	R	**1.6197983**	0.69581413	*BNA3*	Predicted ORF in Assemblies 19, 20 and 21
	Cd36_41720	orf19.4610	4	**1.621369**	0.69721246	*CPS1*	Predicted ORF in Assemblies 19, 20 and 21
	Cd36_83380	orf19.338	3	**1.6213806**	0.6972227	*YMR196W*	Predicted ORF in Assemblies 19, 20 and 21
EBP1	Cd36_61290	orf19.125	6	**1.6220556**	0.6978233	*OYE2*	NADPH oxidoreductase
	Cd36_71170	orf19.6915	7	**1.6223167**	0.6980555	*MRE11*	Predicted ORF in Assemblies 19, 20 and 21
	Cd36_32940	orf19.6137	R	**1.6230861**	0.6987395		Predicted ORF in Assemblies 19, 20 and 21
	Cd36_03990	orf19.1058	1	**1.62395**	0.69950724	*RPN13*	Predicted ORF in Assemblies 19, 20 and 21
	Cd36_83680	orf19.6951	3	**1.6261729**	0.7014806	*DPL1*	Predicted ORF in Assemblies 19, 20 and 21
	Cd36_32430	orf19.1842	R	**1.6272573**	0.7024424	*BUD5*	Predicted ORF in Assemblies 19, 20 and 21
	Cd36_35210	orf19.7598	R	**1.6278181**	0.7029395	*AHC1*	Predicted ORF in Assemblies 19, 20 and 21
PTH2	Cd36_52060	orf19.4231	5	**1.62829**	0.7033577	*YEL007W*	Predicted ORF in Assemblies 19, 20 and 21
	Cd36_52520	orf19.4294	5	**1.6302898**	0.70512843	*CYC2*	Predicted ORF in Assemblies 19, 20 and 21
CRZ2	Cd36_32610	orf19.2356	R	**1.630588**	0.70539236	*CRZ1*	Putative transcription factor
	Cd36_54500	orf19.3977	5	**1.6306845**	0.7054777	*RBG2*	Predicted ORF in Assemblies 19, 20 and 21
CDC28	Cd36_31500	orf19.3856	R	**1.6313223**	0.7060418	*CDC28*	Cyclin-dependent protein kinase, interacts with regulatory subunit Cyb1p
RAD51	Cd36_27150	orf19.3752	R	**1.6341338**	0.70852613	*RAD51*	Predicted ORF in Assemblies 19, 20 and 21
CDC45	Cd36_33370	orf19.1988	R	**1.6350193**	0.7093077	*CDC45*	Protein described as a DNA replication initiation factor
	Cd36_34170	orf19.6431	R	**1.6357604**	0.7099614		Predicted ORF in Assemblies 19, 20 and 21
SUL2	Cd36_42530	orf19.2738	4	**1.6358974**	0.7100823	*SUL1*	Protein described as a sulfate transporter
ALG6	Cd36_32420	orf19.1843	R	**1.6369641**	0.7110226	*ALG6*	Putative glucosyltransferase involved in cell wall mannan biosynthesis
GCD1	Cd36_29270	orf19.481	R	**1.637391**	0.71139884	*GCD1*	Putative translation initiation factor
	Cd36_15950	orf19.2019	2	**1.6375184**	0.71151114	*MRPL16*	Predicted ORF in Assemblies 19, 20 and 21
FAA2-1	Cd36_20470	orf19.4114	2	**1.6377949**	0.7117547	*FAA2*	Predicted long chain fatty acid CoA ligase
	Cd36_25810	orf19.3283	R	**1.6400051**	0.7137003	*OAR1*	Predicted ORF in Assemblies 19, 20 and 21
	Cd36_12430	orf19.4966	1	**1.6402582**	0.713923	*AGC1*	Protein not essential for viability
	Cd36_54330	orf19.3956	5	**1.6414875**	0.7150037	*YMR293C*	Predicted ORF in Assemblies 19, 20 and 21
	Cd36_83710	orf19.6947	3	**1.6422606**	0.715683	*GTT1*	Predicted ORF in Assemblies 19, 20 and 21
	Cd36_54830	orf19.4016	5	**1.6428218**	0.71617603	*COR1*	Predicted ORF in Assemblies 19, 20 and 21
	Cd36_25880	orf19.3273	R	**1.6433991**	0.7166829	*YIH1*	Predicted ORF in Assemblies 19, 20 and 21
	Cd36_35075	orf19.7576	R	**1.6435689**	0.7168319		Protein not essential for viability
	Cd36_32560	orf19.2363	R	**1.644388**	0.71755075	*YOR286W*	Predicted ORF in Assemblies 19, 20 and 21
RBT7	Cd36_42950	orf19.2681	4	**1.6455629**	0.7185812	*RNY1*	Protein with similarity to RNase T2 enzymes, has putative secretion signal
	Cd36_30920	orf19.5845	R	**1.645834**	0.7188188	*RNR1*	Protein described as large subunit of ribonucleotide reductase
	Cd36_28180	orf19.2419	R	**1.6461679**	0.71911144	*DOM34*	Predicted ORF in Assemblies 19, 20 and 21
KTI12	Cd36_28520	orf19.2385	R	**1.6479445**	0.7206676	*KTI12*	Protein similar to S. cerevisiae Kti12p, which associates with Elongator complex
	Cd36_29660	orf19.520	R	**1.648411**	0.721076	*MTL1*	Predicted ORF in Assemblies 19, 20 and 21
	Cd36_71190	orf19.6917	7	**1.6487684**	0.7213888	*ZIM17*	Predicted ORF in Assemblies 19, 20 and 21
	Cd36_73510	orf19.7267	7	**1.6500894**	0.7225442		Predicted ORF in Assemblies 19, 20 and 21
	Cd36_10590	orf19.673	1	**1.6501647**	0.72261	*OYE3*	Predicted ORF in Assemblies 19, 20 and 21
MAL2	Cd36_35540	orf19.7668	R	**1.650753**	0.72312427	*YGR287C*	Alpha-glucosidase that hydrolyzes sucrose
RBR2	Cd36_29770	orf19.532	R	**1.6507598**	0.7231302	*TIP1*	Cell wall protein
	Cd36_13290	orf19.7244	1	**1.6509533**	0.72329926	*YNL168C*	Predicted ORF in Assemblies 19, 20 and 21
	Cd36_30820	orf19.3518	R	**1.6511489**	0.7234702	*ODC1*	Predicted ORF in Assemblies 19, 20 and 21
ECM4	Cd36_27050	orf19.2613	R	**1.6512111**	0.7235246	*ECM4*	Protein similar to S. cerevisiae Ecm4p
	Cd36_87430	orf19.6736	3	**1.6516134**	0.723876	*YOR205C*	Predicted ORF in Assemblies 19, 20 and 21
	Cd36_29940	orf19.549	R	**1.6521746**	0.7243662	*MRPL32*	Predicted ORF in Assemblies 19, 20 and 21
	Cd36_00980	orf19.3292	1	**1.6524597**	0.7246151	*YCL033C*	Predicted ORF in Assemblies 19, 20 and 21
	Cd36_09680	orf19.4898	1	**1.6525564**	0.7246995	*YER004W*	Predicted ORF in Assemblies 19, 20 and 21
	Cd36_80470	orf19.5412	3	**1.6537057**	0.7257025	*ECM9*	Predicted ORF in Assemblies 19, 20 and 21
	Cd36_28020	orf19.2852	R	**1.6556492**	0.72739697	*MRP21*	Predicted ORF in Assemblies 19, 20 and 21
	Cd36_00930		1	**1.6561215**	0.7278085		
UGP1	Cd36_30070	orf19.1738	R	**1.6562594**	0.72792864	*UGP1*	Protein similar to UTP-glucose-1-phosphaturidyl transferase
ADH5	Cd36_27000	orf19.2608	R	**1.656269**	0.727937	*ADH5*	Putative alcohol dehydrogenase
HHF22	Cd36_32340	orf19.1854	R	**1.6580698**	0.7295048	*HHF2/HHF1*	Putative histone H4
QDR1	Cd36_29520	orf19.508	R	**1.6600105**	0.73119235	*QDR1*	Putative transporter of antibiotic resistance
	Cd36_73360	orf19.6690	7	**1.6600474**	0.7312244		Predicted ORF in Assemblies 19, 20 and 21

Gene Name	*C. dubliniensis* Cd36 identifier	*C. albicans* orf19 identifier	C'some	Fold change expression	Normalised Expression	*S. cerevisiae* ortholog	Description
	Cd36_70120	orf19.7065	7	**1.6601057**	0.7312751	*PSF3*	Predicted ORF in Assemblies 19, 20 and 21
	Cd36_26390	orf19.2521	R	**1.6625249**	0.733376		Predicted ORF in Assemblies 19, 20 and 21
	Cd36_20530	orf19.4105	2	**1.662579**	0.733423	*CSM3*	Predicted ORF in Assemblies 19, 20 and 21
AYR2	Cd36_63750	orf19.5615	6	**1.6628696**	0.733675	*AYR1*	Predicted ORF in Assemblies 19, 20 and 21
	Cd36_62760	orf19.5522	6	**1.6629322**	0.73372936		Predicted ORF in Assemblies 19, 20 and 21
	Cd36_54000	orf19.3920	5	**1.6634052**	0.7341397	*MPD1*	Predicted ORF in Assemblies 19, 20 and 21
	Cd36_33290	orf19.6284	R	**1.6641085**	0.73474956	*SRP102*	Predicted ORF in Assemblies 19, 20 and 21
GTT1	Cd36_85600	orf19.6998	3	**1.6649481**	0.7354772	*GTT1*	Protein described as glutathione S-transferase
	Cd36_42640	orf19.2721	4	**1.6661222**	0.7364942	*CDC123*	Predicted ORF in Assemblies 19, 20 and 21
ACH1	Cd36_51850	orf19.3171	5	**1.6663244**	0.7366693	*ACH1*	Soluble protein in hyphae
	Cd36_80220	orf19.5444	3	**1.6664029**	0.73673725	*TIM44*	Predicted ORF in Assemblies 19, 20 and 21
	Cd36_33770	orf19.6374	R	**1.6679031**	0.73803544	*ATP10*	Predicted ORF in Assemblies 19, 20 and 21
YHM1	Cd36_62060	orf19.685	6	**1.6682211**	0.7383106	*GGC1*	Putative mitochondrial carrier protein
YVH1	Cd36_28620	orf19.4401	R	**1.6684244**	0.7384863	*YVH1*	Putative dual specificity phosphatase (phosphoserine/threonine and phosphotyrosine phosphatase)
	Cd36_32360	orf19.1852	R	**1.6694609**	0.73938227	*YIL087C*	Predicted ORF in Assemblies 19, 20 and 21
	Cd36_32490	orf19.2369	R	**1.6712035**	0.7408874	*ORC5*	Predicted ORF in Assemblies 19, 20 and 21
	Cd36_43560	orf19.5037	4	**1.6724476**	0.741961		Protein not essential for viability
	Cd36_07380	orf19.5057	1	**1.6730912**	0.74251604		Predicted ORF in Assemblies 19, 20 and 21
LPD1	Cd36_33030	orf19.6127	R	**1.6731138**	0.7425356	*LPD1*	Putative dihydrolipoamide dehydrogenase
DPS1-1	Cd36_28310	orf19.2407	R	**1.673402**	0.742784	*DPS1*	Putative tRNA-Asp synthetase
	Cd36_51150	orf19.1950	5	**1.6734324**	0.74281025	*POA1*	Predicted ORF in Assemblies 19, 20 and 21
	Cd36_40840	orf19.4162	4	**1.6736845**	0.74302757	*MLH1*	Predicted ORF in Assemblies 19, 20 and 21
	Cd36_86510	orf19.7443	3	**1.67384**	0.7431617		Predicted ORF in Assemblies 19, 20 and 21
	Cd36_29810	orf19.537	R	**1.6743591**	0.74360895	*YBR197C*	Predicted ORF in Assemblies 19, 20 and 21
	Cd36_54740	orf19.4006	5	**1.6760744**	0.7450862	*PAN5*	Predicted ORF in Assemblies 19, 20 and 21
	Cd36_25310	orf19.7507	R	**1.6772745**	0.7461188		Predicted ORF in Assemblies 19, 20 and 21
BTS1	Cd36_53370	orf19.6674	5	**1.6786171**	0.7472732	*BTS1*	Decreased transcription is observed upon benomyl treatment
	Cd36_33230	orf19.6291	R	**1.6786207**	0.7472763	*FUN30*	Predicted ORF in Assemblies 19, 20 and 21
	Cd36_30560	orf19.652	R	**1.6788557**	0.74747825	*YEN1*	Predicted ORF in Assemblies 19, 20 and 21
	Cd36_50620	orf19.927	5	**1.678972**	0.74757814	*CGI121*	Predicted ORF in Assemblies 19, 20 and 21
THI6	Cd36_82850	orf19.277	3	**1.6794811**	0.74801564	*THI6*	Putative thiamin-phosphate pyrophosphorylase, hydroxyethylthiazole kinase
ATS1	Cd36_33910	orf19.6399	R	**1.6810043**	0.74932337	*ATS1*	Induced upon adherence to polystyrene
	Cd36_19790	orf19.3559	2	**1.6810415**	0.7493553	*MRPS35*	Predicted ORF in Assemblies 19, 20 and 21
	Cd36_27740	orf19.2830	R	**1.6812927**	0.74957085	*RRP9*	Predicted ORF in Assemblies 19, 20 and 21
GND1	Cd36_12850	orf19.5024	1	**1.6818106**	0.75001526	*GND1*	Putative 6-phosphogluconate dehydrogenase
	Cd36_23390	orf19.4088	2	**1.6819457**	0.75013113	*GLO2*	Predicted ORF in Assemblies 19, 20 and 21
ERG25	Cd36_27330	orf19.3732	R	**1.681966**	0.75014853	*ERG25*	Putative C-4 methyl sterol oxidase with role in C4-demethylation of ergosterol biosynthesis intermediates, based on similarity to S. cerevisiae Erg25p
	Cd36_73040	orf19.8916	7	**1.6826277**	0.750716		
	Cd36_34020	orf19.6411	R	**1.6826352**	0.7507224	*VAC14*	Predicted ORF in Assemblies 19, 20 and 21
	Cd36_53510	orf19.1116	5	**1.6831917**	0.7511995		Predicted ORF in Assemblies 19, 20 and 21
CDG1	Cd36_34565	orf19.7314	R	**1.6833814**	0.7513621		Protein described as similar to cysteine dioxygenases
	Cd36_34210	orf19.6436	R	**1.6847501**	0.7525346		Predicted ORF in Assemblies 19, 20 and 21
	Cd36_64040			**1.6855327**	0.7532046		
YCP4	Cd36_30710	orf19.5286	R	**1.685626**	0.75328445	*YCP4*	Putative flavodoxin
	Cd36_26160	orf19.3237	R	**1.6857613**	0.7534003	*UFD4*	Predicted ORF in Assemblies 19, 20 and 21
IPP1	Cd36_22980	orf19.3590	2	**1.687632**	0.75500035	*IPP1*	Protein described as inorganic pyrophosphatase
	Cd36_26420	orf19.2527	R	**1.6879746**	0.75529313	*YNL035C*	Predicted ORF in Assemblies 19, 20 and 21
	Cd36_01450	orf19.3348	1	**1.6883501**	0.75561404	*MRPL23*	Predicted ORF in Assemblies 19, 20 and 21
DUR4	Cd36_40540	orf19.5677	4	**1.6899451**	0.7569764	*DUR3*	Putative urea permease
	Cd36_40860	orf19.4160	4	**1.6900738**	0.7570863	*QRI7*	Predicted ORF in Assemblies 19, 20 and 21
DLD1	Cd36_17750	orf19.5805	2	**1.6901306**	0.7571347	*DLD1*	Transcription is specific to white cell type
	Cd36_63070	orf19.5575	6	**1.6905779**	0.7575165	*PEX25*	Predicted ORF in Assemblies 19, 20 and 21
SPR28	Cd36_52310	orf19.4266	5	**1.6907086**	0.7576281	*SPR28*	Septin
	Cd36_83220	orf19.326	3	**1.6915853**	0.7583759		Predicted ORF in Assemblies 19, 20 and 21
PHO81	Cd36_25690	orf19.7475	R	**1.6917533**	0.7585192	*PHO81*	Predicted ORF in Assemblies 19, 20 and 21
	Cd36_40850	orf19.4161	4	**1.6918414**	0.7585943	*NSE4*	Predicted ORF in Assemblies 19, 20 and 21
	Cd36_03250	orf19.3048	1	**1.6925595**	0.75920653	*SCD5*	Predicted ORF in Assemblies 19, 20 and 21
CYP1	Cd36_72170	orf19.6472	7	**1.6934232**	0.75994253	*CPR1*	Peptidyl-propyl cis-trans isomerase (PPIase)
	Cd36_26570	orf19.2549	R	**1.694861**	0.76116705	*SHP1*	Predicted ORF in Assemblies 19, 20 and 21
HYR4	Cd36_25840	orf19.3279	R	**1.6950111**	0.7612947	*DAN4*	Putative GPI-anchored protein of unknown function
YIM1	Cd36_18420	orf19.847	2	**1.695824**	0.7619865	*YIM1*	Protein similar to protease of mitochondrial inner membrane
	Cd36_85480	orf19.6986	3	**1.6959342**	0.7620802	*MSB3*	Predicted ORF in Assemblies 19, 20 and 21
	Cd36_32280	orf19.708	R	**1.6969842**	0.76297307	*SPC97*	Predicted ORF in Assemblies 19, 20 and 21
HWP2	Cd36_43420	orf19.3380	4	**1.6977774**	0.7636473	*MUC1*	Putative GPI-anchored protein
	Cd36_50380	orf19.954	5	**1.6979247**	0.7637725	*YDJ1*	Predicted ORF in Assemblies 19, 20 and 21
INO2	Cd36_25070	orf19.7539	R	**1.7009882**	0.76637316		Transcriptional activator that may be involved in regulation of ribosomal protein genes
MCM6	Cd36_27030	orf19.2611	R	**1.7011058**	0.76647294	*MCM6*	Protein described as part of MCM DNA replication initiation complex
PHB1	Cd36_83720	orf19.6944	3	**1.7013739**	0.76670027	*PHB1*	Protein described as prohibitin
	Cd36_34140	orf19.6423	R	**1.701661**	0.7669437	*FBP26*	Predicted ORF in Assemblies 19, 20 and 21
	Cd36_83600	orf19.357	3	**1.7016962**	0.7669735	*PHB1*	Predicted ORF in Assemblies 19, 20 and 21

Gene Name	*C. dubliniensis* Cd36 identifier	*C. albicans* orf19 identifier	C'some	Fold change expression	Normalised Expression	*S. cerevisiae* ortholog	Description
UBP6	Cd36_00370	orf19.6063	1	**1.702046**	0.7672701	*UBP6*	Predicted ORF in Assemblies 19, 20 and 21
	Cd36_04740	orf19.55	1	**1.7020816**	0.7673001	*IZH2|IZH1*	Predicted ORF in Assemblies 19, 20 and 21
	Cd36_34090	orf19.6418	R	**1.7023338**	0.767514	*YDL063C*	Predicted ORF in Assemblies 19, 20 and 21
	Cd36_31250	orf19.6626	R	**1.7023556**	0.76753247		Predicted ORF in Assemblies 19, 20 and 21
PRP22	Cd36_54970	orf19.4033	5	**1.705908**	0.77053976	*PRP22*	Protein described as an RNA-dependent ATPase
	Cd36_33310	orf19.6283	R	**1.7064476**	0.7709961	*NFU1*	Predicted ORF in Assemblies 19, 20 and 21
	Cd36_26200	orf19.3233	R	**1.7081504**	0.77243495	*HSE1*	Predicted ORF in Assemblies 19, 20 and 21
CCP1	Cd36_82440	orf19.238	3	**1.7093259**	0.7734275	*CCP1*	Similar to cytochrome-c peroxidase N terminus
PUP1	Cd36_35260	orf19.7605	R	**1.7100501**	0.77403855	*PUP1*	Predicted ORF in Assemblies 19, 20 and 21
AUR1	Cd36_51090	orf19.1945	5	**1.7102951**	0.77424526	*AUR1*	Inositolphosphorylceramide (IPC) synthase, catalyzes the key step in the synthesis of sphingolipids
ASH2	Cd36_54390	orf19.3964	5	**1.7113924**	0.77517056	*BRE2*	Predicted ORF in Assemblies 19, 20 and 21
	Cd36_35245	orf19.7603	R	**1.7130692**	0.77658343	*YMR244C-A*	Predicted ORF in Assemblies 19, 20 and 21
	Cd36_35230	orf19.7601	R	**1.7133385**	0.77681017	*MRM2*	Predicted ORF in Assemblies 19, 20 and 21
	Cd36_20750	orf19.5500	2	**1.71342**	0.77687883	*MAK16*	Predicted ORF in Assemblies 19, 20 and 21
	Cd36_08400	orf19.4749	1	**1.713563**	0.77699924		Predicted ORF in Assemblies 19, 20 and 21
IFF6	Cd36_23280	orf19.4072	2	**1.7145828**	0.77785754	*YBL113C*	Putative GPI-anchored protein of unknown function
	Cd36_60920	orf19.91	6	**1.715294**	0.77845585	*YGR053C*	Predicted ORF in Assemblies 19, 20 and 21
	Cd36_10810	orf19.1168	1	**1.7153134**	0.7784722		Predicted zinc-finger protein of unknown function
	Cd36_29730	orf19.528	R	**1.716006**	0.77905464	*SEC26*	Predicted ORF in Assemblies 19, 20 and 21
	Cd36_05740	orf19.2438	1	**1.7161669**	0.7791898	*YNR036C*	Predicted ORF in Assemblies 19, 20 and 21
	Cd36_21240	orf19.2249	2	**1.7170109**	0.7798991	*ATP23*	Predicted ORF in Assemblies 19, 20 and 21
	Cd36_41270	orf19.4659	4	**1.7174512**	0.78026915	*PRP21*	Predicted ORF in Assemblies 19, 20 and 21
	Cd36_18320	orf19.860	2	**1.717834**	0.78059065		Predicted ORF in Assemblies 19, 20 and 21
	Cd36_54290	orf19.3952	5	**1.7184602**	0.7811165	*SRP101*	Predicted ORF in Assemblies 19, 20 and 21
	Cd36_45700	orf19.2921	4	**1.7214341**	0.78361094	*PAC2*	Predicted ORF in Assemblies 19, 20 and 21
	Cd36_32090	orf19.916	R	**1.7219367**	0.7840321	*YNL305C*	Predicted ORF in Assemblies 19, 20 and 21
HHT2	Cd36_32350	orf19.1853	R	**1.7251436**	0.78671646	*HHT2|HHT1*	Protein described as histone H3
POT1-2	Cd36_15720	orf19.2046	2	**1.7255895**	0.78708935	*POT1*	Putative peroxisomal 3-ketoacyl CoA thiolase
HGT18	Cd36_28130	orf19.2425	R	**1.7277733**	0.78891397	*YBR241C*	Putative glucose transporter of the major facilitator superfamily
	Cd36_34300	orf19.6448	R	**1.7279341**	0.7890482		Predicted ORF in Assemblies 19, 20 and 21
PRB1	Cd36_21180	orf19.2242	2	**1.7283894**	0.78942823	*PRB1*	Putative endoprotease B
OSM2	Cd36_12650	orf19.5005	1	**1.7290907**	0.79001355	*OSM1*	Protein described as mitochondrial fumarate reductase
CPR6	Cd36_35470	orf19.7654	R	**1.7299582**	0.79073715	*CPR6*	Predicted ORF in Assemblies 19, 20 and 21
	Cd36_25780	orf19.3287	R	**1.730178**	0.7909205	*BUD22*	Predicted ORF in Assemblies 19, 20 and 21
HGT10	Cd36_64300	orf19.5753	6	**1.730875**	0.7915015	*STL1*	Putative glucose transporter of the major facilitator superfamily
	Cd36_29880	orf19.542.2	R	**1.731313**	0.79186654	*MIM1*	ORF Predicted by Annotation Working Group
	Cd36_28750	orf19.4388	R	**1.7317156**	0.792202	*TAF3*	Predicted ORF in Assemblies 19, 20 and 21
	Cd36_27500	orf19.168	R	**1.7320173**	0.7924533	*MTR3*	Predicted ORF in Assemblies 19, 20 and 21
ERG27	Cd36_26140	orf19.3240	R	**1.7327402**	0.7930553	*ERG27*	3-Keto sterol reductase of ergosterol biosynthesis
	Cd36_81730	orf19.1662	3	**1.73428**	0.7943368	*MRP1*	Predicted ORF in Assemblies 19, 20 and 21
	Cd36_31260	orf19.6625	R	**1.7355084**	0.7953584	*VPS75*	Predicted ORF in Assemblies 19, 20 and 21
LAG1	Cd36_26060	orf19.3249	R	**1.7358963**	0.79568076	*LAG1*	Predicted ORF in Assemblies 19, 20 and 21
EHT1	Cd36_03190	orf19.3040	1	**1.7373105**	0.7968557	*EHT1*	Protein similar to S. cerevisiae Eht1p
	Cd36_33580	orf19.606	R	**1.7380986**	0.7975099	*YLR352W*	Predicted ORF in Assemblies 19, 20 and 21
DUR1,2	Cd36_04410	orf19.780	1	**1.7381191**	0.79752696	*DUR1,2*	Transcription is regulated by Nrg1p
	Cd36_33920	orf19.6400	R	**1.7399626**	0.7990563	*OPI10*	Predicted ORF in Assemblies 19, 20 and 21
SOU2	Cd36_45870	orf19.2897	4	**1.7412809**	0.80014896	*SPS19*	Protein similar to Sou1p
SGT2	Cd36_17540	orf19.5823	2	**1.741415**	0.80026007	*SGT2*	Protein abundance is affected by URA3 expression in the CAI-4 strain background
	Cd36_26490	orf19.2538	R	**1.7423811**	0.8010602	*PTC2*	Predicted ORF in Assemblies 19, 20 and 21
KSR1	Cd36_33010	orf19.6131	R	**1.7434696**	0.8019612	*TSC10*	3-ketosphinganine reductase, catalyzes the second step in phytosphingosine synthesis
EMP46	Cd36_32800	orf19.731	R	**1.7445631**	0.80286574	*EMP47*	Protein similar to S. cerevisiae Emp46p
	Cd36_29720	orf19.527	R	**1.7456428**	0.8037584		Predicted ORF in Assemblies 19, 20 and 21
IFC3	Cd36_27190	orf19.3749	R	**1.7456899**	0.80379725	*OPT2*	Oligopeptide transporter
RSR1	Cd36_27060	orf19.2614	R	**1.7474953**	0.80528855	*RSR1*	RAS-related protein
POL2	Cd36_32530	orf19.2365	R	**1.7479441**	0.80565906	*POL2*	Protein described as DNA polymerase epsilon
MGE1	Cd36_26400	orf19.2524	R	**1.7481203**	0.8058045	*MGE1*	Predicted ORF in Assemblies 19, 20 and 21
PNC1	Cd36_73170	orf19.6684	7	**1.7495315**	0.8069687	*PNC1*	Predicted ORF in Assemblies 19, 20 and 21
DBR1	Cd36_62180	orf19.3506	6	**1.7502369**	0.8075502	*DBR1*	Debranchase
	Cd36_71720	orf19.6530	7	**1.7504721**	0.807744	*SEC63*	Similar to bacterial DnaJ
	Cd36_84270	orf19.5876	3	**1.7552981**	0.8117161		Predicted ORF in Assemblies 19, 20 and 21
	Cd36_28500	orf19.2387	R	**1.7557296**	0.8120706	*YMR098C*	Putative tRNA-Pro synthetase
	Cd36_28400	orf19.2397.3	R	**1.7559981**	0.81229126	*YGR127W*	ORF Predicted by Annotation Working Group
	Cd36_85980	orf19.7386	3	**1.7567215**	0.8128855	*MBA1*	Predicted ORF in Assemblies 19, 20 and 21
ECM42	Cd36_71970	orf19.6500	7	**1.7574158**	0.8134556	*ECM40*	Putative ornithine acetyltransferase
	Cd36_30900	orf19.5847	R	**1.7590595**	0.8148043	*RET1*	Predicted ORF in Assemblies 19, 20 and 21
	Cd36_43490	orf19.1303	4	**1.7600284**	0.8155987	*MRF1*	Predicted ORF in Assemblies 19, 20 and 21
	Cd36_32380	orf19.1849	R	**1.7601453**	0.8156946	*YIL091C*	Predicted ORF in Assemblies 19, 20 and 21
	Cd36_60750	orf19.3644	6	**1.7602012**	0.81574035		Predicted ORF in Assemblies 19, 20 and 21
	Cd36_05380		1	**1.761391**	0.81671524		
PRO3	Cd36_40310	orf19.5650	4	**1.7633952**	0.8183558	*PRO3*	Protein induced during the mating process
	Cd36_29460	orf19.499	R	**1.7642258**	0.8190353	*MTQ1*	Predicted ORF in Assemblies 19, 20 and 21
IFF4	Cd36_25710	orf19.7472	R	**1.7646265**	0.8193629	*MUC1*	Putative GPI-anchored protein
	Cd36_33990	orf19.6406	R	**1.7655869**	0.82014775	*SWS2*	Predicted ORF in Assemblies 19, 20 and 21
	Cd36_00020		1	**1.766416**	0.8208251		

Gene Name	*C. dubliniensis* Cd36 identifier	*C. albicans* orf19 identifier	C'some	Fold change expression	Normalised Expression	*S. cerevisiae* ortholog	Description
	Cd36_43940	orf19.1421	4	**1.7670206**	0.82131886	*DAL3*	Predicted ORF in Assemblies 19, 20 and 21
GNP3	Cd36_35010	orf19.7565	R	**1.7688802**	0.8228364	*AGP1*	Putative high-affinity glutamine permease
	Cd36_31240	orf19.6627	R	**1.769053**	0.8229773		Predicted ORF in Assemblies 19, 20 and 21
MRP17	Cd36_50430	orf19.947	5	**1.7695841**	0.8234103	*MRP17*	Predicted mitochondrial ribosomal protein
	Cd36_25760	orf19.7464	R	**1.7702136**	0.8239234	*YCR045C*	Predicted ORF in Assemblies 19, 20 and 21
	Cd36_71430	orf19.6565	7	**1.7718252**	0.8252363	*OXA1*	Predicted ORF in Assemblies 19, 20 and 21
	Cd36_43740	orf19.5296	4	**1.7729234**	0.82613015	*COA1*	Predicted ORF in Assemblies 19, 20 and 21
IFR1	Cd36_24240	orf19.1763	2	**1.7742077**	0.8271749	*YNL134C*	Predicted ORF in Assemblies 19, 20 and 21
	Cd36_00830	orf19.6017	1	**1.7742121**	0.8271785	*SNF5*	Predicted ORF in Assemblies 19, 20 and 21
	Cd36_25890	orf19.3272	R	**1.7751485**	0.82793975	*STI1*	Predicted ORF in Assemblies 19, 20 and 21
ZRT2	Cd36_17380	orf19.1585	2	**1.7781318**	0.8303623	*ZRT2*	Protein described as predicted zinc transporter
	Cd36_50070	orf19.5698	5	**1.7782006**	0.8304181	*MRPL1*	Predicted ORF in Assemblies 19, 20 and 21
SFL1	Cd36_31370	orf19.454	R	**1.7791145**	0.83115935	*SFL1*	Protein involved in negative regulation of flocculation and filamentous growth
	Cd36_44770	orf19.8361	4	**1.7837315**	0.8348985		
	Cd36_29220	orf19.475	R	**1.7857176**	0.836504	*IPI1*	Predicted ORF in Assemblies 19, 20 and 21
	Cd36_82910	orf19.286	3	**1.7869563**	0.8375044		Decreased transcription is observed upon fluphenazine treatment
NCR1	Cd36_13270	orf19.7242	1	**1.7872871**	0.8377714	*NCR1*	Transcription is regulated by Nrg1p and Mig1p
CSH1	Cd36_03770	orf19.4477	1	**1.7876257**	0.83804464	*YPL088W*	Member of aldo-keto reductase family, similar to aryl alcohol dehydrogenases
	Cd36_26300	orf19.3225	R	**1.788621**	0.83884764	*CWH43*	Predicted ORF in Assemblies 19, 20 and 21
	Cd36_32320	orf19.1857	R	**1.790301**	0.8402021	*SPT10*	Protein not essential for viability
	Cd36_02780	orf19.2989	1	**1.792672**	0.8421116	*GOR1*	Predicted ORF in Assemblies 19, 20 and 21
	Cd36_54180	orf19.3939	5	**1.7940686**	0.843235	*YJR088C*	Predicted ORF in Assemblies 19, 20 and 21
	Cd36_33940	orf19.6403	R	**1.7956362**	0.84449506	*SIL1*	Predicted ORF in Assemblies 19, 20 and 21
	Cd36_52170	orf19.4246	5	**1.7957611**	0.84459543	*YKR070W*	Predicted ORF in Assemblies 19, 20 and 21
	Cd36_26560	orf19.2547	R	**1.7958771**	0.84468865		Predicted ORF in Assemblies 19, 20 and 21
	Cd36_32030	orf19.713	R	**1.7979484**	0.8463516	*YMR074C*	Predicted ORF in Assemblies 19, 20 and 21
	Cd36_28410	orf19.2397	R	**1.7979807**	0.8463775	*TNA1*	Predicted ORF in Assemblies 19, 20 and 21
MSW1	Cd36_52550	orf19.4299	5	**1.7983689**	0.846689	*MSW1*	Protein likely to be essential for growth, based on an insertional mutagenesis strategy
	Cd36_28220	orf19.2417	R	**1.7984259**	0.84673476	*SMC5*	Predicted ORF in Assemblies 19, 20 and 21
	Cd36_35240	orf19.7602	R	**1.7988924**	0.84710884	*AHA1*	Predicted ORF in Assemblies 19, 20 and 21
	Cd36_27310	orf19.3734	R	**1.7991486**	0.84731436	*GEF1*	Predicted ORF in Assemblies 19, 20 and 21
	Cd36_28530	orf19.2384	R	**1.79994**	0.8479488	*MTG1*	Predicted ORF in Assemblies 19, 20 and 21
	Cd36_52340	orf19.4270	5	**1.8014965**	0.84919584	*MNT4*	Predicted ORF in Assemblies 19, 20 and 21
	Cd36_28780	orf19.2376	R	**1.8015201**	0.8492148	*HNT3*	Predicted ORF in Assemblies 19, 20 and 21
ADE17	Cd36_29380	orf19.492	R	**1.8015606**	0.8492472	*ADE17*	Enzyme of adenine biosynthesis
	Cd36_33750	orf19.6371	R	**1.802454**	0.8499625		Predicted ORF in Assemblies 19, 20 and 21
	Cd36_17580	orf19.5826	2	**1.8026814**	0.8501445	*UGA4*	Predicted ORF in Assemblies 19, 20 and 21
	Cd36_54670	orf19.3999	5	**1.8034471**	0.8507571	*YML020W*	Predicted ORF in Assemblies 19, 20 and 21
	Cd36_44300		4	**1.8040502**	0.85123944		
SSC1	Cd36_21650	orf19.1896	2	**1.807238**	0.85378647	*SSC1*	Heat shock protein
	Cd36_84890	orf19.5961	3	**1.8081706**	0.8545308	*NAS6*	Predicted ORF in Assemblies 19, 20 and 21
	Cd36_73900	orf19.7149	7	**1.8093218**	0.85544896	*YMR258C*	Predicted ORF in Assemblies 19, 20 and 21
	Cd36_17300	orf19.1546	2	**1.8115864**	0.85725355		Predicted ORF in Assemblies 19, 20 and 21
CWT1	Cd36_30880	orf19.5849	R	**1.8122364**	0.85777116	*RDS2*	Putative transcription factor
GIT1	Cd36_51400	orf19.1979	5	**1.8123592**	0.8578689	*GIT1*	Putative glycerophosphoinositol permease
HSP70	Cd36_12490	orf19.4980	1	**1.8126404**	0.8580928	*SSA4*	Putative chaperone of Hsp70 family
FCY2	Cd36_83310	orf19.333	3	**1.8138961**	0.85909176	*FCY2*	Putative purine-cytosine permease of pyrimidine salvage
	Cd36_53960	orf19.3914	5	**1.8143835**	0.8594794	*CDC33*	Predicted ORF in Assemblies 19, 20 and 21
	Cd36_33320	orf19.6282	R	**1.8166614**	0.8612895	*NSR1*	Predicted ORF in Assemblies 19, 20 and 21
	Cd36_26690	orf19.2564	R	**1.8205266**	0.8643558	*TMA23*	Predicted ORF in Assemblies 19, 20 and 21
BRF1	Cd36_31000	orf19.6649	R	**1.8210883**	0.86480093	*BRF1*	Component of the general transcription factor for RNA polymerase III (TFIIIB)
	Cd36_32660	orf19.1815	R	**1.8214191**	0.86506295	*TIF6*	Predicted ORF in Assemblies 19, 20 and 21
	Cd36_87300	orf19.6752	3	**1.8232417**	0.86650586	*RSM10*	Predicted ORF in Assemblies 19, 20 and 21
	Cd36_34190	orf19.6434	R	**1.8234894**	0.86670184	*PEX19*	Predicted ORF in Assemblies 19, 20 and 21
	Cd36_42150	orf19.4563	4	**1.8244896**	0.8674929	*YMR310C*	Predicted ORF in Assemblies 19, 20 and 21
	Cd36_73290	orf19.6699	7	**1.8248243**	0.86775756	*HIS2*	Predicted ORF in Assemblies 19, 20 and 21
	Cd36_33220	orf19.6293	R	**1.8254936**	0.8682866	*EMP24*	Predicted ORF in Assemblies 19, 20 and 21
	Cd36_15800	orf19.2038	2	**1.825957**	0.8686527		Predicted ORF in Assemblies 19, 20 and 21
PIF1	Cd36_32990	orf19.6133	R	**1.826028**	0.86870885	*PIF1*	Decreased transcription is observed upon fluphenazine treatment
	Cd36_31770	orf19.3879	R	**1.8275371**	0.8699007		Predicted ORF in Assemblies 19, 20 and 21
PGI1	Cd36_31840	orf19.3888	R	**1.8289427**	0.8710098	*PGI1*	Protein described as glucose-6-phosphate isomerase, enzyme of glycolysis
	Cd36_25550	orf19.7491	R	**1.831964**	0.87339115	*RTT109*	Predicted ORF in Assemblies 19, 20 and 21
	Cd36_31360	orf19.457	R	**1.8332542**	0.8744068	*UBP2*	Predicted ORF in Assemblies 19, 20 and 21
	Cd36_10800	orf19.1169	1	**1.8336184**	0.8746934	*JID1*	Predicted ORF in Assemblies 19, 20 and 21
IDP2	Cd36_27320	orf19.3733	R	**1.8338377**	0.874866	*IDP2*	Putative isocitrate dehydrogenase
	Cd36_32860	orf19.6147	R	**1.8347735**	0.875602	*CHZ1*	Predicted ORF in Assemblies 19, 20 and 21
	Cd36_54550	orf19.3983	5	**1.8359394**	0.8765185	*YGR266W*	Predicted ORF in Assemblies 19, 20 and 21
	Cd36_30810	orf19.3517	R	**1.8399029**	0.8796296	*YOR223W*	Predicted ORF in Assemblies 19, 20 and 21
	Cd36_35566	orf19.7675	R	**1.840769**	0.8803086	*MRPL25*	ORF Predicted by Annotation Working Group
STI1	Cd36_51510	orf19.3192	5	**1.8438178**	0.88269615	*STI1*	Protein that interacts with Cdc37p and Crk1p in the two-hybrid system
ACF2	Cd36_61790	orf19.3417	6	**1.8448603**	0.88351154	*ACF2*	Putative endo-1,3-beta-glucanase

Gene Name	*C. dubliniensis* Cd36 identifier	*C. albicans* orf19 identifier	C'some	Fold change expression	Normalised Expression	*S. cerevisiae* ortholog	Description
GSL2	Cd36_25900	orf19.3269	R	**1.8475385**	0.8856044	*GSC2*	Protein similar to beta-1,3-glucan synthase
	Cd36_54730	orf19.4005	5	**1.8495806**	0.8871982	*YDR196C*	Protein likely to be essential for growth, based on an insertional mutagenesis strategy
	Cd36_84110		3	**1.8502078**	0.8876873		
	Cd36_40580	orf19.4190	4	**1.851843**	0.8889618	*PAM18*	Predicted ORF in Assemblies 19, 20 and 21
	Cd36_26530	orf19.2544	R	**1.8522528**	0.88928103	*PTH2*	Predicted ORF in Assemblies 19, 20 and 21
	Cd36_27280	orf19.3737	R	**1.8528608**	0.88975453	*MUK1*	Predicted ORF in Assemblies 19, 20 and 21
	Cd36_32580	orf19.2361	R	**1.8588098**	0.89437914	*SPT10*	Predicted ORF in Assemblies 19, 20 and 21
	Cd36_22060	orf19.2201	2	**1.8599397**	0.8952558	*CBP6*	Predicted ORF in Assemblies 19, 20 and 21
	Cd36_13000	orf19.7209	1	**1.8627546**	0.8974376	*RDI1*	Predicted ORF in Assemblies 19, 20 and 21
	Cd36_33200		R	**1.863387**	0.8979273		
	Cd36_86840	orf19.6813	3	**1.8646059**	0.8988707		Predicted ORF in Assemblies 19, 20 and 21
	Cd36_24690	orf19.5345	2	**1.8658552**	0.899837	*DSK2*	Predicted ORF in Assemblies 19, 20 and 21
	Cd36_34060	orf19.6416	R	**1.8671689**	0.90085244	*EOS1*	Predicted ORF in Assemblies 19, 20 and 21
	Cd36_19360	orf19.184	2	**1.8683823**	0.90178967	*MDM10*	Predicted ORF in Assemblies 19, 20 and 21
ALS4	Cd36_64610	orf19.4555	6	**1.8717107**	0.90435743	*FLO1*	ALS family protein
	Cd36_32850	orf19.6148	R	**1.8726289**	0.90506506	*USO1*	Predicted ORF in Assemblies 19, 20 and 21
TTR1	Cd36_00420	orf19.6059	1	**1.873045**	0.9053855	*GRX2*	Putative glutaredoxin
	Cd36_54750	orf19.4007	5	**1.8744103**	0.9064368	*RKM2*	Predicted ORF in Assemblies 19, 20 and 21
	Cd36_03330	orf19.3057	1	**1.8745034**	0.90650845	*ILM1*	Predicted ORF in Assemblies 19, 20 and 21
	Cd36_08550	orf19.4763	1	**1.875609**	0.9073591	*FUN14*	Protein not essential for viability
SSA2	Cd36_04050	orf19.1065	1	**1.8775821**	0.90887594	*SSA2*	Cell-surface protein of the HSP70 family
	Cd36_30130	orf19.6316	R	**1.8787354**	0.9097619	*YMR221C*	Predicted ORF in Assemblies 19, 20 and 21
ALG5	Cd36_27850	orf19.2837	R	**1.8788602**	0.90985775	*ALG5*	Putative glucosyltransferase involved in cell wall mannan biosynthesis
	Cd36_25920	orf19.3267	R	**1.8800939**	0.91080475	*SWF1*	Predicted ORF in Assemblies 19, 20 and 21
	Cd36_29650	orf19.519	R	**1.8801154**	0.9108212	*RRN10*	Predicted ORF in Assemblies 19, 20 and 21
	Cd36_87530	orf19.6723	3	**1.8820353**	0.9122937		Predicted ORF in Assemblies 19, 20 and 21
	Cd36_54950	orf19.4030	5	**1.8849217**	0.9145045	*PRI1*	Predicted ORF in Assemblies 19, 20 and 21
ACO1	Cd36_33840	orf19.6385	R	**1.8854176**	0.9148841	*ACO1*	Protein described as aconitase
CYT2	Cd36_42020	orf19.4578	4	**1.8907213**	0.9189367	*CYT2*	Protein described as cytochrome c1 heme lyase
	Cd36_30430	orf19.639	R	**1.8908451**	0.91903114	*RAI1*	Predicted ORF in Assemblies 19, 20 and 21
	Cd36_43920	orf19.1424	4	**1.8913469**	0.91941404	*YMR155W*	Predicted ORF in Assemblies 19, 20 and 21
CDC23	Cd36_34220	orf19.6437	R	**1.8933913**	0.9209726	*CDC23*	Similar to anaphase-promoting complex component
THI4	Cd36_85100	orf19.5986	3	**1.8934122**	0.92098856	*THI4*	Protein repressed during the mating process
ISC1	Cd36_31220	orf19.6629	R	**1.8955517**	0.9226178	*ISC1*	Putative phospholipase C, possible neutral sphingomyelinase
	Cd36_46610	orf19.3091	4	**1.8957348**	0.92275715	*MUC1*	Predicted ORF in Assemblies 19, 20 and 21
	Cd36_25530	orf19.7494	R	**1.8962364**	0.92313886		Predicted ORF in Assemblies 19, 20 and 21
	Cd36_41470	orf19.4639	4	**1.898505**	0.9248638		Predicted ORF in Assemblies 19, 20 and 21
PSA2	Cd36_12220	orf19.4943	1	**1.8985882**	0.924927	*PSA1*	Predicted ORF in Assemblies 19, 20 and 21
	Cd36_21320	orf19.2259	2	**1.8986949**	0.92500806		Predicted ORF in Assemblies 19, 20 and 21
	Cd36_54720	orf19.4004	5	**1.9008882**	0.92667365	*CCT3*	Predicted ORF in Assemblies 19, 20 and 21
	Cd36_26810	orf19.2579	R	**1.9049294**	0.92973757	*MSH4*	Predicted ORF in Assemblies 19, 20 and 21
MRPL6	Cd36_25600	orf19.7486	R	**1.9076091**	0.93176556	*MRPL6*	Putative mitochondrial ribosomal protein
IFG3	Cd36_50460	orf19.944	5	**1.9081476**	0.9321728		Putative D-amino acid oxidase
	Cd36_27020	orf19.2610	R	**1.9083936**	0.93235874	*ARC1*	Predicted ORF in Assemblies 19, 20 and 21
	Cd36_31450	orf19.3851	R	**1.9092385**	0.93299735		Predicted ORF in Assemblies 19, 20 and 21
GLK4	Cd36_33110	orf19.6116	R	**1.9128908**	0.93575454	*GLK1*	Protein described as a glucokinase
	Cd36_34310	orf19.6449	R	**1.913255**	0.9360292		Predicted ORF in Assemblies 19, 20 and 21
	Cd36_26290	orf19.3226	R	**1.9135355**	0.9362407	*NPC2*	Predicted ORF in Assemblies 19, 20 and 21
	Cd36_20540	orf19.4104	2	**1.9146903**	0.937111		Predicted ORF in Assemblies 19, 20 and 21
	Cd36_28630	orf19.4400	R	**1.9147644**	0.9371669		Predicted ORF in Assemblies 19, 20 and 21
GLK1	Cd36_32740	orf19.734	R	**1.9152873**	0.9375608	*GLK1*	Putative glucokinase
	Cd36_27540	orf19.163	R	**1.9205227**	0.941499	*PAN6*	Predicted ORF in Assemblies 19, 20 and 21
	Cd36_17310	orf19.1545	2	**1.9231364**	0.94346106	*MRPS8*	Predicted ORF in Assemblies 19, 20 and 21
	Cd36_50170	orf19.5683	5	**1.93085**	0.94923615	*YHR140W*	Predicted ORF in Assemblies 19, 20 and 21
	Cd36_54640	orf19.3996	5	**1.9309263**	0.94929314	*GPI10*	Putative mannosyltransferase
HSP78	Cd36_18140	orf19.882	2	**1.9316024**	0.9497981	*HSP78*	Protein described as a heat-shock protein
MRPL19	Cd36_06360	orf19.6231	1	**1.9317144**	0.9498818	*MRPL19*	Protein described as a ribosomal protein
ACO2	Cd36_31190	orf19.6632	R	**1.9322007**	0.9502449	*ACO2*	Protein described as aconitate hydratase 2
	Cd36_32570	orf19.2362	R	**1.9325686**	0.95051956	*YOR287C*	Predicted ORF in Assemblies 19, 20 and 21
CTA1	Cd36_61960	orf19.3401	6	**1.9327981**	0.950691	*VPS60*	Protein similar to S. cerevisiae Mos10p, which affects S. cerevisiae filamentous growth
	Cd36_54140	orf19.3936	5	**1.9355652**	0.952755	*GDE1*	Predicted ORF in Assemblies 19, 20 and 21
	Cd36_26130	orf19.3241	R	**1.9362407**	0.9532583	*YDR128W*	Predicted ORF in Assemblies 19, 20 and 21
	Cd36_25320	orf19.7506	R	**1.9363724**	0.95335644		Predicted ORF in Assemblies 19, 20 and 21
	Cd36_41240	orf19.4664	4	**1.9368385**	0.9537037	*NAT4*	Predicted ORF in Assemblies 19, 20 and 21
ALS2	Cd36_64800	orf19.1097	6	**1.9371417**	0.9539294	*FLO1*	ALS family protein
ADP1	Cd36_31330	orf19.459	R	**1.9373071**	0.9540527	*ADP1*	Putative PDR-subfamily ABC transporter
	Cd36_33570	orf19.607	R	**1.9383694**	0.9548435	*RAD26*	Predicted ORF in Assemblies 19, 20 and 21
ARR3	Cd36_46360	orf19.3122	4	**1.9392275**	0.955482	*ARR3*	Protein not essential for viability
ALS2	Cd36_65010	orf19.1097	6	**1.9405152**	0.95643973	*FLO1*	ALS family protein
PEX14	Cd36_30330	orf19.1805	R	**1.9406717**	0.9565561	*PEX14*	Protein not essential for viability
	Cd36_26380	orf19.2520	R	**1.9421113**	0.95762587	*MRPS28*	Predicted ORF in Assemblies 19, 20 and 21
	Cd36_29240	orf19.478	R	**1.9422624**	0.95773816	*MON1*	Predicted ORF in Assemblies 19, 20 and 21
	Cd36_28550	orf19.2382	R	**1.9429386**	0.9582403	*ISM1*	Predicted ORF in Assemblies 19, 20 and 21
	Cd36_54200	orf19.3942	5	**1.9512374**	0.9643893	*VPS25*	Predicted ORF in Assemblies 19, 20 and 21
	Cd36_26150	orf19.3239	R	**1.9513032**	0.96443796	*CTF18*	Predicted ORF in Assemblies 19, 20 and 21

Gene Name	*C. dubliniensis* Cd36 identifier	*C. albicans* orf19 identifier	C'some	Fold change expression	Normalised Expression	*S. cerevisiae* ortholog	Description
FOX3	Cd36_81380	orf19.1704	3	**1.9515854**	0.9646466	*POT1*	Putative peroxisomal 3-oxoacyl CoA thiolase
	Cd36_72220	orf19.6461	7	**1.9517833**	0.96479285	*COX20*	Predicted ORF in Assemblies 19, 20 and 21
	Cd36_33800	orf19.6377	R	**1.9543135**	0.96666193	*PPM1*	Predicted ORF in Assemblies 19, 20 and 21
	Cd36_16600	orf19.1485	2	**1.9546181**	0.96688676	*MRPL31*	Predicted ORF in Assemblies 19, 20 and 21
	Cd36_26270	orf19.3228	R	**1.9564654**	0.96824956	*YER113C*	Predicted ORF in Assemblies 19, 20 and 21
SOU1	Cd36_45880	orf19.2896	4	**1.9566412**	0.96837926	*SPS19*	Enzyme involved in utilization of L-sorbose
	Cd36_31790	orf19.3881	R	**1.9567732**	0.96847653		Predicted ORF in Assemblies 19, 20 and 21
	Cd36_27960	orf19.2847	R	**1.9570862**	0.9687073	*RPC82*	Predicted ORF in Assemblies 19, 20 and 21
	Cd36_85030	orf19.5976	3	**1.9596193**	0.9705734	*YPR152C*	Predicted ORF in Assemblies 19, 20 and 21
UGA2	Cd36_01650	orf19.4543	1	**1.9624236**	0.97263646	*UGA2*	Protein not essential for viability
	Cd36_31860	orf19.3881	R	**1.963058**	0.9731028		Predicted ORF in Assemblies 19, 20 and 21
	Cd36_64240	orf19.5747	6	**1.9647307**	0.9743316	*MRP4*	Predicted ORF in Assemblies 19, 20 and 21
	Cd36_63195	orf19.5564	6	**1.9650658**	0.97457767	*RNH1*	Predicted ORF in Assemblies 19, 20 and 21
	Cd36_33100	orf19.6117	R	**1.9652143**	0.9746866	*YBR287W*	Predicted ORF in Assemblies 19, 20 and 21
SBA1	Cd36_64260	orf19.5749	6	**1.9656433**	0.9750016	*SBA1*	Similar to co-chaperones
THI20	Cd36_18120	orf19.889	2	**1.9663038**	0.9754863	*THI20*	Putative phosphomethylpyrimidine kinase
	Cd36_32750	orf19.733	R	**1.9674659**	0.9763386	*YBR287W*	Predicted ORF in Assemblies 19, 20 and 21
	Cd36_82840	orf19.276	3	**1.9678664**	0.9766323		Predicted ORF in Assemblies 19, 20 and 21
	Cd36_54850	orf19.4018	5	**1.9694844**	0.977818	*RSM7*	Predicted ORF in Assemblies 19, 20 and 21
	Cd36_54400	orf19.3965	5	**1.971637**	0.97939396		Predicted ORF in Assemblies 19, 20 and 21
CAR2	Cd36_40230	orf19.5641	4	**1.9722008**	0.9798064	*CAR2*	Alkaline upregulated
OPT4	Cd36_27420	orf19.176	R	**1.9725391**	0.9800539	*OPT2*	Oligopeptide transporter
RIM13	Cd36_54630	orf19.3995	5	**1.97697**	0.9832909	*RIM13*	Probable protease involved in the pH response pathway, likely to mediate activation of the transcription factor Rim101p via C-terminal cleavage
FMP45	Cd36_72040	orf19.6489	7	**1.9816463**	0.98669946	*FMP45*	Protein induced during the mating process
	Cd36_25670	orf19.7478	R	**1.9848052**	0.98899746	*COQ1*	Predicted ORF in Assemblies 19, 20 and 21
	Cd36_02120	orf19.3684	1	**1.9897863**	0.99261343	*SPS19*	Predicted ORF in Assemblies 19, 20 and 21
	Cd36_28640	orf19.4399	R	**1.995969**	0.9970894	*NCS2*	Predicted ORF in Assemblies 19, 20 and 21
CYP5	Cd36_86110	orf19.7421	3	**1.9960763**	0.9971669	*CPR5*	Protein described as a peptidyl-prolyl cis-trans isomerase
ASR3	Cd36_18460	orf19.842	2	**1.9982893**	0.99876547		Gene regulated by cAMP and by osmotic stress
TRX1	Cd36_35275	orf19.7611	R	**2.0001128**	1.0000813	*TRX1*	Similar to thioredoxin
	Cd36_10460	orf19.2301	1	**2.0114625**	1.0082448	*NAS2*	Predicted ORF in Assemblies 19, 20 and 21
	Cd36_15140	orf19.2116	2	**2.0224204**	1.016083	*NAT2*	Predicted ORF in Assemblies 19, 20 and 21
	Cd36_51460	orf19.585	5	**2.0265374**	1.0190167	*MRPL17*	Predicted ORF in Assemblies 19, 20 and 21
MODF	Cd36_12890	orf19.5029	1	**2.0280094**	1.0200644	*YDR061W*	Predicted ORF in Assemblies 19, 20 and 21
LKH1	Cd36_09880	orf19.992	1	**2.0281434**	1.0201597	*YNL045W*	Protein repressed during the mating process
	Cd36_61780	orf19.3418	6	**2.030097**	1.0215486		Predicted ORF in Assemblies 19, 20 and 21
PRE1	Cd36_54910	orf19.4025	5	**2.0324478**	1.0232184	*PRE1*	Upregulated by Rim101p at acid pH
	Cd36_29760	orf19.530	R	**2.0329738**	1.0235915		Protein not essential for viability
UGA1	Cd36_18820	orf19.802	2	**2.0390089**	1.027868	*UGA1*	Protein described as GABA transaminase
	Cd36_43520	orf19.1300	4	**2.041251**	1.0294536	*OMS1*	Predicted ORF in Assemblies 19, 20 and 21
	Cd36_52800	orf19.4332	5	**2.0419157**	1.0299233		Predicted ORF in Assemblies 19, 20 and 21
NMD3	Cd36_32260	orf19.706	R	**2.0426023**	1.0304084	*NMD3*	Predicted ORF in Assemblies 19, 20 and 21
	Cd36_53970	orf19.3915	5	**2.0446408**	1.0318475	*DUG1*	Predicted ORF in Assemblies 19, 20 and 21
	Cd36_87000	orf19.6793	3	**2.0446553**	1.0318577		Predicted ORF in Assemblies 19, 20 and 21
	Cd36_29080	orf19.4355	R	**2.044877**	1.0320141		Predicted ORF in Assemblies 19, 20 and 21
	Cd36_29890	orf19.543	R	**2.0476332**	1.0339572	*FUM1*	Protein described as fumarate hydratase
MDR1	Cd36_63890	orf19.5604	6	**2.0483031**	1.0344293	*FLR1*	Multidrug efflux pump of plasma membrane
	Cd36_04400	orf19.781	1	**2.050246**	1.035797	*DUR3*	Putative urea transporter
	Cd36_20410	orf19.4121	2	**2.0533092**	1.0379509	*TES1*	Predicted ORF in Assemblies 19, 20 and 21
	Cd36_29450	orf19.498	R	**2.054241**	1.0386055	*NAM9*	Predicted ORF in Assemblies 19, 20 and 21
	Cd36_73450	orf19.7203	7	**2.0577793**	1.0410882	*MRP7*	Predicted ORF in Assemblies 19, 20 and 21
EST1	Cd36_55060	orf19.4045	5	**2.058644**	1.0416944	*EBS1*	Telomerase subunit
	Cd36_54170	orf19.3940	5	**2.0601647**	1.0427597		Predicted ORF in Assemblies 19, 20 and 21
	Cd36_42860	orf19.2693	4	**2.0606406**	1.043093	*URE2*	Increased transcription is observed upon benomyl treatment transcription and in populations of cells exposed to fluconazole over multiple generations
	Cd36_29680	orf19.522	R	**2.0699468**	1.0495937	*PIM1*	Predicted ORF in Assemblies 19, 20 and 21
PUP2	Cd36_32290	orf19.709	R	**2.0709915**	1.0503216	*PUP2*	Alpha5 subunit of the 20S proteasome
DDI1	Cd36_13370	orf19.7258	1	**2.072177**	1.0511472	*DDI1*	Predicted ORF in Assemblies 19, 20 and 21
MAM33	Cd36_73610	orf19.7187	7	**2.074561**	1.0528061	*MAM33*	Predicted ORF in Assemblies 19, 20 and 21
MRP2	Cd36_54890	orf19.4023	5	**2.0764527**	1.054121	*MRP2*	Protein similar to S. cerevisiae Mrp2p, which is a component of the small subunit of the mitochondrial ribosome
HGT8	Cd36_15930	orf19.2021	2	**2.076624**	1.05424	*HXT6*	Putative glucose transporter of the major facilitator superfamily
	Cd36_27370	orf19.3724	R	**2.0779157**	1.0551372	*UTP23*	Predicted ORF in Assemblies 19, 20 and 21
	Cd36_54240	orf19.3946	5	**2.0792255**	1.0560462	*COX18*	Predicted ORF in Assemblies 19, 20 and 21
	Cd36_51270	orf19.1967	5	**2.0810075**	1.0572822	*IMG1*	Predicted ORF in Assemblies 19, 20 and 21
	Cd36_28050	orf19.2857	R	**2.082246**	1.0581405	*SSL2*	Predicted ORF in Assemblies 19, 20 and 21
DES1	Cd36_55070	orf19.4048	5	**2.0822725**	1.0581589		Putative delta-4 sphingolipid desaturase
	Cd36_28650	orf19.4398	R	**2.08376**	1.0591891	*YPR147C*	Predicted ORF in Assemblies 19, 20 and 21
CYP5	Cd36_86340	orf19.7421	3	**2.0849025**	1.0599799	*CPR5*	Protein described as a peptidyl-prolyl cis-trans isomerase
	Cd36_71940	orf19.6503	7	**2.089595**	1.0632235	*MRP49*	Predicted ORF in Assemblies 19, 20 and 21
ILV3	Cd36_55010	orf19.4040	5	**2.0938365**	1.0661488	*ILV3*	Putative dihydroxyacid dehydratase
PTP1	Cd36_33710	orf19.6365	R	**2.0938613**	1.0661659	*PTP1*	Protein not essential for viability
	Cd36_46170	orf19.3139	4	**2.096352**	1.0678811	*YML131W*	Predicted ORF in Assemblies 19, 20 and 21
	Cd36_34320		R	**2.0969517**	1.0682937		
	Cd36_05010	orf19.439	1	**2.098685**	1.0694857	*MHR1*	Predicted ORF in Assemblies 19, 20 and 21

Gene Name	*C. dubliniensis* Cd36 identifier	*C. albicans* orf19 identifier	C'some	Fold change expression	Normalised Expression	*S. cerevisiae* ortholog	Description
	Cd36_01100	orf19.3305	1	**2.0991256**	1.0697885	*UPC2*	Putative transcription factor with zinc cluster DNA-binding motif
LYS9	Cd36_86570	orf19.7448	3	**2.1004105**	1.0706713	*LYS9*	Putative enzyme of lysine biosynthesis
ECM29	Cd36_87170	orf19.6773	3	**2.1115258**	1.0782859	*ECM29*	Protein similar to S. cerevisiae Ecm29p
	Cd36_87250	orf19.6757	3	**2.1152966**	1.0808599	*GCY1*	Predicted ORF in Assemblies 19, 20 and 21
	Cd36_17430	orf19.5809	2	**2.1292145**	1.0903213	*BNA3*	Predicted ORF in Assemblies 19, 20 and 21
IHD1	Cd36_64370	orf19.5760	6	**2.1306605**	1.0913007	*SRP40*	Putative GPI-anchored protein of unknown function
ARO9	Cd36_45160	orf19.1237	4	**2.1308777**	1.0914478	*ARO9*	Predicted ORF in Assemblies 19, 20 and 21
	Cd36_42360	orf19.2754	4	**2.141089**	1.0983447	*TIM13*	Predicted ORF in Assemblies 19, 20 and 21
	Cd36_08700	orf19.4780	1	**2.14134**	1.0985138	*YJR124C*	Predicted ORF in Assemblies 19, 20 and 21
NOT4	Cd36_28580	orf19.2379	R	**2.144547**	1.100673	*MOT2*	Putative E3 ubiquitin-protein ligase
	Cd36_81220	orf19.1723	3	**2.1464436**	1.1019483	*YJL055W*	Predicted ORF in Assemblies 19, 20 and 21
	Cd36_80880	orf19.2500	3	**2.1487412**	1.1034918		Predicted ORF in Assemblies 19, 20 and 21
	Cd36_17720	orf19.5809	2	**2.1533213**	1.1065636	*BNA3*	Predicted ORF in Assemblies 19, 20 and 21
	Cd36_44860	orf19.6859	4	**2.1537602**	1.1068577		Predicted ORF in Assemblies 19, 20 and 21
	Cd36_43180	orf19.3367	4	**2.16556**	1.1147401	*MRPL22*	Predicted ORF in Assemblies 19, 20 and 21
	Cd36_82570	orf19.251	3	**2.1664448**	1.1153295	*HSP31*	Member of ThiJ/Pfpl protein family
	Cd36_21450	orf19.2274	2	**2.1681795**	1.1164842		Predicted ORF in Assemblies 19, 20 and 21
	Cd36_81560	orf19.1676	3	**2.1772125**	1.1224822	*YDL183C*	Predicted ORF in Assemblies 19, 20 and 21
LAP3	Cd36_29830	orf19.539	R	**2.17787**	1.1229179	*LAP3*	Protein described as an aminopeptidase
HSP90	Cd36_71850	orf19.6515	7	**2.1791308**	1.1237528	*HSC82*	Chaperone of Hsp90 family
	Cd36_54460	orf19.3972	5	**2.1795735**	1.1240458	*GOT1*	Predicted ORF in Assemblies 19, 20 and 21
MRPL10	Cd36_19520	orf19.3532	2	**2.1798494**	1.1242285	*MRPL10*	Predicted ORF in Assemblies 19, 20 and 21
	Cd36_31600	orf19.3865	R	**2.1831164**	1.126389	*RFX1*	Predicted ORF in Assemblies 19, 20 and 21
	Cd36_55020	orf19.4041	5	**2.1849816**	1.1276212	*PEX4*	Predicted ORF in Assemblies 19, 20 and 21
	Cd36_25350	orf19.7502	R	**2.188537**	1.1299667		Predicted ORF in Assemblies 19, 20 and 21
	Cd36_53980	orf19.3916	5	**2.1903398**	1.1311548		Predicted ORF in Assemblies 19, 20 and 21
	Cd36_34200	orf19.6435	R	**2.1932638**	1.1330793	*YGR243W*	Predicted ORF in Assemblies 19, 20 and 21
	Cd36_85430	orf19.6982	3	**2.1945477**	1.1339236	*YJL131C*	Predicted ORF in Assemblies 19, 20 and 21
LSC2	Cd36_32310	orf19.1860	R	**2.1985424**	1.1365473	*LSC2*	Protein described as beta subunit of succinate-CoA ligase
	Cd36_29920	orf19.547	R	**2.1989174**	1.1367934	*RAD27*	Predicted ORF in Assemblies 19, 20 and 21
	Cd36_05190	orf19.417	1	**2.2018232**	1.1386986	*MTM1*	Predicted ORF in Assemblies 19, 20 and 21
	Cd36_82020	orf19.1643	3	**2.2018723**	1.1387308	*PCP1*	Predicted ORF in Assemblies 19, 20 and 21
	Cd36_29420	orf19.496	R	**2.2136197**	1.1464074	*MSH1*	Predicted ORF in Assemblies 19, 20 and 21
PRN2	Cd36_05520	orf19.2463	1	**2.2159033**	1.1478949		Predicted ORF in Assemblies 19, 20 and 21
	Cd36_12440		1	**2.2166054**	1.1483519		
YAH1	Cd36_83350	orf19.336	3	**2.2197804**	1.150417	*YAH1*	Similar to oxidoreductases
	Cd36_54570	orf19.3986	5	**2.2231615**	1.1526127	*PPR1*	Putative transcription factor with zinc cluster DNA-binding motif
MSM1	Cd36_54270	orf19.3950	5	**2.2238705**	1.1530728	*MSM1*	Mitochondrial methionyl-tRNA synthetase (MetRS)
	Cd36_28960	orf19.4374	R	**2.22684**	1.154998	*PRP42*	Predicted ORF in Assemblies 19, 20 and 21
	Cd36_53240		5	**2.2280612**	1.1557889		
	Cd36_54070	orf19.3929	5	**2.2295585**	1.1567581	*YJR100C*	Predicted ORF in Assemblies 19, 20 and 21
	Cd36_45350	orf19.1270	4	**2.2359571**	1.1608926	*FRE2*	Predicted ORF in Assemblies 19, 20 and 21
	Cd36_70380	orf19.7106	7	**2.2400057**	1.1635025	*VPS70*	Predicted ORF in Assemblies 19, 20 and 21
PST3	Cd36_30720	orf19.5285	R	**2.2464402**	1.1676407	*PST2*	Putative flavodoxin
RAD14	Cd36_71840	orf19.6517	7	**2.2465947**	1.1677399	*RAD14*	Transcription is regulated upon yeast-hyphal switch
ASF1	Cd36_33540	orf19.3715	R	**2.2486784**	1.1690774	*ASF1*	Protein likely to be essential for growth, based on an insertional mutagenesis strategy
	Cd36_63090	orf19.5573	6	**2.2530468**	1.1718773		Predicted ORF in Assemblies 19, 20 and 21
CSR1	Cd36_44490	orf19.3794	4	**2.258085**	1.1750998	*ZAP1*	Putative DNA-binding transcription factor
	Cd36_08030	orf19.397	1	**2.2622187**	1.1777384	*MRPL28*	Predicted ORF in Assemblies 19, 20 and 21
	Cd36_60980	orf19.95	6	**2.2624903**	1.1779116	*PRM5*	Predicted ORF in Assemblies 19, 20 and 21
	Cd36_84290	orf19.5879	3	**2.2672272**	1.180929	*AYR1*	Predicted ORF in Assemblies 19, 20 and 21
	Cd36_28230	orf19.2415	R	**2.2680213**	1.1814342	*MSE1*	Predicted ORF in Assemblies 19, 20 and 21
	Cd36_31750	orf19.3877	R	**2.2699423**	1.1826556		Predicted ORF in Assemblies 19, 20 and 21
	Cd36_16420	orf19.1465	2	**2.2709599**	1.1833022	*PAA1*	Predicted ORF in Assemblies 19, 20 and 21
	Cd36_28090	orf19.2863	R	**2.2724338**	1.1842382		Predicted ORF in Assemblies 19, 20 and 21
	Cd36_28010	orf19.2851	R	**2.277951**	1.1877367	*ORT1*	Predicted ORF in Assemblies 19, 20 and 21
	Cd36_70950	orf19.7012	7	**2.279471**	1.188699	*MRPS16*	Predicted ORF in Assemblies 19, 20 and 21
	Cd36_35440	orf19.7648	R	**2.2821496**	1.1903933	*YDR338C*	Predicted ORF in Assemblies 19, 20 and 21
	Cd36_63800	orf19.5611	6	**2.2866604**	1.1932421	*GRE2*	Predicted ORF in Assemblies 19, 20 and 21
	Cd36_80310	orf19.5433	3	**2.2899077**	1.1952895	*YDR493W*	Predicted ORF in Assemblies 19, 20 and 21
	Cd36_31980	orf19.718	R	**2.2903075**	1.1955414	*RRN11*	Putative RNA polymerase I subunit
LEU1	Cd36_25490	orf19.7498	R	**2.2905188**	1.1956744	*LEU1*	Protein described as 3-isopropylmalate dehydratase
	Cd36_87240	orf19.6758	3	**2.2907536**	1.1958224	*GCY1*	Predicted ORF in Assemblies 19, 20 and 21
	Cd36_54360	orf19.3960	5	**2.2932754**	1.1974096	*POL31*	Predicted ORF in Assemblies 19, 20 and 21
	Cd36_28820	orf19.4380.1	R	**2.298265**	1.2005451	*YME2*	Predicted ORF in Assembly 20 and 21 (see Locus History)
	Cd36_30960	orf19.6653	R	**2.3016891**	1.202693	*MTG2*	Predicted ORF in Assemblies 19, 20 and 21
RPN5	Cd36_54980	orf19.4032	5	**2.3057272**	1.2052219	*RPN5*	Predicted ORF in Assemblies 19, 20 and 21
	Cd36_10760		1	**2.311334**	1.2087257		
	Cd36_70180	orf19.7073	7	**2.3132706**	1.209934	*YCL002C*	Predicted ORF in Assemblies 19, 20 and 21
PRP13	Cd36_29040	orf19.4379	R	**2.3228798**	1.2159145	*YME2*	Predicted ORF in Assemblies 19, 20 and 21
RPT4	Cd36_29280	orf19.482	R	**2.3248284**	1.2171242	*RPT4*	Predicted ORF in Assemblies 19, 20 and 21
SIS1	Cd36_31550	orf19.3861	R	**2.3253226**	1.2174308	*SIS1*	Predicted ORF in Assemblies 19, 20 and 21
AHP1	Cd36_42290	orf19.2762	4	**2.3257856**	1.2177181	*AHP1*	Putative alkyl hydroperoxide reductase
	Cd36_51940	orf19.4216	5	**2.3273783**	1.2187057	*HSP12*	Predicted ORF in Assemblies 19, 20 and 21
	Cd36_18690	orf19.816	2	**2.329731**	1.2201633	*YLR422W*	Predicted ORF in Assemblies 19, 20 and 21
	Cd36_08340	orf19.4742	1	**2.3325307**	1.221896		Predicted ORF in Assemblies 19, 20 and 21

Gene Name	*C. dubliniensis* Cd36 identifier	*C. albicans* orf19 identifier	C'some	Fold change expression	Normalised Expression	*S. cerevisiae* ortholog	Description
	Cd36_63190	orf19.5565	6	2.3382237	1.225413		Putative 3-hydroxyisobutyrate dehydrogenase
DAL1	Cd36_80170	orf19.5454	3	2.3393023	1.2260783	*DAL1*	Predicted ORF in Assemblies 19, 20 and 21
ARF1	Cd36_34290	orf19.6447	R	2.339655	1.2262957	*ARF1*	ADP-ribosylation factor, probable GTPase involved in intracellular transport
	Cd36_25610	orf19.7485	R	2.3500226	1.2326746	*MRPL9*	Predicted ORF in Assemblies 19, 20 and 21
PRE6	Cd36_29910	orf19.544.1	R	2.3515656	1.2336216	*PRE6*	Protein described as alpha-4 subunit of proteasome
	Cd36_15590	orf19.2064	2	2.3551292	1.2358062		Putative transcription factor with zinc finger DNA-binding motif
	Cd36_32460	orf19.178	R	2.3557634	1.2361946		Predicted ORF in Assemblies 19, 20 and 21
	Cd36_30440	orf19.639.1	R	2.3637834	1.2410978	*MRPL44*	ORF Predicted by Annotation Working Group
	Cd36_54690	orf19.4001	5	2.3640075	1.2412345	*MSS2*	Predicted ORF in Assemblies 19, 20 and 21
	Cd36_03710	orf19.4474	1	2.3743348	1.2475234	*YNL155W*	Protein not essential for viability
CSP37	Cd36_26450	orf19.2531	R	2.380669	1.2513671		Plasma membrane, hyphal cell wall protein
	Cd36_85050	orf19.5978	3	2.3810587	1.2516032	*YNL134C*	Predicted ORF in Assemblies 19, 20 and 21
	Cd36_60480	orf19.4204	6	2.385669	1.2543938	*PET123*	Predicted ORF in Assemblies 19, 20 and 21
PLB4.5	Cd36_16240	orf19.1442	2	2.392372	1.2584417	*PLB3*	Putative phospholipase B
	Cd36_25970	orf19.3263	R	2.3953776	1.2602531	*ADY2*	Predicted ORF in Assemblies 19, 20 and 21
FDH3	Cd36_35225	orf19.7600	R	2.397279	1.2613978	*SFA1*	Putative protein of glycine catabolism
IFA21	Cd36_72810	orf19.5138	7	2.3987138	1.262261		Protein not essential for viability
DAL9	Cd36_83640	orf19.6956	3	2.410671	1.2694348	*DAL5*	Putative allantoate permease
	Cd36_51620	orf19.3205	5	2.4122858	1.2704009	*MRPL36*	Predicted ORF in Assemblies 19, 20 and 21
	Cd36_53190	orf19.2639	5	2.4170568	1.2732514		Predicted ORF in Assemblies 19, 20 and 21
GAD1	Cd36_10950	orf19.1153	1	2.4230862	1.2768457	*GAD1*	Protein described as glutamate decarboxylase
TRP99	Cd36_05140	orf19.424	1	2.4302044	1.2810776	*AHP1*	Protein described as thioredoxin peroxidase/alkyl hydroperoxide reductase
CAR1	Cd36_54130	orf19.3934	5	2.4348018	1.2838044	*CAR1*	Transcription is regulated by Nrg1p, Mig1p, and Tup1p
	Cd36_64900	orf19.1080	6	2.4387946	1.2861682		Predicted ORF in Assemblies 19, 20 and 21
UBC15	Cd36_24750	orf19.5337	2	2.4391103	1.286355	*UBC13*	Predicted ORF in Assemblies 19, 20 and 21
	Cd36_09340	orf19.4861	1	2.4397266	1.2867194		Predicted ORF in Assemblies 19, 20 and 21
ACS2	Cd36_04040	orf19.1064	1	2.4524813	1.2942421	*ACS2*	Probable acetyl-CoA synthetase, similar to known fungal acetyl-CoA synthetases
	Cd36_03660	orf19.4467	1	2.456513	1.2966118		Predicted ORF in Assemblies 19, 20 and 21
	Cd36_84280	orf19.5877	3	2.4587004	1.2978959		Predicted ORF in Assemblies 19, 20 and 21
	Cd36_33350	orf19.1985	R	2.4589896	1.2980657		Predicted ORF in Assemblies 19, 20 and 21
	Cd36_72690	orf19.5158	7	2.4668157	1.30265		Protein with slight similarity to a human gene associated with colon cancer and to orf19.5158
	Cd36_29850	orf19.541	R	2.4907653	1.3165891		Predicted ORF in Assemblies 19, 20 and 21
FAA21	Cd36_82800	orf19.272	3	2.4946864	1.3188584	*FAA2*	Predicted acyl CoA synthetase
	Cd36_28860	orf19.4365	R	2.5043926	1.3244607	*TRM2*	Predicted ORF in Assemblies 19, 20 and 21
	Cd36_73880	orf19.7152	7	2.5074484	1.32622	*YGR012W*	Protein similar to Aspergillus CYSK O-acetylserine sulfhydrylase, suggesting that C. albicans uses an O-acetyl-serine (OAS) pathway of sulfur assimilation
	Cd36_31530	orf19.3859	R	2.514656	1.3303611	*YBR159W*	Predicted ORF in Assemblies 19, 20 and 21
	Cd36_11130	orf19.5279	1	2.5211937	1.3341069	*MRPL51*	Predicted ORF in Assemblies 19, 20 and 21
APG7	Cd36_32270	orf19.707	R	2.5302055	1.3392546	*ATG7*	Protein not essential for viability
SOL3	Cd36_32240	orf19.704	R	2.5401294	1.344902	*SOL3*	Predicted ORF in Assemblies 19, 20 and 21
	Cd36_09920	orf19.999	1	2.5480921	1.3494174	*ROT2*	Predicted ORF in Assemblies 19, 20 and 21
HSP30	Cd36_01850	orf19.4526	1	2.5487576	1.3497941	*HSP30*	Protein described as similar to heat shock protein
	Cd36_71810	orf19.6520	7	2.5500727	1.3505384	*YIL166C*	Putative allantoate permease
GRX1	Cd36_71890	orf19.6510	7	2.5531552	1.3522812	*GRX1*	Protein described as glutaredoxin
TAL1	Cd36_28930	orf19.4371	R	2.5619068	1.357218	*TAL1*	Predicted ORF in Assemblies 19, 20 and 21
TPO4	Cd36_29200	orf19.473	R	2.5631628	1.3579252	*TPO4*	Putative sperimidine transporter
	Cd36_04480		1	2.564292	1.3585606		
	Cd36_28890	orf19.4368	R	2.5666645	1.3598948	*YLL029W*	Predicted ORF in Assemblies 19, 20 and 21
	Cd36_84810	orf19.5952	3	2.5761404	1.3652112		Predicted ORF in Assemblies 19, 20 and 21
PUT1	Cd36_52370	orf19.4274	5	2.582362	1.3686912	*PUT1*	Alkaline upregulated by Rim101p
	Cd36_33420	orf19.3704.1	R	2.5867338	1.3711317	*RSM19*	ORF Predicted by Annotation Working Group
	Cd36_05200	orf19.416	1	2.5960119	1.376297		Predicted ORF in Assemblies 19, 20 and 21
PST1	Cd36_21170	orf19.2241	2	2.5988808	1.3778905	*PST2*	Protein described as 1,4-benzoquinone reductase
	Cd36_34260	orf19.6443	R	2.6010995	1.3791215	*ECI1*	Predicted ORF in Assemblies 19, 20 and 21
	Cd36_30080	orf19.1735	R	2.6085374	1.3832412		Predicted ORF in Assemblies 19, 20 and 21
	Cd36_30250	orf19.6307	R	2.6370428	1.398921		Predicted ORF in Assemblies 19, 20 and 21
MRPL8	Cd36_33020	orf19.6129	R	2.657657	1.4101548	*MRPL8*	Predicted ribosomal protein of the mitochondrial 60S subunit
	Cd36_21350	orf19.2262	2	2.6707814	1.4172618	*ZTA1*	Predicted ORF in Assemblies 19, 20 and 21
	Cd36_32000	orf19.716	R	2.6855557	1.4252206		Predicted ORF in Assemblies 19, 20 and 21
ALG5	Cd36_27860	orf19.2837	R	2.6876988	1.4263715	*ALG5*	Putative glucosyltransferase involved in cell wall mannan biosynthesis
	Cd36_54660	orf19.3998	5	2.7047582	1.4354995		Predicted ORF in Assemblies 19, 20 and 21
YDJ1	Cd36_29510	orf19.506	R	2.7179658	1.4425273	*YDJ1*	Predicted ORF in Assemblies 19, 20 and 21
	Cd36_05700	orf19.2442	1	2.729905	1.4488506		Decreased transcription is observed in an azole-resistant strain that overexpresses MDR1
	Cd36_87050	orf19.6788	3	2.7320614	1.4499899		Predicted ORF in Assemblies 19, 20 and 21
PGA43	Cd36_45820	orf19.2910	4	2.7352688	1.4516827		Putative GPI-anchored protein of unknown function
	Cd36_12200	orf19.4940	1	2.7442386	1.4564059	*HIP1*	Putative histidine permease
	Cd36_54160	orf19.3938	5	2.753468	1.4612498	*RSM26*	Predicted ORF in Assemblies 19, 20 and 21
	Cd36_08270	orf19.4735	1	2.757986	1.4636152	*YGL159W*	Predicted ORF in Assemblies 19, 20 and 21
NCE103	Cd36_81230	orf19.1721	3	2.7784176	1.4742634	*NCE103*	Carbonic anhydrase involved in the conversion of carbon dioxide to bicarbonate

Gene Name	*C. dubliniensis* Cd36 identifier	*C. albicans* orf19 identifier	C'some	Fold change expression	Normalised Expression	*S. cerevisiae* ortholog	Description
SAP10	Cd36_44180	orf19.3839	4	2.7859478	1.4781682	*MKC7*	Secreted aspartyl proteinase
	Cd36_42040	orf19.4577	4	2.7921805	1.4813923	*GPB1*	Predicted ORF in Assemblies 19, 20 and 21
	Cd36_27710	orf19.2828	R	2.7928007	1.4817126	*ALF1*	Predicted ORF in Assemblies 19, 20 and 21
MRPL40	Cd36_29300	orf19.484	R	2.8001995	1.4855297	*MRPL40*	Putative mitochondrial ribosomal protein
PRS	Cd36_26460	orf19.2532	R	2.8414068	1.5066054	*YER087W*	Putative prolyl-tRNA synthetase
	Cd36_32890	orf19.6143	R	2.8573737	1.5146897		Predicted ORF in Assemblies 19, 20 and 21
ALK8	Cd36_32710	orf19.10	R	2.88931	1.530725	*DIT2*	Alkane-inducible cytochrome P450
OYE2	Cd36_61520	orf19.3443	6	2.9196553	1.5457981	*OYE2*	Putative NAPDH dehydrogenase
	Cd36_31350	orf19.458	R	2.9245608	1.5482199	*BCS1*	Predicted ORF in Assemblies 19, 20 and 21
PGA41	Cd36_46040	orf19.2906	4	2.9399116	1.5557728	*CRH1*	Putative GPI-anchored protein of unknown function
	Cd36_71830	orf19.6518	7	2.9617574	1.5664535	*HFD1*	Predicted ORF in Assemblies 19, 20 and 21
	Cd36_23270	orf19.4070	2	2.977629	1.574164		Predicted ORF in Assemblies 19, 20 and 21
	Cd36_34540	orf19.7310	R	2.997629	1.5838218	*MSC1*	Protein similar to S. cerevisiae Gin3p
	Cd36_28870	orf19.4366	R	3.004051	1.5869093		Predicted ORF in Assemblies 19, 20 and 21
CAT1	Cd36_06380	orf19.6229	1	3.0107694	1.5901322	*CTA1*	Catalase
PRN1	Cd36_05500	orf19.2467	1	3.0127323	1.5910724		Protein with similarity to pirins
CUP1	Cd36_54185	orf19.3940.1	5	3.0417478	1.6049006		Metallothionein, involved in copper resistance
	Cd36_04670	orf19.750	1	3.047024	1.6074009		Predicted ORF in Assemblies 19, 20 and 21
HSP31	Cd36_01930	orf19.3664	1	3.0543091	1.610846	*HSP30*	Protein repressed during the mating process
	Cd36_42090	orf19.4570	4	3.0861604	1.625813		Predicted ORF in Assemblies 19, 20 and 21
	Cd36_22390	orf19.2220	2	3.1057308	1.6349328		Predicted ORF in Assemblies 19, 20 and 21
	Cd36_29560	orf19.511	R	3.1147797	1.6391301	*NRK1*	Predicted ORF in Assemblies 19, 20 and 21
	Cd36_87630	orf19.6709	3	3.1409142	1.6511846		Predicted ORF in Assemblies 19, 20 and 21
POT1	Cd36_25170	orf19.7520	R	3.1510446	1.6558301	*POT1*	Putative peroxisomal 3-oxoacyl CoA thiolase
CIP1	Cd36_61180	orf19.113	6	3.1590903	1.6595092		Protein with slight similarity to plant isoflavone reductase
	Cd36_84150	orf19.5862	3	3.2058744	1.680718	*CAR1*	Protein described as related to arginases
TPO3	Cd36_08290	orf19.4737	1	3.2142248	1.6844709	*TPO2*	Possible role in polyamine transport
	Cd36_28240	orf19.2414	R	3.216489	1.6854868	*MPM1*	Predicted ORF in Assemblies 19, 20 and 21
SAP7	Cd36_04610	orf19.756	1	3.2172446	1.6858256	*YPS3*	Member of the secreted aspartyl proteinase family
	Cd36_55050	orf19.4046	5	3.220879	1.6874545		Predicted ORF in Assemblies 19, 20 and 21
WH11	Cd36_19680	orf19.3548.1	2	3.2341878	1.6934035	*HSP12*	Cytoplasmic protein expressed specifically in white phase yeast-form cells
	Cd36_01590	orf19.4550	1	3.254924	1.7026238	*YCR023C*	Predicted ORF in Assemblies 19, 20 and 21
	Cd36_26350	orf19.2517	R	3.2605858	1.7051312	*HOL1*	Predicted ORF in Assemblies 19, 20 and 21
	Cd36_01320	orf19.3330.3	1	3.274837	1.7114232		ORF Predicted by Annotation Working Group
	Cd36_29140	orf19.4358	R	3.3039103	1.7241745	*YDL157C*	Predicted ORF in Assemblies 19, 20 and 21
ECI1	Cd36_34280	orf19.6445	R	3.3320959	1.7364299	*ECI1*	Protein similar to S. cerevisiae Eci1p, which is involved in fatty acid oxidation
SOD1	Cd36_42210	orf19.2770.1	4	3.335822	1.7380424	*SOD1*	Cytosolic copper- and zinc-containing superoxide dismutase, involved in protection from oxidative stress and required for full virulence
	Cd36_71820	orf19.6468	7	3.3769186	1.7557074		Predicted ORF from Assembly 19
HEM14	Cd36_08380	orf19.4747	1	3.4031804	1.7668836	*HEM14*	Putative protoporphyrinogen oxidase involved in heme biosynthesis
	Cd36_52470	orf19.4287	5	3.452462	1.7876256	*XYL2*	Predicted ORF in Assemblies 19, 20 and 21
	Cd36_42400	orf19.2751	4	3.4551108	1.7887319	*MCH4*	Predicted ORF in Assemblies 19, 20 and 21
MUM2	Cd36_55040	orf19.4044	5	3.465394	1.7930194	*MUM2*	Protein similar to S. cerevisiae Mum2p
	Cd36_54110	orf19.3932	5	3.4712894	1.7954717		Predicted ORF in Assemblies 19, 20 and 21
YWP1	Cd36_22720	orf19.3618	2	3.5067647	1.8101406	*FLO5*	Protein with suggested role in dispersal in host
	Cd36_09640	orf19.4894	1	3.5340834	1.821336	*YER010C*	Protein of unknown function, has similarity to S. cerevisiae Yer010cp, which is a protein of unknown function belonging to the prokaryotic RraA family
	Cd36_21190	orf19.2244	2	3.5584788	1.8312607	*YJR096W*	Similar to oxidoreductases and to S. cerevisiae Yjr096wp
MRS2	Cd36_26920	orf19.2597	R	3.5811658	1.8404293	*MRS2*	Putative magnesium ion transporter, mitochondrial
	Cd36_63200	orf19.6690	6	3.7089047	1.8909932		Predicted ORF in Assemblies 19, 20 and 21
	Cd36_29540	orf19.510	R	3.7118747	1.892148	*DEF1*	Predicted ORF in Assemblies 19, 20 and 21
	Cd36_25110	orf19.7531	R	3.7347069	1.900995	*YMR090W*	Predicted ORF in Assemblies 19, 20 and 21
IFR2	Cd36_28420	orf19.2396	R	3.7591155	1.9103932	*YNL134C*	Increased transcription is observed upon benomyl treatment
	Cd36_32950	orf19.6136	R	3.8413208	1.9416025	*MRPL4*	Predicted ORF in Assemblies 19, 20 and 21
GST3	Cd36_31940	orf19.720	R	3.8684618	1.95176		Expression is regulated upon white-opaque switching
	Cd36_24800		2	3.9597888	1.9854234		
	Cd36_40880	orf19.4157	4	3.960658	1.9857402	*SPS19*	Predicted ORF in Assemblies 19, 20 and 21
	Cd36_34340		R	3.9894667	1.9961959		
	Cd36_42120	orf19.4567	4	4.00278	2.0010023		Catechol 1,2-dioxygenase (1,2-CTD), involved in degradation of aromatic compounds
	Cd36_73750	orf19.7167	7	4.0227394	2.0081782		Predicted ORF in Assemblies 19, 20 and 21
DEF1	Cd36_34980	orf19.7561	R	4.031994	2.0114934	*DEF1*	Transcription is induced upon filamentous growth
HXT5	Cd36_28770	orf19.4384	R	4.0662827	2.0237105	*ITR1*	Protein described as a sugar transporter
	Cd36_17890	orf19.5784	2	4.106998	2.0380843		Predicted ORF in Assemblies 19, 20 and 21
AMO2	Cd36_21000	orf19.3152	2	4.114075	2.040568		Protein similar to A. niger predicted peroxisomal copper amino oxidase
	Cd36_86700	orf19.6830	3	4.1159062	2.0412102	*EHD3*	Putative enoyl-CoA hydratase
PXP2	Cd36_81790	orf19.1655	3	4.1234612	2.043856	*POX1*	Putative acyl-CoA oxidase
	Cd36_16310	orf19.1449	2	4.170537	2.060233	*YL335W / YFL061*	Increased transcription is observed in an azole-resistant strain that overexpresses MDR1
	Cd36_73210	orf19.6688	7	4.1761026	2.0621572	*WSC4*	Decreased transcription is observed upon benomyl treatment or in an azole-resistant strain that overexpresses MDR1

Gene Name	*C. dubliniensis* Cd36 identifier	*C. albicans* orf19 identifier	C'some	Fold change expression	Normalised Expression	*S. cerevisiae* ortholog	Description
DCG1	Cd36_82510	orf19.244	3	4.2448015	2.0856972	*DCG1*	Transcription is regulated by Nrg1p and Mig1p
HXT5	Cd36_28610	orf19.4384	R	4.2553596	2.089281	*ITR1*	Protein described as a sugar transporter
	Cd36_13060		1	4.341038	2.11804		
MNN22	Cd36_44410	orf19.3803	4	4.361404	2.1247926	*MNN2*	Protein described as similar to Golgi alpha-1,2-mannosyltransferase
HSP104	Cd36_33850	orf19.6387	R	4.362228	2.125065	*HSP104*	Functional homolog of S. cerevisiae Hsp104p
	Cd36_33480	orf19.3711	R	4.3790593	2.130621		Predicted ORF in Assemblies 19, 20 and 21
	Cd36_54050	orf19.3926	5	4.423245	2.1451051	*RNY1*	Predicted ORF in Assemblies 19, 20 and 21
YMX6	Cd36_63450	orf19.5713	6	4.425792	2.1459358	*NDE1*	Protein described as NADH dehydrogenase
	Cd36_71790	orf19.6469	7	4.43168	2.1478539	*YGR109W-B*	Predicted ORF in Assemblies 19, 20 and 21
	Cd36_62950	orf19.5536	6	4.526183	2.178295	*AMD2*	Predicted ORF in Assemblies 19, 20 and 21
	Cd36_70450	orf19.7098	7	4.5467644	2.1848402	*YKL070W*	Predicted ORF in Assemblies 19, 20 and 21
	Cd36_16390	orf19.1461	2	4.6186237	2.207463		Predicted ORF in Assemblies 19, 20 and 21
	Cd36_50140	orf19.5686	5	4.6400394	2.214137		Predicted ORF in Assemblies 19, 20 and 21
	Cd36_28100	orf19.2863.1	R	4.7377253	2.2441945	*ERV1*	ORF Predicted by Annotation Working Group
PUT2	Cd36_54480	orf19.3974	5	4.87921	2.2866476	*PUT2*	Alkaline upregulated
MRF1	Cd36_11010	orf19.1149	1	4.884085	2.2880883	*ETR1*	Protein similar to mitochondrial respiratory proteins
	Cd36_04210	orf19.6840	1	4.916996	2.2977772		Predicted ORF in Assemblies 19, 20 and 21
	Cd36_54540	orf19.3982	5	5.0297904	2.3304982	*YOL157C*	Maltase
	Cd36_43250	orf19.3373	4	5.1097836	2.3532622	*RIM4*	Predicted ORF in Assemblies 19, 20 and 21
RBR1	Cd36_29780	orf19.535	R	5.329031	2.4138732		Glycosylphosphatidylinositol (GPI)-anchored cell wall protein required for filamentous growth at acidic pH
	Cd36_11890	orf19.6350	1	5.3702517	2.4249897		Predicted ORF in Assemblies 19, 20 and 21
	Cd36_25330	orf19.7504	R	5.3703413	2.4250138	*RTS3*	Predicted ORF in Assemblies 19, 20 and 21
SOD4	Cd36_15610	orf19.2062	2	5.641907	2.496183		Copper- and zinc-containing superoxide dismutase, expression is regulated during white-opaque switching
DDR48	Cd36_23350	orf19.4082	2	5.7685566	2.5282104	*DDR48*	Immunogenic stress-associated protein
OPT7	Cd36_40500	orf19.5673	4	6.1492376	2.6204076	*OPT2*	Putative oligopeptide transporter
	Cd36_02600	orf19.2968	1	6.16676	2.6245127		Predicted ORF in Assemblies 19, 20 and 21
ADH4	Cd36_82790	orf19.271	3	6.5056944	2.701703	*YMR226C*	Protein not essential for viability
FAA2	Cd36_85910	orf19.7379	3	6.5955896	2.7215016	*FAA2*	Predicted acyl CoA synthetase
	Cd36_22050	orf19.2202	2	6.656387	2.7347393	*YKR043C*	Predicted ORF in Assemblies 19, 20 and 21
	Cd36_15160	orf19.2114	2	6.679096	2.7396529		Predicted ORF in Assemblies 19, 20 and 21
	Cd36_53500	orf19.1117	5	6.7741528	2.7600405	*FDH1*	Predicted ORF in Assemblies 19, 20 and 21
	Cd36_72580	orf19.5169	7	7.215125	2.8510244	*AMD2*	Predicted ORF in Assemblies 19, 20 and 21
	Cd36_33900	orf19.6398	R	7.2152014	2.8510396	*JLP1*	Predicted ORF in Assemblies 19, 20 and 21
	Cd36_43010	orf19.2674	4	7.4733105	2.9017475		Putative transcription factor with zinc finger DNA-binding motif
HSP60	Cd36_31990	orf19.717	R	8.06864	3.0123255	*HSP60*	Protein described as mitochondrial heat shock protein
GCA1	Cd36_09690	orf19.4899	1	9.49533	3.2472181	*ROT2*	Predicted extracellular or plasma membrane-associated glucoamylase
	Cd36_00040		1	9.636544	3.2685158		
	Cd36_82040	orf19.1641	3	10.124475	3.339775		Predicted ORF in Assemblies 19, 20 and 21
	Cd36_31810	orf19.3885	R	10.187837	3.3487759		Predicted ORF in Assemblies 19, 20 and 21
PGA58	Cd36_52810	orf19.4334	5	10.190836	3.3492005	*CCW12*	Putative GPI-anchored protein of unknown function
INO1	Cd36_35120	orf19.7585	R	13.987552	3.8060715	*INO1*	Inositol-1-phosphate synthase
LIP4	Cd36_72950	orf19.2133	7	16.270844	4.024217		Secreted lipase, member of a differentially expressed lipase gene family with possible roles in nutrition and/or in creating an acidic microenvironment
ECE1	Cd36_43260	orf19.3374	4	17.181557	4.102789		Protein comprising eight 34-residue repeats
CTA26	Cd36_35580	orf19.7680	R	30.646618	4.937656		Putative transcriptional activator
	Cd36_54120		5	54.675346	5.7728186		

Table S.3. Changes in gene expression greater than 1.5-fold in ΔΔ*tlo* compared to Wü284 at 3 h growth in WS

Gene Name	*C. dubliniensis* Cd36 identifier	*C. albicans* orf19 identifier	C'some	Fold change expression	Normalised Expression	*S. cerevisiae* ortholog	Description
HWP1	Cd36_43360	orf19.1321	4	-26.439566	-4.7246265	*MUC1*	Hyphal cell wall protein
	Cd36_10820	orf19.1167	1	-21.430622	-4.421602	*JLP1*	Predicted ORF in Assemblies 19, 20 and 21
	Cd36_35264	orf19.7608	R	-13.097336	-3.7112014		Predicted ORF in Assemblies 19, 20 and 21
RBT5	Cd36_40190	orf19.5636	4	-10.685766	-3.4176185		GPI-anchored cell wall protein
HMX1	Cd36_00290	orf19.6073	1	-10.585879	-3.4040692	*HMX1*	Heme oxygenase
CSA1	Cd36_70300	orf19.7114	7	-9.236955	-3.2074172	*MUC1*	Surface antigen on elongating hyphae and buds
	Cd36_17020	orf19.1541	2	-9.033015	-3.1752076	*AGA1*	Protein not essential for viability
PGA25	Cd36_60170	orf19.6336	6	-8.579858	-3.1009538	*MUC1*	Putative GPI-anchored protein of unknown function
	Cd36_05550	orf19.2460	1	-7.7972183	-2.9629595		Predicted ORF in Assemblies 19, 20 and 21
GAL10	Cd36_02000	orf19.3672	1	-7.2820797	-2.8643506	*GAL10*	UDP-glucose 4-epimerase, required for galactose utilization
	Cd36_53910	orf19.3905	5	-6.0016913	-2.585369		Predicted ORF in Assemblies 19, 20 and 21
SCW4	Cd36_02380	orf19.2941	1	-5.9898477	-2.5825193	*SCW4*	Putative cell wall protein
FRP1	Cd36_40170	orf19.5634	4	-5.859767	-2.5508432	*FRE5*	Protein similar to ferric reductases
FRP2	Cd36_70310	orf19.7112	7	-5.8277874	-2.5429482	*FRE4*	Protein described as ferric reductase
PRY1	Cd36_07060	orf19.2787	1	-5.529535	-2.467158	*PRY1*	Transcription is opaque specific
OP4	Cd36_12150	orf19.4934	1	-4.765714	-2.2526925		Ala- Leu- and Ser-rich protein
RNR22	Cd36_21850	orf19.1868	2	-4.4490676	-2.153503	*RNR2*	Protein described as ribonucleoside diphosphate reductase
	Cd36_01980		1	-4.4296827	-2.1472034		
	Cd36_08720	orf19.4783	1	-4.1077466	-2.0383472		Predicted ORF in Assemblies 19, 20 and 21
PGA7	Cd36_40180	orf19.5635	4	-3.9890893	-1.9960594	*TIR1*	Protein described as a putative precursor of a hyphal surface antigen
PGA17	Cd36_18100	orf19.893	2	-3.8142228	-1.9313891		Putative GPI-anchored protein of unknown function
FET3	Cd36_60410	orf19.4211	6	-3.7943242	-1.9238429	*FET3*	Multicopper oxidase
GAL7	Cd36_02030	orf19.3675	1	-3.7409916	-1.9034207	*GAL7*	Predicted ORF in Assemblies 19, 20 and 21
GAL1	Cd36_01990	orf19.3670	1	-3.6958232	-1.8858957	*GAL3*	Galactokinase
	Cd36_43670	orf19.1208	4	-3.6887503	-1.8831321		Predicted ORF in Assemblies 19, 20 and 21
SOD6	Cd36_15220	orf19.2108	2	-3.6330318	-1.861174		Copper- and zinc-containing superoxide dismutase
	Cd36_35530	orf19.7666	R	-3.4887218	-1.8026986	*SEO1*	Predicted ORF in Assemblies 19, 20 and 21
PCL2	Cd36_08080	orf19.403	1	-3.4699817	-1.7949281	*PCL2*	Cyclin homolog
PHO84	Cd36_10770	orf19.655	1	-3.4223146	-1.7749724	*PHO84*	Protein similar to high-affinity phosphate transporters
TNA1	Cd36_52840	orf19.4335	5	-3.4145844	-1.77171	*TNA1*	Putative nicotinic acid transporter
RBT1	Cd36_43400	orf19.1327	4	-3.3547301	-1.7461967	*MUC1*	Putative cell wall protein with similarity to Hwp1p, required for virulence
CHT3	Cd36_35130	orf19.7586	R	-3.352441	-1.745212	*CTS1*	Chitinase, major
GAP2	Cd36_85550	orf19.6993	3	-3.306578	-1.7253389	*GAP1*	Protein similar to amino acid permeases
CIP1	Cd36_61180	orf19.113	6	-3.2362478	-1.6943221		Protein with slight similarity to plant isoflavone reductase
	Cd36_82330	orf19.1608	3	-3.200373	-1.6782401		Predicted ORF in Assemblies 19, 20 and 21
CTR1	Cd36_60740	orf19.3646	6	-3.1565707	-1.6583581	*CTR1*	Copper transporter
	Cd36_81870		3	-3.1083965	-1.6361705		
	Cd36_21280	orf19.2253	2	-3.0841231	-1.6248604		Predicted ORF in Assemblies 19, 20 and 21
FGR6-3	Cd36_07280	orf19.4712	1	-3.0699515	-1.6182159	*AGA1*	Protein lacking an ortholog in S. cerevisiae
SOD3	Cd36_70320	orf19.7111.1	7	-3.0626585	-1.6147845	*SOD2*	Cytosolic manganese-containing superoxide dismutase, involved in protection against oxidative stress
	Cd36_81770	orf19.1656	3	-2.9802775	-1.5754467	*PIB2*	Predicted ORF in Assemblies 19, 20 and 21
PHO87	Cd36_05600	orf19.2454	1	-2.9551718	-1.563242	*PHO87*	Protein similar to phosphate permeases
	Cd36_22280	orf19.2175	2	-2.9373994	-1.5545394	*AIF1*	Predicted ORF in Assemblies 19, 20 and 21
	Cd36_63900	orf19.5602	6	-2.9266691	-1.5492597		Predicted ORF in Assemblies 19, 20 and 21
FGR6-4	Cd36_24200	orf19.3490	2	-2.9165676	-1.5442715	*YIL169C*	Protein lacking an ortholog in S. cerevisiae
	Cd36_86820	orf19.6816	3	-2.859652	-1.5158396	*YJR096W*	Predicted ORF in Assemblies 19, 20 and 21
	Cd36_81940		3	-2.8436441	-1.507741		
ERG251	Cd36_41530	orf19.4631	4	-2.828882	-1.500232	*ERG25*	Predicted ORF in Assemblies 19, 20 and 21
	Cd36_85770	orf19.7364	3	-2.8116066	-1.4913948	*FMO1*	Predicted ORF in Assemblies 19, 20 and 21
	Cd36_70700	orf19.1208	7	-2.7900267	-1.480279		Predicted ORF in Assemblies 19, 20 and 21
	Cd36_52980			-2.7840805	-1.477201		
CYS3	Cd36_33930	orf19.6402	R	-2.780083	-1.4751279	*CYS3*	Predicted enzyme of sulfur amino acid biosynthesis
FGR6-3	Cd36_72390	orf19.4712	7	-2.7688925	-1.4693091	*AGA1*	Protein lacking an ortholog in S. cerevisiae
GPD2	Cd36_62130	orf19.691	6	-2.7517862	-1.4603684	*GPD1*	Similar to glycerol 3-P dehydrogenases
	Cd36_24430		2	-2.715519	-1.4412279		
	Cd36_87380	orf19.6741	3	-2.6832726	-1.4239936		Predicted ORF in Assemblies 19, 20 and 21
FGR6-10	Cd36_45130	orf19.1234	4	-2.682677	-1.4236734	*AGA1*	Protein lacking an ortholog in S. cerevisiae
	Cd36_25970	orf19.3263	R	-2.6664982	-1.4149463	*ADY2*	Predicted ORF in Assemblies 19, 20 and 21
	Cd36_64490	orf19.5775	6	-2.664867	-1.4140635	*YIL169C*	Predicted ORF in Assemblies 19, 20 and 21
CHA1	Cd36_16150	orf19.1996	2	-2.6562157	-1.4093723	*CHA1*	Protein similar to serine/threonine dehydratases, catabolic
FRE10	Cd36_43990	orf19.1415	4	-2.6392035	-1.4001026	*FRE4*	Major cell-surface ferric reductase under low-iron conditions
PDR16	Cd36_03560	orf19.1027	1	-2.6370432	-1.3989213	*PDR16*	Phosphatidylinositol transfer protein
	Cd36_04320		1	-2.5758007	-1.365021		
RHR2	Cd36_80290	orf19.5437	3	-2.5730357	-1.3634715	*RHR2*	Putative glycerol 3-phosphatase
	Cd36_80840	orf19.6169	3	-2.5631566	-1.3579216	*ADY2*	Predicted ORF in Assemblies 19, 20 and 21
	Cd36_83580	orf19.355	3	-2.5500317	-1.3505151	*JLP1*	Predicted ORF in Assemblies 19, 20 and 21
TYE7	Cd36_12210	orf19.4941	1	-2.5258315	-1.3367584	*TYE7*	Putative bHLH (basic region, helix-loop-helix) transcription factor
	Cd36_70210	orf19.7077	7	-2.5189943	-1.3328478	*FRE7*	Protein of unknown function
FDH1	Cd36_30420	orf19.638	R	-2.5138385	-1.3298919	*FDH1*	Putative formate dehydrogenase, oxidizes formate to produce CO2

Gene Name	*C. dubliniensis* Cd36 identifier	*C. albicans* orf19 identifier	C'some	Fold change expression	Normalised Expression	*S. cerevisiae* ortholog	Description
	Cd36_52920	orf19.4342	5	-2.4742448	-1.3069882	*SUT1*	Predicted ORF in Assemblies 19, 20 and 21
LTE1	Cd36_21160	orf19.2238	2	-2.4731975	-1.3063774	*LTE1*	Protein similar to S. cerevisiae Lte1p
FRP3	Cd36_20980	orf19.1224	2	-2.431323	-1.2817416	*ATO2*	Upregulated in the presence of human neutrophils
SEO1	Cd36_32190	orf19.700	R	-2.4172468	-1.2733648	*SEO1*	Similar to permeases
MET1	Cd36_17440	orf19.5811	2	-2.390717	-1.2574434	*MET1*	Putative uroporphyrin-3 C-methyltransferase
	Cd36_50410	orf19.951	5	-2.381392	-1.2518051		Predicted ORF in Assemblies 19, 20 and 21
	Cd36_53500	orf19.1117	5	-2.378631	-1.2501315	*FDH1*	Predicted ORF in Assemblies 19, 20 and 21
	Cd36_17710			-2.3570056	-1.2369552		
GIT4	Cd36_51390	orf19.1980	5	-2.356808	-1.2368342	*GIT1*	Putative glycerophosphoinositol permease
RHD1	Cd36_04730	orf19.54	1	-2.3561535	-1.2364335		Putative transmembrane protein with hydrophobic N and C termini and a Ser-Gly rich region
CHL4	Cd36_04310	orf19.6851	1	-2.354718	-1.2355542	*CHL4*	Protein described as having role in chromosome segregation
RTA2	Cd36_20830	orf19.24	2	-2.339071	-1.2259357	*RSB1*	Stress-associated protein
MCD1	Cd36_35370	orf19.7634	R	-2.3285024	-1.2194023	*MCD1*	Protein similar to S. cerevisiae Mcd1p
PI-PLC	Cd36_17810	orf19.5797	2	-2.3279872	-1.2190831		Phosphatidylinositol (PtdIns)-specific phospholipase C PI-PLC)
EFG1	Cd36_33560	orf19.610	R	-2.3246279	-1.2169998	*SOK2*	Transcriptional repressor
HGT6	Cd36_15940	orf19.2020	2	-2.317071	-1.2123022	*HXT6|HXT7*	Putative glucose transporter of major facilitator superfamily
	Cd36_10650	orf19.668	1	-2.314492	-1.2106956	*TOS4*	Predicted ORF in Assemblies 19, 20 and 21
EAP1	Cd36_23630	orf19.1401	2	-2.3005471	-1.201977	*YDL038C*	Cell wall adhesin required for cell-cell adhesion and biofilm formation
FRE7	Cd36_32920	orf19.6139	R	-2.2993567	-1.2012303	*FRE3*	Protein similar to ferric reductase Fre10p
	Cd36_24680	orf19.5346	2	-2.2986536	-1.2007891	*TAF8*	Predicted ORF in Assemblies 19, 20 and 21
	Cd36_53930	orf19.3910	5	-2.2893295	-1.1949251	*RNY1*	Predicted ORF in Assemblies 19, 20 and 21
DOG1	Cd36_62030	orf19.3392	6	-2.2824895	-1.1906083	*DOG2*	Putative 2-deoxyglucose-6-phosphatase
PFK2	Cd36_71630	orf19.6540	7	-2.2777274	-1.1875951	*PFK2*	Beta subunit of phosphofructokinase (PFK), which is a heteromultimer of Pfk1p and Pfk2p
PDC11	Cd36_46050	orf19.2877	4	-2.2733862	-1.1848428	*PDC1*	Protein similar to pyruvate decarboxylase
	Cd36_53430	orf19.6681	5	-2.2697587	-1.1825389	*SAY1*	Predicted ORF in Assemblies 19, 20 and 21
DAG7	Cd36_41020	orf19.4688	4	-2.268287	-1.1816032	*WSC2*	Predicted ORF in Assemblies 19, 20 and 21
	Cd36_07380	orf19.5057	1	-2.2527475	-1.1716856		Predicted ORF in Assemblies 19, 20 and 21
	Cd36_83450	orf19.344	3	-2.2361238	-1.161	*AGA1*	Predicted ORF in Assemblies 19, 20 and 21
ALS1	Cd36_64210	orf19.5741	6	-2.2345333	-1.1599736	*FLO9*	Adhesin
	Cd36_34360	orf19.7279	R	-2.2308114	-1.1575685	*NIT2*	Predicted ORF in Assemblies 19, 20 and 21
WH11	Cd36_19680	orf19.3548.1	2	-2.2107027	-1.144505	*HSP12*	Cytoplasmic protein expressed specifically in white phase yeast-form cells
	Cd36_35450	orf19.7650	R	-2.2049763	-1.1407632	*LTV1*	Predicted ORF in Assemblies 19, 20 and 21
RNR1	Cd36_17930	orf19.5779	2	-2.1983476	-1.1364195	*RNR1*	Protein similar S. cerevisiae Rnr1p, large subunit of ribonucleotide reductase
	Cd36_62620	orf19.3482	6	-2.1885011	-1.1299431	*NPY1*	Predicted ORF in Assemblies 19, 20 and 21
	Cd36_53740	orf19.1287	5	-2.1722116	-1.1191647		Predicted ORF in Assemblies 19, 20 and 21
SYG1	Cd36_04510	orf19.768	1	-2.1664662	-1.1153438	*SYG1*	Protein not essential for viability
PGA32	Cd36_87090	orf19.6784	3	-2.1663523	-1.1152679	*DAN4*	Putative GPI-anchored protein of unknown function
GPH1	Cd36_70860	orf19.7021	7	-2.1658814	-1.1149542	*GPH1*	Putative glycogen phosphorylase
	Cd36_12610		1	-2.1650376	-1.114392		
TEM1	Cd36_02880	orf19.3001	1	-2.1627064	-1.1128378	*TEM1*	Protein similar to S. cerevisiae Tem1p, which is a GTPase involved in termination of the M phase of the cell cycle
JEN2	Cd36_43830	orf19.5307	4	-2.154008	-1.1070235	*JEN1*	Protein described as carboxylic acid transporter
	Cd36_16780	orf19.1510	2	-2.1528013	-1.1062151	*YOL019W*	Protein not essential for viability
ACS1	Cd36_24410	orf19.1743	2	-2.1497667	-1.1041801	*ACS1*	Putative acetyl-CoA synthetase, similar to S. cerevisiae Acs2p
	Cd36_72490	orf19.5180	7	-2.1404395	-1.0979071	*PRX1*	Protein described as a putative cysteine peroxidase
MAF1	Cd36_22300	orf19.2173	2	-2.1332514	-1.0930539	*MAF1*	Protein described as affecting nucleocytoplasmic transport and synthesis of RNA Polymerase III
	Cd36_21860	orf19.1867	2	-2.1296024	-1.0905842	*SSU1*	Putative malate permease
GRP2	Cd36_52640	orf19.4309	5	-2.1275115	-1.0891669	*GRE2*	Similar to S. cerevisiae Gre2p (methylglyoxal reductase)
	Cd36_17790	orf19.5799	2	-2.109503	-1.0769031	*CAF120*	Predicted ORF in Assemblies 19, 20 and 21
	Cd36_73550	orf19.7196	7	-2.1082637	-1.0760553	*PRB1*	Protein described as a vacuolar protease
	Cd36_08690	orf19.4779	1	-2.1069171	-1.0751336	*YKR105C*	Putative transporter
DSE1	Cd36_22620	orf19.3629	2	-2.1028097	-1.0723183	*DSE1*	Predicted cell wall protein
	Cd36_60160	orf19.6329	6	-2.099919	-1.0703337	*HPF1*	Predicted ORF in Assemblies 19, 20 and 21
RNR21	Cd36_17780	orf19.5801	2	-2.099892	-1.0703151	*RNR2*	Protein described as similar to ribonucleoside-diphosphate reductase
	Cd36_18720	orf19.813	2	-2.0998378	-1.0702779	*NAB3*	Predicted ORF in Assemblies 19, 20 and 21
	Cd36_63630	orf19.5626	6	-2.0981839	-1.0691411	*RLM1*	Predicted ORF in Assemblies 19, 20 and 21
KTR2	Cd36_19160	orf19.4494	2	-2.0948048	-1.0668159	*KTR2*	Protein with similarity to S. cerevisiae Ktr2p, which is a mannosyltransferase
ENO1	Cd36_08010	orf19.395	1	-2.0940354	-1.0662858	*ENO1*	Enolase (2-phospho-D-glycerate-hydrolyase), enzyme of glycolysis and gluconeogenesis
	Cd36_61660	orf19.3430	6	-2.0887787	-1.0626596		Predicted ORF in Assemblies 19, 20 and 21
HOF1	Cd36_40430	orf19.5664	4	-2.0850537	-1.0600846		Protein not essential for viability
	Cd36_53880	orf19.3901	5	-2.0845103	-1.0597085		Putative benzene desulfurase
HTA2	Cd36_03930	orf19.1051	1	-2.0808353	-1.0571628	*HTA1*	Protein described as histone H2A
WOR2	Cd36_85150	orf19.5992	3	-2.0700996	-1.0497003	*AGA1*	Transcriptional regulator of white-opaque switching
HGT19	Cd36_80200	orf19.5447	3	-2.0689957	-1.0489306	*HXT3*	Putative glucose/myo-inositol transporter of major facilitator superfamily
	Cd36_44550	orf19.3788	4	-2.0686445	-1.0486858		Predicted ORF in Assemblies 19, 20 and 21
	Cd36_42860	orf19.2693	4	-2.066797	-1.0473967	*URE2*	Increased transcription is observed upon benomil treatment transcription and in populations of cells exposed to fluconazole over multiple generations
FBA1	Cd36_41650	orf19.4618	4	-2.0494132	-1.0352108	*FBA1*	Putative fructose-bisphosphate aldolase

Gene Name	*C. dubliniensis* Cd36 identifier	*C. albicans* orf19 identifier	C'some	Fold change expression	Normalised Expression	*S. cerevisiae* ortholog	Description
	Cd36_43440	orf19.1308	4	-2.0455284	-1.0324736	*VBA1*	Predicted ORF in Assemblies 19, 20 and 21
CRP1	Cd36_08730	orf19.4784	1	-2.039457	-1.0281851	*CCC2*	Copper transporter of the plasma membrane
SAP6	Cd36_63420	orf19.5542	6	-2.0185807	-1.0133412	*YPS3*	Secreted aspartyl proteinase
SUR2	Cd36_17510	orf19.5818	2	-2.0149567	-1.0107489	*SUR2*	Protein described as similar to ceramide hydroxylase
	Cd36_80160	orf19.5455	3	-2.012754	-1.0091708	*VTC1*	Predicted ORF in Assemblies 19, 20 and 21
ARF3	Cd36_81390	orf19.1702	3	-2.0096848	-1.0069692	*ARF3*	Transcription is filament induced
CAM1	Cd36_85940	orf19.7382	3	-2.0048769	-1.0035136	*CAM1*	Putative translation elongation factor eEF1 gamma
	Cd36_12290	orf19.4952	1	-1.9947213	-0.9961872		Predicted ORF in Assemblies 19, 20 and 21
CDR3	Cd36_43320	orf19.1313	4	-1.9939485	-0.9956281	*PDR5*	Transporter of the Pdrp/Cdrp family of the ATP-binding cassette (ABC) superfamily
	Cd36_83050	orf19.304	3	-1.9820483	-0.9869921	*YOR378W*	Putative transporter similar to MDR proteins
	Cd36_84530	orf19.5915	3	-1.9500244	-0.96349216	*DUR3*	Predicted ORF in Assemblies 19, 20 and 21
	Cd36_61820	orf19.3414	6	-1.9491106	-0.962816	*SUR7*	Predicted ORF in Assemblies 19, 20 and 21
CFL5	Cd36_50970	orf19.1930	5	-1.9431034	-0.9583627	*FRE3*	Protein similar to ferric reductase Fre10p
ARG3	Cd36_63830	orf19.5610	6	-1.9408872	-0.9567163	*ARG3*	Alkaline downregulated
SSU81	Cd36_08610	orf19.4772	1	-1.9359068	-0.9530095	*SHO1*	Predicted adaptor protein involved in activation of MAP kinase-dependent signaling pathways
CPA1	Cd36_41540	orf19.4630	4	-1.929153	-0.9479675	*CPA1*	Alkaline downregulated
ASR1	Cd36_10070	orf19.2344	1	-1.9279858	-0.94709444	*HPF1*	Protein described as similar to heat shock proteins
SNQ2	Cd36_64350	orf19.5759	6	-1.9235462	-0.9437685	*SNQ2*	Protein similar to S. cerevisiae Snq2p transporter
PGA62	Cd36_42270	orf19.2765	4	-1.9218819	-0.94251966	*FLO1*	Putative GPI-anchored protein
RPS3	Cd36_30190	orf19.6312	R	-1.9164071	-0.9384041	*RPS3*	Putative ribosomal protein
	Cd36_06520	orf19.6211	1	-1.9147502	-0.9371562		Predicted ORF in Assemblies 19, 20 and 21
	Cd36_71330	orf19.6580	7	-1.9077394	-0.93186414		Predicted ORF in Assemblies 19, 20 and 21
FGR41	Cd36_09790	orf19.4910	1	-1.9073408	-0.93156266	*DSE2*	Putative GPI-anchored protein
RAD53	Cd36_83790	orf19.6936	3	-1.9002038	-0.92615414	*RAD53*	Protein involved in regulation of DNA-damage-induced filamentous growth
	Cd36_23940	orf19.1365	2	-1.898126	-0.9245758		Predicted ORF in Assemblies 19, 20 and 21
	Cd36_45340	orf19.1272	4	-1.8977487	-0.924289	*YGR111W*	Predicted ORF in Assemblies 19, 20 and 21
OYE32	Cd36_46240	orf19.3131	4	-1.8905997	-0.918844	*OYE3*	Protein of NAD(P)H oxidoreductase family
OSM2	Cd36_12650	orf19.5005	1	-1.8898588	-0.91827846	*OSM1*	Protein described as mitochondrial fumarate reductase
	Cd36_82930	orf19.288	3	-1.8886021	-0.9173188	*MET13*	Predicted ORF in Assemblies 19, 20 and 21
GUT2	Cd36_46220	orf19.3133	4	-1.8834407	-0.9133706	*GUT2*	Predicted ORF in Assemblies 19, 20 and 21
	Cd36_23170	orf19.206	2	-1.8823105	-0.9125047	*MUC1*	Predicted ORF in Assemblies 19, 20 and 21
CLN3	Cd36_51220	orf19.1960	5	-1.8785684	-0.90963364	*CLN3*	G1 cyclin
FOX2	Cd36_80740	orf19.1288	3	-1.8776096	-0.90889716	*FOX2*	Predicted 3-hydroxyacyl-CoA epimerase, required for fatty acid beta-oxidation
CHT2	Cd36_53830	orf19.3895	5	-1.8734322	-0.90568376	*CTS1*	Chitinase
URA1	Cd36_09160	orf19.4836	1	-1.8643332	-0.8986597	*URA1*	Dihydroorotate dehydrogenase (DHODH)
	Cd36_46250	orf19.3130	4	-1.8625649	-0.8972907	*YLR243W*	Predicted ORF in Assemblies 19, 20 and 21
	Cd36_04250	orf19.6845	1	-1.8613964	-0.8963853		Putative transcription factor with bZIP DNA-binding motif
DOT5	Cd36_80440	orf19.5417	3	-1.8587981	-0.8943701	*DOT5*	Alkaline downregulated
	Cd36_87550	orf19.6720	3	-1.8574878	-0.89335275	*YDR090C*	Predicted ORF in Assemblies 19, 20 and 21
CLB4	Cd36_73620	orf19.7186	7	-1.8497937	-0.8873644	*CLB4*	B-type mitotic cyclin
NOP1	Cd36_46180	orf19.3138	4	-1.8497249	-0.88731074	*NOP1*	Nucleolar protein
	Cd36_00300	orf19.6072	1	-1.8496739	-0.8872709		Predicted ORF in Assemblies 19, 20 and 21
CHT1	Cd36_25200	orf19.7517	R	-1.8483981	-0.88627553	*CTS1*	Chitinase
	Cd36_60980	orf19.95	6	-1.8466833	-0.88493645	*PRM5*	Predicted ORF in Assemblies 19, 20 and 21
	Cd36_09170	orf19.4837	1	-1.8404244	-0.8800385		Predicted ORF in Assemblies 19, 20 and 21
CAM1-1	Cd36_53070	orf19.2651	5	-1.8393557	-0.87920046	*CAM1*	Putative translation elongation factor
	Cd36_50820	orf19.4148	5	-1.827318	-0.86972773	*RTS1*	Predicted ORF in Assemblies 19, 20 and 21
KTR4	Cd36_03720	orf19.4475	1	-1.8268436	-0.8693532	*KTR4*	Protein with similarity to mannosyltransferases
GUK1	Cd36_53520	orf19.1115	5	-1.8267789	-0.86930203	*GUK1*	Putative guanylate kinase
	Cd36_02020	orf19.3674	1	-1.8241034	-0.8671875	*GAL10*	Predicted ORF in Assemblies 19, 20 and 21
	Cd36_33900	orf19.6398	R	-1.8227823	-0.8661423	*JLP1*	Predicted ORF in Assemblies 19, 20 and 21
DLD1	Cd36_17750	orf19.5805	2	-1.8203906	-0.86424804	*DLD1*	Transcription is specific to white cell type
ARO9	Cd36_45160	orf19.1237	4	-1.8183045	-0.8625939	*ARO9*	Predicted ORF in Assemblies 19, 20 and 21
ENA21	Cd36_72570	orf19.5170	7	-1.8139994	-0.859174	*ENA2*	Predicted ORF in Assemblies 19, 20 and 21
ILV2	Cd36_82300	orf19.1613	3	-1.8100173	-0.8560035	*ILV2*	Protein described as acetolactate synthase
SAM2	Cd36_10740	orf19.657	1	-1.8059112	-0.85272694	*SAM2*	S-adenosylmethionine synthetase, localizes to surface of hyphal cells, but not yeast-form cells
BAT22	Cd36_85560	orf19.6994	3	-1.8043778	-0.85150146	*BAT2*	Protein described as a branched chain amino acid aminotransferase
YOR1	Cd36_24060	orf19.1783	2	-1.8034948	-0.85079527	*YOR1*	Protein similar to S. cerevisiae Yor1p, which is a plasma membrane transporter of the ATP-binding cassette (ABC) family involved in resistance to aureobasidin A
	Cd36_04720	orf19.53	1	-1.8027886	-0.8502302	*MNN4*	Predicted ORF in Assemblies 19, 20 and 21
	Cd36_04420	orf19.779	1	-1.8019787	-0.84958196	*HAT1*	Predicted ORF in Assemblies 19, 20 and 21
	Cd36_04640	orf19.753	1	-1.7980789	-0.8464563	*MNT4/MNT2*	Predicted ORF in Assemblies 19, 20 and 21
PIL1	Cd36_04430	orf19.778	1	-1.7910215	-0.84078264	*PIL1*	Echinocandin-binding protein
	Cd36_44620	orf19.3781	4	-1.7908031	-0.8406067	*YBR147W*	Predicted ORF in Assemblies 19, 20 and 21
	Cd36_52430	orf19.4283	5	-1.7894986	-0.8395554		Predicted ORF in Assemblies 19, 20 and 21
	Cd36_84450	orf19.5905	3	-1.7828645	-0.83419704	*YBL028C*	Predicted ORF in Assemblies 19, 20 and 21
	Cd36_05260	orf19.411	1	-1.7815579	-0.8331394	*SRP40*	Similar to GTPase regulators
HTA3	Cd36_83230	orf19.327	3	-1.7794623	-0.8314414	*HTZ1*	Protein described as histone H2A
PGA56	Cd36_53620	orf19.1105.2	5	-1.7754105	-0.82815266		Regulator of sorbose utilization
POX1-3	Cd36_81950	orf19.1652	3	-1.7720449	-0.82541513	*POX1*	Predicted acyl-CoA oxidase
	Cd36_20970	orf19.1223	2	-1.7675086	-0.82171726	*DBF2*	Predicted ORF in Assemblies 19, 20 and 21

Gene Name	*C. dubliniensis* Cd36 identifier	*C. albicans* orf19 identifier	C'some	Fold change expression	Normalised Expression	*S. cerevisiae* ortholog	Description
GCF1	Cd36_08060	orf19.400	1	-1.7646414	-0.81937504		Protein that binds the regulatory region in the HWP1 pomoter
ADE4	Cd36_07230	orf19.1233	1	-1.7643402	-0.81912875	*ADE4*	Predicted ORF in Assemblies 19, 20 and 21
MLS1	Cd36_09130	orf19.4833	1	-1.7620019	-0.81721544	*MLS1*	Malate synthase
	Cd36_28920	orf19.4370	R	-1.7619143	-0.8171437		Predicted ORF in Assemblies 19, 20 and 21
PGA6	Cd36_08570	orf19.4765	1	-1.7612563	-0.81660485	*FLO1*	Putative GPI-anchored cell-wall protein of unknown function
	Cd36_50370	orf19.955	5	-1.7611914	-0.8165517		Predicted ORF in Assemblies 19, 20 and 21
	Cd36_06070	orf19.6264.3	1	-1.7606932	-0.8161435	*YIP3*	ORF Predicted by Annotation Working Group
	Cd36_22770		2	-1.7601311	-0.8156829		
	Cd36_01020	orf19.3296	1	-1.758486	-0.8143339		Predicted ORF in Assemblies 19, 20 and 21
ARG5,6	Cd36_08760	orf19.4788	1	-1.7577884	-0.8137615	*ARG5,6*	Arginine biosynthetic enzyme activities
	Cd36_42800	orf19.2701	4	-1.7575688	-0.8135812		Predicted ORF in Assemblies 19, 20 and 21
MNN3	Cd36_09470	orf19.4874	1	-1.7501369	-0.8074677	*MNN2*	Predicted Golgi alpha-1,2-mannosyltransferase
KEL1	Cd36_00150	orf19.6092	1	-1.7493987	-0.80685914	*KEL2*	Protein containing a Kelch repeat domain, similar to S. cerevisiae Kel1p
CEK1	Cd36_45970	orf19.2886	4	-1.7452921	-0.80346847	*FUS3*	ERK-family protein kinase, required for wild-type yeast hyphal switching, mating efficiency, and virulence in a mouse model
	Cd36_20030	orf19.6869	2	-1.7429345	-0.8015183	*AST2*	Predicted ORF in Assemblies 19, 20 and 21
CSH1	Cd36_03770	orf19.4477	1	-1.7407112	-0.7996769	*YPL088W*	Member of aldo-keto reductase family, similar to aryl alcohol dehydrogenases
GCN4	Cd36_24010	orf19.1358	2	-1.7404671	-0.7994745	*GCN4*	Transcriptional activator of general amino acid control response
	Cd36_02860	orf19.2998	1	-1.7402505	-0.79929495	*TSR2*	Predicted ORF in Assemblies 19, 20 and 21
	Cd36_45180	orf19.1239	4	-1.7376285	-0.7971196		Predicted ORF in Assemblies 19, 20 and 21
MDN1	Cd36_40990	orf19.4697	4	-1.7371544	-0.796726	*MDN1*	Protein induced during the mating process
	Cd36_00850	orf19.6014	1	-1.7311916	-0.79176545	*RRS1*	Predicted ORF in Assemblies 19, 20 and 21
MIG1	Cd36_52720	orf19.4318	5	-1.7295974	-0.79043627	*MIG1*	Transcriptional repressor
TUB4	Cd36_45170	orf19.1238	4	-1.7253485	-0.78688776	*TUB4*	Putative gamma-tubulin
	Cd36_17140	orf19.1569	2	-1.7221982	-0.7842512	*UTP22*	Predicted ORF in Assemblies 19, 20 and 21
CFL2	Cd36_45400	orf19.1264	4	-1.722177	-0.78423345	*FRE4*	Iron utilization protein
	Cd36_87200	orf19.6769	3	-1.7179673	-0.7807026	*YHL029C*	Predicted ORF in Assemblies 19, 20 and 21
	Cd36_83590	orf19.356	3	-1.7177927	-0.78055596	*GTT1*	Predicted ORF in Assemblies 19, 20 and 21
	Cd36_87040	orf19.6789	3	-1.7167889	-0.7797127	*NUD1*	Predicted ORF in Assemblies 19, 20 and 21
	Cd36_09890	orf19.993	1	-1.7144669	-0.77776		Predicted ORF in Assemblies 19, 20 and 21
	Cd36_17160	orf19.1566	2	-1.7130712	-0.7765851	*UTP21*	Predicted ORF in Assemblies 19, 20 and 21
	Cd36_46550	orf19.3100	4	-1.7116243	-0.77536607	*SPC110*	Predicted ORF in Assemblies 19, 20 and 21
CDR11	Cd36_84000	orf19.918	3	-1.711135	-0.7749536	*PDR5*	Putative transporter of PDR subfamily of ABC family
	Cd36_09670	orf19.4897	1	-1.7099138	-0.77392364	*SFH5*	Predicted ORF in Assemblies 19, 20 and 21
CAN2	Cd36_61160	orf19.111	6	-1.708167	-0.772449	*CAN1*	Putative amino acid permease
	Cd36_42610	orf19.2726	4	-1.7072002	-0.7716322	*SFK1*	Predicted ORF in Assemblies 19, 20 and 21
	Cd36_08790	orf19.4792	1	-1.7023803	-0.7675533	*AGA1*	Predicted ORF in Assemblies 19, 20 and 21
DUT1	Cd36_01230	orf19.3322	1	-1.7022351	-0.7674303	*DUT1*	dUTP pyrophosphatase
	Cd36_51050	orf19.1941	5	-1.7009076	-0.76630473	*NUF2*	Predicted ORF in Assemblies 19, 20 and 21
HIT1	Cd36_42620	orf19.2723	4	-1.6980386	-0.7638693	*HIT1*	Protein not essential for viability
ARG8	Cd36_44690	orf19.3770	4	-1.6973931	-0.7633207	*ARG8*	Predicted ORF in Assemblies 19, 20 and 21
HGT2	Cd36_01970	orf19.3668	1	-1.69696	-0.76295257	*RGT2*	Putative glucose transporter of the major facilitator superfamily
	Cd36_84010		3	-1.6960412	-0.76217127		
CSA2	Cd36_46390	orf19.3117	4	-1.6941289	-0.7605436		Predicted ORF in Assemblies 19, 20 and 21
	Cd36_72920	orf19.5126	7	-1.6870118	-0.75447005	*SRO9*	Predicted ORF in Assemblies 19, 20 and 21
	Cd36_81350	orf19.1709	3	-1.6868259	-0.7543111		Predicted ORF in Assemblies 19, 20 and 21
	Cd36_85890	orf19.7377	3	-1.685361	-0.75305766	*ASE1*	Predicted ORF in Assemblies 19, 20 and 21
	Cd36_80760	orf19.6155	3	-1.6848787	-0.7526447	*CDC9*	Predicted ORF in Assemblies 19, 20 and 21
PMA1	Cd36_80660	orf19.5383	3	-1.6831775	-0.7511873	*PMA1*	Plasma membrane H(+)-ATPase
	Cd36_35524	orf19.7664	R	-1.681605	-0.7498388	*YCR087C-A*	Predicted ORF in Assemblies 19, 20 and 21
VAC7	Cd36_44040	orf19.1409	4	-1.6811423	-0.74944186	*VAC7*	Protein not essential for viability
SWE1	Cd36_09410	orf19.4867	1	-1.6807334	-0.7490909	*SWE1*	Functional homolog of S. cerevisiae Swe1p
SPE2	Cd36_50700	orf19.568	5	-1.6792567	-0.74782276	*SPE2*	Predicted ORF in Assemblies 19, 20 and 21
	Cd36_03170	orf19.3037	1	-1.6763872	-0.74535537	*PAB1*	Protein described as poly(A)-binding protein
	Cd36_17430	orf19.5809	2	-1.6752373	-0.74436545	*BNA3*	Predicted ORF in Assemblies 19, 20 and 21
AHP2	Cd36_72180	orf19.6470	7	-1.6718081	-0.7414093	*AHP1*	Predicted ORF in Assemblies 19, 20 and 21
	Cd36_70380	orf19.7106	7	-1.6706843	-0.7404392	*VPS70*	Predicted ORF in Assemblies 19, 20 and 21
CEF3	Cd36_50780	orf19.4152	5	-1.6702589	-0.7400718	*HEF3*	Translation elongation factor 3 (EF-3)
YTM1	Cd36_08970	orf19.4815	1	-1.6687313	-0.73875165	*YTM1*	Protein similar to S. cerevisiae Ytm1p, which is involved in biogenesis of the large ribosomal subunit
ICL1	Cd36_04240	orf19.6844	1	-1.6680671	-0.7381773	*ICL1*	Isocitrate lyase
	Cd36_01530	orf19.3356	1	-1.6680213	-0.7381377	*ESP1*	Predicted ORF in Assemblies 19, 20 and 21
	Cd36_83220	orf19.326	3	-1.6663784	-0.73671603		Predicted ORF in Assemblies 19, 20 and 21
AAT1	Cd36_19740	orf19.3554	2	-1.6662033	-0.7365644	*AAT1*	Protein described as aspartate aminotransferase
	Cd36_04100	orf19.5203	1	-1.6656767	-0.7361084	*CCW14*	Predicted ORF in Assemblies 19, 20 and 21
	Cd36_86280	orf19.7413	3	-1.6655009	-0.7359561	*MMS21*	Predicted ORF in Assemblies 19, 20 and 21
	Cd36_12660	orf19.5006	1	-1.6630067	-0.733794	*GCV3*	Predicted ORF in Assemblies 19, 20 and 21
GAR1	Cd36_10840	orf19.1164	1	-1.6619074	-0.73284006	*GAR1*	Predicted ORF in Assemblies 19, 20 and 21
	Cd36_28490	orf19.2389	R	-1.6610276	-0.73207605	*SLD2*	Predicted ORF in Assemblies 19, 20 and 21
	Cd36_16490	orf19.1473	2	-1.6609758	-0.7320311	*YPL113C*	Predicted ORF in Assemblies 19, 20 and 21
	Cd36_06060	orf19.6264.4	1	-1.660703	-0.731794	*RPL39*	ORF Predicted by Annotation Working Group
	Cd36_70590	orf19.7082	7	-1.6578493	-0.7293129	*PET8*	Predicted ORF in Assemblies 19, 20 and 21
CSI2	Cd36_11540	orf19.5232	1	-1.6569153	-0.7284999	*BRX1*	Protein essential for growth
VAN1	Cd36_87410	orf19.6738	3	-1.6565701	-0.72819924	*VAN1*	Member of Mnn9p family

Gene Name	*C. dubliniensis* Cd36 identifier	*C. albicans* orf19 identifier	C'some	Fold change expression	Normalised Expression	*S. cerevisiae* ortholog	Description
	Cd36_20920	orf19.35	2	-1.6544293	-0.7263336	*SKY1*	Predicted ORF in Assemblies 19, 20 and 21
LEU4	Cd36_00180	orf19.6086	1	-1.6527667	-0.7248831	*LEU4*	Putative 2-isopropylmalalate synthase
MIT1	Cd36_23310	orf19.4077	2	-1.649839	-0.7223253	*SUR1|CSH1*	Protein involved in sphingolipid biosynthesis
	Cd36_62770		6	-1.648305	-0.72098327		
	Cd36_04520		1	-1.6480174	-0.7207315		
PGA39	Cd36_30290	orf19.6302	R	-1.6455026	-0.7185283	*AGA1*	Putative GPI-anchored protein of unknown function
POL30	Cd36_41670	orf19.4616	4	-1.6444589	-0.717613	*POL30*	Protein described as proliferating cell nuclear antigen (PCNA)
	Cd36_19420	orf19.4125	2	-1.6420342	-0.71548414	*PZF1*	Putative transcription factor with zinc finger DNA-binding motif
CCC1	Cd36_83700	orf19.6948	3	-1.6404735	-0.7141123	*CCC1*	Protein described as predicted manganese transporter
	Cd36_15800	orf19.2038	2	-1.6403593	-0.71401185		Predicted ORF in Assemblies 19, 20 and 21
	Cd36_71400	orf19.6569	7	-1.6382718	-0.7121747		Predicted ORF in Assemblies 19, 20 and 21
HHT21	Cd36_04010	orf19.1061	1	-1.6380256	-0.71195793	*HHT2|HHT1*	Putative histone H3
	Cd36_41080	orf19.4680	4	-1.6377	-0.7116711		Predicted ORF in Assemblies 19, 20 and 21
	Cd36_84230	orf19.5871	3	-1.6373596	-0.7113712	*SNF5*	Predicted ORF in Assemblies 19, 20 and 21
CDC5	Cd36_00900	orf19.6010	1	-1.6372497	-0.7112744	*CDC5*	Polo-like kinase
	Cd36_71490	orf19.6559	7	-1.6369501	-0.71101034	*TFC7*	Predicted ORF in Assemblies 19, 20 and 21
	Cd36_61710	orf19.3425	6	-1.6341043	-0.7085	*MED2*	Predicted ORF in Assemblies 19, 20 and 21
	Cd36_51210	orf19.1959	5	-1.6329441	-0.7074754	*OTU2*	Predicted ORF in Assemblies 19, 20 and 21
NUP49	Cd36_12540	orf19.4987	1	-1.6329327	-0.7074653	*NUP49*	Nuclear pore protein
ADO1	Cd36_63990	orf19.5591	6	-1.6308322	-0.70560837	*ADO1*	Predicted ORF in Assemblies 19, 20 and 21
	Cd36_45480	orf19.1277	4	-1.6303537	-0.70518494	*MUC1*	Predicted ORF in Assemblies 19, 20 and 21
	Cd36_73000	orf19.1340	7	-1.6291113	-0.7040851	*YDL124W*	Predicted ORF in Assemblies 19, 20 and 21
CDC47	Cd36_23200	orf19.201	2	-1.6290792	-0.70405674		Protein described as having role in control of cell division
	Cd36_17720	orf19.5809	2	-1.6290208	-0.704005	*BNA3*	Predicted ORF in Assemblies 19, 20 and 21
MET6	Cd36_26580	orf19.2551	R	-1.6286055	-0.7036371	*MET6*	5-methyltetrahydropteroyltriglutamate-homocysteine methyltransferase (cobalamin-independent methionine synthase)
	Cd36_02060	orf19.3678	1	-1.6276475	-0.70278835		Protein not essential for viability
	Cd36_09320	orf19.4857	1	-1.626375	-0.7016599		Predicted ORF in Assemblies 19, 20 and 21
RPS7A	Cd36_81410	orf19.1700	3	-1.6247567	-0.7002237	*RPS7A*	Predicted ribosomal protein
HSP70	Cd36_12490	orf19.4980	1	-1.619767	-0.69578624	*SSA4*	Putative chaperone of Hsp70 family
	Cd36_07470	orf19.5066	1	-1.6186099	-0.6947553	*YDR412W*	Predicted ORF in Assemblies 19, 20 and 21
	Cd36_62940	orf19.5535	6	-1.6182729	-0.6944549	*FEN2*	Predicted ORF in Assemblies 19, 20 and 21
	Cd36_44070		4	-1.6156504	-0.69211507		
	Cd36_09050	orf19.4824	1	-1.6154381	-0.6919255		Predicted ORF in Assemblies 19, 20 and 21
	Cd36_13200	orf19.7232	1	-1.6141196	-0.6907475	*IRR1*	Predicted ORF in Assemblies 19, 20 and 21
CTN1	Cd36_01580	orf19.4551	1	-1.613335	-0.6900461	*YAT1*	Predicted carnitine acetyl transferase
	Cd36_80120	orf19.5465	3	-1.612165	-0.6889994	*YJU2*	Predicted ORF in Assemblies 19, 20 and 21
ILV5	Cd36_60880	orf19.88	6	-1.6115787	-0.68847466	*ILV5*	Protein described as ketol-acid reductoisomerase
DED81	Cd36_73270	orf19.6702	7	-1.6108427	-0.68781567	*DED81*	Putative tRNA-Asn synthetase
	Cd36_00170	orf19.6090	1	-1.6108047	-0.6877816	*NSR1*	Predicted ORF in Assemblies 19, 20 and 21
	Cd36_06240	orf19.6245	1	-1.6094309	-0.6865506		Predicted ORF in Assemblies 19, 20 and 21
RNH35	Cd36_71460	orf19.6562	7	-1.6086886	-0.6858851	*RNH201*	Predicted ORF in Assemblies 19, 20 and 21
	Cd36_35560	orf19.7672	R	-1.607232	-0.6845782	*DFM1*	Predicted ORF in Assemblies 19, 20 and 21
	Cd36_15150	orf19.2115	2	-1.6062483	-0.68369484	*YKL027W*	Putative molybdopterin-converting factor
ALD5	Cd36_17740	orf19.5806	2	-1.6059988	-0.6834707	*ALD5*	Protein described as an aldehyde dehydrogenase
	Cd36_09120	orf19.4831	1	-1.6053852	-0.6829195		Predicted ORF in Assemblies 19, 20 and 21
GPX2	Cd36_60850	orf19.85	6	-1.6045319	-0.6821525	*HYR1*	Similar to glutathione peroxidase
	Cd36_07330	orf19.5051	1	-1.6043301	-0.68197095		Predicted ORF in Assemblies 19, 20 and 21
CTN3	Cd36_83950	orf19.2809	3	-1.6038402	-0.6815305	*YAT2*	Predicted peroxisomal carnitine acetyl transferase
	Cd36_02070	orf19.3679	1	-1.6028332	-0.68062425	*YNL200C*	Predicted ORF in Assemblies 19, 20 and 21
AAF1	Cd36_86430	orf19.7436	3	-1.6021862	-0.6800418	*DEF1*	Possible regulatory protein
ADE8	Cd36_17860	orf19.5789	2	-1.6019005	-0.67978454	*ADE8*	Predicted enzyme of amino acid biosynthesis
	Cd36_44990	orf19.1791	4	-1.6008219	-0.67881274	*MAK11*	Predicted ORF in Assemblies 19, 20 and 21
	Cd36_19050	orf19.4513	2	-1.6006514	-0.6786591		Protein not essential for viability
	Cd36_42230	orf19.2769	4	-1.6006403	-0.6786492	*PBI2*	Predicted ORF in Assemblies 19, 20 and 21
CDC21	Cd36_19690	orf19.3549	2	-1.6004009	-0.6784334	*CDC21*	Predicted ORF in Assemblies 19, 20 and 21
GCV1	Cd36_62730	orf19.5519	6	-1.5989473	-0.67712235	*GCV1*	Protein described as T subunit of glycine decarboxylase
SIN3	Cd36_00880	orf19.6011	1	-1.5980438	-0.6763069	*SIN3*	Protein similar to S. cerevisiae Sin3p (transcriptional corepressor involved in histone deacetylase recruitment)
	Cd36_64670	orf19.1091	6	-1.597062	-0.6754203	*NOP8*	Putative ortholog of S. cerevisiae Nop8p, which is a nucleolar protein required for 60S ribosomal subunit biogenesis
	Cd36_53470	orf19.1121	5	-1.59552	-0.6740267		Predicted ORF in Assemblies 19, 20 and 21
TRP4	Cd36_46560	orf19.3099	4	-1.5955101	-0.6740178	*TRP4*	Predicted enzyme of amino acid biosynthesis
YST1	Cd36_85350	orf19.6975	3	-1.5937041	-0.6723838	*RPS0A*	Ribosome-associated protein
	Cd36_22340	orf19.2168.3	2	-1.5930479	-0.67178965	*YOP1*	ORF Predicted by Annotation Working Group
RPL27A	Cd36_11610	orf19.5225.2	1	-1.5917753	-0.67063665	*RPL27A*	Predicted ribosomal protein
EFB1	Cd36_44190	orf19.3838	4	-1.5903364	-0.669332	*EFB1*	Translation elongation factor EF-1 beta
	Cd36_42910	orf19.2686	4	-1.589736	-0.66878724	*CPS1*	Predicted ORF in Assemblies 19, 20 and 21
	Cd36_44560	orf19.3787	4	-1.5892512	-0.6683471	*KAE1*	Predicted ORF in Assemblies 19, 20 and 21
	Cd36_34470	orf19.7297	R	-1.5888063	-0.66794324	*YHR112C*	Predicted ORF in Assemblies 19, 20 and 21
	Cd36_62200	orf19.3505	6	-1.5887845	-0.66792345	*SLM2*	Predicted ORF in Assemblies 19, 20 and 21
ERG13	Cd36_34550	orf19.7312	R	-1.5879917	-0.6672034	*ERG13*	Protein similar to S. cerevisiae Erg13p, which is involved in ergosterol biosynthesis
	Cd36_50290	orf19.969	5	-1.5872171	-0.6664995	*PRS1*	Predicted ORF in Assemblies 19, 20 and 21
	Cd36_15360	orf19.2092	2	-1.5863178	-0.66568184	*STR3*	Predicted ORF in Assemblies 19, 20 and 21
	Cd36_46170	orf19.3139	4	-1.5859799	-0.6653745	*YML131W*	Predicted ORF in Assemblies 19, 20 and 21
	Cd36_12810	orf19.5020	1	-1.5854621	-0.6649034	*DEF1*	Predicted ORF in Assemblies 19, 20 and 21

Gene Name	*C. dubliniensis* Cd36 identifier	*C. albicans* orf19 identifier	C'some	Fold change expression	Normalised Expression	*S. cerevisiae* ortholog	Description
CNH1	Cd36_40100	orf19.367	4	-1.5851847	-0.6646509	*NHA1*	Na+/H+ antiporter
	Cd36_83090	orf19.308	3	-1.5848255	-0.66432405	*SNG1*	Predicted ORF in Assemblies 19, 20 and 21
RPS24	Cd36_80110	orf19.5466	3	-1.5841293	-0.6636901	*RPS24B|RPS24A*	Predicted ribosomal protein
	Cd36_73050	orf19.1335	7	-1.5841097	-0.6636722	*MTR4*	Predicted ORF in Assemblies 19, 20 and 21
	Cd36_20630		2	-1.5826826	-0.662372		
MP65	Cd36_24090	orf19.1779	2	-1.5813651	-0.6611705	*SCW4*	Cell surface mannoprotein
	Cd36_15970	orf19.2018	2	-1.5809752	-0.66081476	*JJJ3*	Predicted ORF in Assemblies 19, 20 and 21
	Cd36_08780	orf19.4791	1	-1.5796577	-0.65961194		Predicted ORF in Assemblies 19, 20 and 21
PHO86	Cd36_22080	orf19.2199	2	-1.5796317	-0.6595882	*PHO86*	Predicted ORF in Assemblies 19, 20 and 21
	Cd36_13050	orf19.7215	1	-1.5771369	-0.65730786	*UTP10*	Predicted ORF in Assemblies 19, 20 and 21
	Cd36_00750		1	-1.5766034	-0.6568198		
	Cd36_17560	orf19.5825	2	-1.5763234	-0.6565635	*NCB2*	Predicted ORF in Assemblies 19, 20 and 21
AGA1	Cd36_50540	orf19.935	5	-1.5759071	-0.6561825	*MUC1*	Protein with some similarity to agglutinin subunit
	Cd36_22270	orf19.2177	2	-1.5758322	-0.656114		ORF Predicted by Annotation Working Group
	Cd36_12120	orf19.4931.1	1	-1.5739421	-0.65438247	*RPL14A|RPL14B*	ORF Predicted by Annotation Working Group
	Cd36_15050	orf19.1917	2	-1.5730879	-0.65359926	*SAY1*	Predicted ORF in Assemblies 19, 20 and 21
	Cd36_07000	orf19.2794	1	-1.5701802	-0.65093017	*YBL036C*	Protein regulated by Gcn4p
	Cd36_09520	orf19.4882	1	-1.5696391	-0.6504328	*TFA2*	Predicted ORF in Assemblies 19, 20 and 21
	Cd36_53660	orf19.3218	5	-1.5695368	-0.6503389	*YJR124C*	Putative multidrug resistance protein
	Cd36_62020	orf19.3393	6	-1.5691991	-0.65002835	*DBP9*	Putative DEAD-box helicase
	Cd36_87420	orf19.6737	3	-1.5681975	-0.6491072		Protein not essential for viability
	Cd36_87330	orf19.6748	3	-1.5675056	-0.64847064		Predicted ORF in Assemblies 19, 20 and 21
	Cd36_28370	orf19.2399	R	-1.5661427	-0.6472156	*JJJ1*	Putative transcription factor with zinc finger DNA-binding motif
GCV2	Cd36_07910	orf19.385	1	-1.5660137	-0.6470969	*GCV2*	Putative protein of glycine catabolism
	Cd36_02840	orf19.2995	1	-1.5649551	-0.64612126	*LOT5*	Predicted ORF in Assemblies 19, 20 and 21
	Cd36_10720	orf19.660	1	-1.5644819	-0.6456849		Predicted ORF in Assemblies 19, 20 and 21
GIN4	Cd36_10690	orf19.663	1	-1.5635687	-0.6448426	*GIN4*	Kinase involved in pseudohyphal-to-hyphal switch
	Cd36_09660	orf19.4896	1	-1.5623788	-0.64374423	*RPA34*	Predicted ORF in Assemblies 19, 20 and 21
ARG4	Cd36_73220	orf19.6689	7	-1.5622355	-0.6436119	*ARG4*	Argininosuccinate lyase, catalyzes the final step in the arginine biosynthesis pathway
	Cd36_70370	orf19.7107	7	-1.5617262	-0.6431415	*ALB1*	Predicted ORF in Assemblies 19, 20 and 21
	Cd36_83770	orf19.6938	3	-1.5607852	-0.642272	*MEU1*	Predicted ORF in Assemblies 19, 20 and 21
ALR1	Cd36_82340	orf19.1607	3	-1.5588442	-0.6404767	*ALR1*	Putative transporter of divalent cations
ARO4	Cd36_04870	orf19.4060	1	-1.5586798	-0.6403246	*ARO4*	3-Deoxy-D-arabinoheptulosonate-7-phosphate synthase
	Cd36_44740		4	-1.5571117	-0.63887244		
	Cd36_00250	orf19.6077	1	-1.5565662	-0.63836694	*PNS1*	Predicted ORF in Assemblies 19, 20 and 21
IFE1	Cd36_04500	orf19.769	1	-1.5544492	-0.63640344	*BDH2*	Protein not essential for viability
HOG1	Cd36_18080	orf19.895	2	-1.5543479	-0.6363094	*HOG1*	MAP kinase of osmotic-, heavy metal-, and core stress response
APT1	Cd36_16300	orf19.1448	2	-1.5538424	-0.6358402	*APT1*	Predicted ORF in Assemblies 19, 20 and 21
	Cd36_23960	orf19.1363	2	-1.5535127	-0.63553405	*YOR338W*	Predicted ORF in Assemblies 19, 20 and 21
	Cd36_62600	orf19.3481	6	-1.5532879	-0.6353252	*MRH4*	Predicted ORF in Assemblies 19, 20 and 21
SOL1	Cd36_83830	orf19.6930	3	-1.5526875	-0.63476753		Cell cycle regulator
IMH3	Cd36_20770	orf19.18	2	-1.5526072	-0.6346929	*IMD4*	Inosine monophosphate (IMP) dehydrogenase
	Cd36_08800	orf19.4793	1	-1.5523281	-0.6344335	*TMA16*	Predicted ORF in Assemblies 19, 20 and 21
EIF4E	Cd36_35334	orf19.7626	R	-1.5502831	-0.63253164	*CDC33*	Putative translation initiation factor eIF4E
	Cd36_34520	orf19.7306	R	-1.5493431	-0.63165665	*YPR127W*	Protein of aldo-keto reductase family
	Cd36_50080	orf19.5693	5	-1.5491812	-0.63150597	*GAA1*	Predicted ORF in Assemblies 19, 20 and 21
MSH6	Cd36_12230	orf19.4945	1	-1.5485742	-0.63094056	*MSH6*	Protein similar to S. cerevisiae Msh6p, which is involved in mismatch repair
USO5	Cd36_83070	orf19.306	3	-1.5485628	-0.6309298	*MYO1*	Protein of unknown function
	Cd36_45000	orf19.1792	4	-1.5481713	-0.63056505	*CDC16*	Predicted ORF in Assemblies 19, 20 and 21
ERG1	Cd36_08100	orf19.406	1	-1.548148	-0.6305435	*ERG1*	Squalene epoxidase, catalyzes epoxidation of squalene to 2,3(S)-oxidosqualene in the ergosterol biosynthetic pathway
	Cd36_12860		1	-1.5476763	-0.6301038		
	Cd36_43870	orf19.1430	4	-1.546293	-0.62881374		Predicted ORF in Assemblies 19, 20 and 21
	Cd36_24540		2	-1.5458465	-0.628397		
BUD31	Cd36_09300	orf19.4855	1	-1.5444193	-0.62706447	*BUD31*	Not subject to mating-type regulation, in contrast to the S. cerevisiae ortholog, which has a role in specification of the bud site
RPL19A	Cd36_84440	orf19.5904	3	-1.5439671	-0.626642	*RPL19A|RPL19B*	Predicted ribosomal protein
	Cd36_10210	orf19.2330	1	-1.5435405	-0.62624335	*UTP6*	Predicted ORF in Assemblies 19, 20 and 21
CCC2	Cd36_52780	orf19.4328	5	-1.5422786	-0.6250634	*CCC2*	Copper-transporting P-type ATPase of Golgi
HOL1	Cd36_02800	orf19.2991	1	-1.5418591	-0.624671	*HOL1*	Predicted ORF in Assemblies 19, 20 and 21
KAR9	Cd36_12730	orf19.5011	1	-1.5416344	-0.6244607	*KAR9*	Protein similar to S. cerevisiae Kar9p, which has role in mitotic spindle positioning
	Cd36_46320	orf19.3124	4	-1.5403227	-0.6232326	*MAP1*	Predicted ORF in Assemblies 19, 20 and 21
	Cd36_83900		3	-1.5400695	-0.6229954		
	Cd36_51240	orf19.1963	5	-1.5396432	-0.622596	*GDS1*	Predicted ORF in Assemblies 19, 20 and 21
	Cd36_52360	orf19.4273	5	-1.5385089	-0.6215328		Predicted ORF in Assemblies 19, 20 and 21
DUR3	Cd36_53230	orf19.6656	5	-1.5375559	-0.62063885	*DUR3*	Alkaline downregulated
	Cd36_81120		3	-1.537049	-0.6201632		
RCK2	Cd36_21410	orf19.2268	2	-1.5366285	-0.6197684	*RCK2*	Predicted ORF in Assemblies 19, 20 and 21
	Cd36_02830		1	-1.5363067	-0.6194663		
	Cd36_73590	orf19.7190	7	-1.5362451	-0.61940837	*OGG1*	Predicted ORF in Assemblies 19, 20 and 21
	Cd36_82490	orf19.242.2	3	-1.5358735	-0.61905944	*YSY6*	ORF Predicted by Annotation Working Group
	Cd36_72830	orf19.5136	7	-1.5356156	-0.6188171	*YGR017W*	Predicted ORF in Assemblies 19, 20 and 21

Gene Name	*C. dubliniensis* Cd36 identifier	*C. albicans* orf19 identifier	C'some	Fold change expression	Normalised Expression	*S. cerevisiae* ortholog	Description
	Cd36_08680	orf19.4778	1	-1.5348866	-0.6181321	*LYS14*	Putative transcription factor with zinc cluster DNA-binding motif
	Cd36_70090	orf19.7062	7	-1.5338305	-0.6171391	*RPA135*	Predicted ORF in Assemblies 19, 20 and 21
	Cd36_86710	orf19.6829	3	-1.5319015	-0.61532354		Predicted ORF in Assemblies 19, 20 and 21
	Cd36_81670	orf19.1667.1	3	-1.5314263	-0.6148759	*YLR218C*	ORF Predicted by Annotation Working Group
	Cd36_09710	f19.4902; orf19.49	1	-1.5312421	-0.6147024		
	Cd36_81800	orf19.1654	3	-1.5303891	-0.6138985		Predicted ORF in Assemblies 19, 20 and 21
NIP7	Cd36_62570	orf19.3478	6	-1.5300144	-0.6135452	*NIP7*	Protein described as a nucleolar protein with role in ribosomal assembly
RAD57	Cd36_22290	orf19.2174	2	-1.5297976	-0.61334074	*RAD57*	Essential protein
	Cd36_11970	orf19.6343	1	-1.5296657	-0.6132164	*FEN1*	Predicted ORF in Assemblies 19, 20 and 21
DBF4	Cd36_72610	orf19.5166	7	-1.5294862	-0.6130471	*DBF4*	Predicted ORF in Assemblies 19, 20 and 21
PST1	Cd36_21170	orf19.2241	2	-1.528976	-0.61256576	*PST2*	Protein described as 1,4-benzoquinone reductase
AXL2	Cd36_43700	orf19.5292	4	-1.5273128	-0.61099553	*AXL2*	Protein not essential for viability
	Cd36_63370	orf19.5550	6	-1.5271235	-0.6108167	*MRT4*	Predicted ORF in Assemblies 19, 20 and 21
	Cd36_03530	orf19.1030	1	-1.526358	-0.61009336	*FPR3*	Predicted ORF in Assemblies 19, 20 and 21
	Cd36_82720	orf19.263.1	3	-1.5259633	-0.60972023	*YBR056W-A*	Predicted ORF in Assembly 20 and 21
VRG4	Cd36_07220	orf19.1232	1	-1.5255494	-0.6093289	*VRG4*	GDP-mannose transporter
	Cd36_04770	orf19.58	1	-1.5253209	-0.60911274	*RRP6*	Predicted ORF in Assemblies 19, 20 and 21
CYS4	Cd36_01710	orf19.4536	1	-1.523439	-0.60733175	*CYS4*	Predicted enzyme of sulfur amino acid biosynthesis
SSC1	Cd36_21650	orf19.1896	2	-1.5234151	-0.6073091	*SSC1*	Heat shock protein
	Cd36_22530	orf19.1434	2	-1.5233666	-0.6072631	*DPB11*	Predicted ORF in Assemblies 19, 20 and 21
	Cd36_50850	orf19.4145	5	-1.5228337	-0.60675836	*HAP1*	Predicted zinc-finger protein of unknown function
	Cd36_24770		2	-1.5224489	-0.6063938		
	Cd36_60570	orf19.4193	6	-1.5221436	-0.6061045	*YDR063W*	Predicted ORF in Assemblies 19, 20 and 21
	Cd36_52320	orf19.4268	5	-1.5216061	-0.6055949	*UTP13*	Predicted ORF in Assemblies 19, 20 and 21
	Cd36_87740	orf19.6183	3	-1.5215794	-0.6055696	*TIM8*	Predicted ORF in Assemblies 19, 20 and 21
	Cd36_62440	orf19.3466	6	-1.5210384	-0.6050566	*MRM2*	Predicted ORF in Assemblies 19, 20 and 21
SMC2	Cd36_22690	orf19.3623	2	-1.5207068	-0.60474205	*SMC2*	Protein similar to S. cerevisiae Smc2p, which is a component of the condensin complex involved in mitotic chromosome condensation
	Cd36_86370	orf19.7425	3	-1.5204763	-0.6045234	*UNG1*	Predicted ORF in Assemblies 19, 20 and 21
	Cd36_86390	orf19.7427	3	-1.520342	-0.60439587	*YML018C*	Predicted ORF in Assemblies 19, 20 and 21
	Cd36_10970		1	-1.5197717	-0.60385466		
	Cd36_21040	orf19.3148	2	-1.5193125	-0.6034186	*IXR1*	Predicted ORF in Assemblies 19, 20 and 21
NOP5	Cd36_60320	orf19.1199	6	-1.5189414	-0.6030662	*NOP58*	Protein similar to S. cerevisiae Nop5p protein of small nucleolar ribonucleoprotein complex
	Cd36_62640	orf19.5510	6	-1.5176705	-0.6018586	*ITC1*	Predicted ORF in Assemblies 19, 20 and 21
KRR1	Cd36_10710	orf19.661	1	-1.5173495	-0.60155344	*KRR1*	Decreased transcription is observed upon benomyl treatment or in an azole-resistant strain that overexpresses MDR1
	Cd36_71140	orf19.6910	7	-1.5170934	-0.6013099	*PSF1*	Predicted ORF in Assemblies 19, 20 and 21
	Cd36_50630	orf19.926	5	-1.5162622	-0.6005192	*EXO1*	Predicted ORF in Assemblies 19, 20 and 21
GUA1	Cd36_08950	orf19.4813	1	-1.5162206	-0.6004796	*GUA1*	Predicted ORF in Assemblies 19, 20 and 21
MET28	Cd36_70670	orf19.7046	7	-1.5154462	-0.59974265	*MET4*	Protein induced during the mating process
	Cd36_09150	orf19.4835	1	-1.5148839	-0.59920716	*UTP7*	Predicted ORF in Assemblies 19, 20 and 21
CPY1	Cd36_73010	orf19.1339	7	-1.5138905	-0.5982609	*PRC1*	Carboxypeptidase Y
MNT1	Cd36_81700	orf19.1665	3	-1.5125494	-0.59698224	*KTR1*	Alpha-1,2-mannosyl transferase
MLT1	Cd36_07740	orf19.5100	1	-1.5124464	-0.596884	*BPT1*	Vacuolar membrane transporter: MRP subfamily of ABC family
	Cd36_08580	orf19.4766	1	-1.5123619	-0.5968034	*ARG81*	Putative transcription factor with zinc cluster DNA-binding motif
	Cd36_85930	orf19.7381	3	-1.511683	-0.59615564	*LYS14*	Predicted zinc-finger protein of unknown function
	Cd36_11990	orf19.6341	1	-1.5111974	-0.59569216	*RIB7*	Predicted ORF in Assemblies 19, 20 and 21
	Cd36_50330	orf19.964	5	-1.5107837	-0.5952971	*SMC4*	Predicted ORF in Assemblies 19, 20 and 21
	Cd36_70960	orf19.7011	7	-1.5101559	-0.5946975	*RRP12*	Predicted ORF in Assemblies 19, 20 and 21
	Cd36_64640	orf19.1089	6	-1.5097576	-0.59431696	*PEX11*	Predicted ORF in Assemblies 19, 20 and 21
	Cd36_03960	orf19.1054	1	-1.509576	-0.5941434	*YLL023C*	Predicted ORF in Assemblies 19, 20 and 21
PGA1	Cd36_35332	orf19.7625	R	-1.5091585	-0.5937443		Putative GPI-anchored protein of unknown function
NEP1	Cd36_10670	orf19.665	1	-1.5087734	-0.59337616	*EMG1*	Protein of unknown function
	Cd36_35420	orf19.7645	R	-1.5086417	-0.5932503	*BPL1*	Predicted ORF in Assemblies 19, 20 and 21
RPL35	Cd36_84940	orf19.5964.2	3	-1.5064152	-0.5911195	*RPL35A|RPL35E*	Protein described as a ribosomal protein
RPL8B	Cd36_85230	orf19.6002	3	-1.5057112	-0.59044504	*RPL8B*	Predicted ribosomal protein
	Cd36_81860	orf19.5773	3	-1.5052862	-0.5900378	*YOL057W*	Predicted ORF in Assemblies 19, 20 and 21
RPS5	Cd36_52860	orf19.4336	5	-1.504338	-0.58912873	*RPS5*	Predicted ribosomal protein
	Cd36_00220		1	-1.5042139	-0.58900976		
ADH1	Cd36_54650	orf19.3997	5	-1.5033795	-0.58820915	*ADH3*	Alcohol dehydrogenase
RPS6A	Cd36_41260	orf19.4660	4	-1.5029204	-0.58776855	*RPS6A|RPS6B*	Predicted ribosomal protein
FCY21	Cd36_24020	orf19.1357	2	-1.5026541	-0.58751297	*FCY2*	High affinity, high capacity, hypoxanthine-adenine-guanine-cytosine/ H+ symporter
	Cd36_05410	orf19.2478	1	-1.5006113	-0.5855503		Predicted ORF in Assemblies 19, 20 and 21
IRO1	Cd36_81290	orf19.1715	3	-1.5005808	-0.585521	*YJL225C*	Putative transcription factor
	Cd36_03250	orf19.3048	1	-1.5000653	-0.5850253	*SCD5*	Predicted ORF in Assemblies 19, 20 and 21
	Cd36_86200	orf19.7404	3	1.5005535	0.58549476	*CHA1*	Predicted ORF in Assemblies 19, 20 and 21
	Cd36_26950	orf19.2605	R	1.5014281	0.5863354	*PRK1*	Predicted ORF in Assemblies 19, 20 and 21
	Cd36_05580	orf19.2457	1	1.501452	0.5863583		Predicted ORF in Assemblies 19, 20 and 21
	Cd36_87450	orf19.6732	3	1.5014738	0.5863793	*YCR015C*	Predicted ORF in Assemblies 19, 20 and 21
	Cd36_21540	orf19.2284	2	1.5023956	0.5872648		Predicted ORF in Assemblies 19, 20 and 21
	Cd36_32090	orf19.916	R	1.5030339	0.5878775	*YNL305C*	Predicted ORF in Assemblies 19, 20 and 21
	Cd36_70270	orf19.7118	7	1.5039482	0.5887549	*ADK2*	Predicted ORF in Assemblies 19, 20 and 21

Gene Name	*C. dubliniensis* Cd36 identifier	*C. albicans* orf19 identifier	C'some	Fold change expression	Normalised Expression	*S. cerevisiae* ortholog	Description
DPP2	Cd36_10930	orf19.1155	1	1.5040358	0.58883893	*DPP1*	Predicted ORF in Assemblies 19, 20 and 21
	Cd36_33790	orf19.6376	R	1.5040923	0.5888932	*PTC5*	Predicted ORF in Assemblies 19, 20 and 21
PDE1	Cd36_52100	orf19.4235	5	1.5040971	0.5888977	*PDE1*	Cyclic nucleotide phosphodiesterase (PDEase), low affinity
TRP1	Cd36_00130	orf19.6096	1	1.5049218	0.58968854	*TRP1*	Phosphoribosylanthranilate isomerase
	Cd36_25980	orf19.3260	R	1.5049598	0.589725	*YKL088W*	Predicted ORF in Assemblies 19, 20 and 21
	Cd36_32370	orf19.1850	R	1.505136	0.5898938	*SIW14*	Predicted ORF in Assemblies 19, 20 and 21
	Cd36_27670	orf19.2825	R	1.5062251	0.5909374	*DRE2*	Predicted ORF in Assemblies 19, 20 and 21
GSY1	Cd36_25850	orf19.3278	R	1.5062871	0.59099674	*GSY1*	Protein described as glycogen synthase
CDR2	Cd36_84860	orf19.5958	3	1.5069376	0.59161973	*PDR5*	Multidrug transporter, ATP-binding cassette (ABC) superfamily
	Cd36_63110	orf19.5572	6	1.5071976	0.59186864		Predicted ORF in Assemblies 19, 20 and 21
LYS12	Cd36_26410	orf19.2525	R	1.5078666	0.5925088	*LYS12*	Protein described as mitochondrial homoisocitrate dehydrogenase
APG7	Cd36_32270	orf19.707	R	1.5085076	0.593122	*ATG7*	Protein not essential for viability
	Cd36_32500	orf19.2368	R	1.5088295	0.5934298	*LIN1*	Predicted ORF in Assemblies 19, 20 and 21
INO2	Cd36_25070	orf19.7539	R	1.5097113	0.5942726		Transcriptional activator that may be involved in regulation of ribosomal protein genes
	Cd36_70150	orf19.7069	7	1.5098138	0.5943706	*YBR261C*	Predicted ORF in Assemblies 19, 20 and 21
	Cd36_27780	orf19.2832	R	1.5112524	0.5957446	*YNL152W*	Predicted ORF in Assemblies 19, 20 and 21
	Cd36_32930	orf19.6138	R	1.5117342	0.5962045	*FRE4*	Predicted ORF in Assemblies 19, 20 and 21
SAP99	Cd36_18360	orf19.853	2	1.512369	0.5968102	*MKC7*	Putative secreted aspartyl protease
	Cd36_08400	orf19.4749	1	1.5130671	0.597476		Predicted ORF in Assemblies 19, 20 and 21
	Cd36_00030		1	1.5131906	0.5975938		
PDB1	Cd36_43720	orf19.5294	4	1.5133835	0.5977776	*PDB1*	Protein described as similar to pyruvate dehydrogenase
	Cd36_35190	orf19.7596	R	1.5139986	0.5983639	*PMU1*	Predicted ORF in Assemblies 19, 20 and 21
MNT3	Cd36_30630	orf19.1010	R	1.5142387	0.59859264	*KTR1*	Protein with similarity to mannosyltransferases
PRE1	Cd36_54910	orf19.4025	5	1.5149419	0.5992625	*PRE1*	Upregulated by Rim101p at acid pH
	Cd36_30560	orf19.652	R	1.5150148	0.59933186	*YEN1*	Predicted ORF in Assemblies 19, 20 and 21
	Cd36_71830	orf19.6518	7	1.5151422	0.5994532	*HFD1*	Predicted ORF in Assemblies 19, 20 and 21
	Cd36_06700	orf19.4450	1	1.5166669	0.6009042	*YJL103C*	Predicted zinc-finger protein of unknown function
	Cd36_51750	orf19.3183	5	1.5172297	0.6014395		Predicted ORF in Assemblies 19, 20 and 21
	Cd36_82860	orf19.278	3	1.5173277	0.6015327		Predicted ORF in Assemblies 19, 20 and 21
BCR1	Cd36_31890	orf19.723	R	1.520256	0.6043143	*USV1*	Transcription factor required for wild-type biofilm formation
	Cd36_29250	orf19.479.2	R	1.5202733	0.6043308	*SEC22*	ORF Predicted by Annotation Working Group
CTR2	Cd36_08130	orf19.4720	1	1.5219234	0.60589576	*CTR2*	Predicted ORF in Assemblies 19, 20 and 21
	Cd36_33880	orf19.6393	R	1.5219246	0.60589695	*GTS1*	Predicted ORF in Assemblies 19, 20 and 21
	Cd36_60610	orf19.3659	6	1.5223116	0.60626364	*YER139C*	Predicted ORF in Assemblies 19, 20 and 21
	Cd36_29490	orf19.504	R	1.5224419	0.60638714	*ARP5*	Predicted ORF in Assemblies 19, 20 and 21
	Cd36_40850	orf19.4161	4	1.5227928	0.6067197	*NSE4*	Predicted ORF in Assemblies 19, 20 and 21
ECM29	Cd36_87170	orf19.6773	3	1.5240885	0.60794663	*ECM29*	Protein similar to S. cerevisiae Ecm29p
	Cd36_27540	orf19.163	R	1.5250001	0.60880935	*PAN6*	Predicted ORF in Assemblies 19, 20 and 21
	Cd36_86880	orf19.6809	3	1.5253813	0.60916996	*PMU1*	Predicted ORF in Assemblies 19, 20 and 21
	Cd36_32980	orf19.6134	R	1.5262188	0.60996175	*SEC39*	Predicted ORF in Assemblies 19, 20 and 21
	Cd36_26160	orf19.3237	R	1.5265235	0.61024976	*UFD4*	Predicted ORF in Assemblies 19, 20 and 21
	Cd36_29980	orf19.551	R	1.5265626	0.6102867		Predicted ORF in Assemblies 19, 20 and 21
PHO13	Cd36_23590	orf19.1405	2	1.527594	0.6112611	*PHO13*	Transcription is regulated upon yeast-hyphal switch
	Cd36_31170	orf19.6635	R	1.5290107	0.6125984		Predicted ORF in Assemblies 19, 20 and 21
	Cd36_54870	orf19.4021	5	1.5291235	0.612705		Predicted ORF in Assemblies 19, 20 and 21
	Cd36_54740	orf19.4006	5	1.5294193	0.61298394	*PAN5*	Predicted ORF in Assemblies 19, 20 and 21
	Cd36_85520	orf19.6990	3	1.5300907	0.6136172	*CPR5*	Predicted ORF in Assemblies 19, 20 and 21
ARC40	Cd36_31710	orf19.3873	R	1.530446	0.61395216	*ARC40*	Protein similar to S. cerevisiae Arc40p, which is involved in actin filament organization in S. cerevisiae
FGR32	Cd36_33660	orf19.593	R	1.5327529	0.6161251	*SWA2*	Protein described as similar to S. cerevisiae Swa2p
	Cd36_28260	orf19.2411	R	1.5331136	0.6164646	*SYN8*	Predicted ORF in Assemblies 19, 20 and 21
	Cd36_26310		R	1.5332332	0.61657715		
	Cd36_33770	orf19.6374	R	1.5333594	0.6166959	*ATP10*	Predicted ORF in Assemblies 19, 20 and 21
	Cd36_27020	orf19.2610	R	1.5336624	0.616981	*ARC1*	Predicted ORF in Assemblies 19, 20 and 21
	Cd36_26120	orf19.3242	R	1.5339228	0.6172259	*TAF10*	Predicted ORF in Assemblies 19, 20 and 21
PGM2	Cd36_27900	orf19.2841	R	1.5354118	0.61862564	*PGM2*	Protein not essential for viability
	Cd36_23750	orf19.1387	2	1.5354671	0.6186776	*CFD1*	Predicted ORF in Assemblies 19, 20 and 21
	Cd36_11480	orf19.5239	1	1.5356611	0.6188599	*YNL040W*	Predicted ORF in Assemblies 19, 20 and 21
	Cd36_34170	orf19.6431	R	1.5361837	0.6193508		Predicted ORF in Assemblies 19, 20 and 21
	Cd36_25310	orf19.7507	R	1.5366155	0.6197562		Predicted ORF in Assemblies 19, 20 and 21
	Cd36_31650		R	1.5367534	0.6198857		
	Cd36_01070	orf19.3302	1	1.5371243	0.6202338	*GAC1*	Predicted ORF in Assemblies 19, 20 and 21
	Cd36_26190	orf19.3234	R	1.5371518	0.62025964	*OYE3*	Predicted ORF in Assemblies 19, 20 and 21
	Cd36_43840	orf19.5308	4	1.5388892	0.62188935		Predicted ORF in Assemblies 19, 20 and 21
	Cd36_52800	orf19.4332	5	1.5395182	0.62247896		Predicted ORF in Assemblies 19, 20 and 21
	Cd36_29610	orf19.516	R	1.5396063	0.62256145	*RFT1*	Predicted ORF in Assemblies 19, 20 and 21
DPS1-1	Cd36_28310	orf19.2407	R	1.5398995	0.6228361	*DPS1*	Putative tRNA-Asp synthetase
	Cd36_52460	orf19.4286	5	1.5403787	0.62328506		Predicted ORF in Assemblies 19, 20 and 21
	Cd36_00200	orf19.6084	1	1.5404037	0.62330854		Predicted ORF in Assemblies 19, 20 and 21
	Cd36_02580	orf19.2966	1	1.541606	0.624434	*YDL086W*	Predicted ORF in Assemblies 19, 20 and 21
	Cd36_30430	orf19.639	R	1.5425373	0.6253054	*RAI1*	Predicted ORF in Assemblies 19, 20 and 21
	Cd36_30140	orf19.6315	R	1.5450774	0.6276791		Predicted ORF in Assemblies 19, 20 and 21
CPP1	Cd36_09400	orf19.4866	1	1.5463219	0.6288406	*MSG5*	MAPK phosphatase of the VH1 family
HRT2	Cd36_41600	orf19.4624	4	1.546896	0.6293762	*YMR027W*	Protein described as having a role in Ty3 transposition
HYR4	Cd36_25840	orf19.3279	R	1.5473318	0.62978256	*DAN4*	Putative GPI-anchored protein of unknown function

Gene Name	*C. dubliniensis* Cd36 identifier	*C. albicans* orf19 identifier	C'some	Fold change expression	Normalised Expression	*S. cerevisiae* ortholog	Description
FAS2	Cd36_84800	orf19.5949	3	**1.5475751**	0.6300094	*FAS2*	Alpha subunit of fatty-acid synthase
	Cd36_54690	orf19.4001	5	**1.549326**	0.6316407	*MSS2*	Predicted ORF in Assemblies 19, 20 and 21
	Cd36_23660	orf19.1396	2	**1.5494841**	0.631788	*AGE2*	Predicted ORF in Assemblies 19, 20 and 21
	Cd36_25180	orf19.7519	R	**1.5496355**	0.6319289		Predicted ORF in Assemblies 19, 20 and 21
	Cd36_52500	orf19.4292	5	**1.5505219**	0.63275385	*PEP12*	Predicted ORF in Assemblies 19, 20 and 21
	Cd36_26360	orf19.2518	R	**1.551233**	0.63341546	*SEC17*	Predicted ORF in Assemblies 19, 20 and 21
	Cd36_72230	orf19.6460	7	**1.5543046**	0.6362692	*PEX1*	Predicted ORF in Assemblies 19, 20 and 21
	Cd36_30990	orf19.6650	R	**1.5543197**	0.6362833		Predicted ORF in Assemblies 19, 20 and 21
	Cd36_52470	orf19.4287	5	**1.5548341**	0.6367607	*XYL2*	Predicted ORF in Assemblies 19, 20 and 21
	Cd36_29220	orf19.475	R	**1.556209**	0.6380358	*IPI1*	Predicted ORF in Assemblies 19, 20 and 21
MRPL40	Cd36_29300	orf19.484	R	**1.5565603**	0.63836145	*MRPL40*	Putative mitochondrial ribosomal protein
	Cd36_28800	orf19.4382	R	**1.5571536**	0.63891125	*RET3*	Predicted ORF in Assemblies 19, 20 and 21
NTG1	Cd36_07730	orf19.5098	1	**1.557229**	0.6389811	*NTG2*	Similar to DNA repair glycosylase
	Cd36_54930	orf19.4028	5	**1.5574884**	0.63922143	*RER2*	Predicted ORF in Assemblies 19, 20 and 21
GSG1	Cd36_11700	orf19.3764	1	**1.5579897**	0.63968575	*GSG1*	Protein not essential for viability
SRP54	Cd36_26110	orf19.3243	R	**1.5588027**	0.6404383	*SRP54*	Predicted ORF in Assemblies 19, 20 and 21
	Cd36_33070	orf19.6121	R	**1.5593414**	0.64093685	*YER130C*	Similar to S. cerevisiae Yer130cp
	Cd36_25770	orf19.7460	R	**1.5595282**	0.6411097	*TRM13*	Predicted ORF in Assemblies 19, 20 and 21
IFD3	Cd36_01150	orf19.3311	1	**1.560352**	0.64187145	*YPL088W*	Transcription is regulated by Mig1p
	Cd36_28640	orf19.4399	R	**1.5608352**	0.64231825	*NCS2*	Predicted ORF in Assemblies 19, 20 and 21
OBPA	Cd36_51550	orf19.3198	5	**1.5617156**	0.64313173	*OSH7*	Similar to oxysterol binding protein
	Cd36_53510	orf19.1116	5	**1.5621963**	0.64357567		Predicted ORF in Assemblies 19, 20 and 21
	Cd36_26080	orf19.3247	R	**1.5653138**	0.64645195	*LAA1*	Predicted ORF in Assemblies 19, 20 and 21
AHP1	Cd36_42290	orf19.2762	4	**1.5665188**	0.647562	*AHP1*	Putative alkyl hydroperoxide reductase
	Cd36_54940	orf19.4029	5	**1.5669806**	0.64798737	*SQT1*	Predicted ORF in Assemblies 19, 20 and 21
PGA4	Cd36_54990	orf19.4035	5	**1.5673629**	0.6483393	*GAS5*	Putative cell-surface protein, predicted to carry a glycosylphosphatidylinositol (GPI) lipid anchor
	Cd36_28150	orf19.2423	R	**1.5675901**	0.64854836	*YBR239C*	Putative DNA-binding transcription factor
	Cd36_87630	orf19.6709	3	**1.5678675**	0.6488037		Predicted ORF in Assemblies 19, 20 and 21
GYP7	Cd36_73150	orf19.6706	7	**1.568671**	0.6495428	*GYP7*	Predicted ORF in Assemblies 19, 20 and 21
	Cd36_50170	orf19.5683	5	**1.5702835**	0.65102506	*YHR140W*	Predicted ORF in Assemblies 19, 20 and 21
	Cd36_54110	orf19.3932	5	**1.5706004**	0.65131617		Predicted ORF in Assemblies 19, 20 and 21
	Cd36_52410	orf19.4280	5	**1.5707787**	0.65147996		Predicted ORF in Assemblies 19, 20 and 21
SSD1	Cd36_54350	orf19.3959	5	**1.5712546**	0.651917	*SSD1*	Functional homolog of S. cerevisiae Ssd1p, which suppresses various mutant phenotypes
ECM331	Cd36_52240	orf19.4255	5	**1.5737369**	0.65419436	*ECM33*	Putative GPI-anchored protein
	Cd36_29750	orf19.529	R	**1.5743086**	0.6547184	*MUC1*	Predicted ORF in Assemblies 19, 20 and 21
	Cd36_11500	orf19.5237	1	**1.5747768**	0.6551473	*VPH2*	Predicted ORF in Assemblies 19, 20 and 21
	Cd36_32330	orf19.1856	R	**1.5749238**	0.655282	*SDS3*	Predicted ORF in Assemblies 19, 20 and 21
	Cd36_04090	orf19.1070	1	**1.5760441**	0.65630794	*YMR010W*	Predicted ORF in Assemblies 19, 20 and 21
MHP1	Cd36_31300	orf19.6621	R	**1.5778198**	0.6579325	*MHP1*	Protein similar to S. cerevisiae Mhp1p, which is involved in microtubule stabilization
	Cd36_15580	orf19.2065	2	**1.5783477**	0.6584151	*DAL2*	Predicted ORF in Assemblies 19, 20 and 21
	Cd36_34660	orf19.7328	R	**1.5805048**	0.6603854		Gene transcription regulated by Mig1p and Tup1p
	Cd36_31270	orf19.6624	R	**1.582785**	0.66246533		Predicted ORF in Assemblies 19, 20 and 21
YME1	Cd36_45280	orf19.1252	4	**1.5829788**	0.662642	*YME1*	Protein not essential for viability
HST7	Cd36_29180	orf19.469	R	**1.5839529**	0.6635294	*STE7*	MAP kinase kinase, involved in signal transduction pathways for mating and hyphal growth
	Cd36_45320		4	**1.5845542**	0.66407704		
	Cd36_01760	orf19.4531	1	**1.5845791**	0.6640997	*YOL075C*	Putative PDR-subfamily ABC transporter
EXG2	Cd36_02450	orf19.2952	1	**1.584713**	0.6642215	*EXG1*	Protein similar to S. cerevisiae Exg2p, which is an exo-1,3-beta-glucosidase
	Cd36_84270	orf19.5876	3	**1.5855415**	0.66497564		Predicted ORF in Assemblies 19, 20 and 21
	Cd36_26490	orf19.2538	R	**1.585562**	0.66499424	*PTC2*	Predicted ORF in Assemblies 19, 20 and 21
	Cd36_85280	orf19.6966	3	**1.5875319**	0.6667856	*CKI1*	Predicted ORF in Assemblies 19, 20 and 21
SDH2	Cd36_30410	orf19.637	R	**1.5875869**	0.66683555	*SDH2*	Succinate dehydrogenase, Fe-S subunit
	Cd36_32750	orf19.733	R	**1.5888045**	0.6679416	*YBR287W*	Predicted ORF in Assemblies 19, 20 and 21
	Cd36_15460	orf19.2078	2	**1.5888493**	0.66798234	*APM2*	Predicted ORF in Assemblies 19, 20 and 21
	Cd36_45350	orf19.1270	4	**1.590484**	0.6694659	*FRE2*	Predicted ORF in Assemblies 19, 20 and 21
MRP2	Cd36_54890	orf19.4023	5	**1.590776**	0.66973066	*MRP2*	Protein similar to S. cerevisiae Mrp2p, which is a component of the small subunit of the mitochondrial ribosome
	Cd36_34240	orf19.6440	R	**1.591759**	0.6706219	*ASI1*	Predicted ORF in Assemblies 19, 20 and 21
SMX4	Cd36_32960	orf19.6135.1	R	**1.5922128**	0.67103314	*LSM3*	ORF Predicted by Annotation Working Group
PGA44	Cd36_81300	orf19.1714	3	**1.5924587**	0.67125595	*AGA1*	Putative GPI-anchored protein of unknown function
	Cd36_25120	orf19.7529	R	**1.5931506**	0.6718826	*EPL1*	Predicted ORF in Assemblies 19, 20 and 21
RHD3	Cd36_43810	orf19.5305	4	**1.5934179**	0.6721246		Putative GPI-anchored protein that localizes to the cell wall
	Cd36_08040	orf19.398	1	**1.5939264**	0.672585	*YDL012C*	Predicted ORF in Assemblies 19, 20 and 21
SFT2	Cd36_10100	orf19.2342	1	**1.5947126**	0.67329645	*SFT2*	Transcription is regulated by Mig1p
TIP20	Cd36_54710	orf19.4003	5	**1.5955647**	0.67406714		Protein interacting with Sec20p, possibly involved in retrograde transport between the Golgi and the endoplasmic reticulum
	Cd36_53240		5	**1.5961636**	0.6746085		
ATP3	Cd36_26320	orf19.3223	R	**1.5964962**	0.6749091	*ATP3*	Predicted ORF in Assemblies 19, 20 and 21
	Cd36_70520	orf19.7091	7	**1.5966117**	0.67501354		Predicted ORF in Assemblies 19, 20 and 21
	Cd36_25130	orf19.7527	R	**1.5978091**	0.676095		Predicted ORF in Assemblies 19, 20 and 21
	Cd36_11810	orf19.6360	1	**1.6009046**	0.67888737	*CWC15*	Predicted ORF in Assemblies 19, 20 and 21
	Cd36_33670	orf19.592	R	**1.6017011**	0.679605	*YNL092W*	Predicted ORF in Assemblies 19, 20 and 21
FBP1	Cd36_87700	orf19.6178	3	**1.6022155**	0.68006825	*FBP1*	Fructose-1,6-bisphosphatase, a key enzyme of gluconeogenesis

Gene Name	*C. dubliniensis* Cd36 identifier	*C. albicans* orf19 identifier	C'some	Fold change expression	Normalised Expression	*S. cerevisiae* ortholog	Description
	Cd36_33100	orf19.6117	R	1.6025208	0.68034315	*YBR287W*	Predicted ORF in Assemblies 19, 20 and 21
PXA1	Cd36_25450	orf19.7500	R	1.6029462	0.68072593	*PXA1*	Putative peroxisomal, half-size adrenoleukodystrophy protein (ALD or ALDp) subfamily ABC family transporter
	Cd36_28940	orf19.4372	R	1.6031145	0.68087745	*YDL206W*	Predicted ORF in Assemblies 19, 20 and 21
	Cd36_51480	orf19.583	5	1.6052704	0.68281627	*BNA2*	Putative indoleamine 2,3-dioxygenase (IDO)
	Cd36_21190	orf19.2244	2	1.6057854	0.68327904	*YJR096W*	Similar to oxidoreductases and to S. cerevisiae Yjr096wp
	Cd36_28180	orf19.2419	R	1.6060202	0.68349004	*DOM34*	Predicted ORF in Assemblies 19, 20 and 21
PEX14	Cd36_30330	orf19.1805	R	1.6075503	0.6848638	*PEX14*	Protein not essential for viability
	Cd36_42410	orf19.2749	4	1.6082916	0.685529	*YDR132C*	Predicted ORF in Assemblies 19, 20 and 21
	Cd36_30160	orf19.6313.2	R	1.610995	0.68795204		ORF Predicted by Annotation Working Group
RFG1	Cd36_27640	orf19.2823	R	1.6117034	0.68858624	*ROX1*	Transcriptional regulator of filamentous growth and hyphal genes
HEM4	Cd36_24400	orf19.1744	2	1.6119391	0.68879724	*HEM4*	Protein described as uroporphyrinogen I!I synthase
CGR1	Cd36_42630	orf19.2722	4	1.6119598	0.68881583	*YBR053C*	Possible negative regulator of yeast-form growth
VID21	Cd36_46690	orf19.3077	4	1.6124909	0.689291	*EAF1*	Predicted ORF in Assemblies 19, 20 and 21
	Cd36_26170	orf19.3235	R	1.6141039	0.69073343	*CAP1*	Predicted ORF in Assemblies 19, 20 and 21
GCD1	Cd36_29270	orf19.481	R	1.6144096	0.69100666	*GCD1*	Putative translation initiation factor
	Cd36_02790		1	1.6151947	0.6917081		
	Cd36_25790	orf19.3286	R	1.6158694	0.6923106	*GTB1*	Predicted ORF in Assemblies 19, 20 and 21
	Cd36_27590		R	1.6189238	0.6950351		
HSP60	Cd36_31990	orf19.717	R	1.6220207	0.6977923	*HSP60*	Protein described as mitochondrial heat shock protein
	Cd36_27710	orf19.2828	R	1.6221529	0.69790983	*ALF1*	Predicted ORF in Assemblies 19, 20 and 21
GLN3	Cd36_53950	orf19.3912	5	1.6226956	0.6983924	*GLN3*	GATA transcription factor involved in regulation of filamentous growth induced by nitrogen starvation
	Cd36_29730	orf19.528	R	1.6229968	0.69866014	*SEC26*	Predicted ORF in Assemblies 19, 20 and 21
CYP5	Cd36_86110	orf19.7421	3	1.6232666	0.6989	*CPR5*	Protein described as a peptidyl-prolyl cis-trans isomerase
	Cd36_27340	orf19.3730	R	1.6248201	0.70027995	*KRE27*	Protein similar to S. cerevisiae Kre27p, which has a role in resistance to killer toxin
	Cd36_84280	orf19.5877	3	1.6254576	0.70084596		Predicted ORF in Assemblies 19, 20 and 21
SEC18	Cd36_12570	orf19.4993	1	1.6257373	0.70109415	*SEC18*	Functional homolog of S. cerevisiae Sec18p, which acts in protein transport
	Cd36_72680	orf19.5159	7	1.6261113	0.701426	*DUG3*	Predicted ORF in Assemblies 19, 20 and 21
	Cd36_32430	orf19.1842	R	1.626689	0.7019384	*BUD5*	Predicted ORF in Assemblies 19, 20 and 21
	Cd36_34460	orf19.7296	R	1.6273019	0.702482		Predicted ORF in Assemblies 19, 20 and 21
ABP1	Cd36_42810	orf19.2699	4	1.6289308	0.7039254	*ABP1*	Protein similar to S. cerevisiae Abp1p, which is an actin-binding protein of the cortical actin cytoskeleton
TPS1	Cd36_31110	orf19.6640	R	1.6320468	0.70668244	*TPS1*	Trehalose-6-phosphate synthase
	Cd36_31860	orf19.3881	R	1.6326063	0.7071769		Predicted ORF in Assemblies 19, 20 and 21
ALG6	Cd36_32420	orf19.1843	R	1.6334909	0.70795846	*ALG6*	Putative glucosyltransferase involved in cell wall mannan biosynthesis
YWP1	Cd36_22720	orf19.3618	2	1.6341223	0.7085159	*FLO5*	Protein with suggested role in dispersal in host
ATP17	Cd36_25290	orf19.7509.1	R	1.6347296	0.7090521	*ATP17*	Protein described as a component of mitochondrial ATPase complex
SOK1	Cd36_31410	orf19.451	R	1.6364247	0.7105472	*SOK1*	Transcription is induced in response to alpha pheromone in SpiderM medium
PRE6	Cd36_29910	orf19.544.1	R	1.6377012	0.71167207	*PRE6*	Protein described as alpha-4 subunit of proteasome
	Cd36_28650	orf19.4398	R	1.6411077	0.71466994	*YPR147C*	Predicted ORF in Assemblies 19, 20 and 21
FRP6	Cd36_61540	orf19.3441	6	1.6412148	0.7147641	*ATO2*	Transcription is regulated by Nrg1p and Tup1p
	Cd36_28100	orf19.2863.1	R	1.6429502	0.7162887	*ERV1*	ORF Predicted by Annotation Working Group
	Cd36_10860		1	1.6430047	0.7163366		
	Cd36_18040	orf19.899	2	1.6432812	0.71657944		Predicted ORF in Assemblies 19, 20 and 21
	Cd36_33440	orf19.3706	R	1.643954	0.71717	*AST2*	Predicted ORF in Assemblies 19, 20 and 21
GRR1	Cd36_54220	orf19.3944	5	1.6448772	0.7179799	*GRR1*	Protein involved in the negative control of pseudohyphal growth
	Cd36_23610	orf19.1403	2	1.645285	0.71833754	*SAL1*	Predicted ORF in Assemblies 19, 20 and 21
	Cd36_33550	orf19.612	R	1.6461495	0.71909535	*YML050W*	Predicted ORF in Assemblies 19, 20 and 21
	Cd36_33090	orf19.6118	R	1.6467526	0.7196238	*DSS4*	Predicted ORF in Assemblies 19, 20 and 21
	Cd36_54860	orf19.4019	5	1.6473508	0.72014785	*PSY4*	Predicted ORF in Assemblies 19, 20 and 21
	Cd36_53570	orf19.1110	5	1.647577	0.720346	*THI80*	Predicted ORF in Assemblies 19, 20 and 21
	Cd36_32660	orf19.1815	R	1.6478668	0.72059965	*TIF6*	Predicted ORF in Assemblies 19, 20 and 21
	Cd36_53980	orf19.3916	5	1.6479921	0.7207093		Predicted ORF in Assemblies 19, 20 and 21
	Cd36_25780	orf19.3287	R	1.6490875	0.721668	*BUD22*	Predicted ORF in Assemblies 19, 20 and 21
RPD3	Cd36_27810	orf19.2834	R	1.651368	0.72366166	*RPD3*	Histone deacetylase
	Cd36_26040	orf19.3251	R	1.6520542	0.72426105	*ARC19*	Predicted ORF in Assemblies 19, 20 and 21
	Cd36_28860	orf19.4365	R	1.652703	0.7248275	*TRM2*	Predicted ORF in Assemblies 19, 20 and 21
	Cd36_27350	orf19.3728	R	1.6527687	0.72488487	*DAN4*	Predicted ORF in Assemblies 19, 20 and 21
	Cd36_16740	orf19.1504	2	1.6529871	0.7250755	*TGL4*	Putative patatin-like phospholipase
	Cd36_32840	orf19.6151	R	1.6540654	0.7260163	*ARC15*	Predicted ORF in Assemblies 19, 20 and 21
	Cd36_11760	orf19.3758	1	1.6549034	0.72674704	*TMS1*	Predicted ORF in Assemblies 19, 20 and 21
ADP1	Cd36_31330	orf19.459	R	1.6551521	0.72696376	*ADP1*	Putative PDR-subfamily ABC transporter
	Cd36_04800		1	1.6557026	0.7274436		
GUT1	Cd36_30600	orf19.558	R	1.656629	0.7282505	*GUT1*	Protein described as glycerol kinase
	Cd36_30910	orf19.5846	R	1.6568203	0.72841716	*TFB2*	Predicted ORF in Assemblies 19, 20 and 21
ADH5	Cd36_27000	orf19.2608	R	1.6574426	0.72895885	*ADH5*	Putative alcohol dehydrogenase
	Cd36_60080	orf19.1178	6	1.6575773	0.72907615		Putative transcription factor with bZIP DNA-binding motif
MNT4	Cd36_30170	orf19.6313	R	1.6610758	0.7321179	*MNT4*	Transcriptionally regulated by iron
	Cd36_30620	orf19.1007	R	1.6613643	0.73236847	*KCS1*	Putative transcription factor with bZIP DNA-binding motif
	Cd36_33200		R	1.6624138	0.7332796		
CYP5	Cd36_86340	orf19.7421	3	1.6631062	0.7338803	*CPR5*	Protein described as a peptidyl-prolyl cis-trans isomerase

Gene Name	*C. dubliniensis* Cd36 identifier	*C. albicans* orf19 identifier	C'some	Fold change expression	Normalised Expression	*S. cerevisiae* ortholog	Description
	Cd36_25150	orf19.7522	R	**1.665471**	0.7359302	*BNA3*	Predicted ORF in Assemblies 19, 20 and 21
	Cd36_73490	orf19.7199	7	**1.6667218**	0.73701334	*YBR137W*	Predicted ORF in Assemblies 19, 20 and 21
	Cd36_26390	orf19.2521	R	**1.6681467**	0.7382462		Predicted ORF in Assemblies 19, 20 and 21
	Cd36_31790	orf19.3881	R	**1.6695199**	0.7394333		Predicted ORF in Assemblies 19, 20 and 21
	Cd36_50610	orf19.928	5	**1.6698767**	0.73974156		Predicted ORF in Assemblies 19, 20 and 21
	Cd36_87050	orf19.6788	3	**1.670421**	0.7402117		Predicted ORF in Assemblies 19, 20 and 21
	Cd36_54020	orf19.3922	5	**1.6718463**	0.7414422	*SDT1*	Predicted ORF in Assemblies 19, 20 and 21
	Cd36_29190	orf19.470	R	**1.6727597**	0.7422302	*TAF12*	Predicted ORF in Assemblies 19, 20 and 21
MET2	Cd36_27110	orf19.2618	R	**1.6732094**	0.7426181	*MET2*	Putative homoserine acetyltransferase
	Cd36_71750	orf19.6527	7	**1.6741607**	0.743438	*PRM10*	Predicted ORF in Assemblies 19, 20 and 21
	Cd36_31350	orf19.458	R	**1.6771293**	0.74599385	*BCS1*	Predicted ORF in Assemblies 19, 20 and 21
SHE3	Cd36_33180	orf19.729	R	**1.6775863**	0.746387		Protein similar to S. cerevisiae She3p
	Cd36_09800	orf19.4911	1	**1.6778636**	0.7466254		Predicted ORF in Assemblies 19, 20 and 21
LSM6	Cd36_25280	orf19.7509.2	R	**1.678142**	0.7468648	*LSM6*	ORF Predicted by Annotation Working Group
	Cd36_11140	orf19.5278	1	**1.6803014**	0.74872005	*YJR111C*	Predicted ORF in Assemblies 19, 20 and 21
	Cd36_54670	orf19.3999	5	**1.6813276**	0.7496009	*YML020W*	Predicted ORF in Assemblies 19, 20 and 21
	Cd36_31150	orf19.6637	R	**1.6825818**	0.75067663		Predicted ORF in Assemblies 19, 20 and 21
	Cd36_29260	orf19.480	R	**1.6829913**	0.7510277	*YJR056C*	Predicted ORF in Assemblies 19, 20 and 21
	Cd36_33800	orf19.6377	R	**1.6836616**	0.7516022	*PPM1*	Predicted ORF in Assemblies 19, 20 and 21
	Cd36_33570	orf19.607	R	**1.6848431**	0.75261426	*RAD26*	Predicted ORF in Assemblies 19, 20 and 21
	Cd36_54550	orf19.3983	5	**1.6867111**	0.75421286	*YGR266W*	Predicted ORF in Assemblies 19, 20 and 21
	Cd36_34020	orf19.6411	R	**1.6870843**	0.7545321	*VAC14*	Predicted ORF in Assemblies 19, 20 and 21
RPN5	Cd36_54980	orf19.4032	5	**1.6894902**	0.756588	*RPN5*	Predicted ORF in Assemblies 19, 20 and 21
	Cd36_84850	orf19.5956	3	**1.6896876**	0.75675654	*PIN3*	Predicted ORF in Assemblies 19, 20 and 21
	Cd36_81840		3	**1.692565**	0.7592112		
	Cd36_86920	orf19.6802	3	**1.6937747**	0.760242	*PFA3*	Predicted ORF in Assemblies 19, 20 and 21
	Cd36_26100	orf19.3244	R	**1.6939421**	0.76038456	*COX23*	Predicted ORF in Assemblies 19, 20 and 21
PRP22	Cd36_54970	orf19.4033	5	**1.6978744**	0.7637298	*PRP22*	Protein described as an RNA-dependent ATPase
	Cd36_54170	orf19.3940	5	**1.6988728**	0.76457787		Predicted ORF in Assemblies 19, 20 and 21
	Cd36_31980	orf19.718	R	**1.6989211**	0.7646189	*RRN11*	Putative RNA polymerase I subunit
	Cd36_83680	orf19.6951	3	**1.6992016**	0.76485705	*DPL1*	Predicted ORF in Assemblies 19, 20 and 21
HTS1	Cd36_55080	orf19.4051	5	**1.7010295**	0.7664082	*HTS1*	Putative tRNA-His synthetase
	Cd36_86630	orf19.7455	3	**1.7013816**	0.7667067		Predicted ORF in Assemblies 19, 20 and 21
	Cd36_29840	orf19.540	R	**1.7014859**	0.76679516		Predicted ORF in Assemblies 19, 20 and 21
	Cd36_34140	orf19.6423	R	**1.7027708**	0.76788425	*FBP26*	Predicted ORF in Assemblies 19, 20 and 21
	Cd36_29820	orf19.538	R	**1.7040429**	0.76896167	*GPI2*	Predicted ORF in Assemblies 19, 20 and 21
FLC2	Cd36_32680	orf19.1813	R	**1.704491**	0.769341	*FLC2*	Protein involved in heme uptake
UGP1	Cd36_30070	orf19.1738	R	**1.7057269**	0.7703867	*UGP1*	Protein similar to UTP-glucose-1-phosphaturidyl transferase
ACO2	Cd36_31190	orf19.6632	R	**1.7058276**	0.7704718	*ACO2*	Protein described as aconitate hydratase 2
	Cd36_16380	orf19.1460	2	**1.7066306**	0.7711508	*QNS1*	Predicted ORF in Assemblies 19, 20 and 21
	Cd36_34210	orf19.6436	R	**1.7072916**	0.77170944		Predicted ORF in Assemblies 19, 20 and 21
PEX5	Cd36_40220	orf19.5640	4	**1.707539**	0.77191854	*PEX5*	Protein of the Pex5p family, required for fatty acid beta-oxidation
PRP13	Cd36_29040	orf19.4379	R	**1.7075664**	0.77194166	*YME2*	Predicted ORF in Assemblies 19, 20 and 21
PXP2	Cd36_81790	orf19.1655	3	**1.7086947**	0.7728946	*POX1*	Putative acyl-CoA oxidase
IFC3	Cd36_27190	orf19.3749	R	**1.7092463**	0.77336025	*OPT2*	Oligopeptide transporter
	Cd36_10460	orf19.2301	1	**1.7113514**	0.775136	*NAS2*	Predicted ORF in Assemblies 19, 20 and 21
SSY5	Cd36_34130	orf19.6422	R	**1.7129248**	0.77646184	*SSY5*	Protein similar to S. cerevisiae Ssy5p, which is a component of a complex that senses external amino acids
	Cd36_28320	orf19.2406	R	**1.7136261**	0.7770524	*GTR2*	Predicted ORF in Assemblies 19, 20 and 21
	Cd36_52330	orf19.4269	5	**1.7136426**	0.77706623	*YLR253W*	Predicted ORF in Assemblies 19, 20 and 21
	Cd36_53320	orf19.6668	5	**1.7150425**	0.77824426	*CUE1*	Predicted ORF in Assemblies 19, 20 and 21
IRS4	Cd36_83660	orf19.6953	3	**1.7153018**	0.7784624	*TAX4*	Protein with roles in cell wall integrity, systemic (but not oral) murine infection, adherence, hyphal growth, and agar-embedded filamentous growth
	Cd36_31360	orf19.457	R	**1.7185761**	0.78121376	*UBP2*	Predicted ORF in Assemblies 19, 20 and 21
ALG5	Cd36_27860	orf19.2837	R	**1.7186139**	0.78124547	*ALG5*	Putative glucosyltransferase involved in cell wall mannan biosynthesis
	Cd36_54620	orf19.3994	5	**1.7190187**	0.7815852	*OST3*	Predicted ORF in Assemblies 19, 20 and 21
	Cd36_25800	orf19.3285	R	**1.7209496**	0.7832049		Predicted ORF in Assemblies 19, 20 and 21
	Cd36_34040	orf19.6414	R	**1.7222198**	0.78426933		Predicted ORF in Assemblies 19, 20 and 21
	Cd36_11510	orf19.5236	1	**1.724899**	0.7865119	*SRT1*	Predicted ORF in Assemblies 19, 20 and 21
IFF4	Cd36_25710	orf19.7472	R	**1.7261169**	0.7875302	*MUC1*	Putative GPI-anchored protein
	Cd36_54960	orf19.4031	5	**1.7272432**	0.7884712	*YIR007W*	Predicted ORF in Assemblies 19, 20 and 21
	Cd36_54730	orf19.4005	5	**1.7281554**	0.78923297	*YDR196C*	Protein likely to be essential for growth, based on an insertional mutagenesis strategy
	Cd36_54150	orf19.3937	5	**1.7282286**	0.789294	*TIP41*	Predicted ORF in Assemblies 19, 20 and 21
	Cd36_54290	orf19.3952	5	**1.7288204**	0.789788	*SRP101*	Predicted ORF in Assemblies 19, 20 and 21
	Cd36_26240	orf19.3231	R	**1.7290972**	0.79001904	*CDC27*	Predicted ORF in Assemblies 19, 20 and 21
YVH1	Cd36_28620	orf19.4401	R	**1.7294376**	0.790303	*YVH1*	Putative dual specificity phosphatase (phosphoserine/threonine and phosphotyrosine phosphatase)
	Cd36_33870	orf19.6392	R	**1.7300948**	0.7908511		Predicted ORF in Assemblies 19, 20 and 21
	Cd36_20390	orf19.5217	2	**1.7301146**	0.79086757	*TES1*	Predicted ORF in Assemblies 19, 20 and 21
	Cd36_82960	orf19.292	3	**1.7302086**	0.790946		Predicted ORF in Assemblies 19, 20 and 21
CDC45	Cd36_33370	orf19.1988	R	**1.7310222**	0.7916243	*CDC45*	Protein described as a DNA replication initiation factor
	Cd36_13160	orf19.7227	1	**1.7336401**	0.7938044	*YPI1*	Predicted ORF in Assemblies 19, 20 and 21
	Cd36_43710	orf19.5293	4	**1.7338718**	0.7939973		Predicted ORF in Assemblies 19, 20 and 21

Gene Name	*C. dubliniensis* Cd36 identifier	*C. albicans* orf19 identifier	C'some	Fold change expression	Normalised Expression	*S. cerevisiae* ortholog	Description
SOD1	Cd36_42210	orf19.2770.1	4	**1.7351557**	0.79506516	*SOD1*	Cytosolic copper- and zinc-containing superoxide dismutase, involved in protection from oxidative stress and required for full virulence
	Cd36_82890	orf19.284	3	**1.7365875**	0.7962551		Predicted ORF in Assemblies 19, 20 and 21
THI4	Cd36_85100	orf19.5986	3	**1.7369193**	0.7965307	*THI4*	Protein repressed during the mating process
	Cd36_54470	orf19.3973	5	**1.7388297**	0.7981167	*HUA1*	Predicted ORF in Assemblies 19, 20 and 21
	Cd36_28010	orf19.2851	R	**1.7413269**	0.8001871	*ORT1*	Predicted ORF in Assemblies 19, 20 and 21
ACF2	Cd36_61790	orf19.3417	6	**1.7413629**	0.8002169	*ACF2*	Putative endo-1,3-beta-glucanase
	Cd36_43940	orf19.1421	4	**1.7415352**	0.8003596	*DAL3*	Predicted ORF in Assemblies 19, 20 and 21
PUP2	Cd36_32290	orf19.709	R	**1.743737**	0.80218244	*PUP2*	Alpha5 subunit of the 20S proteasome
	Cd36_31830	orf19.3887	R	**1.7441877**	0.8025553	*YML108W*	Predicted ORF in Assemblies 19, 20 and 21
	Cd36_34060	orf19.6416	R	**1.7447695**	0.80303645	*EOS1*	Predicted ORF in Assemblies 19, 20 and 21
	Cd36_33290	orf19.6284	R	**1.7450702**	0.8032851	*SRP102*	Predicted ORF in Assemblies 19, 20 and 21
	Cd36_18010	orf19.904	2	**1.7472734**	0.80510545		Predicted ORF in Assemblies 19, 20 and 21
	Cd36_26200	orf19.3233	R	**1.7478505**	0.8055818	*HSE1*	Predicted ORF in Assemblies 19, 20 and 21
	Cd36_08340	orf19.4742	1	**1.7479656**	0.8056768		Predicted ORF in Assemblies 19, 20 and 21
	Cd36_28820	orf19.4380.1	R	**1.749285**	0.8067653	*YME2*	Predicted ORF in Assembly 20 and 21 (see Locus History)
	Cd36_28050	orf19.2857	R	**1.7508823**	0.8080821	*SSL2*	Predicted ORF in Assemblies 19, 20 and 21
RPT4	Cd36_29280	orf19.482	R	**1.7511361**	0.8082912	*RPT4*	Predicted ORF in Assemblies 19, 20 and 21
	Cd36_28840	orf19.4362	R	**1.7519544**	0.8089652	*MSP1*	Predicted ORF in Assemblies 19, 20 and 21
	Cd36_81810	orf19.1653	3	**1.7525705**	0.80947244		Predicted ORF in Assemblies 19, 20 and 21
	Cd36_30810	orf19.3517	R	**1.7542385**	0.8108449	*YOR223W*	Predicted ORF in Assemblies 19, 20 and 21
ATG15	Cd36_61830	orf19.3412	6	**1.7543826**	0.8109634	*ATG15*	Putative lipase
TAL1	Cd36_28930	orf19.4371	R	**1.7571507**	0.8132379	*TAL1*	Predicted ORF in Assemblies 19, 20 and 21
	Cd36_26790	orf19.2574	R	**1.7574542**	0.81348705	*YFL034W*	Predicted ORF in Assemblies 19, 20 and 21
	Cd36_71720	orf19.6530	7	**1.759011**	0.8147645	*SEC63*	Similar to bacterial DnaJ
	Cd36_86900	orf19.6804	3	**1.7590168**	0.81476927	*SRP68*	Predicted ORF in Assemblies 19, 20 and 21
	Cd36_45310	orf19.1255	4	**1.7628741**	0.8179295	*HAP1*	Putative transcription factor with zinc cluster DNA-binding motif
	Cd36_25810	orf19.3283	R	**1.763261**	0.818246	*OAR1*	Predicted ORF in Assemblies 19, 20 and 21
	Cd36_26510	orf19.2541	R	**1.7655246**	0.82009697	*YBL055C*	Predicted ORF in Assemblies 19, 20 and 21
	Cd36_27400	orf19.3720	R	**1.7658535**	0.82036567	*BCY1*	Predicted ORF in Assemblies 19, 20 and 21
	Cd36_80850	orf19.2496	3	**1.7661695**	0.8206239	*ADY2*	Predicted ORF in Assemblies 19, 20 and 21
SAP1	Cd36_63430	orf19.5714	6	**1.7664922**	0.82088745	*YPS3*	Secreted aspartyl proteinase
	Cd36_29680	orf19.522	R	**1.7696393**	0.82345533	*PIM1*	Predicted ORF in Assemblies 19, 20 and 21
	Cd36_52710		5	**1.7697029**	0.8235072		
	Cd36_25730	orf19.7468	R	**1.7725937**	0.82586193	*VHR1*	Predicted ORF in Assemblies 19, 20 and 21
	Cd36_26710	orf19.2565	R	**1.7763796**	0.8289399	*MDM1*	Predicted ORF in Assemblies 19, 20 and 21
IFR1	Cd36_24240	orf19.1763	2	**1.7788029**	0.8309066	*YNL134C*	Predicted ORF in Assemblies 19, 20 and 21
	Cd36_40970		4	**1.7821352**	0.83360684		
	Cd36_33760	orf19.6373	R	**1.7836384**	0.83482313	*DCP2*	Predicted ORF in Assemblies 19, 20 and 21
	Cd36_28360	orf19.2400	R	**1.7852257**	0.83610654	*SQS1*	Predicted ORF in Assemblies 19, 20 and 21
PGA37	Cd36_54030	orf19.3923	5	**1.7860506**	0.8367729		Putative GPI-anchored protein of unknown function
EHT1	Cd36_03190	orf19.3040	1	**1.788377**	0.83865094	*EHT1*	Protein similar to S. cerevisiae Eht1p
FTH2	Cd36_26280	orf19.3227	R	**1.78909**	0.839226	*FTH1*	Putative iron transporter
LIP3	Cd36_09310	orf19.4856	1	**1.7915792**	0.8412318		Secreted lipase, member of a lipase gene family whose members are expressed differentially in response to carbon source and during infection
	Cd36_22050	orf19.2202	2	**1.7931464**	0.8424933	*YKR043C*	Predicted ORF in Assemblies 19, 20 and 21
	Cd36_54680	orf19.4000	5	**1.794345**	0.84345734	*PHO2*	Predicted ORF in Assemblies 19, 20 and 21
	Cd36_54380	orf19.3963	5	**1.7948402**	0.8438554	*YER182W*	Predicted ORF in Assemblies 19, 20 and 21
SYS3	Cd36_28270	orf19.2410	R	**1.7963654**	0.84508085	*IMH1*	Protein similar to S. cerevisiae Sys3p
HST2	Cd36_26820	orf19.2580	R	**1.7966807**	0.84533405	*HST2*	Predicted ORF in Assemblies 19, 20 and 21
LPD1	Cd36_33030	orf19.6127	R	**1.7972043**	0.8457544	*LPD1*	Putative dihydrolipoamide dehydrogenase
	Cd36_82910	orf19.286	3	**1.7976933**	0.8461468		Decreased transcription is observed upon fluphenazine treatment
	Cd36_84590	orf19.5924	3	**1.8001735**	0.84813595	*VRP1*	Predicted zinc-finger protein of unknown function
RIM13	Cd36_54630	orf19.3995	5	**1.8029349**	0.8503473	*RIM13*	Probable protease involved in the pH response pathway, likely to mediate activation of the transcription factor Rim101p via C-terminal cleavage
	Cd36_53970	orf19.3915	5	**1.803724**	0.8509786	*DUG1*	Predicted ORF in Assemblies 19, 20 and 21
	Cd36_28630	orf19.4400	R	**1.8054546**	0.85236216		Predicted ORF in Assemblies 19, 20 and 21
RAD14	Cd36_71840	orf19.6517	7	**1.8075614**	0.8540447	*RAD14*	Transcription is regulated upon yeast-hyphal switch
GSL2	Cd36_25900	orf19.3269	R	**1.8123565**	0.85786676	*GSC2*	Protein similar to beta-1,3-glucan synthase
	Cd36_02600	orf19.2968	1	**1.8139226**	0.859113		Predicted ORF in Assemblies 19, 20 and 21
	Cd36_01680	orf19.4539	1	**1.815651**	0.860487	*RDI1*	Predicted ORF in Assemblies 19, 20 and 21
	Cd36_51740	orf19.3184	5	**1.8158041**	0.8606086	*SFT2*	Predicted ORF in Assemblies 19, 20 and 21
	Cd36_26570	orf19.2549	R	**1.8175613**	0.86200404	*SHP1*	Predicted ORF in Assemblies 19, 20 and 21
	Cd36_27450	orf19.173	R	**1.8197689**	0.8637552	*AZF1*	Putative transcription factor with zinc finger DNA-binding motif
OPI1	Cd36_17040	orf19.1543	2	**1.8208579**	0.8646183	*OPI1*	Functional homolog of S. cerevisiae Opi1p, which is a transcriptional repressor of INO1 involved in inositol biosynthesis
	Cd36_62150	orf19.692	6	**1.8216585**	0.8652525	*ENT2*	Predicted ORF in Assemblies 19, 20 and 21
	Cd36_54280	orf19.3951	5	**1.821859**	0.8654113	*YIP1*	Predicted ORF in Assemblies 19, 20 and 21
	Cd36_32890	orf19.6143	R	**1.8284255**	0.8706019		Predicted ORF in Assemblies 19, 20 and 21
PCL5	Cd36_54790	orf19.4012	5	**1.8288383**	0.8709276		Protein similar to S. cerevisiae Pcl5p and other cyclins for Pho85p kinase
	Cd36_31420	orf19.3848	R	**1.8307226**	0.87241316		Predicted ORF in Assemblies 19, 20 and 21

Gene Name	*C. dubliniensis* Cd36 identifier	*C. albicans* orf19 identifier	C'some	Fold change expression	Normalised Expression	*S. cerevisiae* ortholog	Description
SPT14	Cd36_29330	orf19.487	R	1.8309549	0.87259626	*SPT14*	Putative DNA-binding transcription factor
	Cd36_54060	orf19.3928	5	1.8309671	0.8726058	*AZF1*	Putative transcription factor with zinc finger DNA-binding motif
	Cd36_33310	orf19.6283	R	1.8374025	0.87766767	*NFU1*	Predicted ORF in Assemblies 19, 20 and 21
	Cd36_28410	orf19.2397	R	1.8380673	0.87818956	*TNA1*	Predicted ORF in Assemblies 19, 20 and 21
	Cd36_10960		1	1.8393458	0.8791927		
	Cd36_31730	orf19.3876	R	1.8404529	0.8800608		Predicted zinc-finger protein of unknown function
	Cd36_86960	orf19.6797	3	1.8407959	0.8803296		Predicted ORF in Assemblies 19, 20 and 21
YDJ1	Cd36_29510	orf19.506	R	1.8434498	0.88240814	*YDJ1*	Predicted ORF in Assemblies 19, 20 and 21
	Cd36_61780	orf19.3418	6	1.8445685	0.8832834		Predicted ORF in Assemblies 19, 20 and 21
	Cd36_84890	orf19.5961	3	1.8450567	0.8836651	*NAS6*	Predicted ORF in Assemblies 19, 20 and 21
KSR1	Cd36_33010	orf19.6131	R	1.8476276	0.885674	*TSC10*	3-ketosphinganine reductase, catalyzes the second step in phytosphingosine synthesis
YHB1	Cd36_33450	orf19.3707	R	1.8482909	0.88619184	*YHB1*	Nitric oxide dioxygenase
	Cd36_34310	orf19.6449	R	1.8504308	0.88786125		Predicted ORF in Assemblies 19, 20 and 21
	Cd36_05200	orf19.416	1	1.8506477	0.88803023		Predicted ORF in Assemblies 19, 20 and 21
	Cd36_25890	orf19.3272	R	1.8528352	0.8897345	*STI1*	Predicted ORF in Assemblies 19, 20 and 21
	Cd36_54240	orf19.3946	5	1.8542556	0.89084005	*COX18*	Predicted ORF in Assemblies 19, 20 and 21
	Cd36_34665	orf19.7329	R	1.8567473	0.89277744	*UBC7*	Predicted ORF in Assemblies 19, 20 and 21
LSC1	Cd36_01550	orf19.3358	1	1.8574878	0.89335275	*LSC1*	Protein described as succinate-CoA ligase subunit
	Cd36_26130	orf19.3241	R	1.8578832	0.89365983	*YDR128W*	Predicted ORF in Assemblies 19, 20 and 21
	Cd36_32230	orf19.703	R	1.8641212	0.8984957	*CPD1*	Predicted ORF in Assemblies 19, 20 and 21
	Cd36_26090	orf19.3245	R	1.8644801	0.89877343		Predicted ORF in Assemblies 19, 20 and 21
	Cd36_32690	orf19.8	R	1.8678108	0.90134835		Predicted ORF in Assemblies 19, 20 and 21
MGE1	Cd36_26400	orf19.2524	R	1.873931	0.90606785	*MGE1*	Predicted ORF in Assemblies 19, 20 and 21
OSH3	Cd36_43340	orf19.1317	4	1.8748089	0.9067435	*OSH3*	Protein required for wild-type filamentation
MDR1	Cd36_63890	orf19.5604	6	1.8795279	0.91037035	*FLR1*	Multidrug efflux pump of plasma membrane
	Cd36_54640	orf19.3996	5	1.880593	0.91118765	*GPI10*	Putative mannosyltransferase
MKC1	Cd36_25140	orf19.7523	R	1.8817896	0.9121053	*SLT2*	MAP kinase
	Cd36_33690	orf19.590	R	1.886394	0.91563106		Predicted ORF in Assemblies 19, 20 and 21
	Cd36_18690	orf19.816	2	1.8865786	0.9157722	*YLR422W*	Predicted ORF in Assemblies 19, 20 and 21
	Cd36_25880	orf19.3273	R	1.888458	0.9172087	*YIH1*	Predicted ORF in Assemblies 19, 20 and 21
DAL9	Cd36_83640	orf19.6956	3	1.8993044	0.9254711	*DAL5*	Putative allantoate permease
	Cd36_35075	orf19.7576	R	1.901537	0.927166		Protein not essential for viability
	Cd36_28250	orf19.2412	R	1.9084626	0.93241096	*VPS55*	Predicted ORF in Assemblies 19, 20 and 21
RNH1	Cd36_63220	orf19.5563	6	1.9092633	0.93301606	*RNH1*	Protein described as Ribonuclease H (RNAse H)
EBP1	Cd36_61290	orf19.125	6	1.9096596	0.9333155	*OYE2*	NADPH oxidoreductase
	Cd36_28240	orf19.2414	R	1.9119961	0.9350796	*MPM1*	Predicted ORF in Assemblies 19, 20 and 21
	Cd36_29600	orf19.515	R	1.9129794	0.9358213	*YER137C*	Predicted ORF in Assemblies 19, 20 and 21
THI20	Cd36_18120	orf19.889	2	1.9162687	0.9382999	*THI20*	Putative phosphomethylpyrimidine kinase
	Cd36_63195	orf19.5564	6	1.9175137	0.9392369	*RNH1*	Predicted ORF in Assemblies 19, 20 and 21
	Cd36_54460	orf19.3972	5	1.9185778	0.94003725	*GOT1*	Predicted ORF in Assemblies 19, 20 and 21
	Cd36_01100	orf19.3305	1	1.9187589	0.9401734	*UPC2*	Putative transcription factor with zinc cluster DNA-binding motif
	Cd36_28480	orf19.2391	R	1.9204811	0.94146776	*YKR023W*	Predicted ORF in Assemblies 19, 20 and 21
	Cd36_34190	orf19.6434	R	1.9207598	0.9416771	*PEX19*	Predicted ORF in Assemblies 19, 20 and 21
	Cd36_40880	orf19.4157	4	1.9209429	0.94181466	*SPS19*	Predicted ORF in Assemblies 19, 20 and 21
	Cd36_28230	orf19.2415	R	1.9226519	0.9430976	*MSE1*	Predicted ORF in Assemblies 19, 20 and 21
	Cd36_26810	orf19.2579	R	1.9229205	0.94329906	*MSH4*	Predicted ORF in Assemblies 19, 20 and 21
	Cd36_29110	orf19.4357	R	1.9229354	0.94331026	*YMR115W*	Predicted ORF in Assemblies 19, 20 and 21
	Cd36_32580	orf19.2361	R	1.9231279	0.94345474	*SPT10*	Predicted ORF in Assemblies 19, 20 and 21
	Cd36_31960	orf19.719	R	1.9238838	0.9440217	*HRD1*	Predicted ORF in Assemblies 19, 20 and 21
	Cd36_20540	orf19.4104	2	1.9241892	0.9442507		Predicted ORF in Assemblies 19, 20 and 21
	Cd36_84290	orf19.5879	3	1.925017	0.9448712	*AYR1*	Predicted ORF in Assemblies 19, 20 and 21
DAL1	Cd36_80170	orf19.5454	3	1.9277905	0.9469483	*DAL1*	Predicted ORF in Assemblies 19, 20 and 21
	Cd36_07510	orf19.5070	1	1.9290534	0.94789314	*AGA1*	Predicted ORF in Assemblies 19, 20 and 21
	Cd36_29650	orf19.519	R	1.9327953	0.95068884	*RRN10*	Predicted ORF in Assemblies 19, 20 and 21
SMF3	Cd36_15540	orf19.2069	2	1.9350344	0.9523592	*SMF3*	Protein described as vacuolar iron transporter
PTP1	Cd36_33710	orf19.6365	R	1.9351463	0.95244265	*PTP1*	Protein not essential for viability
	Cd36_30790	orf19.3515	R	1.9382604	0.95476246	*BNA1*	Predicted ORF in Assemblies 19, 20 and 21
	Cd36_16110	orf19.2001	2	1.94334	0.9585383		Predicted ORF in Assemblies 19, 20 and 21
PHO15	Cd36_06770	orf19.4444	1	1.943746	0.95883965	*PHO13*	Protein described as 4-nitrophenyl phosphatase
	Cd36_29460	orf19.499	R	1.9519663	0.96492815	*MTQ1*	Predicted ORF in Assemblies 19, 20 and 21
	Cd36_55020	orf19.4041	5	1.9552782	0.96737385	*PEX4*	Predicted ORF in Assemblies 19, 20 and 21
	Cd36_31570	orf19.3862	R	1.9558353	0.9677849	*LST8*	Predicted ORF in Assemblies 19, 20 and 21
	Cd36_34300	orf19.6448	R	1.9585972	0.96982074		Predicted ORF in Assemblies 19, 20 and 21
	Cd36_10750		1	1.9587038	0.9698992		
	Cd36_28780	orf19.2376	R	1.962397	0.9726169	*HNT3*	Predicted ORF in Assemblies 19, 20 and 21
	Cd36_05610	orf19.2452	1	1.9647138	0.9743192		Transcriptionally regulated by iron
ALS4	Cd36_64610	orf19.4555	6	1.9657656	0.9750913	*FLO1*	ALS family protein
	Cd36_22120	orf19.2194	2	1.9677866	0.9765737	*APM4*	Predicted ORF in Assemblies 19, 20 and 21
	Cd36_54180	orf19.3939	5	1.9702588	0.9783852	*YJR088C*	Predicted ORF in Assemblies 19, 20 and 21
	Cd36_02850	orf19.2996	1	1.9752567	0.98204017		Predicted ORF in Assemblies 19, 20 and 21
YAH1	Cd36_83350	orf19.336	3	1.9769038	0.98324263	*YAH1*	Similar to oxidoreductases
ALK8	Cd36_32710	orf19.10	R	1.9772731	0.98351216	*DIT2*	Alkane-inducible cytochrome P450
HGT1	Cd36_01840	orf19.4527	1	1.9792837	0.9849784	*HXT11*	High-affinity glucose transporter, member of major facilitator superfamily
CWT1	Cd36_30880	orf19.5849	R	1.9799436	0.9854593	*RDS2*	Putative transcription factor

Gene Name	*C. dubliniensis* Cd36 identifier	*C. albicans* orf19 identifier	C'some	Fold change expression	Normalised Expression	*S. cerevisiae* ortholog	Description
	Cd36_22200	orf19.2184	2	1.9846721	0.98890066	*YNL168C*	Predicted ORF in Assemblies 19, 20 and 21
	Cd36_29810	orf19.537	R	1.9847156	0.98893225	*YBR197C*	Predicted ORF in Assemblies 19, 20 and 21
	Cd36_86490	orf19.7441	3	1.9860771	0.98992157	*BRR6*	Predicted ORF in Assemblies 19, 20 and 21
	Cd36_33940	orf19.6403	R	1.9886233	0.99177	*SIL1*	Predicted ORF in Assemblies 19, 20 and 21
DAP1	Cd36_29350	orf19.489	R	1.9906346	0.99322844	*DAP1*	Protein similar to S. cerevisiae Dap1p, which is a protein related to mammalian membrane-associated progesterone receptors involved in response to DNA damage
	Cd36_31210	orf19.6630	R	1.9930142	0.99495196	*YLR104W*	ORF Predicted by Annotation Working Group
	Cd36_84810	orf19.5952	3	1.9941126	0.99574685		Predicted ORF in Assemblies 19, 20 and 21
	Cd36_41750	orf19.4607	4	1.9954559	0.9967184		Predicted ORF in Assemblies 19, 20 and 21
	Cd36_46100	orf19.2870	4	1.9966128	0.99755454		Predicted ORF in Assemblies 19, 20 and 21
	Cd36_12430	orf19.4966	1	1.9997257	0.9998021	*AGC1*	Protein not essential for viability
	Cd36_29760	orf19.530	R	2.0005114	1.0003688		Protein not essential for viability
	Cd36_80590	orf19.5393	3	2.002183	1.0015738		Putative cysteine sulfinate decarboxylase
	Cd36_29360	orf19.490	R	2.0187712	1.0134773	*NAT5*	Predicted ORF in Assemblies 19, 20 and 21
DES1	Cd36_55070	orf19.4048	5	2.0204554	1.0146805		Putative delta-4 sphingolipid desaturase
ARR3	Cd36_46360	orf19.3122	4	2.0209622	1.0150423	*ARR3*	Protein not essential for viability
	Cd36_55050	orf19.4046	5	2.0236893	1.0169878		Predicted ORF in Assemblies 19, 20 and 21
AGE1	Cd36_03270	orf19.3050	1	2.0242817	1.01741	*AGE1*	Protein described as a GTPase activator
	Cd36_11040	orf19.1142	1	2.027077	1.0194008	*AVT4*	Predicted ORF in Assemblies 19, 20 and 21
	Cd36_28500	orf19.2387	R	2.0277634	1.0198894	*YMR098C*	Putative tRNA-Pro synthetase
SLC1	Cd36_82560	orf19.250	3	2.0280228	1.0200738	*SLC1*	Protein repressed during the mating process
TPO3	Cd36_08290	orf19.4737	1	2.0280273	1.020077	*TPO2*	Possible role in polyamine transport
AOX2	Cd36_08630	orf19.4773	1	2.030958	1.0221603		Alternative oxidase
	Cd36_41280	orf19.4658	4	2.0418718	1.0298922		Protein not essential for viability
	Cd36_25350	orf19.7502	R	2.0471885	1.033644		Predicted ORF in Assemblies 19, 20 and 21
ILV3	Cd36_55010	orf19.4040	5	2.0503755	1.0358882	*ILV3*	Putative dihydroxyacid dehydratase
	Cd36_27280	orf19.3737	R	2.0534716	1.038065	*MUK1*	Predicted ORF in Assemblies 19, 20 and 21
RIB1	Cd36_28080	orf19.2862	R	2.0578094	1.0411093	*RIB1*	Putative GTP cyclohydrolase II
	Cd36_04740	orf19.55	1	2.0591602	1.0420561	*IZH2|IZH1*	Predicted ORF in Assemblies 19, 20 and 21
TPO4	Cd36_29200	orf19.473	R	2.0657008	1.0466313	*TPO4*	Putative sperimidine transporter
	Cd36_33580	orf19.606	R	2.0820088	1.0579762	*YLR352W*	Predicted ORF in Assemblies 19, 20 and 21
	Cd36_72930	orf19.5125	7	2.0879428	1.0620823	*YLR149C*	Predicted ORF in Assemblies 19, 20 and 21
	Cd36_25510	orf19.7497	R	2.090422	1.0637941	*CDC53*	Predicted ORF in Assemblies 19, 20 and 21
	Cd36_30650	orf19.1012	R	2.0912707	1.0643798	*APS1*	Predicted ORF in Assemblies 19, 20 and 21
PRS	Cd36_26460	orf19.2532	R	2.097693	1.0688035	*YER087W*	Putative prolyl-tRNA synthetase
PGA61	Cd36_64390	orf19.5762	6	2.1091006	1.0766279	*CCW14*	Putative GPI-anchored protein of unknown function
	Cd36_41270	orf19.4659	4	2.1102457	1.0774109	*PRP21*	Predicted ORF in Assemblies 19, 20 and 21
RGD3	Cd36_33170	orf19.729.1	R	2.1168928	1.0819483	*RGD2*	Putative Rho GTPase activating protein
TPO2	Cd36_73910	orf19.7148	7	2.1246402	1.0872186	*TPO1*	Putative polyamine transport protein
	Cd36_72450	orf19.2669	7	2.1293545	1.0904161	*R161W-B|YFL0(*	Predicted ORF in Assemblies 19, 20 and 21
AMO2	Cd36_21000	orf19.3152	2	2.130739	1.0913539		Protein similar to A. niger predicted peroxisomal copper amino oxidase
	Cd36_15590	orf19.2064	2	2.138872	1.09685		Putative transcription factor with zinc finger DNA-binding motif
TEC1	Cd36_84480	orf19.5908	3	2.1401353	1.097702	*TEC1*	TEA/ATTS transcription factor involved in regulation of hypha-specific genes
HGT14	Cd36_33400	orf19.2633	R	2.1434603	1.0999417	*HXT4*	Putative glucose transporter of the major facilitator superfamily
	Cd36_32810	orf19.730	R	2.1442816	1.1004944	*RGD2*	Predicted ORF in Assembly 20 and 21 (see Locus History)
	Cd36_73880	orf19.7152	7	2.1476183	1.1027377	*YGR012W*	Protein similar to Aspergillus CYSK O-acetylserine sulfhydrylase, suggesting that C. albicans uses an O-acetyl-serine (OAS) pathway of sulfur assimilation
	Cd36_30890	orf19.5848	R	2.1497588	1.1041749		Predicted ORF in Assemblies 19, 20 and 21
OPT7	Cd36_40500	orf19.5673	4	2.1501908	1.1044648	*OPT2*	Putative oligopeptide transporter
PLB4.5	Cd36_16240	orf19.1442	2	2.1511025	1.1050763	*PLB3*	Putative phospholipase B
	Cd36_72060	orf19.6487	7	2.155358	1.1079276		Predicted ORF in Assemblies 19, 20 and 21
	Cd36_24390	orf19.1745	2	2.1598723	1.1109459		Predicted ORF in Assemblies 19, 20 and 21
FCR1	Cd36_86810	orf19.6817	3	2.161174	1.1118153	*CAT8*	Putative zinc cluster transcription factor
HSP104	Cd36_33850	orf19.6387	R	2.1632705	1.113214	*HSP104*	Functional homolog of S. cerevisiae Hsp104p
	Cd36_71520	orf19.6556	7	2.1690083	1.1170355	*AGA1*	Predicted ORF in Assemblies 19, 20 and 21
	Cd36_31770	orf19.3879	R	2.1726024	1.1194242		Predicted ORF in Assemblies 19, 20 and 21
	Cd36_09700	orf19.4900	1	2.1748474	1.1209142	*MNT4|MNT2*	Predicted ORF in Assemblies 19, 20 and 21
SFT1	Cd36_26180	orf19.3234.1	R	2.179742	1.1241574	*SFT1*	ORF Predicted by Annotation Working Group
	Cd36_29140	orf19.4358	R	2.1800797	1.1243808	*YDL157C*	Predicted ORF in Assemblies 19, 20 and 21
	Cd36_51150	orf19.1950	5	2.1826987	1.1261129	*POA1*	Predicted ORF in Assemblies 19, 20 and 21
	Cd36_80010		3	2.1856923	1.1280904		
	Cd36_46720		4	2.1908233	1.1314731		
	Cd36_17200	orf19.1562	2	2.2060626	1.1414738		Predicted ORF in Assemblies 19, 20 and 21
	Cd36_00010		1	2.232283	1.15852		
	Cd36_08550	orf19.4763	1	2.243199	1.1655576	*FUN14*	Protein not essential for viability
	Cd36_31750	orf19.3877	R	2.256542	1.1741136		Predicted ORF in Assemblies 19, 20 and 21
	Cd36_11890	orf19.6350	1	2.256839	1.1743035		Predicted ORF in Assemblies 19, 20 and 21
	Cd36_01870	orf19.4524	1	2.2606099	1.176712	*ASG1*	Predicted zinc-finger protein of unknown function
	Cd36_28870	orf19.4366	R	2.265403	1.1797677		Predicted ORF in Assemblies 19, 20 and 21
	Cd36_50580	orf19.931	5	2.2665823	1.1805185		Predicted ORF in Assemblies 19, 20 and 21
	Cd36_25940		R	2.266687	1.1805851		
NOT4	Cd36_28580	orf19.2379	R	2.2783246	1.1879733	*MOT2*	Putative E3 ubiquitin-protein ligase
	Cd36_28730	orf19.4391	R	2.2827492	1.1907723		Predicted ORF in Assemblies 19, 20 and 21

Gene Name	*C. dubliniensis* Cd36 identifier	*C. albicans* orf19 identifier	C'some	Fold change expression	Normalised Expression	*S. cerevisiae* ortholog	Description
CDC4	Cd36_26650	orf19.2559	R	2.285887	1.192754	*CDC4*	F-box subunit of SCF(CDC4) ubiquitin ligase
	Cd36_30130	orf19.6316	R	2.3014362	1.2025344	*YMR221C*	Predicted ORF in Assemblies 19, 20 and 21
	Cd36_04650	orf19.752	1	2.3026562	1.203299		Predicted ORF in Assemblies 19, 20 and 21
	Cd36_46730		4	2.303094	1.2035732		
	Cd36_42120	orf19.4567	4	2.3045719	1.2044988		Catechol 1,2-dioxygenase (1,2-CTD), involved in degradation of aromatic compounds
	Cd36_26440	orf19.2529	R	2.3263066	1.2180412		Predicted ORF in Assemblies 19, 20 and 21
	Cd36_50010		5	2.340554	1.22685		
SKN1	Cd36_85750	orf19.7362	3	2.340625	1.2268939	*KRE6*	Protein with predicted role in beta-1,6-glucan synthesis
DUR1,2	Cd36_04410	orf19.780	1	2.352441	1.2341585	*DUR1,2*	Transcription is regulated by Nrg1p
MDL1	Cd36_27070	orf19.2615	R	2.3612595	1.2395566	*MDL1*	Putative mitochondrial, half-size MDR-subfamily ABC transporter
MNN22	Cd36_44410	orf19.3803	4	2.3682203	1.2438034	*MNN2*	Protein described as similar to Golgi alpha-1,2-mannosyltransferase
SGA1	Cd36_81250	orf19.1719	3	2.3821158	1.2522436	*SGA1*	Putative glucoamylase
FMP45	Cd36_72040	orf19.6489	7	2.384302	1.253567	*FMP45*	Protein induced during the mating process
SAP7	Cd36_04610	orf19.756	1	2.399078	1.26248	*YPS3*	Member of the secreted aspartyl proteinase family
	Cd36_29880	orf19.542.2	R	2.4008715	1.2635581	*MIM1*	ORF Predicted by Annotation Working Group
PGA12	Cd36_35200	orf19.7597	R	2.4096186	1.2688048	*PMU1*	Putative GPI-anchored protein of unknown function
	Cd36_65120	orf19.2125	6	2.4206796	1.2754121		Predicted ORF in Assemblies 19, 20 and 21
HSP30	Cd36_01850	orf19.4526	1	2.4576826	1.2972987	*HSP30*	Protein described as similar to heat shock protein
	Cd36_10140	orf19.2336	1	2.4676385	1.3031311	*PRY3*	Predicted ORF in Assemblies 19, 20 and 21
	Cd36_28380	orf19.2398	R	2.4745576	1.3071706		Predicted ORF in Assemblies 19, 20 and 21
	Cd36_25010		R	2.4746218	1.3072081		
PDC12	Cd36_41740	orf19.4608	4	2.4869592	1.3143828	*PDC1*	Putative pyruvate decarboxylase
	Cd36_43690	orf19.5291	4	2.4971397	1.3202765	*SCS3*	Predicted ORF in Assemblies 19, 20 and 21
HIS3	Cd36_19370	orf19.183	2	2.5164313	1.3313792	*HIS3*	Imidazoleglycerol-phosphate dehydratase, enzyme of histidine biosynthesis
YMX6	Cd36_63450	orf19.5713	6	2.5172648	1.331857	*NDE1*	Protein described as NADH dehydrogenase
	Cd36_16030	orf19.2010	2	2.524791	1.336164		Predicted ORF in Assemblies 19, 20 and 21
	Cd36_63090	orf19.5573	6	2.5482895	1.3495291		Predicted ORF in Assemblies 19, 20 and 21
	Cd36_81220	orf19.1723	3	2.553246	1.3523326	*YJL055W*	Predicted ORF in Assemblies 19, 20 and 21
IFR2	Cd36_28420	orf19.2396	R	2.5542352	1.3528914	*YNL134C*	Increased transcription is observed upon benomyl treatment
CUP1	Cd36_54185	orf19.3940.1	5	2.5684662	1.3609071		Metallothionein, involved in copper resistance
	Cd36_01880	orf19.4523	1	2.5799718	1.3673552	*FAU1*	Predicted ORF in Assemblies 19, 20 and 21
LSC2	Cd36_32310	orf19.1860	R	2.5923426	1.3742564	*LSC2*	Protein described as beta subunit of succinate-CoA ligase
	Cd36_29890	orf19.543	R	2.595124	1.3758035	*FUM1*	Protein described as fumarate hydratase
FCY2	Cd36_83310	orf19.333	3	2.6019652	1.3796017	*FCY2*	Putative purine-cytosine permease of pyrimidine salvage
CDG1	Cd36_34565	orf19.7314	R	2.6239815	1.3917575		Protein described as similar to cysteine dioxygenases
	Cd36_16390	orf19.1461	2	2.626228	1.3929923		Predicted ORF in Assemblies 19, 20 and 21
	Cd36_07860	orf19.5114	1	2.6265883	1.3931901	*SNX3*	Predicted ORF in Assemblies 19, 20 and 21
PGA30	Cd36_43790	orf19.5303	4	2.627979	1.3939538	*DAN4*	Putative GPI-anchored protein of unknown function
	Cd36_50520	orf19.938	5	2.6314006	1.3958309		Predicted ORF in Assemblies 19, 20 and 21
	Cd36_21700	orf19.1888	2	2.6371152	1.3989606	*URH1*	Predicted ORF in Assemblies 19, 20 and 21
	Cd36_32460	orf19.178	R	2.6372955	1.3990592		Predicted ORF in Assemblies 19, 20 and 21
IFF11	Cd36_80550	orf19.5399	3	2.6387358	1.3998469	*WSC4*	Secreted protein required for normal cell wall structure and for virulence
	Cd36_25110	orf19.7531	R	2.640623	1.4008784	*YMR090W*	Predicted ORF in Assemblies 19, 20 and 21
ACS2	Cd36_04040	orf19.1064	1	2.6828732	1.4237789	*ACS2*	Probable acetyl-CoA synthetase, similar to known fungal acetyl-CoA synthetases
	Cd36_73900	orf19.7149	7	2.6966183	1.4311514	*YMR258C*	Predicted ORF in Assemblies 19, 20 and 21
	Cd36_29540	orf19.510	R	2.6997259	1.4328129	*DEF1*	Predicted ORF in Assemblies 19, 20 and 21
SOL3	Cd36_32240	orf19.704	R	2.7297509	1.4487693	*SOL3*	Predicted ORF in Assemblies 19, 20 and 21
	Cd36_31600	orf19.3865	R	2.732035	1.449976	*RFX1*	Predicted ORF in Assemblies 19, 20 and 21
	Cd36_27310	orf19.3734	R	2.7354345	1.4517701	*GEF1*	Predicted ORF in Assemblies 19, 20 and 21
	Cd36_42100	orf19.4569	4	2.7410257	1.4547158		Predicted ORF in Assemblies 19, 20 and 21
PGA43	Cd36_45820	orf19.2910	4	2.763265	1.4663739		Putative GPI-anchored protein of unknown function
	Cd36_31820	orf19.3886	R	2.7957652	1.4832432		Predicted ORF in Assemblies 19, 20 and 21
IDP2	Cd36_27320	orf19.3733	R	2.8006892	1.4857819	*IDP2*	Putative isocitrate dehydrogenase
	Cd36_70450	orf19.7098	7	2.828694	1.5001361	*YKL070W*	Predicted ORF in Assemblies 19, 20 and 21
	Cd36_15160	orf19.2114	2	2.8560822	1.5140375		Predicted ORF in Assemblies 19, 20 and 21
	Cd36_15700	orf19.2048	2	2.8625627	1.5173073		Transcription is positively regulated by Sfu1p
	Cd36_19630	orf19.3544	2	2.8950331	1.5335798	*YML131W*	Predicted ORF in Assemblies 19, 20 and 21
PHO89	Cd36_41830	orf19.4599	4	2.9060578	1.5390635	*PHO89*	Putative phosphate permease
	Cd36_17880	orf19.5785	2	2.927362	1.5496012		Predicted ORF in Assemblies 19, 20 and 21
DAL7	Cd36_12840	orf19.5023	1	2.9297187	1.5507622	*DAL5*	Putative allantoate permease
GDH3	Cd36_45660	orf19.4716	4	2.9395502	1.5555954	*GDH3*	Protein described as similar to NADP-glutamate dehydrogenase
LEU1	Cd36_25490	orf19.7498	R	2.950859	1.561135	*LEU1*	Protein described as 3-isopropylmalate dehydratase
	Cd36_28400	orf19.2397.3	R	2.9699526	1.5704399	*YGR127W*	ORF Predicted by Annotation Working Group
PGA41	Cd36_46040	orf19.2906	4	2.9953728	1.5827355	*CRH1*	Putative GPI-anchored protein of unknown function
GAL4	Cd36_24740	orf19.5338	2	3.0635285	1.6151943	*GAL4*	Putative transcription factor with zinc cluster DNA-binding motif
NCE103	Cd36_81230	orf19.1721	3	3.0875173	1.6264472	*NCE103*	Carbonic anhydrase involved in the conversion of carbon dioxide to bicarbonate
SFL1	Cd36_31370	orf19.454	R	3.100988	1.6327279	*SFL1*	Protein involved in negative regulation of flocculation and filamentous growth
	Cd36_54570	orf19.3986	5	3.1072736	1.6356493	*PPR1*	Putative transcription factor with zinc cluster DNA-binding motif

Gene Name	*C. dubliniensis* Cd36 identifier	*C. albicans* orf19 identifier	C'some	Fold change expression	Normalised Expression	*S. cerevisiae* ortholog	Description
	Cd36_85030	orf19.5976	3	3.1219387	1.6424422	*YPR152C*	Predicted ORF in Assemblies 19, 20 and 21
ZCF25	Cd36_42110	orf19.4568	4	3.1386409	1.6501399	*PUT3*	Putative transcription factor with zinc cluster DNA-binding motif
	Cd36_44300		4	3.1495943	1.655166		
	Cd36_03280	orf19.3051	1	3.1937735	1.675262	*YJR116W*	Predicted ORF in Assemblies 19, 20 and 21
	Cd36_43010	orf19.2674	4	3.1983697	1.6773367		Putative transcription factor with zinc finger DNA-binding motif
	Cd36_32000	orf19.716	R	3.2006361	1.6783587		Predicted ORF in Assemblies 19, 20 and 21
DEF1	Cd36_34980	orf19.7561	R	3.2212634	1.6876266	*DEF1*	Transcription is induced upon filamentous growth
	Cd36_34200	orf19.6435	R	3.2718213	1.710094	*YGR243W*	Predicted ORF in Assemblies 19, 20 and 21
	Cd36_72580	orf19.5169	7	3.3094814	1.7266052	*AMD2*	Predicted ORF in Assemblies 19, 20 and 21
	Cd36_73210	orf19.6688	7	3.3377097	1.7388585	*WSC4*	Decreased transcription is observed upon benomyl treatment or in an azole-resistant strain that overexpresses MDR1
	Cd36_63200	orf19.6690	6	3.3548985	1.7462691		Predicted ORF in Assemblies 19, 20 and 21
ACH1	Cd36_51850	orf19.3171	5	3.3906572	1.761565	*ACH1*	Soluble protein in hyphae
HEM14	Cd36_08380	orf19.4747	1	3.4449947	1.7845018	*HEM14*	Putative protoporphyrinogen oxidase involved in heme biosynthesis
MUM2	Cd36_55040	orf19.4044	5	3.4677074	1.7939821	*MUM2*	Protein similar to S. cerevisiae Mum2p
	Cd36_09720	orf19.4903	1	3.5546274	1.8296983	*GPI12*	Predicted ORF in Assemblies 19, 20 and 21
	Cd36_17890	orf19.5784	2	3.5720603	1.8367565		Predicted ORF in Assemblies 19, 20 and 21
	Cd36_26350	orf19.2517	R	3.6274056	1.8589381	*HOL1*	Predicted ORF in Assemblies 19, 20 and 21
SOD4	Cd36_15610	orf19.2062	2	3.6319273	1.8607353		Copper- and zinc-containing superoxide dismutase, expression is regulated during white-opaque switching
GNP3	Cd36_35010	orf19.7565	R	3.699621	1.8873775	*AGP1*	Putative high-affinity glutamine permease
YHB5	Cd36_33470	orf19.3710	R	3.7324653	1.9001288	*YHB1*	Protein related to flavohemoglobins
	Cd36_19360	orf19.184	2	3.7452574	1.9050648	*MDM10*	Predicted ORF in Assemblies 19, 20 and 21
	Cd36_42400	orf19.2751	4	3.7837968	1.9198346	*MCH4*	Predicted ORF in Assemblies 19, 20 and 21
	Cd36_73980	orf19.7130	7	3.8029642	1.9271244		Predicted ORF in Assemblies 19, 20 and 21
	Cd36_05640	orf19.2449	1	3.9192472	1.9705765	*MUC1*	Predicted ORF in Assemblies 19, 20 and 21
	Cd36_24800		2	3.9362442	1.9768198		
GCA1	Cd36_09690	orf19.4899	1	4.052068	2.0186584	*ROT2*	Predicted extracellular or plasma membrane-associated glucoamylase
ARF1	Cd36_34290	orf19.6447	R	4.073013	2.0260963	*ARF1*	ADP-ribosylation factor, probable GTPase involved in intracellular transport
	Cd36_04210	orf19.6840	1	4.1207323	2.0429008		Predicted ORF in Assemblies 19, 20 and 21
	Cd36_12200	orf19.4940	1	4.169186	2.0597658	*HIP1*	Putative histidine permease
	Cd36_54050	orf19.3926	5	4.331947	2.1150155	*RNY1*	Predicted ORF in Assemblies 19, 20 and 21
	Cd36_29560	orf19.511	R	4.335034	2.1160433	*NRK1*	Predicted ORF in Assemblies 19, 20 and 21
	Cd36_31810	orf19.3885	R	4.3400373	2.1177075		Predicted ORF in Assemblies 19, 20 and 21
HSP31	Cd36_01930	orf19.3664	1	4.5587273	2.188631	*HSP30*	Protein repressed during the mating process
	Cd36_34320		R	4.6342154	2.212325		
UBC15	Cd36_24750	orf19.5337	2	4.6967745	2.2316704	*UBC13*	Predicted ORF in Assemblies 19, 20 and 21
	Cd36_28430	orf19.2395	R	4.7755203	2.255658	*IME2*	Predicted ORF in Assemblies 19, 20 and 21
	Cd36_33480	orf19.3711	R	4.7761455	2.2558467		Predicted ORF in Assemblies 19, 20 and 21
	Cd36_54120		5	5.196872	2.3776436		
PGA58	Cd36_52810	orf19.4334	5	5.2602386	2.3951283	*CCW12*	Putative GPI-anchored protein of unknown function
	Cd36_43450	orf19.1307	4	5.265162	2.396478	*THI74*	Predicted ORF in Assemblies 19, 20 and 21
HGT17	Cd36_41060	orf19.4682	4	5.295716	2.4048257	*HXT17*	Putative glucose transporter of the major facilitator superfamily
ECE1	Cd36_43260	orf19.3374	4	5.332768	2.4148846		Protein comprising eight 34-residue repeats
HGT13	Cd36_70500	orf19.7093	7	5.4570436	2.4481196	*STL1*	Putative glucose transporter of the major facilitator superfamily
	Cd36_25330	orf19.7504	R	5.7147803	2.514698	*RTS3*	Predicted ORF in Assemblies 19, 20 and 21
MNN1	Cd36_52400	orf19.4279	5	5.740784	2.5212479	*MNN1*	Putative alpha-1,3-mannosyltransferase, a component of mannosyltransferase complex
	Cd36_43250	orf19.3373	4	5.903606	2.5615964	*RIM4*	Predicted ORF in Assemblies 19, 20 and 21
PGA13	Cd36_34100	orf19.6420	R	5.925389	2.5669098	*DAN4*	Putative GPI-anchored protein
FGR2	Cd36_70160	orf19.7071	7	6.0519524	2.5974007		Protein similar to phosphate transporters
	Cd36_34340		R	6.454561	2.690319		
	Cd36_28690	orf19.4394	R	6.45593	2.690625		Predicted ORF in Assemblies 19, 20 and 21
	Cd36_27950	orf19.2846	R	6.705009	2.7452393		Predicted ORF in Assemblies 19, 20 and 21
HGT10	Cd36_64300	orf19.5753	6	7.2212887	2.8522563	*STL1*	Putative glucose transporter of the major facilitator superfamily
	Cd36_33320	orf19.6282	R	7.584961	2.9231417	*NSR1*	Predicted ORF in Assemblies 19, 20 and 21
	Cd36_73750	orf19.7167	7	8.107295	3.0192206		Predicted ORF in Assemblies 19, 20 and 21
	Cd36_54780	orf19.4011	5	8.119587	3.0214064	*SAY1*	Predicted ORF in Assemblies 19, 20 and 21
	Cd36_20990	orf19.1225	2	9.723123	3.2814198		Predicted ORF in Assemblies 19, 20 and 21
	Cd36_54540	orf19.3982	5	11.992067	3.5840085	*YOL157C*	Maltase
	Cd36_00040		1	13.706082	3.7767444		
LIP4	Cd36_72950	orf19.2133	7	17.03029	4.090031		Secreted lipase, member of a differentially expressed lipase gene family with possible roles in nutrition and/or in creating an acidic microenvironment
CTA26	Cd36_35580	orf19.7680	R	40.62084	5.344148		Putative transcriptional activator